The Dissertation Committee for Craig Eugene Quadrato certifies that this is the approved version of the following dissertation:

Stability of Skewed I-Shaped Girder Bridges

Using Bent Plate Connections

Committee:

Todd A. Helwig, Supervisor

Michael D. Engelhardt

Karl H. Frank

Eric B. Williamson

Kenneth M. Liechti

Stability of Skewed I-Shaped Girder Bridges

Using Bent Plate Connections

by

Craig Eugene Quadrato, B.S.; M.S.

Dissertation

Presented to the Faculty of the Graduate School of

The University of Texas at Austin

in Partial Fulfillment

of the Requirements

for the Degree of

Doctor of Philosophy

The University of Texas at Austin

May 2010

Dedication

To my wife and best friend Kristi

for all your undying love,

enduring encouragement and

unyielding support.

Acknowledgements

I would like to thank my dissertation committee for all the support that sustained me throughout this research study. Dr. Helwig's guidance formed the cornerstone of my graduate experience and will continue into the rest of my academic career. Dr. Engelhardt's insight and experience into structural analysis, testing, and finite element modeling made the project successful beyond my wildest expectations. Dr. Frank's extensive bridge engineering and laboratory testing knowledge saved at least a year's worth of searching for the right answer. Dr. Williamson's finite element modeling experience proved to be the key to getting the model to match the laboratory results so closely. Dr. Liechti's mentorship in experimental methods gave me the experimental background I sorely lacked to perform the laboratory testing required.

The Staff and Faculty of the Ferguson Structural Engineering Laboratories at The University of Texas at Austin were absolutely critical in performing the connection and large scale girder testing. Blake Stasney, Dennis Fillip, Andrew Valentine, Mike Wason, and Eric Schell gave me the freedom to work, guidance when needed, and kept me safe from myself. Without them, the testing would not have happened.

Also, the "platoon" of other students that worked on the project was invaluable to its completion. Thanks to Rangsan Wongjeeraphat, Anthony Battistini, Wei Wang, Andrew Wahr, Sean Donahue, Ryan Hall, and Loren Campos. Their diligent work allowed the timely completion of this study

Finally, nothing happens without great administrative support. I would sincerely like to thank Ms. Barbara Howard and Ms. Jessica Hanten for keeping the financing straight and the parts flowing.

April 29, 2010

Stability of Skewed I-Shaped Girder Bridges Using Bent Plate Connections

Publication No. _____

Craig Eugene Quadrato, Ph.D.
The University of Texas at Austin, 2010

Supervisor: Todd A. Helwig

Lateral bracing systems consisting of cross frames and their connections play a significant role in the elastic buckling strength of steel girder bridges. By providing lateral and torsional stability, they prevent lateral torsional buckling of the girder during bridge construction prior to the concrete bridge deck curing. To perform this function, the bracing system must possess adequate strength and stiffness. And since each component of the bracing system acts in series, the overall stiffness of the system is less than the least stiff component.

In skewed bridges, cross frames at the ends of the girders are installed parallel to the bridge skew angle, and their connection to the girder requires that the cross frames be at an angle that prohibits welding a stiffener from the cross frame directly to the girder

web. To make this connection, many states use a bent plate to span the angle between the web stiffener and cross frame.

While this bent plate connection is now being widely used, it has never been rationally designed to account for its strength or stiffness in the bracing system. Results from field studies show that the bent plate connection may be limiting the cross frame stiffness thereby hampering its ability to provide stability to the girder during construction. The result is significant girder end rotations. The purpose of this research is to classify the impact of the bent plate connection on the end cross frame stiffness in skewed straight steel girder bridges and propose methods to improve the end cross frame's structural efficiency.

This research uses laboratory testing, finite element modeling, and parametric studies to recommend design guidance and construction practices related to the end cross frames of skewed steel girder bridges. In addition to recommending methods to stiffen the existing bent plate connection, an alternative pipe stiffener connection is evaluated. The pipe stiffener not only offers the possibility of a stiffer connection, but can also provide warping restraint to the end of the girder which may significantly increase the girder elastic buckling capacity.

Table of Contents

List of Tables

List of Figures

CHAPTER 1
Introduction

1.1 PROBLEM DESCRIPTION

Cross frames serve an important role in steel bridges by causing adjacent girder lines to resist applied loads as a unit, thereby enhancing torsional stiffness of the system and providing overall stability. The critical stage for cross frames is generally during construction before the concrete deck has cured, since at this stage the steel girders must support all of the applied loads. After the concrete deck has cured, cross frames help resist lateral loads during the service life of the bridge. The cross frame spacing is typically controlled by the construction loading case prior to the concrete deck curing. While The American Association of State Highways and Transportation Officials (AASHTO) design guidelines (American Association of State Highway and Transportation Officials 2007) allow a rational analysis to determine cross frame spacing, many states and jurisdictions use rules based on previous experience to set intermediate cross frame spacing.

Although the primary purpose of the majority of the cross frames is served for just a few short weeks while the bridge is under construction, their fabrication and erection represent substantial cost in materials and labor. Additionally, each cross frame attached to the girder must be periodically inspected for fatigue cracking, which causes additional cost and risk during the bridge service life.

Cross frames in skewed bridges present additional challenges. A skewed bridge is one with supporting elements across the width of the bridge that intersect the bridge cross section at an angle other than 90 degrees (see Figure 1.1 and Figure 1.2). The necessity of the skewed supports is typically related to geometric issues with intersecting roadways or the surrounding terrain. The skewing of a bridge requires that the abutments not be perpendicular to the girder's longitudinal axis. This causes an offset to the support in each adjacent girder. This offset is shown in Figure 1.3 for a bridge with a nearly 60°

skew angle. The left exterior girder has a 70' offset to the support while the right exterior girder has no offset at the highlighted intermediate cross frame line.

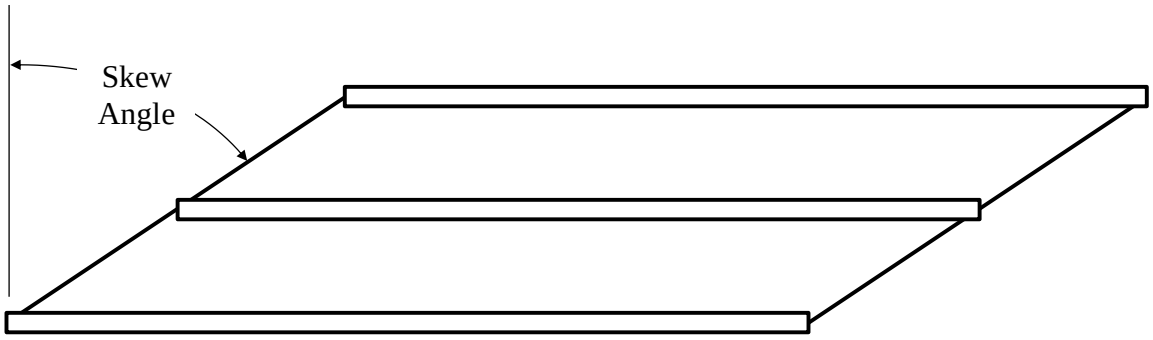

Figure 1.1: Skewed bridge plan view showing positive skew angle

Figure 1.2: Skewed straight steel girder bridge

As trucks pass over the bridge, the support offset causes differential deflections between the adjacent girders and makes the bridge twist along the contiguous line of intermediate cross frames inducing live load forces in the cross frame members. In turn,

these cyclic live load forces cause additional fatigue risk not experienced in unskewed bridges.

Figure 1.3: Skewed bridge support offset

Additionally, since the girders are generally connected through a series of end cross frames, the skewed end brace has components directed along both the longitudinal and transverse direction on the girder end. As the girders experience a strong axis rotation at the skewed support, forces are induced in the cross frame that produce girder end twist (Figure 1.4). Accounting for this end twist complicates both the fabrication and erection of cross frames. Also, excessive girder end twist is likely to reduce the buckling capacity of the girder.

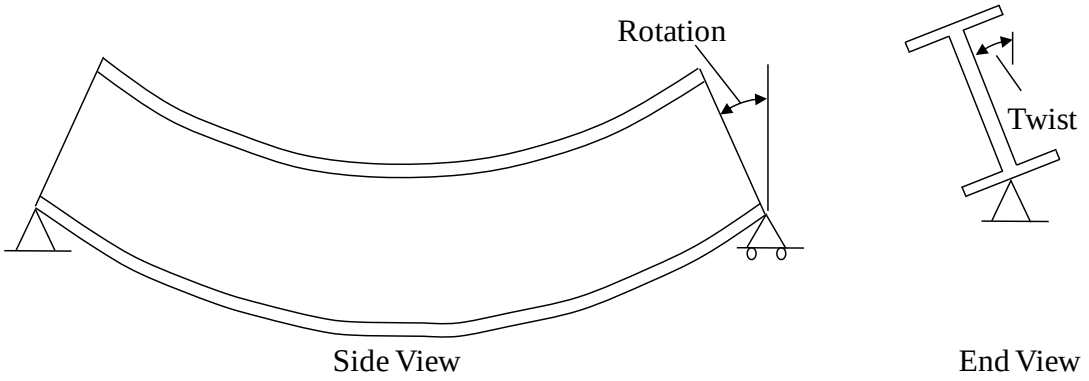

Figure 1.4: Girder rotation and end twist

1.2 PREVIOUS AND PROPOSED SOLUTIONS

Several methods may be taken to mitigate the live load induced cross frame fatigue issues. First, the intermediate cross frame line may be skewed to match the bridge skew angle. However, AASHTO only allows this for skew angles less than or equal to 20° since the cross frame stiffness perpendicular to the girder drops significantly as the skew increases. The lower stiffness reduces the effectiveness of the cross frame and may result in dangerous conditions on the bridge. This was the case in the Churchman Road Bridge in Delaware where skewed intermediate cross frames at an angle of approximately 60° (significantly larger than the 20° limit in AASHTO) were used as shown in Figure 1.5. The subsequent reduction in stiffness caused excessive girder twist under steel dead load alone. This twist required significant retrofit before the concrete slab could be placed (Winterling 2007).

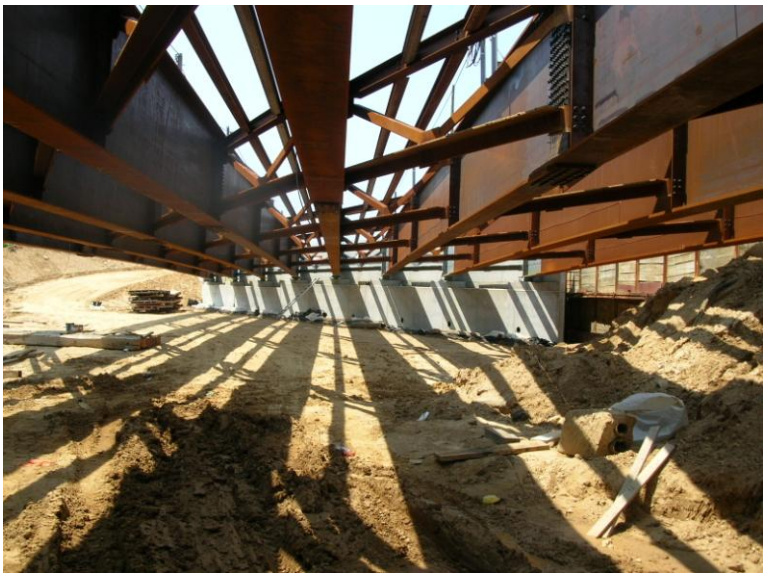

Figure 1.5: Churchman Road Bridge Delaware skewed intermediate cross frames

Another method to mitigate the intermediate live load forces is to use a lean-on bracing system as pictured in Figure 1.3. In the lean-on bracing system, the diagonal members of some cross frames are removed so the cross frame no longer represents a rigid support line across the width of the bridge. Therefore, as the bridge twists, the intermediate cross frames attract less live load force and thus reduce the associated fatigue issues (Herman, Helwig and Chong 2007) (Wang 2002).

Finally, another mitigation measure may be to make the cross frames at the abutments and intermediate piers more efficient in stabilizing the girder end so the first row of intermediate cross frames may be moved farther from the abutment and intermediate piers. By doing this, the intermediate cross frames will be moved to a region that has less differential deflection which will reduce the live load forces they attract. Additionally, if the end cross frames are stiffened; they will be more effective in limiting the girder end twist previously described. This will make cross frame fit up easier and aid in keeping the girder webs plumb after concrete deck placement.

However, making the end cross frames more efficient cannot be done by adjusting their skew angle because AASHTO requires that the end cross frames be parallel to the bridge skew angle to support the slab edge and transfer any lateral forces to the bearings

(American Association of State Highway and Transportation Officials 2007). Therefore another method must be found to stiffen the end cross frames.

1.3 SKEWED END CROSS FRAME CONNECTIONS

In order to most efficiently stiffen the skewed end cross frames, the least stiff component of the cross frame should be identified because stiffening this component will have the greatest effect. While previous research has quantified the stiffness of the brace members, girder in-plane stiffness, and the girder cross sectional stiffness, only limited research exists on the stiffness of the cross frame to girder connection.

Many states, like Texas, have allowed a bent plate to connect the cross frame to the girder parallel to the skew angle (AASHTO/NSBA Steel Bridge Collaboration 2003) as shown in Figure 1.6 and Figure 1.7. The bent plate and the connection plate it attaches to, appear to be relatively flexible and, if they represent the least stiff component in the cross frame system, will be the limiting factor in the cross frame stiffness.

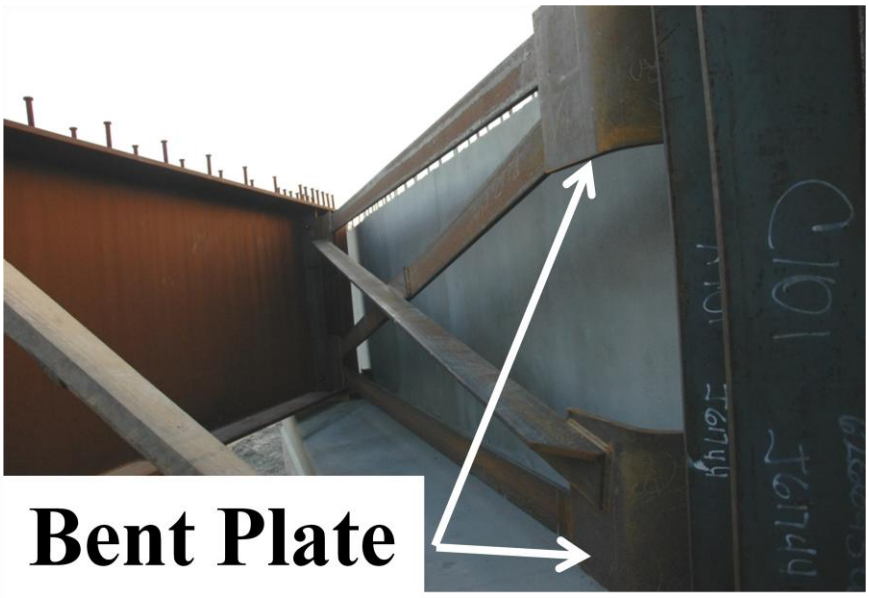

Figure 1.6: Bent plate end cross frame connection elevation view

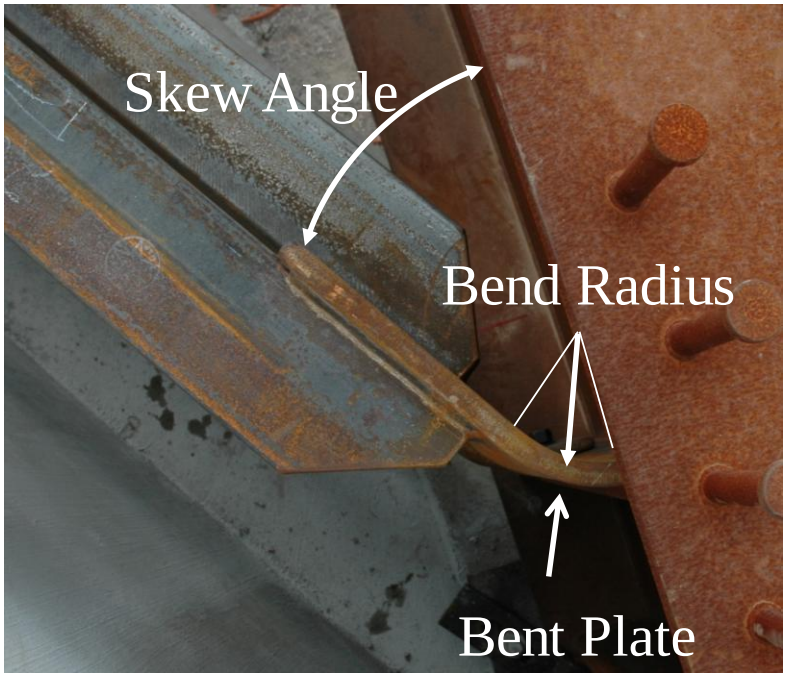

Figure 1.7: Bent plate end cross frame connection plan view

If the bent plate connection is the least stiff cross frame component, then it will limit the force the cross frame attracts. This effect was investigated during concrete deck placement of a nearly 60° skewed bridge in Lubbock, Texas. One end cross frame was instrumented with strain gages so the brace member forces could be monitored during the concrete deck placement.

The results for the top strut of the end cross frame are shown in Figure 1.8. The results show that the axial force never exceeded 4 kips in the cross frame member. Additionally, no end cross frame member's axial force exceeded 4 kips during the concrete placement (Battistini 2009). One of the reasons for this may have been the bent plate's flexibility. By limiting the cross frame's stiffness, the bent plate keeps the end cross frame from attracting higher forces. It therefore may also allow the girder to rotate an excessive amount relative to the support. If the bent plate connection could be stiffened, then the end cross frame would attract more force and therefore be used more efficient in the skewed bridge bracing system.

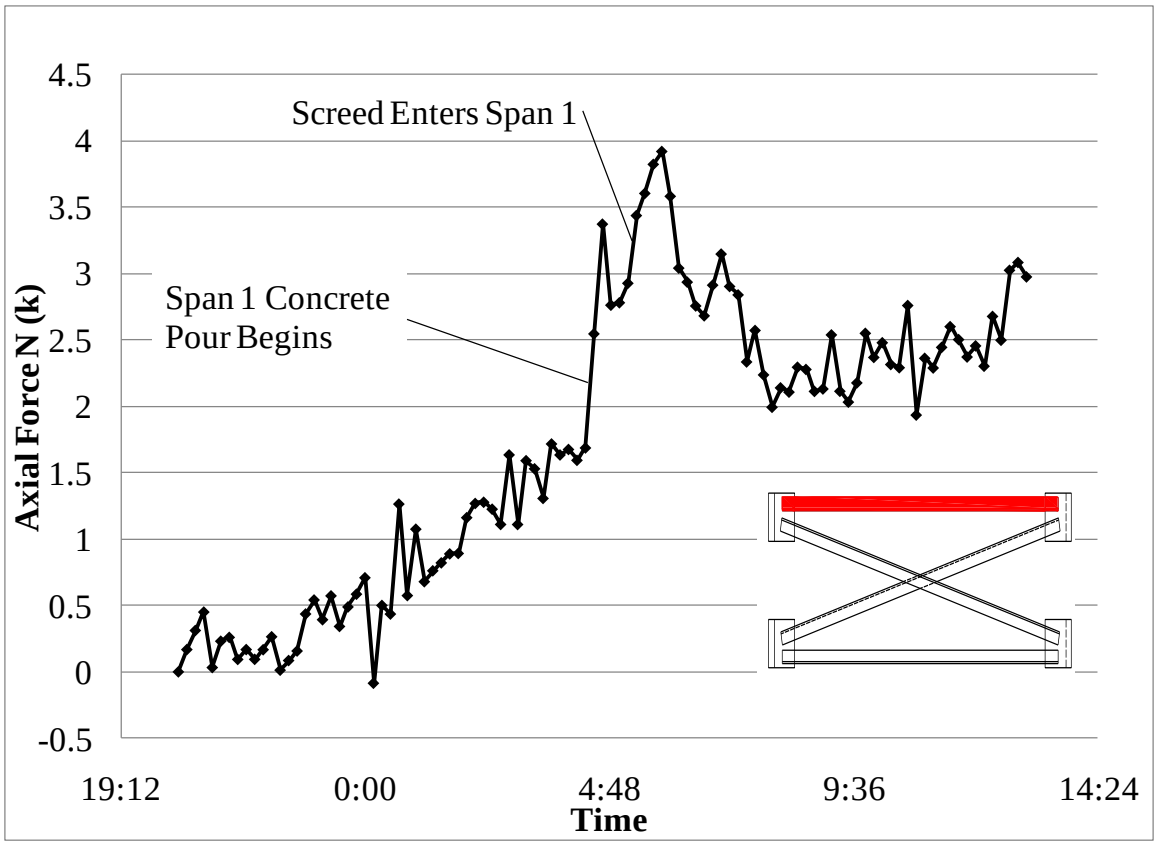

Figure 1.8: Top strut axial force during concrete placement

1.4 RESEARCH PURPOSE

The purpose of this research is to propose methods to make the end cross frames more structurally efficient so they reduce girder end twist and allow the first row of intermediate cross frames to be moved further from the abutment region. Moving the first row of intermediate cross frames farther from the abutment is likely to decrease live load induced fatigue forces and mitigate fatigue cracking.

The research outlined in this dissertation primarily focuses on stiffening the end cross frame connection to the girder. In addition to recommending measures to stiffen the existing bent plate connection, a new connection has been proposed consisting of a pipe, split in half, and then each half welded to the girder web and flanges as shown in Figure 1.9. Besides offering the possibility of a stiffer connection, the split pipe also

offers warping restraint which has been shown to significantly increase girder elastic buckling capacity (Ojalvo and Chambers 1977). Increasing the girder buckling strength will result in larger permissible unbraced lengths and allow the first row of intermediate cross frames to be moved farther from the abutment region.

Figure 1.9: Split pipe end frame connection (53° skew)

1.5 RESEARCH METHODS

The methods used in this study include laboratory tests, finite element modeling and parametric studies. The laboratory tests consisted of small scale connection testing,

fatigue testing, and large scale single girder lateral load tests, as well as large scale two and three girder buckling tests.

The laboratory tests in this study were used to directly compare the impact of varying key parameters used in the experiments. In addition to demonstrating the fundamental behavior of cross frames in skewed bridges, the laboratory results provided valuable data that could be used to validate the finite element models created with the three-dimensional finite element program ANSYS® Academic Research, Release 11.0. This model was then used, in conjunction with the laboratory results, to conduct parametric studies that formed the basis for design guidance and recommendations.

1.6 REPORT ORGANIZATION

This report is organized into six chapters. An overview of previous research along with pertinent background information that is used in the subsequent chapters is provided in Chapter 2. A description of the experimental program including the connection, fatigue, and large scale girder lateral and buckling tests is provided in Chapter 3. Chapter 4 covers the modeling techniques used to create the finite element model as well as the analytic and experimental results used to validate the model. A description of the parametric studies performed as well as the analytic equations and conclusions derived from the parametric studies and laboratory experiments is provided in Chapter 5. Finally, the summary and conclusions are provided in Chapter 6 along with recommendations for future research efforts.

CHAPTER 2
Background

2.1 INTRODUCTION

The flexural strength of a girder can be controlled by several limit states, including the cross sectional yield strength (typically expressed as a yield or fully plastic moment capacity) or local or global instability of the girder. Local instabilities include local flange or web buckling, both of which are controlled by the respective plate slenderness. The global stability is governed by lateral torsional buckling of the girders, which consists of a simultaneous twist and lateral deflection of the girder as depicted in Figure 2.1. The global buckling strength is a function of the boundary conditions of the girder as well as the spacing between braces. To stabilize a girder and permit an increase in the buckling strength, a variety of bracing schemes may be employed to limit the laterally or torsionally unsupported length.

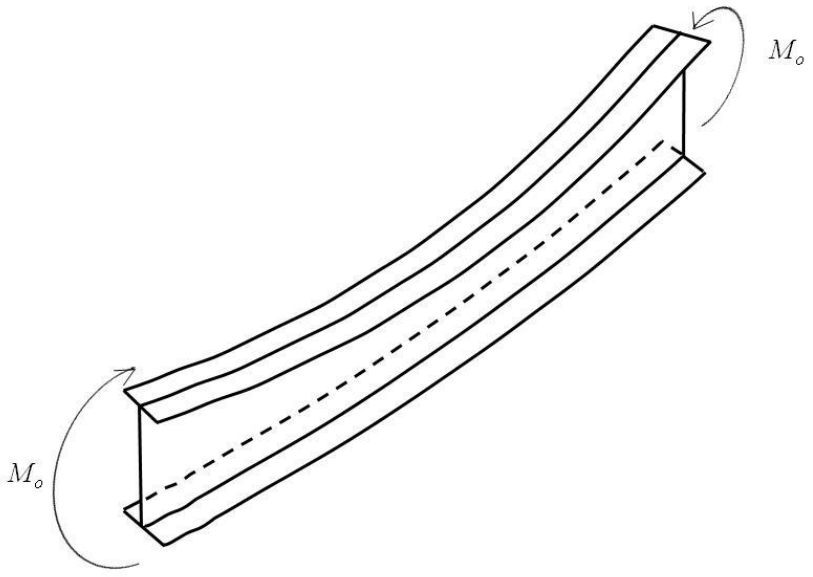

Figure 2.1: Girder lateral torsional buckling (Zhou, 2006).

For most boundary conditions, the compression flange of a girder experiences the largest lateral deformation as the beam buckles. Regions of the beam in tension do not tend to drive the buckling, and therefore the cross section also experiences torsional deformations. A beam's resistance to lateral torsional buckling can be improved by providing restraints at the ends of the beam or at locations along the length of the beam. The primary focus of the research documented in this dissertation is the role of bracing at the ends of the girder.

2.2 BASIC ELASTIC BEAM BUCKLING STRENGTH

Timoshenko and Gere (1961) used equilibrium and elastic theory to derive the critical lateral torsional buckling moment for an unbraced doubly symmetric beam under uniform moment with simple supports, no twist at the ends, and no warping restraint at the ends (Figure 2.2).

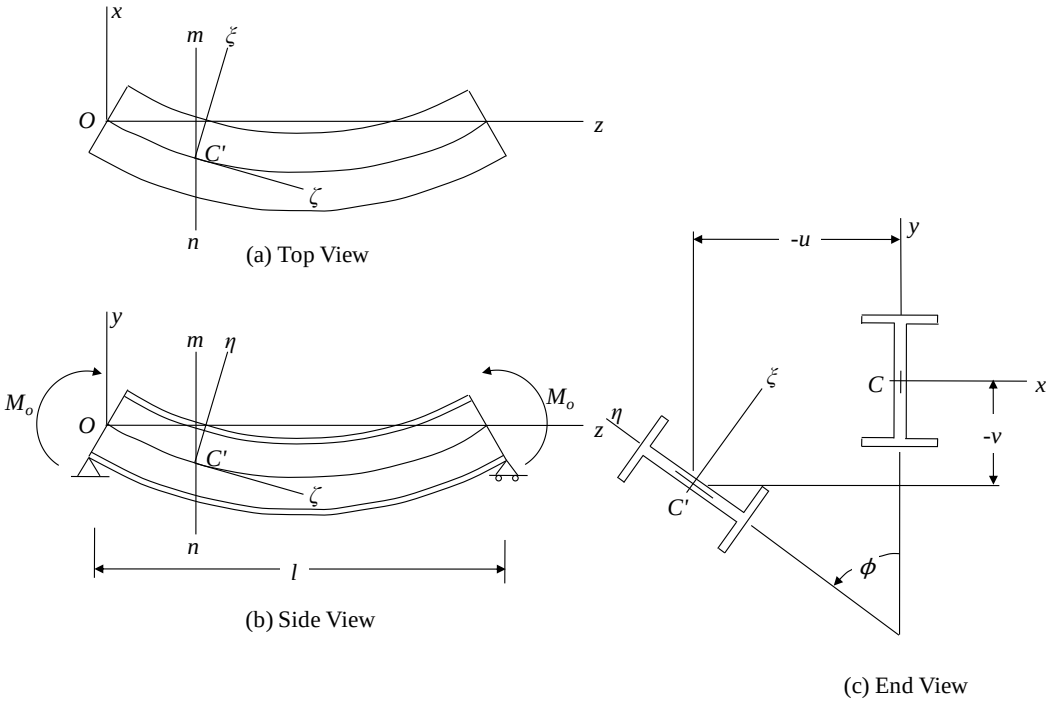

Figure 2.2: (a) Top, (b) side, and (c) end view of buckled beam.

For small deflections and rotations, Timoshenko and Gere transformed the moment about the *x*-axis (M_o) into the rotated coordinate system giving the moment components shown below.

$$M_\xi = M_o \tag{2.1}$$

$$M_\eta = \phi M_o \tag{2.2}$$

$$M_\zeta = -\frac{du}{dz} M_o \tag{2.3}$$

Then by using the equation for elastic curvature about each axis and the equation for twist of an open thin walled cross section, they found the following governing differential equations for vertical deflection (v), lateral translation (u), and twist (ϕ).

$$EI_\xi \frac{d^2v}{dz^2} - M_o = 0 \tag{2.4}$$

$$EI_\eta \frac{d^2u}{dz^2} - \phi M_o = 0 \tag{2.5}$$

$$GJ\frac{d\phi}{dz} - EC_w \frac{d^3\phi}{dz^3} + \frac{du}{dz} M_o = 0 \tag{2.6}$$

where

E = elastic modulus

I_ξ = strong-axis moment of inertia for the rotated cross section

I_η = weak-axis moment of inertia for the rotated cross section

G = shear modulus of elasticity

J = torsional constant

C_w = torsional warping constant

Equation 2.4 defines the bending behavior of a beam about the strong axis. Equations 2.5 and 2.6 contain cross terms of the lateral deformation (u) and angle of twist

of the beam (ϕ). By differentiating Equation (2.6) with respect to the z-axis and using Equation (2.5), the differential equation for the angle of twist becomes:

$$EC_w \frac{d^4\phi}{dz^4} - GJ\frac{d^2\phi}{dz^2} - \frac{{M_o}^2}{EI_\eta}\phi = 0 \tag{2.7}$$

Equation (2.7) is a fourth order homogenous equation with constant coefficients that can be solved using the differential operator technique to find two real and two complex roots. To perform this operation Equation (2.7) can be recast to simplify the final result.

$$\frac{d^4\phi}{dz^4} - 2\alpha\frac{d^2\phi}{dz^2} - \beta\phi = 0 \tag{2.8}$$

where

$$\alpha = \frac{GJ}{2EC_w} \tag{2.9}$$

$$\beta = \frac{{M_o}^2}{EI_\eta EC_w} \tag{2.10}$$

Then using the differential operator (D) Equation (2.8) becomes

$$D^4 - D^2 2\alpha - \beta = 0 \tag{2.11}$$

The roots for the auxiliary equation for Equation (2.11) are, respectively

$$m_1, m_2 = \pm i\sqrt{-\alpha + \sqrt{\alpha^2 + \beta}} \tag{2.12}$$

$$m_3, m_4 = \pm\sqrt{\alpha + \sqrt{\alpha^2 + \beta}} \tag{2.13}$$

So the solution becomes

$$\phi = A_1 e^{m_1 z} + A_2 e^{m_2 z} + A_3 e^{m_3 z} + A_4 e^{m_4 z} \tag{2.14}$$

Using Euler's formula the complex roots can be rewritten in terms of trigonometric functions giving the solution to the angle of twist as

$$\phi = A_1 \sin(m_1 z) + A_2 \cos(m_2 z) + A_3 e^{m_3} + A_4 e^{m_4} \tag{2.15}$$

The boundary conditions Timoshenko used at the end of the beam consisted of a simply supported beam free to warp with no twist. Applying these boundary conditions of no twist shown in Equation(2.16) provides a solution for the constants (A_1, A_2, A_3, and A_4) and the resulting solution for M_o in Equation (2.17).

$$\phi = \frac{d^2\phi}{d\phi^2} = 0 \tag{2.16}$$

$$M_{ocr} = \pi / L_b \sqrt{E I_y G J + \pi^2 E^2 C_w I_y / L_b^2} \tag{2.17}$$

where

M_{ocr} = buckling moment

L_b = unbraced length

I_y = weak-axis moment of inertia

Timoshenko's solution in Equation 2.17 is applicable to uniform moment loading on simply supported beams with twist prevented at the ends. However, depending on the bracing details that are used in practice, significant twist may occur at the ends of the beam. For example, in girders with skewed supports, the ends will twist to some degree and some warping restraint will be provided to the girder from the bracing. The amount of warping restraint, depends on the cross-frame-to-girder connection used. A discussion of how these two departures from the assumptions in Equation (2.17) may impact the basic girder buckling strength in skewed steel bridges is provided in the following two sections.

2.3 GIRDER END ROTATION IN SKEWED BRIDGES

The elastic buckling strength equation discussed in the preceding section was developed with the assumption that the girder ends do not twist. However, in a bridge with skewed supports, the girder ends are likely to twist. This twist occurs because the girder is part of the end cross frame system. As the girder deflects vertically, it induces a rotation perpendicular to its web. However, at the girder ends, the girder cannot rotate perpendicular to its web due to the high in-plane stiffness of the cross frame system. Instead, the cross frame twists about the abutment center line and induces a twist on the girder end (Ude 2009). The rotation vectors for this system are shown in Figure 2.3

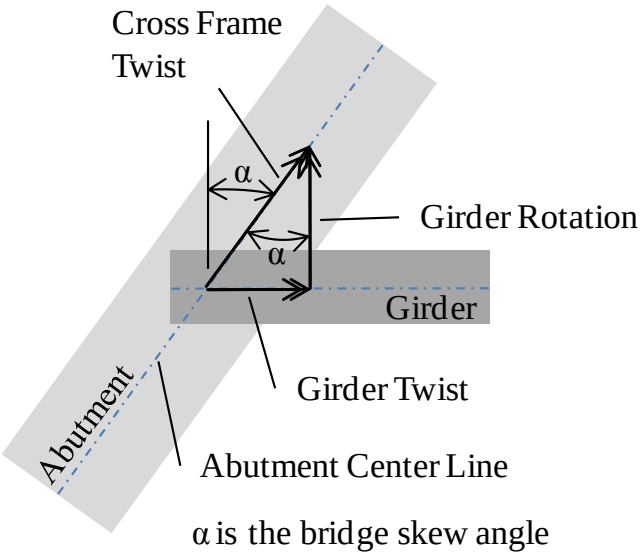

Figure 2.3: Cross frame twist induced by strong axis girder rotation.

One purpose of the end cross frames on a skewed bridge is to resist twist, but they will not completely prevent twist as assumed in Timoshenko's solution. The cross frame will prevent twist of the girder end by the couple imposed by the braces' axial stiffness and by the individual braces' flexural stiffnesses.

2.4 END CROSS FRAME STIFFNESS

To accurately account for the impact of end cross frames as well as intermediate frames on girder buckling capacities, equations quantifying the cross frame stiffness must be developed. Cross frames are a series of component stiffnesses and the overall cross frame stiffness can be calculated by adding, in series, the stiffness contribution of each component (Yura, 2001) as shown in Equation (2.18). An explanation for each cross frame component stiffness (brace, girder web, and girder in-plane stiffness,) is given below. Additionally a proposed solution to quantify the connection stiffness is given.

$$\frac{1}{\beta_T} = \frac{1}{\beta_{br}} + \frac{1}{\beta_{sec}} + \frac{1}{\beta_g} \tag{2.18}$$

where

β_{br} = stiffness of attached brace

β_T = discrete brace system stiffness

β_{sec} = web stiffness including any stiffeners

β_g = attached girder stiffness

2.4.1 Brace Stiffness (β_{br})

2.4.1.1 Introduction

The torsional resistance of the braces making up the cross frame system consists of an axial component and a bending component. The axial component comes from the brace's axial stiffness acting on the girder cross section with a separation typically described as the height of brace. The axial stiffnesses and related forces separated by the height of brace exert a stabilizing couple resisting the twist of the cross section. Additionally, the flexural stiffness of each brace member in the cross frame system will

also resist the twist of the cross section as long as they are connected to the cross section with a connection capable of transferring moment. So, in order for the girder cross section to twist, each connected brace must bend. The deflected shape of such a cross frame is shown in Figure 2.4.

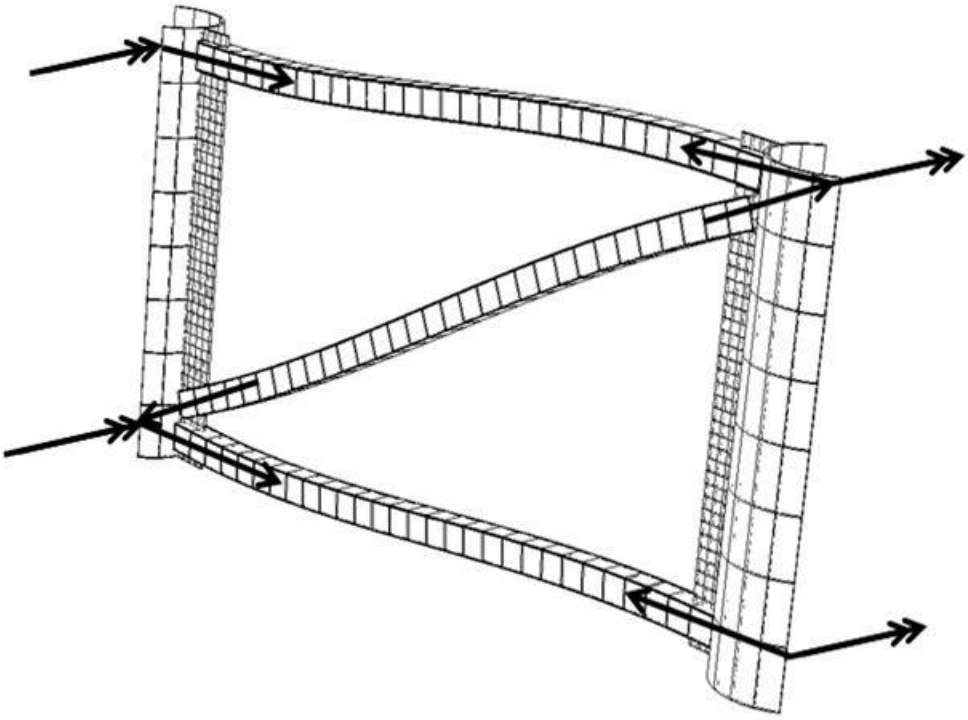

Figure 2.4: Cross frame with brace member axial force and moment vectors

2.4.1.2 Brace Axial Component of Torsional Stiffness

The equation describing the torsional restraint of the cross frame system due to the axial stiffnesses of its braces can be found in previous research for several different cross frame configurations (Yura, 2001) The complete derivation for a single diagonal cross frame is given below since it is typically used in the laboratory study. The derivation begins with the free body diagram of a cross frame shown in Figure 2.5. Although most conventional cross frames have two diagonals, these diagonals are often

composed of angles that have a relatively low buckling strength compared to the tensile strength. Therefore the cross frames are often modeled as a tension-only system, which is why the cross frame in Figure 2.5 only has a single diagonal.

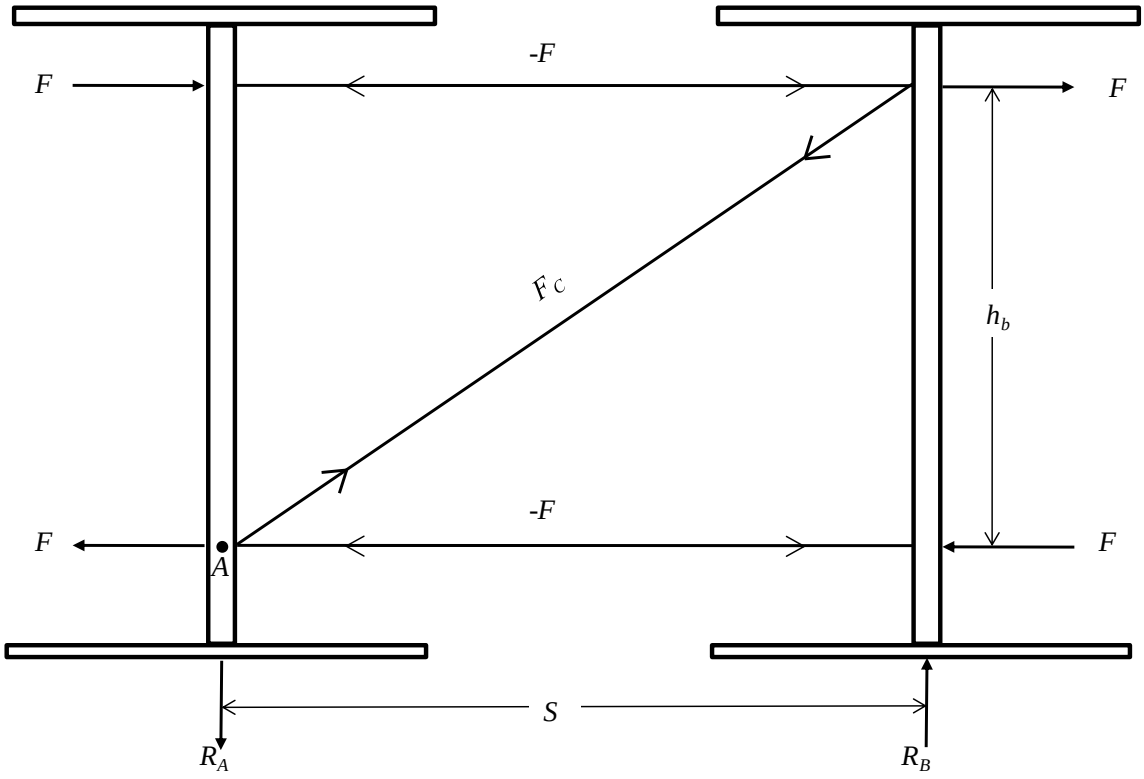

Figure 2.5. Single diagonal cross frame free body diagram

Using equilibrium the reactions at *A* and *B* (R_A and R_B) are solved by summing moments about point *A* then summing vertical forces using the free body diagram of joint *A* gives the force in the diagonal member (F_c).

$$R_A = R_B = \frac{2Fh_b}{S} \tag{2.19}$$

$$F_C = \frac{2FL_c}{S} \tag{2.20}$$

Then to find deflections in terms of the forces above, the deflected shape of the cross frame is drawn with all deflections taken on one side of the cross frame as shown in Figure 2.6.

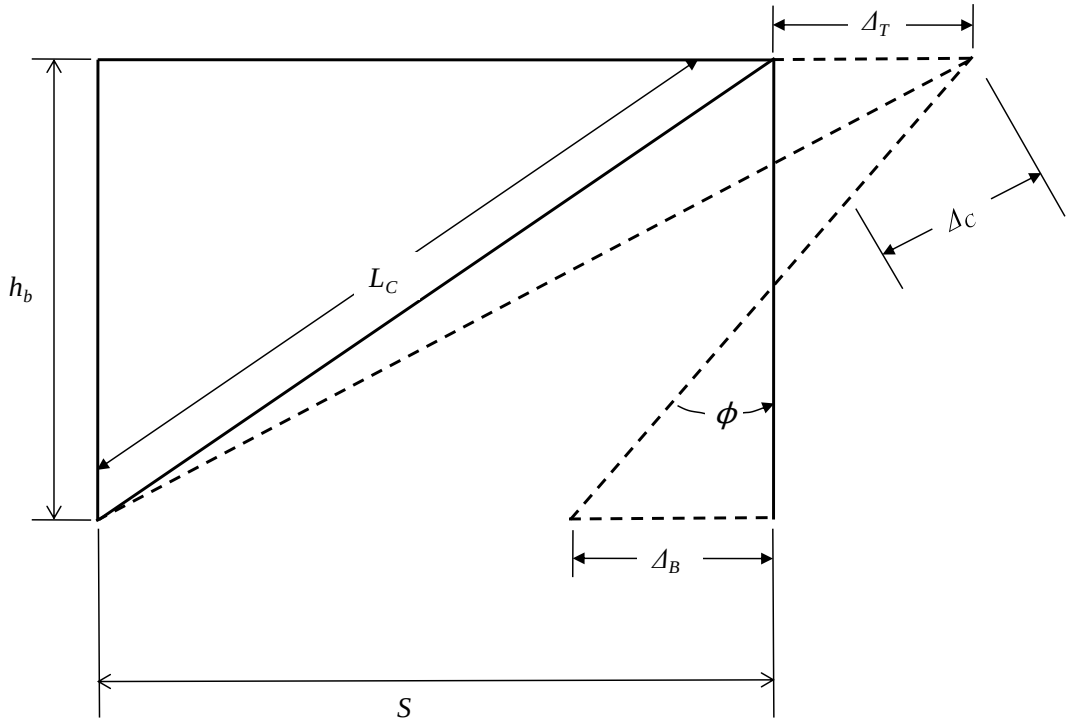

Figure 2.6: Tension-only cross frame deflected shape.

The deflected shape in Figure 2.6 is used to find the deflections in terms of forces. First the deflection of the diagonal (Δ_C) is found in terms of the top horizontal deflection (Δ_T) using similar triangles. Then the top and bottom (Δ_B) deflections are found in terms of the strut force (F).

$$\Delta_C = \frac{S}{L_C}\Delta_T \tag{2.21}$$

$$F_C = k_C\Delta_C = \left(\frac{AE}{L}\right)_C \Delta_C = \left(\frac{AE}{L}\right)_C \frac{S}{L_C}\Delta_T \tag{2.22}$$

Setting Equation (2.22) equal to Equation (2.20) yields the top deflection in terms of the strut force. A similar procedure is used to find the bottom deflection in terms of the strut force.

$$\Delta_T = \frac{2FL_C^3}{(AE)_c S^2} \tag{2.23}$$

$$\Delta_B = \frac{FS}{(AE)_S} \tag{2.24}$$

Defining the girder twist in terms of the top and bottom deflection gives the following relationship.

$$\phi = \frac{\Delta_T + \Delta_B}{h_b} \tag{2.25}$$

Now substituting Equations (2.23) and (2.24) gives:

$$\phi = \frac{2FL_C^3}{h_b S^2 (AE)_c} + \frac{FS}{h_b (AE)_S} \tag{2.26}$$

Then defining the axial portion of the cross frame stiffness in terms of the moment the cross frame imposes on the girder gives:

$$\beta_{braxial} = \frac{M}{\phi} \tag{2.27}$$

where

$$M = Fh_b \tag{2.28}$$

And now substituting Equations (2.26) and (2.28) into Equation (2.27) gives:

$$\beta_{braxial} = \frac{Eh_b^2}{\frac{2L_C^3}{A_c S^2} + \frac{S}{A_S}} \tag{2.29}$$

Finally by multiplying the second term in the denominator by $(S/S)^2$ and simplifying gives the final result for the tension-only cross frame stiffness due to the axial stiffness of the braces as:

$$\beta_{braxial} = \frac{Eh_b^2 S^2}{\frac{2L_C^3}{A_c} + \frac{S^3}{A_S}} \tag{2.30}$$

Equation (2.30) is valid if the cross frame is normal to the girder. A skewed cross frame with skew angle α is shown in Figure 2.7. From the figure the relationships between the normal and skewed cross frame members and forces are shown below.

$$F' = \frac{F}{cos\,\alpha} \tag{2.31}$$

$$L'_C = \frac{L_C}{\cos\alpha} \tag{2.32}$$

$$S' = \frac{S}{cos\,\alpha} \tag{2.33}$$

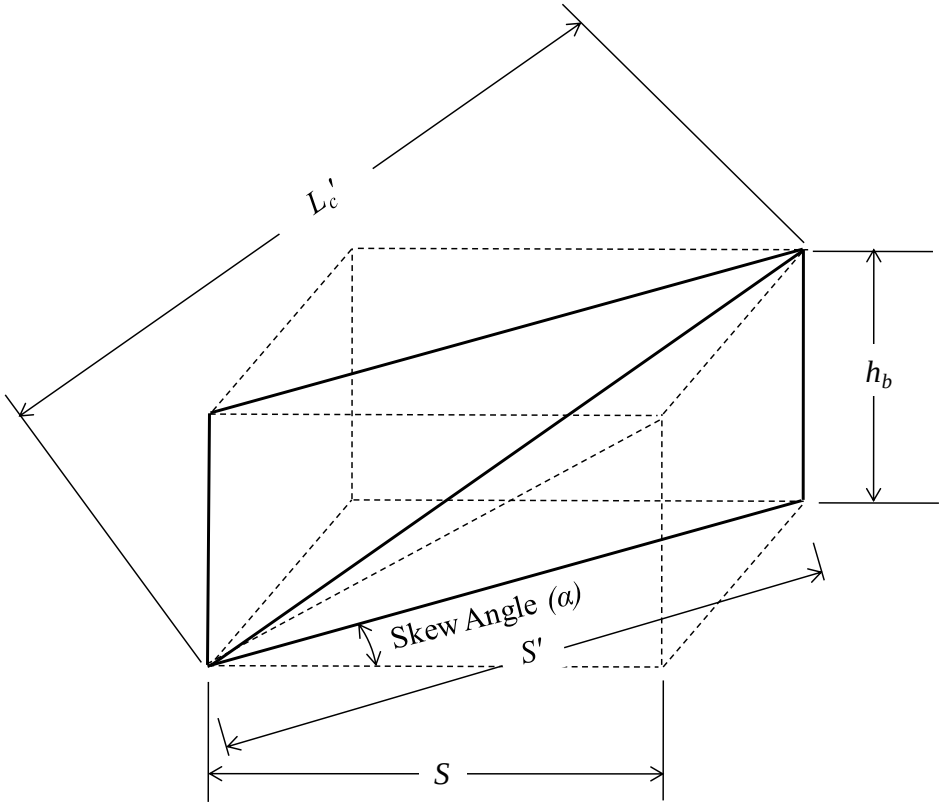

Figure 2.7: Skewed cross frame.

Now the top and bottom cross frame deflections in Equations (2.23) and (2.24) can be written including the skew angle α.

$$\Delta'_T = \frac{2F'L'^3_C}{(AE)_c S'^2} = \frac{2FL_C^3 \cos^2\alpha}{(AE)_c S^2 \cos^4\alpha} = \frac{2FL_C^3}{(AE)_c S^2 \cos^2\alpha} \tag{2.34}$$

$$\Delta'_B = \frac{F'S'}{(AE)_S} = \frac{FS}{(AE)_S \cos^2\alpha} \tag{2.35}$$

And the girder twist given by Equation (2.26) is used with the deflections of Equations (2.34) and (2.35) giving the girder twist in the skewed coordinate system.

$$\phi' = \left[\frac{2FL_C^3}{h_b S^2 (AE)_c} + \frac{FS}{h_b (AE)_S}\right] \frac{1}{\cos^2\alpha} = \frac{\phi}{\cos^2\alpha} \tag{2.36}$$

Now using the final result of Equation (2.36) the skewed cross frame stiffness can be written as (Wang and Helwig, Stability Bracing Requirements for Steel Bridge Girders with Skewed Supports 2008):

$$\beta_{braxialskew} = \frac{M}{\phi'} = \frac{M}{\phi} cos^2 \alpha = \beta_{braxial} cos^2 \alpha \tag{2.37}$$

2.4.1.3 Brace Bending Component of Torsional Stiffness

As the girder cross section twists, it will cause the cross frame members to bend in reverse curvature if the braces are connected to the girder with a moment resisting connection (Figure 2.4) and the brace height extends above midheight of the girder. From basic mechanics the bending stiffness of a brace in the plane of the cross frame is described in Equation (2.38).

$$\beta_{brbend} = \frac{6EI_{br}}{L_{br}} \tag{2.38}$$

where

I_{br} = Brace moment of inertia in plane of the cross frame

L_{br} = Brace member length

The inclusion of the bending stiffness of the braces simply requires that the bending stiffness of each brace be added to the result of Equation (2.30) giving the brace stiffness shown in Equation (2.39).

$$\beta_{br} = \frac{Eh_b^2 S^2}{\frac{2L_C^3}{A_c} + \frac{S^3}{A_S}} + 2\frac{6EI_{strut}}{S} + \frac{6EI_{diagonal}}{L_c} \tag{2.39}$$

To account for the impact of support skew on the bending stiffness of the braces, a similar procedure to that for the brace axial stiffness is followed as described below.

The girder twist shown in Figure 2.3 is resisted by a corresponding cross frame twist and brace rotation. The twist and rotation vector triangle for the girder twist and cross frame resistance are shown in Figure 2.8. The geometry from this vector triangle leads to the transformation of the girder twist to the brace rotation.

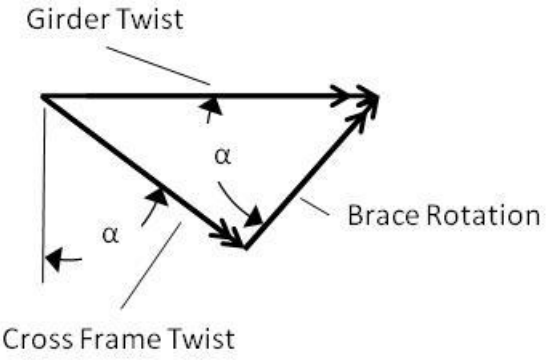

Figure 2.8: Girder and brace twist/rotation triangle (α is the bridge skew angle).

$$\theta_{brace\ rotation} = \theta_{girder\ twist} \cos\alpha \tag{2.40}$$

Therefore

$$M_{brace} = \beta_{brbend}\theta_{girder\ twist} \cos\alpha \tag{2.41}$$

where

M_{brace} = bending moment applied to brace in cross frame plane

Additionally, the length of the brace is also impacted by the skew angle as shown in Equation (2.32). Combining this skew impact into Equation (2.38) and substituting into Equation (2.41) gives

$$M_{brace} = \beta_{brbend}\theta_{girder\ twist} \cos^2\alpha \tag{2.42}$$

Therefore

$$\beta_{brbendskew} = \beta_{brbend} \cos^2\alpha \tag{2.43}$$

And finally, combining Equations (2.43) and (2.37) yields

$$\beta_{brskew} = \left[\frac{Eh_b^2 S^2}{\frac{2L_C^3}{A_c} + \frac{S^3}{A_S}} + 2\frac{6EI_{strut}}{S} + \frac{6EI_{diagonal}}{L_c} \right] \cos^2 \alpha \tag{2.44}$$

2.4.2 Web Stiffness (β_{sec})

If the cross frame attaches directly to the girder web, then web distortion (out of the web's plane) will reduce the overall stiffness of the cross frame stiffness. The web's contribution to the cross frame stiffness is calculated using Equation (2.45) (Yura, Phillips, et al. 1992). If the cross frame attaches at a full depth web stiffener, then the web stiffness typically may be taken as infinite as there will be insignificant web distortion. Similarly, when modeling a cross frame in a finite element program, connecting the cross frame directly to the web-flange interface allows the web stiffness to be taken as infinite.

$$\beta_{sec} = \frac{3.3E}{h}\left(\frac{(\mathrm{N} + 1.5h)t_w^3}{12} + \frac{t_s b_s^3}{12} \right) \tag{2.45}$$

where

E = Young's Modulus

h = web depth

N = brace contact area with flange

t_w = web thickness

t_s = stiffener thickness

b_s = stiffener width

2.4.3 Attached girder stiffness (β_g)

As the girders begin to twist during buckling, the cross frame is forced to resist the couple created. In turn, the cross frame's resisting moment is countered by vertical reactions on the girders. These vertical reactions cause the girder to deflect in the girder's strong plane and the girder's in-plane flexibility will also affect the stiffness of the cross frame system. The impact of the girder's in-plane flexibility is given by Equation (2.46) (Helwig, Yura and Frank, Bracing Forces in Daphragms and Cross Frames 1993).

$$\beta_g = \frac{12S^2EI_x}{L^3} \tag{2.46}$$

where

S = spacing between girders

E = Young's modulus

I_x = girder moment of inertia about its strong axis

L = girder length

2.4.4 Connection Stiffness ($\beta_{conntors}$)

The stiffness of the cross frame will also be affected by its connections. This component is not yet reflected in Equation (2.18). The development of connection stiffness parallels that of the brace stiffness since the force and geometry are the same for each and is given below. The derivation begins with Equation (2.22) and then substitutes the connection stiffness rather than the brace's axial stiffness. Of course this assumes the axial stiffness of the connection perpendicular to the girder is known.

Using the same deflected geometry as in the brace stiffness derivation (Figure 2.6) the top and bottom connection displacements are given below.

$$\Delta_{Tconn} = \frac{2FL_C^2}{\beta_{conn}S^2} \tag{2.47}$$

$$\Delta_{Bconn} = \frac{F}{\beta_{conn}} \tag{2.48}$$

where

β_{conn} = axial connection stiffness perpendicular to the girder

Using these deflections and substituting them into Equation (2.25) then simplifying gives the connection torsional stiffness perpendicular to the girder shown below.

$$\beta_{conntors} = \frac{\beta_{conn}\, h_b^2}{\frac{2L_c^2}{S^2} + 1} \tag{2.49}$$

Equation (2.49) assumes that the axial connection stiffness perpendicular to the girder is known. As outlined in Chapter 1, a common connection that is used to simplify fabrication for cross frame connections at skewed supports is the bent plate detail. To develop the connection stiffness perpendicular to the girder web for a bent plate the axial and lateral stiffness of the bent plate must be quantified and then transformed into a component perpendicular to the girder. These quantities are explored through laboratory testing and finite element modeling and developed in Chapter 5 (Parametric Studies and Design Guidance).

2.5 IMPACT OF GIRDER END TWIST ON ELASTIC BUCKLING STRENGTH

Previous research has shown that as a girder's end is allowed to twist due to support rotation, its buckling strength is reduced (Flint 1951) (Schmidt 1965) (Bose

1982). The relationship between support rotation and buckling strength is given by Flint (1951) as

$$\frac{M_{cr}}{M_o} = 1 - \frac{4}{3}\left[\frac{\left(\theta/_T\right)_{support}}{\left(L/_{JG}\right)_{girder}}\right] \tag{2.50}$$

where

M_{cr} = girder buckling strength with support rotation

M_o = girder buckling strength with no support rotation

θ = support rotation due to torque (T)

Rearranging the terms and using the cross frame stiffness rather than the support stiffness parameters, Equation (2.50) can be recast to account for the girder cross section torsional stiffness relative to the cross frame stiffness. This formulation is shown in Equation (2.51).

$$n = 1 - \frac{4}{3}\left(\frac{GJ}{L}\right)_{girder}\left(\frac{1}{\beta_T}\right) \tag{2.51}$$

While subsequent analytical studies have shown that the reduction in buckling capacity is negligible if the support stiffness is 20 times the girder's torsional stiffness (Schmidt 1965), Equation (2.50) has been found to overestimate the girder buckling capacity when end twist is allowed (Bose 1982). Additionally it is not specific to cross frames, rather its derivation comes from support twist. Therefore, Equation (2.51) will be investigated in Chapter 5 using a parametric study to determine its accuracy when end cross frame stiffnesses rather than support stiffnesses are used.

2.6 GIRDER WARPING RESTRAINT IN SKEWED BRIDGES

Typical end cross frames are connected to girders via connection plates or bearing stiffeners (AASHTO/NSBA Steel Bridge Collaboration 2003) that offer negligible restraint to girder end warping. However, the integration of a warp restraining device into the girder-end frame connection can provide significant warping restraint and dramatically increase the girder's buckling capacity.

Such warp restraining devices have previously been studied (Hunt 1973). One analytical study found that the use of a pipe connecting the girder flanges (Figure 2.9) can provide as much as a 70% increase in the buckling capacity (Ojalvo and Chambers 1977).

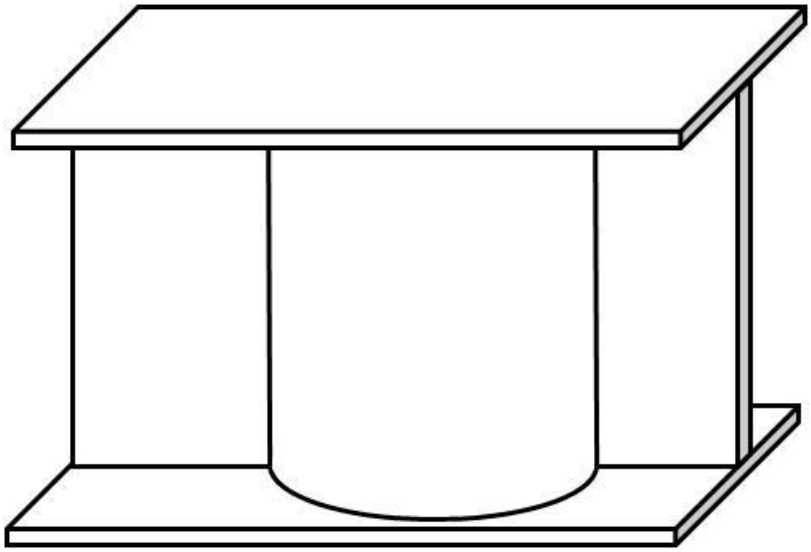

Figure 2.9: Wide flange shape with pipe stiffener.

The reason a pipe stiffener is effective in increasing the girder buckling capacity is shown in Figure 2.10. As the girder twists during buckling, the flanges undergo differential twist about the vertical axis through the web. The differential twist of the flanges is often referred to as warping deformation. The relative flange twist is

represented in the figure by the flange ends rotating in opposite directions. For the flanges to twist relatively to one another, they must twist the pipe that connects them. Since the pipe is a closed shape it is torsionally stiff and provides a significant source of warping restraint that adds to the stability of the girder.

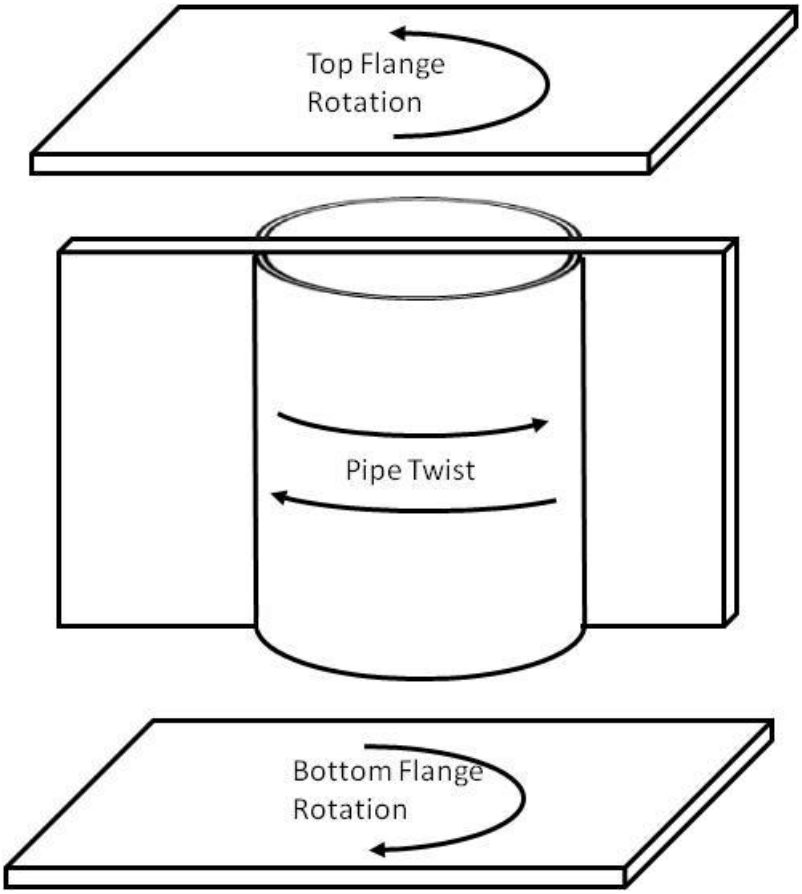

Figure 2.10: Pipe stiffener twist due to girder flange end rotation.

Ojalvo and Chambers (1977) analytically investigated the increase in buckling strength due to pipe stiffeners at the ends of girders and developed a method to calculate this contribution. By incorporating the resistance the pipe provides to each flange into

the boundary conditions for Equation (2.15) an iterative numerical integration can be used to calculate the increase in buckling strength. This procedure is described below.

Using the coordinate system shown in Figure 2.2 and equating the rotation of the bottom flange plus the angle of twist in the tube to the rotation of the top flange Ojalvo and Chambers derive the following compatibility equation:

$$u' + \frac{d}{2}\phi' - \frac{d^2}{2}\frac{E}{GJ}I_f\phi'' = u' - \frac{d}{2}\phi' \tag{2.52}$$

where

d = distance between flange centroids

I_f = flange strong axis moment of inertia

From Equation (2.52) and the simply supported end conditions, the following boundary conditions for the simply supported beams with warping restraint are developed.

$$\phi = u = u'' = 0 \tag{2.53}$$

$$\phi' - \left(EI_f/2GJ\right)d\phi'' = 0 \tag{2.54}$$

With the above boundary conditions, Ojalvo and Chambers used a numerical integration technique to solve Equations (2.5) and (2.6) as an initial value problem for the critical buckling moment for six rolled shapes using both an infinitely stiff tube and a tube with a ¼" thick wall as the warping restraint. While this analysis produces accurate results and shows that such a warping restraint device provides a near warping fixed end condition, this method requires an iterative solution of four simultaneous equations to converge on a buckling solution.

Another possibility in calculating the girder buckling strength due to warping restraint provided by a pipe stiffener is to consider the two sources of stability defined in Equation (2.17). An examination shows that the terms under the radical define both

components of the girder's resistance to lateral torsional buckling. The first term defines the uniform (St. Venant) torsional resistance and the second term defines the torsional warping resistance. Therefore, the warping resistance provided by a pipe stiffener can be incorporated into the second term as an effective torsional length factor (K_z) as shown in Equation (2.55). Such a method has previously been employed to calculate the impact of warping restraint provided by adjacent unbraced girder lengths (Structural Stability Research Council 1988). Of course a suitable selection for K_z must be made.

$$M_{cr} = \mathrm{C_b}\pi/L_b\sqrt{EI_yGJ + \pi^2E^2C_wI_y/(K_zL_b)^2} \tag{2.55}$$

where

C_b = moment gradient coefficient

K_z = effective length factor for torsion

The critical parameter in determining K_z for a pipe stiffener lies in the relative rotational stiffness of the girder's compression flange about its strong axis ($2EI_f/L$ where I_f is the flange's strong axis moment of inertia) to the torsional stiffness of the pipe (GJ/L). If the torsional stiffness of the pipe is much greater than that of the girder flange then K_z will approach 0.5 with no intermediate bracing and 0.7 with intermediate bracing (torsionally fixed). For the case with intermediate bracing, the warping restraint is taken as zero to maintain consistency with typical design specifications. Likewise if the pipe's stiffness is much smaller than the flange's stiffness then K_z will approach 1.0 (torsionally free). This is analogous to a sidesway inhibited column where the torsional stiffness of the pipe is considered as the flexural stiffness of a girder framing into the end of the column. Approaching the problem in this way allows the sidesway inhibited alignment chart (American Institute of Steel Construction 2001) for columns to be used to select an

appropriate K_z where the relative rotational stiffness of the girder flange to the torsional stiffness of the pipe is used to calculate G_A or G_B at the girder's pipe stiffened end.

In order to use the alignment chart, the chart's assumption that the stiffening girders bend in single curvature with *2EI/L* stiffness must be considered in terms of the pipe stiffener. If the pipe is much stiffer than the girder flanges, then as the flanges attempt to warp in opposite directions the very rigid pipe will limit the flange warping to a very small amount. This condition will result in a very high effective torsional stiffness similar to the *6EI/L* of beams bent in reverse curvature which is three times the assumed value of *2EI/L* in the chart. Likewise as the stiffness of the pipe declines relative to the flange flexural stiffness, the pipe will allow more flange rotation thereby reducing its effectiveness in increasing girder buckling strength. So, in general *G* may be defined as:

$$G_{A\ or\ B} = \left(\frac{EI}{L_b}\right)_{flange} \Big/ m\left(\frac{GJ}{L}\right)_{pipe} \tag{2.56}$$

where

I = flange strong axis moment of inertia

m = pipe stiffness multiplier based on relative stiffness of pipe to flange

L = pipe length

The difficulty in assessing the value of m comes from the indeterminate nature of the pipe boundary conditions. Since the boundary conditions depend on the relative torsional stiffness of the pipe to the flexural stiffness of the flange and in turn the flexural stiffness of the flange depends on the torsional stiffness of the pipe there is no simple solution to define m. Therefore, to determine a value for m based on the pipe to flange stiffness a finite element parametric study will be used to establish values of m for

corresponding ratios of the pipe torsional stiffness to the girder flange flexural stiffness. This study is described in Chapter 5 (Parametric Studies and Design Guidance).

2.7 ESTIMATION OF GIRDER BUCKLING STRENGTH WITH INITIAL IMPERFECTIONS

Equation (2.17) considers only a linear elastic solution to the girder buckling problem; however, real girders have initial imperfections which will affect the buckling strength. To incorporate the impact of initial imperfections, a large deflection analysis can be used rather than an eigenvalue buckling analysis, but determining the buckling load then becomes a challenge since the deflections continue to increase as the load increases and approaches, but never reaches the eigenvalue buckling load.

Meck (1977) built on the method Southwell proposed to solve such a problem for columns in 1932 (Southwell 1932). By solving for equilibrium on an Euler column with an initial imperfection, Southwell was able to develop an explicit relationship between critical load, deflection, and initial imperfection shown in Equation (2.57).

$$P_{cr}\left(\frac{x_c}{P}\right) = x_c + x_{oc} \tag{2.57}$$

where

x_c = lateral deflection at midspan of column under load P

x_{oc} = initial lateral imperfection at midspan of column.

By putting Equation (2.57) into slope-intercept form and plotting x_c/P versus x_{oc} a straight line plot is found whose slope is the critical buckling load and y-intercept is the initial imperfection.

Following a similar pattern, Meck used Timoshenko's equilibrium equations for beam buckling and then applied an energy method to solve them for buckling under a point load at mid-span which produced the following simultaneous equations

$$\alpha \frac{\emptyset_c}{P} = u_c + \overline{u_c} \tag{2.58}$$

$$\beta \frac{u_c}{P} = \emptyset_c + \overline{\emptyset_c} \tag{2.59}$$

where

$$\alpha = \frac{2\left(GJ + \frac{\pi^2 E C_w}{L}\right)}{\left(\frac{1}{4} + \frac{1}{\pi^2}\right) L} \tag{2.60}$$

ϕ_c is the twist at girder midspan

u_c is the lateral deflection of the girder centroid at midspan

$\overline{u_c}$ is the initial lateral imperfection of the girder centroid at midspan

P is the load applied to the centroid of the cross section

$$\beta = \frac{2\pi^2 E I_y}{\left(\frac{1}{4} + \frac{1}{\pi^2}\right) L^3} \tag{2.61}$$

Similar to Southwell's column procedure two plots are produced and their slopes are α and β. Then by setting the initial lateral and twist imperfections to zero in Equations (2.58) and (2.59) and solving for P_{cr} yields the following relationship.

$$P_{cr}{}^2 = \alpha\beta \tag{2.62}$$

So, the product of the slopes of the two graphs becomes the buckling load. However, few girders have point loads applied at their centroids. So to account for top flange loading, Meck recommended that Equation (2.58) becomes

$$\alpha \frac{\emptyset_c}{P} = (u_c + e\emptyset_c) + \left(\overline{u_c} + e\overline{\emptyset_c}\right) \tag{2.63}$$

where

e is the vertical distance from the centroid to the point of load application.

Then ϕ_c/P is plotted against $u_c+e\phi_c$ and the slope of the straight line plot is α. Then finally the critical buckling load is found by solving the following quadratic equation.

$$P_{cr}^2 + \beta e P_{cr} - \alpha\beta = 0 \quad (2.64)$$

2.8 CURRENT CODE PROVISIONS AND CONSTRUCTION PRACTICES

The preceding theoretical discussion forms the basis for skewed steel bridge girder end cross frame design as codified in a number of national and Texas state specific publications. These provisions are summarized below.

2.8.1 2007 AASHTO Bridge Design Provisions (American Association of State Highway and Transportation Officials 2007)

2.8.1.1 Section 6.7.4.1 Diaphragms and Cross-Frames - General

In the first edition of the LRFD Specification, AASHTO removed the arbitrary requirement that diaphragms be spaced at no more than 25 feet (AASHTO LRFD 1994). Instead a rational analysis is recommended to establish acceptable diaphragm spacing. While not directly specified in AASHTO, a rational analysis should ensure that the brace has both adequate stiffness and strength to provide girder stability as well as meeting other requirements that the braces provide to the bridge. The specification requires that cross frames be spaced to provide:

- Transfer of lateral wind loads to the bearings
- Stability of the bottom flange when in compression
- Stability of the top flange when in compression
- Consideration of any flange lateral bending effects

- Distribution of vertical dead and live loads

Additionally, where there is a discontinuity in the slab or at the edge of the slab, the slab is required to be supported by diaphragms or other edge supports (Section 9.4.4) to stiffen the deck for wheel loads at the edge of the slab.

2.8.1.2 Section 6.6.1.3 Distortion Induced Fatigue

The AASHTO specification requires transverse connection plates to be bolted or welded to both the girder web and flange when the connection plates are attached to diaphragms or cross frames. Attaching the connection plate to the flanges reduces the problems with distortional fatigue around the cross frame regions. The commentary states that for skewed bridges, the diaphragm forces should be determined by analysis and references Keating, et al., (1990).

For lateral connection plates (such as a bent plate), the specification limits the placement of plates to a vertical distance not less than one-half the width of the flange above or below the flange on stiffened webs and at least six inches above or below the flanges on unstiffened webs. These provisions are intended to minimize the effect of weld terminations on fatigue strength and prevent distortion induced fatigue on the web to flange weld.

2.8.1.3 Section 6.7.4.2 Diaphragms and Cross-Frames – I-Section Members

The specification allows intermediate diaphragms or cross-frames on bridges with supports skewed 20° or less to be placed parallel to the skew. However, when the supports are skewed more than 20° the intermediate diaphragms or cross-frames are required to be placed normal to the girders. The braces can be placed either along a continuous bracing line or can also be staggered along a line parallel to the skew angle.

End diaphragms are required to be designed for forces and distortions transmitted by the deck to the bearings.

2.8.2 2004 AASHTO Bridge Construction Specification (American Association of State Highway and Transportation Officials 2004)

2.8.2.1 Section 11.4.3.3 Bent Plates

Minimum bend radii of cold bent plates are given in Table 11.4.3.3.2-1 of the AASHTO Specification. The specification recommends that the bend line be oriented perpendicular to the final rolling directions. If this is not possible the minimum radius should be multiplied by 1.5. If a smaller radius than that allowed by cold bending is required, then hot bending is required in accordance with the specification provisions.

2.8.3 2003 AASHTO/NSBA Guidelines for Design for Constructability (AASHTO/NSBA Steel Bridge Collaboration 2003)

2.8.3.1 Section1.6.1 Deflections for Straight Structures on Skewed Piers and Abutments

The guidelines point out that differential girder deflections and twist on bridges with highly skewed supports must be evaluated for the load under which diaphragms must fit (no-load, steel only, or non-composite dead load). The differential deflections are caused by the differing distance to the supports for adjacent girders. Girder twist becomes an issue because the twist is normal to the skewed pier and not the web causing the top flange to deflect away from the bottom flange resulting in the web being out of plumb and the flanges to be unlevel.

2.8.4 2007 TxDOT LRFD Bridge Design Manual (Texas Department of Transportation 2007)

2.8.4.1 Chapter 3 Section 12 Straight Plate Girders

Guidelines for TxDOT bridges on bracing permit the cross-frame spacing to be a maximum of 30 feet and at least two interior bearings must have a diaphragm intersecting them at each bent. The manual also confirms the AASHTO provisions on aligning diaphragms with a skew 20° or less and normal to girders for larger skews.

2.8.5 2007 TxDOT Preferred Practices for Steel Bridge Design, Fabrication, and Erection (Texas Steel Quality Council 2007)

2.8.5.1 Section 2.6 Diaphragms and Cross Frames

TxDOT has preferred field welding to connect diaphragms and cross frames to girders due to erection tolerances. TxDOT plans utilize standard drawings for cross frames and diaphragms that are published on the Miscellaneous Details Steel Girders and Beams (SGMD) sheets (Texas Department of Transportation 2006). These standard details cover bridge skews up to 45° and any skew over 45° requires additional details to show the girder to cross-frame connections. Cross-frames are allowed to be spaced more than 25 feet if this spacing can be attained without temporary bracing and all other limit states are satisfied.

According to TxDOT preferred practices fabricators prefer single equal leg angles to all other types of members for cross-frames. Also, due to the use of Dart welders, welding stiffener and connection plates at more than a 20° to the girder is problematic.

2.8.6 Current Texas Cross Frame Connection Fabrication Practices

Based on the preceding national and state guidance, Texas bridge fabricators are given significant leeway in creating end cross frame connections on steel girder bridges. The connection found in the TxDOT SGMD plan sheet (Texas Department of Transportation 2006) uses an integral bearing stiffener connection plate to connect bent plates that support the cross frame brace members for skew angles between 20° and 45° and straight connection plates for skews 20° and under (Figure 2.11).

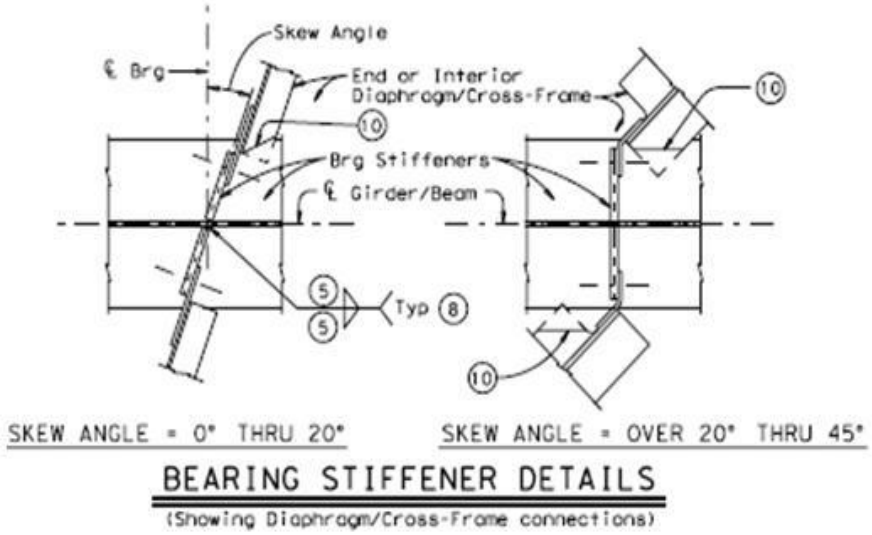

Figure 2.11: TxDoT standard skewed cross frame connection (from SGMD sheet 1)

However, fabricators have used other connection details successfully. One of the most common departures from the standard plans is to use separate cross frame connection plates and bearing stiffeners (Figure 2.12) so the cross frame forces are collinear.

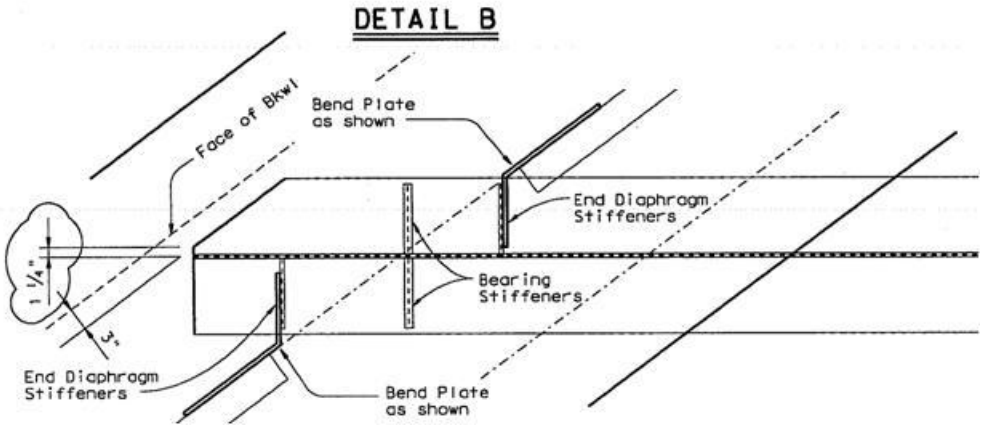

Figure 2.12: Cross frame connection for US 82 at 9th St. underpass Lubbock, TX

In addition to using bent plates to account for the bridge skew angle, additional connections such as those utilizing pipes for the web stiffeners have been tried (Figure 2.13 and Figure 2.14). The pipe stiffener allows a connection plate to be welded at any angle thereby standardizing the connection no matter what the skew angle. It can also provide warping restraint as previously described in this chapter.

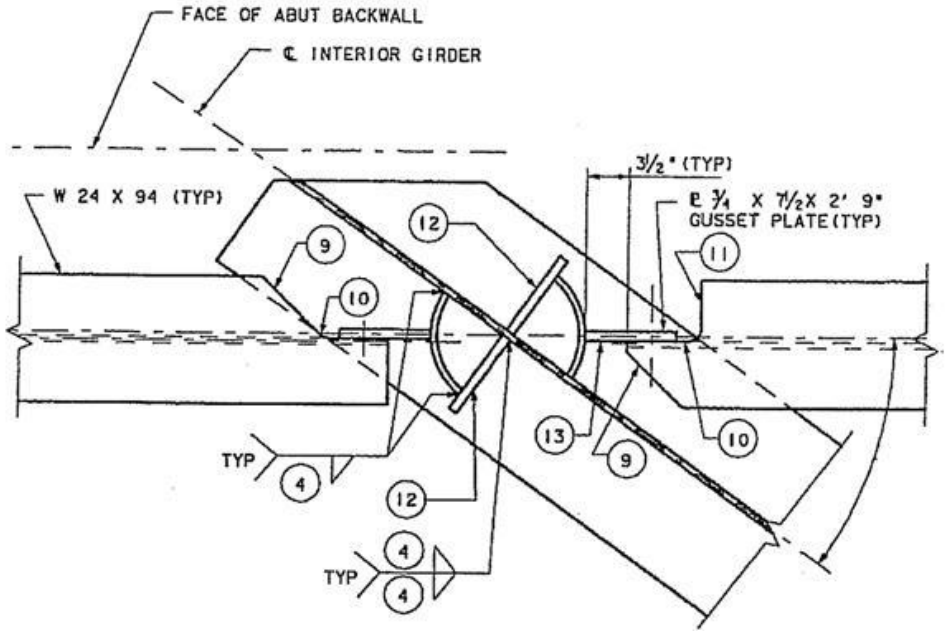

Figure 2.13: Quarter pipe end cross frame connection

Figure 2.14: Full pipe end cross frame connection

2.9 BACKGROUND SUMMARY

This chapter has described the current state of research and code provisions for skewed steel girder bridge bracing. Most of this research has focused on intermediate cross frame bracing perpendicular and parallel to the bridge skew angle. The current research also assumes a rigid connection between the cross frame and girder and that the girder ends are free to warp and do not twist. These assumptions have been adopted into the current codes and standard practices outlined in this chapter.

In Chapter 3 (Experimental Program), several series of connection and large scale experiments will be described that tested the impact of these assumptions on girder buckling strength, end twist and cross frame forces. Additionally Chapter 3 briefly describes pipe stiffener fatigue test results comparing the pipe stiffener to the currently used plate stiffener detail. These experimental results will then be used to validate the finite element modeling techniques developed in Chapter 4 (Finite Element Modeling), and in Chapter 5 (Parametric Studies and Design Guidance) the validated model will be used in several parametric studies to extend the experimental results.

CHAPTER 3
Experimental Program

3.1 INTRODUCTION

The experimental program consisted of three different series of laboratory tests. First, small scale connection testing was performed for the bent plate and split pipe stiffener connections. Next, a fatigue test was run on several split pipe and plate stiffeners to compare the fatigue performance of each. Then, large scale buckling and lateral load tests were performed on various girder systems using plate and split pipe stiffeners at the supports. The buckling tests were conducted on single-, twin-, and three-girder systems. In addition to varying the connection details at the end cross frames, intermediate cross frame details were also considered.

The primary purpose of the small and large scale tests was to validate the finite element modeling techniques used in the parametric studies. Additionally, each specimen was compared to the others to show the impact of the varying parameters in the laboratory tests. These comparisons are described in this chapter. A discussion of the validation of the finite element model using the laboratory results is provided in Chapter 4.

3.2 CONNECTION TESTING

The connection testing program is covered in detail in a related research report (Battistini 2009). The key results and conclusions are summarized here.

3.2.1 Small Scale Connection Test Set Up

The connection test frame with a bent plate connection assembly is shown in Figure 3.1. The test frame was designed to accept a W135x55 girder segment with a bent plate or split pipe stiffener connection assembly at skew angles of 0°, 15°, 30°, 45°, or 60°. Once in the frame, a loading ram was used to deliver a tension load to a single angle attached to the connection assembly.

Figure 3.1: Small scale test set up – south (left) and east (right))

3.2.2 Connection Specimens

There were six different bent plate specimens tested with differing skew angles and bend radii and two split pipe stiffeners tested with different skew angles. The bent plates were 5/16" thick and the pipe had a 10.75" outside diameter with a 0.34" wall thickness. Each connection assembly was welded to a W135x55 girder segment. Four of the bent plate

specimens are shown in Figure 3.2 and the 45° split pipe specimen is shown in Figure 3.3. The specimens tested are summarized in Table 3.1.

Figure 3.2: Bent plate connection specimens

Figure 3.3: 45° Split pipe connection specimen

Table 3.1: Small scale test specimens

Connection	Skew Angle	Bend Radius
Bent Plate	15°	0.50"
Bent Plate	30°	0.84"
Bent Plate	45°	0.59"
Bent Plate	45°	0.94"
Bent Plate	45°	2.41"
Bent Plate	60°	0.63"
Split pipe	0°	N/A
Split pipe	45°	N/A

During the test, a tension load was applied to each specimen and the lateral and vertical deflections of the bent plate and split pipe connection plate were measured so the deflections could be used to validate the finite element model of each connection. The results were also directly compared and some key conclusions were made based on the laboratory tests. In each of the graphs shown below, the error bars show the minimum and maximum values for each test while the line plotted is the average value.

3.2.3 Connection Testing Key Results

The results of the vertical and lateral deflections measured at the top of bent plate specimens top are shown in Figure 3.4 and Figure 3.5, respectively. The 45° skew specimen data shown are for the 0.59" bend radius. The vertical deflection results clearly show that despite the varying bend radius, larger skew angles increase the plate flexibility. These results are not quite as clear for the lateral deflection data due to the small deflections of the 45° degree specimen. The reasons for these small deflections were a result of the specimen imperfection, relatively small bend radius, and ram offset in the test frame. These anomolies are explained in the previously mentioned research report (Battistini 2009). However, all other specimens show that similar to the vertical deflection, larger skew angles resulted in an increase in lateral deflection. Finally, the larger variability in the 30° specimen was due to not carefully aligning the loading ram, connection clevis and specimen. These were the first tests run and initially it was thought that the applied load would align the ram, clevis and specimen, but the friction between the parts did allow some small offset. In subsequent tests this condition was monitored

more closely to ensure the proper alignment occurred, resulting in less variablity in the data.

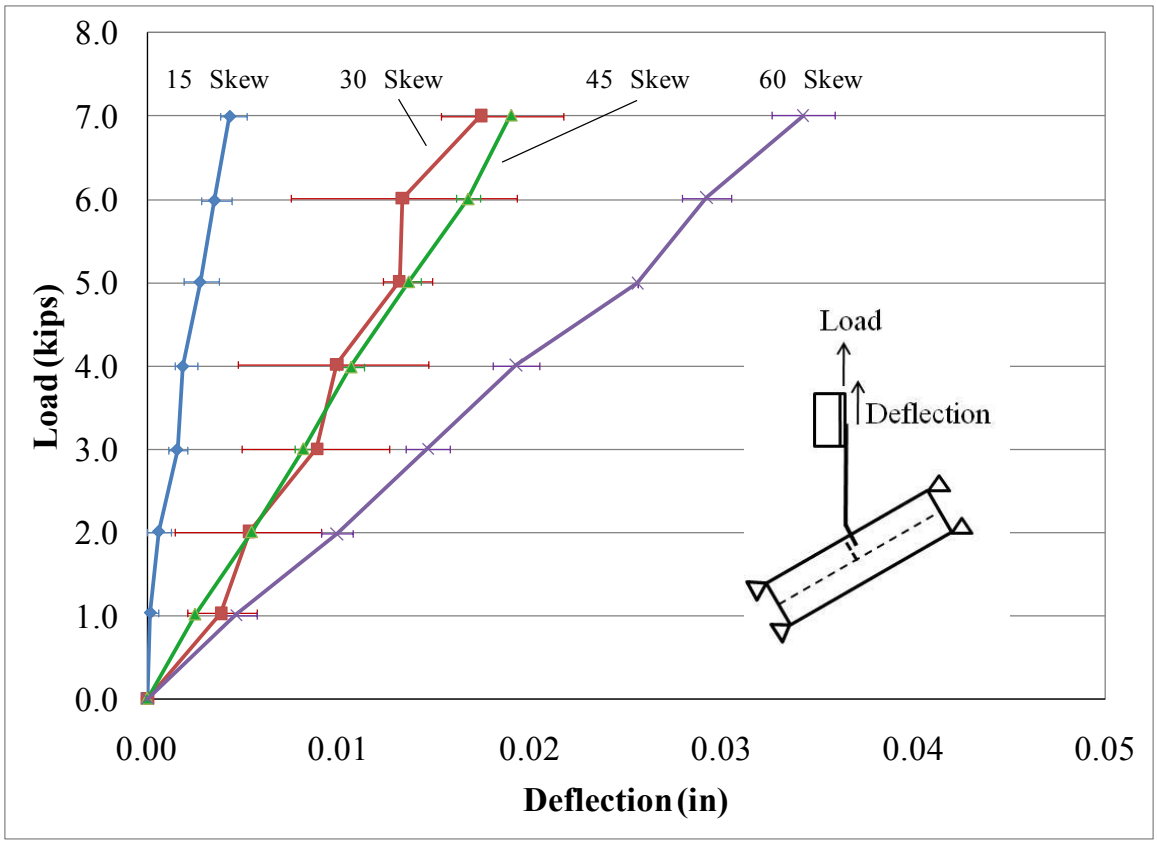

Figure 3.4: Bent plate top vertical deflection

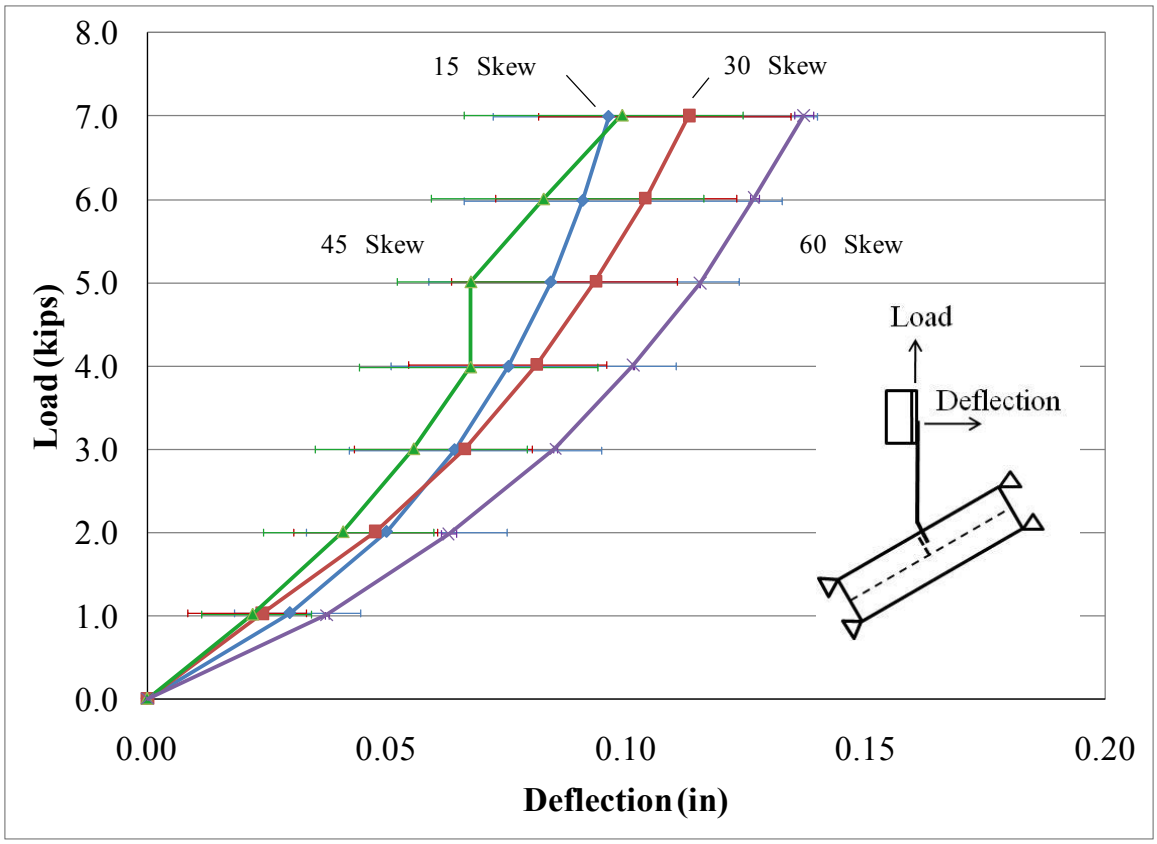

Figure 3.5: Bent plate top lateral deflection

The impact of the bend radii on the vertical deflection for the 45° specimens are shown in Figure 3.6 and Figure 3.7. The specimens with the larger bend radius had larger axial deflections for a given load level. Therefore, in addition to the impact of skew angle on the stiffness of the plate, the bend radius also affects the plate axial flexibility. The lateral deflection results do not show this same pattern as the 2.41" radius specimen deflects less than the 0.94" radius specimen as shown in Figure 3.7. It was unclear whether this difference was due to the previously mentioned anomalies in the specimen and test set up or if it was a result of the difference in bend radius.

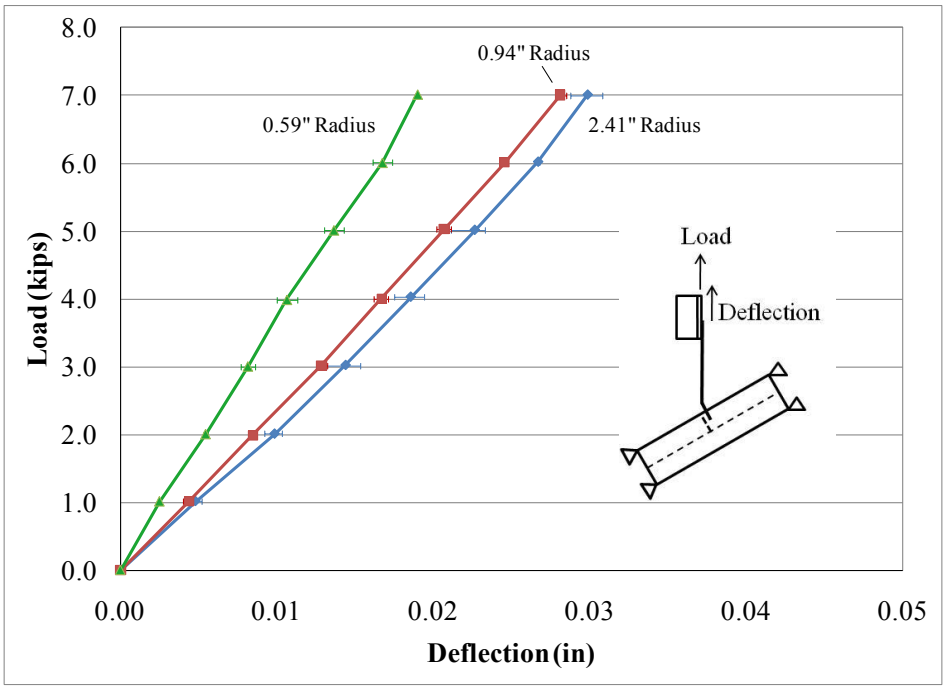

Figure 3.6: 45° skew bent plate vertical deflection

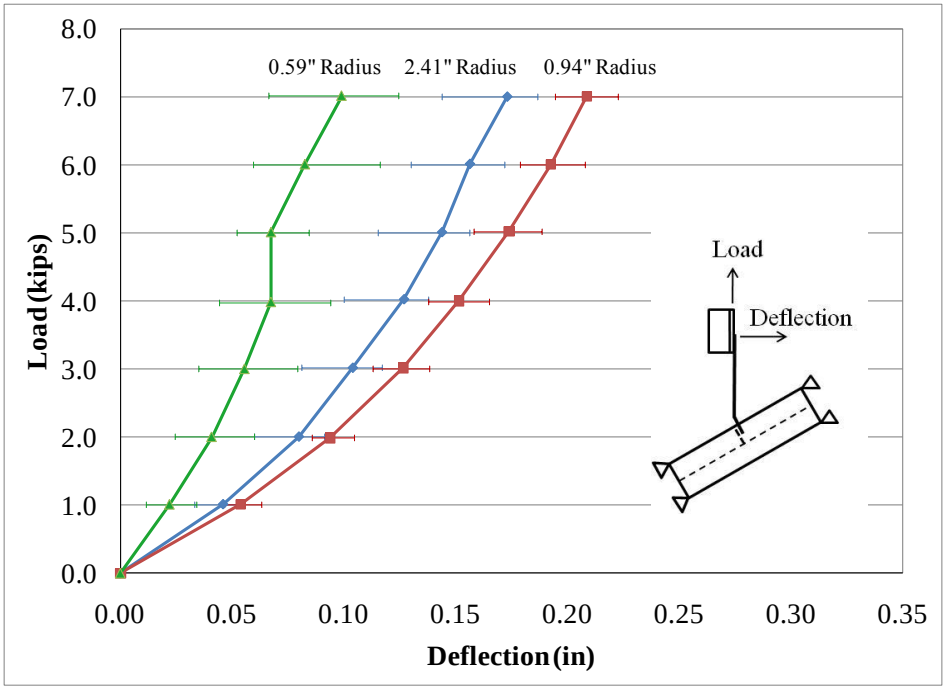

Figure 3.7: 45° skew bent plate lateral deflection

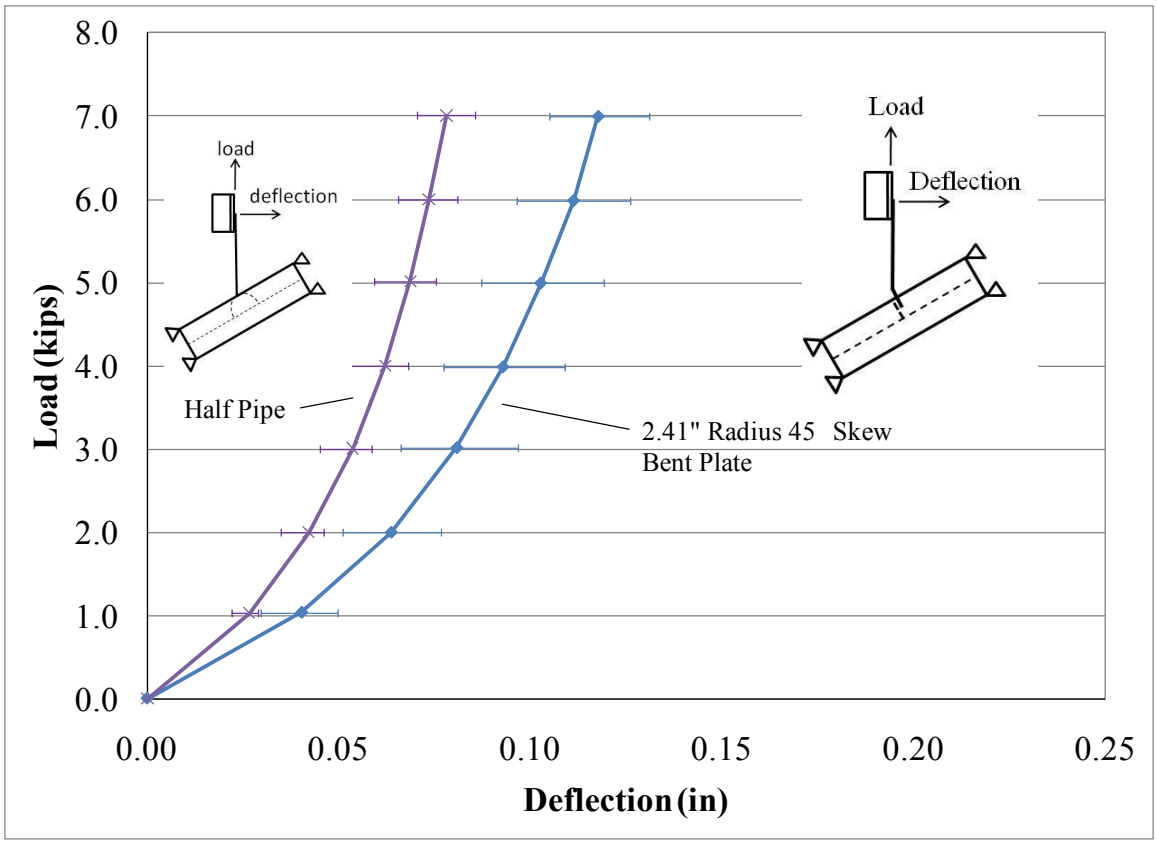

Figure 3.8: 45° skew lateral deflection comparison

The comparison between the 45° skew bent plate and split pipe stiffener connection are shown in Figure 3.8. From the figure it can be seen that the split pipe specimen had significantly smaller deflections than the bent plate detail. The results shown are typical of all of the bent plate and split pipe stiffener tests that were conducted. The difference between the bent plate and split pipe stiffener vertical deflections were found to be negligible. The tests showed that the split pipe stiffeners were stiffer than the bent plate details and that the difference in the stiffness increased with larger skew angles.

3.3 FATIGUE TESTING

Fatigue testing was conducted to make sure the split pipe stiffener did not introduce a detail that was more prone to maintenance issues than the plate stiffener details. While split pipe stiffeners at the abutments of exterior spans are not located at a region of high moment, stiffeners at the interior piers of continuous girders are located at regions with very high moments. Therefore gaining a measure of the fatigue performance relative to the plate stiffeners that have been traditionally used is an important step in this research. In addition to comparing the split pipe stiffeners to normal stiffeners, plate stiffeners that were skewed were also considered since some engineers or fabricators may propose such a detail in lieu of the bent plate.

A complete summary of the fatigue testing program will be in a separate thesis to be written by (Wahr 2010). A brief description and key findings are reported in this dissertation.

3.3.1 Fatigue Test Set Up

Fatigue testing was completed on four W21x101 girder segments. Each segment had three separate stiffener specimens: a split pipe stiffener, a normal plate stiffener, and a skewed plate stiffener. The skewed stiffeners were angled at 30° for two of the specimens and a 60° for the other two. Plan views of the two types of specimens are shown in Figure 3.9 and Figure 3.10.

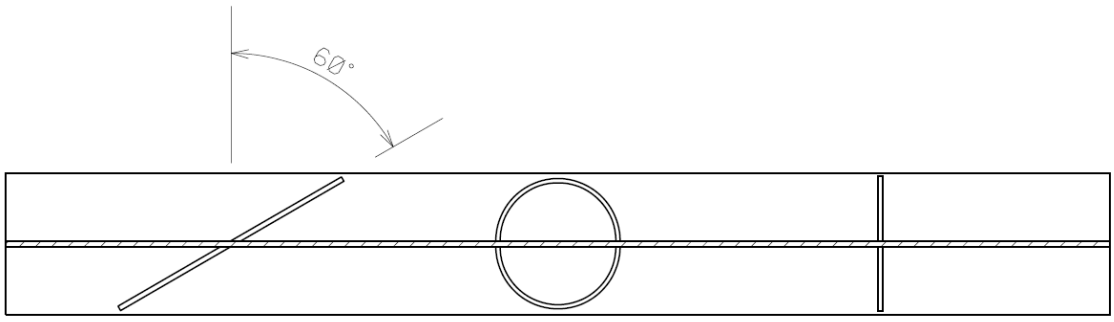

Figure 3.9: Fatigue specimen with 60° skewed stiffener

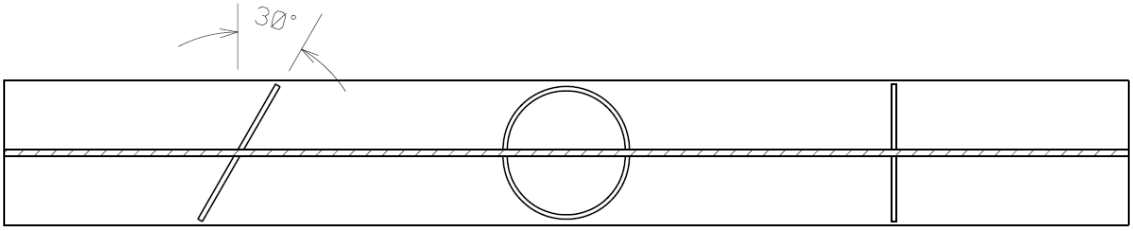

Figure 3.10: Fatigue specimen with 30° skewed stiffener

The test frame was constructed so that all three stiffeners were in a constant moment region so that the flange stresses were uniform among the different stiffeners. The load was cycled at approximately 1 Hz, and the load was set to give a tension flange stress range meeting AASHTO fatigue category C values for three of the tests and category B values for one test. A picture of the test set up is shown in Figure 3.11.

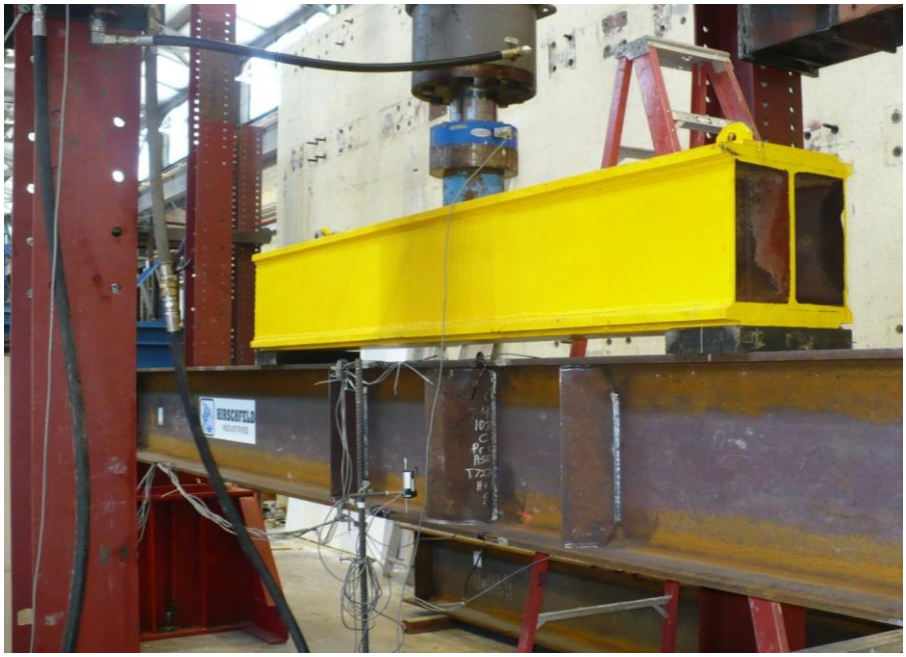

Figure 3.11: Fatigue test set up

3.3.2 Fatigue Testing Key Results

A chart summarizing the results of the fatigue testing is shown in Figure 3.12. The results show that all tested stiffeners met the required AASHTO category C detail. The skewed stiffeners failed first after meeting the category C threshold while the normal and split pipe stiffeners showed no visible cracks well after the category C threshold had been met. The tests that did not exhibit cracking were stopped at approximately 3 million cycles. Destructive testing was used to determine if any cracking had started in the split pipe and normal stiffeners during the fatigue tests. No evidence of cracking was found in any of the split pipe stiffeners, but one normal stiffener did have incipient cracking.

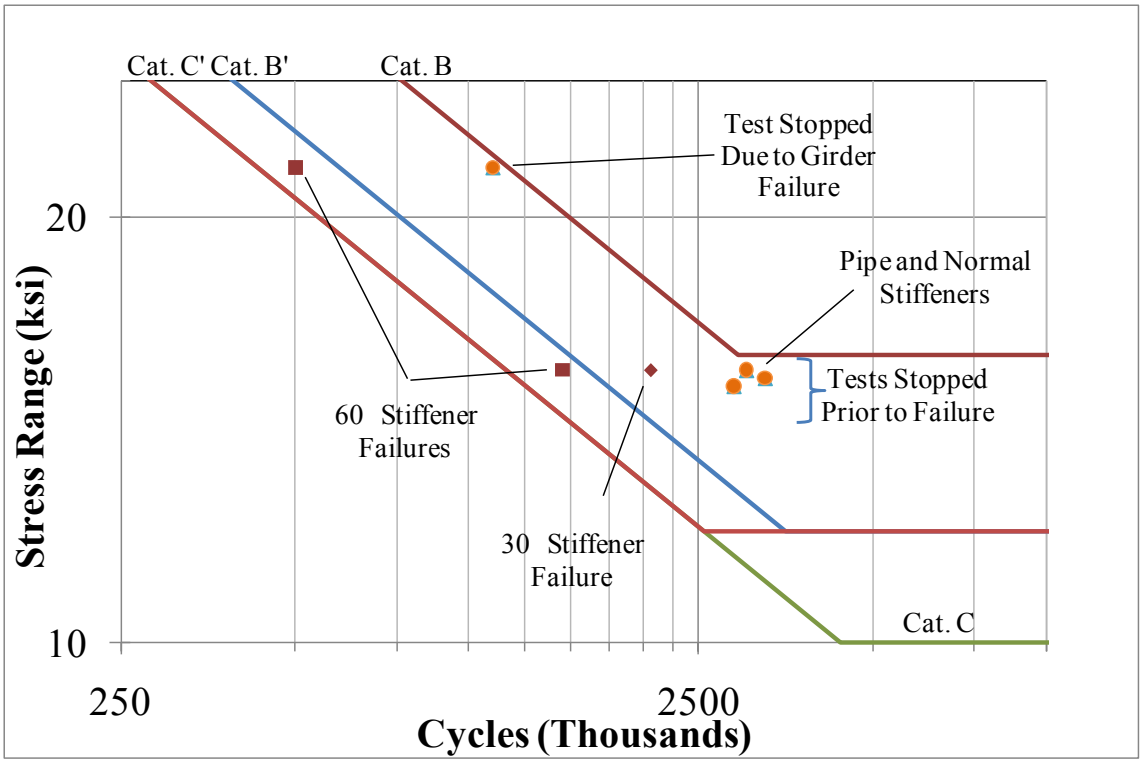

Figure 3.12: Fatigue test results

Therefore, the split pipe stiffener meets the required category C detail and performs at least as well as the currently used detail. The final fatigue report to be presented by Wahr (2010) will contain parametric studies to extend these results to other connection and girder sizes.

3.4 LARGE SCALE TESTING

The large scale testing program consisted of single, two, and three girder tests. The purpose of the testing was to validate the finite element modeling as well as compare the performance of the split pipe stiffener and bent plate connection under a variety of support and bracing conditions.

3.4.1 Single and Twin Girder Testing

The purpose of the test on single and twin girder systems was to validate the finite element modeling of the girder as well as the plate and split pipe bearing stiffeners. Additionally, the tests were used to measure the impact of the split pipe stiffener warping resistance on the girder buckling strength.

3.4.1.1 Single and Twin Girder Testing Program

Four total girders were tested in two pairs. The first girder pair had plate bearing stiffeners as shown in Figure 3.13. These two girders were named Girder Bent Plate (GBP) 1 and 2. The second girder pair had split pipe bearing stiffeners as shown in Figure 3.14 and were named Girder Split Pipe (GSP) 1 and 2. A plan view of the whole test specimen is shown in Figure 3.15. A picture of a typical twin girder buckling test set up is shown in Figure 3.16.

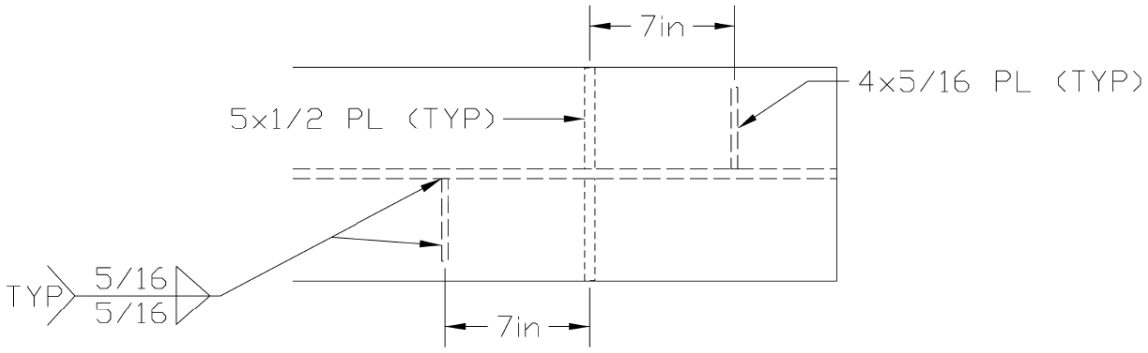

Figure 3.13: Bent plate connection plate stiffener detail

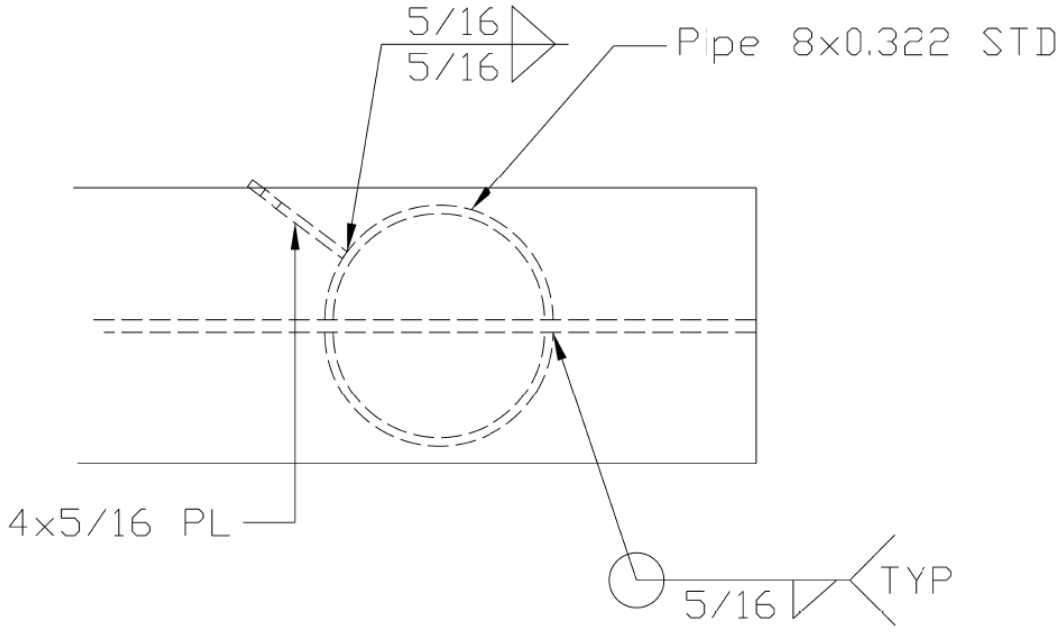

Figure 3.14: Split pipe stiffener connection detail

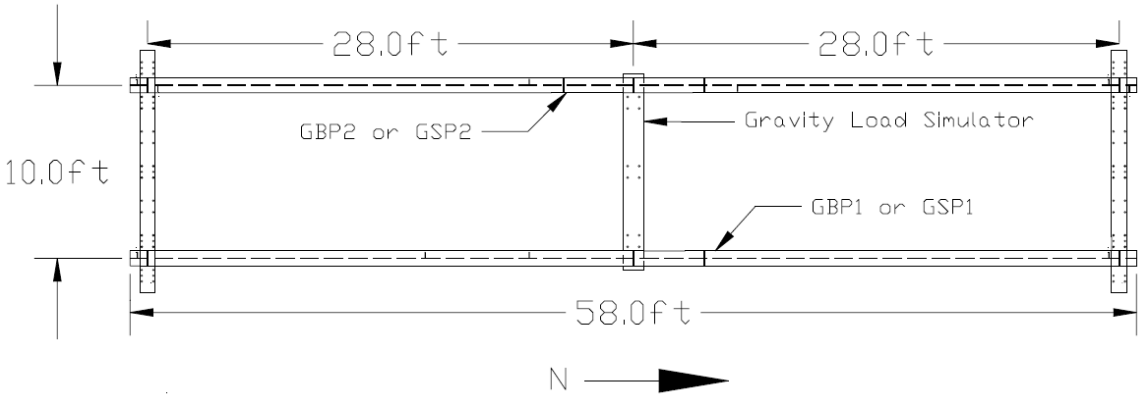

Figure 3.15: Twin girder test specimen plan view (plate stiffened specimen shown)

Figure 3.16: GBP1 and GBP2 in the twin girder buckling test frame (looking north)

In addition to the basic tests used to measure the girders buckling strength and strong axis flexural resistance, lateral tests were conducted with lateral loads applied to gain a measure of the lateral and torsional stiffness of the girder system. The lateral loads were applied with and without vertical loads to assess the degree of restraint that may have been provided by the gravity load simulator. Additionally, a series of lateral and torsional tests were run on GBP2 and GSP2 individually to compare with the twin girder lateral and torsional tests. A summary of all twin and single girder testing is provided in Table 3.2.

Table 3.2: Single and twin girder tests

Girders Tested	Test Type	Number of Tests
GSP1 and 2	Buckling	2
GSP1 and 2	Lateral With No Vertical Load	2
GSP1 and 2	Lateral With 2k Vertical Load	2
GSP1 and 2	Lateral Eccentric With 2k Vertical Load	2
GSP2	Lateral With No Vertical Load	2
GSP2	Lateral Eccentric With No Vertical Load	2
GBP1 and 2	Buckling	2
GBP1 and 2	Lateral With No Vertical Load	2
GBP1 and 2	Lateral With 2k Vertical Load	2
GBP1 and 2	Lateral Eccentric With 2k Vertical Load	2
GBP2	Lateral With No Vertical Load	2
GBP2	Lateral Eccentric With No Vertical Load	2

3.4.1.2 Specimen Fabrication

Each specimen was fabricated from a 58' long W30x90 girder. The span length was 56' with a 1' overhang on each end. The plate bearing and load point stiffeners were fabricated from 5"x1/2" plate and all connection plates were fabricated from 4"x5/16" plate. All welds used to connect the plates were 5/16" fillet welds. The connection plates for the end and intermediate cross frame connection locations were welded to the girders

prior to the twin girder tests in anticipation of the three girder tests when cross frames were to be installed.

3.4.1.2.1 Split Pipe Stiffener Fabrication

The split pipe stiffener detail is shown in Figure 3.14. The split pipe stiffener was fabricated at Ferguson Structural Laboratory from a standard 8" x 0.322" pipe purchased from a local pipe supplier. The cross frame connection plate (as shown in Figure 3.14) was welded to the pipe prior to welding the pipe to the girder to facilitate weld access. For larger skew angles and smaller pipe diameters, the connection plate will be very near the girder web making the web side weld difficult if not done prior to attaching the pipe to the girder. Each connection plate was positioned so the cross frame would overlap the connection plate on the side away from the girder web, again to ensure weld access for future cross frame connection.

Fabricating the split pipe stiffener consisted of splitting the pipe in half with a track torch, saw cutting the pipe to length, grinding it to fit, then welding the connection plate to the pipe, and finally welding the pipe to the girder. The following figures show the key steps in this process.

Figure 3.17: Splitting the pipe stiffener with a track torch

Figure 3.17 shows the pipe splitting process. To prevent the pipe from expanding after cutting the first side, the torch was started before the beginning of the pipe and ended prior to the end of the pipe leaving a short uncut portion on each end of the pipe (as seen on the left pipe in Figure 3.17). The pipe was then turned 180° and the opposite side was then completely split with the torch (as seen on the right pipe in Figure 3.17). Finally the pipe was rotated again and the first cut was completed to sever the pipe into two halves. This process kept the cuts even and maintained a uniform cross section throughout the pipe length after the cuts were completed.

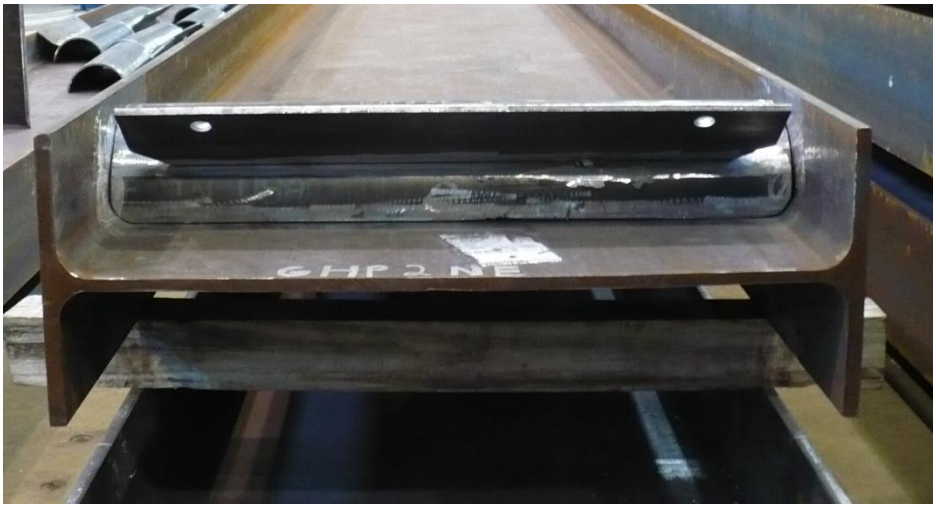

Figure 3.18: Split pipe stiffener prepared for welding

Figure 3.18 shows a completed split pipe with connection plate prepared for welding to the girder. To achieve the appropriate fit, each split pipe was ground to match the fillet area of the girder. This process seldom took more than one-half hour for each split pipe. During welding, the girder was rotated so each weld could be made in the horizontal position. Each split pipe was welded by hand with a continuous feed welder and took approximately 20 minutes of welding time (not including time to rotate the girder). All welds were 5/16" fillet welds based on the typical weld size specified by TxDOT to connect cross frames to girders (Texas Department of Transportation 2006).

3.4.1.2.2 Plate Stiffener Fabrication

The plate stiffener detail is shown in Figure 3.13. The detail consists of four plates. The two offset plates are for the bent plate cross frame connections and the central plates are the bearing stiffeners. While TxDoT allows the bearing stiffener to be used as the bent plate cross frame connection plate, most Texas fabricators prefer to offset the cross frame connection plates to align the cross frame forces. Therefore, this method was selected for

the test specimens. The amount of connection plate offset is determined by the skew angle and distance between adjacent girders. Figure 3.13 shows the detail for a 53° skew with approximately 7" between the bearing stiffeners and cross frame connection plates.

3.4.1.3 Twin and Single Girder Test Frame Set-Up

An end view of the test setup prior to testing was shown in Figure 3.16. Figure 3.19 shows the twin girder test frame during a buckling test. The test setup used for all single and twin girder tests was essentially the same. Only the method of load application differed between the lateral load tests and the buckling test. The basic boundary conditions used were simple supports with no twist and unrestrained warping at the girder ends. Vertical loads were delivered via a gravity load simulator while lateral loads were imparted using a rod and turnbuckle system. The following sections describe these aspects of the test set-up.

Figure 3.19: Twin girder buckling test (looking north)

3.4.1.3.1 Test Frame Boundary Conditions

The wide flange sections shown in Figure 3.16 that were used to support the girders provide a good model of simply supported conditions since the flexibility allows movement in the longitudinal direction of the girders. The girders rested on 4" diameter thrust washers as shown in Figure 3.20, to minimize warping restraint. The thrust washer allows the girder flange to rotate in its strong plane, but since it has a small diameter relative to the flange width, it provides only modest tipping restraint.

Figure 3.20: Thrust washer bearing

To prevent twist at the girder ends, threaded rods were used on both sides of the top and bottom flange. After the girders were set in place, the rods were advanced until they came into contact with the flanges. The rods were then adjusted to plumb the girder ends prior to testing. The ends of the rods in contact with the girder flanges were rounded to minimize any warping restraint they may have provided to the girder. Figure 3.21 shows the threaded rods prior to plumbing the girders (note the top rod is not yet in contact with the left flange) and the thrust washer bearing at the south end of GBP1.

Figure 3.21: Threaded rods and thrust washer

3.4.1.3.2 Load Application

The vertical loads were applied via a gravity load simulator as shown in Figure 3.22. The gravity load simulator delivers load and then translates and rotates with the specimens as they buckle in order to keep the applied load vertical. In doing so, the gravity load simulator does not impart a restoring force on the specimen and should therefore not add any stability to the specimens. The displacement of the gravity load simulator while the loading ram maintains its vertical orientation is evident in Figure 3.22. More information about the gravity load simulator may be found in Yarimici, et al (1966).

In the twin girder buckling tests, the gravity load simulator was centered between the beams, so its total load was delivered evenly to the two specimens and was measured via a load cell positioned between the loading ram and load beam. Because the gravity load simulator is a mechanism, two adjustable struts are used to keep the apparatus stable with

no load is applied. Once load is applied to the beams, the gravity load simulator displaces laterally with the girder. In the buckling tests, , the gravity load simulator was first loaded with 1 kip and then the lateral stops were removed in order to keep the simulator stable until enough friction between the knife edges and the top flange of the beams to link the apparatus to the beams.

Figure 3.22: Gravity load simulator applying vertical load (looking south)

The concentrated load from the gravity load simulator was delivered to each specimen at its mid-span through a knife edge. A thrust washer was placed between the knife edge and the loading beam to minimize warping restraint from the point of load contact. The use of the knife edge minimized any torsional restraint provided to the girder from the load point. This assembly was loosely held in place by four bolts which acted to prevent the knife edge from shifting under low loads, but still allowed the loading assembly to

rotate as required. Figure 3.23 shows a picture of the knife edge and thrust washer assembly.

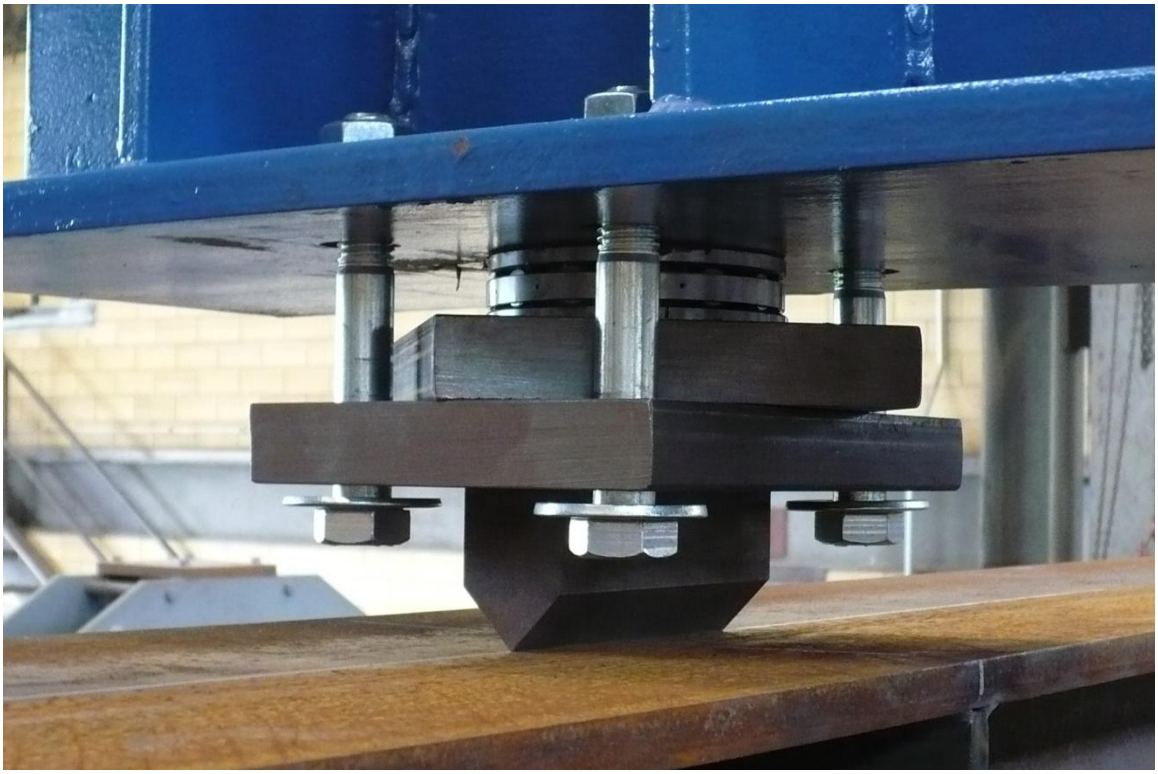

Figure 3.23: Knife edge and thrust washer assembly

The loads for the lateral load tests were applied to the mid-span of girders GBP2 and GSP2 (the western girders). Two load positions on the cross section were used. In the first case, the load was applied at the cross section mid-height, while in the second case, the load was applied at 25.75" above the centroid of the bottom flange (a point just below the top flange). The first load case resulted in weak axis bending while the second case resulted in bending and twisting. The loads were delivered via a turnbuckle and rod system shown in Figure 3.24. As the turnbuckle was rotated by hand, the lateral load on

the girder increased and was read by a load cell reacting against the web of the reaction column.

Figure 3.24: Torsional load test turnbuckle loading system

3.4.1.3.3 Strain and Deflection Measurements

Strain gages, string potentiometers, linear potentiometers, and tilt sensors were used to gather specimen data. Measurements were taken at mid-span, and the ends of the girders were also instrumented to monitor the twist and lateral deformations. Although the supports are assumed to rigidly prevent lateral deformation and twist, the effects of

realistic support details on the deformational behavior at the supports was of interest in the project.

3.4.1.3.3.1 Buckling Test Measurements

At girder mid-span, four strain gages, one at each flange edge, were used so that flange bending stresses could be calculated. This also allowed the calculation of load delivered to each girder to check that the gravity load simulator was delivering the same load to each girder. Also at mid-span, the top and bottom flange lateral deflections were measured using 6" linear potentiometers. This data was also used to calculate the girder mid-span twist. This calculated twist was checked by a tilt sensor that was mounted at the girder mid-span. Finally a 4" linear potentiometer was mounted below the girder bottom flange to measure vertical deflection. In order to minimize friction between the linear potentiometers and the specimen, glass or Teflon plates were mounted to the specimen to ensure the specimen deformations did not disturb the alignment of the linear potentiometer.

Girder end twist monitored by measuring the top and bottom flange lateral translations. The top flanges were instrumented with string potentiometers while the bottom flanges were instrumented with 2" linear potentiometers. No significant end twist was detected during any of the testing when the end brackets were used. When cross frames were used on the three girder systems, deformation at the supports did occur.

3.4.1.3.3.2 Lateral Load Test Measurements

During the lateral load testing, girder twist and lateral translations were measured at mid-span. Also, as in the buckling tests, the girder ends were monitored for twist. The lateral translations were measured using a linear potentiometer at mid-height of the cross

section, and twist was measured at the same location using a tilt sensor. This instrumentation configuration is shown in Figure 3.25.

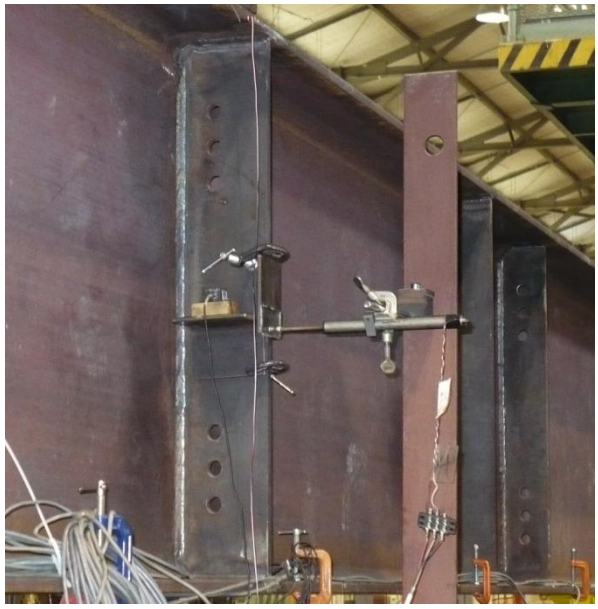

Figure 3.25 Lateral load test instrumentation

3.4.1.3.4 Initial Imperfection Measurements

To model the girder buckling behavior, an initial imperfection measurement was taken for each specimen. To capture both the initial twist and sweep of the girder, the lateral deviations from the girder bottom flange end points were measured for both sides of the top and bottom flanges. The two side measurements for each flange were then averaged to arrive at the initial imperfection for each flange.

Figure 3.26 shows the calculations used to arrive at the initial imperfections on the east and west side of the girders. The reference line used to measure the flange imperfections was a music wire strung along each side of the girder's bottom flange. The wire passed

over threaded rods clamped to the ends of the girder. Weights were hung from the wire to keep it taut during the measurements. The bottom flange deviations from the wire (d_{BFLW} and d_{BFLE}) were measured directly using calipers. A plumb bob and calipers were then used to measure the deviation of the top flange from the bottom flange of the girder ($d_{TFLW-BFLW}$ and $d_{TFLE-BFLE}$). The top flange deviations (d_{TFLW} and d_{TFLE}) were then calculated as shown in Figure 3.26. After the top and bottom flange deviations were measured and calculated, they were linearly adjusted to account for the offset in the wire from each end of the girder. Graphs of the initial imperfections used during testing can be found in Appendix A (Large Scale Experimental Results)

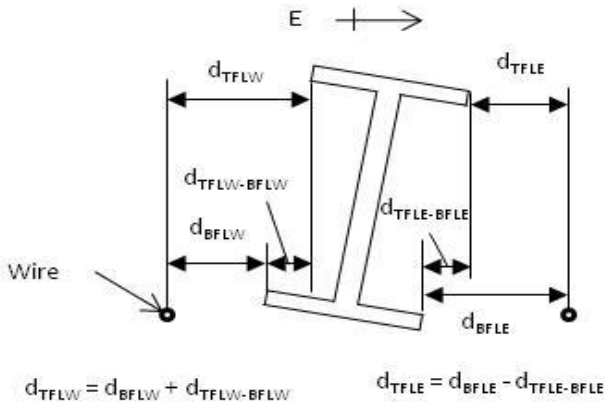

Figure 3.26: Initial imperfection calculations

3.4.1.4 Single and Twin Girder Test Results

Single girder testing consisted of lateral load tests, while the twin girder tests consisted of both lateral load tests and buckling tests as listed in Table 3.2. The results for each of these tests are reported below. Each of the laboratory results are depicted by a series of error bars showing the minimum, average, and maximum values at the reported load

levels for each of the two tests. Where analytic solutions are available they are plotted with dotted lines. Where no analytical solutions exist, the average of each test specimen is plotted with a solid line.

3.4.1.4.1 Single Girder Lateral and Torsional Test Results

A picture of a typical single girder lateral load test is shown in Figure 3.27. The results of the lateral load tests for the plate stiffened girder (GBP2) and split pipe stiffened girder (GSP2) are shown in Figure 3.28.

Figure 3.27: Typical single girder lateral load test

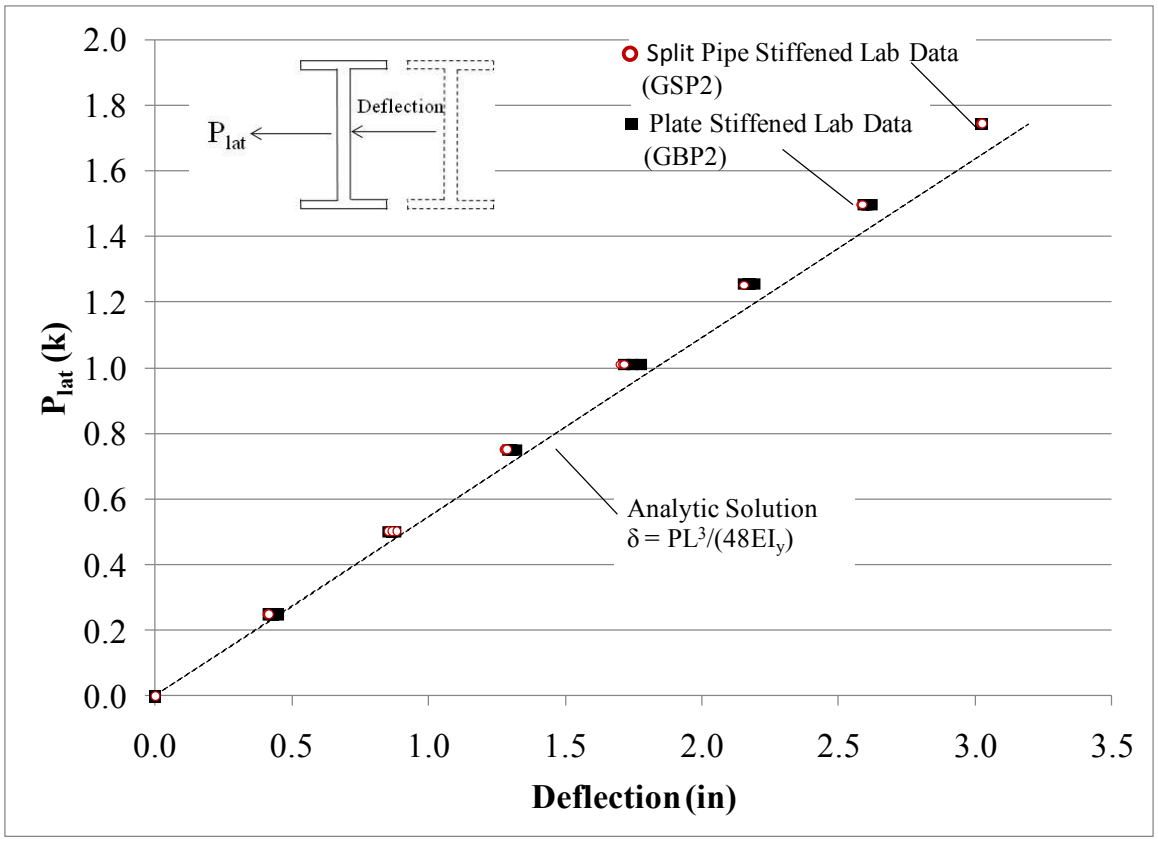

Figure 3.28: Single girder lateral load test results

From Figure 3.28 it can be seen that there is negligible difference between the plate and split pipe stiffened girder lateral stiffness. This is to be expected as both the top and bottom flanges rotate the same amount at their ends during the test causing the stiffeners to undergo only a rigid body rotation (no twist). Therefore the type of stiffener does not change the girder's behavior. When compared to the analytic solution, both girders appear to be stiffer by a small amount. The most likely reason is the friction generated between the threaded rods at the girder ends. As the lateral load increases, the friction between the girder flanges and the threaded rods increase which adds restraint to the girders.

The results for the lateral load tests with the eccentric load are shown in Figure 3.29. From the figure it can be seen that the split pipe stiffened girder (GSP2) is nearly 50% stiffer than the plate stiffened girder. This is due to the warping restraint provided by the split pipe. The variability in the plate stiffened data was due to the tilt sensor registering the vibrations of the turnbuckle being hand tightened. Since the data was gathered continuously, it was being recorded as the turnbuckle was being turned to increase the load. This procedure was changed to record data discretely during the split pipe stiffened data gathering so the specimen was static during data collection. This resulted in a much smaller variability in the split pipe stiffened specimen data.

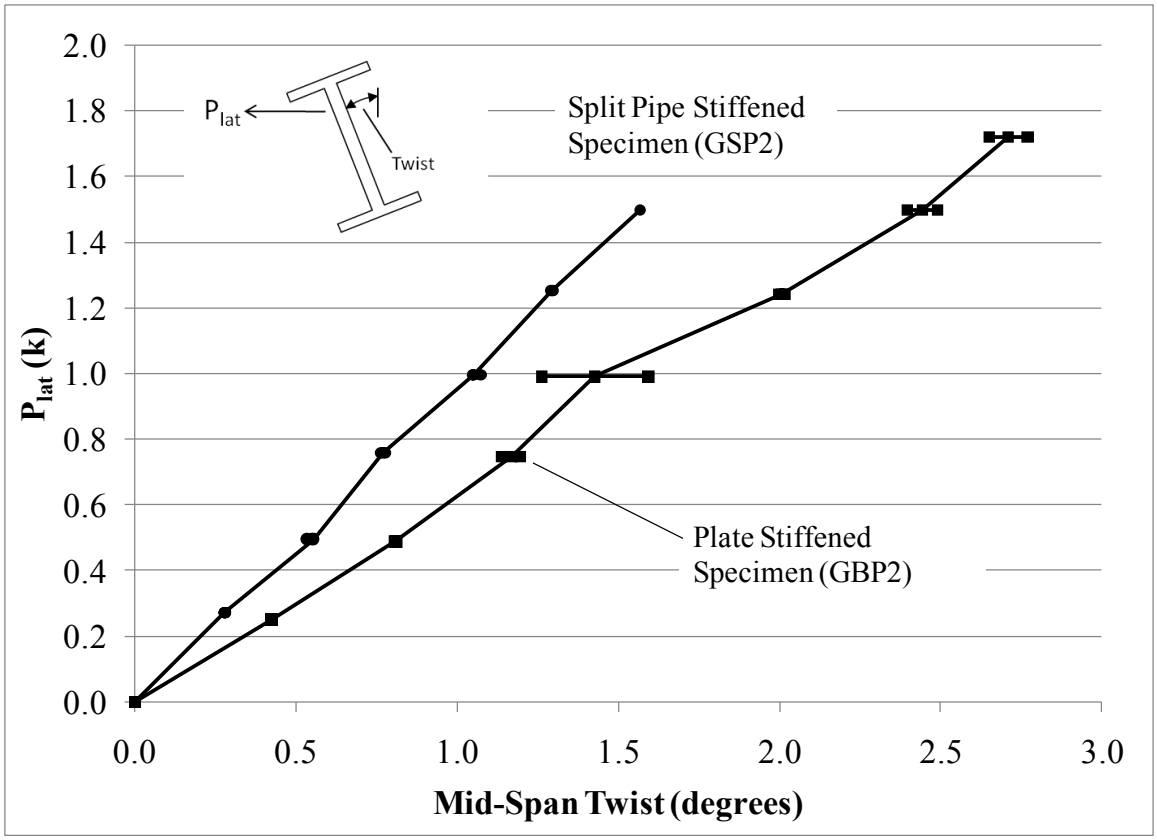

Figure 3.29: Single girder torsional test results

3.4.1.4.2 Twin Girder Lateral and Torsional Test Results

The twin girder lateral load tests were conducted with and without vertical loads applied by the gravity load simulator. For the twin girder lateral tests, flexible single angle members were clamped to each girder's top and bottom flange so the lateral load applied through a turn buckle on one side of the test setup was distributed to both girders. A picture of the typical test set up with vertical load is shown in Figure 3.30.

Figure 3.30: Twin girder lateral load test under vertical load

A gravity load of two kips was applied to the two girders. A comparison of the systems with and without applied vertical loads for the plate stiffened girders is shown in Figure 3.31. These results show that the presence of the gravity load simulator and vertical load does not add any significant lateral stiffness to the system.

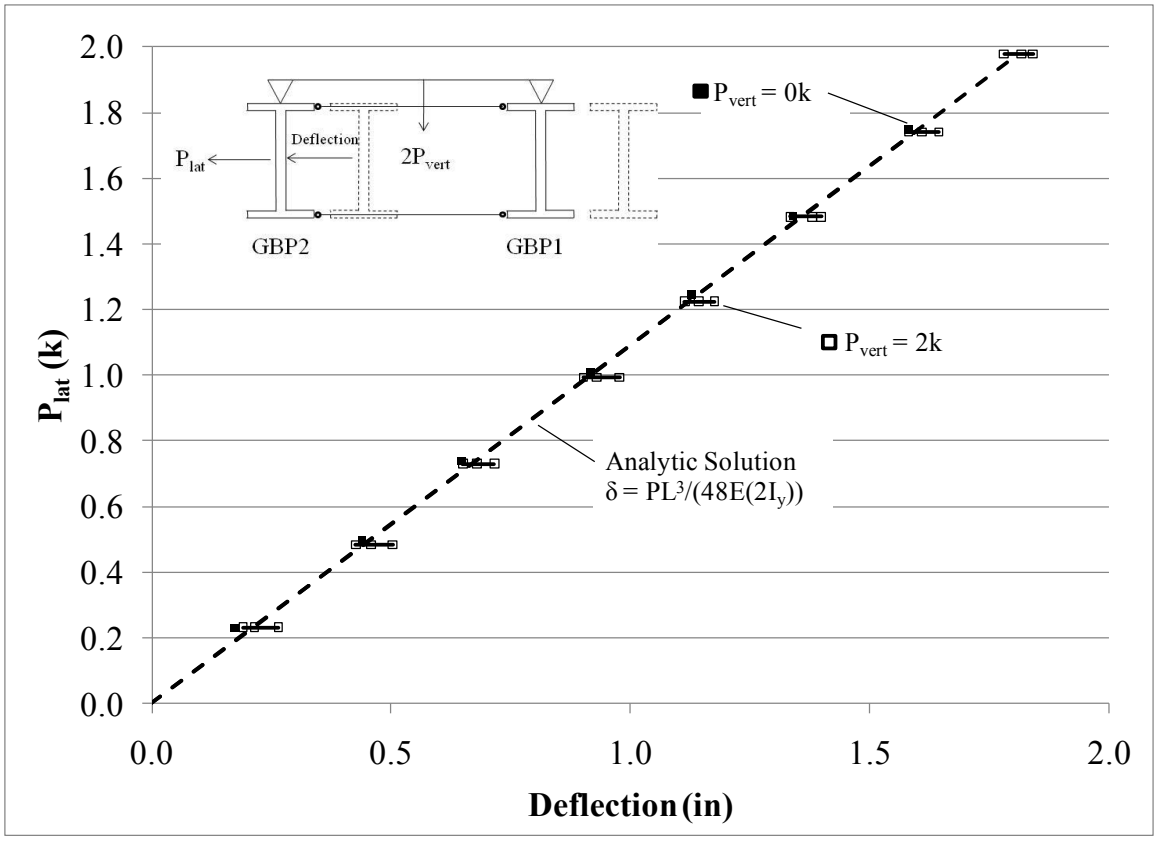

Figure 3.31: Plate stiffened twin girder lateral load test mid-span results

The data for the split pipe stiffened girders with and without vertical load is shown in Figure 3.32. These results show that under vertical load, the split pipe stiffened section is about 17% stiffer than under no vertical load. This goes against expectations since the presence of the compressive stresses associated with the strong axis bending moment

would tend to reduce the stiffness of the girders. In this case, the effect on the stiffness would be very small since the applied load was less than 11% of the buckling capacity. One possible reason for the larger stiffness has to do with the initial twist of GSP2. It is the only girder in the tests that has a twist in the direction of the applied lateral load. Therefore when vertical load is applied, it will begin to displace laterally in this direction giving it a larger initial imperfection in the lateral load direction and increase the reaction against the threaded rods. The increased reaction will increase the friction between the girder and the lateral supports and stiffen the system resulting in the higher stiffness seen in Figure 3.32.

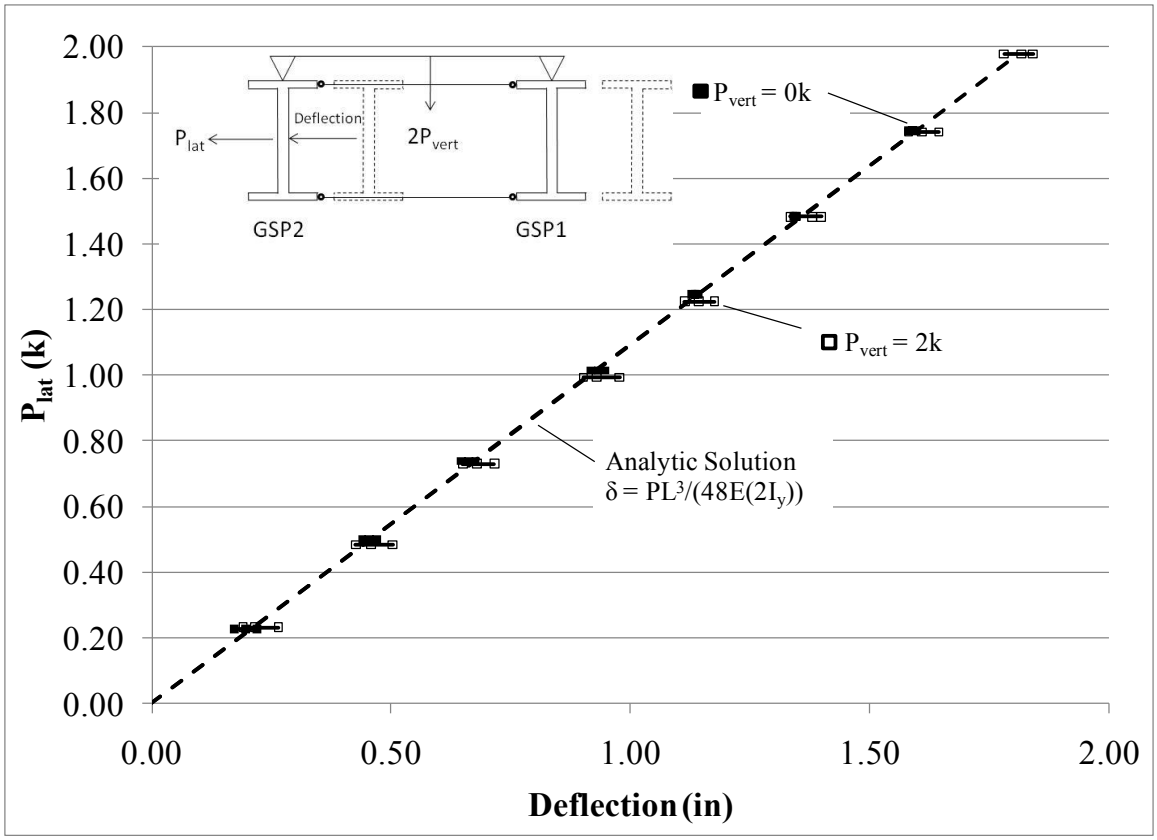

Figure 3.32: Split pipe stiffened twin girder lateral load test results

The eccentric lateral load tests on the twin girders were conducted with two kips of vertical load on each girder. Additionally, the single angles fastened to the girder flanges in the lateral tests were removed so they would not act as torsional restraints between the girders. The results for these tests are shown in Figure 3.33.

The variability in the plate stiffened data was caused by the tilt sensor reading data continuously during the manual turning of the turnbuckle (the same issue as in the single girder torsional test). This procedure was corrected during the split pipe stiffener specimen data collection resulting in a much smaller variability. As with the single girder torsional test, the split pipe stiffened girders are over 70% torsionally stiffer than the plate stiffened girders.

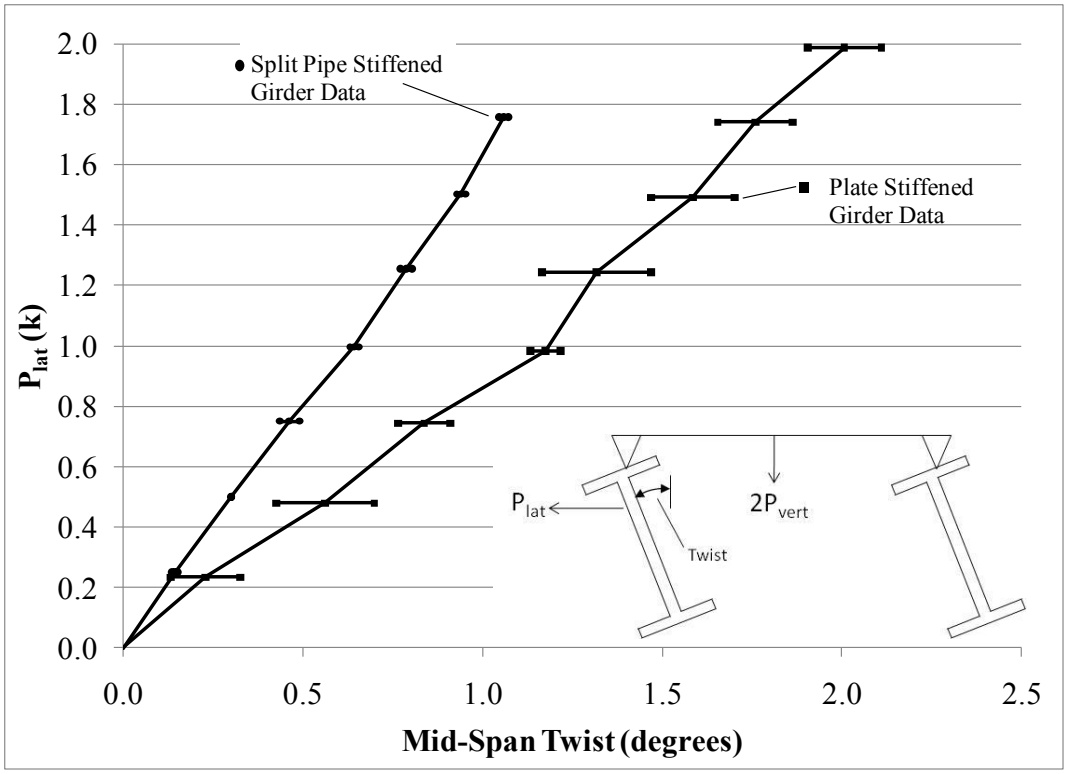

Figure 3.33: Twin girder torsional mid-span test results

3.4.1.4.3 Twin Girder Buckling Test Results

The top flange lateral deflection results for the split pipe and plate stiffened girder are shown in Figure 3.34. The deflections shown in the figure are the absolute values so that both specimens could be compared directly. The results show that the buckling capacity of the split pipe stiffened section increased the buckling capacity by over 50% relative to the plate stiffened specimens. This is due to the warping restraint provided by the split pipe. Graphs of all the deflections, twist, and stresses for each specimen are provided in Appendix A (Large Scale Experimental Results).

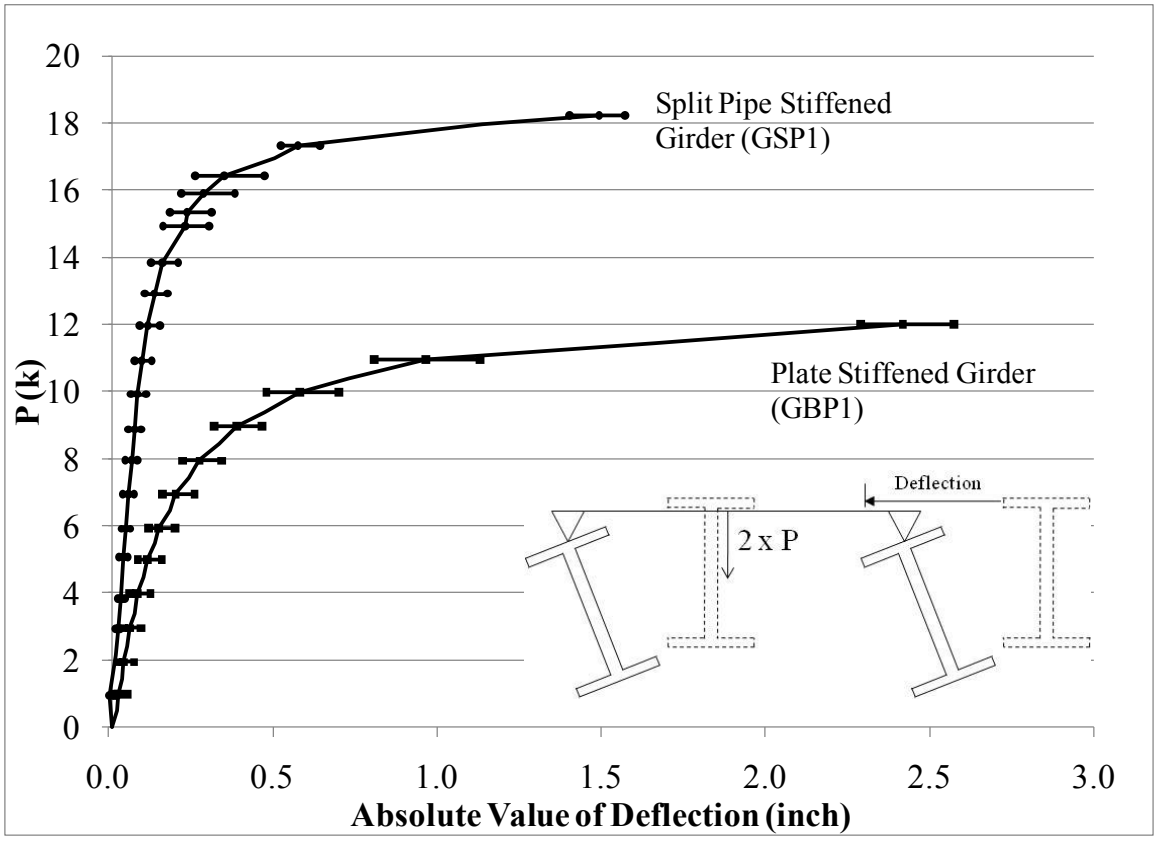

Figure 3.34: Twin girder buckling test mid-span top flange deflections

3.4.2 Three Girder Testing

The purpose of the three girder test program was to measure the buckling capacity, brace forces, and girder end twst for girders with realistic details for the bracing and support conditions. Both split pipe stiffeners and plate stiffeners with bent plate cross frame connections were considered in order to compare the specimen responses and validate the cross frame finite element model. The tests were developed to measure the effects of the support skew as well as the bracing details for both intermediate and support cross frames. The split pipe stiffened cross frame specimen is covered in this dissertation and the results from the bent plate specimen will included in a separate publication.

The girders tested in the three girder testing program were the split pipe stiffened W30x90 specimens (GSP1, GSP2, and GSP3) a picture of the typical test set up is shown in Figure 3.35. In the figure GSP1 is on the left (east), GSP2 is in the middle and GSP3 is on the right (west). A plan view of the test specimen with the key components labeled is shown in Figure 3.36

The testing program, measurements taken, and results are described below. The same girder specimens used for the two girder tests were used again in the three girder tests, so their fabrication is not covered in this section. Also the initial imperfection measurements were performed in the same manner as the twin girder testing, so it is not described in this section.

Figure 3.35: Three girder test (53° skew and no intermediate frames- looking south)

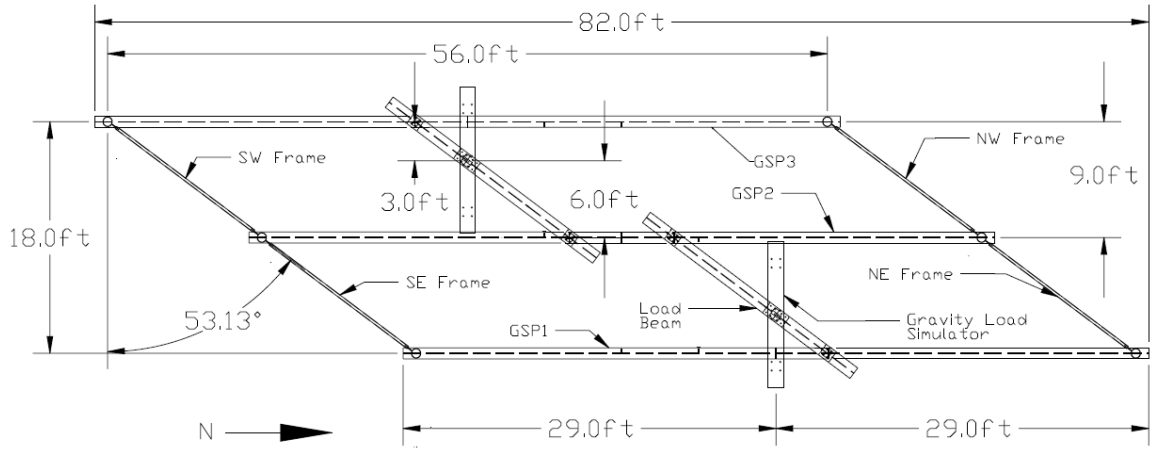

Figure 3.36: Three girder test specimen plan view (no intermediate frames)

3.4.2.1 Three Girder Testing Program

The parameters varied for the three testing were the placement of intermediate cross frames. Tests were performed with no intermediate frames and with intermediate frames continuous across the width of the girders (centered at misdpan of GSP2), and staggered along the skew angle. The cross frame placement was varied to determine the effects of their placement on the end and intermediate frame forces and girder end twist. The tests conducted are listed in Table 3.3.

Table 3.3: Three girder test program

Intermediate Cross Frames	Bearing Type	Number of Tests
None	Thrust Washer	3
Staggered	Thrust Washer	2
Continuous	Thrust Washer	2

3.4.2.2 Cross Frame Fabrication

The cross frames that were used at the supports and intermediate locations were fabricated at The Ferguson Structural Engineering Laboratory. All cross frames had single diagonals with two struts all constructed from HSS2.5x2.5x1/4 tubes. Although cross frame members are often composed of angles, the use of tubular members had two benefits: 1) higher axial buckling strength 2) permitted concentric connections that made member force measurement easier. The two diagonal cross frames made from angle

systems are usually modeled as tension only systems due to the low buckling strength of angles. With the higher buckling strength, the cross frames composed from the tubes only required a single diagonal. The intermediate frames were bolted to connection plates perpendicular to the girders while the end frames were bolted to the connection plate on the split split pipe stiffener parallel to the skew angle.

The details used to construct the end cross frames are shown in Figure 3.37, and a picture of a completed split pipe end cross frame is shown in Figure 3.38. The details used to construct the intermediate cross frames are shown in Figure 3.39, and a picture of a completed intermediate cross frame is shown in Figure 3.40.

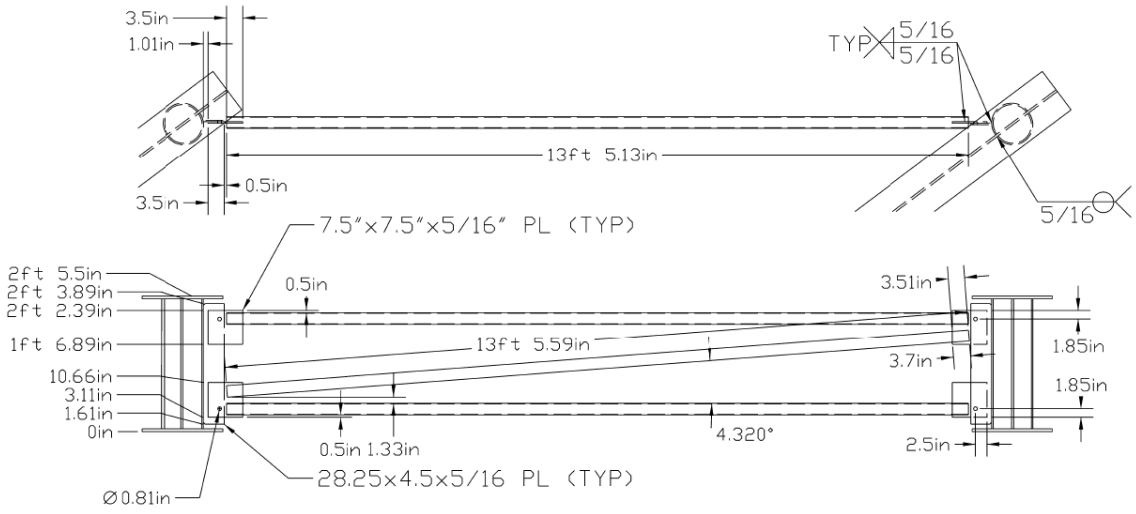

Figure 3.37: Split pipe end cross frame detail

Figure 3.38: Split pipe end cross frame (SE cross frame shown)

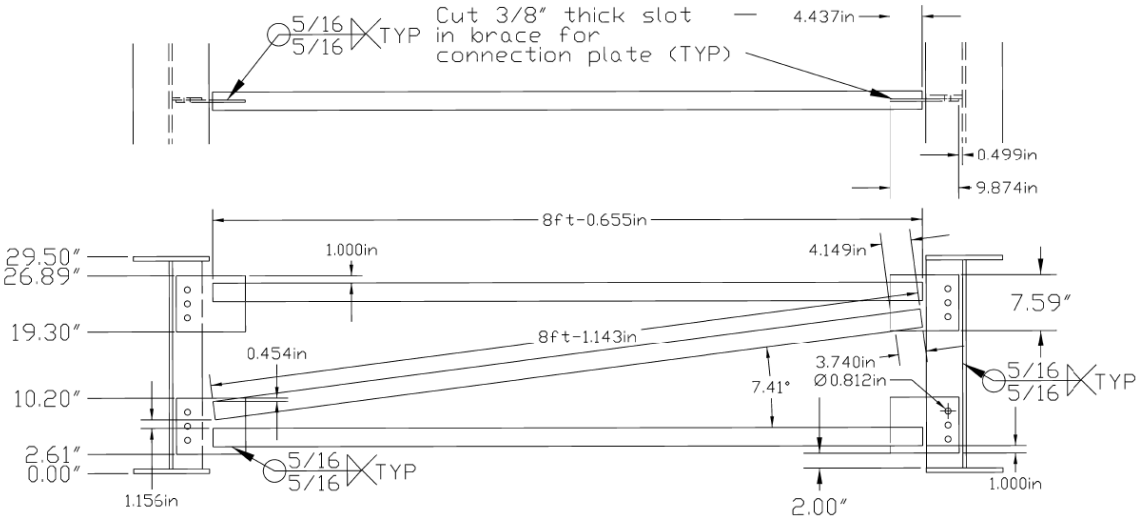

Figure 3.39: Intermediate cross frame detail

Figure 3.40: Intermediate cross frame (western frame shown)

3.4.2.3 Test Frame Set-Up

The three girder test setup is shown in Figure 3.35. Many of the aspects of the three girder test set up are the same as the two girder test set up. The similarities and differences are covered below.

3.4.2.3.1 Test Frame Boundary Conditions

The girder bearing boundary conditions were covered in Section 3.4.1.3.1 of this chapter. The load point boundary conditions used the knife edge bearing surface described in Section 3.4.1.3.2 of this chapter.

A major difference between the three and two girder test was the source of the girder end twist restraint. In the single and twin girder tests, twist was restrained at the ends of the girders by a set of rigid threaded rods connected to a bracket anchored to the supports. As noted earlier in this chapter, the end restraints were very stiff and the one- and two-girder systems experienced no significant translation. In the three girder test, the twist restraint was provided by the end cross frames. The supports were also skewed, which can lead to significant out of plane deformations.

3.4.2.3.2 Load Application

The load was delivered to the girders via gravity load simulators in a similar fashion in the twin girder test (see Section 3.4.1.3.2). As shown in Figure 3.36, the load beams were offset four feet either side of the center of GSP2 so they would not interfere with their placement on GSP2. Finally, each gravity load simulator was placed between the girders they loaded and offset 1/3 of the girder spacing toward the exterior girder. Since the load beams was essentially simply supported on top of the girders, 2/3 of the gravity load simulators force was applied to the exterior girder and 1/3 of the force was applied to GSP2. Therefore each of the girders received essentially the same magnitude of the total load.

3.4.2.3.3 Strain and Deflection Measurements

The girders and cross frames were instrumented to gather the required structural responses. As in the twin girder test each girder was monitored at mid-span for vertical deflection, top flange lateral deflection, bottom flange lateral deflection, twist, and the strains on both sides of the top and bottom flange. In addition to these measurements the girder end twist was measured with tilt sensors and by measuring the top and bottom flange translation with a string and linear potentiometers, respectively.

Each cross frame brace was instrumented with a strain gage on the top and bottom of each member at the ¼ and ¾ points along the member lengths. This allowed the axial force to be calculated in two locations and allowed the calculation of the maximum and minimum moment in each brace member. Typical cross frame strain gage locations are indicated in Figure 3.41.

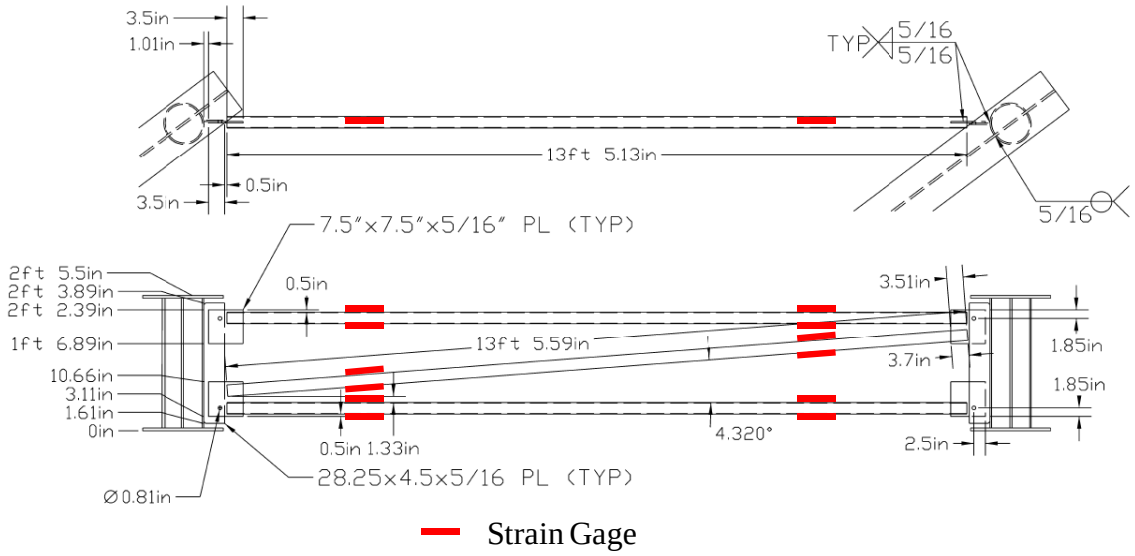

Figure 3.41: Cross frame strain gage locations

3.4.2.4 Three Girder Split Pipe Specimen Test Results

The results for the three girder split pipe specimen tests are presented below. A complete series of graphs of all the structural responses recorded for each test are provided in Appendix A (Large Scale Experimental Results).

3.4.2.4.1 Thrust Washer Bearing and No Intermediate Cross Frames

The vertical deflection results for GSP2 are shown in Figure 3.42 along with the analytic solution for the mid-span vertical deflection of a simply supported beam. The figure shows that the girder is a bit stiffer than the analytic solution. This is to be expected as the cross frames provide a small amount of rotational support to the girder ends and help stiffen the girder against vertical deflection.

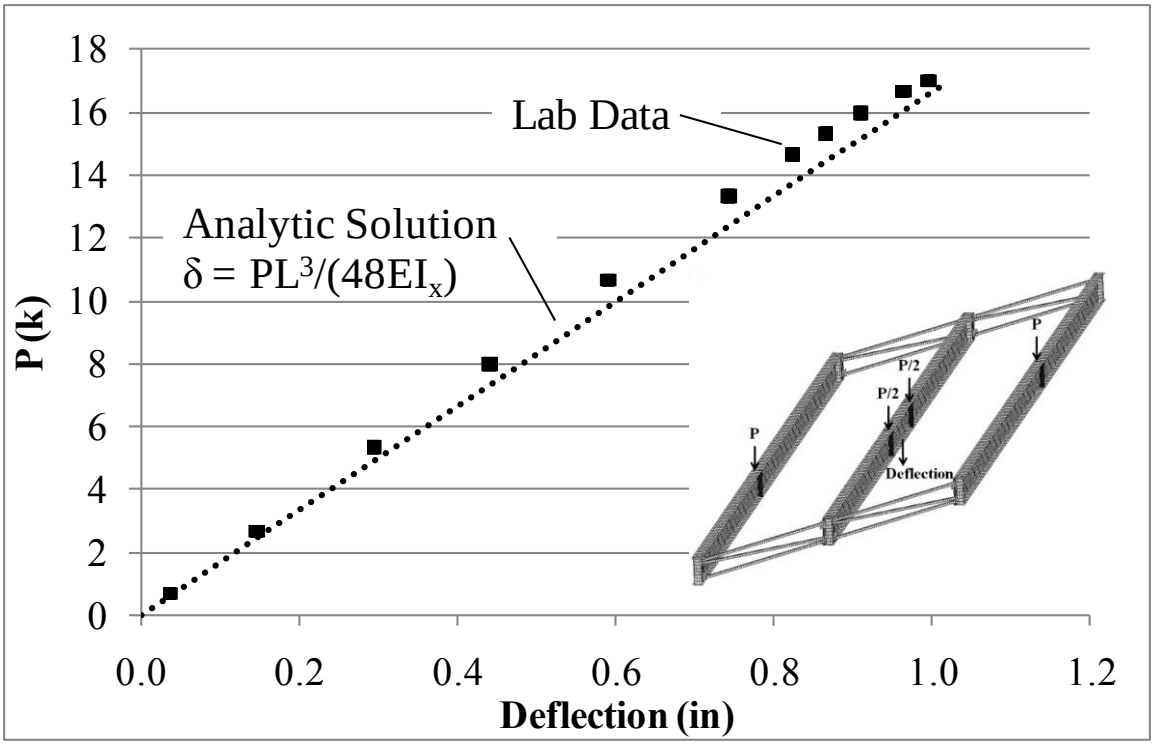

Figure 3.42: GSP2 mid-span vertical deflection laboratory results

A comparison plot for GSP2 mid-span top flange lateral deflection is shown in Figure 3.43. Note that the plot shows the absolute value of deflection since the deflections were opposite one another during the two tests. As discussed in Chapter 2, the impact of allowing twist at the girder end does decrease the girder strength. Using the apparent buckling capacities from Figure 3.43, allowing end twist reduces the girder buckling strength by only about 7%. Such a small decrease in strength is consistent with the previous research discussed in Chapter 2 (Background). There is a small difference in the loading conditions between the twin and three girder tests which also may account for some of the difference (see Section 3.4.2.3.2).

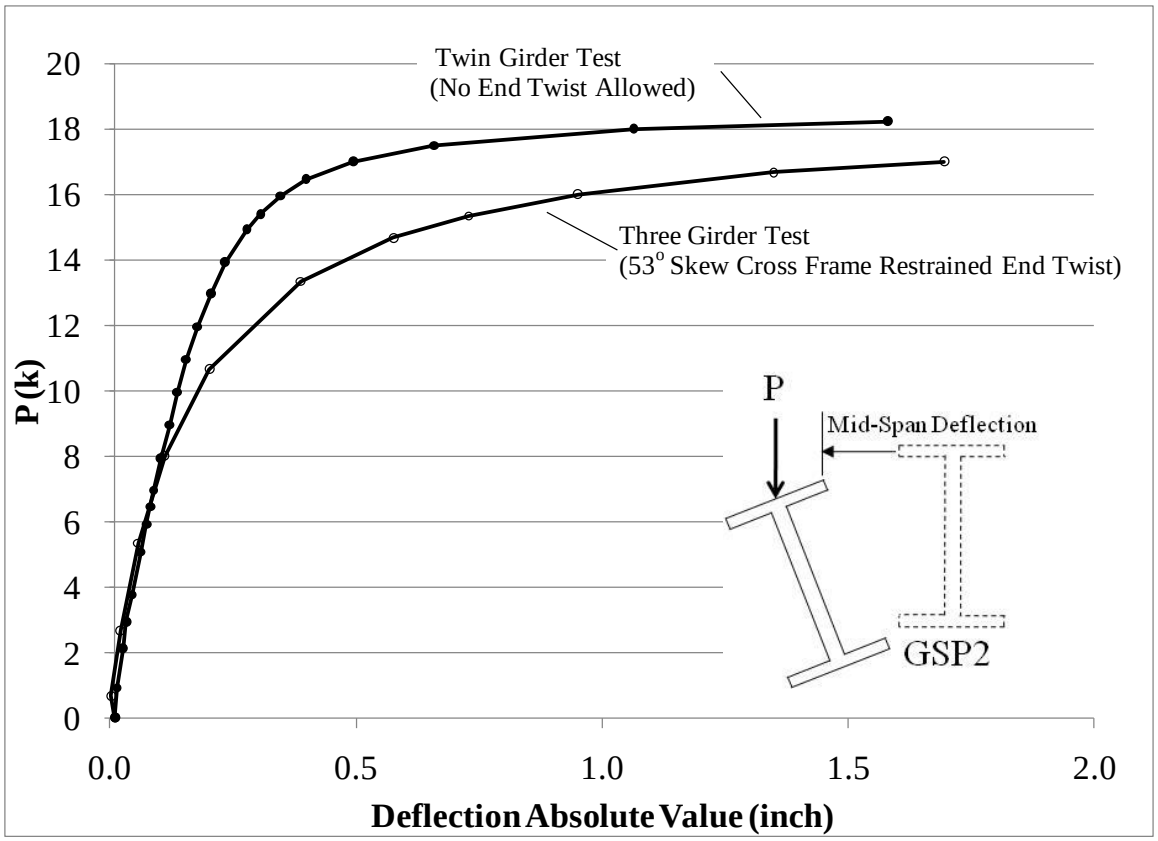

Figure 3.43: GSP2 mid-span top flange lateral deflection with and without end twist

The end twist from the north and south ends of GSP 2 are shown in Figure 3.44. As explained in Chapter 2 (Background) the girder twist due to the skewed abutments are opposite one another on each girder end. However, the impact of the stability forces can also be seen. The girder mid-span buckling twist is clockwise looking north as shown in Figure 3.45. This is the same direction as the north end twist from the skew effect. The buckling twist on the south end is actually opposite to the direction of the skew effect. As a result, the twist at the north end is larger than at the south end due to the combination of the skew and buckling effects. A similar response can be seen in the cross frame forces.

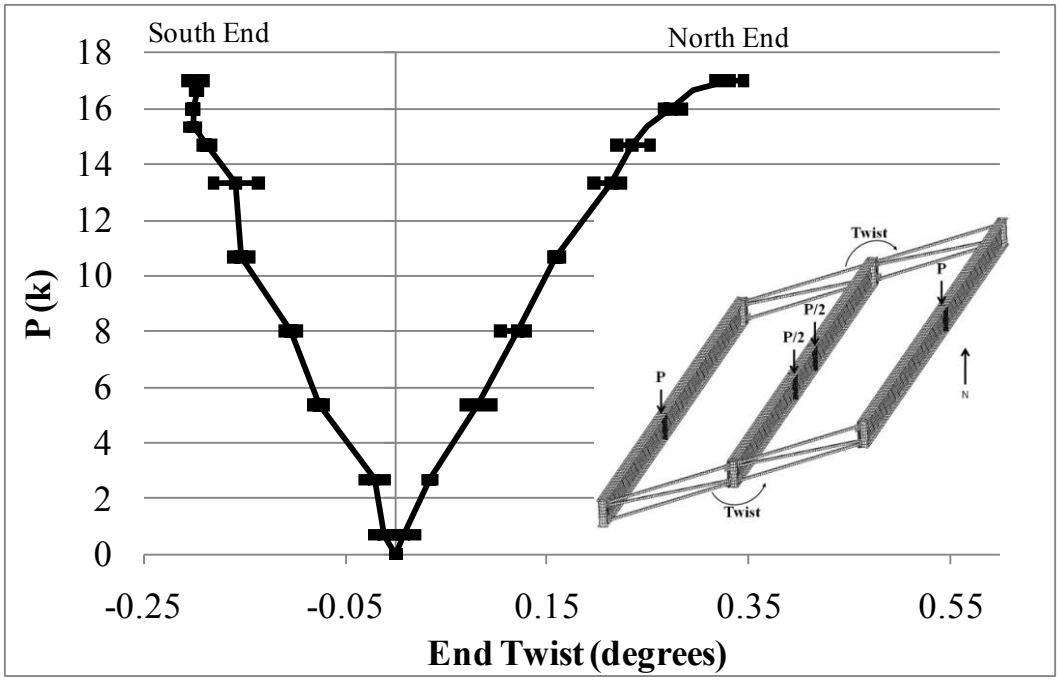

Figure 3.44: GSP2 north and south end twist

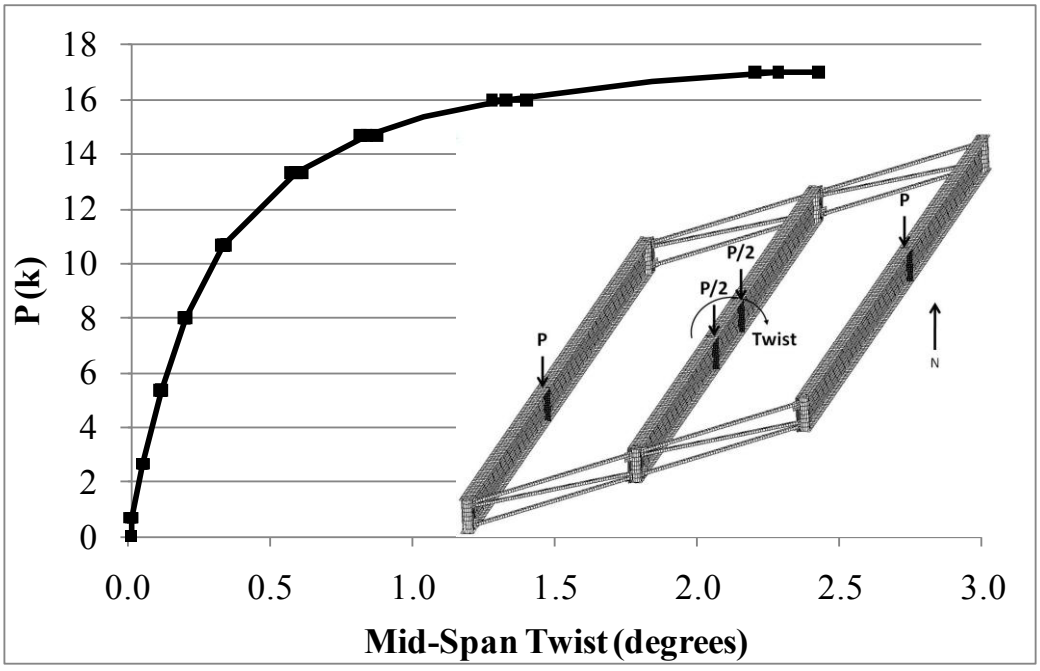

Figure 3.45: GSP2 mid-span twist

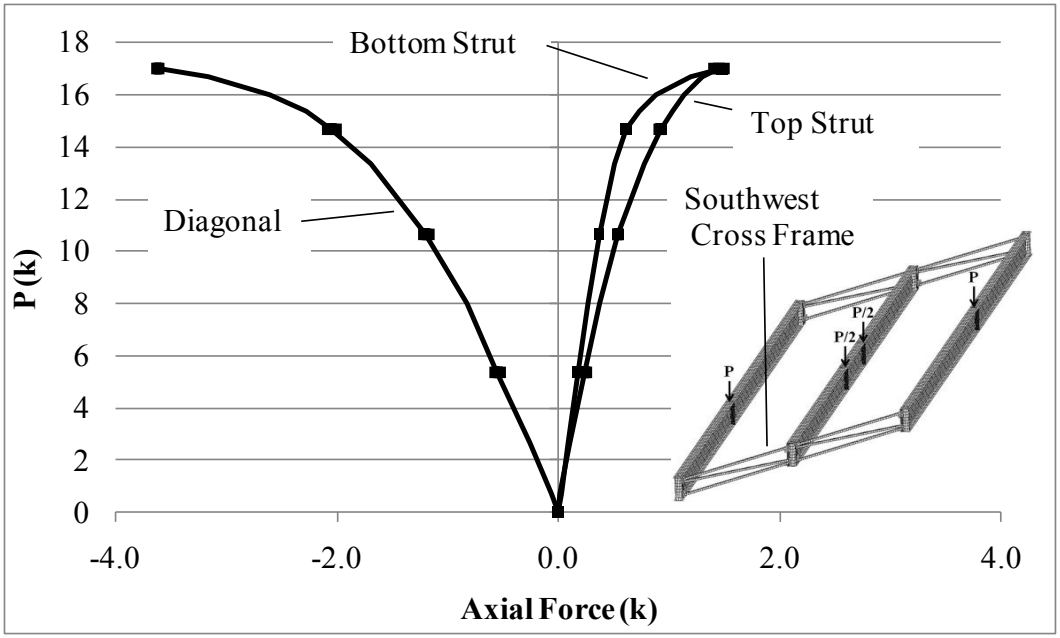

Figure 3.46: Southwest cross frame axial brace forces

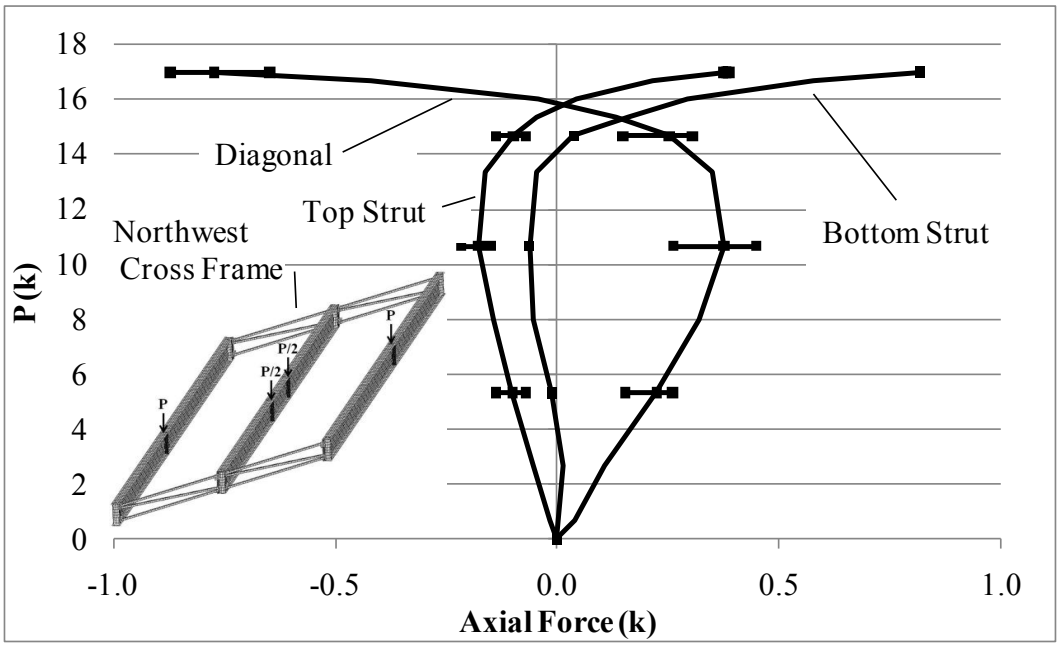

Figure 3.47: Northwest cross frame axial brace forces

The axial brace forces for the southwest and northwest cross frames are shown in Figure 3.46 and Figure 3.47 respectively. The skew and stability force interaction can be seen in the graphs. For the south end cross frame forces, the skew and stability forces add and the forces never change their direction. However on the north end, the skew and stability forces work against each other and as the specimen load increases the stability forces increase and cause a force reversal in the braces.

3.4.2.4.2 Thrust Washer Bearing and Staggered Intermediate Cross Frames

A picture of the staggered intermediate cross frame specimen is shown in Figure 3.48, and a plan view drawing is shown in Figure 3.49. The test set up was identical to the case with no intermediate cross frames with the exception of one intermediate cross frame in each bay. The intermediate cross frames were staggered parallel to the skew angle which positioned them 6' either side of the center of GSP2.

One of the purposes of the test was to compare the end cross frame forces and girder end twist with and without intermediate cross frames. Figure 3.50 shows a comparison of the southwest end cross frame forces without intermediate cross frames and with staggered intermediate cross frames. The only difference between the end cross frame forces in the two bracing schemes is the magnitude of the stability forces in the case without intermediate cross frames. Since the intermediate cross frames reduce the unbraced length, the end cross frames do not attract significant stability forces at the applied load level.

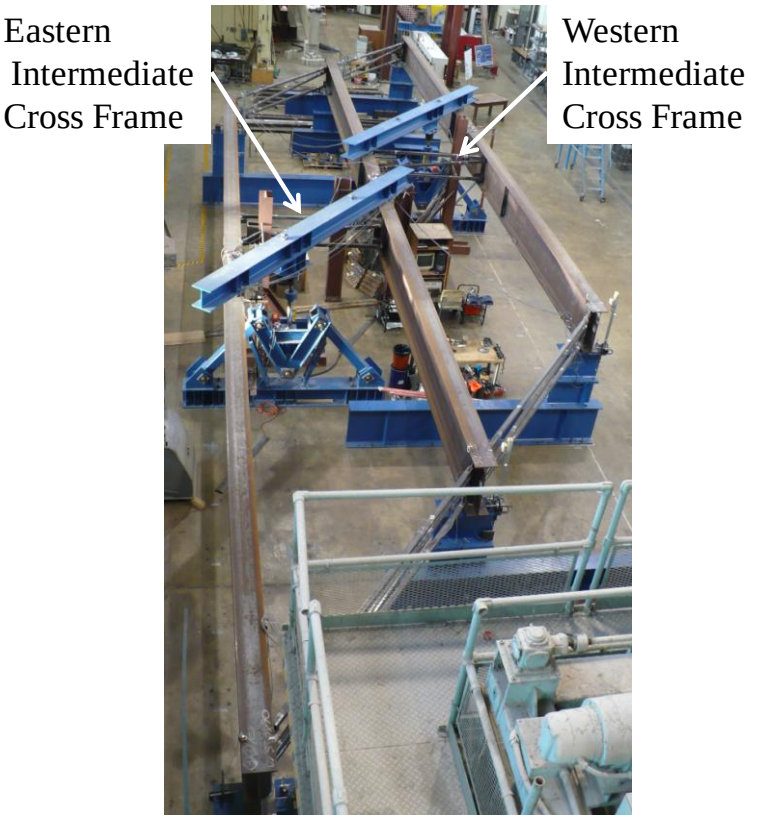

Figure 3.48: 53° Skew specimen with staggered int. cross frames (looking south)

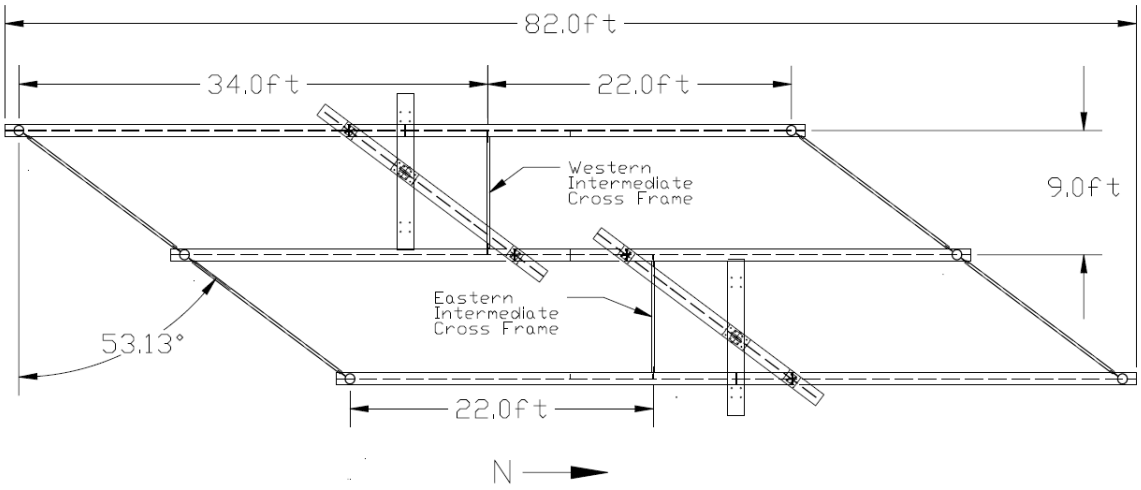

Figure 3.49: Plan view 53° skew specimen with staggered intermediate cross frames

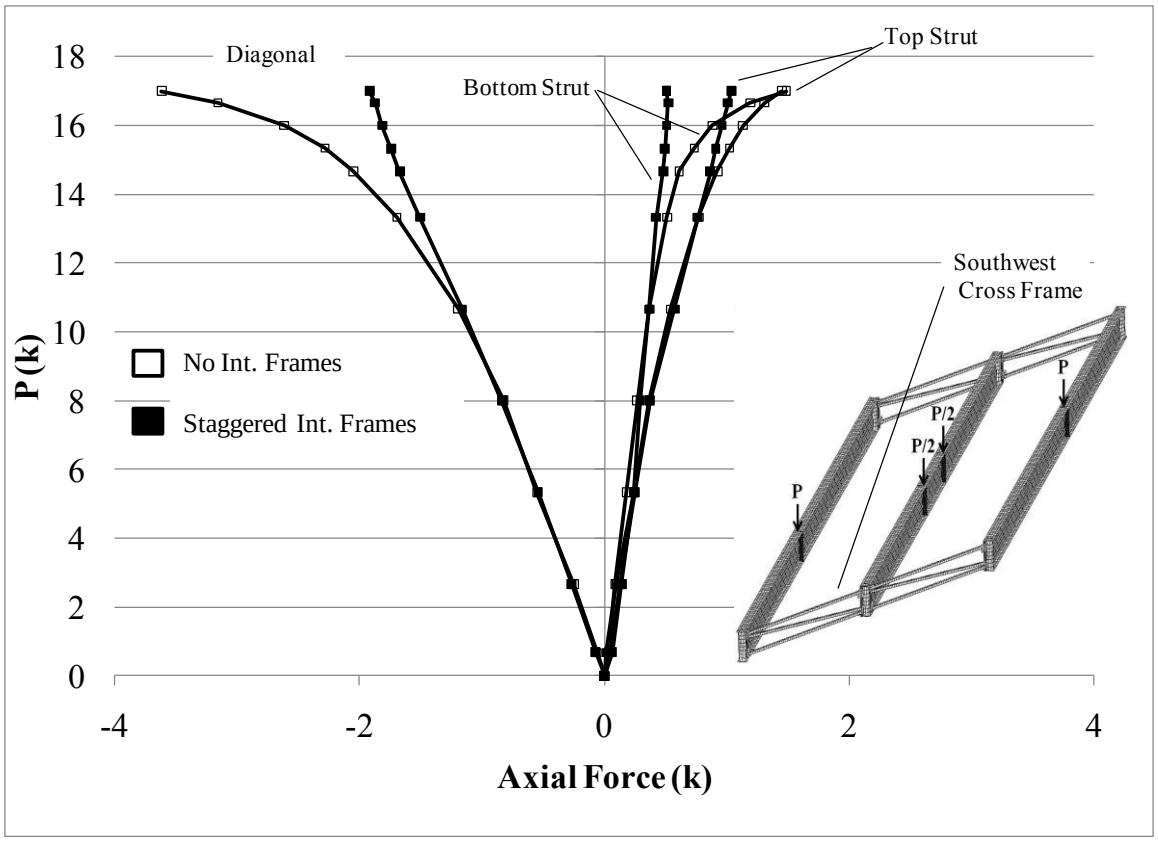

Figure 3.50: Southwest cross frame forces with and without staggered int. frames

A similar pattern can be seen in the girder end twist for GSP2 shown in Figure 3.51. The specimen with the staggered intermediate bracing shows a nearly equal and opposite twist at the girder ends, while the unbraced (and therefore buckling specimen) shows the previously mentioned impact of stability forces causing the end twist to be unequal. Therefore, these laboratory results show that adding intermediate cross frames reduces the stability forces in the end cross frames, but the skew forces remain relatively unchanged. The complete series of graphs showing the cross frame forces and girder end twist for the staggered cross frame layout are given in Appendix A (Large Scale Experimental Results). The mid-span lateral deflections and twist were negligible and are therefore not included in this dissertation.

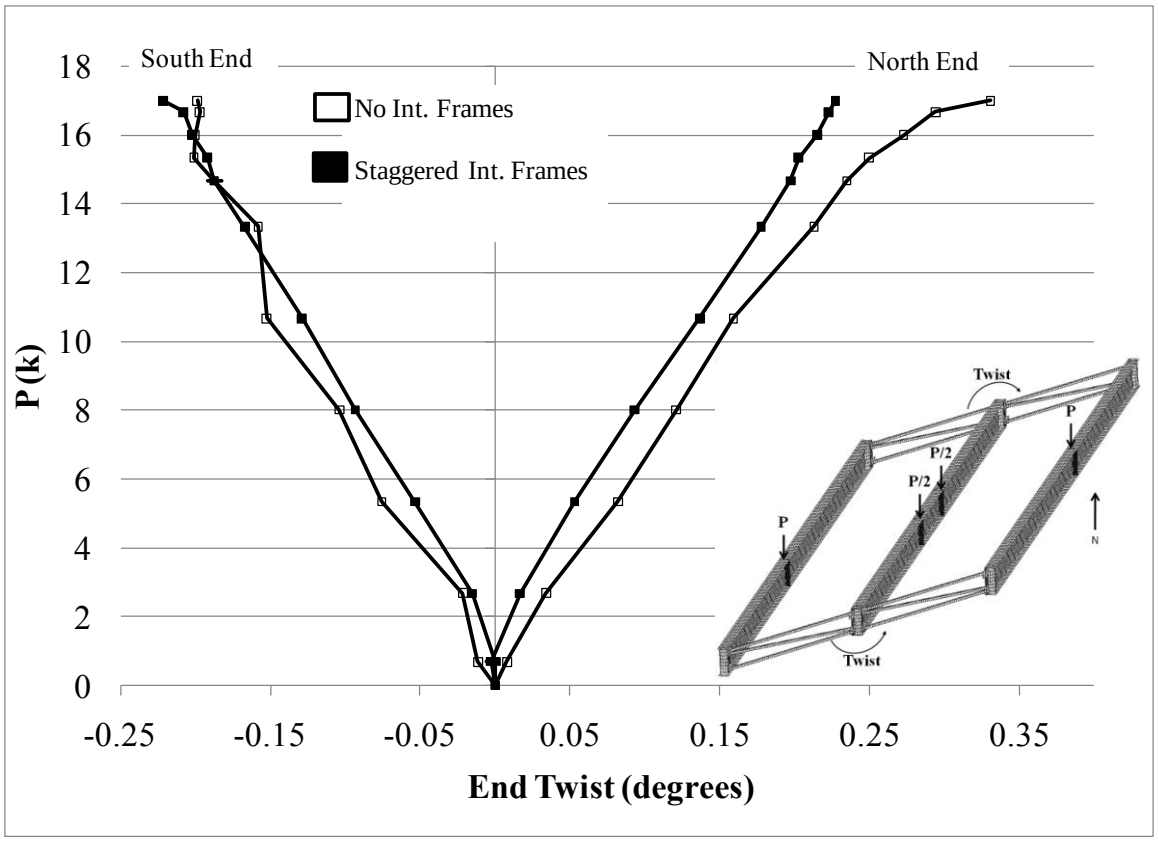

Figure 3.51: GSP2 end twist with and without staggered int. cross frames

3.4.2.4.3 Thrust Washer Bearing Continuous Intermediate Cross Frames

The effect of the layout of the intermediate cross frames were also considered during the large scale testing. Tests were conducted with the braces oriented continuous across the bridge width and also a staggered layout where the braces were perpendicular to the individual girders, but were laid out along a line parallel to the skew angle. A plan view drawing of the continuous intermediate cross frame layout is shown in Figure 3.52. As noted earlier, the braces were positioned so that they framed into Girder GSP2 at mid-span but were offset by 12 feet from the middle of the other two girders for the case of a 53° skew angle.

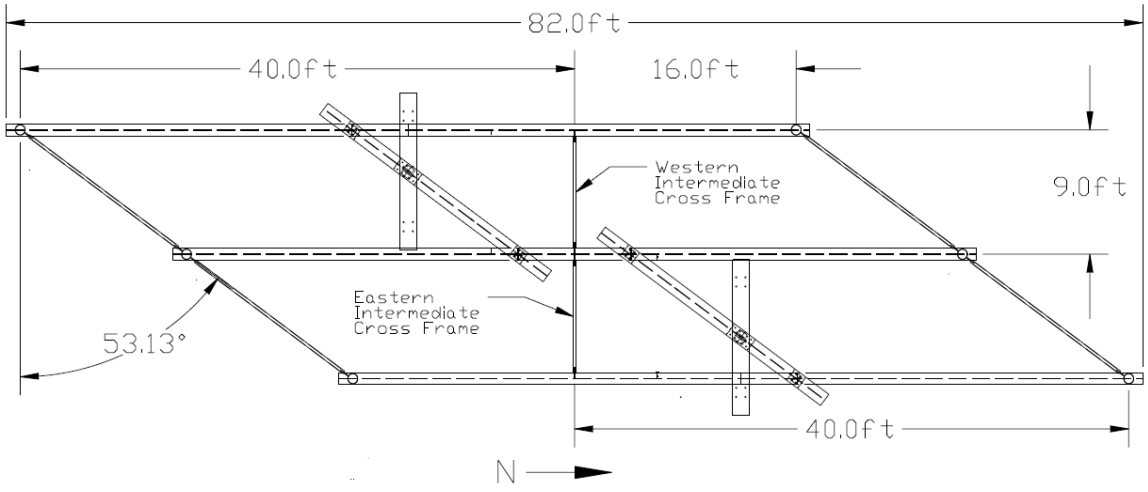

Figure 3.52: Plan view 53° skew specimen with continuous intermediate cross frames

As explained in Chapter 2 (Background), staggering the intermediate cross frames is done in an attempt to reduce the cross frame forces. The graphs in Figure 3.53 show that for this test, staggering the intermediate cross frames parallel to the skew angle resulted in a significant reduction in the cross frame forces relative to the case where the braces were continuous across the bridge width.

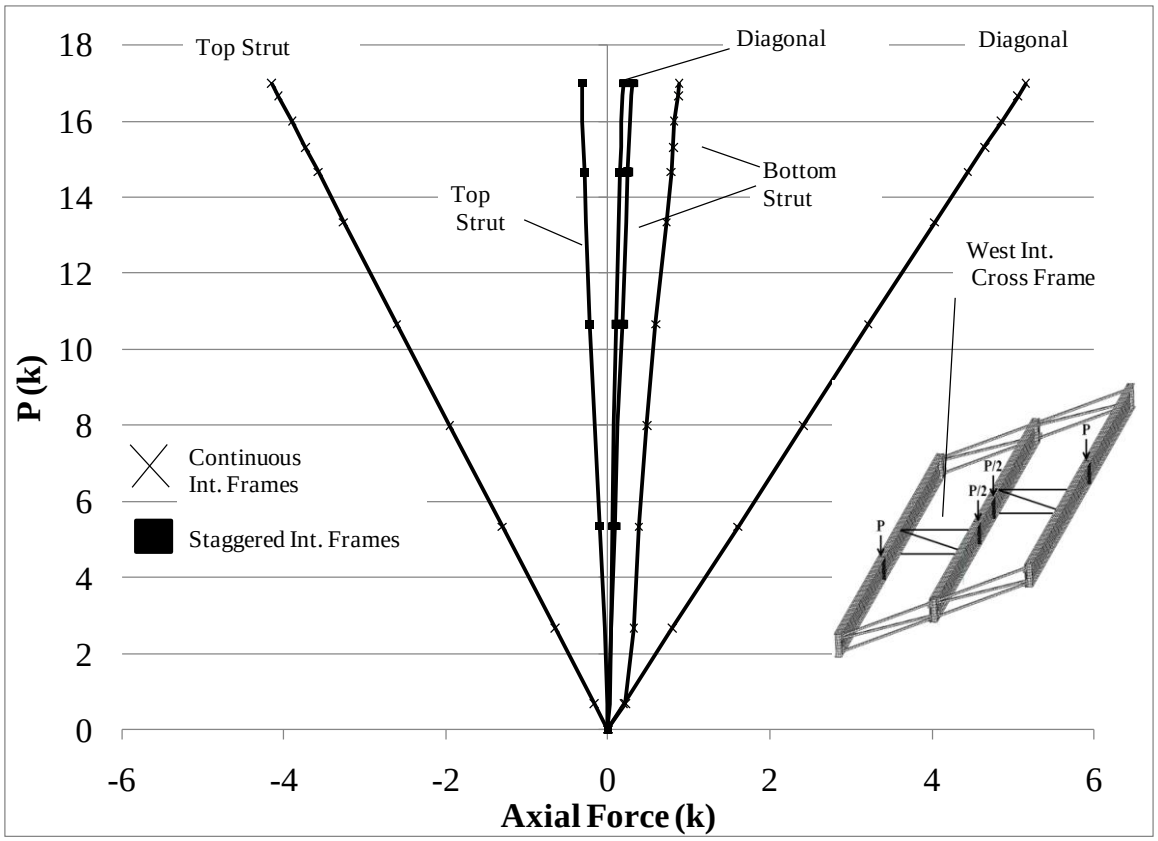

Figure 3.53: Staggered and continuous western intermediate cross frame forces

However, as shown in Figure 3.54, the staggering of the cross frames does not appear to change the skew induced girder end twist. So, at the unbraced length used in this experiment, staggering the cross frames has no apparent affect on the girder end twist. Of course it may be expected that this result would change as the intermediate frames are moved closer to the abutment.

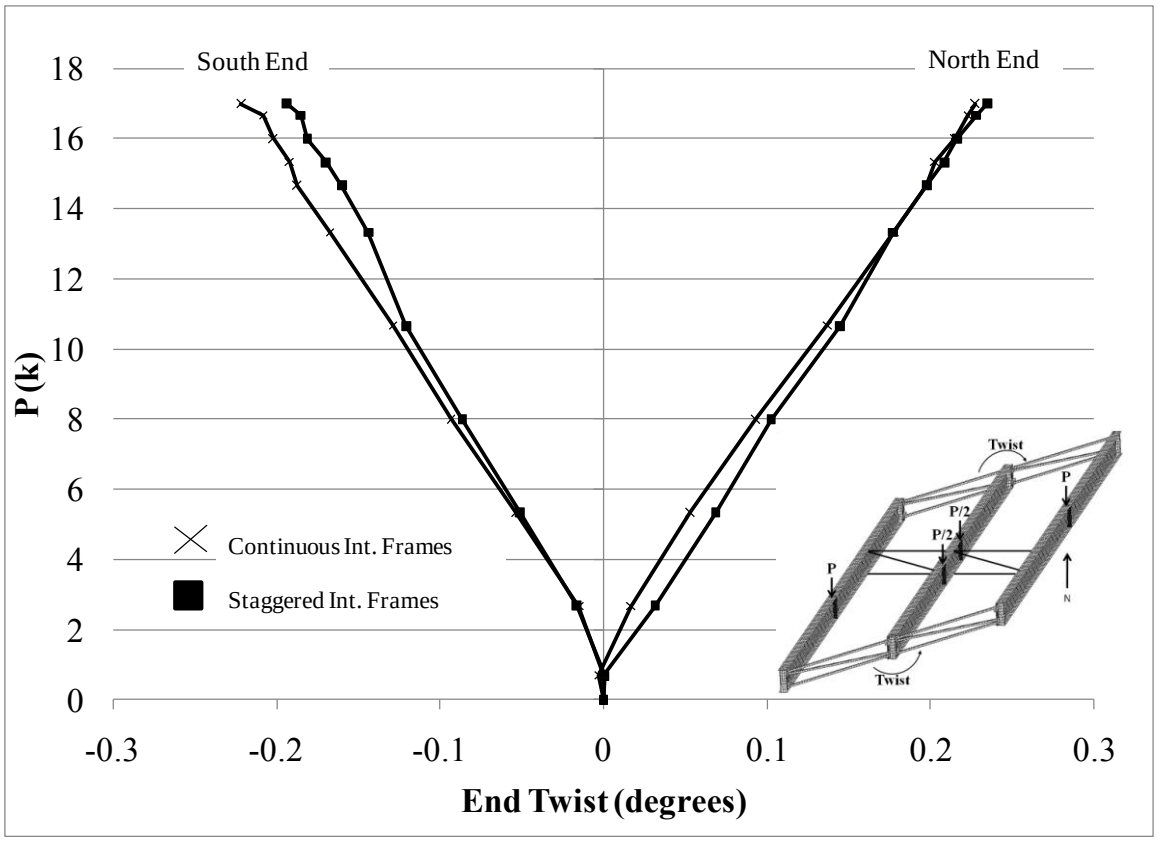

Figure 3.54: GSP2 end rotations for staggered and continuous int. cross frames

3.5 EXPERIMENTAL PROGRAM SUMMARY

The experimental program has given several important results. First the connection tests demonstrated that the split pipe stiffener is stiffer than the bent plate connection when a simple tension load is applied. The split pipe stiffener performed at least as well as a plate stiffener normal to the girder web, which is the current standard for the bent plate connection.

Several important lessons were also learned during the large scale testing. First, the split pipe adds warping restraint to the girder ends and can significantly increases the elastic buckling capacity. Next, forces induced by skewed supports twist the ends of a girder in equal but opposite directions. And the stability forces will interact with these

skew forces limiting the skew induced twist that is opposite to the buckling twist and increasing the skew induced twist that is in the same direction to the buckling twist. Finally, the impact of staggering intermediate cross frames significantly decreases the cross frame forces, while the skew induced girder twist appears to be insensitive to intermediate cross frame stagger.

The above mentioned results are specific to the test parameters described in this chapter. In Chapter 4 (Finite Element Modeling) the laboratory results from this chapter are used to validate the finite element modeling techniques used to create a skewed bridge substructure finite element model. This validated model can then be used to extend the experimental results in this chapter to a wider array of geometric and loading parameters.

CHAPTER 4
Finite Element Modeling

4.1 INTRODUCTION

This chapter includes a description of the finite element modeling techniques used to develop models of laboratory specimens described in Chapter 3 (Experimental Program). The purpose for developing these models was to validate the modeling techniques used in order to employ these techniques in the parametric studies described in Chapter 5 (Parametric Studies and Design Recommendations). The three-dimensional finite element program ANSYS® Academic Research, Release 11.0 was used to create these models. Using the ANSYS Parametric Design Language (APDL) allowed a computer code to be developed that was used to conduct the parametric studies.

This chapter begins with a general discussion of the modeling and analysis techniques used and then describes the specific components used to build the overall connection, cross frame, and bridge substructure models. Where analytic solutions and laboratory results were used to validate the modeling techniques, they are covered in the applicable section describing the component. Additional validation results can be found in Appendix B (Finite Element Modeling Validation Results).

4.2 GENERAL MODELING AND ANALYSIS TECHNIQUES

Most of the girder and cross frame components investigated in this study were modeled as steel plates connected at their mid-thicknesses (such as a web-flange interface) or overlapped at their surfaces (such as a basic tension splice). Once these basic plates and connections were created to form the finite element model, three different types of analyses were conducted. These were a first order elastic analysis, an elastic critical load analysis (eigenvalue buckling analysis), and a second-order elastic analysis (non-linear geometric analysis). The basic plate and connection components are described in the following sections.

4.2.1 Steel Plate Modeling

The element used to create the steel plates for the models was the 8-node shell element (ANSYS SHELL93). This element has been successfully used in previous girder buckling research to model the flat plates that make up most girders (Helwig 1994) (Wang 2002) (Whisenhunt 2004). In this current study, this element was also used to model curved surfaces. Since the element has mid-side nodes, it models curved shells well and supports non-linear geometric analysis (ANSYS Inc. 2010).

The SHELL93 element has six degrees of freedom at each node and allows the user to define its thickness at each corner. Since it does not require multiple rows of nodes to define its thickness, it is much more computationally efficient than using a solid element to model the components in this study. Additionally, its aspect ratio is defined in two dimensions rather than three, which eases maintaining an element aspect ratio near unity. Providing an aspect ratio near unity can be important in maintaining accuracy in the finite element solution. Since the shape functions in a quadrilateral element are derived for a square element in isoperimetric coordinates, excessive deviations from this assumed aspect ratio can result in significant error.

In this study, the finite element analytical (FEA) model was not formed directly by initially creating nodes and elements, but was instead derived from meshing geometric entities, such as key points, lines, and areas created to represent the component geometry. This meant that the SHELL93 element aspect ratios took on the underlying aspect ratios of the areas from which they were meshed. To ensure an element aspect ratio as near unity as possible, and accurately represent the component geometry, an algorithm in the APDL code was used that formed nearly square areas for every component.

The algorithm computed the number of square areas required to construct the underlying plate. Any overage or underage along the length of the plate was then calculated. This overage or underage was then distributed among each of the areas along the length so all areas had the same aspect ratio. The aspect ratio was always less than two and usually very near unity. Once the areas were created, they were then meshed

with a user-provided mesh density to create the number of elements per line requested. A mesh density of two creates four elements in each area since the elements were created along the length and the height of the area.

4.2.2 Plate Connections

The method of connection between the different components was a primary concern in the development of the FEA model. Due to complex curved and angled geometries in this study as well as the offset between the shell nodes at its outer surface, these connections presented a significant challenge. Three different methods were used to connect the shell elements. They were coincident nodes, constraint equations, and multipoint constraint elements. The primary factors in deciding which method was used were the component mesh density, the point of contact between the elements, and the relative deformation expected between the elements.

Coincident nodes were used where plates intersected at their mid-thicknesses and the component mesh densities were the same. An example of this was the web-flange interface of an I-shaped girder like the one shown in Figure 4.1. Of course this assumes the mesh density of the flange is the same as the web along the length of the girder. In this study the mesh density of the web was used to control the mesh density of the flange in order to enforce the nodal coincidence for both plates. A major advantage of this method is that the elements share the same nodes and have the same degrees of freedom, and as a result, no further measures are needed to create an accurate representation of the plate connections. A disadvantage of the method is that the flange density is set by the web. The previously described algorithm to create near unity element aspect ratios was not directly applied to the flange. To mitigate this, two areas were used along the web depth, which allowed the flange elements to have aspect ratios between one and two for the girder geometries used in the study.

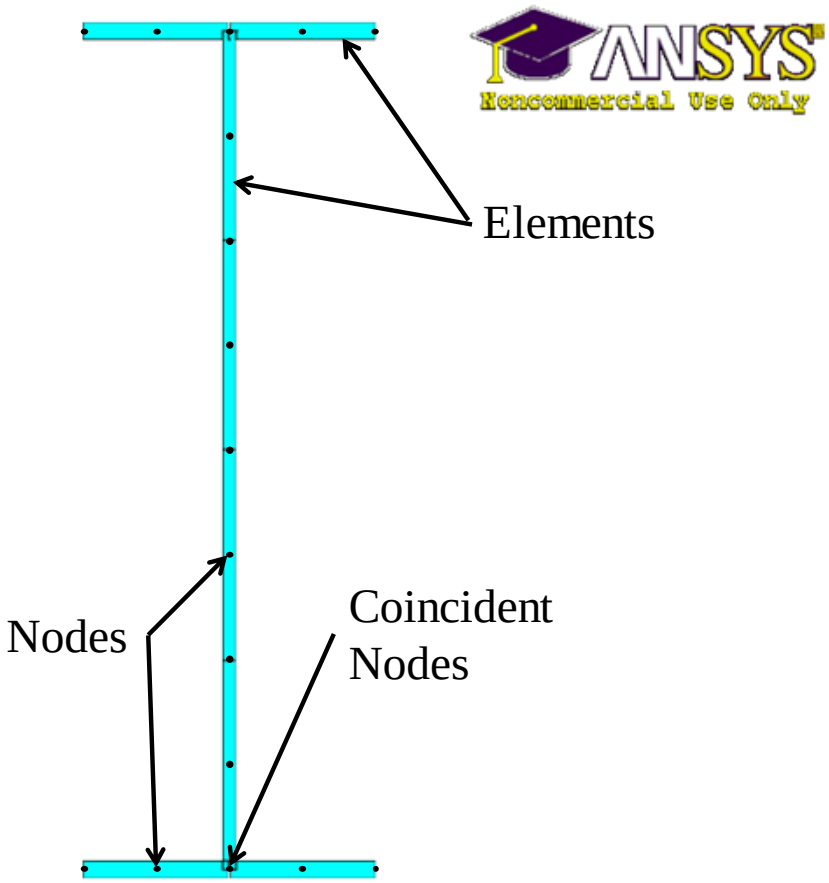

Figure 4.1: Girder cross section nodes and elements

Constraint equations were used where the plates intersected at their mid-thickness, had different mesh densities, and where little relative deformation was expected between the connected components. An example was where the braces intersected the connection plates. Constraint equations are equations that constrain nodes between two elements. Therefore the constrained node's response is governed by the shape functions of the constraining element. This means the constraint equation is generated based on the location of the constrained node relative to the constrained element. The advantages of this connection method is that it is computationally efficient (no additional elements or nodes are generated), it allows the mesh densities of the connected components to be different, and ANSYS has built in functions that allow these equations to be easily developed.

The major disadvantage of the constraint equation connection is the equation is not updated as the relative position of the node changes with respect to its constraining element during a non-linear analysis. For this reason, the constraint equations were only used on this project where little relative deformation was expected between elements. Another disadvantage is that if the constraining node does not lie along the constraining element's mid-thickness, when the constraining element undergoes a rigid body rotation a virtual reaction can develop between the constraining element's nodes and the constrained node. This may cause the structure to appear not to be in equilibrium. Therefore another criterion employed for the use of constraint equations in the modeling was to limit their use only to cases where plate components intersected at their mid-thicknesses.

If large relative deformation was expected between plates with differing mesh densities not intersecting at their mid-thickness, then a multi-point constraint element with 6 degrees of freedom at each end node (ANSYS MPC184 – rigid beam) was used to model the connection. This element does have non-linear capabilities (therefore it updates the geometric relationship between its nodes during a non-linear analysis) and does not impose virtual reactions if rigid body rotation occurs. This element was particularly well suited to model welds in cases where the size of the weld was an important consideration. A table summarizing the types of connections and when they were used can be found below.

Table 4.1: Model plate connection parameters

Connection Type	Plate Intersection		Mesh Density		Relative Deformation	
	Mid-thickness	Not Mid-thickness	Same	Different	Little	Significant
Coincident Node	X		X		X	X
Constraint Equation	X			X	X	
Multi-Point Constraint Element		X		X		X

4.3 CONNECTION MODELING AND VALIDATION

One of the purposes of the study was to compare the stiffnesses of the bent plate and split pipe stiffener connections. To do this computationally, finite element models of the bent plate and split pipe connections were created and then validated with laboratory results. The laboratory data used was from the connection tests described in Chapter 3 (Experimental Program). This section describes the creation and validation of the models for both the bent plate and split pipe stiffener models.

4.3.1 Bent Plate Connection Modeling

The bent plate connection model was created based on the geometry of the laboratory specimen and the general modeling techniques previously described in this chapter. A picture of the model with some of the key aspects called out is shown in Figure 4.2.

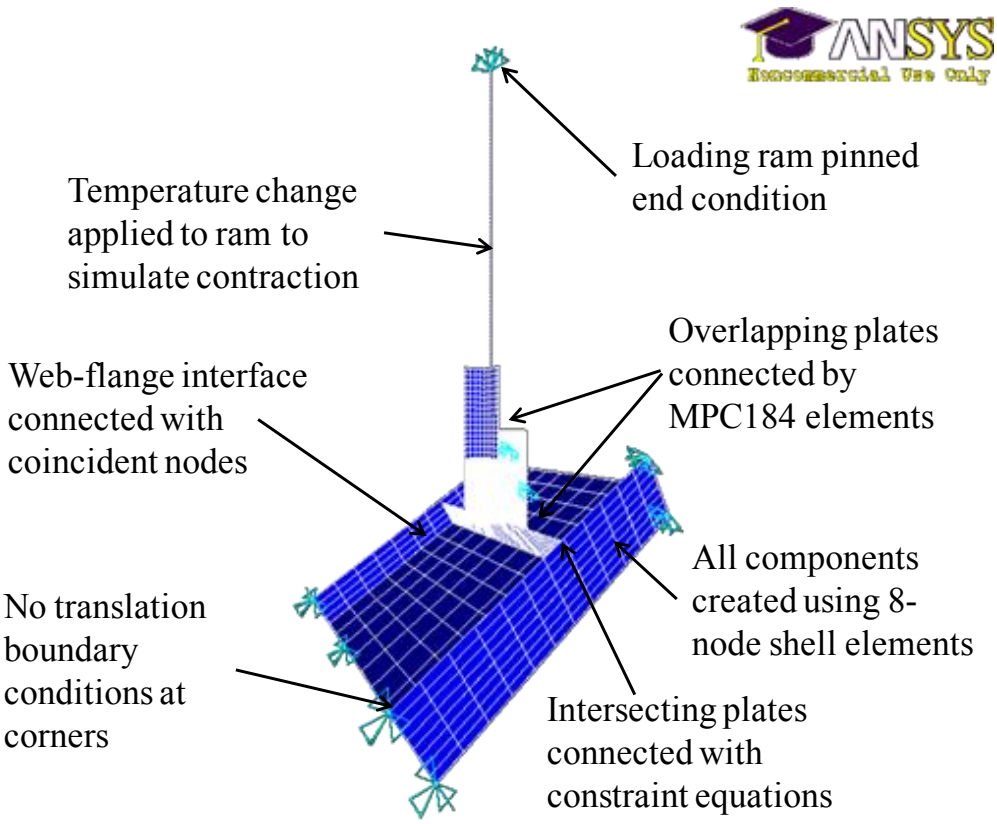

Figure 4.2: Bent plate connection finite element model

Figure 4.2 indicates the locations were the connection methods outlined in the last section were used in the model. The line marked as the "ram" in the figure consisted of a truss element connected to the angle in the model. To simulate the ram applying the tension load to the specimen, a temperature contraction was supplied to the ram with the end of the ram being pinned as it was in the specimen test frame. This allowed the model to account for the restoring force the ram applied to the specimen as the angle and bent plate experienced lateral deflection.

A critical feature in the model was accurately capturing the weld between the connection plate and bent plate at the bend in the plate. Comparisons between the model and the FEA solutions, demonstrated that the weld provided significant stiffening to the connection since it increased the effective thickness at the bend in the plate. Including the weld into the model resulted in good agreement between the laboratory test results

and the FEA solution. A picture of the multi-point constraint elements used to model the weld at the bend and the constraint equations connecting the connection plate and girder are shown in Figure 4.3. Additional lessons learned during model validation are covered in the small scale testing validation section of this chapter.

The bend in the bent plate was spanned by four elements as seen in Figure 4.3. This was done to ensure that there was at least one element per 15° of arc in accordance with the recommendation found in the ANSYS documentation for modeling curved surfaces (ANSYS Inc. 2010).

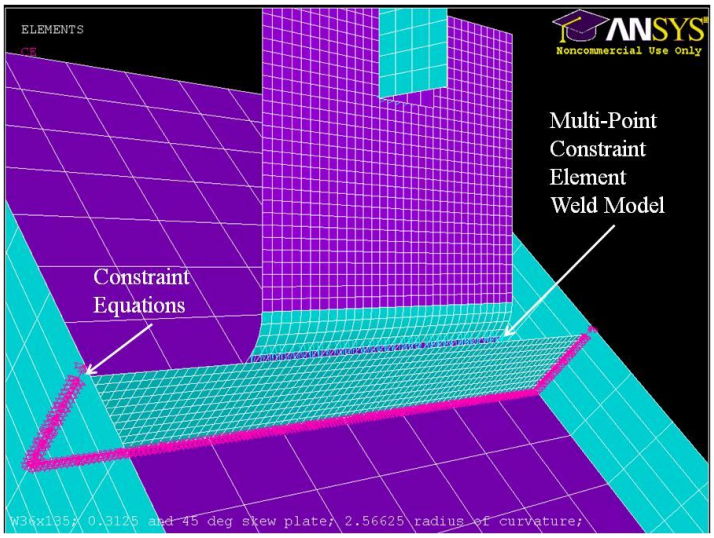

Figure 4.3: Bent plate connection weld models

4.3.2 Bent Plate Connection Modeling Validation

The laboratory results from the bent plate connection tests were used to validate the bent plate finite element model. Both the vertical and lateral deflections of the plate were compared to assure the behavior of the bent plate, connection plate to the girder web, as well as the connections between the plates were being appropriately modeled. All specimens listed in the connection testing section of the previous chapter were used to validate the bent plate connection modeling techniques.

One parameter that was identified to be particularly important was the ratio of the bend radius to element thickness of the bend in the bent plate. ANSYS allows this ratio to be 0.5 or larger, but issues a warning if this ratio is below five because this approaches the limit of the plate theory on which ANSYS SHELL93 element is based. Therefore the three 45° skew specimens were used to find how small the ratio could be and still have good agreement between the model and test results.

The results of the validation showed that as long as the bend radius to element thickness was greater than three, the model had good agreement with the specimen lateral translation. An example of this is shown in Figure 4.4 where the bend ratio to element thickness is 3.2 (the bent plate was 5/16" thick with a 1" bend radius) and there is good agreement.

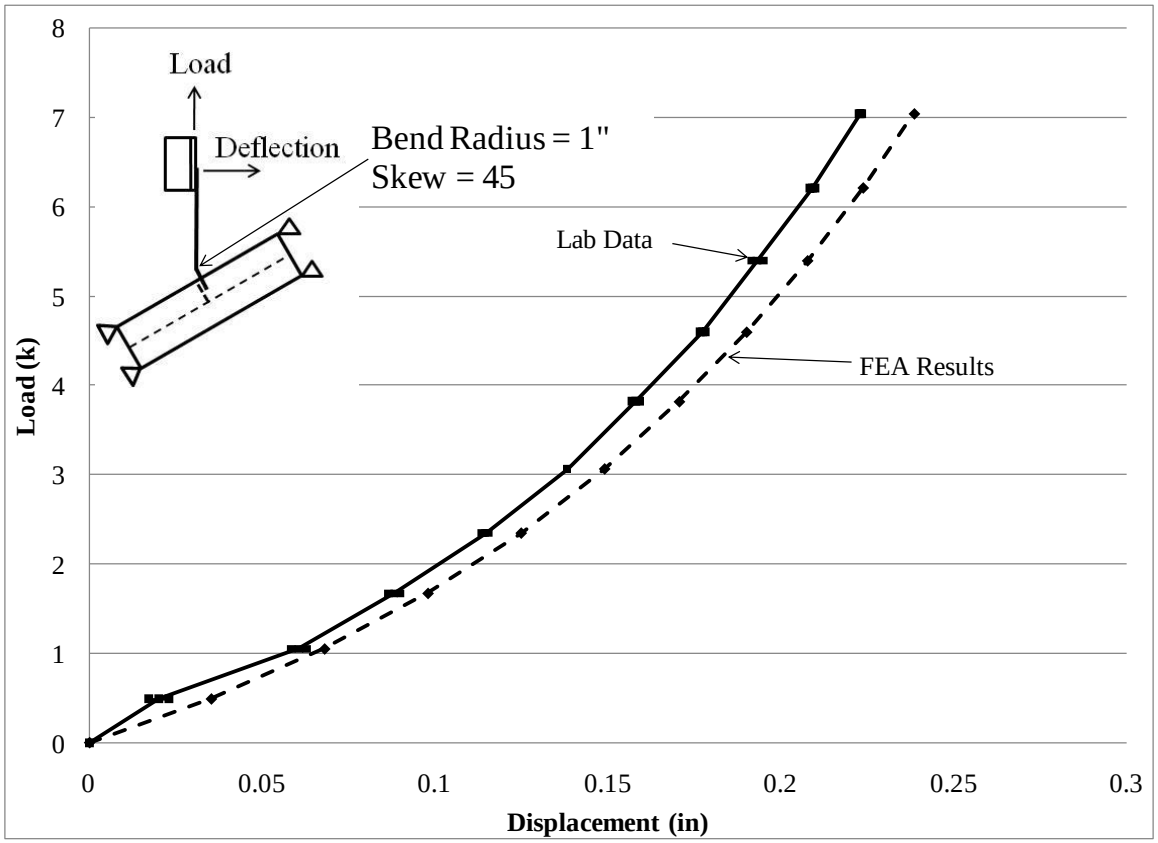

Figure 4.4: 45° specimen lateral results with 3.2 bend radius to thickness ratio

However, if the bend ratio to element thickness ratio was below three, poor agreement between the specimen and model lateral deflection generally resulted as shown in Figure 4.5 for a bend ratio to element thickness of 1.9. An additional case where this occurred was with the 60° specimen which can be found in Appendix B (Finite Element Model Validation Results).

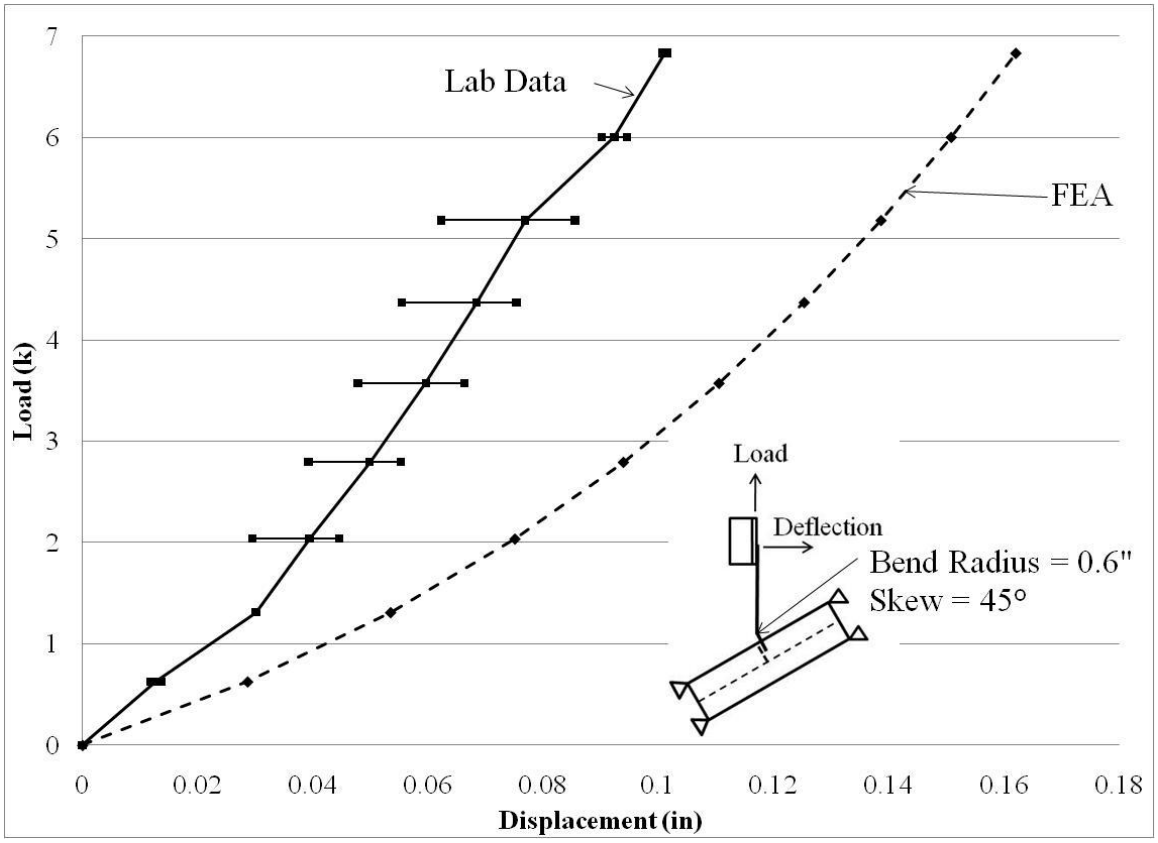

Figure 4.5: 45° specimen lateral results with 1.9 bend radius to thickness ratio

Finally, if the bend radius to element thickness was larger than three then the vertical deflections also showed good agreement demonstrated by the graph of results in Figure 4.6.

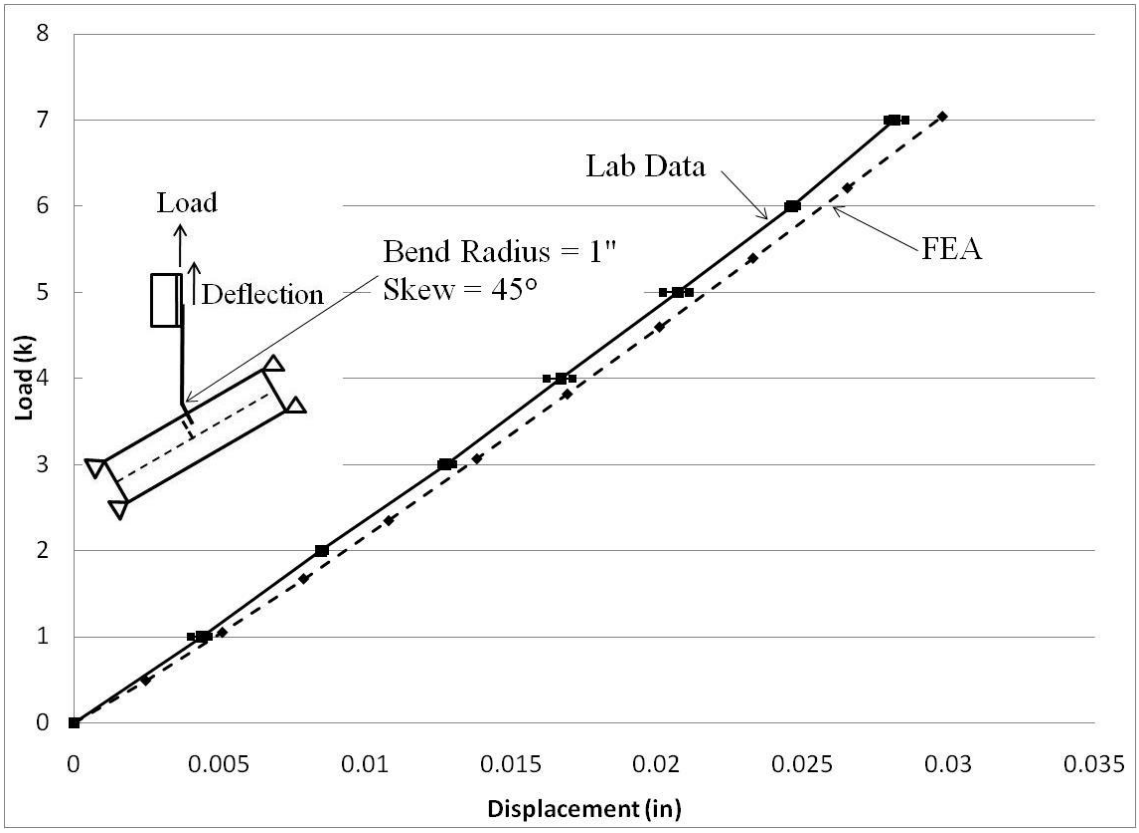

Figure 4.6: 45° specimen vertical results with 3.2 bend radius to thickness ratio

All other cases showed good agreement between the model and specimen deflections except for the axial deformation in the 15° skew specimen. The poor comparison in this case was likely due to fact that the deflections were relatively small (less than five thousandths of an inch) therefore measuring them was extremely difficult. Charts of this case as well as all others can be found in Appendix B (Finite Element Model Validation Results).

4.3.3 Split Pipe Connection Modeling

The 0° and 45° split pipe specimens described in the previous chapter were used to validate the split pipe connection model. A picture of the model and specimen is shown in Figure 4.7. The same techniques used in the bent plate model were again used in the split pipe model. This section provides an overview of the comparisons between

the test results and computational solutions used to validate the FEA modeling techniques.

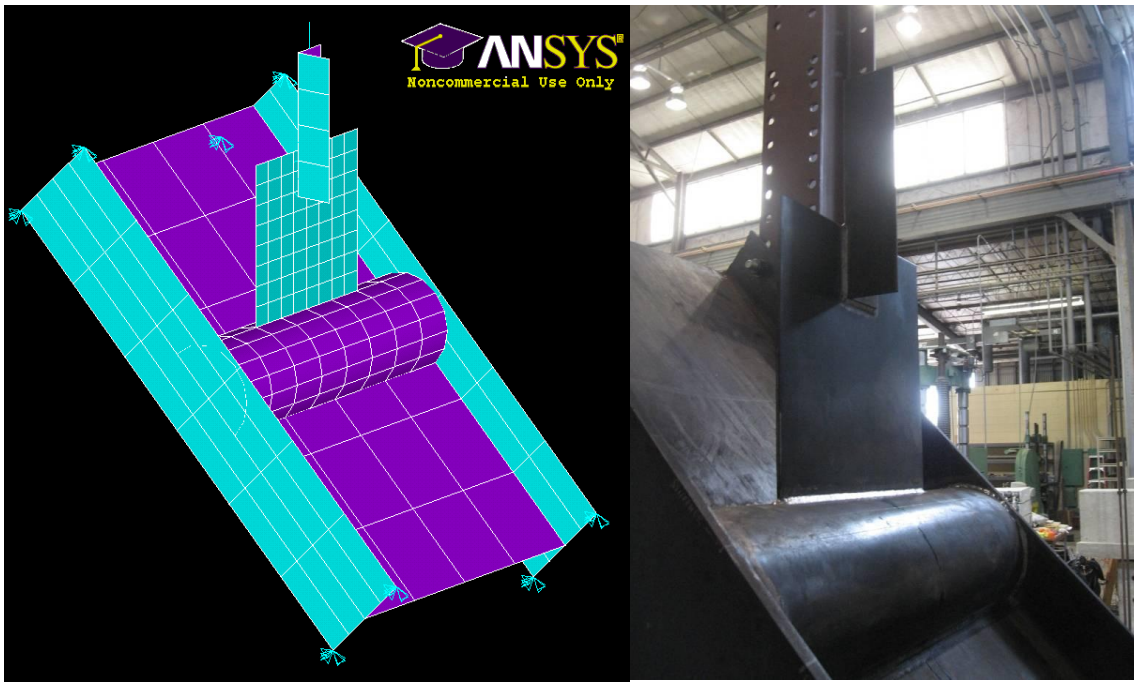

Figure 4.7: 45° connection model (left) and specimen (right)

The 0° skew lateral deflection results are shown in Figure 4.8. The lateral deflection in this case primarily occurred due to the eccentricity in the connection between the angle and the plate welded to the split pipe. Although there was difference between the FEA solution and the measurements, the model did have a similar shape to the measurements. The 45° lateral deflection results are shown in Figure 4.9. The 45° specimen deflected less than the 0° specimen since the connection plate was closer to the pipe–web interface. The model reflects this as well and shows good agreement with the laboratory specimen. While the model results between the two skew cases may seem inconsistent since it predicts a stiffer connection than the lab results in the 0° skew case and a more flexible connection than the lab results in the 45° case, two factors must be considered. First, the differences between the laboratory results are only 0.02" which is near the expected error of the measuring device and test frame. Secondly, the model assumes no imperfections, while there is certainly some imperfection in the laboratory

specimens that most likely would account for a majority of the difference between the laboratory results. The vertical deflection results are provided in Appendix B (Finite Element Validation Results).

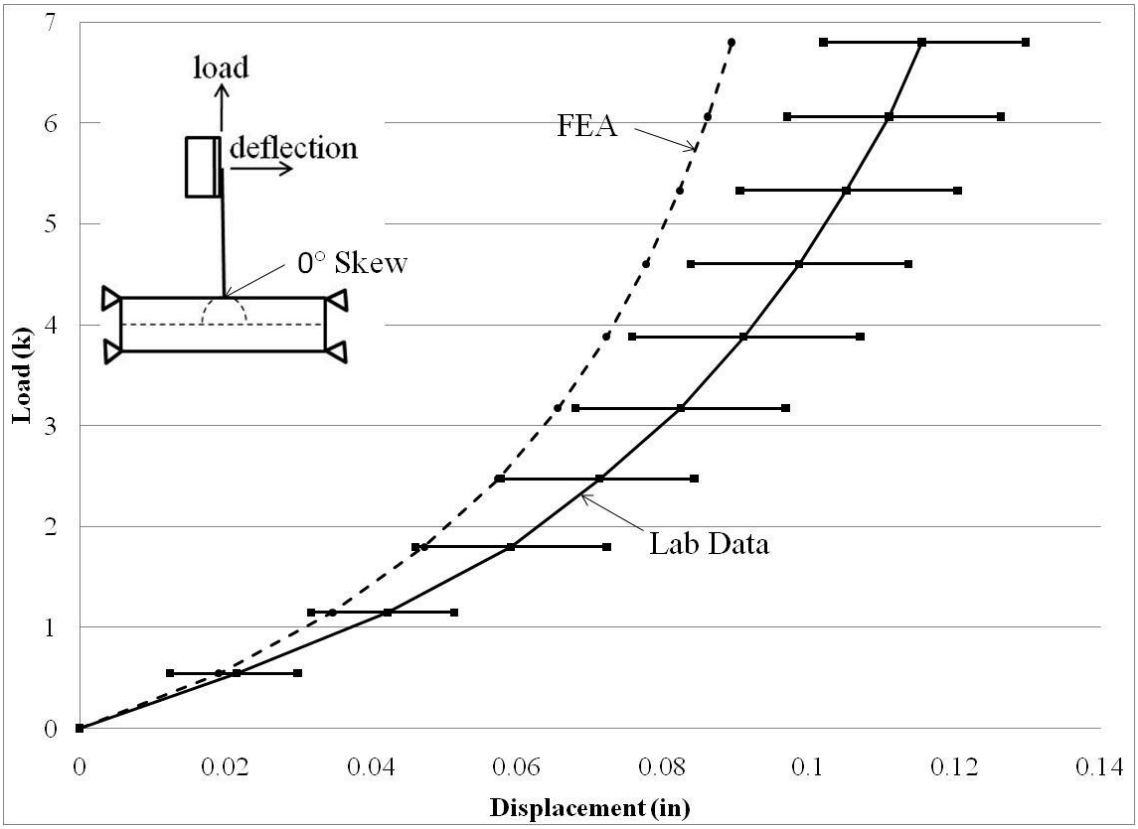

Figure 4.8: 0° skew split pipe lateral deflection FEA and specimen results

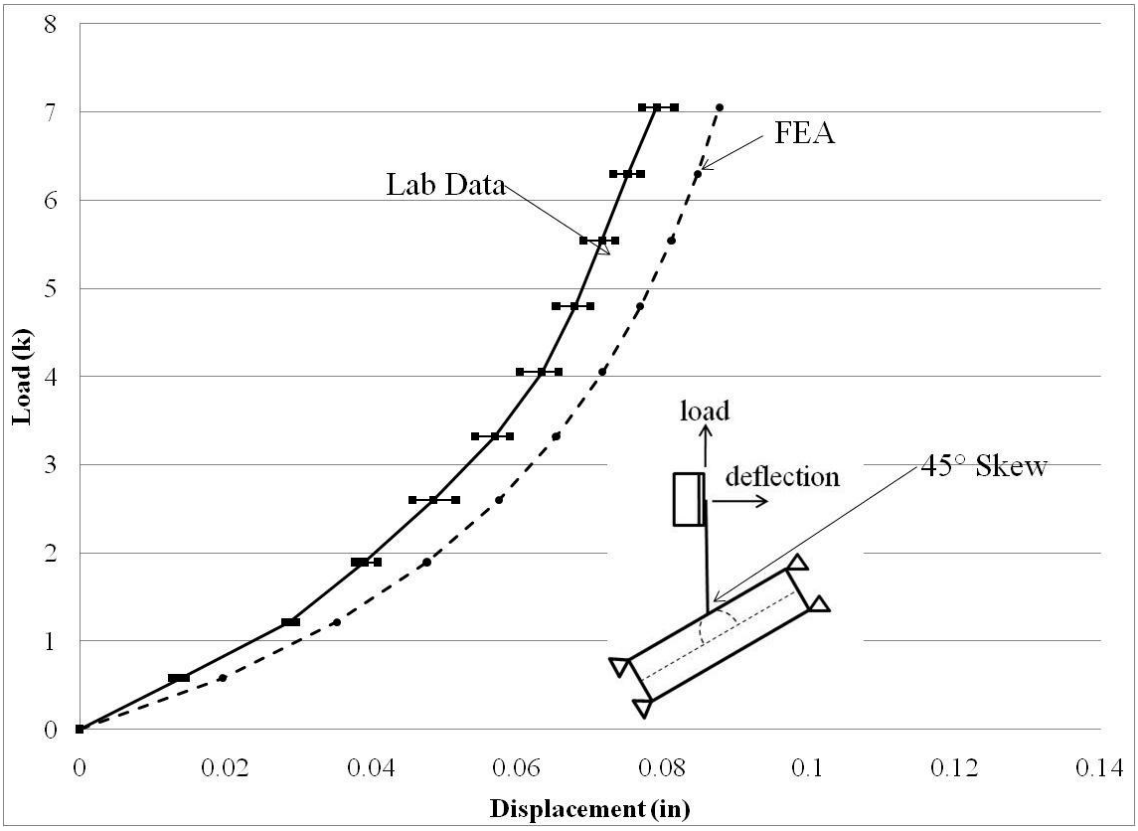

Figure 4.9: 45° skew split pipe lateral deflection FEA and specimen results

4.4 GIRDER MODELING

After confidence had been gained in the modeling of the bent plate and split pipe connection models, the next step in the modeling was to create a finite element model of the full girder system. Validation comparisons were conducted by comparing the model with eigenvalue and non-linear geometric buckling results from both analytic solutions and laboratory test results. This section describes the modeling techniques used to create the girder model, stiffeners, connection plates, and split pipe stiffener as well as the analytic and laboratory validation data.

4.4.1 Girder Cross Section

The girder cross section was constructed using the basic techniques described in Section 4.2 by considering the girder cross section to be composed of three plate

elements including the top flange plate, the bottom flange plate, and the web plate. As previously mentioned the plates were connected using coincident nodes. Figure 4.10 shows a W30x90 girder segment model. In the left part of the figure are the areas used to create the model. The right side of the figure shows the model elements when a web mesh density per area of two is used. Note there are four elements along the depth of the web since two areas make up the web depth.

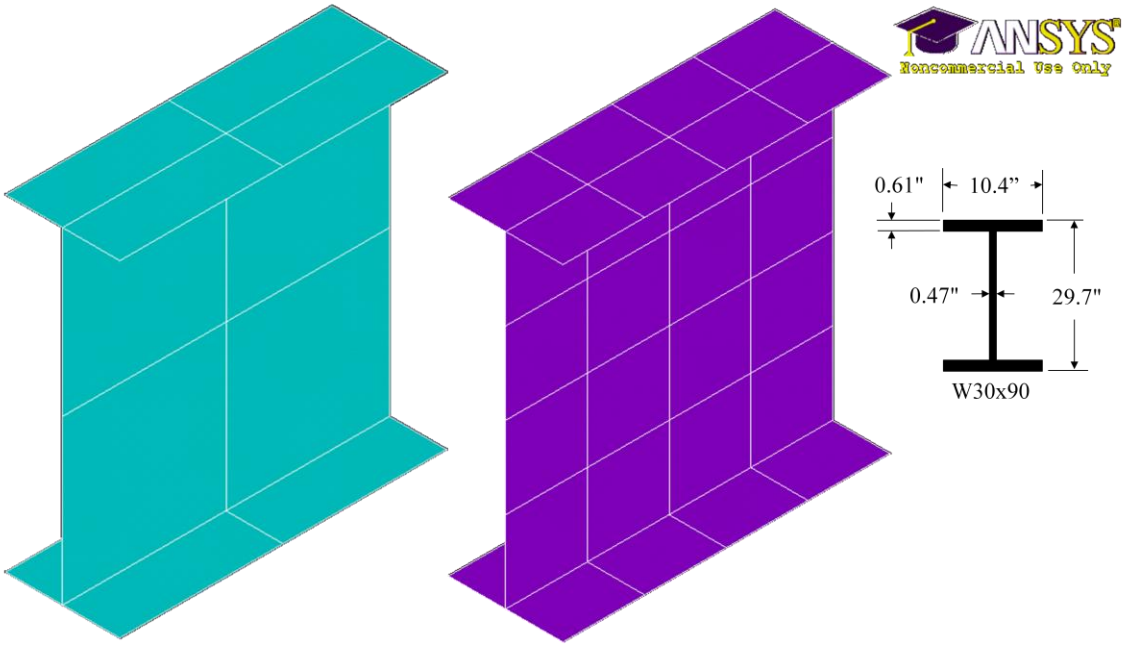

Figure 4.10: W30x90 finite element model girder segment areas (left) elements (right)

Accounting for the fillets in a rolled shape must be accomplished to get an accurate model of the laboratory specimen. While the model uses plates to build the girders, the geometric properties of the fillet between the flange and web are modeled by using beam elements (ANSYS BEAM4) connected between each node along the length of the web-flange interfaces. The geometric properties of the beam elements (area, torsional constant, etc.) are assigned by calculating the properties as if the rolled shape were a plate girder and then subtracting them from the rolled shape values as given in the AISC Steel Construction Manual (American Institute of Steel Construction 2005).

4.4.2 Plate Stiffeners

Plate stiffeners were used in several different applications in this study, including bearing stiffeners, concentrated load stiffeners, and cross frame connection plates. They are all modeled in the same way using the plate modeling technique previously discussed with the stiffeners intersecting the web and flange plates at their mid-thicknesses. The most important consideration was found to be the method of attaching the stiffeners to the girder cross section.

Two different stiffener to girder connections were used depending on whether the FEA solution was being compared to analytic solutions or to actual conditions. The plate stiffeners do actually provide some warping restraint; however the analytic solutions that were used to validate the model accuracy did not account for the warping restraint provided by the plate stiffeners. Therefore, if minimal warping restraint was desired then constraint equations were used to connect the stiffeners to the girders. This was the typical application if an eigenvalue buckling analysis was being used to compare with an analytic solution.

However, in the case of comparisons between the FEA models and test results, the test data included the increased warping stiffness provided by the plate stiffeners. To obtain an estimate of the actual warping restraint provided by the stiffener, multi-point constraint elements were used to model the welds that attached the stiffeners to the girders. The multipoint constraint equations were used to connect nodes on the stiffeners and girders that were connected via fillet welds. The lengths of the multipoint constraint equations were set by the half thicknesses of the plates they connected and the size of the weld. Figure 4.11 shows both connection types. The left side shows the constraint equation connection and the right depicts the weld modeled by multi-point constraint elements.

When using element welds, their size was set by the connected component mesh densities. Therefore, an adequate mesh density had to be selected to ensure the weld

element sizes and orientations were accurate. In some cases, a denser mesh was required than typically used, which added to the computational time on larger models.

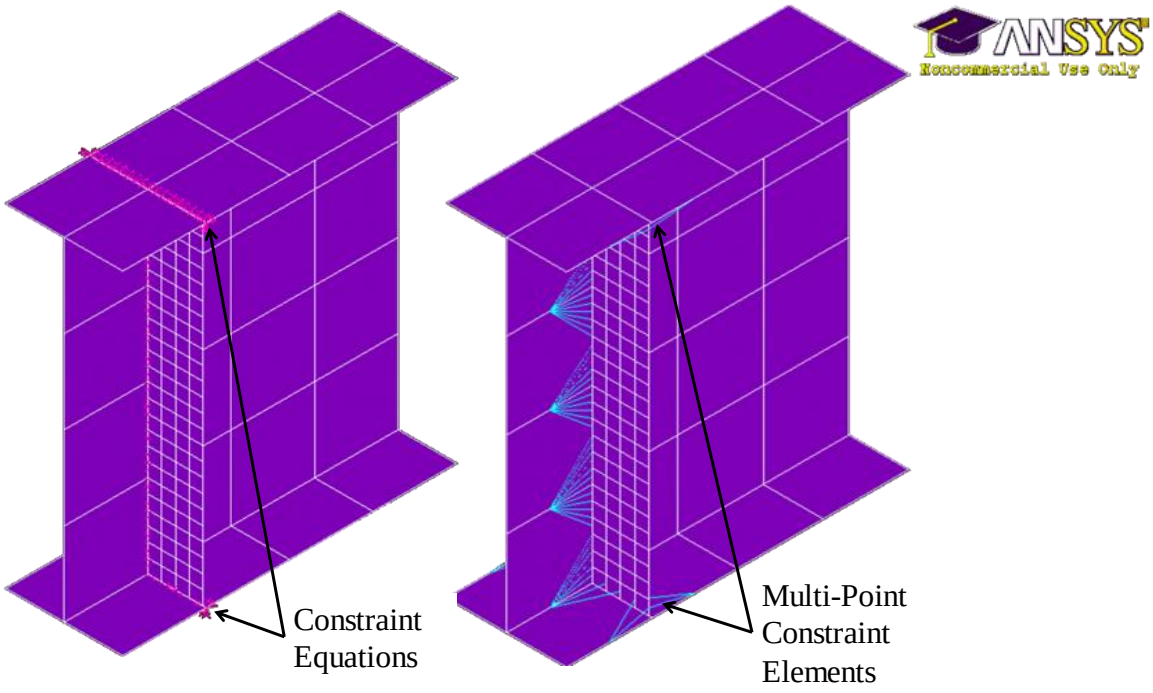

Figure 4.11: Plate stiffener connections

4.4.3 Split pipe Stiffeners

The split pipe stiffeners were modeled using the basic steel plate modeling techniques previously described in Section 4.2.1 with the additional curved surface modeling considerations as described in Section 4.3.1. The split pipes were connected to the girder web and flanges using constraint equations. Figure 4.12 shows split pipe bearing stiffeners connected to a girder segment.

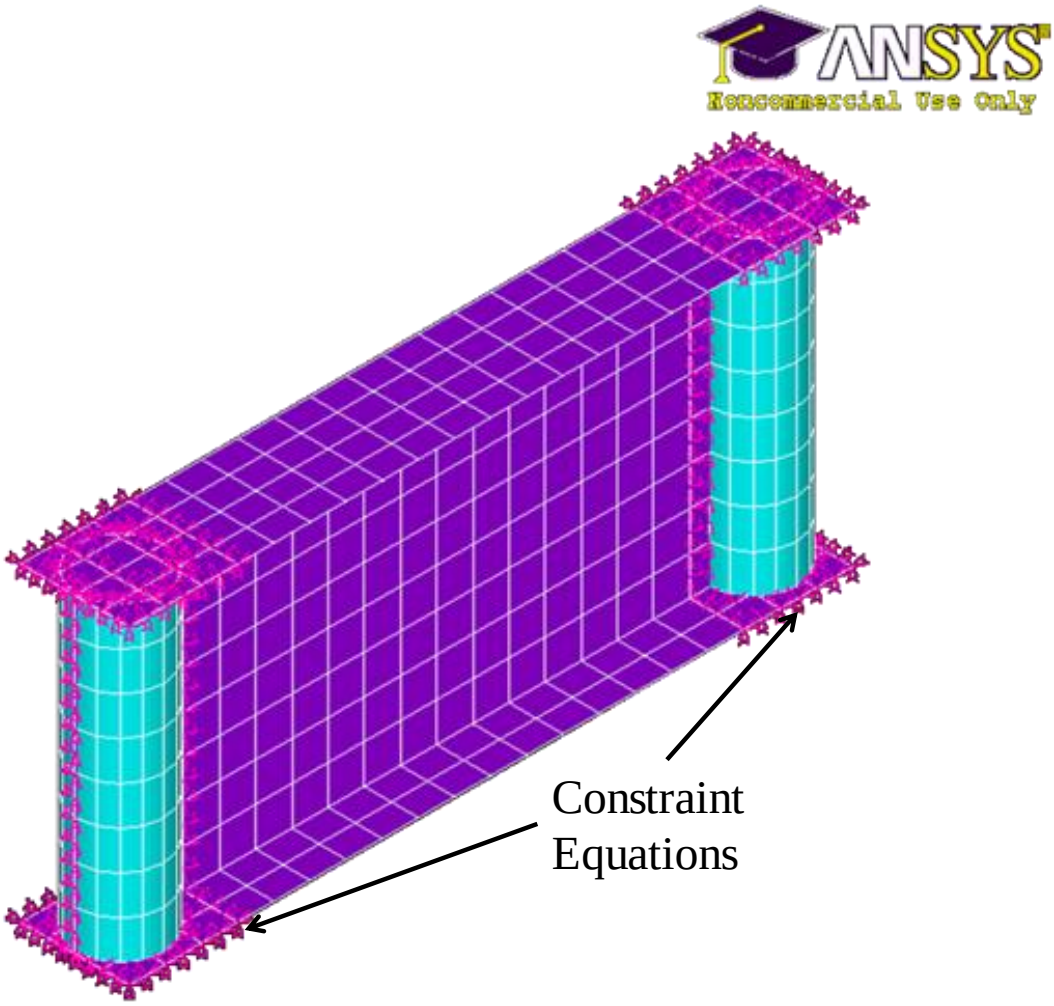

Figure 4.12: Split pipe stiffener model

4.4.4 Steel Self-Weight

The self weight of the steel was accounted for by applying a gravitational acceleration to the model. The density of the steel was included as one of the material properties which ANSYS used to formulate a lumped mass matrix for each element that was included in the analysis via the inertial loads it created.

One exception to this was the self weight of the loading beam. Its self weight was accounted for by using a concentrated mass element (MASS21) at the point of contact

between the load beam and girder. The reason for this is explained in the next section. A picture of the load beam in the twin girder model is shown in Figure 4.13.

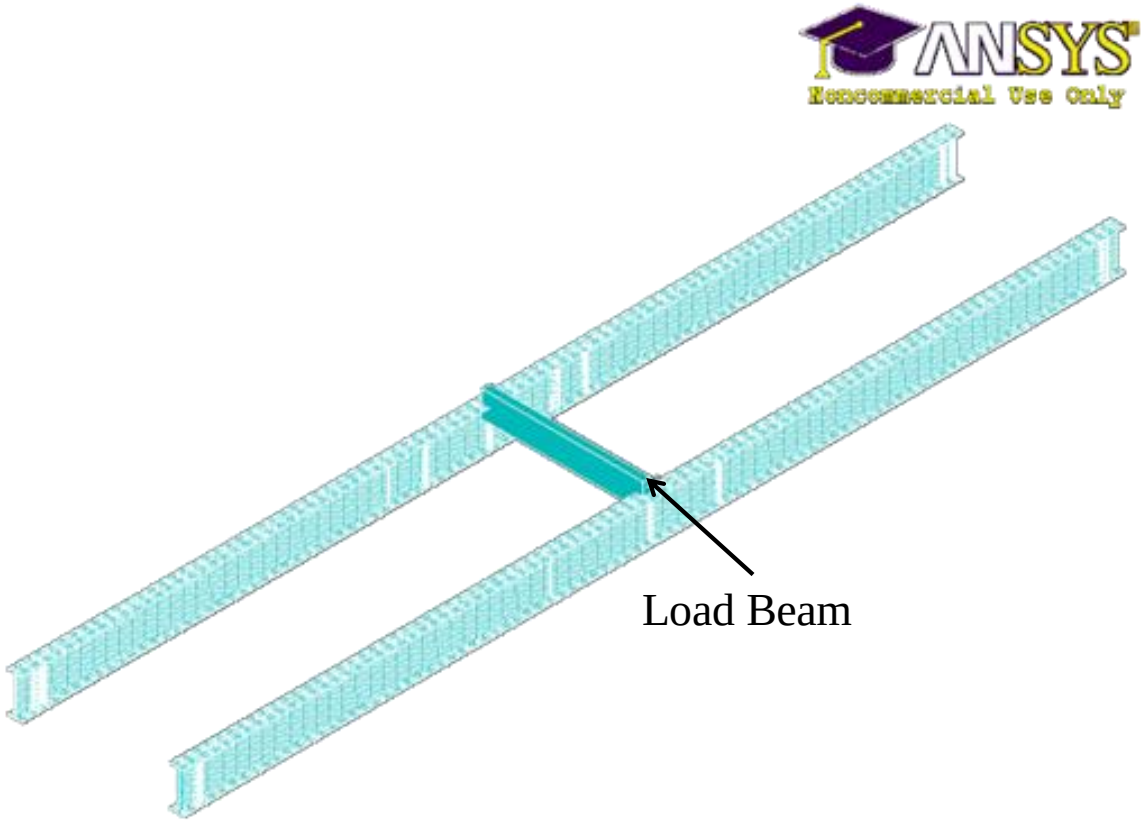

Figure 4.13: Twin girder model with load beam

4.4.5 Loading and Load Beam

The load beam was modeled as a zero mass beam element (BEAM4) with negligible flexural stiffness. This allowed a simple coincident node connection between the girders and load beam and acted to couple the translation of the girder top flanges. Although, using a coupled node equation would typically work well in this situation, constraint equations and coupling cannot be simultaneously used on nodes. Since the load stiffeners were connected to the girder with constraint equations or multi-point constraint elements (see Section 4.4.2), at the same location as the load beam reaction, load coupling could not be used. Therefore the beam element was used to couple the

girders. Since the beam element had no mass and negligible flexural stiffness, it did not act as a torsional brace between the girders or apply a torque to the girders. The individual load beam reactions were directly applied to the top flange of the girder model.

4.4.6 Initial Imperfections

To model the laboratory girder specimens, their initial imperfections were measured as described in the previous chapter. These imperfections were included in the model by imposing displacements on the top and bottom flanges to capture the initial sweep and twist of the girder along the length. An analysis was performed to generate the initial imperfection geometry. Results from the analysis that generated the initial imperfection were used to define the geometry for the non-linear geometric buckling analysis using the UPGEOM command. The UPGEOM command uses the deformed shape from a previous analysis to define the basic geometry of a model. The model showing the initial imperfections of GBP1 and GBP2 is in Figure 4.14.

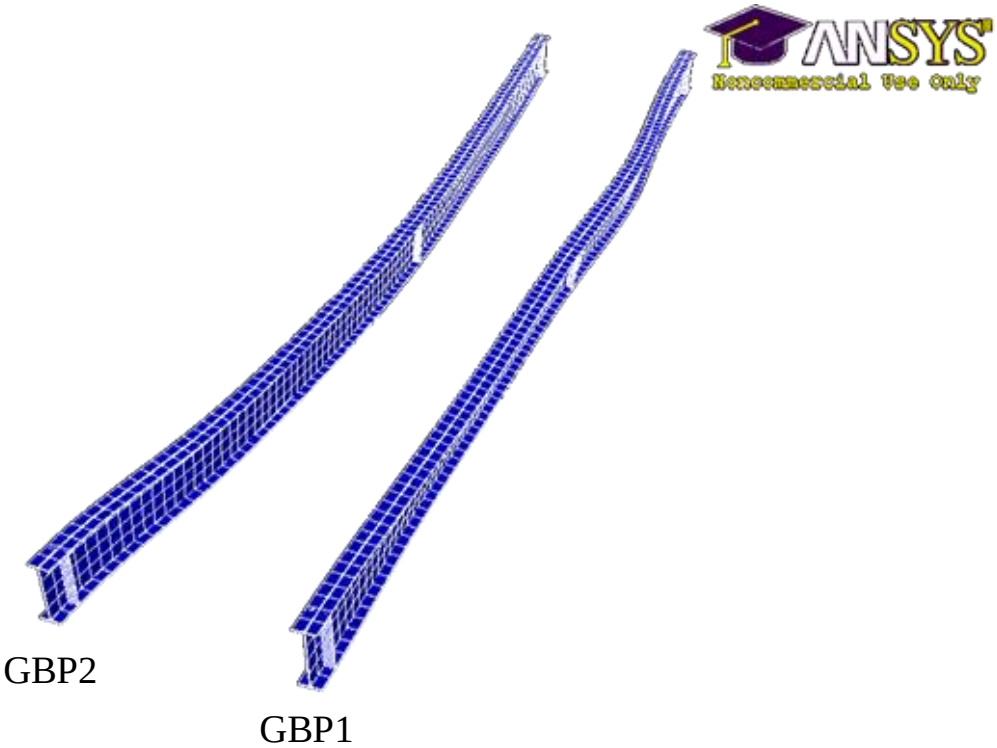

Figure 4.14: GBP1 and GBP2 initial imperfections (magnified 60x)

One issue that had to be considered was the impact the self weight had on the initial imperfection. Since the specimen initial imperfection was measured with the girders installed in the test frame, the imperfection included the effects of the girder self weight. In the nonlinear geometrical buckling analysis, gravity was not added to the model's initial imperfection until the first load step. If the imperfection measured in the laboratory was directly used in the model, at the conclusion of the first load step, the model initial imperfection would be larger than the actual specimen's initial imperfection.

This was accounted for by putting a reduction factor on the initial imperfection applied to the model. An iterative solution was used to determine the magnitude of the correction factor applied to the initial imperfection that was necessary so that once gravity was applied to the model would match the measured imperfection. Typical reduction factors were between 0.86 and 0.89.

4.4.7 Bearings

The bearing model to represent the 4" diameter thrust washer was built from a series of compression-only line elements (LINK10) distributed around the outside diameter of the thrust washer. The compression-only elements allowed the girder to rotate up on the edge of the washer in the same location as the specimen and provide a moderate amount of tipping restraint. The base of the bearing elements were fixed in the vertical direction and coupled in the horizontal direction to the top of the elements to prevent vertical movement at the bottom and differential lateral movement between the top and bottom of the thrust washer model. Finally one node at the middle of the girder was supported in the lateral and longitudinal direction (on the far end only the lateral direction was fixed) to prevent the girder from sliding off the bearing. The top nodes of the thrust washer line elements were connected to the girder bottom flange via vertical constraint equations. With this modeling technique, the arrangement of the bearing elements did not depend on the bottom flange node locations.

4.4.8 Girder Model Validation

The validation of the girder model was done with both analytic solutions and single and twin girder laboratory data. The analytic solution used was the basic buckling strength covered in Chapter 2 (Background), with a coefficient (C_b) added to account for moment gradient and load height effects (SSRC 1998). The expression is repeated here for convenience.

$$M_{ocr} = \mathrm{C_b}\pi/L_b\sqrt{EI_yGJ + \pi^2E^2C_wI_y/L_b^2} \tag{4.1}$$

where

$C_b = AB^{2y/h}$

A = 1.35 for mid-span point load or 1.12 for distributed load

$B = 1 - 0.180W^2+0.649W$ for mid-span point load or $1 - 0.154W^2+.535W$ for distributed load

$W = \frac{\pi}{L}\sqrt{\frac{EC_w}{GJ}}$

y = distance from mid-height to load (negative if above or positive if below)

h = distance between flange centroids

All other variables remain as defined in Chapter 2 (Background).

A W30x90 cross section was used to check the model against the analytic solution for top flange, bottom flange and centroidal loading for cases of point loads, uniform distributed loads, as well as the uniform moment case. Unless otherwise noted, the fillets were not accounted for in the finite element model (FEM) or analytic solution. Simple supports were used in all cases and span to depth ratios considered ranged from 10 to 40.

The results for the uniform moment case are given in Table 4.2. From the table it can be seen that the model has good agreement (within 2%) with the analytic solution in all cases. Fillets were accounted for in the model as described in Section 4.4.1. The model was also checked against the analytic solution that used the AISC rolled shape quantities. These results are given in Table 4.3. These results show that accounting for

the fillets with beam elements works well giving results within 1% of the analytic solution.

Table 4.2: Uniform moment FEA analytic validation

L/D	$M_{cr(analytic)}$	$M_{cr(FEM)}$	$M_{cr(FEM)}/M_{(analytic)}$
10	6400	6310	0.99
20	2150	2110	0.98
30	1260	1240	0.98
40	900	880	0.98

Table 4.3: Uniform moment FEA analytic validation – fillets included

L/D	$M_{cr(analytic)}$	$M_{cr(FEM)}$	$M_{cr(FEM)}/M_{cr(analytic)}$
10	6420	6410	0.99
20	2200	2180	0.99
30	1310	1290	0.99
40	935	925	0.99

Top flange loading for the mid-span point load and distributed load results are given in Table 4.4 and Table 4.5, respectively. Both load cases show that the finite element model has very good agreement with the analytic solution.

Table 4.4: Top flange mid-span point load FEA analytic validation

L/D	$P_{cr(analytic)}$	$P_{cr(FEM)}$	$P_{cr(FEM)}/P_{cr(analytic)}$
10	73.6	70.6	0.96
20	13.8	13.5	0.98
30	5.9	5.7	0.98
40	3.3	3.2	0.98

Table 4.5: Top flange mid-span point load FEA analytic validation

L/D	$W_{cr(analytic)}$	$W_{cr(FEM)}$	$W_{cr(FEM)}/W_{cr(analytic)}$
10	6420	6410	0.99
20	2200	2180	0.99
30	1310	1290	0.99
40	935	925	0.99

The split pipe stiffened girder model was validated using the previous analytic solutions developed by Ojalvo and Chambers (1977). The models used the same parameters as the original Ojalvo solutions that used simple supports and uniform moments with pipe diameters equal to the girder flange width and 1/4" wall thickness and a shear modulus of 12,000 ksi. The results for the W30x99 and W18x50 cross sections are given in Table 4.6 and Table 4.7, respectively.

The most likely reasons for the trend in the FEA model predicted buckling strength decreasing with respect to the Ojalvo solution as the span increases are the shear stiffness of the girder and warping restraint provided by the web. The FEA model accounts for these, while the Ojalvo solution does not. As the span increases these factors become less important allowing the Ojalvo solution to predict a stiffer response than the FEA at longer girder lengths.

Table 4.6: W30x99 Split pipe stiffened girder buckling comparison

L/D	$M_{cr(Ojalvo)}$	$M_{cr(FEM)}$	$M_{cr(FEM)}/M_{(Ojalvo)}$
10	12970	13090	1.01
15	6390	6350	0.99
20	3970	3890	0.98
25	2800	2720	0.97
30	2140	2060	0.96

Table 4.7: W18x50 Split pipe stiffened girder buckling comparison

L/D	$M_{cr(Ojalvo)}$	$M_{cr(FEM)}$	$M_{cr(FEM)}/M_{(Ojalvo)}$
10	6750	6800	1.01
15	3300	3300	0.99
20	2070	2030	0.98
25	1460	1420	0.97
30	1120	1080	0.96

Prior to proceeding to large scale laboratory testing, a mesh density study was conducted to ensure the appropriate density was used and that going to a denser mesh would neither improve nor degrade the analytic validation significantly. To do this the W30x99 split pipe stiffened cross section was selected so the split pipe and girder densities could be checked. As in the previous studies simple supports were used and the case of uniform moment was considered.

The density used to give the previous results was four elements per web area, two elements per flange area and four elements per pipe area, or 4-2-4. Therefore this density was increased to 6-3-6 and compared to the 4-2-4 density results. The results of this study provided in Table 4.8. From the table it can be seen that when the buckling moment is expressed to the nearest k-in, there is no difference in the results and the 4-2-4 density is sufficient.

Table 4.8: W30x99 Split pipe stiffened girder mesh density study

L/D	$M_{cr(4-2-4)}$	$M_{cr(6-3-6)}$	$M_{cr(6-3-6)}/M_{(4-2-4)}$
10	13090	13090	1.00
15	6350	6350	1.00
20	3890	3890	1.00
25	2720	2710	1.00
30	2060	2060	1.00

4.4.9 Large Scale Laboratory Test Validation

Once good agreement was achieved between the model and the analytic solutions, the model was then compared to the laboratory results from the single and twin girder lateral and buckling tests described in Chapter 3 (Experimental Program). This section provides a description of the results of this validation.

4.4.9.1 Single Girder Validation Results

The single girder model was run for lateral tests as described in Chapter 3 (Experimental Program). A picture of the finite element model with some of the key features called out is shown in Figure 4.15. Note that the 6-3-6 element density was used to correctly size the stiffener welds.

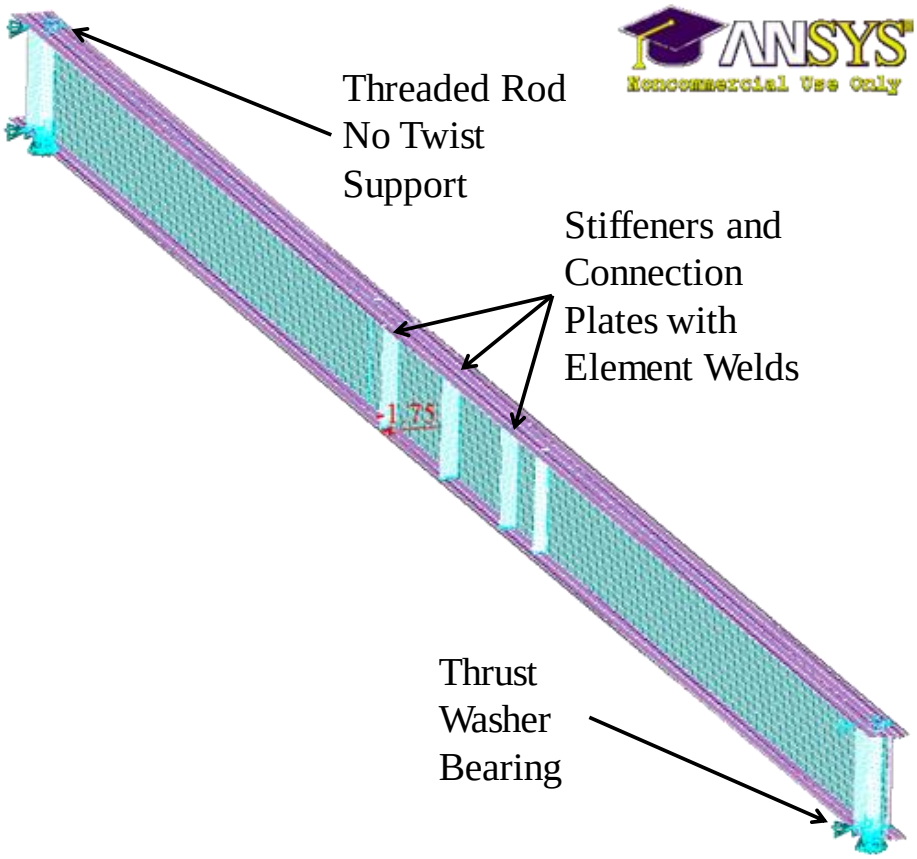

Figure 4.15: W30x90 single girder (GBP2) lateral deflection finite element model

The lateral load test validation results for both the plate (GBP2) and split pipe (GSP2) stiffened girders are shown in Figure 4.16 for the case of the lateral load applied at midheight. As would be expected, the results for both the plate and split pipe stiffened model show good agreement with the laboratory results. This shows that the bearing stiffener models behaved appropriately since the model correctly predicts that each simply undergoes a nearly rigid body twist while the girder mid-span deflects in a pure lateral mode.

The results do show that the split pipe stiffener model is slightly stiffer than the plate stiffened model. A similar trend was observed in the laboratory data. This is most likely due to a small deviation in the point of load application or deflection measurement point between the two specimens.

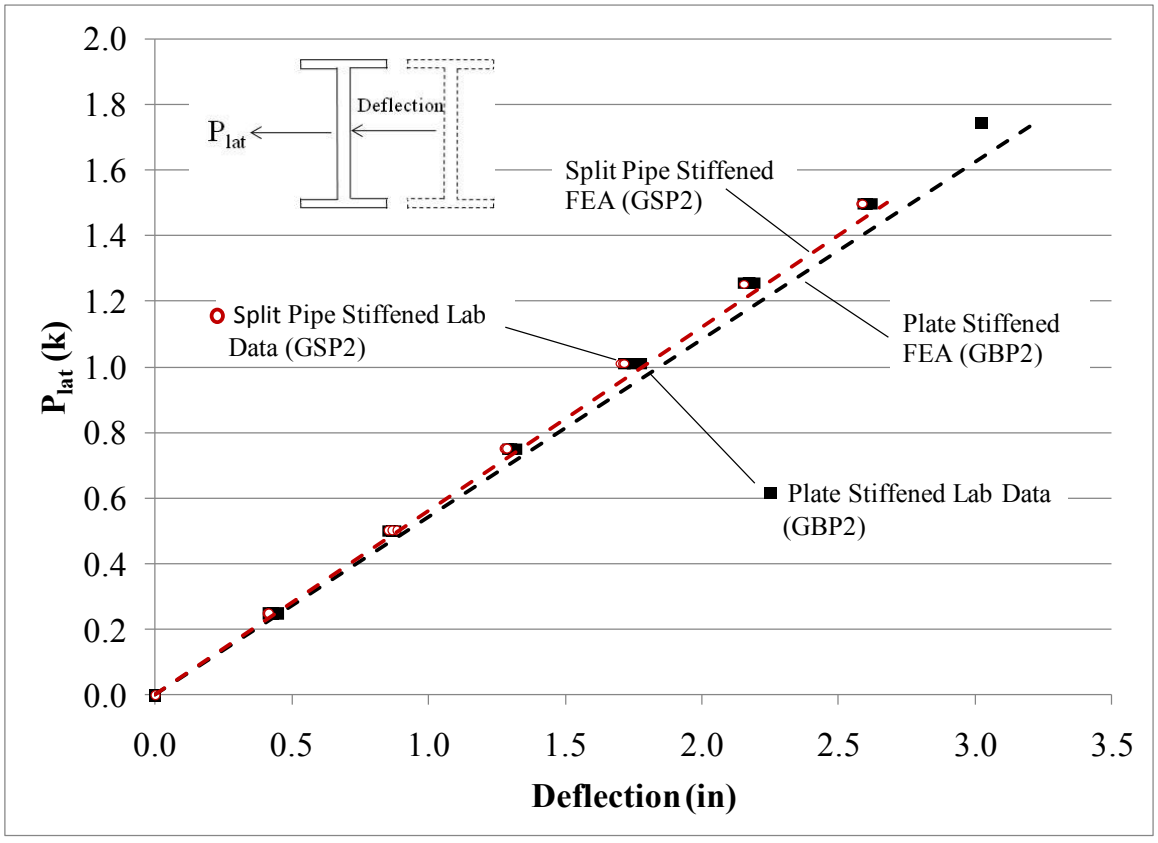

Figure 4.16: Single girder lateral load test results

Finally, it can be seen that the laboratory test specimens were slightly stiffer than the FEA models. Such a result is typically not the case in finite element modeling where the computational error usually results in the model being stiffer than the specimen. This counterintuitive result is most likely due to some friction between the threaded rods and the girder flanges on the side where the girder bears against the rods. In the model, the threaded rods are considered a friction free surface and the girder can slide freely against the support, while in the laboratory specimen friction between the girder flange and the rod results in a reaction that stiffens the system slightly. While this may be an issue in the lateral test where the girders were pulled directly against the threaded rods, during a buckling test, these reactions are relatively small and should have little effect on the results.

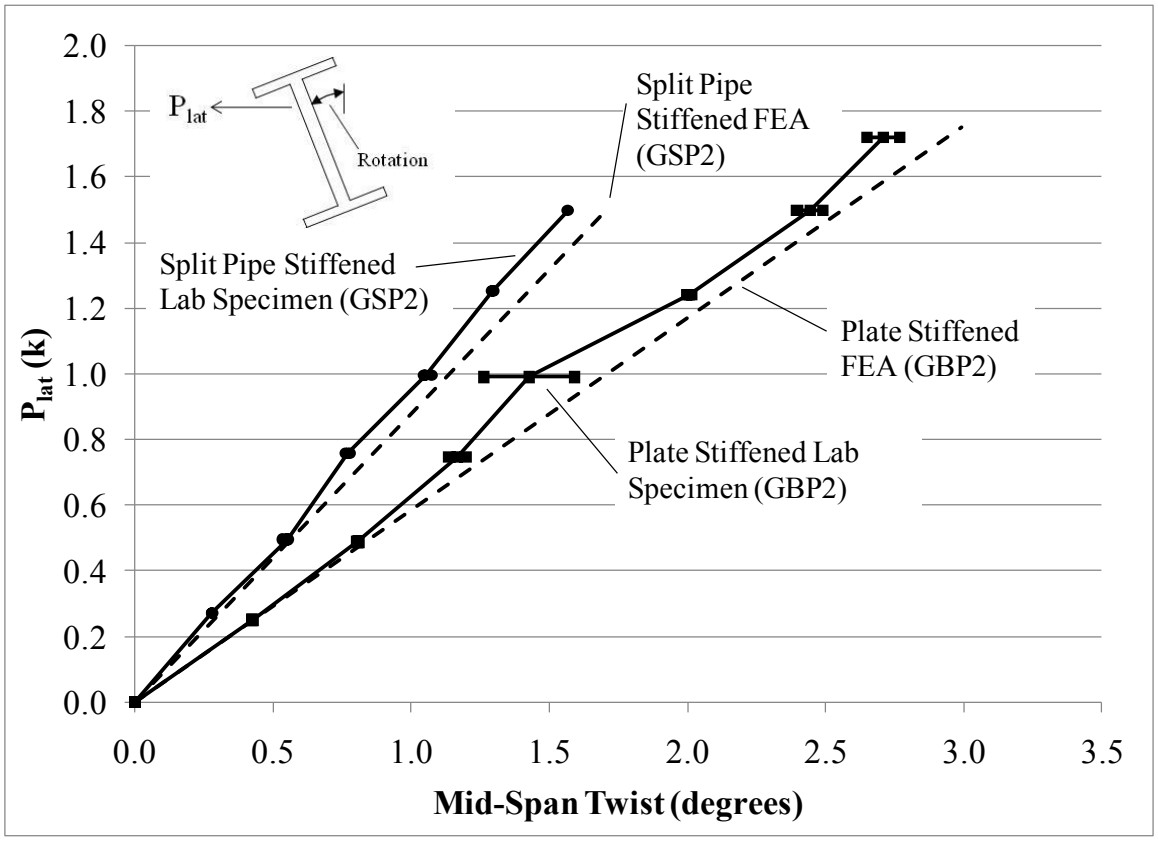

Figure 4.17: Single girder FEA to lab specimen comparison for top flange lateral load

Next the single girder models were validated for a lateral load applied at the top flange. Since the lateral load is not applied at the shear center of the section, the loading results in both lateral deformation and twisting. The model was adjusted from the pure lateral test by moving the load to 25.75" above the bottom flange centroid and modeling a no slip condition along the top flange-threaded rod interface. Since the applied load was near the top of the cross section, the top threaded rods bore very tightly against the top flange and increased the friction. When these two adjustments were made to the models, good agreement was achieved between the FEA solutions and the laboratory data as shown in Figure 4.17

4.4.9.2 Twin Girder Validation Results

Once good agreement was achieved between the FEA models and laboratory test results for the lateral load tests on the single girder, the series of twin girder buckling tests described in Chapter 3 (Experimental Program) were used to validate the finite element girder models. These comparisons provided insight into the accuracy of the modeling techniques for the load beam and gravity load simulators as well as ensured the girders were modeled appropriately. A picture of the model is shown in Figure 4.13. This section describes the results of these validations.

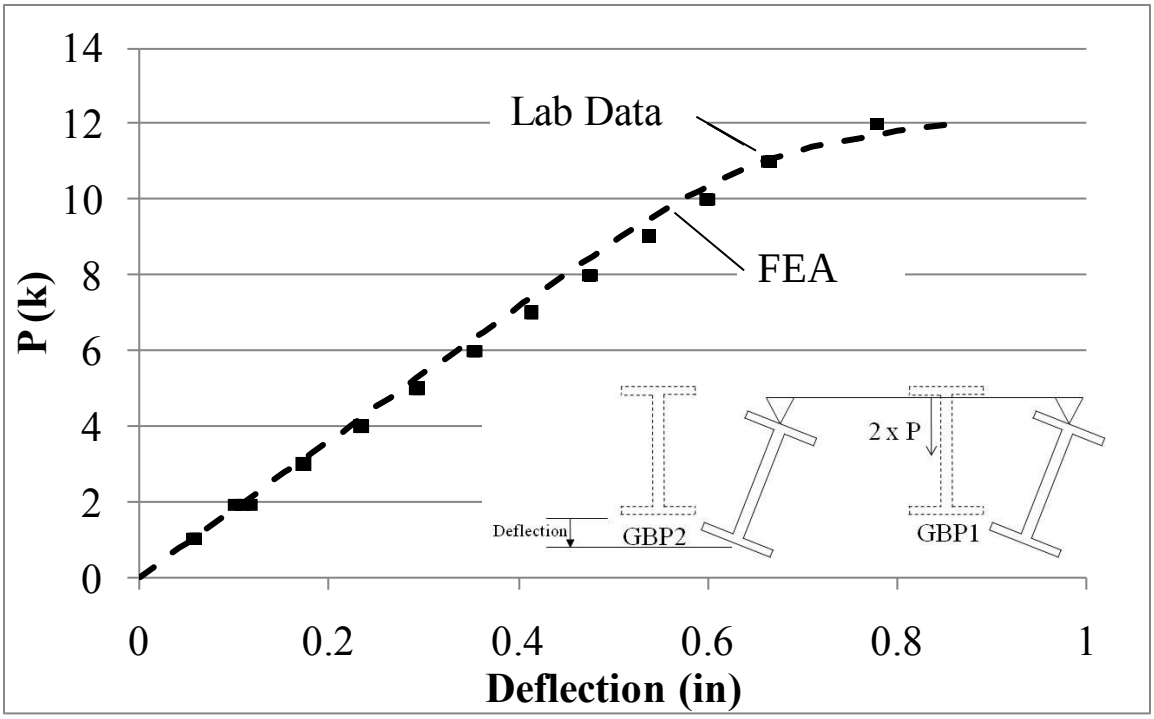

Figure 4.18: GBP2 mid-span vertical deflection FEA validation

The plate stiffened girders (GBP1 and GBP2) were validated first and GBP2's vertical deflection results are shown in Figure 4.18. The results show that the FEA model has good agreement with the laboratory specimen. The FEA, and specimen results become non-linear at the onset of buckling since the twist and translation of the cross section begin to counteract the vertical deflection. The validation data for GBP1 is similar and can be found in Appendix B (Finite Element Model Validation Data).

The mid-span top flange lateral deflection validation data for GBP2 is shown in Figure 4.19. The results show that there is good agreement between the model and the laboratory specimen. Based upon the maximum laboratory specimen loading, the model is 7% conservative. GBP1 had similar results for its top flange lateral deflection. It and all the other twin girder validation results are provided in Appendix B (Finite Element Model Validation Data).

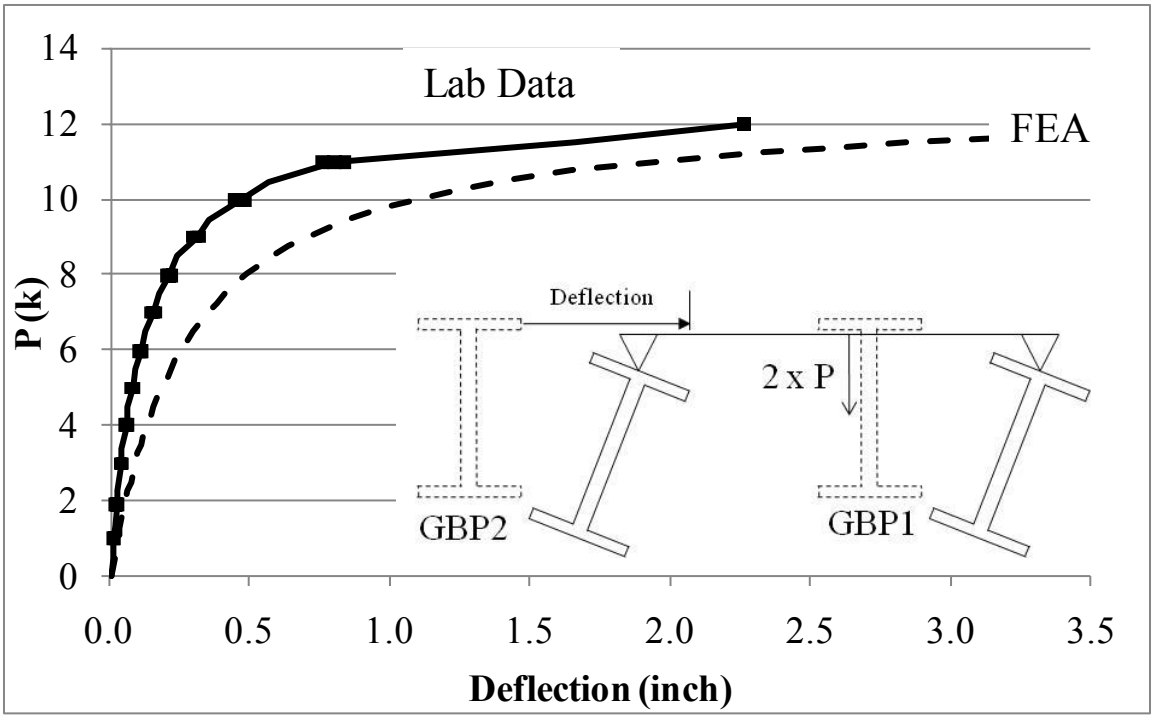

Figure 4.19: GBP2 mid-span top flange lateral deflection FEA validation

4.5 CROSS FRAME MODELING

After the connections and girder models were validated, bent plate and split pipe stiffener cross frame models were developed using the validated connection models. These models were used to classify the impact of each connection on the cross frame stiffness as well as compare the stiffness values of the cross frames as discussed in Chapter 5 (Parametric Studies and Design Recommendations).

4.5.1.1 Bent Plate End Cross Frame Model

A picture of the bent plate cross frame model is provided in Figure 4.20. The cross frame in Figure 4.20 is designed to fit a pair of W30x90 girders (shown in the diagram for reference only – they were not part of this model) spaced 9' apart with a 53° skew angle. The cross frame uses a single diagonal brace system that is capable of carrying tension and compression. The additional features of the bent plate cross frame model are described below.

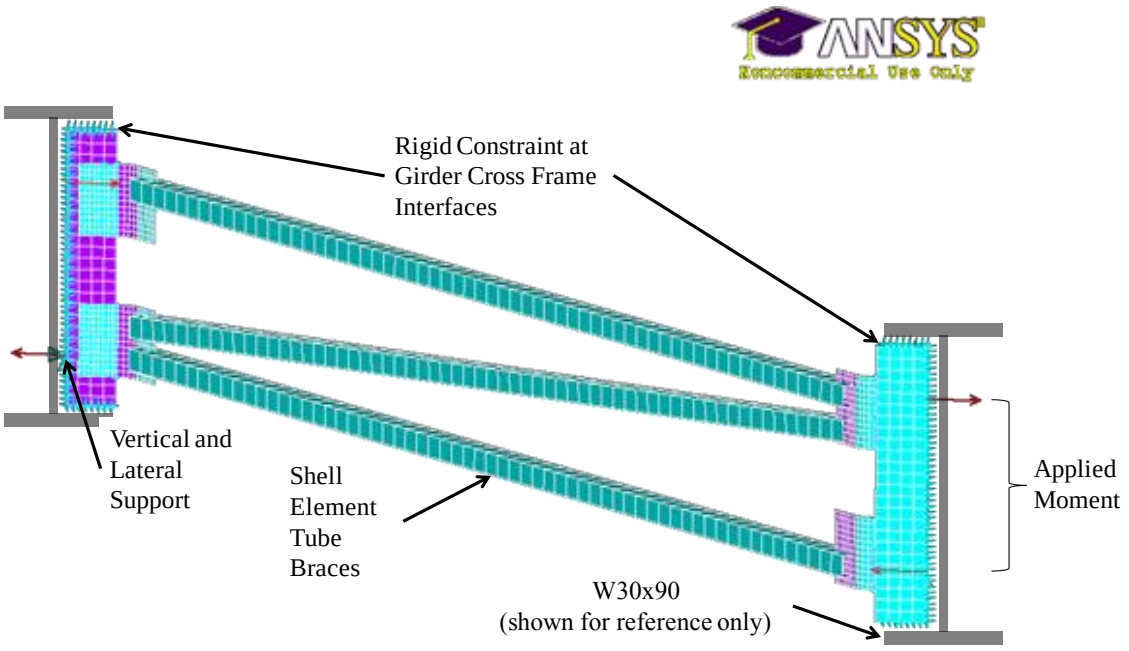

Figure 4.20: Bent plate cross frame model (53° skew)

As shown in Figure 4.20, the boundary conditions for the cross frame model consisted of a rigid constraint at the cross frame-girder interface for rotation. This causes the edge of the connection plates to rotate as a rigid body about the girder's longitudinal axis. Additionally, longitudinal restraint is applied at the same interface to prevent the cross frame from moving along the length of the girder longitudinal axis. There is one node on the left connection plate that serves as the vertical and lateral support provided by the girder. There is a corresponding node on the right connection plate that provides vertical support.

To simulate the girder twist, a moment was applied to the end of each cross frame in the plane of the girder's cross section as shown in Figure 4.20. Once an analysis was run, the rotation of the cross frame was measured and then the cross frame stiffness was calculated using Equation (2.27) (repeated below for convenience).

$$\beta_{braxial} = \frac{M}{\phi} \tag{2.27}$$

The brace members were square hollow tubes composed of four shell elements (SHELL93). Therefore, since ANSYS does not directly provide forces for shell elements, the stresses were taken from the middle of the top and bottom brace shell elements and averaged to compensate for bending then multiplied by the brace area to recover the brace force. To retrieve the stresses at any cross section along the length of the brace, the ANSYS PATH command was used since it maps any structural response to a defined path. This allowed the stresses to be measured at the ¼ and ¾ points along each brace's length (the same location as the strain gages on the test specimen) regardless of node placement.

4.5.1.2 Unskewed Cross Frame Model

An unskewed cross frame model was constructed with shell elements to find the stiffness of the cross frame brace members with rigid connections normal to the girder. This model was constructed such that all out of plane deformations were restricted and the connection plates and tabs connecting the braces to the connection plates were formed from a rigid material. A picture of this cross frame is shown in Figure 4.21 with the standard cross frame component nomenclature used in this dissertation.

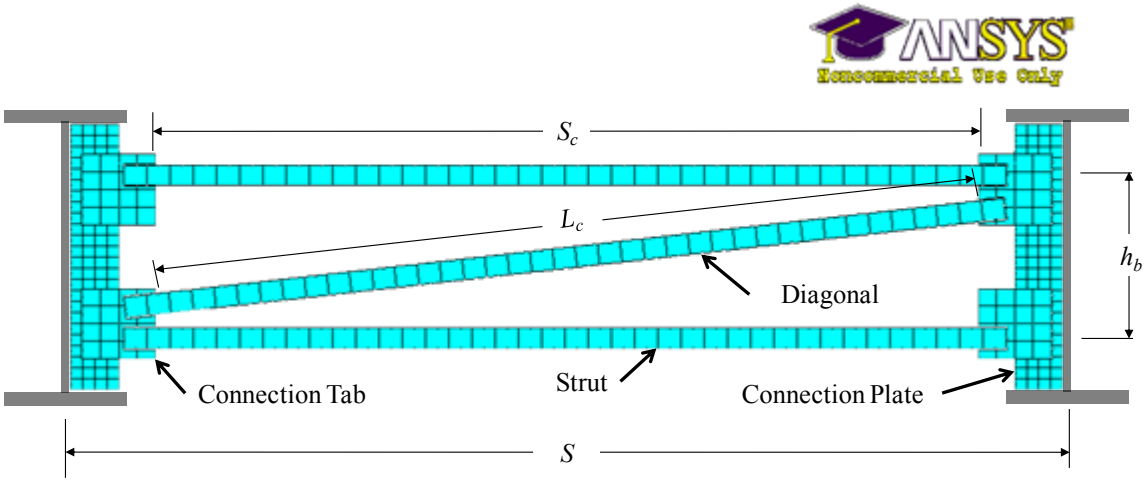

Figure 4.21: Unskewed cross frame model

The unskewed cross frame was used to calculate the axial and flexural cross frame stiffness with a rigid connection condition. While this is the same quantity calculated using Equation (2.44), there are some differences between the FEA solution and the equation. The analytic solution only considers brace axial and flexural stiffness, while the shell elements used in the model account for other structural responses such as shear strength and axial force and moment interaction. Therefore, the cross frame would likely be expected to be stiffer than the analytic solution for smaller girder spacings (*S*) and this difference should become smaller as *S* gets larger and the cross frame deformation is dominated by bending with a relatively small axial force.

Table 4.9 shows the comparison of cross frame stiffness as calculated by the FEA model and the analytic solution of Equation (2.44). A W30x90 girder cross section with HSS2.5x2.5x1/4 braces were used in the comparison. The comparison shows that the FEA solution is relatively conservative for smaller values of the girder spacing and closes to within 10% for a girder spacing of 15'. In general, for most common values of the girder spacing in Texas (8'-10'), the analytic solution of the cross frame stiffness is approximately 20% conservative relative to the FEA model. The FEA model is used rather than the analytic solution in the next chapter to calculate the stiffness of the cross frame braces to be consistent with the models used in the cross frame connection stiffness calculations.

Table 4.9: FEA to analytic cross frame stiffness comparison

Girder Spacing (ft)	$\beta_{Total(FEA)}/\beta_{Total(Analytic)}$
8	1.23
9	1.19
10	1.16
15	1.08

4.5.1.3 Split Pipe Cross Frame Model

The split pipe cross frame model is shown in Figure 4.22. It was created using the previously mentioned techniques. The only difference was that the moment application was divided in half and distributed to each side of the split pipe. The next section describes the validation of the split pipe cross frame model using large scale laboratory test data.

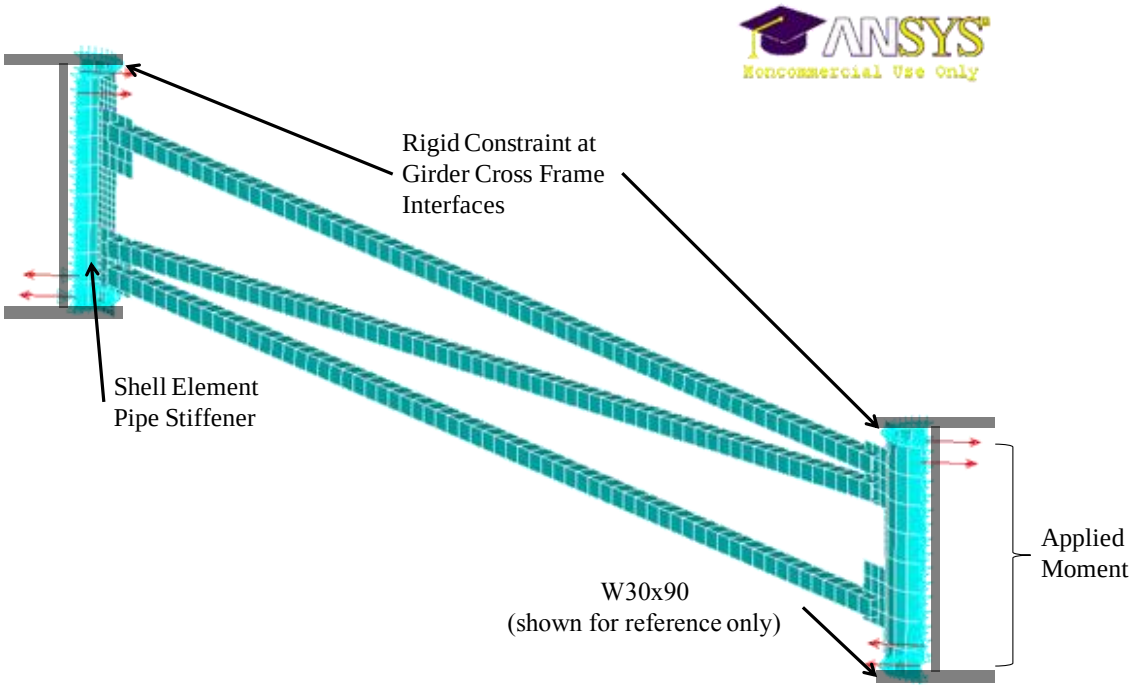

Figure 4.22: Split pipe cross frame model (53° skew)

4.5.1.4 Split-Pipe Cross Frame Large Scale Laboratory Test Validation

To validate the split-pipe cross frame model, a three girder finite element model was used. The three girder finite element model was built using the techniques covered in the previous sections of this chapter. The model geometry was based on the 53° skew, three girder split-pipe end frame laboratory specimen described in Chapter 3 (Experimental Program). A picture showing the finite element model is given in Figure 4.23. In the figure areas are shown (not elements) and the load beams have been removed for clarity.

Figure 4.23: Three girder finite element model with split pipe-stiffener end frames

The large scale laboratory tests described in Chapter 3 (Experimental Program) were used to validate the girder and cross frame models. The key parameters for validation were the end twist of the girders as well as the cross frame forces. The overall three-girder model provided an opportunity to put all the previous components together to ensure the model captured the full system behavior.

The mid-span vertical deflection validation results for GSP2 are shown in Figure 4.24. The model had good general agreement with the laboratory specimen. The FEA results show the same effect of the cross frame resistance to the end twist of the girder as the laboratory data by plotting slightly stiffer than the analytic solution.

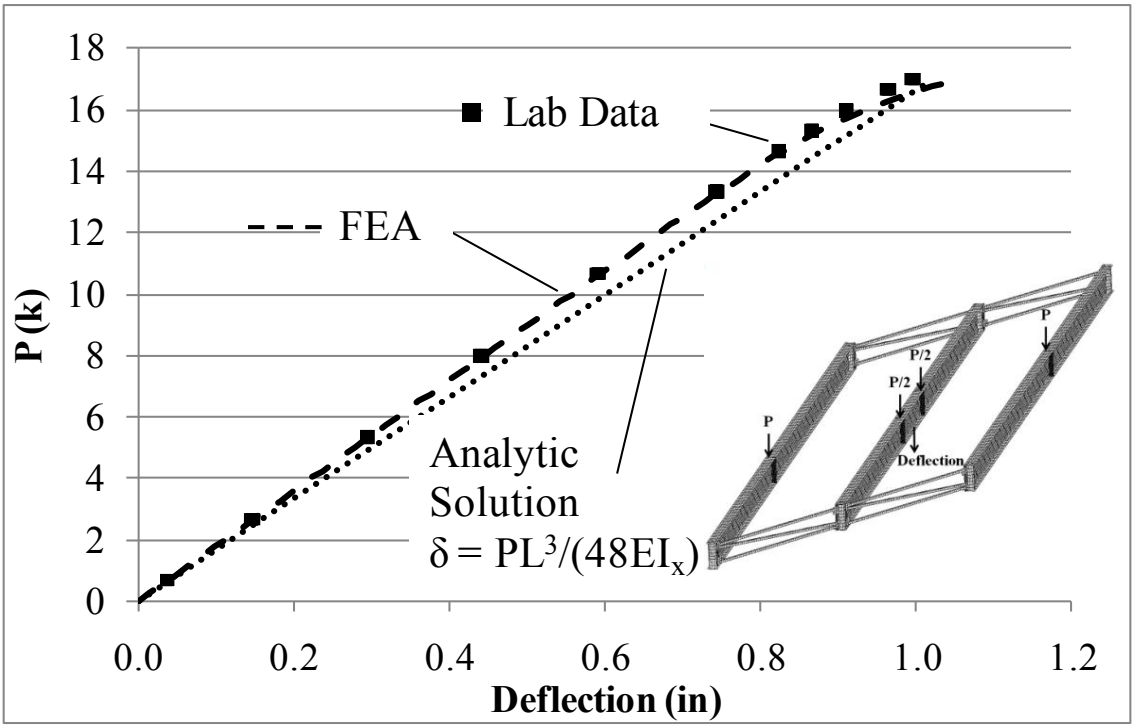

Figure 4.24: GSP2 Mid-span vertical deflection FEA to lab specimen comparison

A plot of GSP 2's mid-span top flange lateral translation is shown in Figure 4.25. Again the model had good agreement with the laboratory test data. Similarly, the model had good agreement with the GSP2 end twist shown in Figure 4.26 and the northwest and southwest end cross frame forces shown in Figure 4.27 and Figure 4.28, respectively. The slight differences in cross frame forces appear to be due to the slightly conservative buckling load predicted by the model.

Similar agreement was found among all other measured structural responses. Plots of all validation data are given in Appendix B (Finite Element Model Validation Results).

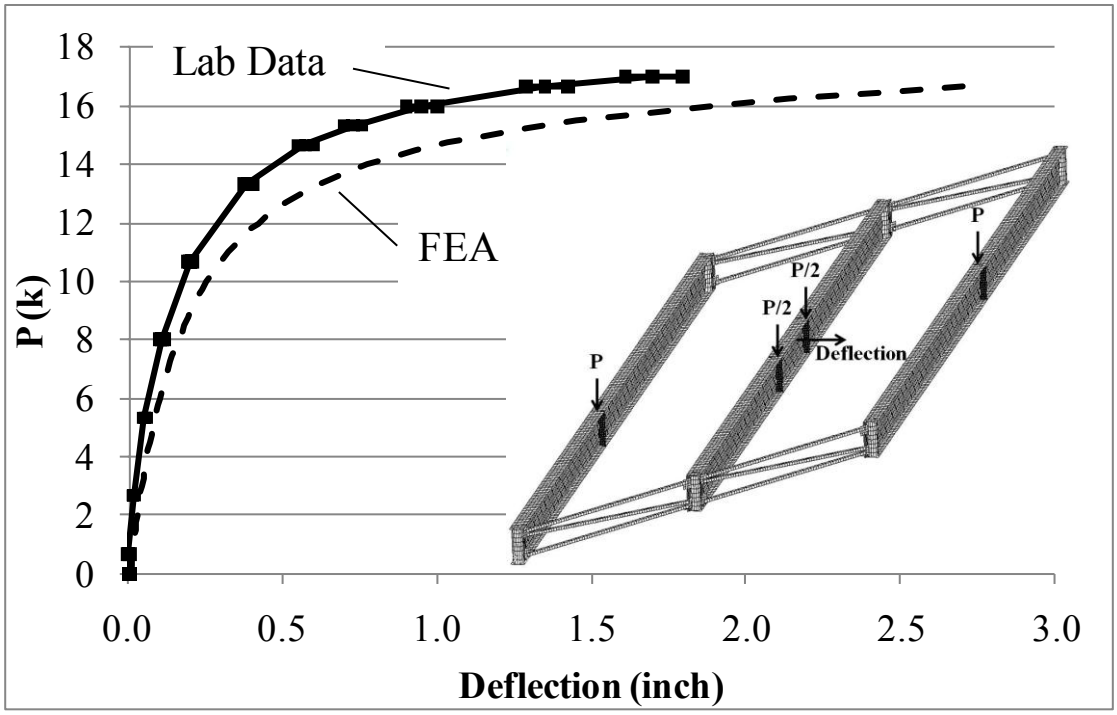

Figure 4.25: GSP2 top flange lateral deflection FEA to lab specimen comparison

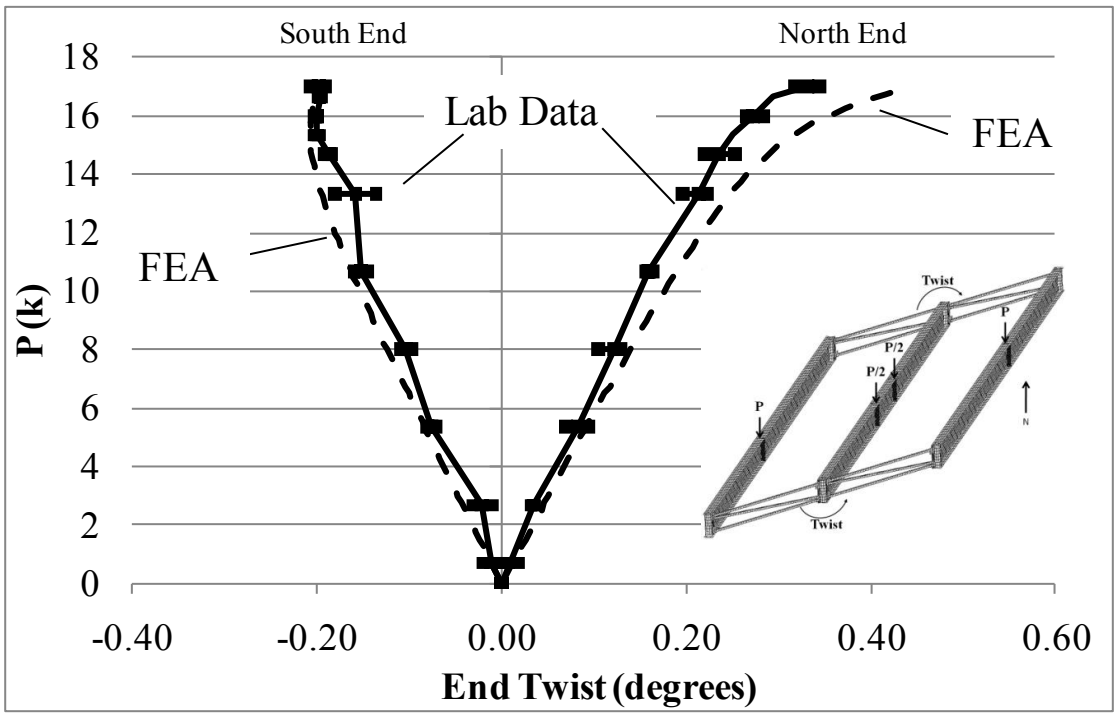

Figure 4.26: GSP2 end twist FEA to lab specimen comparison

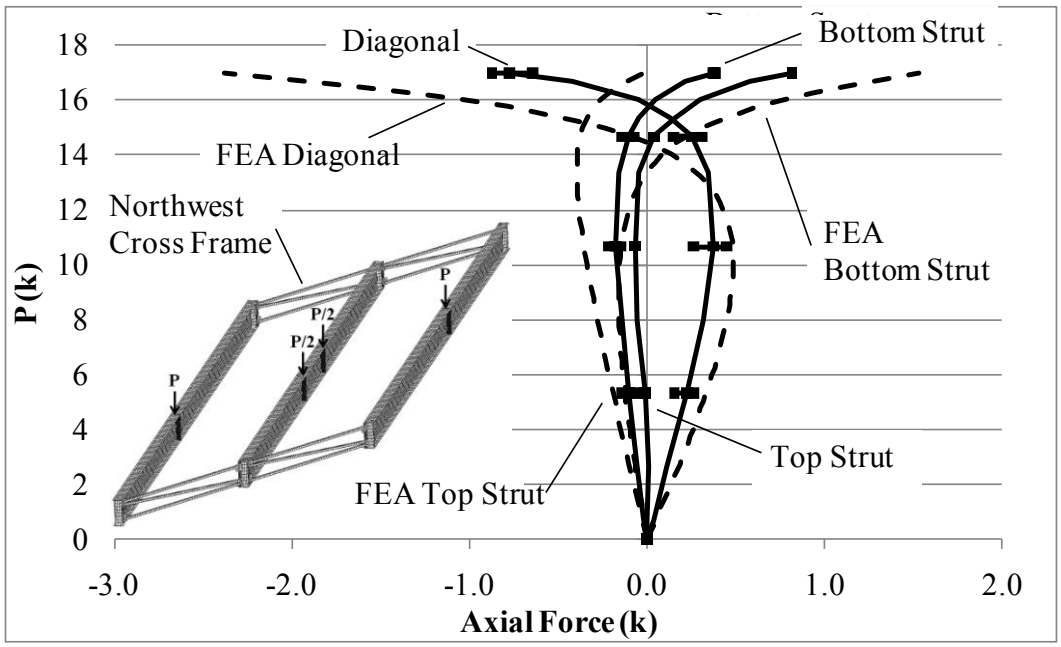

Figure 4.27: Northwest end cross frame FEA to lab specimen force comparison

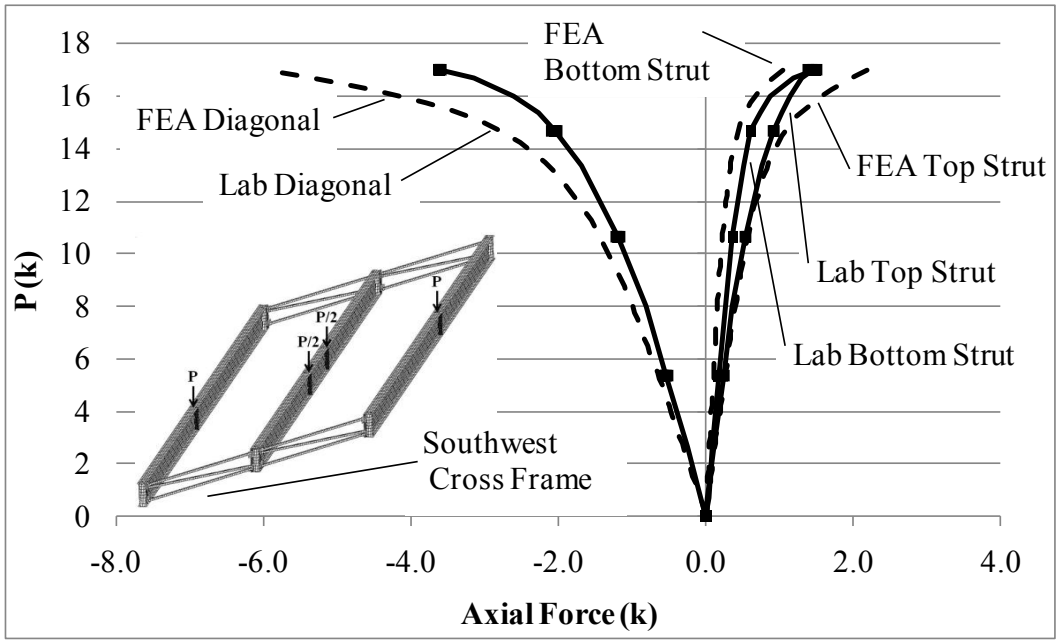

Figure 4.28: Southwest end cross frame FEA to lab specimen force comparison

4.5.1.5 Intermediate Cross Frame Model

A simplified intermediate cross frame model was constructed using truss elements (ANSYS LINK8) to investigate the impact of bracing patterns on girder behavior. This technique has been used successfully in previous research and has been found a very computationally efficient way to accurately match analytic results (Yura, Helwig, et al. 2008), (Wang and Helwig 2008).

A picture of a typical intermediate cross frame is shown in Figure 4.29. The model uses a coincident node connection at the girder web-flange interface. A shell element full depth stiffener is incorporated into the model to prevent web distortion. This model differs from the actual cross frame in two important ways. First the model assumes a rigid connection. This assumption is reasonable for a cross frame perpendicular to the girder since connection plates have their strong axis aligned with the cross frame forces. Second, the model assumes that the braces have no flexural stiffness. This is also a good assumption as long as the axial stiffness is large enough to significantly limit cross section twist. Finally, the model assumes the height of brace is the distance between flange centroids. In reality the height of the brace will be smaller. The impact of this assumption is that the axial brace forces may be smaller in the model since the distance between the axial forces that create the restraining couple is larger.

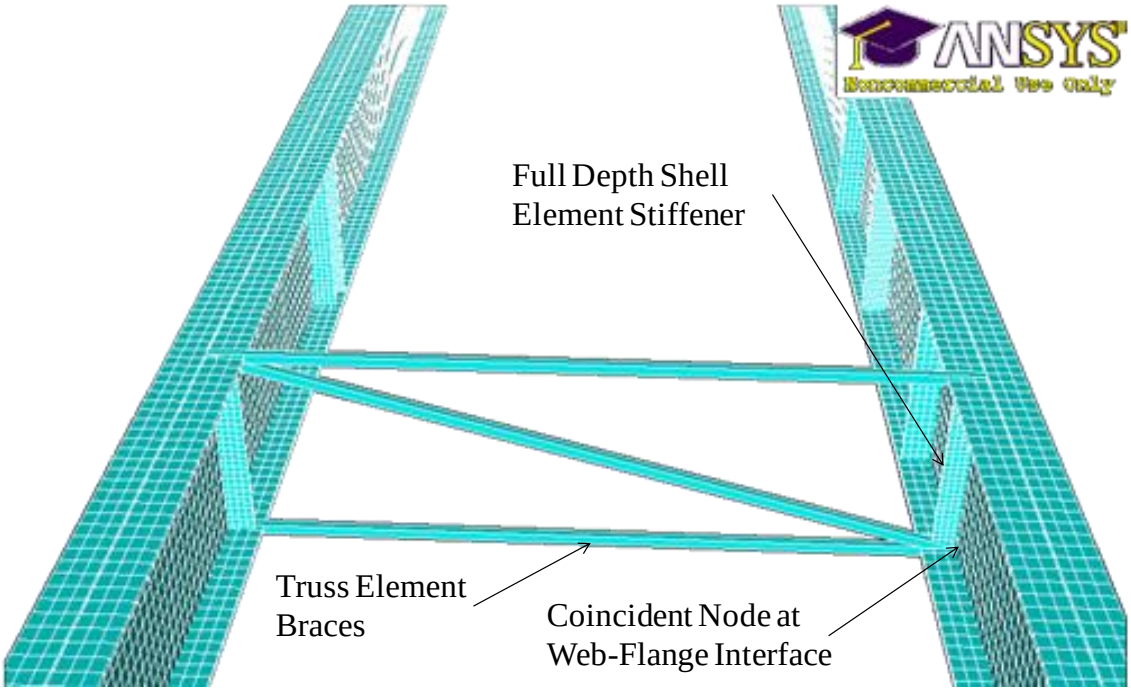

Figure 4.29: Truss element intermediate cross frame model

The intermediate cross frame model was validated using the staggered and continuous layouts for intermediate cross frame specimens described in Chapter 3. Since the girders were braced and had significantly smaller unbraced lengths than the no intermediate cross frame case, buckling did not occur (the test was kept in the elastic range so buckling was not allowed). Therefore, mid-span lateral deflections and twist were negligible (in the thousandths of an inch) and not compared. The key responses used for validation were the end and intermediate cross frame forces as well the twist at the girder ends. These results are discussed below.

The axial force validation results for the southwest staggered intermediate cross frame are shown in Figure 4.30. The results show that the model has a reasonable agreement with the top strut force, but some deviation between the bottom strut and diagonal. A similar pattern was found in the northeastern intermediate cross frame (see Appendix B for these results). While the measured force levels are small in these members (no more than 200lbs), there is a significant difference between the FEA and

laboratory specimen. The difference between the model and FEA most likely has two primary sources.

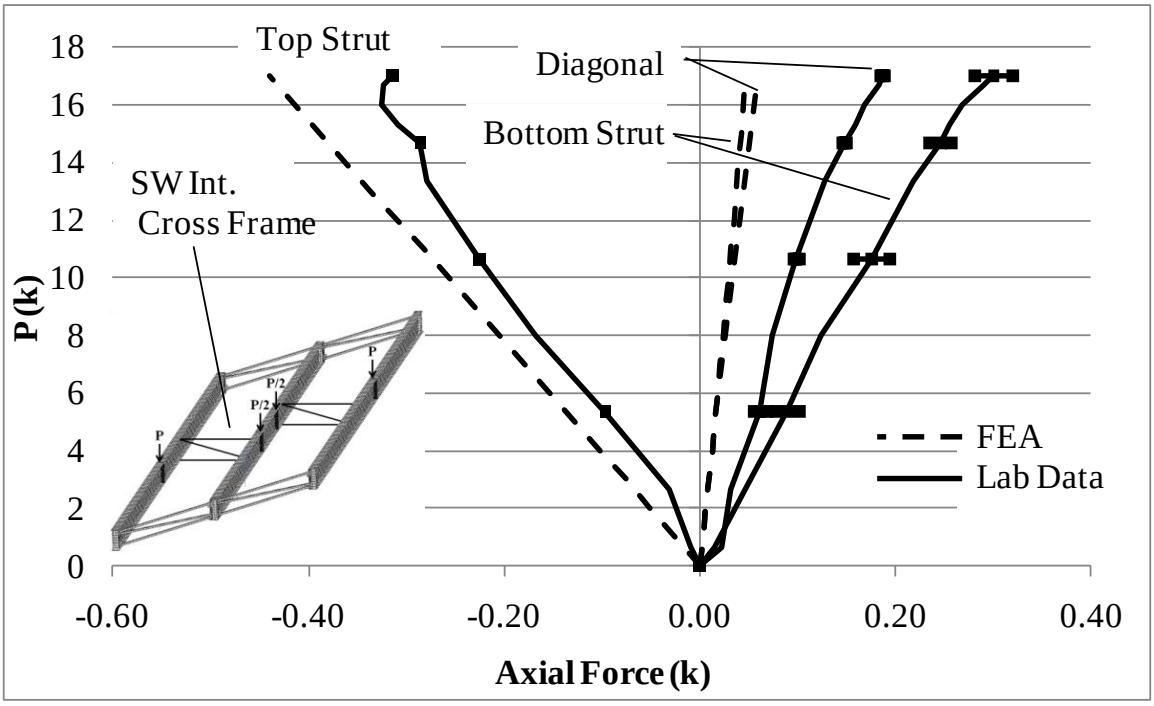

Figure 4.30: SW intermediate cross frame axial force FEA validation

The first source was the previously discussed difference between the finite element model and specimen. As mentioned, it is likely that the brace forces would be smaller in the model, and this is the case for the diagonal and bottom strut. Second, at the conclusion of testing it was noticed that the girders had shifted slightly (about 0.25" east) on their bearings. This most likely occurred during the installation of the intermediate cross frames since this shift was not detected during testing.

Despite these anomalies, the measured and predicted end cross frame forces had good agreement. The results for the southeastern end cross frame are shown in Figure 4.31. Similar results were found for all the other end cross frames and are provided in Appendix B (Finite Element Model Validation Results).

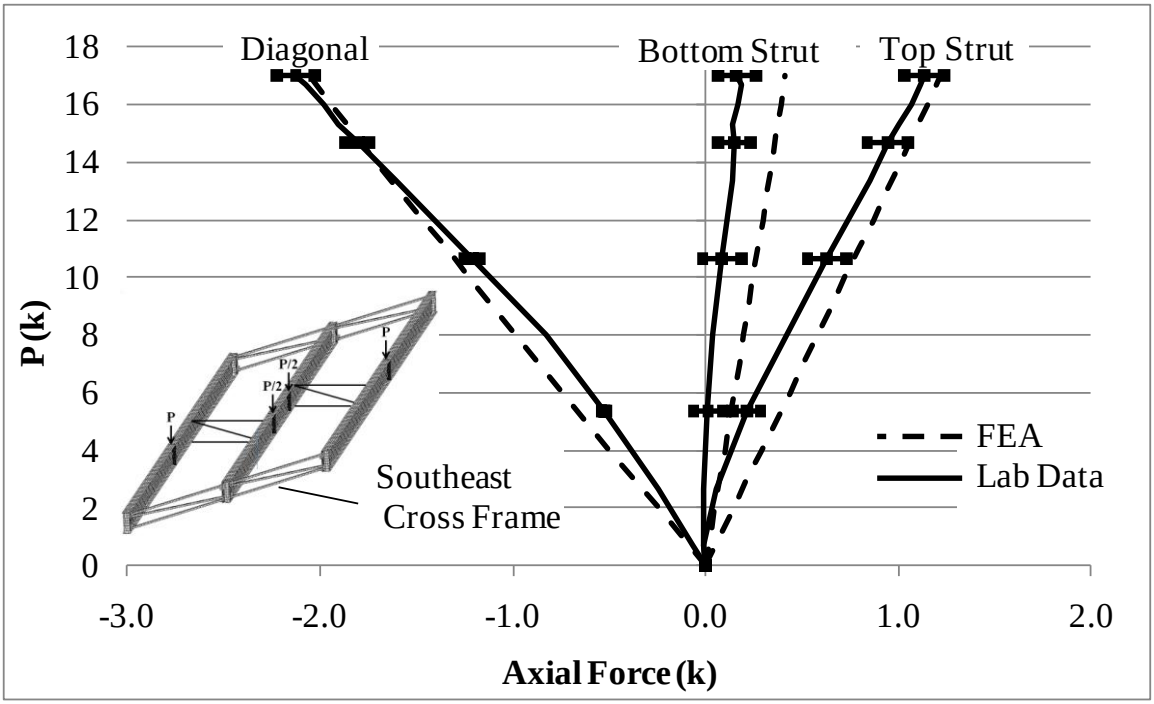

Figure 4.31: SE end cross frame force validation (staggered intermediate frames)

Similar to the end cross frame force results, the laboratory test and FEA results for the girder end twist had good agreement for the staggered intermediate cross frame model. Results for GSP2 end twist are shown in Figure 4.32. Similar results were found for the other two girders and are provided in Appendix B (Finite Element Model Validation Results).

Before the staggered intermediate cross frame tests were conducted, the girders were centered on their thrust washer bearings to eliminate this possible source of error. This plus the higher force levels present in the continuous layout of intermediate cross frame members significantly improved the validation results.

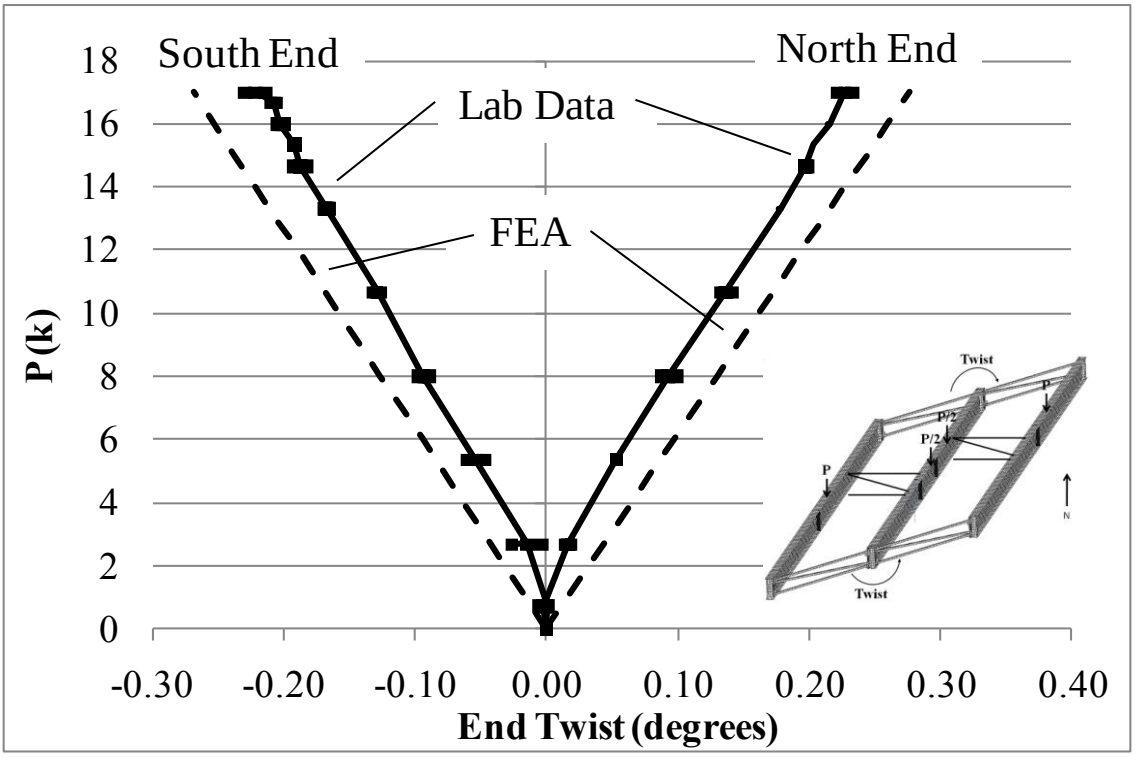

Figure 4.32: GSP2 end twist (staggered intermediate cross frames)

The validation results for the western intermediate cross frame for the continuous cross frame layout are given in Figure 4.33. The figure shows good agreement between the model and finite element results. Similar good agreement can be seen in the southeastern cross frame axial forces as shown in Figure 4.34 and girder GSP2 end twist shown in Figure 4.35. All other validation results showed good agreement with the exception of two cross frame members discussed below. All other validation results for the continuous cross frame case are provided in Appendix B (Finite Element Model Results).

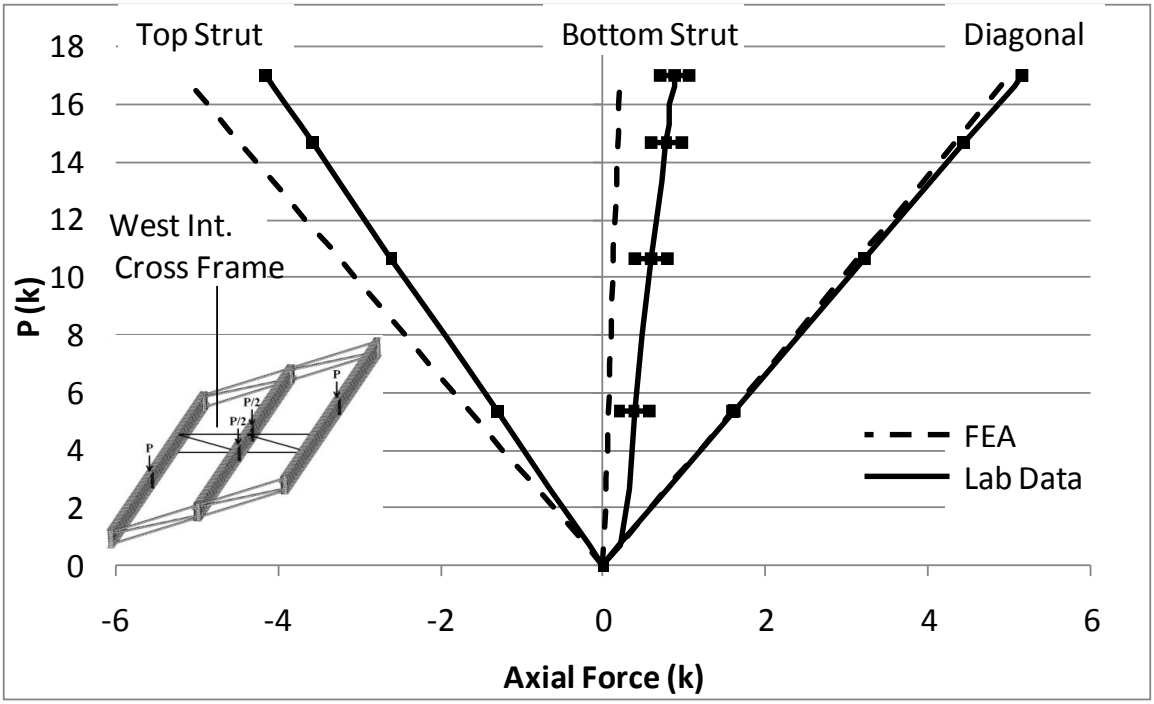

Figure 4.33: Western continuous intermediate cross frame axial force validation

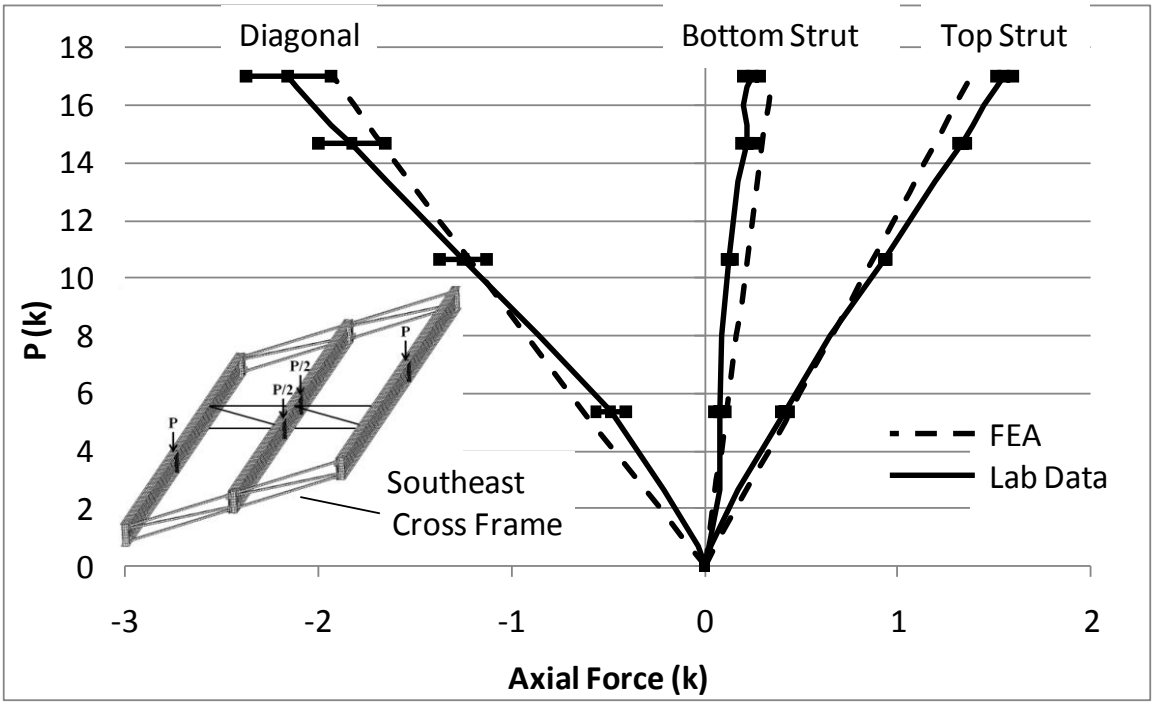

Figure 4.34: SE end cross frame axial force validation (continuous int. cross frame)

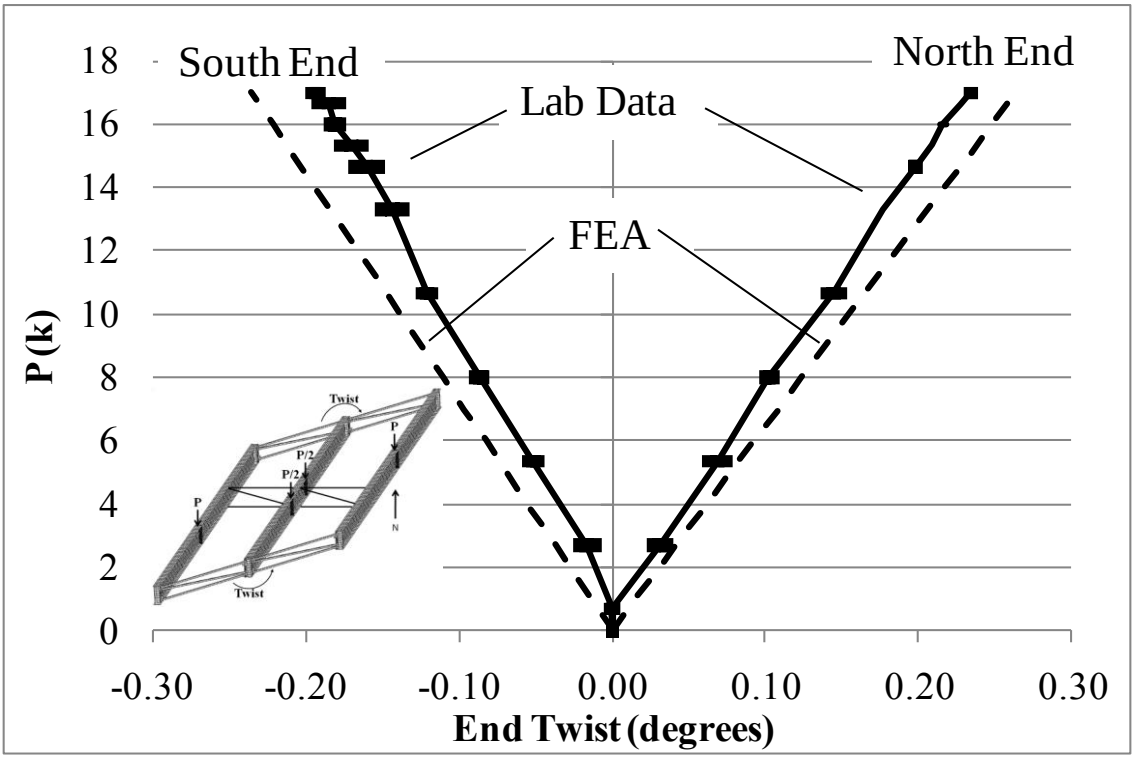

Figure 4.35: GSP2 end twist (continuous intermediate cross frames)

The only significant anomalies in the continuous cross frame model validation data are seen in the bottom struts in the northern end cross frames. The axial force validation data charts for the northeastern and northwestern cross frames are given in Figure 4.36 and Figure 4.37, respectively. The northeastern bottom strut shows a sudden jump in force in the first load step and then the force remains constant, while the FEA shows a linear progression to the final load level. The reason for this may be the FEA bearing model. As mentioned in Section 4.4.7 the bottom flange at the FEA bearing is fixed against translation. This assumes that the specimen has enough friction between the flange and the bearing not to slide. If this is not the case, then the reaction is passed through the brace into the next bearing.

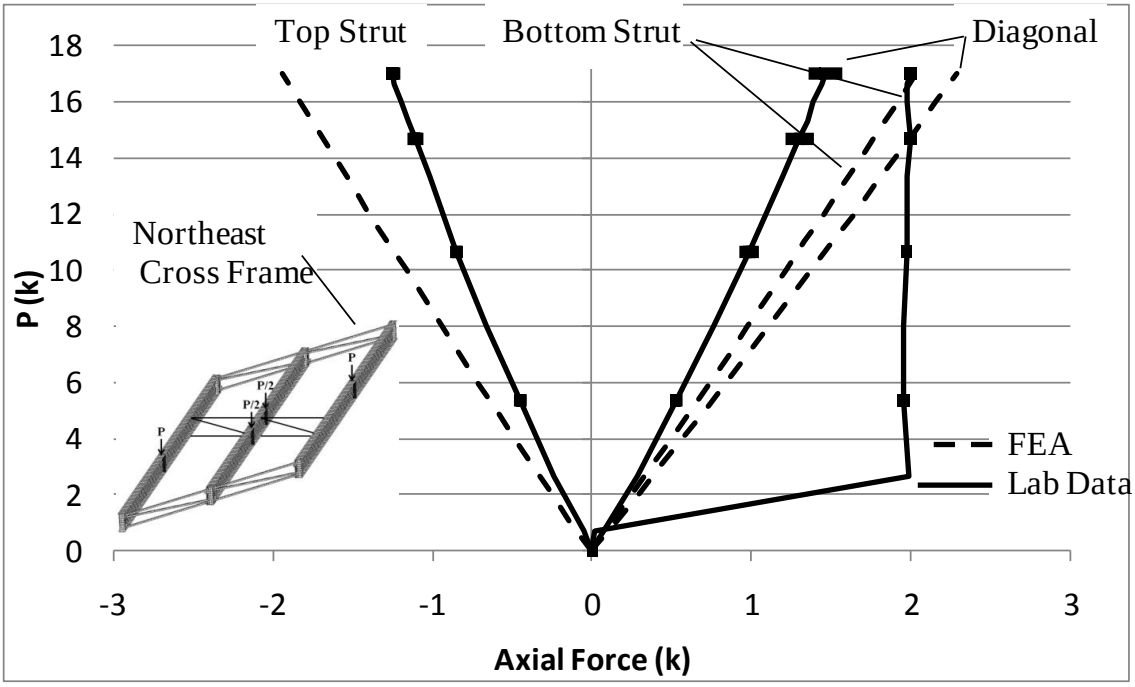

Figure 4.36: NE end cross frame axial force validation (continuous int. frames)

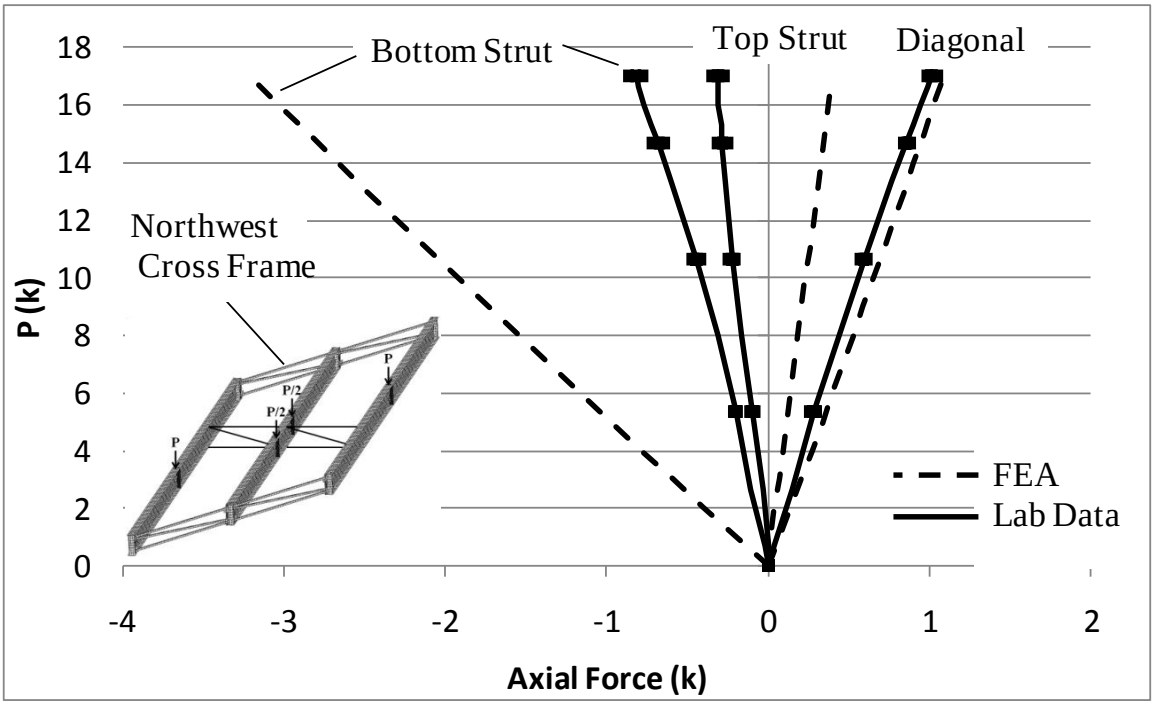

Figure 4.37: NE end cross frame axial force validation (continuous int. frames)

In the case shown in Figure 4.36 and Figure 4.37, if the north end of GSP2 slides it will pull on the north east cross frame bottom strut as shown in Figure 4.36. As the analysis progresses, the northeastern cross frame's bottom strut counters the skew forces and therefore relieves the load on the northwestern cross frame's bottom strut as shown in Figure 4.37.

While this explanation is plausible, it certainly may not be the only reason for the anomaly. However, the results from the staggered and continuous validation show that the overall model has good agreement with the laboratory specimen and the agreement between the two is very sensitive to the girders not sliding on the bearing.

4.6 FINITE ELEMENT MODELING SUMMARY

The results from the finite element model validation show that overall the modeling techniques used have a good agreement with the analytic equations and laboratory test results. Several important lessons were learned during the validation.

From the small scale tests it was learned that modeling the curved surfaces, like the bent plate, in ANSYS with shell elements requires a bend to element thickness ratio greater than three. A ratio below three resulted in poor agreement with laboratory results. The connection testing validation also showed that modeling welds can be important. The weld between the bent plate and connection plate add significantly to the bent plate stiffness and when modeled gave good agreement between the FEA and laboratory data.

A similar lesson about welds was learned from the large scale buckling tests. During the girder validation, it was learned that fastening the stiffeners to the connection plates via constraint equations did not engage the warping restraint the plate stiffeners provide to the girders. Although this restraint is relatively small, it can significantly affect the girder buckling strength. When these welds were modeled using multi-point constraint elements, the FEA solutions had good agreement with the laboratory results.

However, there is a place for using constraint equations to connect the stiffeners and girders. During the analytic solution validation, it was learned that the constraint equations do prevent alternate modes of failure not accounted for in the analytic solutions

used (such as local buckling) but do not affect the warping restraint provided by the stiffeners. Since the warping restraining provided by the stiffeners are generally not reflected in the analytic solution, when comparing with these solutions it may be desirable to have a model that does not engage the warping stiffness provided by the stiffeners.. Modeling the stiffeners in this way for the analytic validations gave good agreement between the model and analytic results.

Finally, it was shown that modeling intermediate cross frames perpendicular to the girders with truss elements gives good results compared to the laboratory data. This is especially important for modeling larger bridges with numerous intermediate cross frames. Using truss elements is very computationally efficient in these cases where creating the intermediate cross frames from shell elements could make the computational effort prohibitive in many cases.

Using the above lessons learned, the overall model performed well during validation. These models and techniques were then used to perform parametric studies to understand skewed steel girder buckling behavior and draw conclusions that can be applied to design guidance. These studies and guidance are covered in Chapter 5 (Parametric Studies and Design Recommendations).

CHAPTER 5
Parametric Studies and Design Recommendations

5.1 INTRODUCTION

The validated finite element model that was outlined in Chapter 4 (Finite Element Modeling) was used to perform several parametric studies to establish guidelines for the design of skewed end cross frame connections. This chapter provides an overview of those studies and the proposed design guidelines. Some of the key factors that were considered and summarized in this chapter include the impact the cross frame connection has on the overall brace stiffness, the skew angle at which the connection stiffness becomes the limiting component for the cross frame stiffness, the effect of girder end twist on buckling strength, and an investigation on the increase in buckling strength due to warping restraint provided by the split pipe stiffener.

5.2 GENERAL PARAMETRIC STUDY METHOD

The parametric studies summarized in this chapter were based on the five representative cross sections shown in Figure 5.1. These cross sections were created considering current TxDoT guidelines (Texas Steel Quality Council 2007), previous research (Zhou 2006), and a survey of bridge plans provided by TxDoT. In each section of the chapter, a brief description is provided of the FEA model that was used, along with the constant and variable parameters investigated. Results of the study are presented along with proposed guidelines for current design and construction practices. Results that are not shown in this chapter are provided in Appendix C (Parametric Study Results).

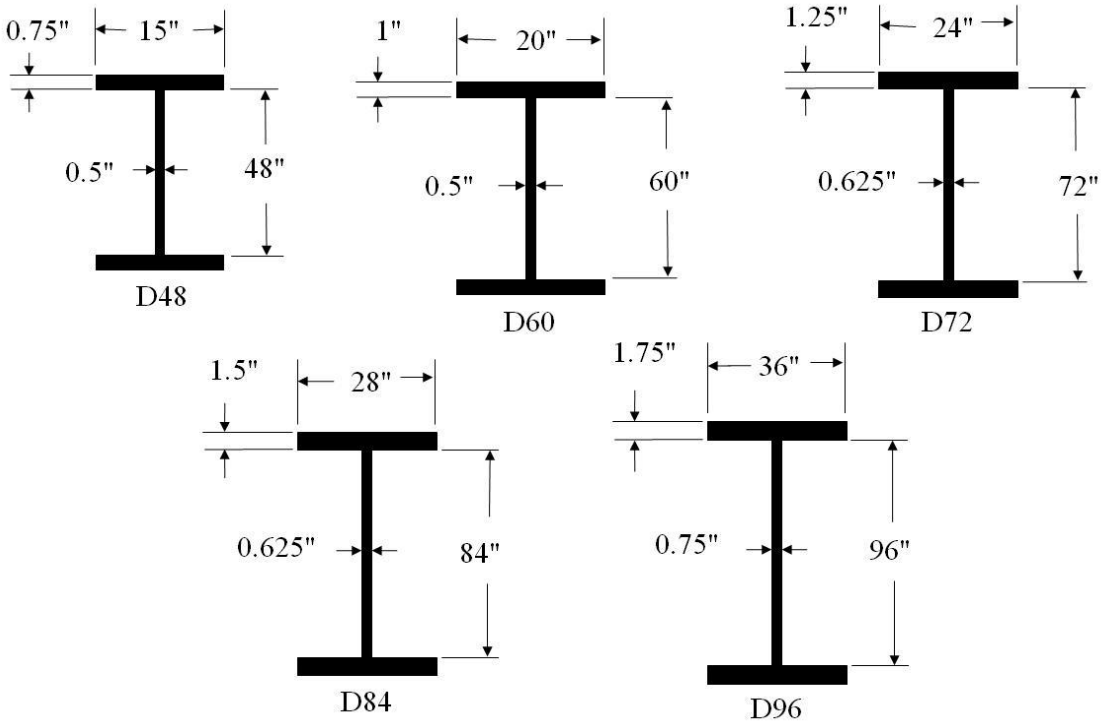

Figure 5.1: Parametric study cross sections

5.3 CROSS FRAME STIFFNESS PARAMETRIC STUDY

The purpose of the cross frame stiffness parametric study is twofold. First, it was used to determine at what skew angle the bent plate begins to limit the cross frame stiffness so that an equation to describe the bent plate stiffness could be developed. This quantity was used in Equation (2.49) to calculate the impact of the bent plate connection on the overall cross frame stiffness. Second, the parametric study was used to compare the stiffness of a cross frame using the bent plate connection against one using the split split pipe stiffener connection.

5.3.1 Bent Plate Stiffness

The bent plate stiffness was determined for a ½" thick bent plate and ½" thick connection plate since this is the smallest bent plate and connection plate that meet current TxDoT guidelines (Texas Steel Quality Council 2007). A 2.5" bend radius was

used in the study. The impact of varying these parameters on cross frame stiffness was also considered.

The impact of the stiffness of various components of the bracing system on the overall cross frame stiffness (β_T) was presented in Equation (2.18). Chapter 2 also contains the derivation of the connection stiffness ($\beta_{conn\text{-}tors}$) contribution to the overall cross frame stiffness and the adjustment to the brace axial stiffness for skew (β_{brskew}). Adding the connection stiffness to the other system components results in the expression provided in Equation (2.18).

$$\frac{1}{\beta_T} = \frac{1}{\beta_{brskew}} + \frac{1}{\beta_{sec}} + \frac{1}{\beta_g} + \frac{1}{\beta_{conn-tors}} \tag{5.1}$$

A typical bent plate cross frame has four bent plates and two connection plates whose combined axial stiffnesses together affect the cross frame torsional stiffness ($\beta_{conn\text{-}tors}$) as shown in Figure 5.2. Quantifying $\beta_{conn\text{-}tors}$ in Equation (5.1) requires an assessment of the axial stiffness of the four individual bent plate connections perpendicular to the girder. The axial stiffness of the individual bent plate to connection plate connection is referred to as β_{conn}. Once β_{conn} is known, it is used in Equation (2.49) to calculate the connection torsional stiffness of ($\beta_{conn\text{-}tors}$). The connection torsional stiffness is then used in Equation (2.18) to calculate the overall cross frame stiffness. The challenge in this process is to accurately calculate β_{conn}. Therefore, the parametric study was used to first assess $\beta_{conn\text{-}tors}$ and then use it to calculate β_{conn} to see if the process would give similar values of the bent plate connection stiffness for different cross frame geometries. This serves as a check on the accuracy of the method. This process is described below.

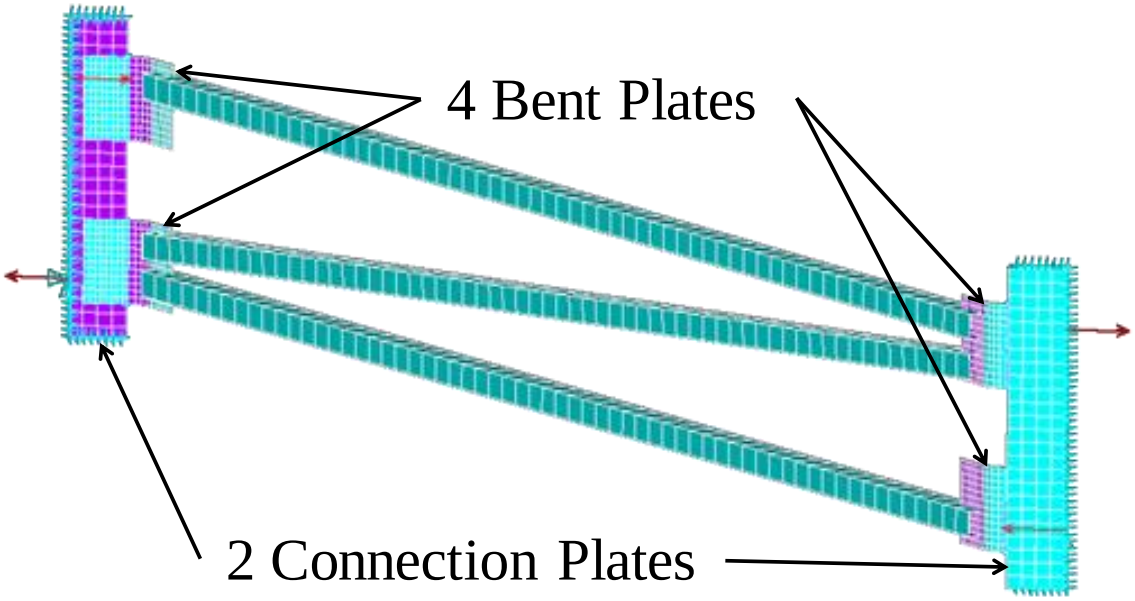

Figure 5.2: Components comprising the cross frame connection stiffness ($\beta_{conn\text{-}tors}$)

Estimating the bent plate connection stiffness begins with Equation (2.49), which defines the connection contribution to the cross frame connection torsional stiffness ($\beta_{conn\text{-}tors}$) in terms of the values of the individual connection stiffness (β_{conn}) and cross frame geometry. This equation is repeated below for convenience.

$$\beta_{conn-tors} = \frac{\beta_{conn}\, h_b^2}{\frac{2L_c^2}{S^2} + 1} \tag{2.49}$$

By rearranging the equation, the individual connection stiffness can be isolated as shown in Equation (5.2).

$$\beta_{conn} = \frac{\left(\frac{2L_c^2}{S^2} + 1\right)\beta_{conn-tors}}{h_b^2} \tag{5.2}$$

Using the bent plate cross frame model and the unskewed cross frame finite element model described in Chapter 4, $\beta_{conn\text{-}tors}$ can be found using Equation (2.18) once the total brace stiffness is found from a finite element analysis. In the bent plate cross frame models, the girder cross section stiffness (β_{sec}) and girder in-plane stiffness (β_g) are infinite and can be dropped from Equation (2.18). This matches the case of an end cross frame, since the girder does not deflect vertically at the abutment, and a full depth cross frame is typically used to connect the cross frame to the girder. The skewed brace stiffness (β_{brskew}) can be found by using the unskewed cross frame model described in Section 4.5.1.2 and then multiplying the finite element brace stiffness given from this model by the cosine squared of the skew angle as described in Equation (2.43). The total cross frame stiffness (β_T) can then be found by using the bent plate cross frame model described in Section 4.5.1.1. Once these values are known, Equation (5.1) can be used to solve for $\beta_{conn\text{-}tors}$ and then substituted into Equation (5.2) to solve for the bent plate connection stiffness (β_{conn}).

It is important to note that the final result from this procedure is not the actual stiffness value of the individual bent plates, but is instead the combined effect of all four bent plates and the two connection plates on the cross frame stiffness. Calculating the actual stiffness of each of the four bent plates in the cross frame would require knowledge of the forces and deformations of each plate. Since each plate may have tension and compression members connected to it at various angles, the state of force and deformation in each plate is unique, non-linear, and complicated. Rather, the proposed method relies on small deflection assumption to assume linearity and considers the overall impact of all the plates as a whole on the cross frame stiffness. This approach is a reasonable assumption based upon the small scale testing that showed if the forces in the

braces remain relatively low (below 5 kips for the 5/16" thick plates in the small scale testing) then the deformation response of the plate is nearly linear.

If the finite element analysis is run for various cross frame geometries for the same bent plate, the bent plate stiffness should vary only slightly due to the differing brace height, diagonal orientation and other geometric differences that affect the size and the forces entering the plate. To check this condition a parametric study was performed using the five cross sections shown in Figure 5.1 for skew angles ranging from 15° to 60° in 15° increments. The girder spacings used were 10', 8', and 6' since 10' is the maximum recommended plate girder spacing in Texas (Texas Steel Quality Council 2007). The cross frames were made up of HSS3.5x3.5x3/8 members, which is a similar brace area used in the Texas standard plans (Texas Department of Transportation 2006). All connection plates were half as wide as the flange width. A check of the individual bent plate connection stiffness is shown in Figure 5.3 for an 8' girder spacing.

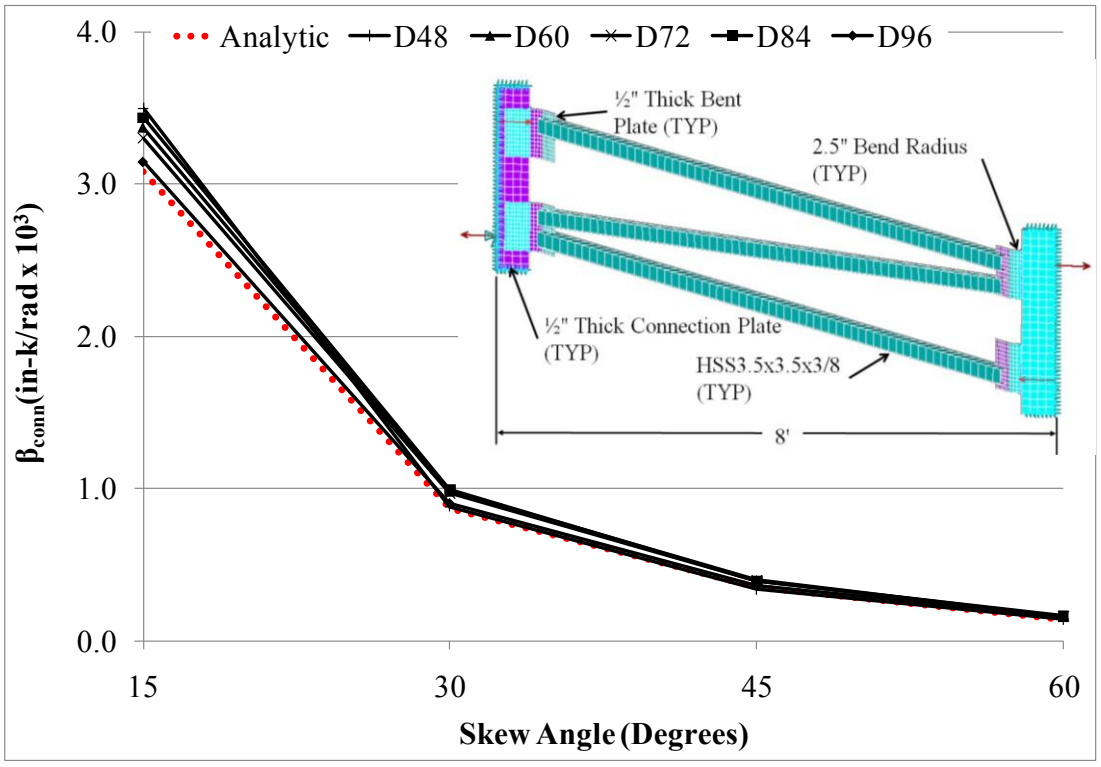

Figure 5.3: Bent plate connection stiffness parametric study result (S=8')

From the results in Figure 5.3 it can be seen that, the bent plate connection stiffness from Equation (5.2) only varies a small amount between the different girder geometries. This shows the plate stiffness is not very sensitive to the girder geometry at an 8' girder spacing, which was expected and shows that Equation (5.2) does a reasonable job of predicting the bent plate stiffness at the 8' girder spacing. To develop an equation describing the bent plate stiffness, an exponential curve fit was used for the minimum bent plate stiffness values at each skew angle from 15° to 60°. The analytic equation is plotted with the FEA results in Figure 5.3 and is given as Equation (5.3).

$$\beta_{conn} = (70\alpha + 5000)e^{-q\alpha} \tag{5.3}$$

where

$q = 0.045 + (\alpha - 15)/100 \leq 0.07$

α = *skew angle in degrees* ($15° \leq \alpha \leq 60°$)

The limits on α above do not necessarily mean that the expressions will not work for skew angles outside this range, but instead reflect the range of angles considered in the study. With the individual connection stiffness defined, the total cross frame stiffness for each cross section was calculated using Equations (5.3), (2.49), and (2.18), normalized with respect to the zero skew case and plotted against the skew angle. This stiffness was compared to the cross frame stiffness results from the FEA models. Results for the D48 and D72 cross sections shown in Figure 5.1 are given in Figure 5.4 and Figure 5.5, respectively.

From the figures it can be seen that Equation (5.3) has good agreement with the finite element model results. The results for the 8' girder spacing for all cross sections tested (D60, D84, and D96 shown in Figure 5.1) can be found in Appendix C (Parametric Study Results). All other cross sections had the same good agreement between the FEA and analytic solutions.

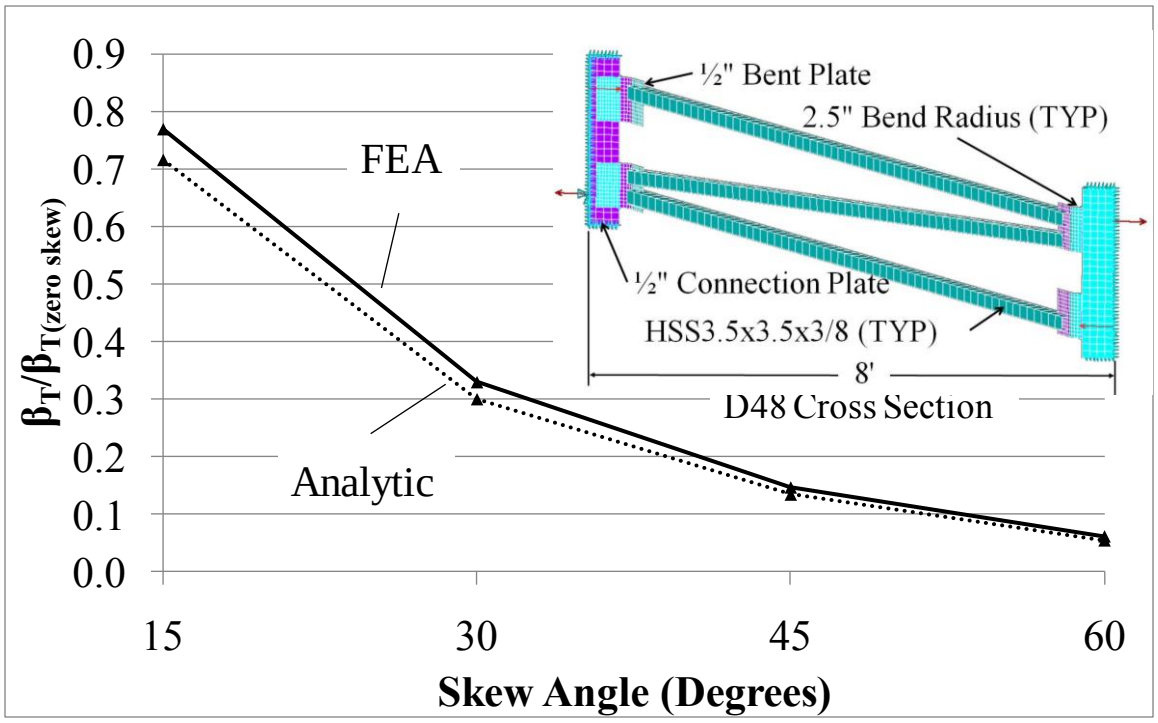

Figure 5.4: Analytic to FEA cross frame stiffness comparison (cross section D48)

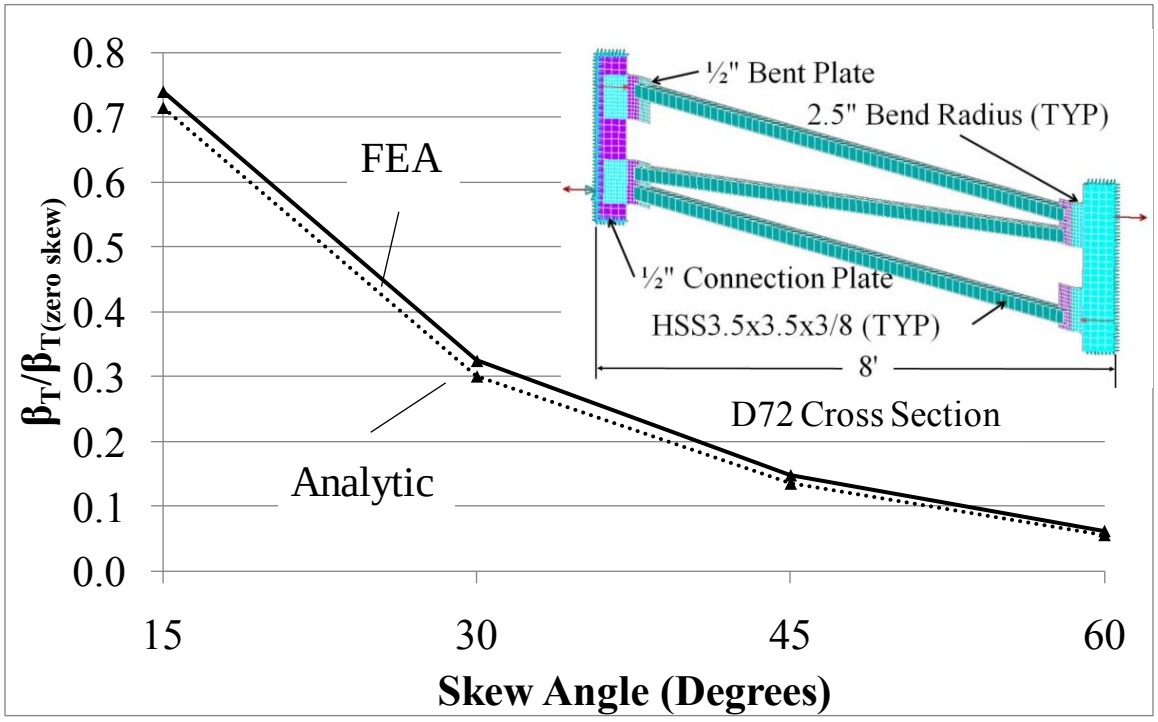

Figure 5.5: Analytic to FEA cross frame stiffness comparison (cross section D72)

In addition to the 8' girder spacing, an additional study was run using a 10' girder spacing. The results for the D96 cross sections are shown in Figure 5.6. The figure shows that the analytic equation over-estimates the cross frame stiffness by about 20% at a 15° skew and about 100% at a 60° skew when a 10' spacing is used. Similar poor agreement was found in the shallower cross sections as well.

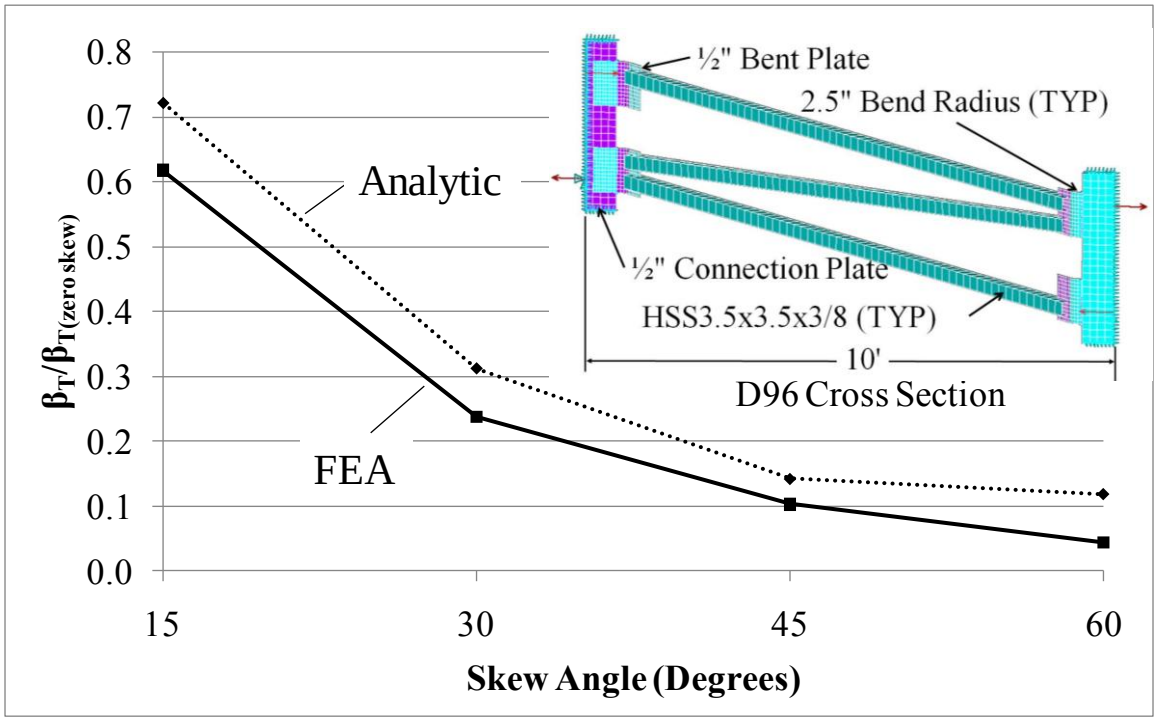

Figure 5.6: Analytic to FEA cross frame stiffness comparison (cross section D96)

To more accurately extend Equation (5.3) to girder spacings other than 8', the equation is multiplied by the ratio of the 8' spacing for which it was derived to the desired girder spacing. The resulting equation is shown in Equation (5.4).

$$\beta_{conn} = \frac{8}{S}(70\alpha + 5000)e^{-q\alpha} \tag{5.4}$$

where

S = girder spacing in feet

All variables remain as previously defined.

The cross frame stiffness using Equation (5.4) for the connection stiffness compared to the FEA solution for the D48 and D96 cross section are plotted in Figure 5.7 and Figure 5.8, respectively. The analytic solution now shows good agreement with the FEA solution. All other cross sections show agreement and can be found in Appendix C (Parametric Study Results).

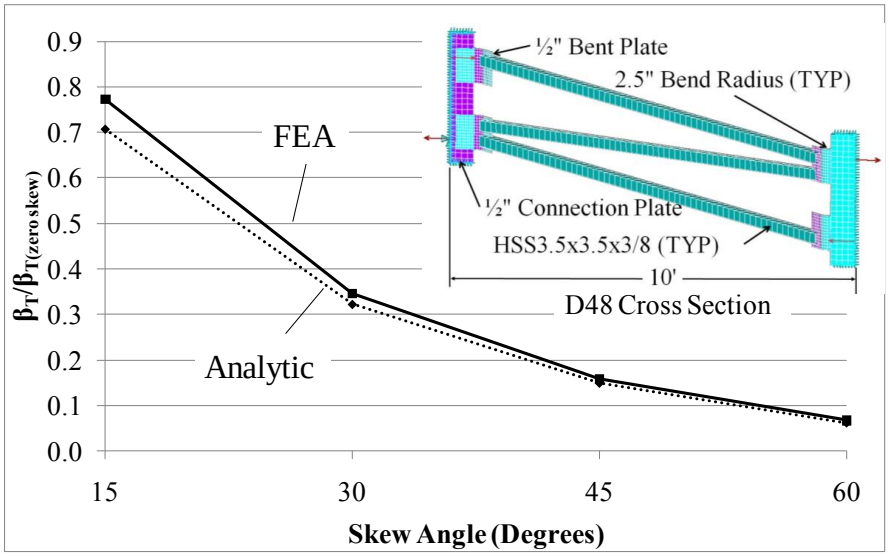

Figure 5.7: Analytic to FEA cross frame stiffness comparison (cross section D48)

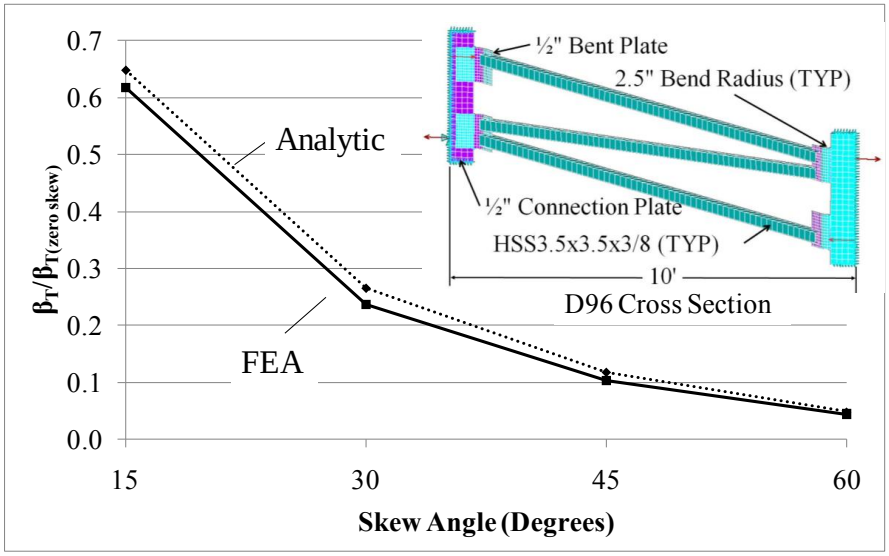

Figure 5.8: Analytic to FEA cross frame stiffness comparison (cross section D96)

Finally, the case where the girder spacing is smaller than 8' was checked. The analysis was run again for the D48 and D60 cross section at a 6' spacing and compared to the analytical solution using Equation (5.4) to calculate the connection stiffness. The results are shown in Figure 5.9 and Figure 5.10. Again, the analytic results show good agreement with the FEA results.

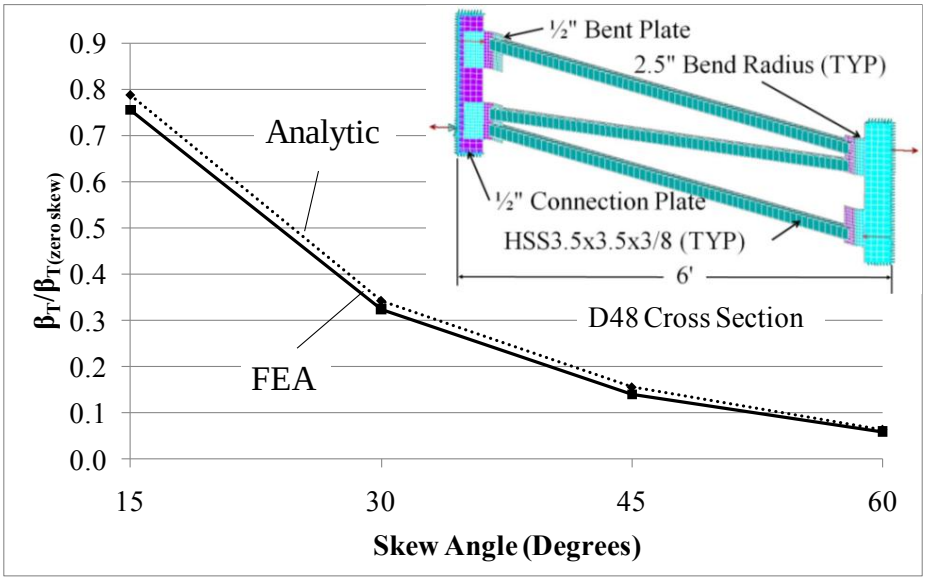

Figure 5.9: Analytic to FEA cross frame stiffness comparison (cross section D48)

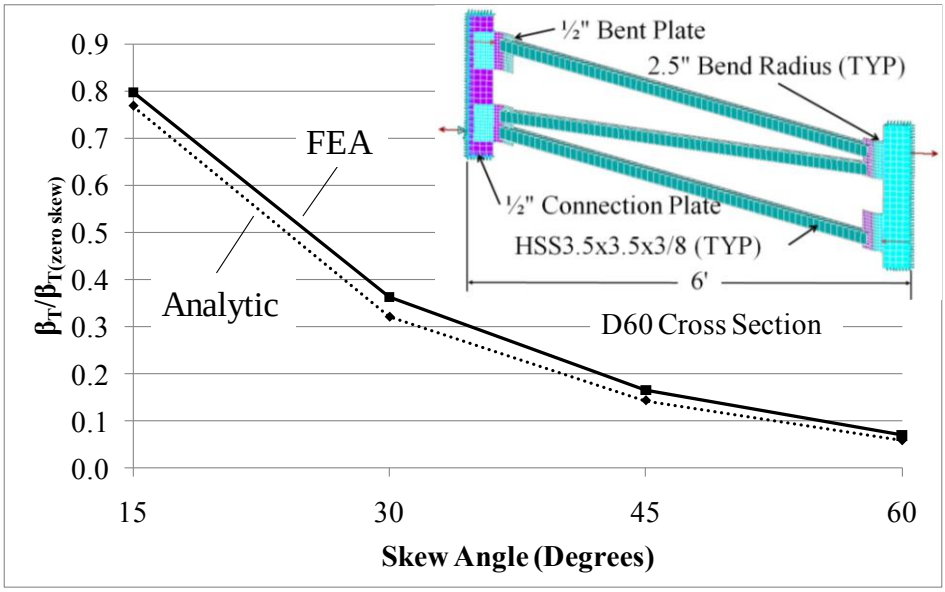

Figure 5.10: Analytic to FEA cross frame stiffness comparison (cross section D60)

5.3.2 Critical Bent Plate Connection Stiffness Skew Angle

While the previous cross frame connection stiffness equations are useful in quantifying cross frame stiffness, an important aspect of the connection stiffness is to determine what angle the connection stiffness begins to limit the cross frame stiffness. Identifying the limiting angle provides designers the ability to determine the most efficient action to stiffen a cross frame. If the connection governs, then stiffening the connection is the most efficient alternative. Similarly if the brace stiffness is the limiting component, then stiffening the brace has the most impact. For girders with full depth stiffeners and end cross frame values of the in-plane and cross sectional girder stiffness are near infinity; therefore, the remaining terms of Equation (2.18) (the brace and connection stiffnesses) are the limiting components for the total cross frame stiffness. By forming the ratio of the connection stiffness ($\beta_{conn\text{-}tors}$) to brace stiffness (β_{brskew}) and plotting this ratio against the skew angle for each of the parametric cross sections, the range of skew angles where the connection stiffness limits the cross frame stiffness can be identified by tracing the horizontal line where the ratio equals one.

An example of such a plot is given in Figure 5.11. Where the plots are above the red horizontal line, the HSS3.5x3.5x3/8 brace limits the cross frame stiffness and below the line the connection limits the stiffness. The range of skew angles where the connection begins to limit the cross frame stiffness is centered around 20°. Of course the plot shown is specific to the brace size, bent plate and girder spacing shown in the figure.

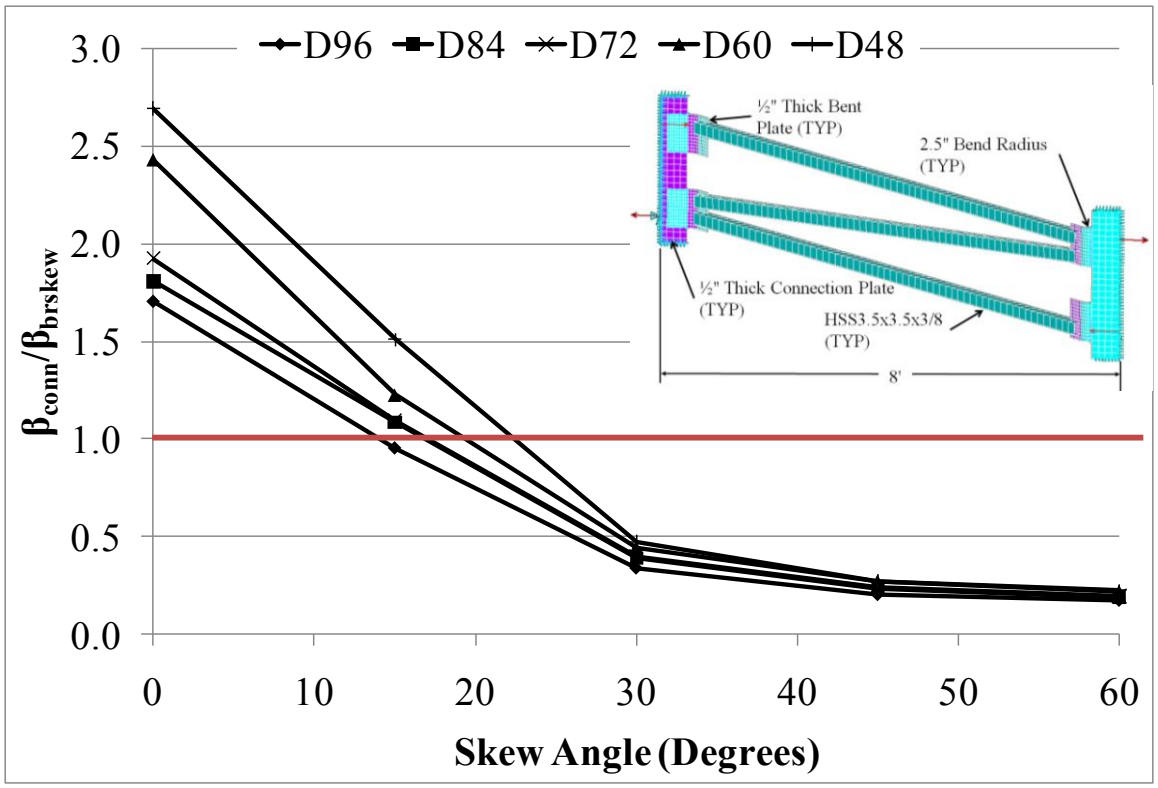

Figure 5.11: Bent Plate cross frame limiting stiffness ratio

5.3.3 Plate Thickness and Bend Radius Impact on Cross Frame Stiffness

Since much of the previous analysis in this chapter has been specific to a ½" thick bent plate and ½" connection plate, varying these parameters was also checked to ensure that increasing the plate thickness can stiffen the connection sufficiently to improve the behavior. Primarily designers will be most interested in which portion of the connection (the bent plate or connection plate) has the greatest impact on the connection's overall stiffness. Therefore, beside the basic case of ½" thick bent plate and connection plate the cases of ¾" bent plates and connection plates were checked.

The results of varying the bent plate and connection plate thickness from ½" to ¾" are shown in Figure 5.12 for the D72 cross section. The results are normalized by the ½" thick bent plate and connection plate standard case ($\beta_{T(standard)}$) used in the previous analysis. As can be seen from the figure, stiffening one or both of the plates does stiffen

the connection, so the previous equations developed are conservative if used for these additional cases. Also, stiffening the connection plate is generally more effective than just stiffening the bent plate. Increasing the thickness from 0.5 in. to 0.75 in. as much as doubled the stiffness of the overall connection depending on the skew angle. Results for the other parametric cross study sections are provided in Appendix C (Parametric Study Results).

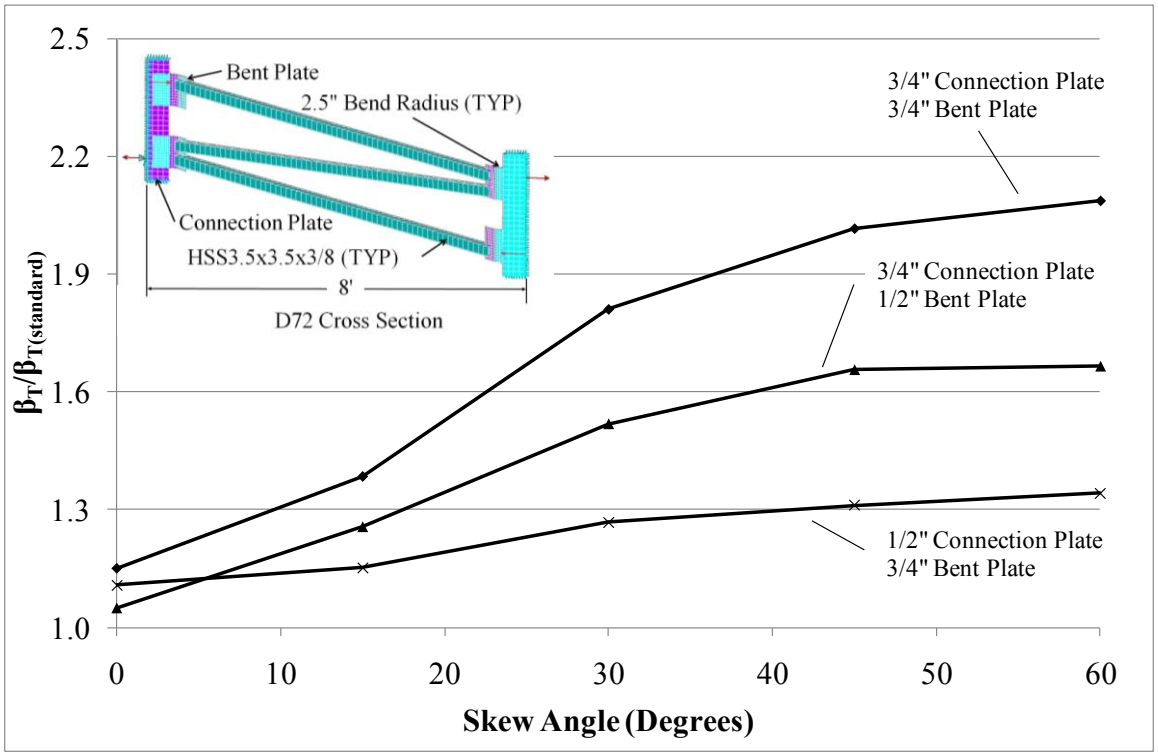

Figure 5.12: Plate thickness impact on bent plate connection (2.5" bend radius)

Another parameter that may impact the bent plate stiffness is the bend radius. The connection tests outlined in Chapter 3 showed that the bend radius of the bent plate did impact the connection stiffness. Therefore, another set of cases were run with a bend radius of 3.5" to compare to the 2.5" bend radius cases. The results of the analysis are shown in Figure 5.13 with the percent change in cross frame stiffness due to increasing the bend radius from 2.5" to 3.5" plotted against skew angle. From the figure it can be

seen that increasing the bend radius from 2.5" to 3.5" can decrease the cross frame stiffness nearly 10% at the larger skew angles. At skew angles less than 30°, the cross frame stiffness actually increases slightly since increasing the bend radius shortens the brace length a small amount. The plots for the other cross sections considered in this analysis are given in Appendix C (Parametric Study Results).

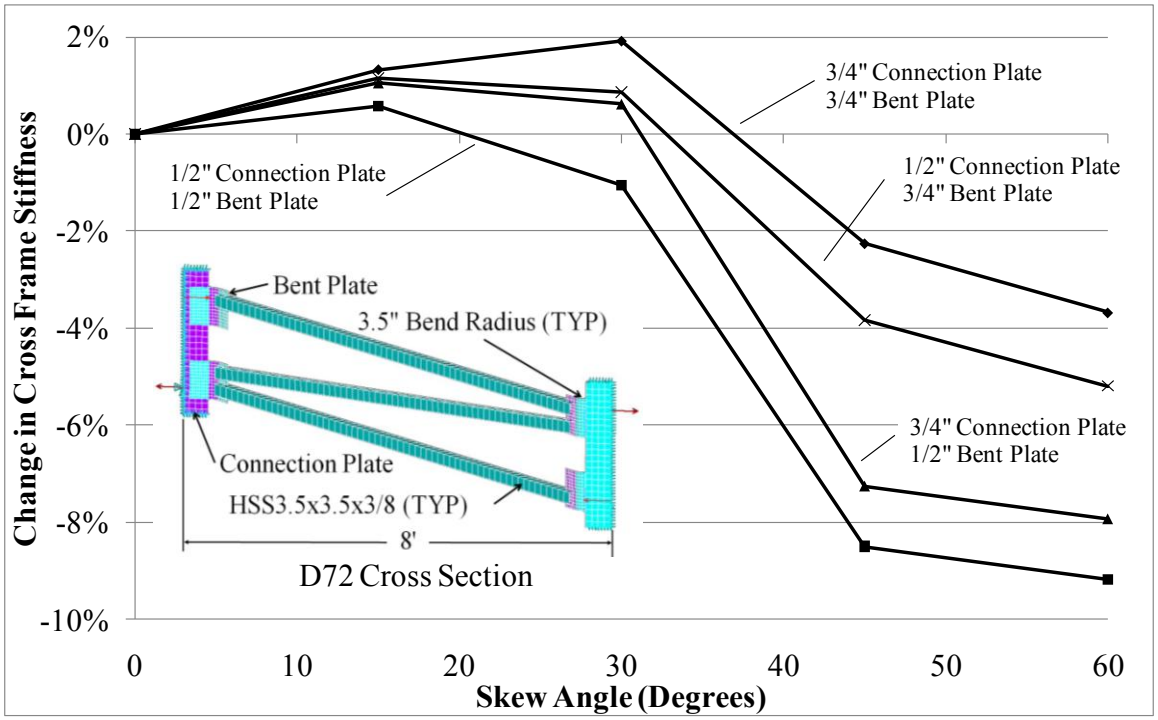

Figure 5.13: Change in cross frame stiffness for 2.5" and 3.5" bend radii

5.3.4 Cross Frame Connection Comparison

To compare the bent plate and split pipe stiffener cross frame connections, a similar analysis used in the previous section was run using the split pipe cross frame model described in Chapter 4. The parameters for the split pipe stiffener cross frame were the same as for the bent plate cross frame. In both cases the connection plate was ½" thick, and the bent plate and split pipe connection tabs were also ½" thick. The height of brace (h_b) was also held constant for both connections. A ½" thick pipe was considered, and like the bent plate cases, the brace members were HSS3.5x3.5x3/8. The

only parameter common to the two cross frame types that changed was the length of the braces. Since the split pipe connection requires a longer connection length, the split pipe connection brace members were about 6" shorter than the bent plate brace members. In the comparisons below, the standard bent plate case with the 2.5" bend radius was considered.

The results of the analysis for all five parametric study cross sections with pipe diameters 2 inches less than the flange width (BFL) are shown in Figure 5.14. The split pipe cross frame stiffness values have been normalized by the bent plate cross frame stiffness values. Therefore the data on the vertical axis represents the increase in stiffness of the split pipe cross frame compared to the bent plate cross frame stiffness

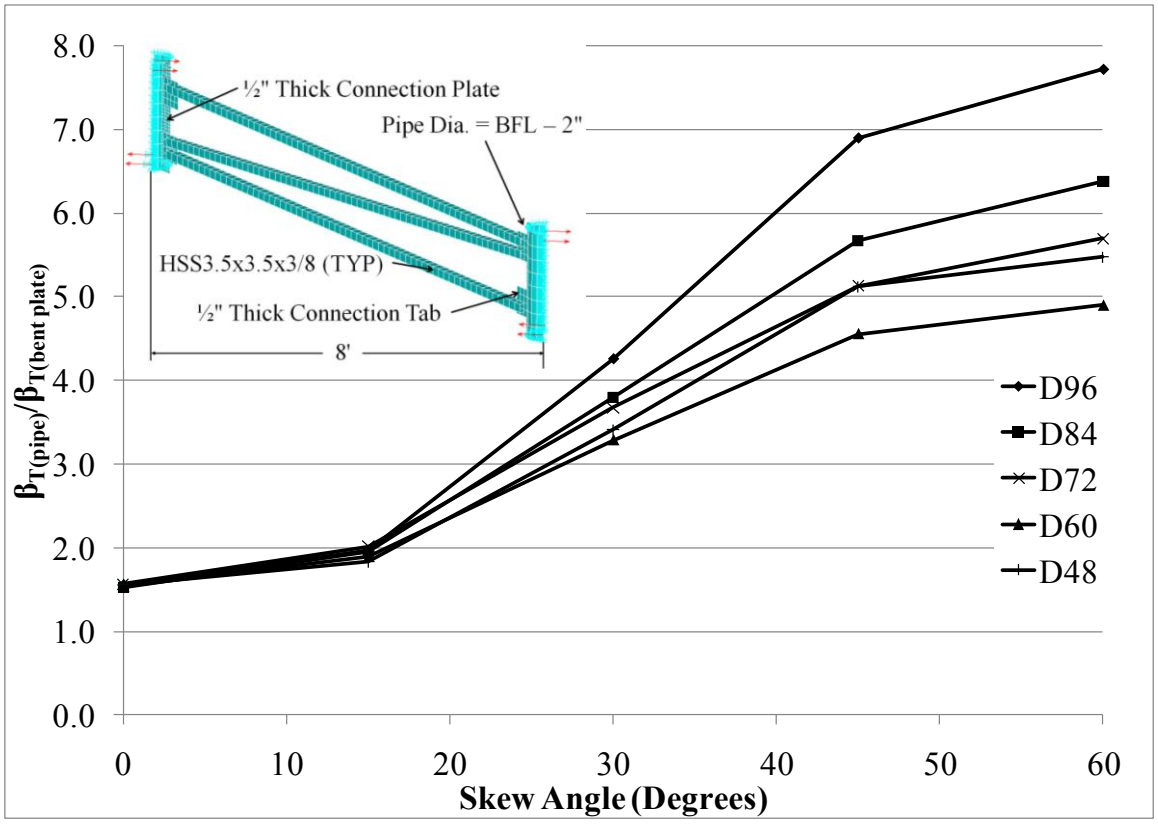

Figure 5.14: Split pipe to bent plate connection cross frame stiffness (BFL-2)

From the figure it can be seen that the split pipe detail is much stiffer than the bent plate detail. At the larger skew angles the split pipe stiffener cross frame reaches from 5 to 8 times as stiff depending on the depth of the girder cross section.

In the previous study the pipe diameter was as large as physically possible to fit the girder (2 inches less than the flange width). To check a lower bound on the split pipe cross frame stiffness, the pipe diameter was reduced to half the flange width. These results are plotted in Figure 5.15. The figure shows a moderate reduction in the stiffness of the split pipe connection relative to the bent plate connection, which is expected since the braces must get longer as the pipe diameter decreases. However, even with this stiffness reduction, the split pipe stiffener shows a significant increase in stiffness over the bent plate detail.

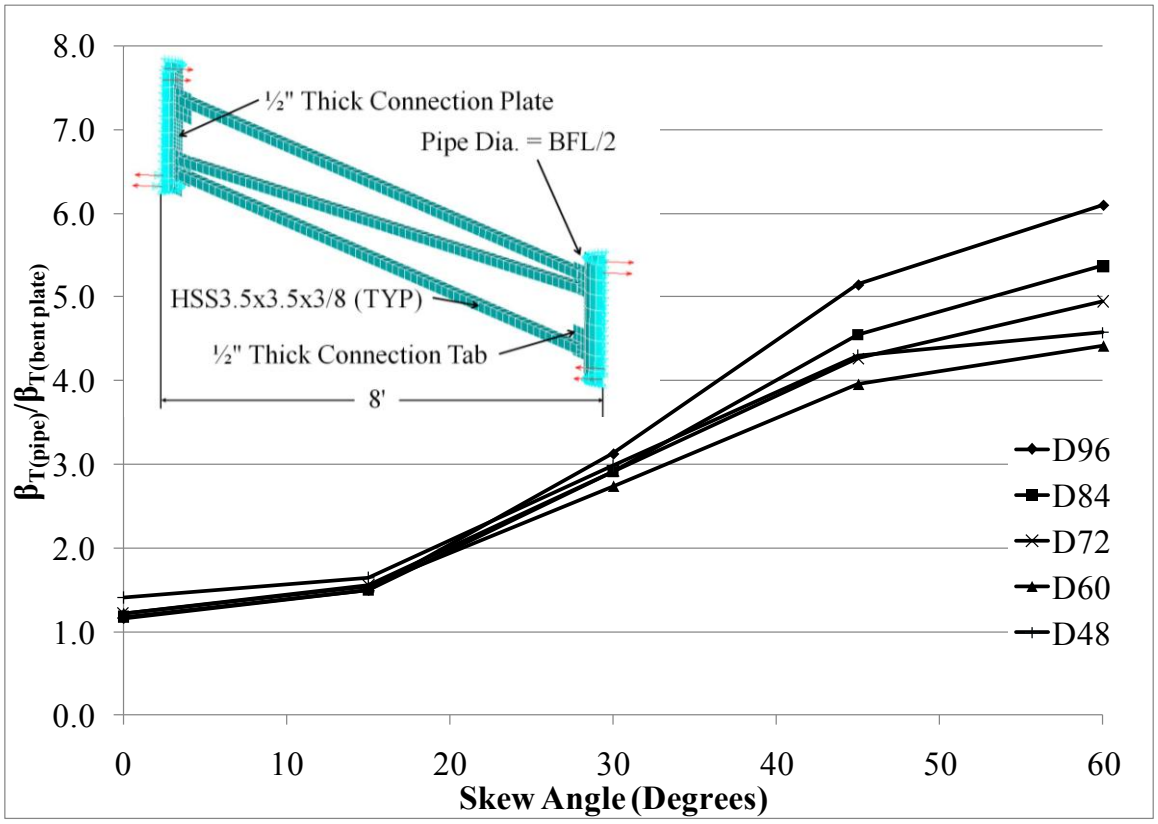

Figure 5.15: Split pipe to bent plate connection cross frame stiffness (BFL-2)

5.3.5 Critical Split Pipe Connection Skew Angle

The next analysis performed was to determine at what skew angle the split pipe stiffener would be the limiting stiffness component. A plot similar to that used in the previous section for the bent plate analysis was created. The analysis results are given in Figure 5.16 and show that for the cross sections and braces considered, the split pipe connection is not the limiting component stiffness in any case.

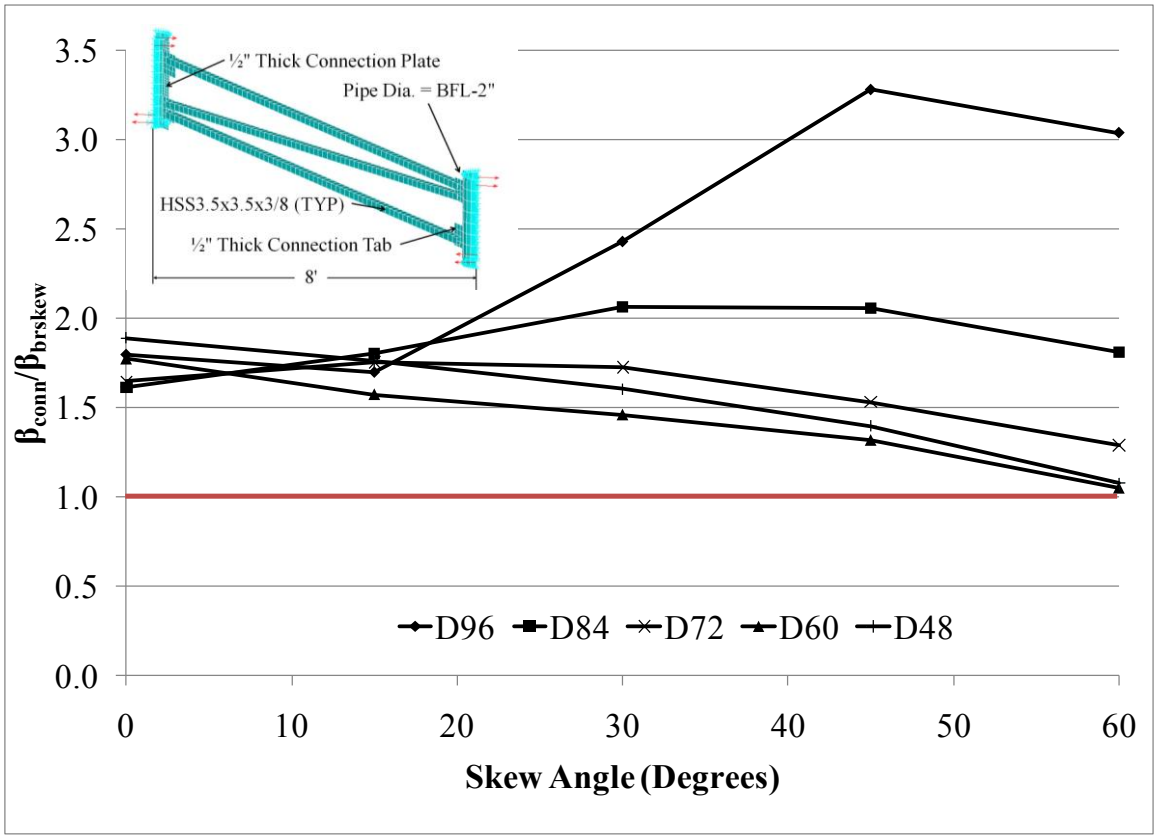

Figure 5.16: Split pipe cross frame limiting stiffness ratio

However, even though the split pipe connection may not be the limiting component stiffness, it does still have a finite stiffness that does result in a decrease of the total cross frame stiffness. To determine the impact of the split pipe connection on the cross frame stiffness, the total cross frame stiffness (including the split pipe cross frame connection stiffness) was normalized by the cross frame with an infinite connection stiffness and plotted against the skew angle. The results are shown in Figure 5.17.

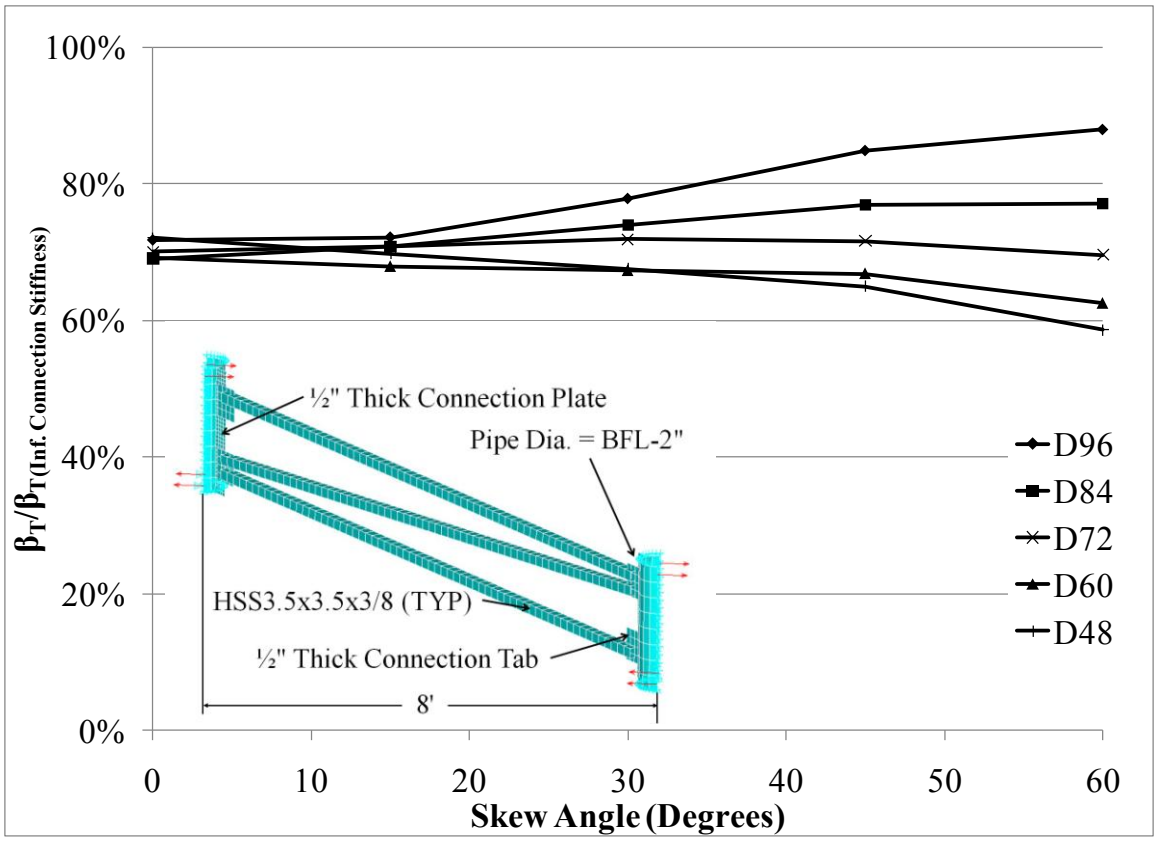

Figure 5.17: Split pipe connection impact on cross frame stiffness (BFL-2)

The results show that the impact of the split pipe connection on the cross frame stiffness is fairly uniform until the 30° skew is reached. For skews larger than 30°, the cross section depth becomes an important factor. A reasonable estimate of the reduction in cross frame stiffness due to the split pipe connection flexibility for cross sections at least 72" deep is 30%. For cross sections less than 72" the reduction can be taken as 30% for skews up to 30° and 40% for skews between 30° and 60°. These recommendations are based upon the assumption of standard conditions of an end cross frame, namely that the girder in-plane and cross-sectional stiffness are large and therefore not included in the total cross frame stiffness calculation.

5.3.6 Connection Stiffness Summary

The preceding analysis demonstrated that the split pipe stiffener connection is much stiffer than the bent plate connection, especially at larger skew angles. Therefore, the split pipe connection provides better control of twist at the end of skewed steel girder bridges. While the stiffer connection will certainly help mitigate construction issues such as cross frame to girder fit-up, there is still some question as to whether limiting twist will improve the girder's elastic buckling strength. In Chapter 2 the impact of girder twist was discussed in terms of previous research efforts, which found that the buckling strength is not greatly affected by moderate twist at the end of the girders. The next section presents results demonstrating the effect of end twist as a function of the cross frame stiffness.

5.4 GIRDER END TWIST PARAMETRIC STUDY

The purpose of this portion of the parametric study was to determine if Equation (2.51) (repeated below for convenience) is accurate in terms of predicting the decrease in buckling strength due to girder end twist allowed by skewed cross frames. Since this equation was formulated from an equation for support twist rather than twist allowed by cross frames, it must be validated to determine its accuracy.

$$n = 1 - \frac{4}{3}\left(\frac{GJ}{L}\right)_{girder}\left(\frac{1}{\beta_T}\right) \tag{2.51}$$

where

n = ratio of buckling strengths with and without end twist M_{cr}/M_o (M_{cr} = strength with end twist, M_o is strength without end twist).

To validate the equation accuracy, a parametric study was conducted using a twin girder finite element model with the same end cross frames from the cross frame stiffness parametric study. A picture of the bent plate and split pipe cross frame models are given in Figure 5.18 and Figure 5.19.

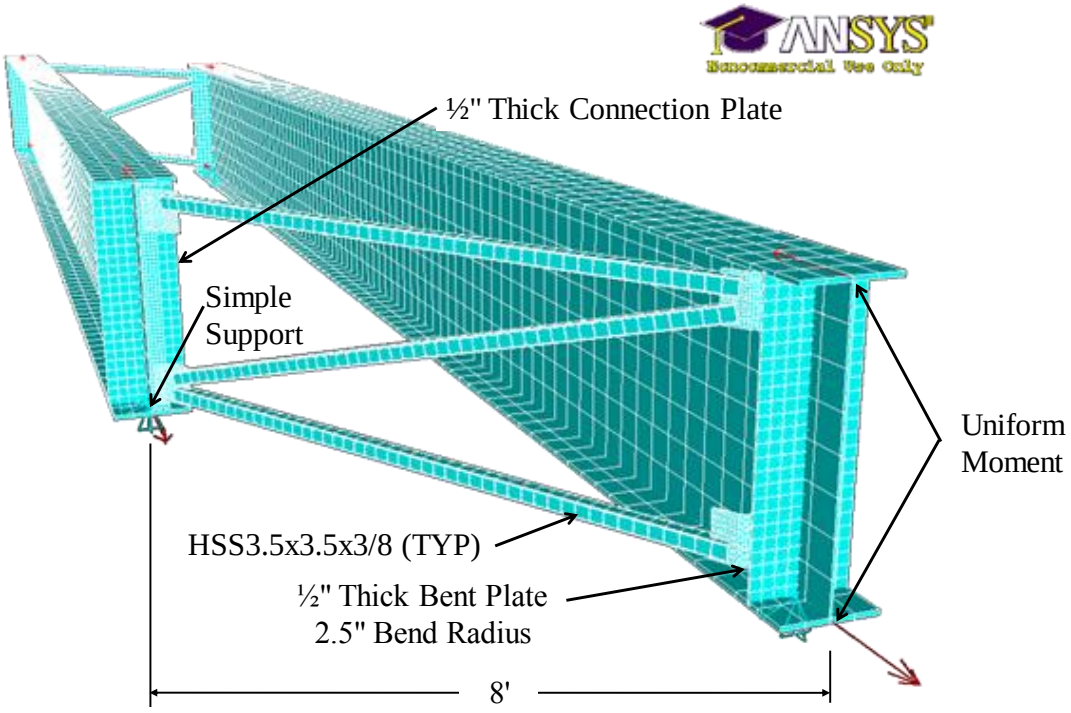

Figure 5.18: Bent plate cross frame twin girder model

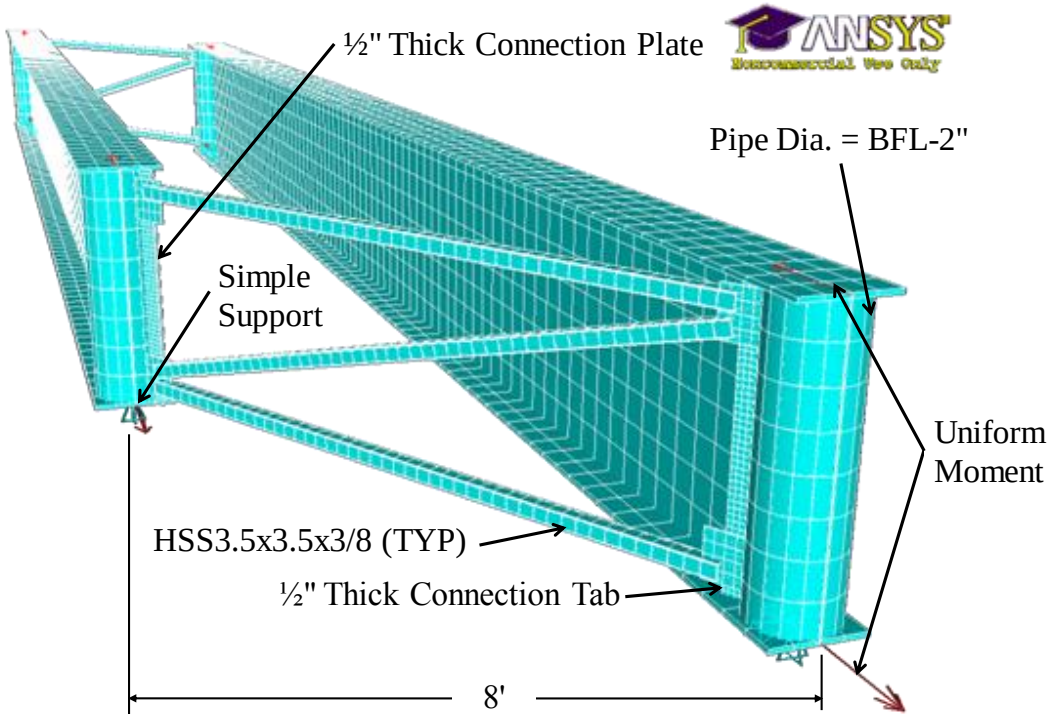

Figure 5.19: Split pipe cross frame twin girder model

The parameters in this study remained the same as in the base cases from the cross frame stiffness study with the bent plate and its connection plates as well as the split pipe and its connection plate and tabs all being ½" thick. The brace members were HSS3.5x3.5x3/8 and the split pipe diameters were taken as 2" less than the flange width. The twin girder model was subjected to a uniform moment, and an eigenvalue buckling analysis was conducted to determine the critical buckling moment for span-to-depth ratios ranging from 10-40 and skew angles of 15°, 30°, 45°, and 60°. The data shown below are normalized with respect to the no twist case (M_o) for each model.

Figure 5.20 and Figure 5.21 show the results for the D60 and D72 cross sections with bent plate cross frames. From the figures it can be seen that as the skew and associated end twist increase, the buckling capacity decreases. This effect is the most significant at the shorter span-to-depth ratios, but the decrease in buckling capacity is minimal. The D60 cross section at the span-to-depth ratio of 10 and 60° skew is the largest decrease in buckling capacity at just over 6%. At a span-to-depth ratio of 10, the beam is likely to experience significant yielding prior to buckling. All other cases were typically less than 4%. Results for other cross sections with the bent plate cross frame connection are provided in Appendix C (Parametric Study Results).

With the decrease in buckling capacity due to end twist being small when the bent plate connection is used, the current practice of simply ignoring reductions in buckling capacity due to end twist appears to be justified. When Equation (2.51) is applied to predict the buckling capacity reduction, it underestimates the reduction significantly, seldom resulting in a reduction greater than 1%. While better results can be achieved by changing the 4/3 constant in the equation to a value close to 30, the results are still not consistent. In some cases the equation with a constant of 30 over-predicts the reduction by 3% and in others it under-predicts it by 5%. With such small actual reductions, such variability makes such an equation unnecessary. As in current practice, ignoring the end twist effect on the girder buckling strength is acceptable, especially since tipping restraint provided by the bearing was conservatively ignored in the analysis and will generally more than compensate for the loss of buckling strength due to end twist.

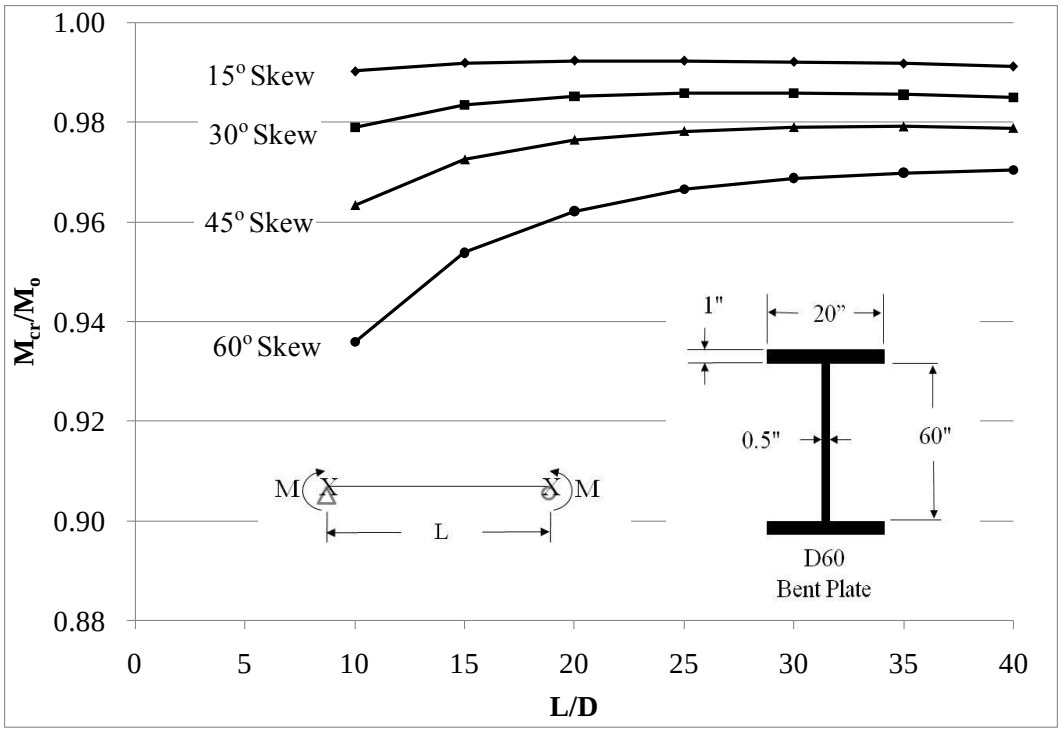

Figure 5.20: D60 cross section buckling strength with end twist

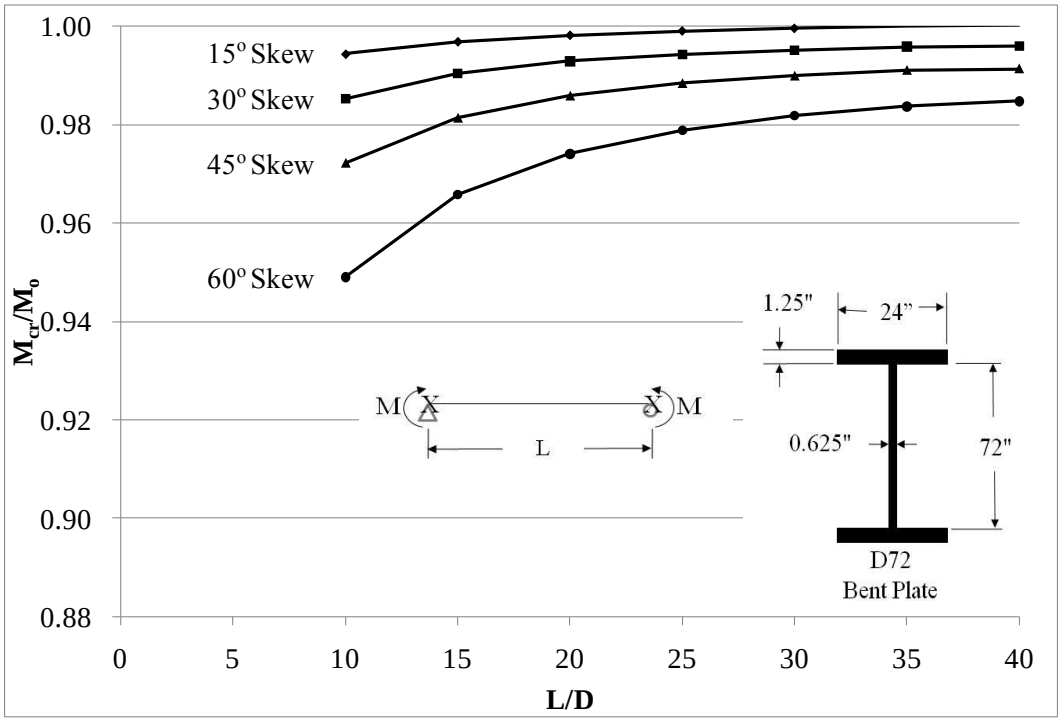

Figure 5.21: D72 cross section buckling strength with end twist

In addition to the bent plate details, the same cases for the split pipe stiffener were investigated using the finite element model shown in Figure 5.19. The results for the D84 cross section are shown in Figure 5.22. As shown in the previous section of this report, the split pipe connection is significantly stiffer than the bent plate connection and should limit twist better than the bent plate connection. The results of the larger stiffness are demonstrated with the very small buckling strength reductions shown in Figure 5.22. In no case did the buckling of a split pipe stiffened section drop below 98% of the no twist case. In some cases (such as the 15° skew case below) the cross frame provides some warping restraint and the buckling capacity is greater than the no twist case. The results from the other cross sections considered are provided in Appendix C (Parametric Study Results).

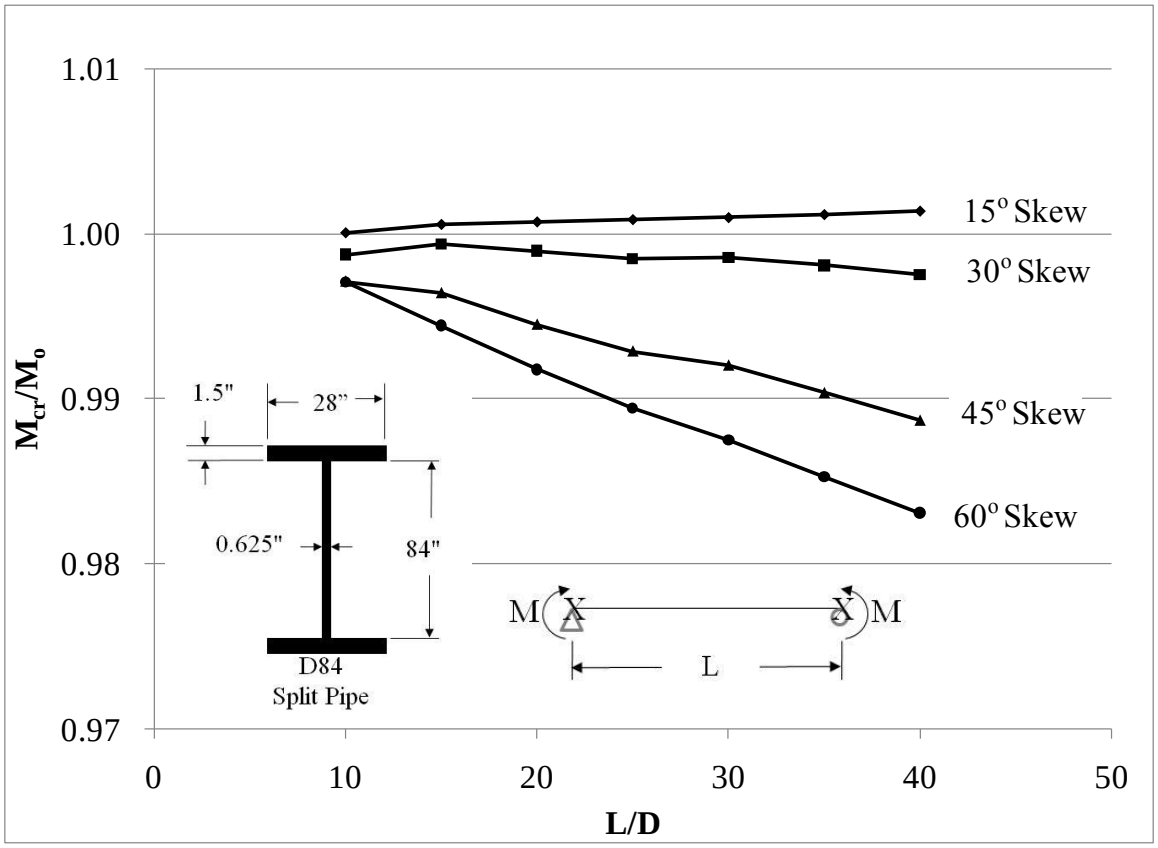

Figure 5.22: D84 cross section buckling strength with end twist

To directly assess the impact of the connection type on end twist and girder strength, a non-linear geometric analysis was conducted to check the end twist and cross frame forces to the D60 cross section at an L/D of 30 (150' length). The same models pictured in Figure 5.18 and Figure 5.19 were used to compare the responses between the bent plate and split pipe stiffener connections.

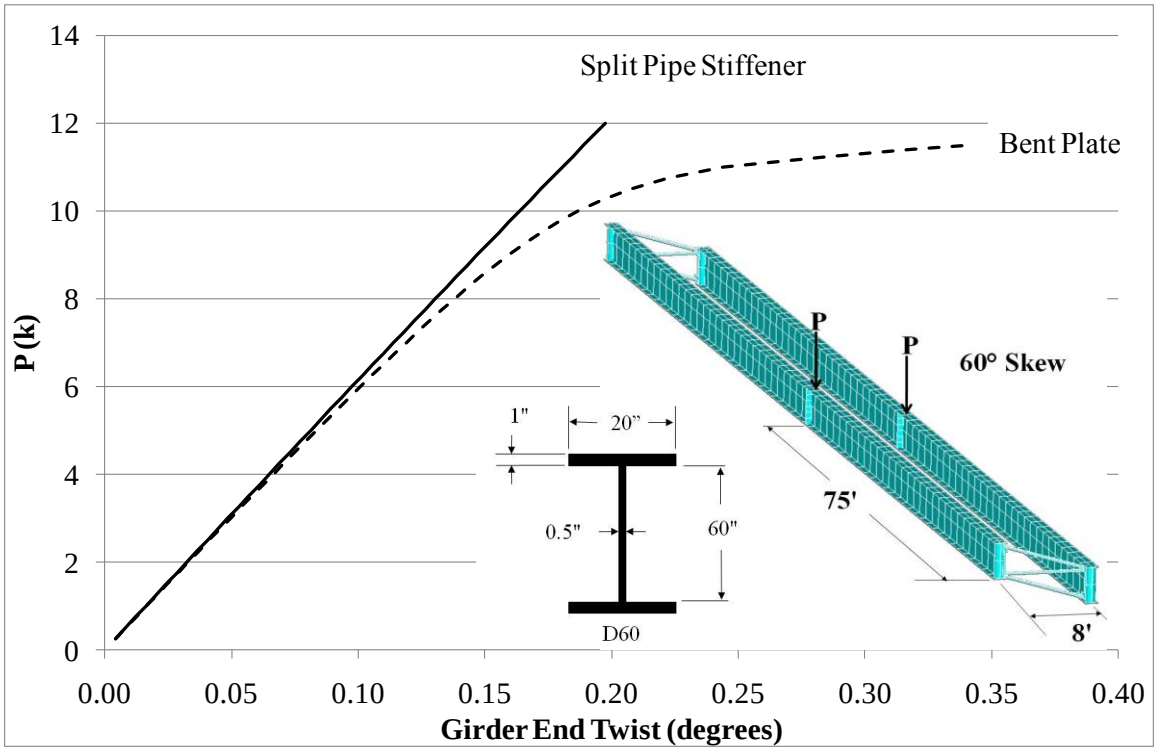

Figure 5.23: Girder end twist comparison

The results for the end twist comparison are provided in Figure 5.23. The data in the figure demonstrate that the split pipe stiffener connection is slightly better at limiting girder twist prior to the onset of buckling. As the girder with the bent plate connection buckles, the end twist rapidly increase as would be expected during buckling. A corresponding response can be seen in the end cross frame diagonal forces as shown in Figure 5.24.

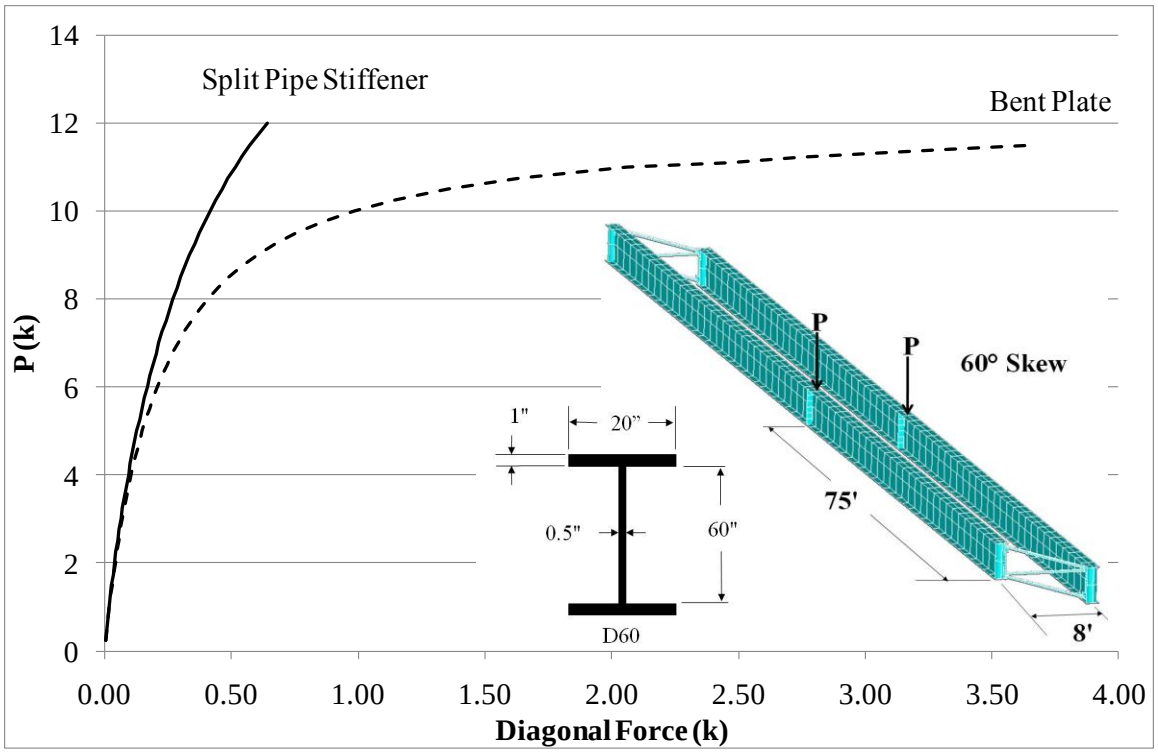

Figure 5.24: Cross frame diagonal force comparison

The two preceding figures show that the split pipe stiffener connection does reduce the girder end twist and the corresponding brace forces compared to the bent plate connection. While this is in part due to the higher connection stiffness, the majority of the reduction is due to the increase in buckling strength as a result of the warping restraint provided by the split pipe stiffener.

5.4.1 End Twist Summary

The end twist parametric study demonstrated that end twist does results in a slight decrease in the elastic buckling capacity of the girder. For the common bent plate connection, the reduction is small and can be neglected as has been done in the past. The slight reduction in capacity is typically offset by the tipping restraint provided by the bearings. The reduction in buckling capacity for the split pipe stiffener is even smaller than the bent plate and typically does not exceed 2%, which can generally be disregarded.

The split pipe stiffener has been shown to be a much stiffer connection than the bent plate and will therefore better control girder end twist. While this may not significantly enhance the girder buckling strength, it will help mitigate construction fit-up issues and aid in keeping the girder web plumb during the concrete deck placement. Finally, while the stiffness of the split pipe connection does help stabilize the girder end, the majority of its benefit seems to be the warping restraint the detail provides. This impact is discussed in the next section.

5.5 SPLIT PIPE STIFFENER WARPING RESTRAINT PARAMETRIC STUDY

The results of the twin girder buckling tests described in Chapter 3 (Experimental Program) showed that the split pipe stiffener significantly increased the buckling capacity of the girders in the laboratory. To extend these results to other cross sections and pipe sizes and find an analytic equation to calculate the increased girder buckling capacity due to the warping restraint provided by a split pipe stiffener, a parametric study was conducted using the cross section, pipe diameter and span-to-depth ratio as the primary variables.

In Chapter 2 (Background) a method to predict the buckling capacity of a split pipe stiffened girder was proposed. This method used a torsional effective length factor (K_z) in the non-uniform torsional resistance portion of the basic buckling strength equation as shown in Equation (2.55) (repeated below for convenience).

$$M_{cr} = \mathrm{C_b}\pi/L_b\sqrt{EI_yGJ + \pi^2E^2C_wI_y/(K_zL_b)^2} \tag{2.55}$$

To determine K_z the use of the no sway alignment chart from the AISC Manual of Steel Construction was proposed with G_z values as given in Equation (2.56) (repeated below). However, to properly calculate G_z, the split pipe boundary conditions must be known. Therefore a multiplier (m) was proposed to account for the changes in the relative flexural stiffness of the girder flange to pipe torsional stiffness. The purpose of

this parametric study was to find suitable values for *m* that give good agreement between the finite element model and Equation (2.55) and to determine if the increase in buckling capacity due to the split pipe warping restraint was significant when the girder and pipe geometries were varied.

$$G_z = \left(\frac{EI}{L_b}\right)_{flange} \Big/ m\left(\frac{GJ}{L}\right)_{pipe} \tag{2.56}$$

The parametric study focused on a single girder with simple supports and no twist at the end. The cross section, loading condition, pipe diameter, and span lengths were all varied during the study. The girder cross sections used were those pictured in Figure 5.1. A variety of loads were considered including, uniform moment, a point load at mid-span, and distributed loads. The point loads and gravity loads were applied at midheight of the cross section. Pipes ranged in diameter from half the flange width to two inches less than the flange width and were ½" thick. Span-to-depth ratios that were considered ranged from 10 through 40.

After running all the cases, a trial and error analysis was employed to find values of *m* for ranges of the ratio of the pipe torsional stiffness to the flange flexural stiffness. The results of this analysis are summarized in Table 5.1. Results for three cross sections and three different loading conditions are given in Figure 5.25, Figure 5.26, and Figure 5.27 for the largest and smallest pipe diameters considered. The results are normalized by the non-stiffened buckling capacity of the cross section at the span-to-depth ratios plotted. Results for the other cross sections and load cases that were considered are provided in Appendix C (Parametric Study Results).

Table 5.1: m-values

m	$\frac{\left(\frac{GJ}{L}\right)_{pipe}}{\left(\frac{EI}{L}\right)_{flange}}$
1.0	< 4
1.5	≥4 and <6
3.0	≥ 6

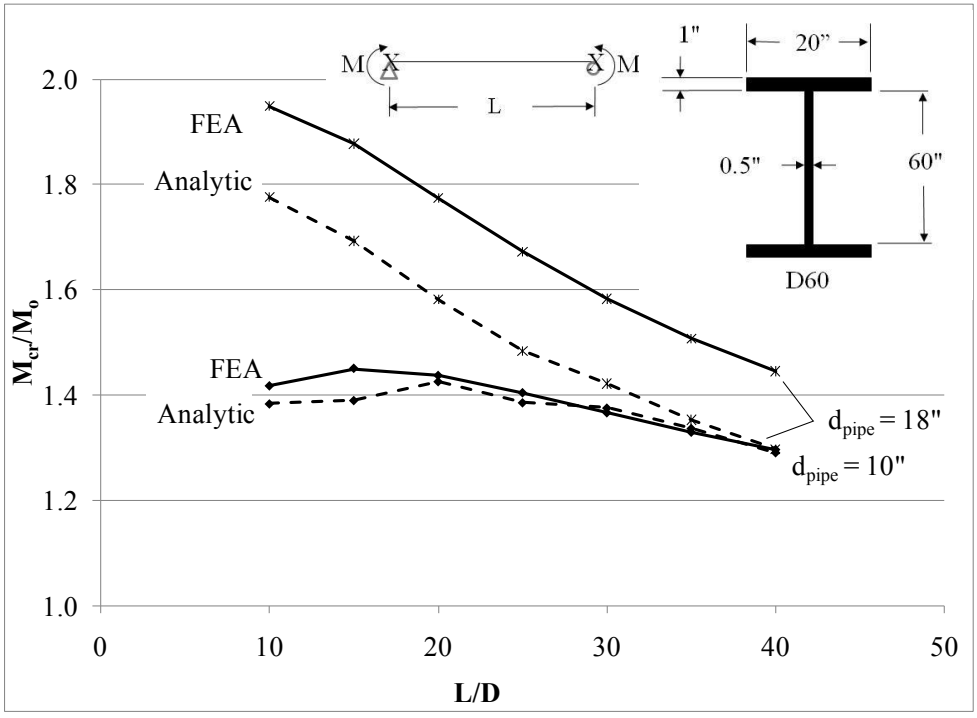

Figure 5.25: D60 split pipe stiffened buckling capacity (uniform moment)

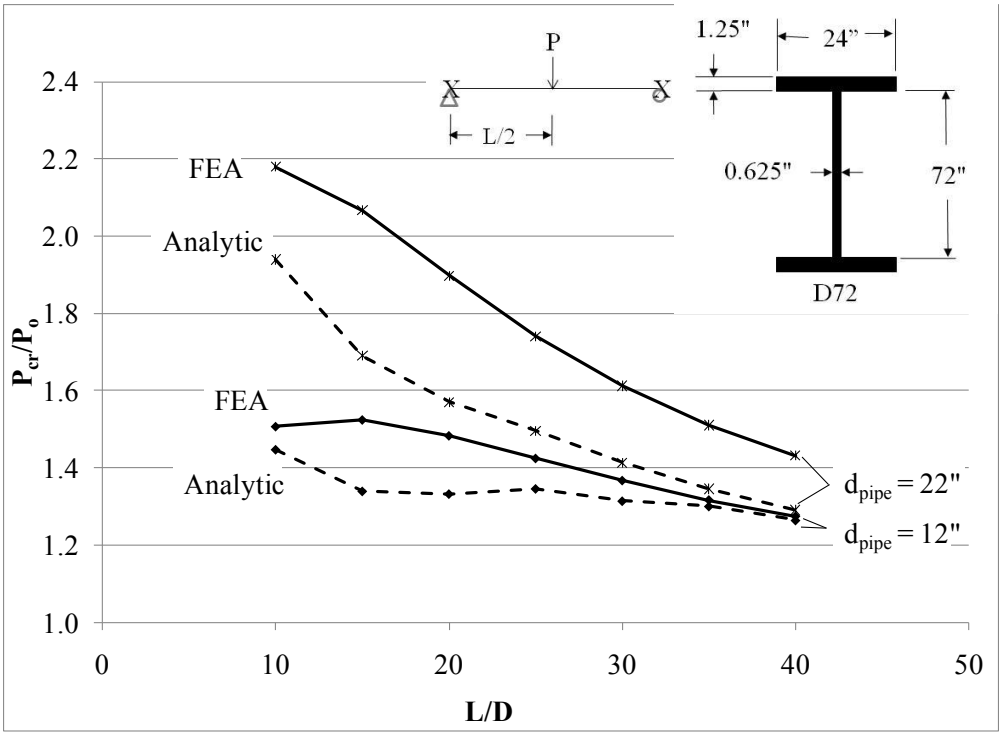

Figure 5.26: D72 split pipe stiffened buckling capacity (mid-span point load)

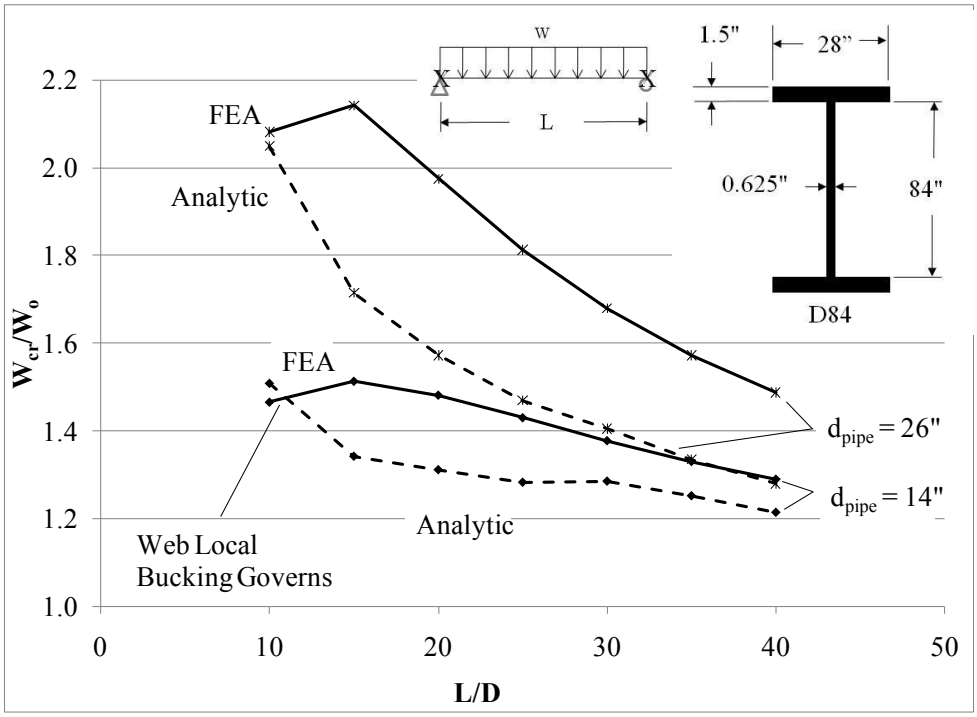

Figure 5.27: D84 split pipe stiffened buckling capacity (distributed load)

The results in the preceding three charts show good agreement between the FEA model and the analytic solution. All other cases, including the pipe diameter values between the ones displayed, show similar good agreement. From the graphs it can be seen that, as in the twin girder laboratory buckling results, the warping restraint provided by the split pipe significantly strengthens the elastic buckling capacity of the girders from 40% to 80% in the 20-30 span-to-depth ratio range. Also, the analytic solution is moderately conservative when larger pipe sizes are used and less so when smaller pipe sizes are used. The reasons for these deviations can be explained based on the underlying assumptions made in formulating the analytic solution.

Equation (2.55) is based upon the assumption that the split pipe stiffener will only impact the warping resistance of the cross section. However by adding the split pipe stiffener to the girder cross section, the torsional constant at the ends of the girder is changed from that of an open I-shaped section to a closed shape and the rate of change of the twist in the cross section is reduced at the end regions. Therefore the uniform torsional resistance of the cross section increases significantly at the girder ends (Heins and Potocko 1979). This increase is reflected in the near uniform difference of about 20% between the analytic solution, which does not account for this increase, and the FEA solution. As the pipe diameter decreases, so does the increase in the girder's uniform torsional resistance. This is reflected in the much smaller difference between the analytic solution and the FEA results at the smaller pipe diameters.

Another source of deviation between Equation (2.55) and the FEA solution is the discrete *m*-values selected to determine G_z. The *m*-value will actually vary between the discrete ratio limits shown in Table 5.1. As the values of $(GJ/L)_{pipe}/(EI/L)_{girder}$ are closer to the limits given in Table 5.1, the accuracy of the analytic solution improves. This can be seen from the values shown on the graphs in Figure 5.28 and Figure 5.29. Where the relative stiffness ratio (value shown on the upper horizontal axis) is close to the limits of 4 and 6, the solution is very accurate. As the relative stiffness ratios get farther from the Table 5.1 values, the analytic solution becomes more conservative.

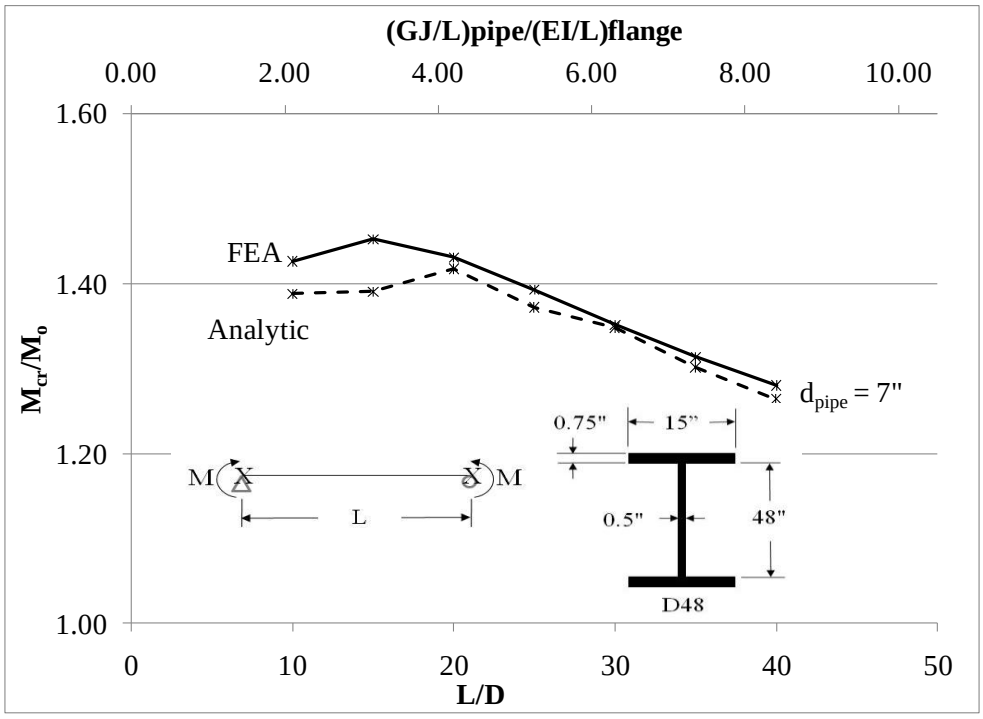

Figure 5.28: D48 split pipe stiffened buckling capacity (uniform moment)

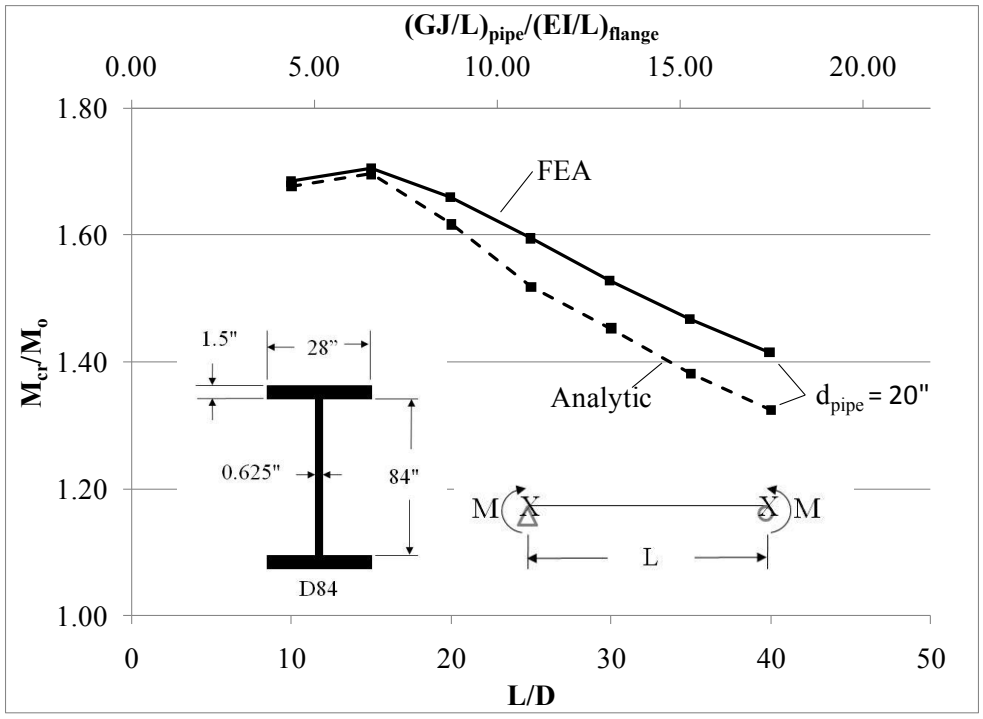

Figure 5.29: D84 split pipe stiffened buckling capacity (uniform moment)

5.5.1 Warping Restraint Summary

As was demonstrated with the laboratory testing results discussed in Chapter 3 (Experimental Program), warping restraint applied at the ends of the section can provide a significant increase in a girder's elastic buckling capacity in the wide range of girder and pipe geometries investigated. The use of Equation (2.55) with the *m*-values given in Table 5.1 had good agreement with the finite element results and can be used to calculate the increase in buckling capacity due to a split pipe stiffener at the girder end. The results summarized in this chapter have focused on the elastic buckling behavior. The recommendations should be applicable up to the elastic limit of the material.

5.6 PARAMETRIC STUDY RESULTS CONCLUSIONS

Several conclusions can be drawn from the results of the parametric studies. Most importantly, the skewed cross frame connection stiffness is not infinite as currently assumed. Whether a split pipe or bent plates are used, the connection stiffness is finite and in the cases studied can decrease the cross frame stiffness by 20% or more.

Designers have several options possible to increase the stiffness of connections in skewed end cross frames. First, if a bent plate is used, the bent plate and connection plate thickness can be increased. Increasing the thickness of the connection plate is generally more efficient than just increasing the bent plate thickness. The most effective result was increasing the thickness of both the bent plate and the connection plate. Second, the designer may choose to use a split pipe stiffener connection rather than the bent plate.

The split pipe stiffener connection was shown to significantly increase the connection stiffness and reduce twist at the girder ends. While end twist was not a significant factor in decreasing the girder buckling strength, reducing girder end twist will help ease cross frame fit-up issues during erection and help achieve a vertical web at the girder ends when the concrete slab is placed. However, the largest source of stability for the split pipe stiffener comes from the warping restraint provide to the girder end.

The impact of warping restraint was shown to be significant in all the cases investigated. By increasing the elastic buckling strength in the end spans, the first row of

intermediate cross frames may be moved farther from the abutment and therefore reduce the differential deflections along the first row of intermediate cross frames. This in turn will mitigate the fatigue issues in connecting the intermediate cross frames to the girder tension flange.

CHAPTER 6
Conclusions and Recommendations

6.1 CONCLUSIONS

The results of this research demonstrated that the split pipe stiffener cross frame connection is much stiffer than the current bent plate connection detail. Using the stiffer split pipe connection will help limit girder end rotations compared to the current bent plate connection detail. In addition to a stiffer connection, the split pipe stiffener offers warping restraint to the end of the girder which significantly increases the girder elastic buckling strength and corresponding unbraced length. Therefore, using the split pipe stiffener to increase the girder buckling capacity near the abutments will likely allow the first row of intermediate cross frames to be moved farther away from the abutment. Doing so will move the intermediate cross frames into a region of smaller differential girder deflections and therefore reduce the live load forces induced in the cross frames and mitigate the potential for associated fatigue cracking.

In arriving at the above conclusion, many lessons were learned and several recommendations can be made. These lessons and recommendations are divided among the finite element modeling and design of the bent plate and split pipe stiffener connections and summarized below.

6.1.1 Finite Element Modeling Lessons and Recommendations

Several lessons were learned while modeling the girders and cross frames for this research. First, the ANSYS SHELL93 element proved to be a computationally efficient way to model I-shaped girder buckling. In addition to modeling the flat plates that make up the cross section, the shell element was very accurate in modeling the curved surfaces of the bent plate and split pipe stiffener as long as the bend radius to element thickness ratio was three or greater.

However, using shell elements presents a challenge in appropriately modeling the interface between the elements when the structural components do not intersect at their midsections or have differing mesh densities. It is recommended that if shell elements intersect at their mid-thicknesses with differing mesh densities and little deformation is expected between the elements, constraint equations be used to connect the elements. If the elements do not intersect at their mid-thicknesses or large deformations are expected, then rigid beam elements (ANSYS MPC 184) should be used to make the connection.

Another lesson learned in modeling the connections was the importance of considering the effect of weld geometry on the plate connection stiffness. Two examples where the weld geometry was important in this research were at the bend in the bent plate to connection plate overlap and the plate stiffener to girder welds. It is recommended that weld models using rigid beam elements should be used if there is the possibility that a weld will significantly stiffen a connection. Additionally, when modeling a laboratory specimen with plate stiffeners, the welds should be modeled. In this research, the stiffener to flange welds were found to more accurately engage the warping restraint provided by the stiffeners if the actual weld geometry was included in the model. And finally, if trying to match an analytic solution with a finite element model containing web stiffeners, then constraint equations should be used at the girder to stiffener interface so the finite element model does not contain warping restraint not predicted by the analytic solution.

Modeling the end cross frames with a very detailed shell element model was required in this study to accurately capture the connection stiffness of the skewed cross frames. However, simply modeling the non-skewed intermediate cross frames with truss elements connected at the girder web to flange interface were sufficiently accurate for predicting the laboratory specimen brace forces and girder rotations. Therefore it is recommended that truss elements be used for unskewed cross frame members rather than shell elements as the truss members provide an accurate and computationally efficient solution.

6.1.2 Bent Plate and Split Pipe Stiffener Connection Recommendations

The results of this research demonstrated that the connection stiffness has a significant impact on the end cross frame stiffness and can be the limiting component stiffness at skew angles of 20° or greater. Therefore it is recommended that the connection stiffness be considered in calculating the stiffness of the skewed cross frames for skew angles of 20° or larger using Equation (5.1) below.

$$\frac{1}{\beta_T} = \frac{1}{\beta_{brskew}} + \frac{1}{\beta_{sec}} + \frac{1}{\beta_g} + \frac{1}{\beta_{conn-tors}} \tag{5.1}$$

The torsional stiffness of the bent plates is given in Equation (2.49).

$$\beta_{conn-tors} = \frac{\beta_{conn}\, h_b^2}{\frac{2L_c^2}{S^2} + 1} \tag{2.49}$$

And the effective axial stiffness on an individual bent plate perpendicular to the girder is given in Equation (5.4) and all other variables remain as defined in Chapters 2 and 5.

$$\beta_{conn} = \frac{8}{S}(70\alpha + 5000)e^{-q\alpha} \tag{5.4}$$

If it is found that the bent plate connection needs to be stiffened, it is recommended that the thickness of both the connection plate and bent plate be increased from the standard 1/2" thickness to 3/4" thickness, or that a split pipe stiffener connection be considered as an alternative. The split pipe stiffener offers several advantages over the bent plate stiffener as outlined below.

The split pipe stiffener allows perpendicular connection between the split pipe and the cross frame connection tab for any magnitude skew angle. The detail has the potential to standardize the cross frame connection across a wide variety of bridge applications. Such standardization removes the bent plate variables such as bend radius and plate size that were shown to affect connection stiffness. Also, by serving as a bearing stiffener, the split pipe connection provides good weld access and essentially requires similar total lengths weld compared to the current connection details employed

in Texas that consist of two bearing plate stiffeners and two cross frame connection plates.

The split pipe stiffener also provides warping restraint to the girder which can result in significant increases in the girder buckling capacity. As previously mentioned, the split pipe detail may help alleviate the potential for fatigue issues associated with cross frame locations in skewed bridges. In addition, the split pipe details may reduce the overall number of intermediate cross frames in the abutment region relieving this congested area and leaving fewer connections to inspect during the bridge service life.

Beside the above advantages, the fatigue performance of the split pipe stiffener was found to be at least as good as the current plate stiffener detail and met the AASHTO guidelines for use on highway bridges. However, to preserve this fatigue performance should the split pipe connection be used at an intermediate pier, it is recommended that the cross frame connection plate be welded to the pipe only and not the girder flanges. This will avoid a skewed weld to the tension flange which was found to not perform as well as the split pipe or normal plate stiffener weld.

Finally, laboratory testing showed that for the loading pattern used, intermediate cross frames staggered with the skew angle had much lower brace forces than cross frames that had a continuous layout across the width of the bridge. While further testing needs to be performed to establish this pattern for other loading conditions, staggering the intermediate cross frames offers the possibility to further limit live load cross frame forces and reduce fatigue cracking in skewed bridges.

6.2 RECOMMENDATIONS FOR FUTURE WORK

Based on this study, several additional laboratory tests should be conducted and additional parametric studies should be considered. These recommendations are detailed below.

6.2.1 Recommended Laboratory Tests

Additional full scale three girder laboratory tests should be run at the 53° degree skew angle using bent plate cross frames so that the differences in buckling strength, end rotations, and brace forces can be compared to the split pipe stiffener specimen already tested. Additionally, two other specimens, one with split pipe stiffener cross frames and one with bent plate connections, should be tested at a smaller skew angle to obtain laboratory data to confirm the accuracy of the finite element model at reduced skew angles.

Tests with different girder bearing conditions should also be run to assess the impact of tipping restraint on the bent plate and split pipe connection. While it has been reasonably assumed that tipping restraint is a significant source of girder stability, no known laboratory data exists to check the impact on end cross frame forces and girder end rotations in skewed bridges.

Laboratory testing should be considered to improve the connection between the brace member and the connection plate welded to the split pipe stiffener. The current split tube connection may not offer the best transfer of forces, may have fatigue issues, and may not be easily fabricated. While this current connection may be adequate, significant efficiency could be gained if a better connection was found.

Finally, if the split pipe stiffener is to be used away from the support region, distortional fatigue tests should be run to check the gap region between the flange and connection plate weld. If there is significant deformation allowed in this region then fatigue cracking may be an issue. Finally, if the brace member is used to provide significant support to the slab edge at the abutment, then distortional fatigue may be an issue at the abutment as well.

6.2.2 Recommended Parametric Studies

Several other parametric studies should be run to assess the effect of the split pipe stiffener and intermediate bracing patterns on the brace forces and girder end rotations in skewed bridges. Expanded loading conditions could be checked with the staggered and

continuous bracing patterns used in this study to check how the intermediate brace forces change with different loading patterns. Additionally, studies could be run to assess the impact of the split pipe stiffener at the negative moment region of an intermediate support as well as its impact on singly symmetric I-shaped sections. Finally, a parametric study could be used to verify the equations used to predict girder end twist in order to aid in ensuring girder webs are plumb after concrete deck placement.

APPENDIX A

Large Scale Experimental Results

A.1 GIRDER INITIAL IMPERFECTIONS

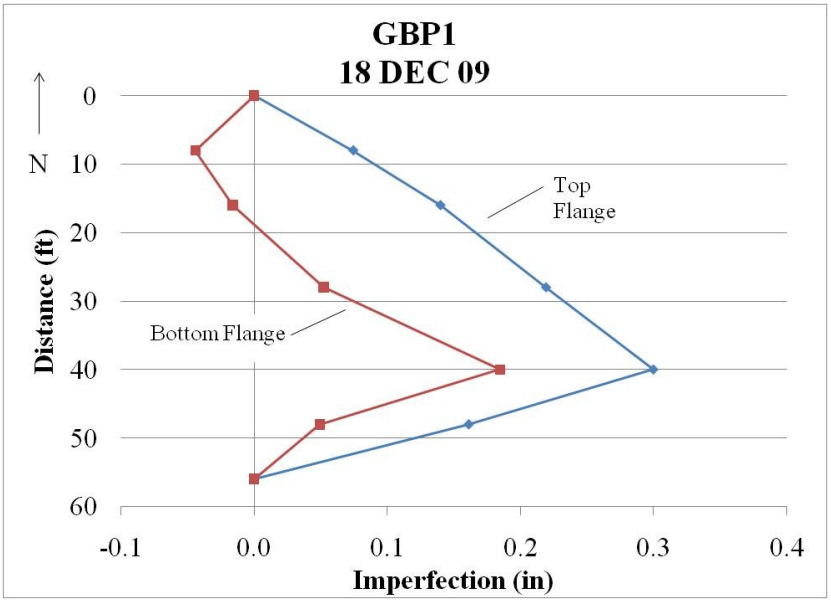

Figure A.1: Girder GBP1 Initial Imperfection as of 18 DEC 09

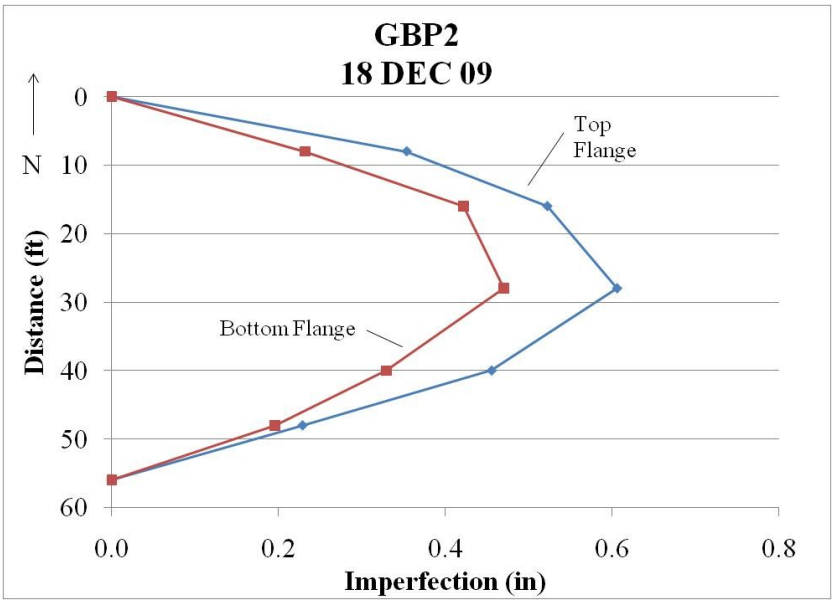

Figure A.2: Girder GBP2 Initial Imperfection as of 18 DEC 09

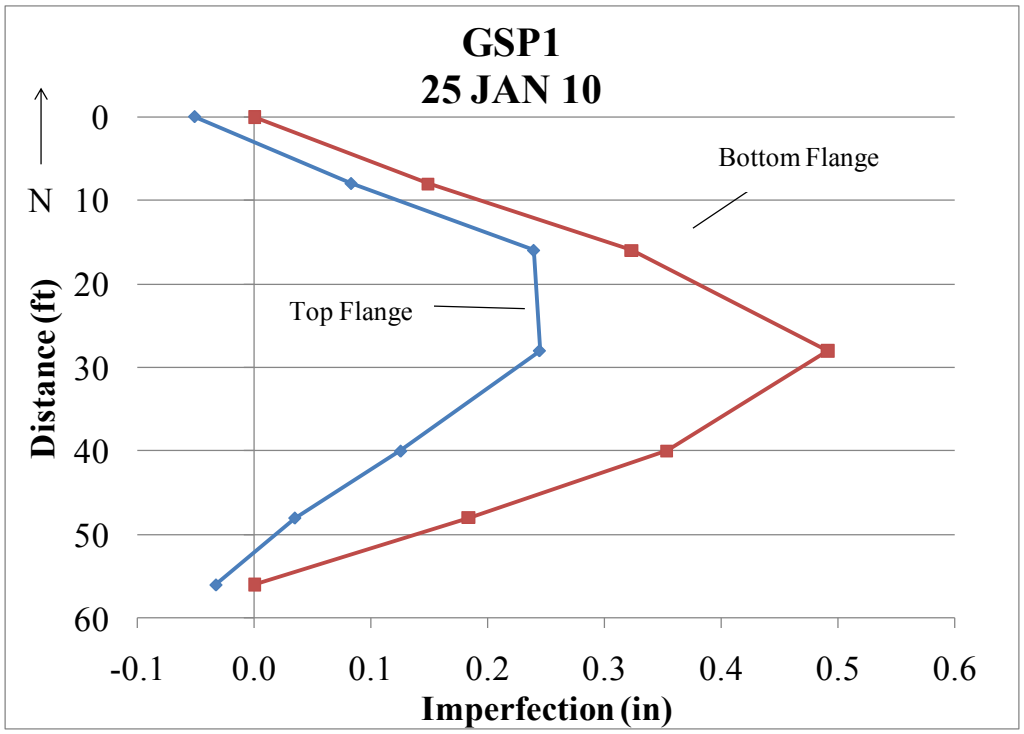

Figure A.3: Girder GSP1 Imperfection as of 25 JAN 10

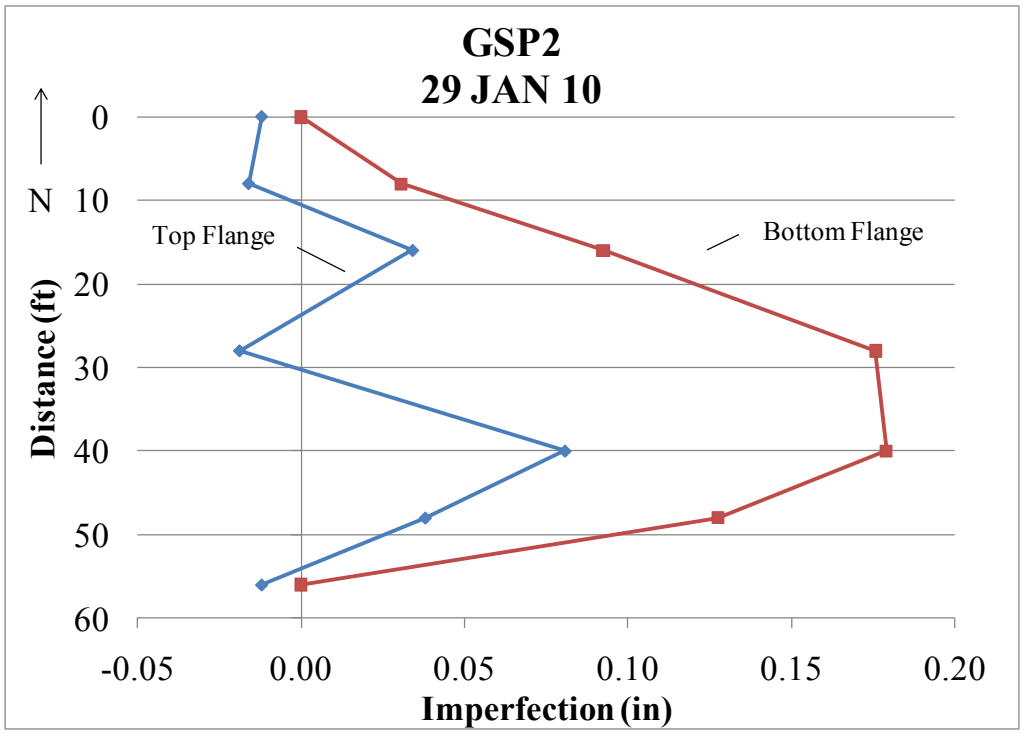

Figure A.4: Girder GSP2 Imperfection as of 25 JAN 10

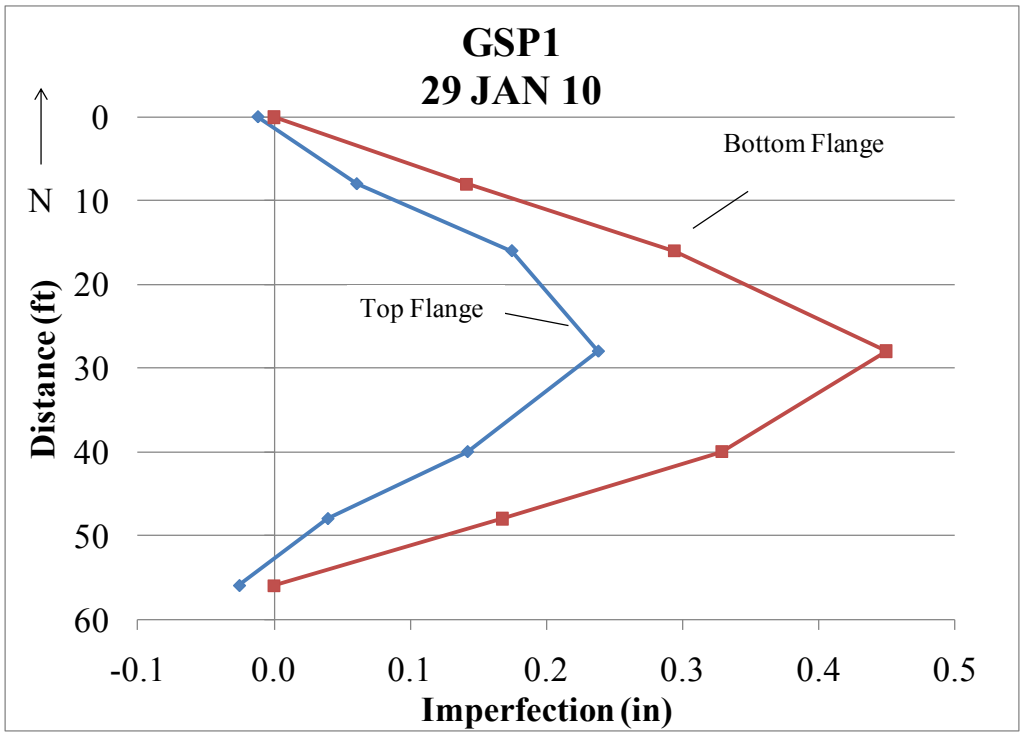

Figure A.5: Girder GSP1 Imperfection as of 29 JAN 10

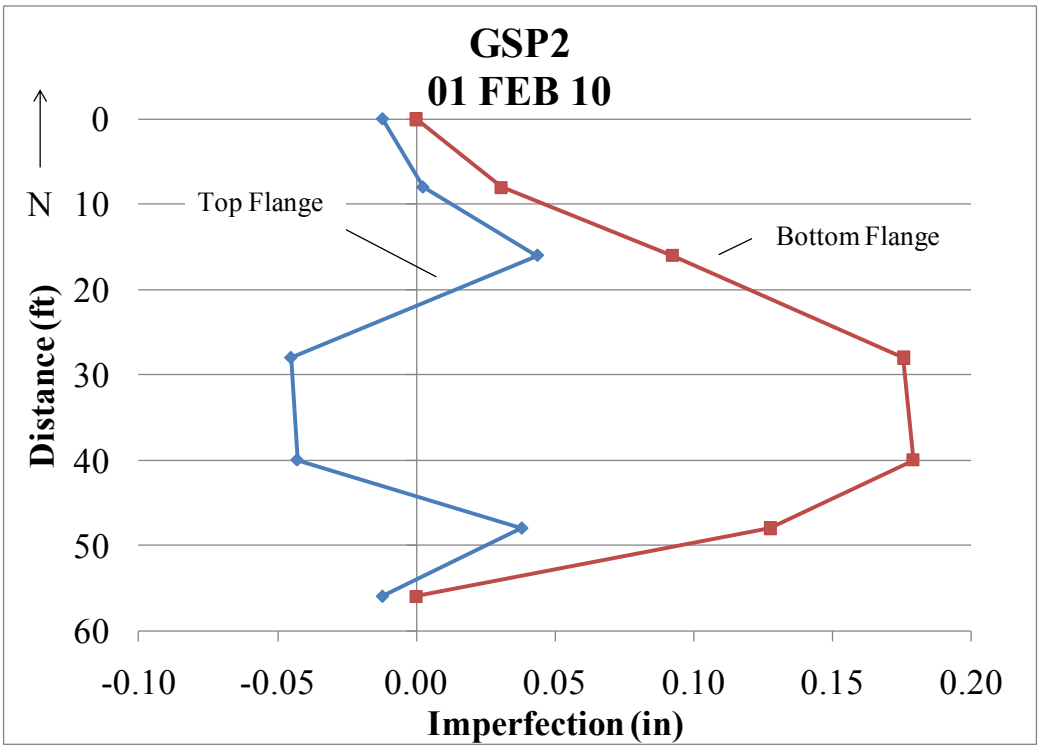

Figure A.6: Girder GSP2 Imperfection as of 1 FEB 10

A.2 TWIN GIRDER BUCKLING TEST RESULTS

A.2.1 Plate Stiffened Specimens (GBP1 and GBP2)

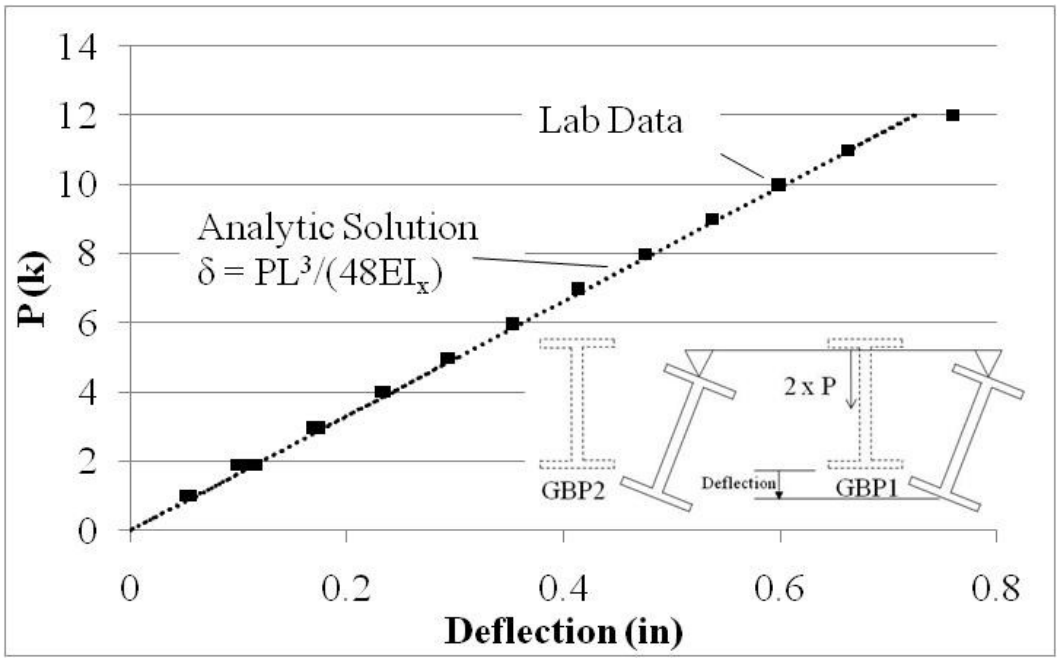

Figure A.7: GBP1 mid-span vertical deflection (down is positive)

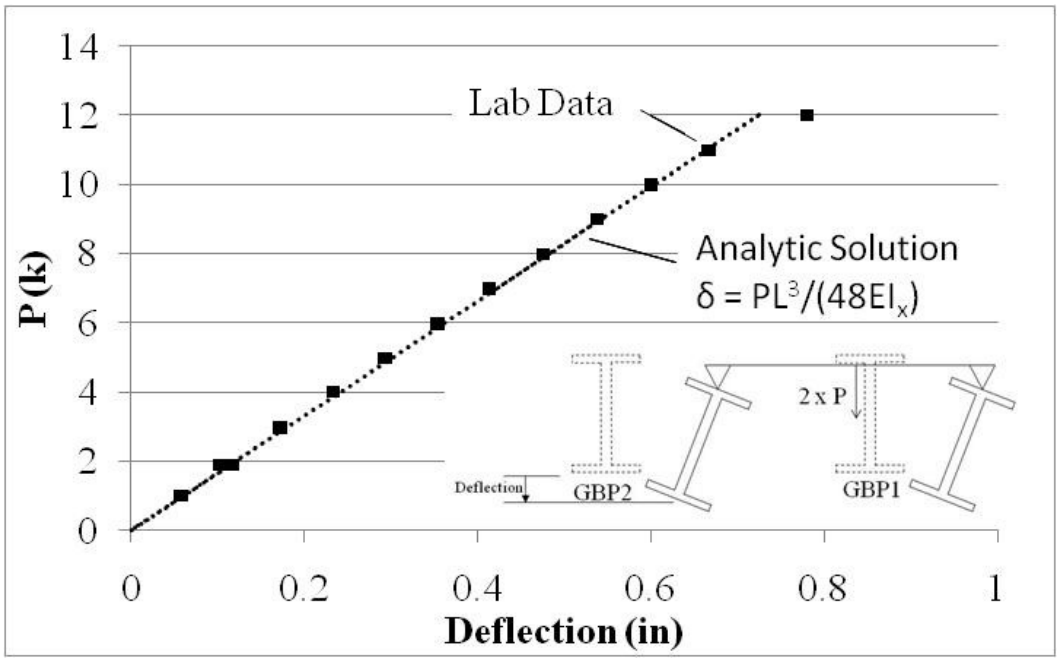

Figure A.8: GBP2 mid-span vertical deflection (down is positive)

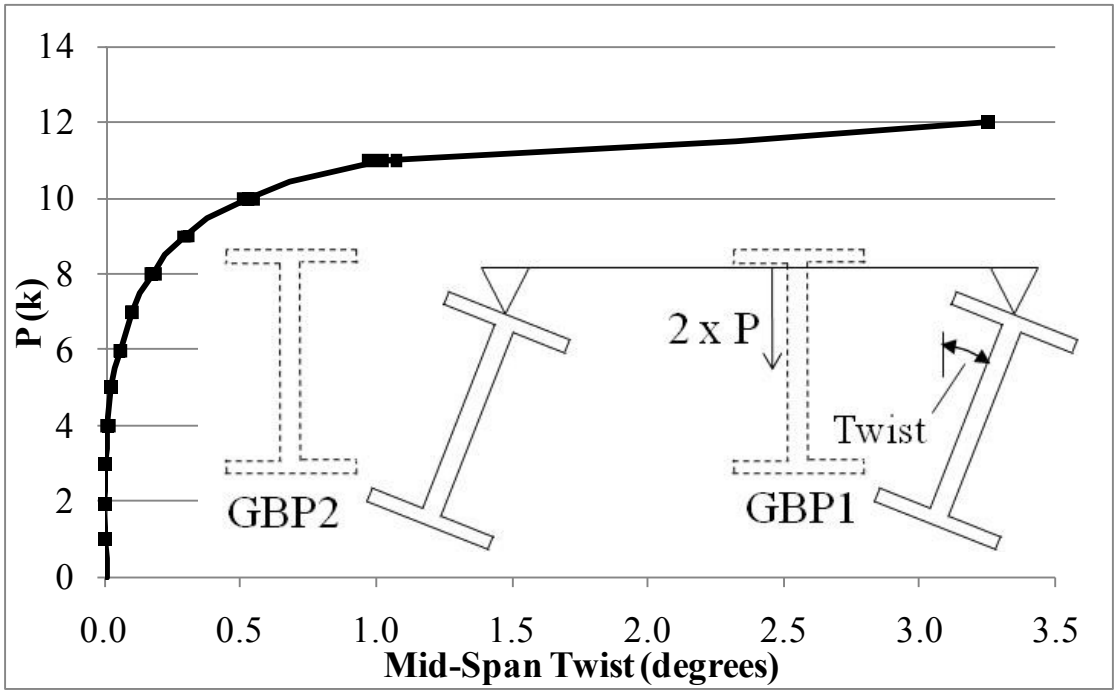

Figure A.9: GBP1 mid-span twist (CW looking north is positive)

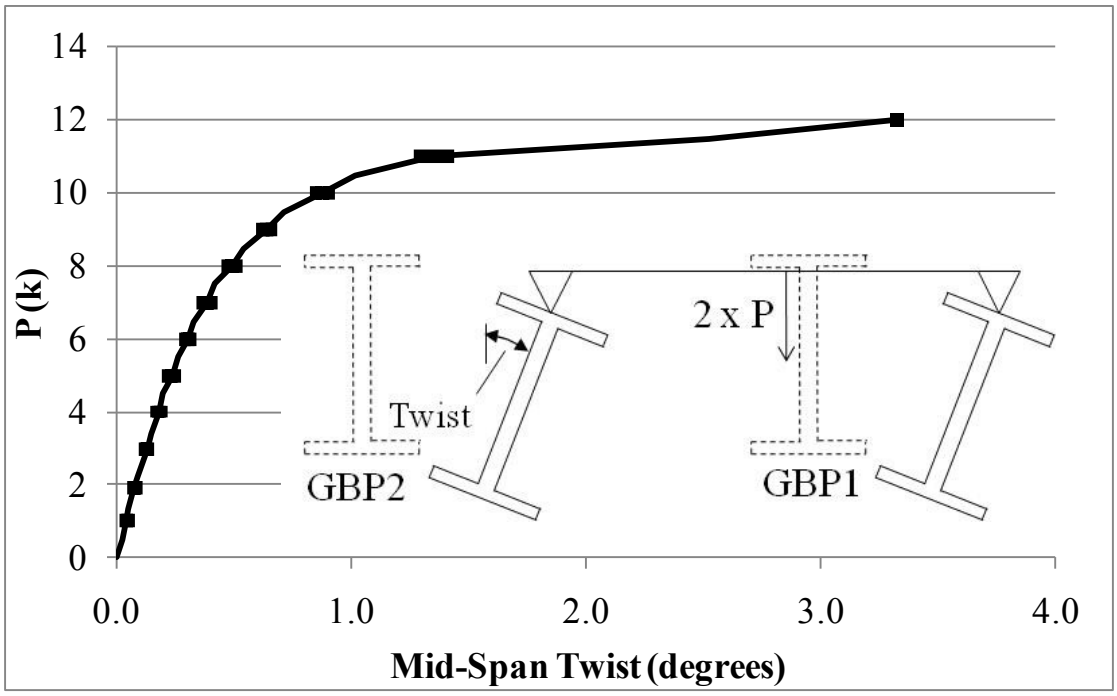

Figure A.10: GBP2 mid-span twist (CW looking north is positive)

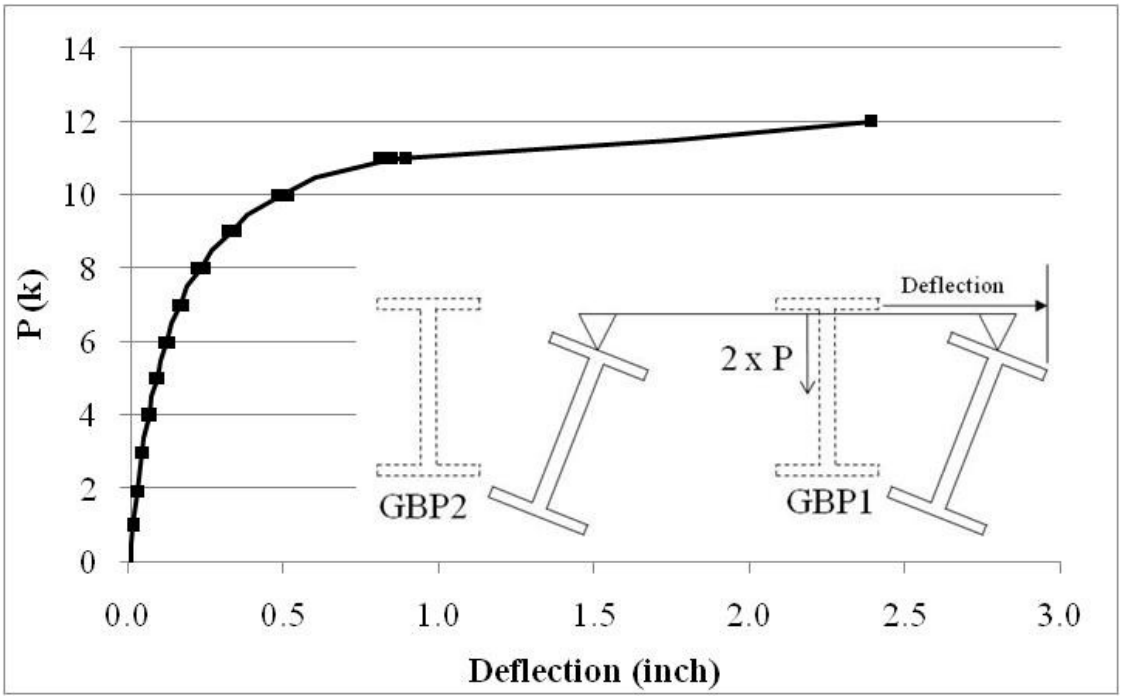

Figure A.11: GBP1 mid-span top flange lateral deflection (east is positive)

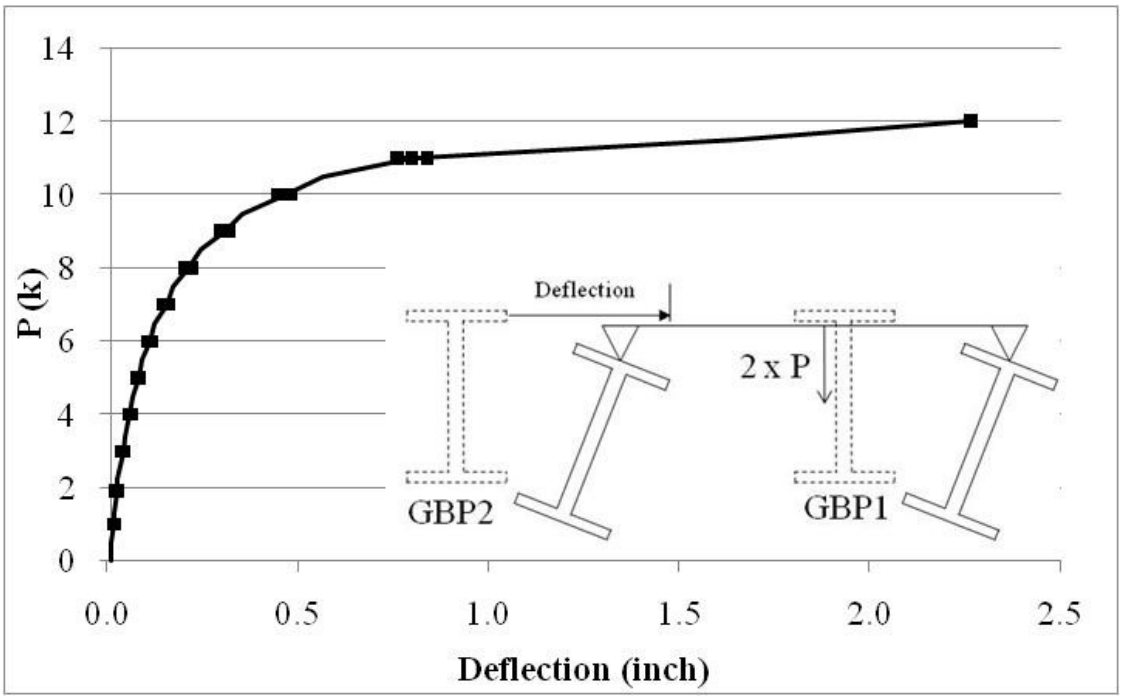

Figure A.12: GBP2 mid-span top flange lateral deflection (east is positive)

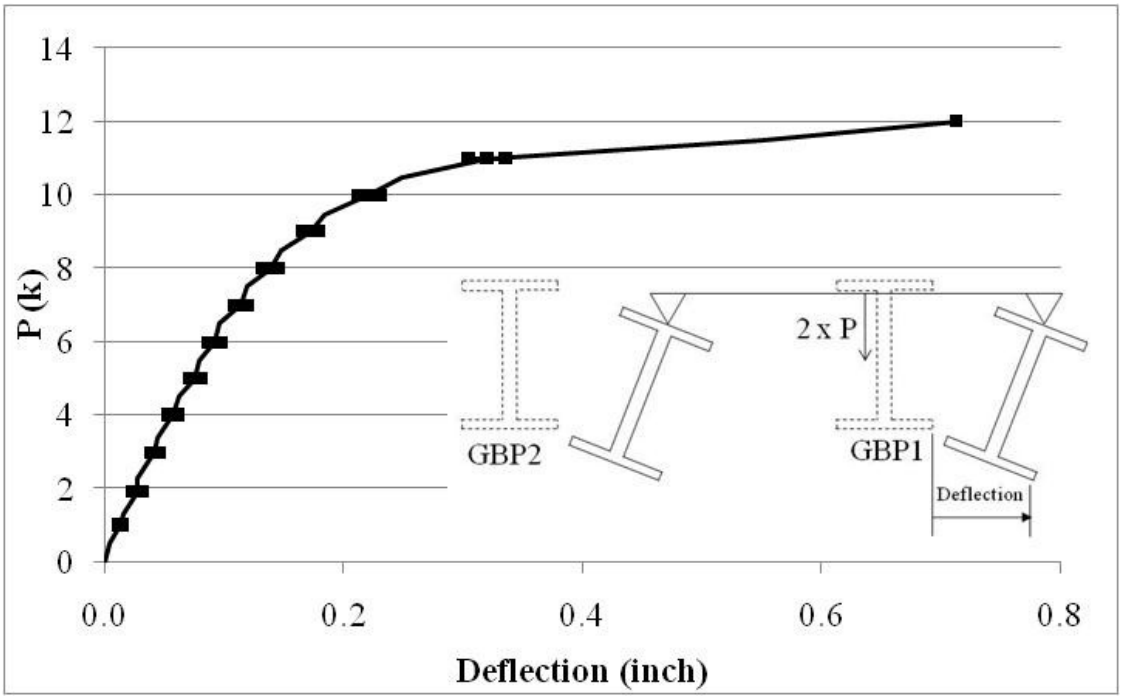

Figure A.13: GBP1 mid-span bottom flange lateral deflection (east is positive)

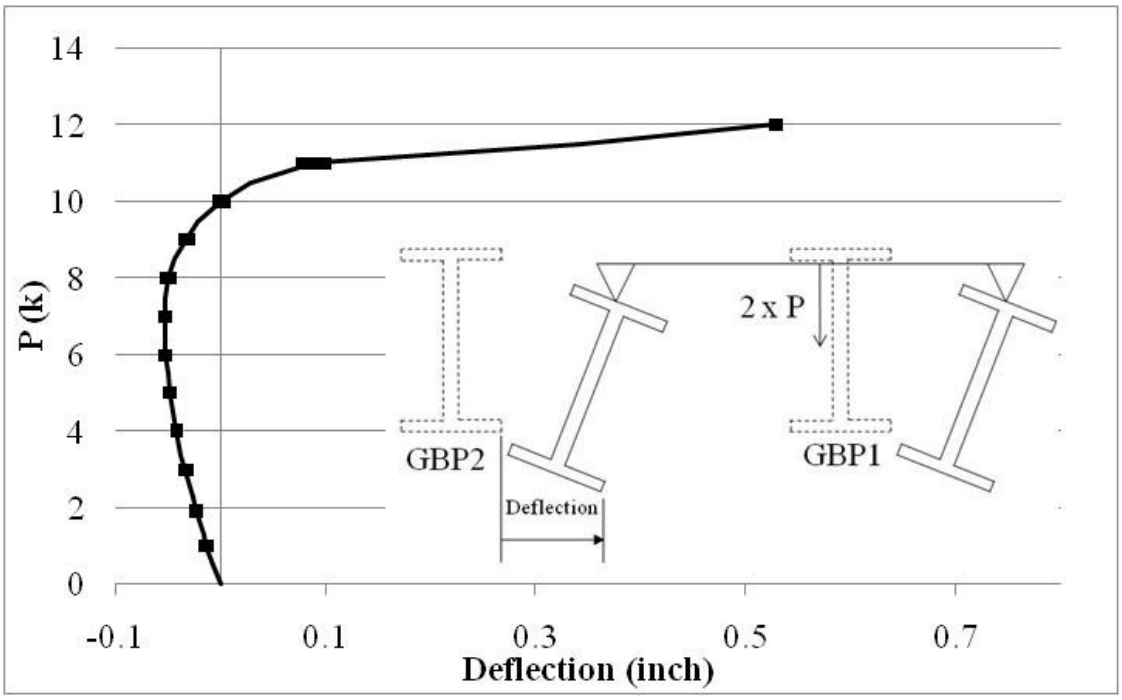

Figure A.14: GBP2 bottom flange mid-span lateral deflection (east is positive)

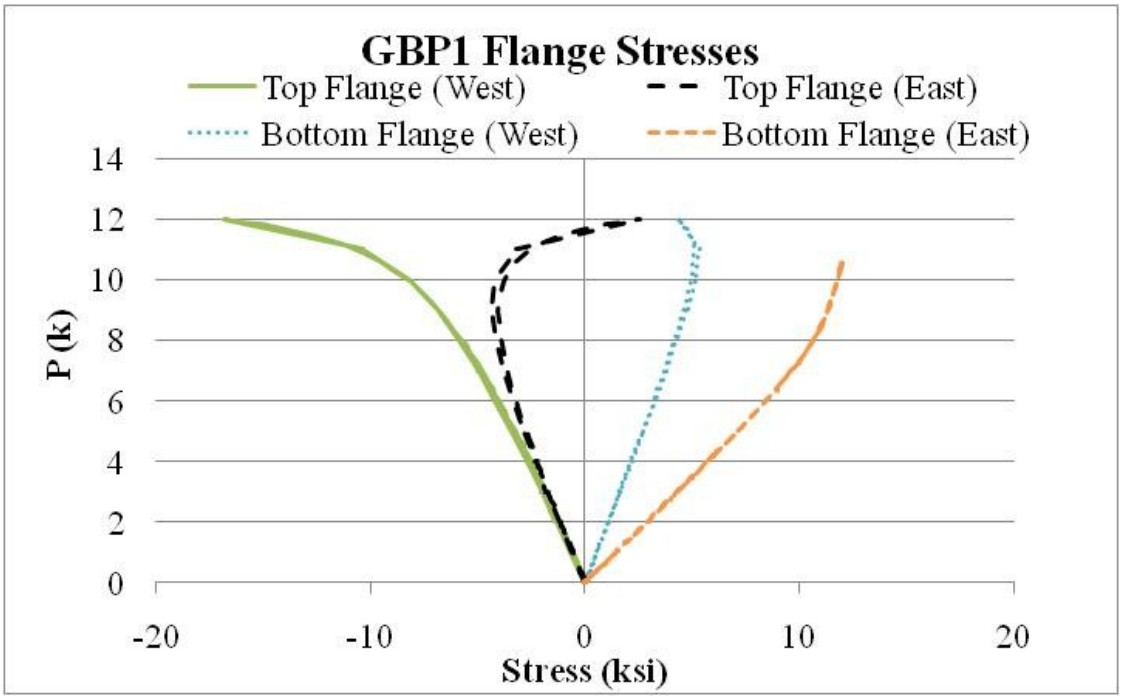

Figure A.15: GBP1 mid-span flange stresses (tension is positive)

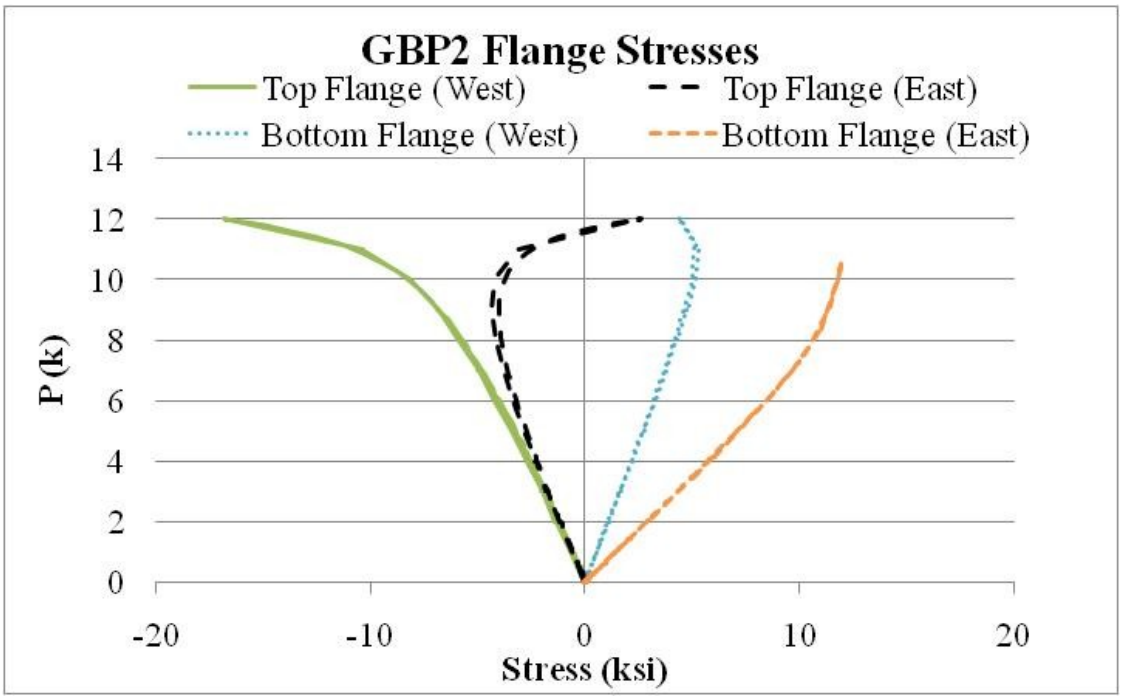

Figure A.16: GBP2 mid-span flange stresses (tension is positive)

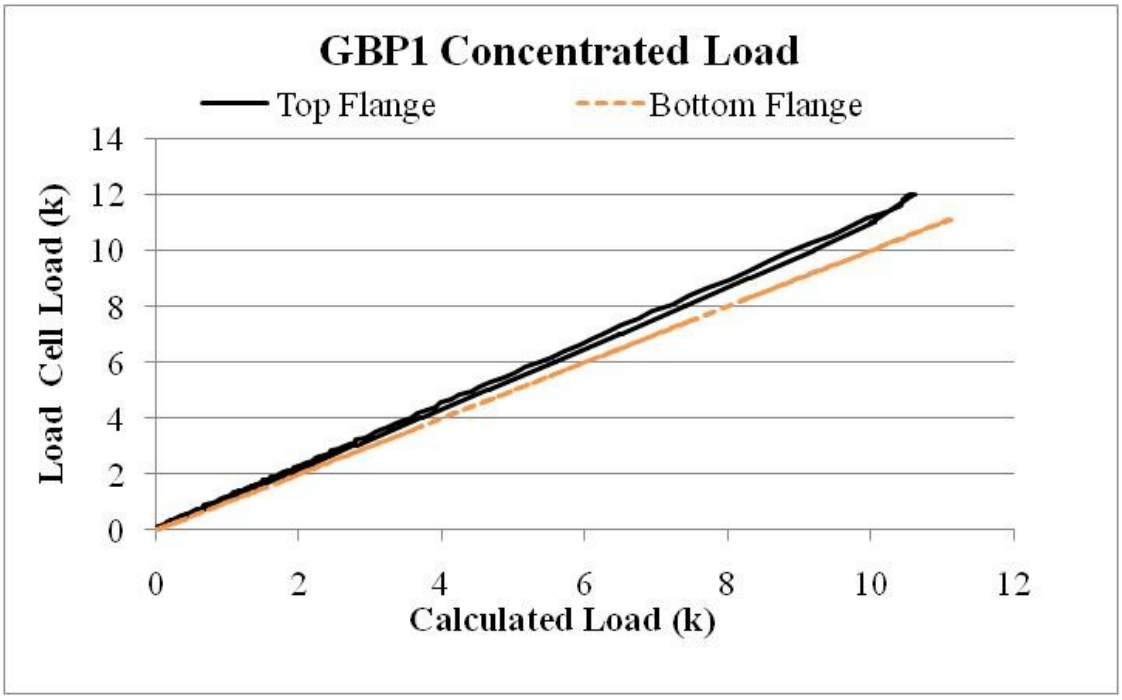

Figure A.17: GBP1 calculated applied load from mid-span flange stresses

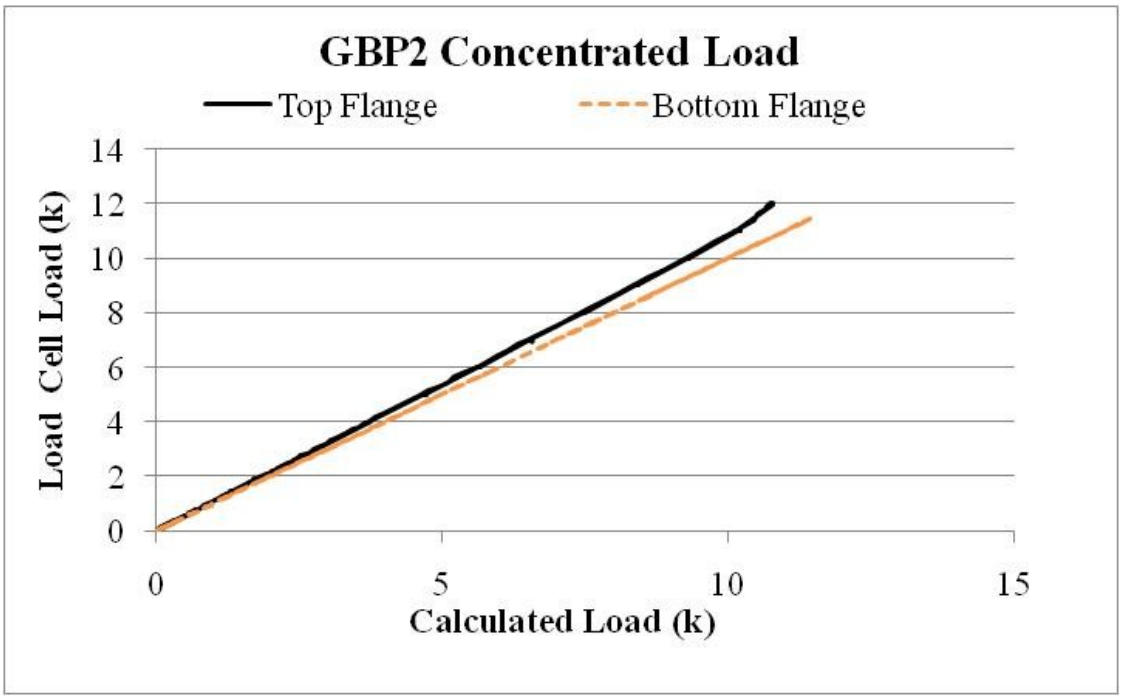

Figure A.18: GBP2 calculated applied load from mid-span flange stresses

A.2.2 Pipe Stiffened Specimens (GSP1 and GSP2)

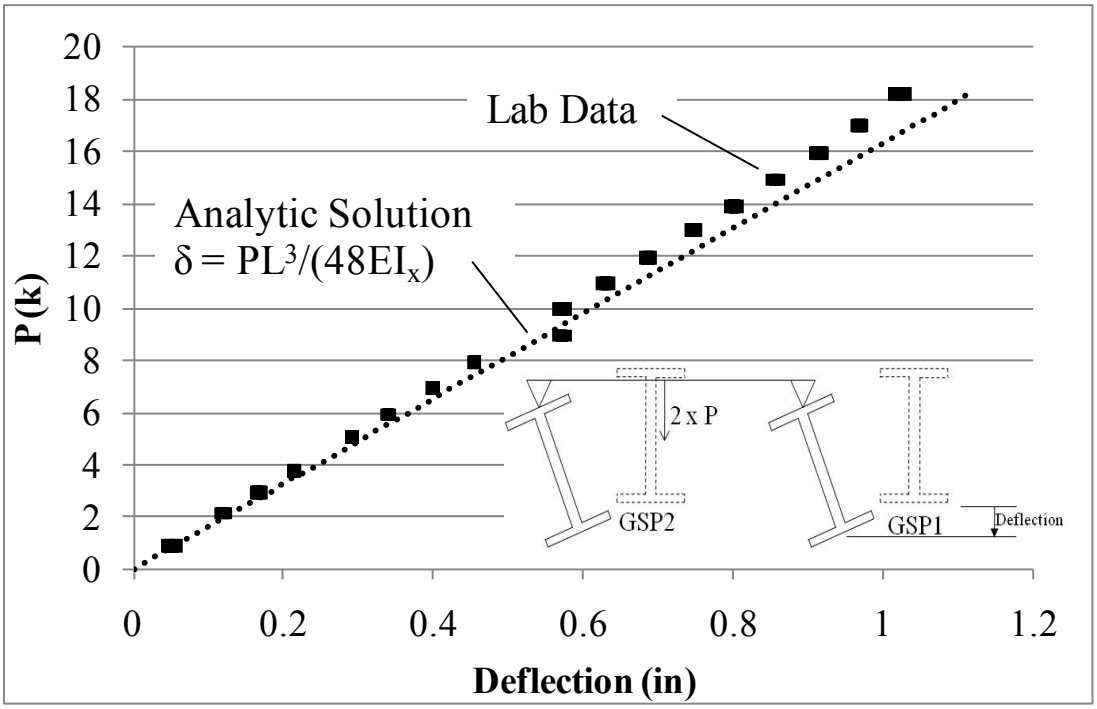

Figure A.19: GSP1 mid-span vertical deflection (down is positive)

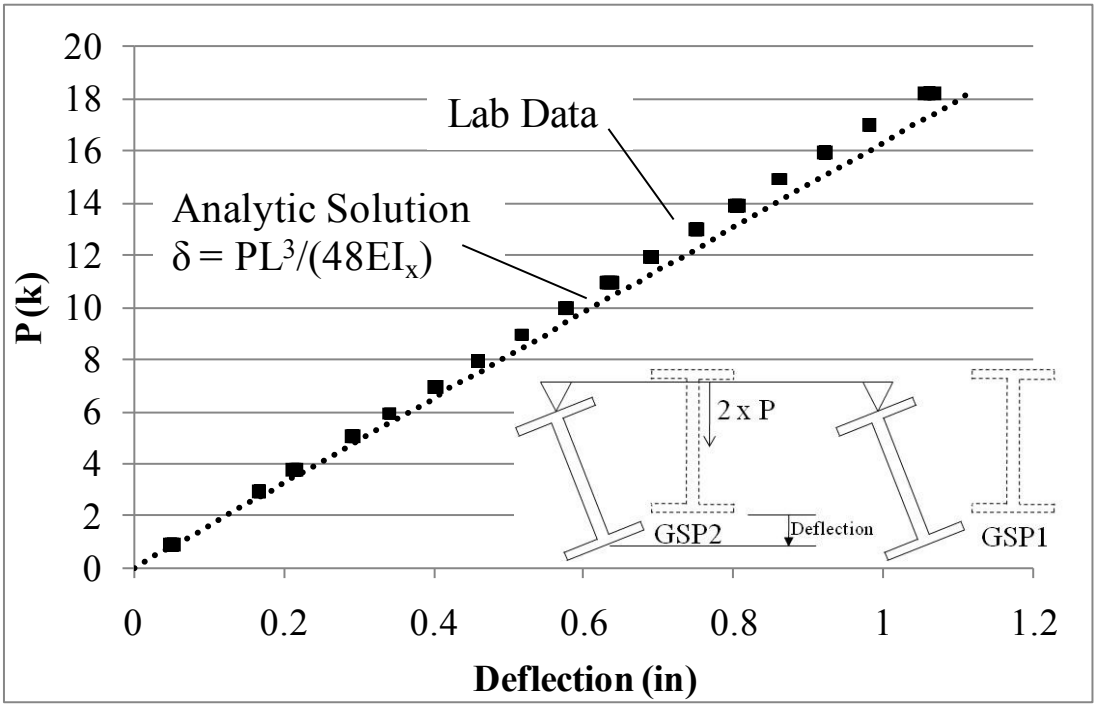

Figure A.20: GSP2 mid-span vertical deflection (down is positive)

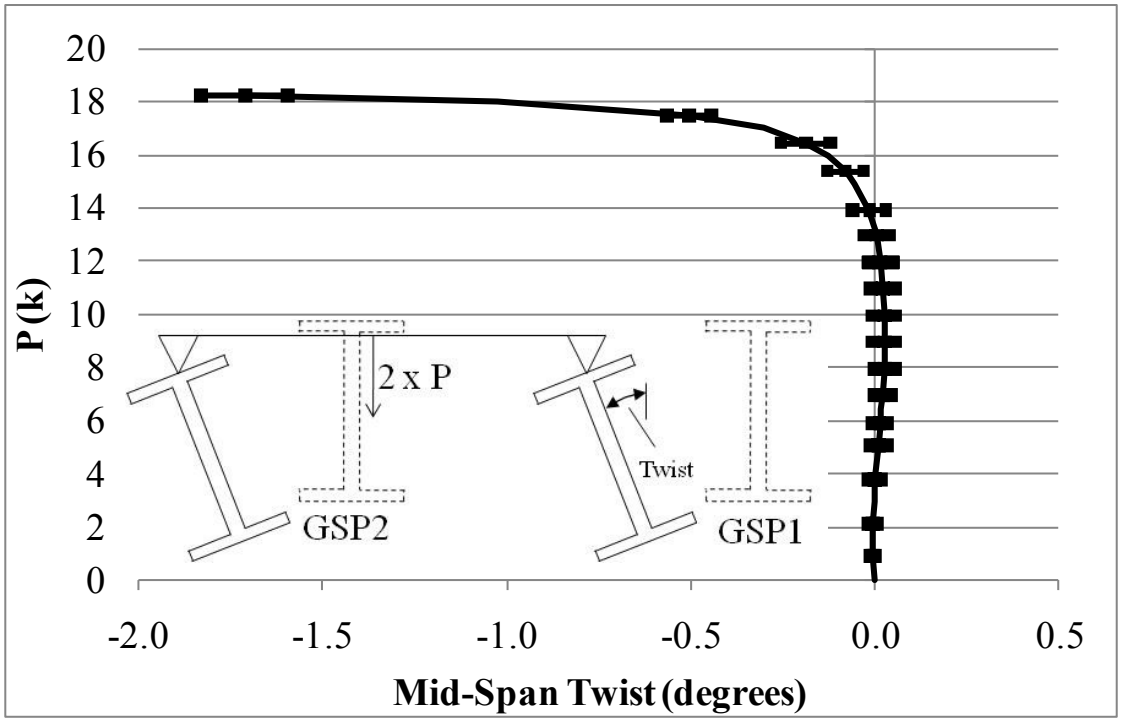

Figure A.21: GSP1 mid-span twist (CW looking north is positive)

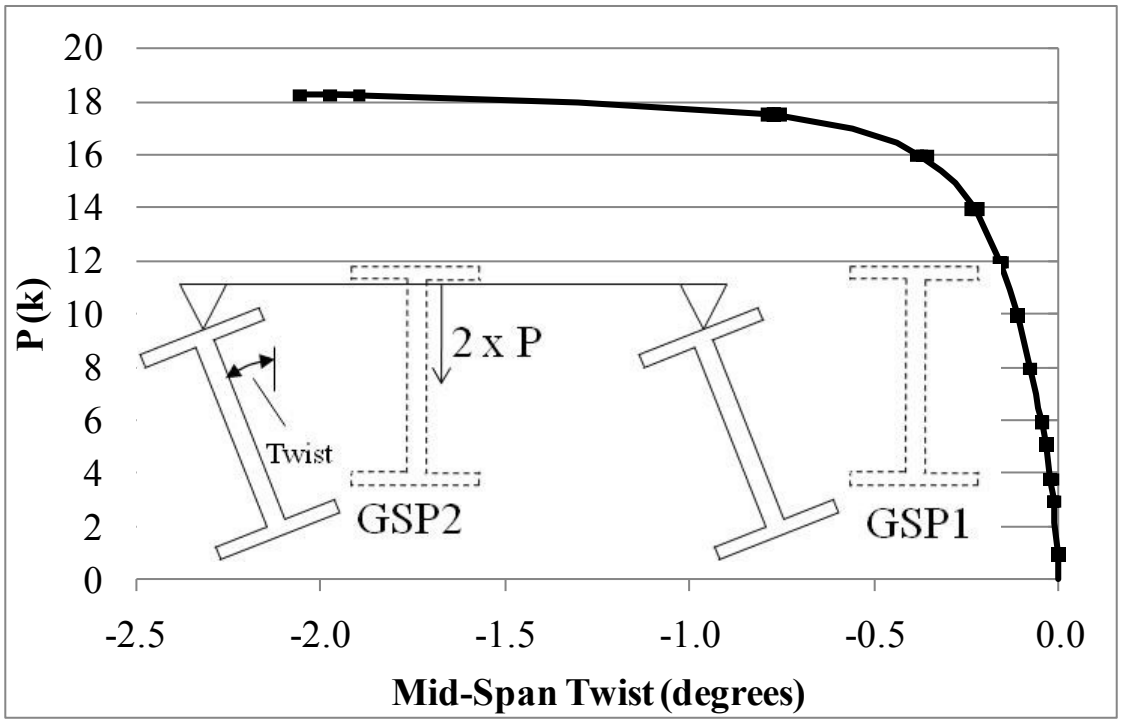

Figure A.22: GSP2 mid-span twist (CW looking north is positive)

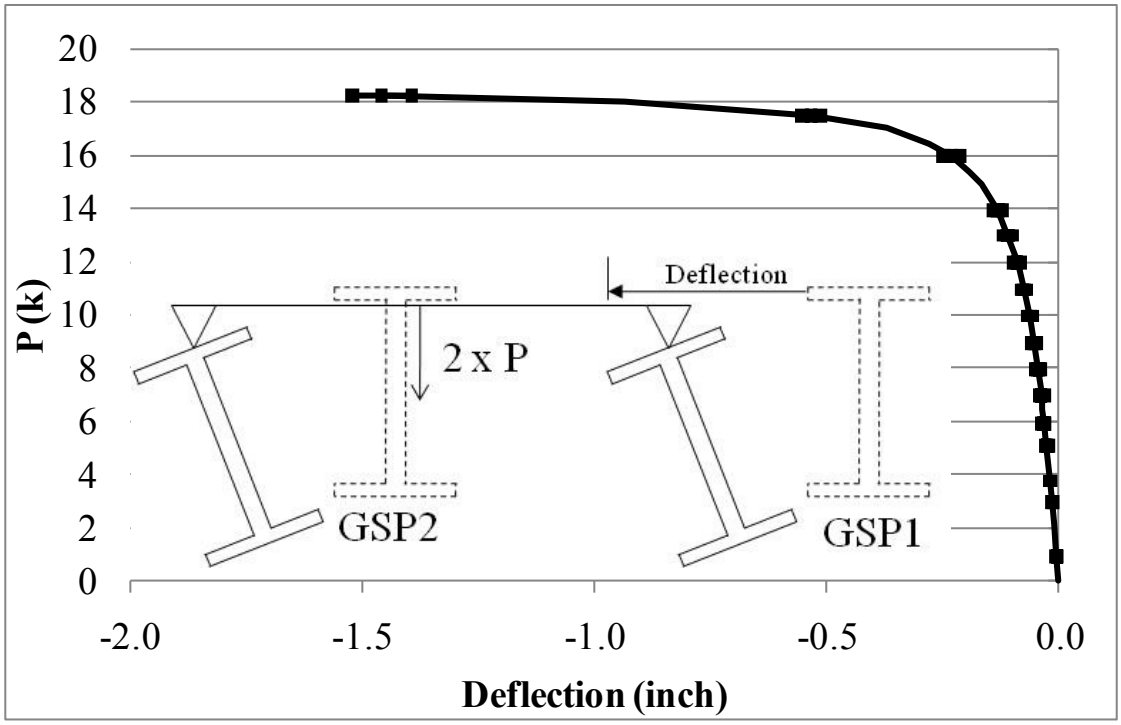

Figure A.23: GSP1 mid-span top flange lateral deflection (east is positive)

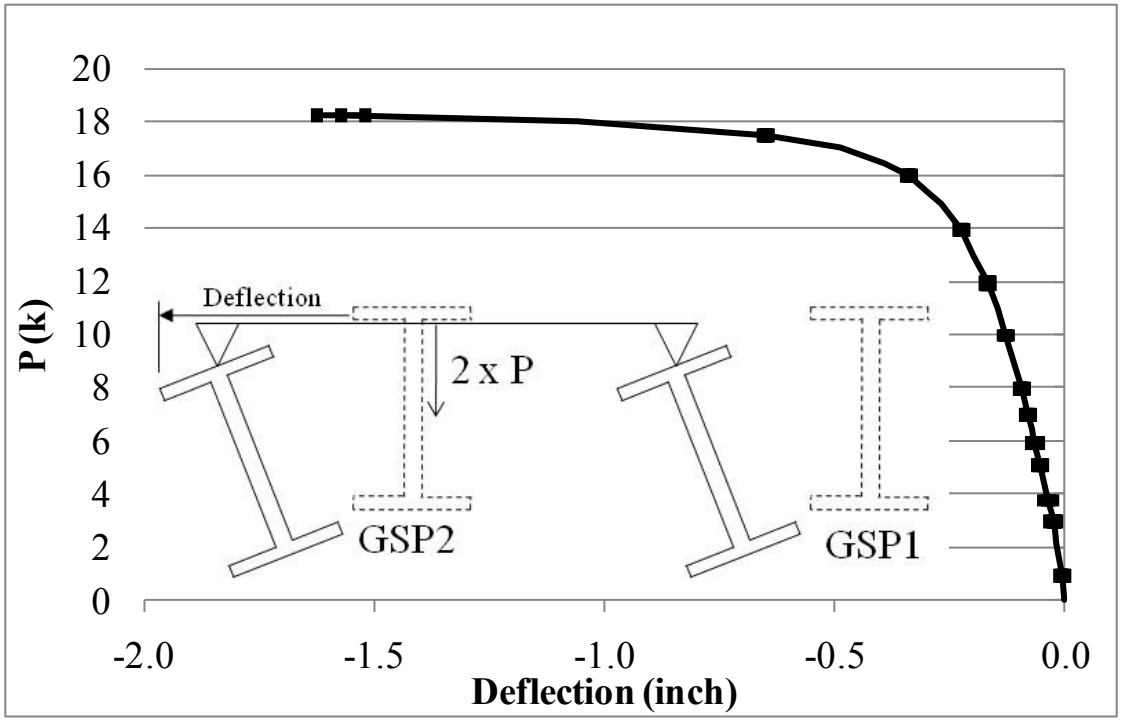

Figure A.24: GSP2 mid-span top flange lateral deflection (east is positive)

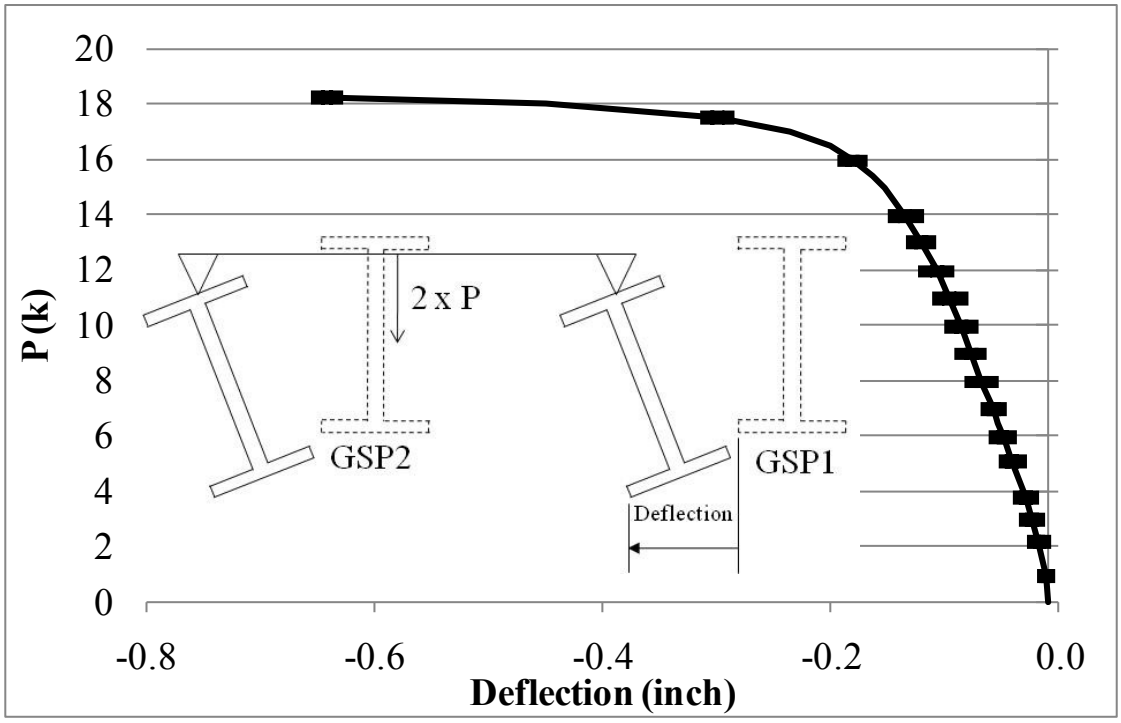

Figure A.25: GSP1 mid-span bottom flange lateral deflection (east is positive)

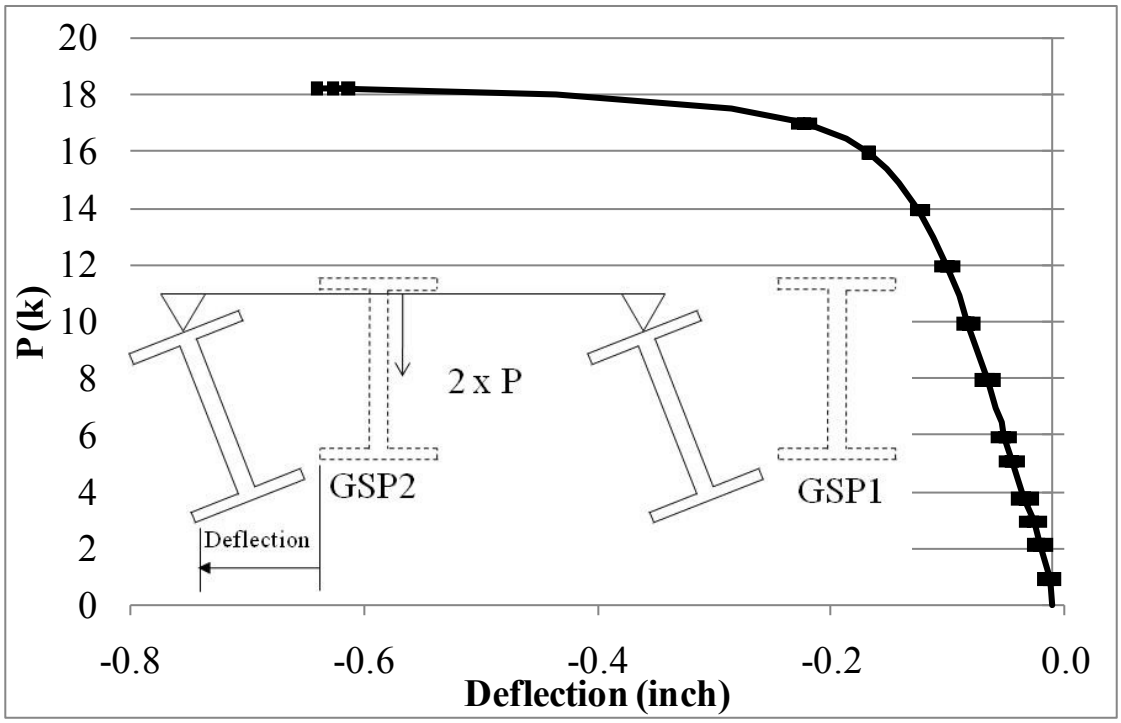

Figure A.26: GSP2 bottom flange mid-span lateral deflection (east is positive)

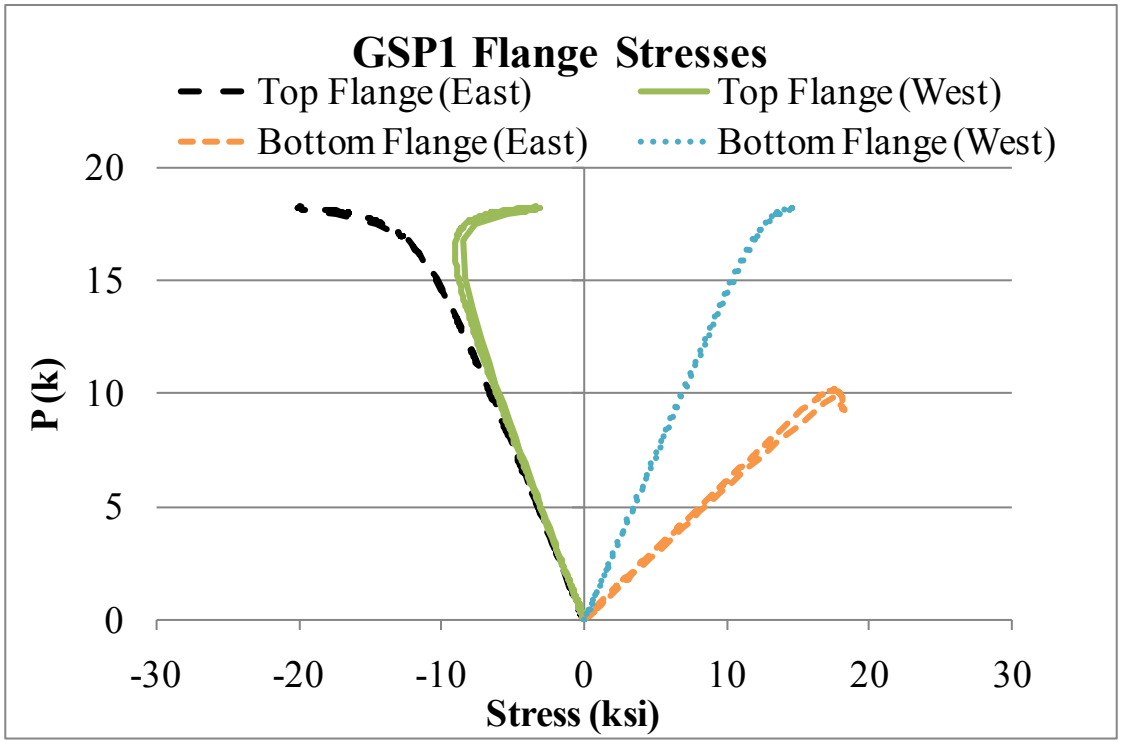

Figure A.27: GSP1 mid-span flange stresses (tension is positive)

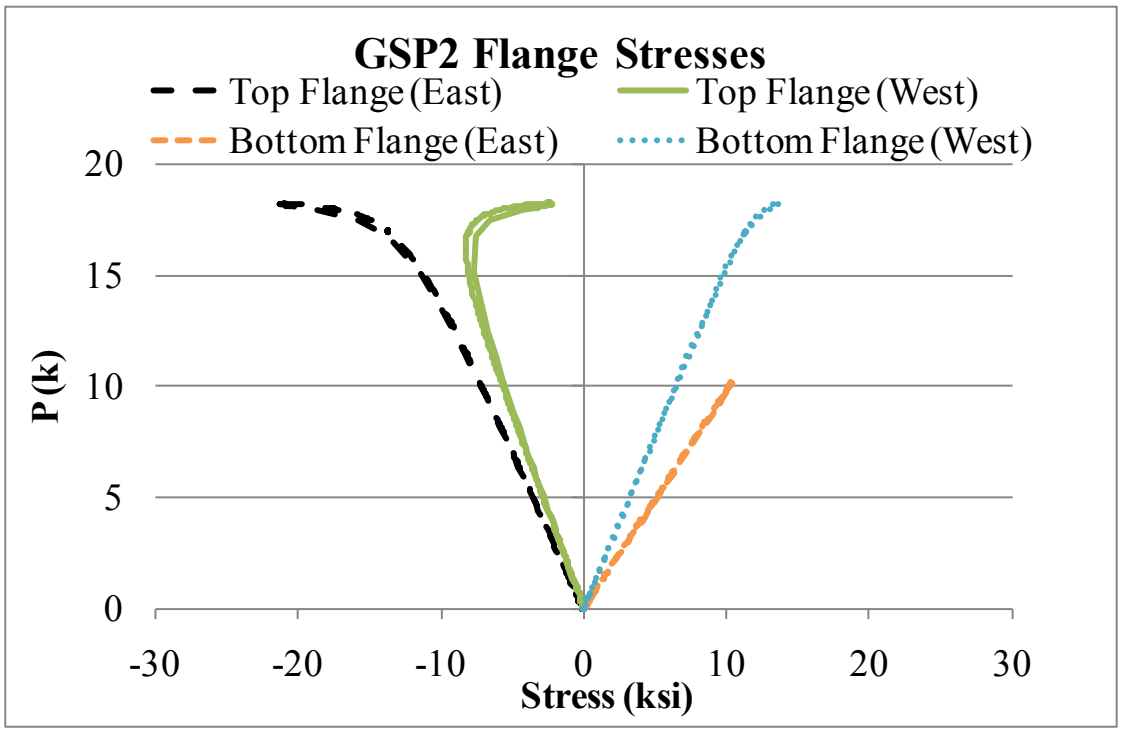

Figure A.28: GSP2 mid-span flange stresses (tension is positive)

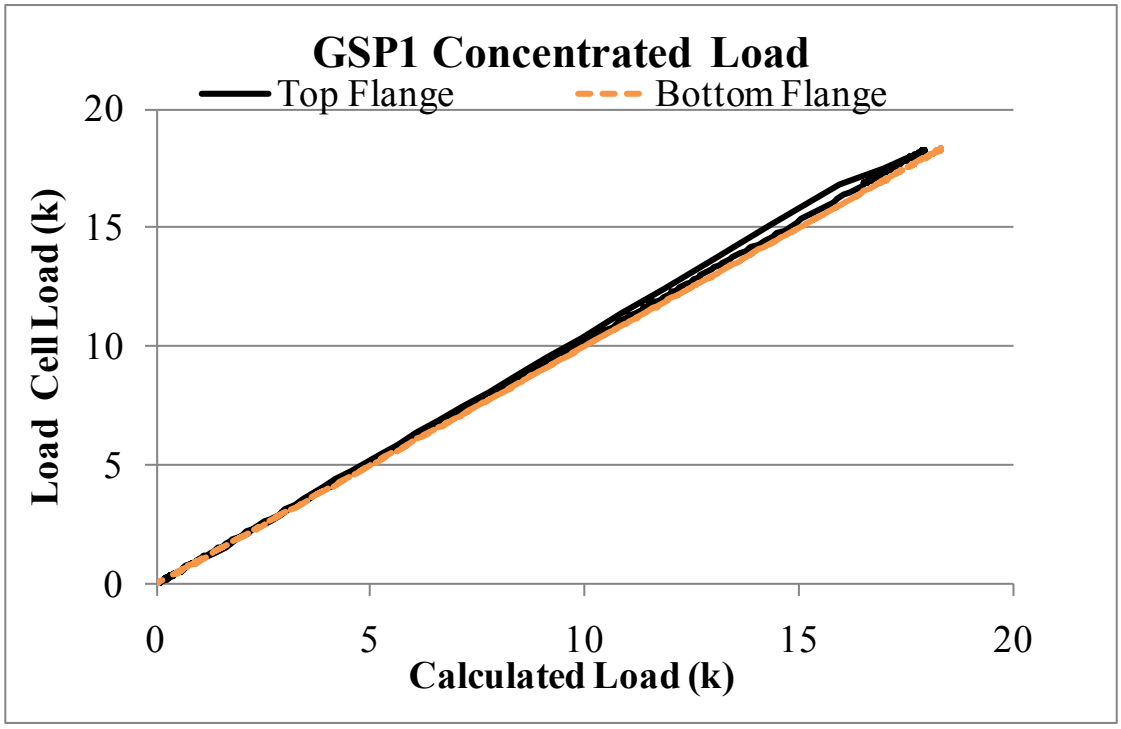

Figure A.29: GSP1 calculated applied load from mid-span flange stresses

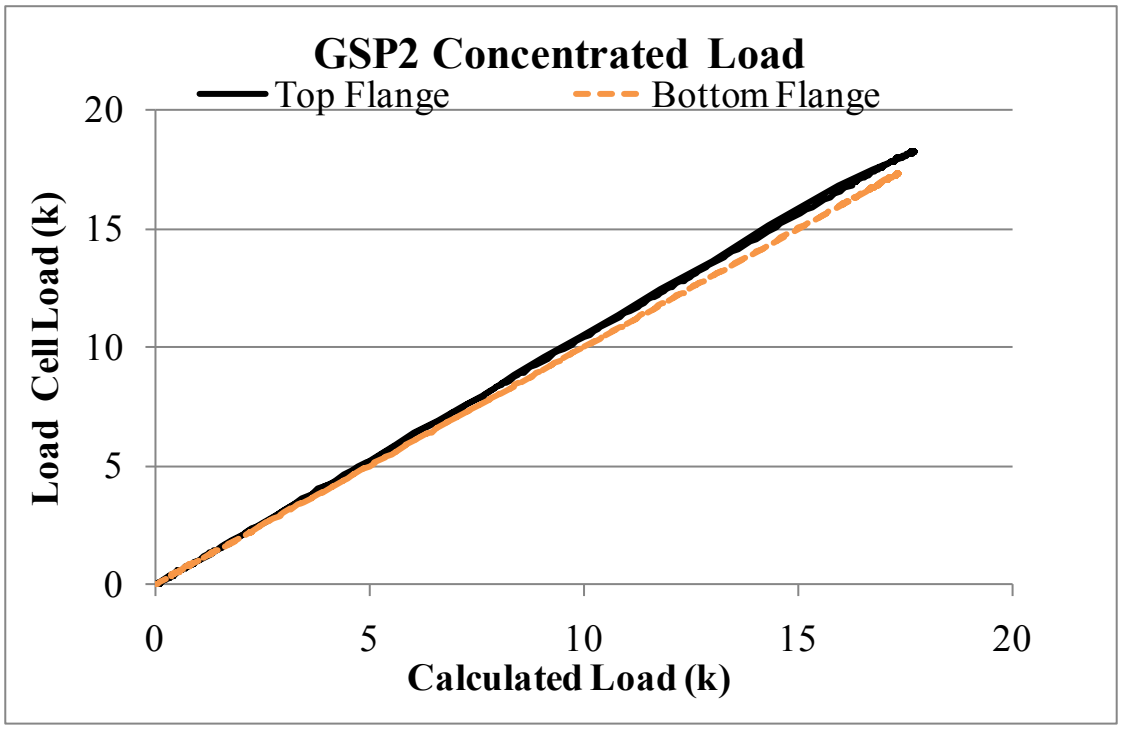

Figure A.30: GSP2 calculated applied load from mid-span flange stresses

A.3 THREE GIRDER HALF-PIPE END FRAME TEST RESULTS

A.3.1 Thrust Washer Bearing with No Intermediate Cross Frames

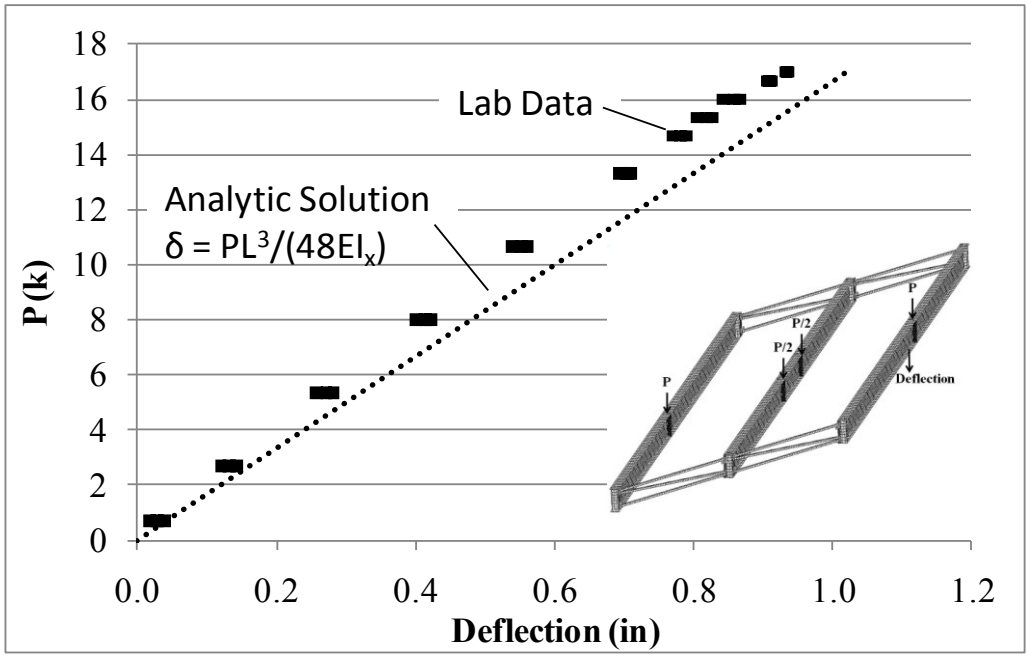

Figure A.31: GSP1 mid-span vertical deflection

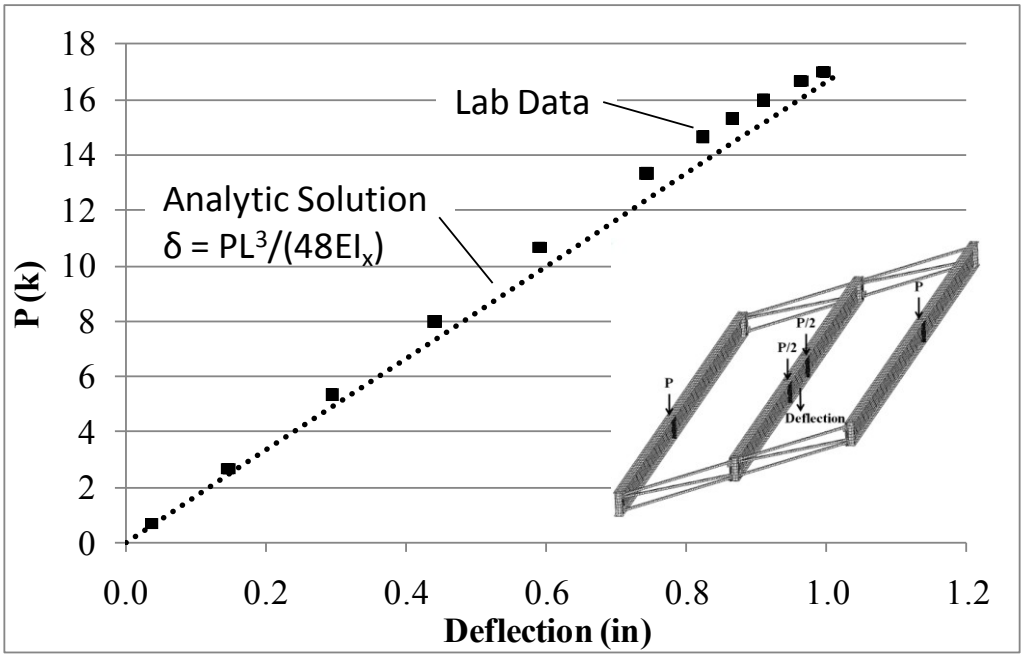

Figure A.32: GSP2 mid-span vertical deflection

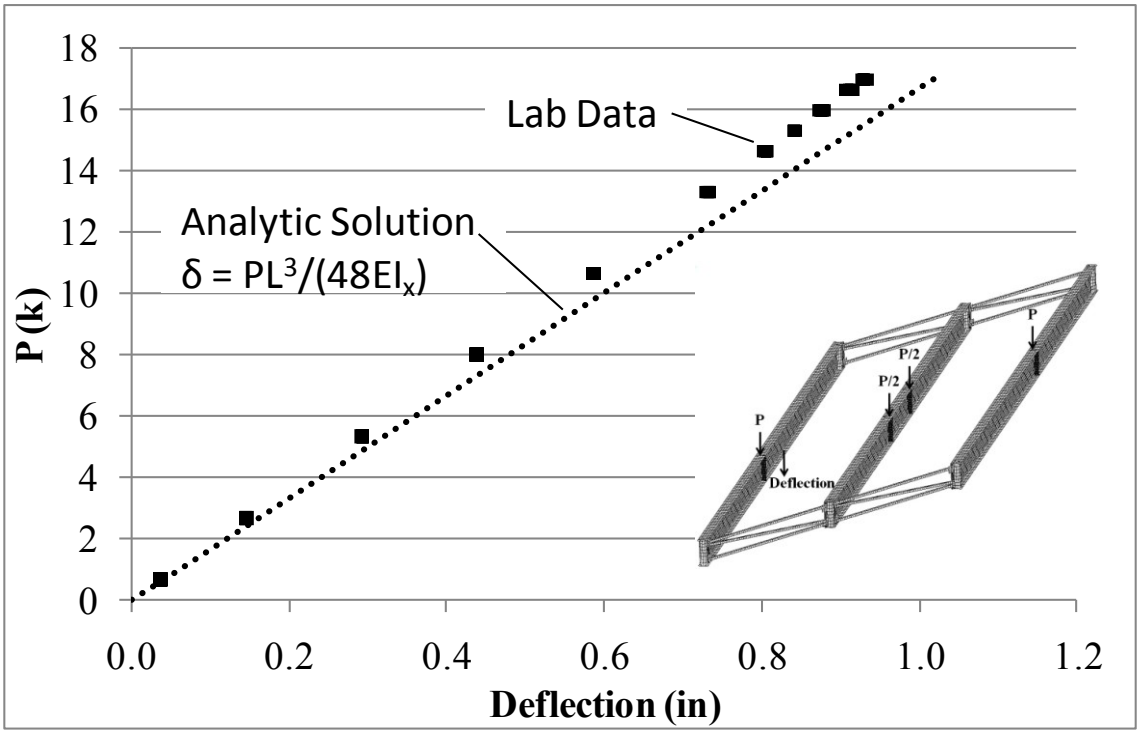

Figure A.33: GSP3 mid-span vertical deflection

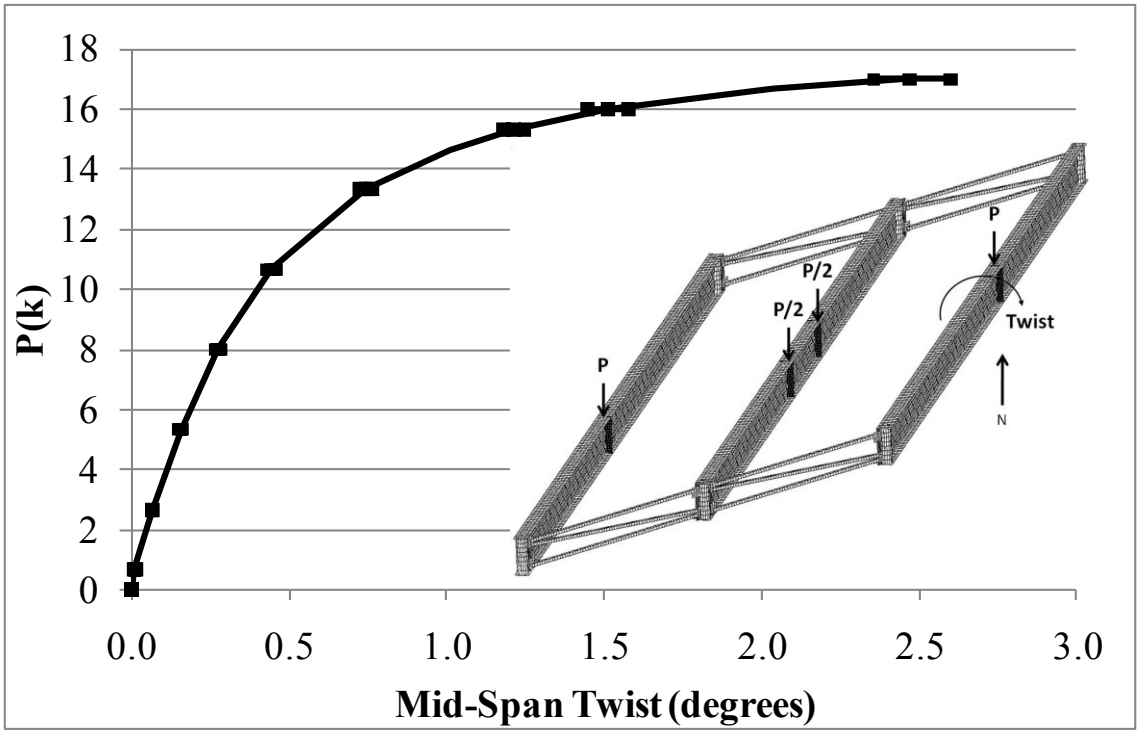

Figure A.34: GSP1 mid-span twist

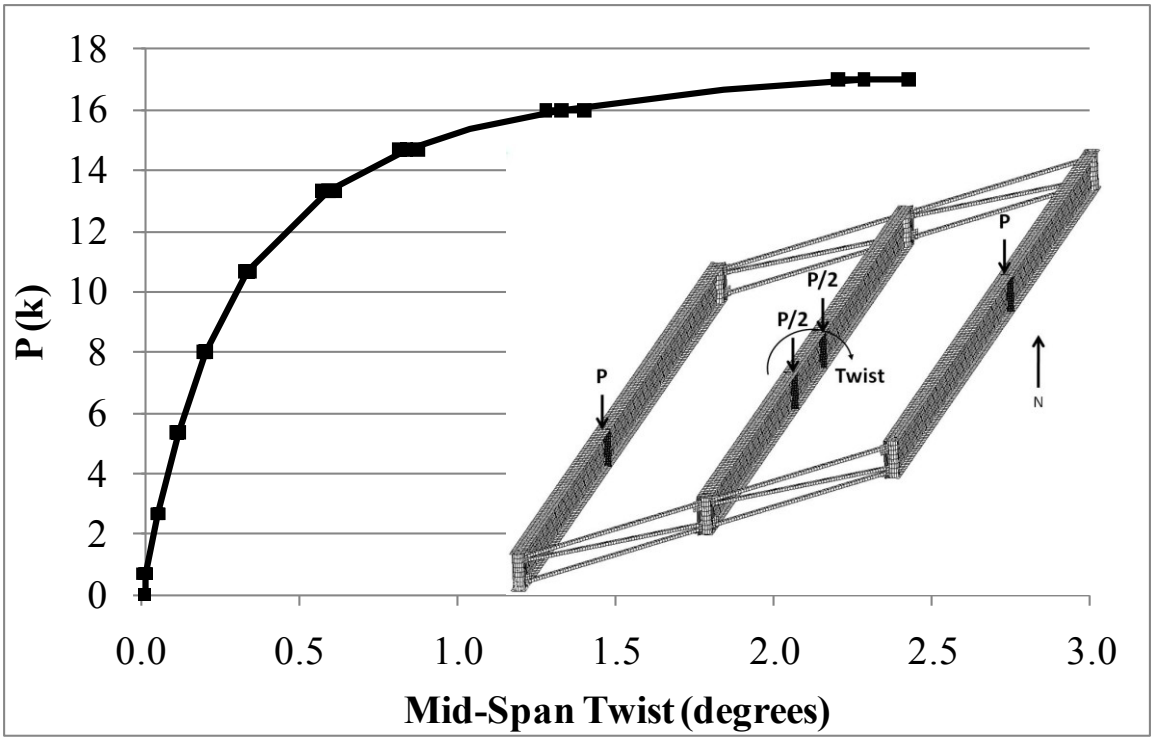

Figure A.35: GSP2 mid-span twist

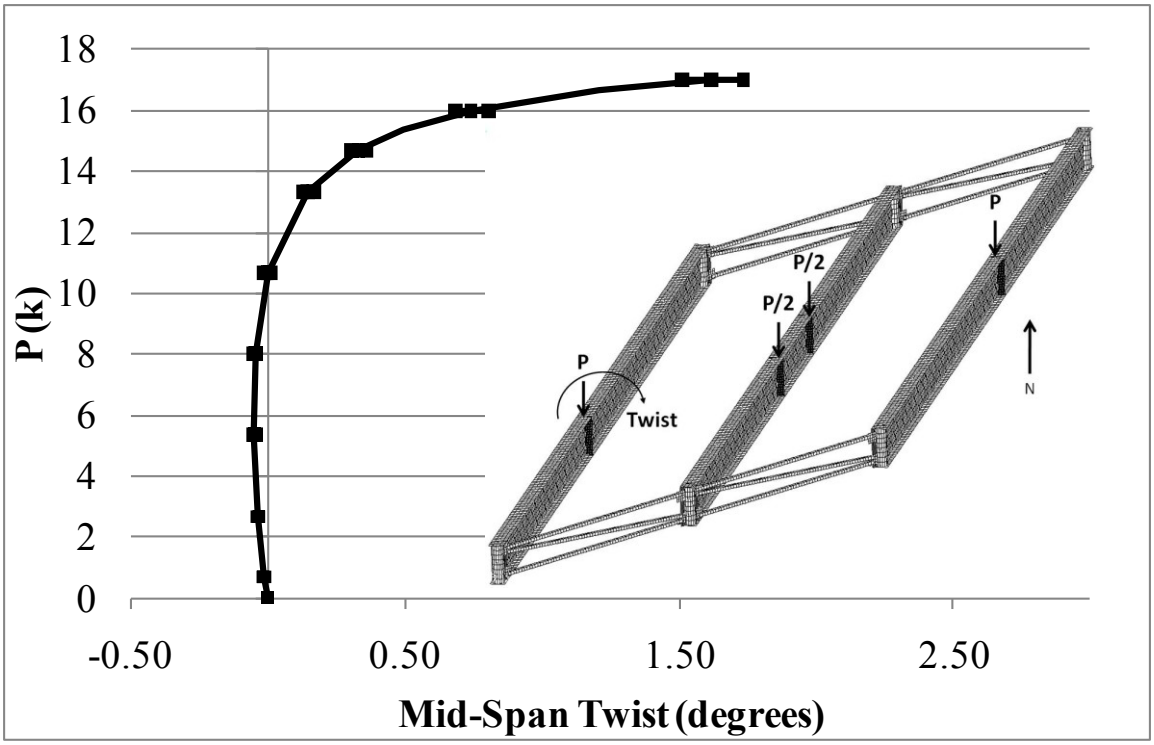

Figure A.36: GSP3 mid-span twist

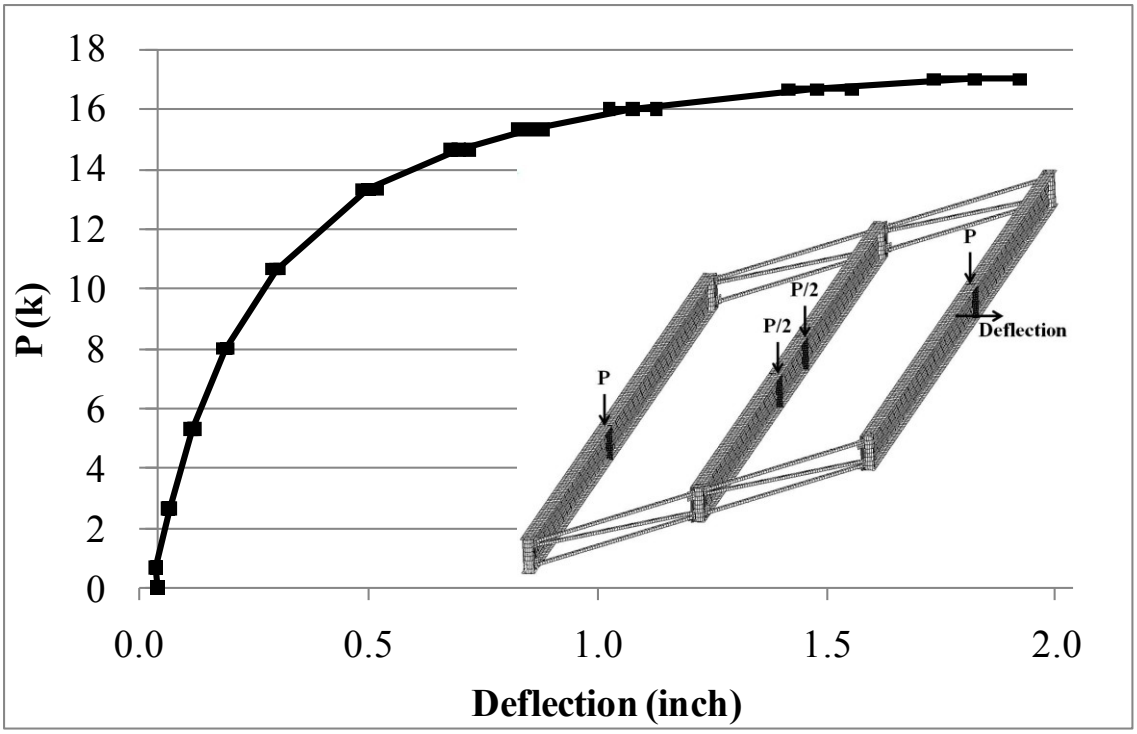

Figure A.37: GSP1 mid-span top flange lateral deflection

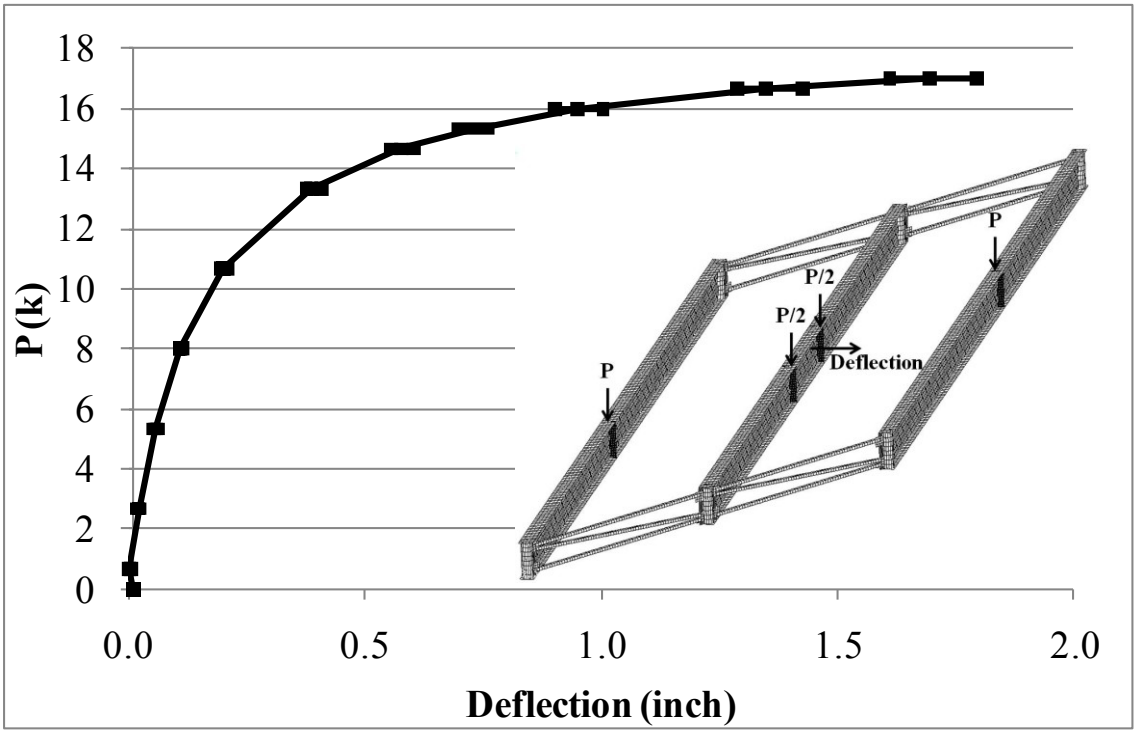

Figure A.38: GSP2 mid-span top flange lateral deflection

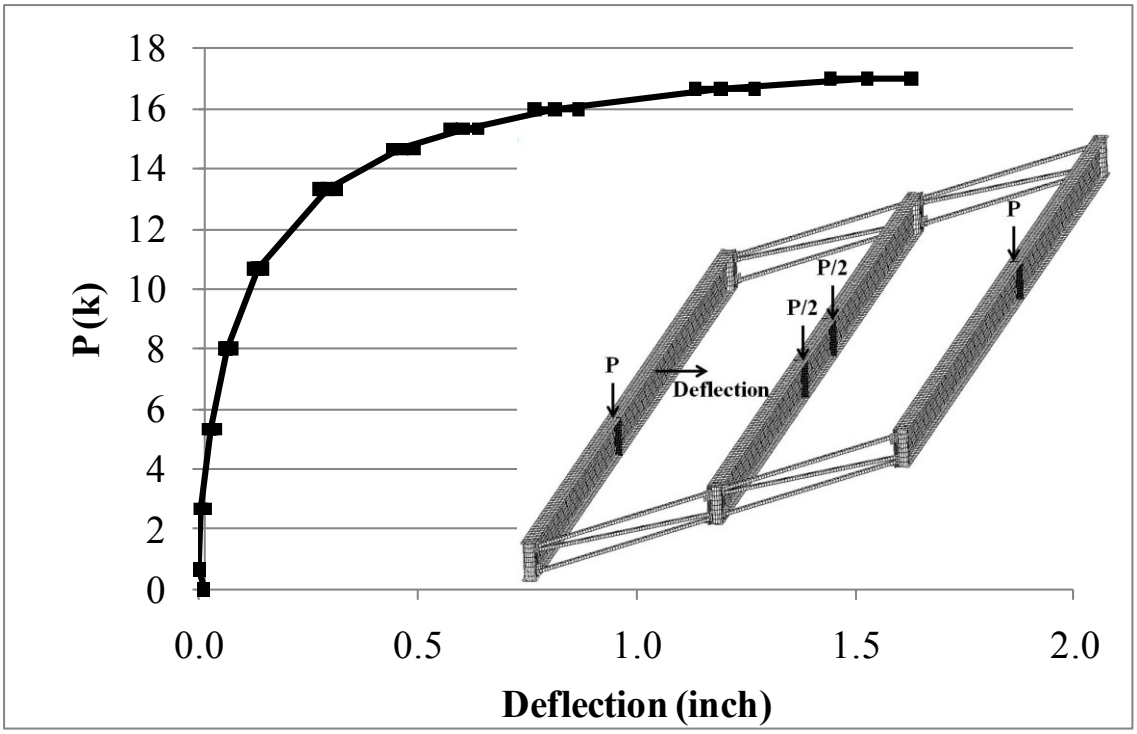

Figure A.39: GSP3 mid-span top flange lateral deflection

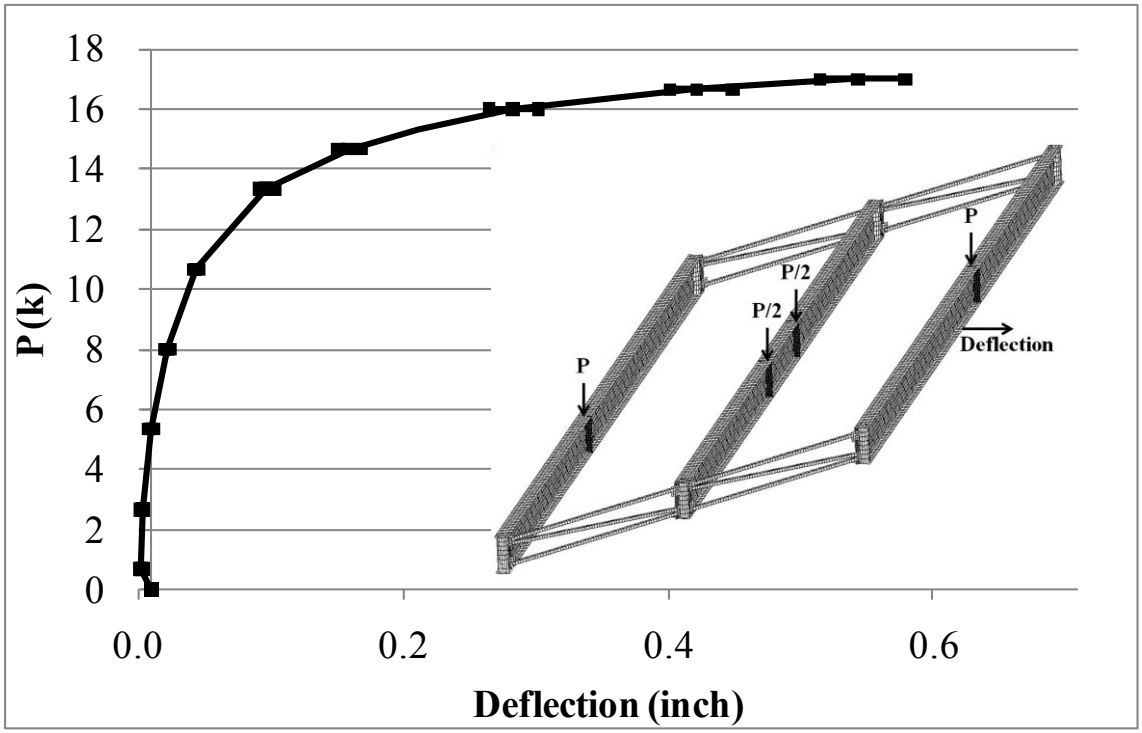

Figure A.40: GSP1 mid-span bottom flange lateral deflection

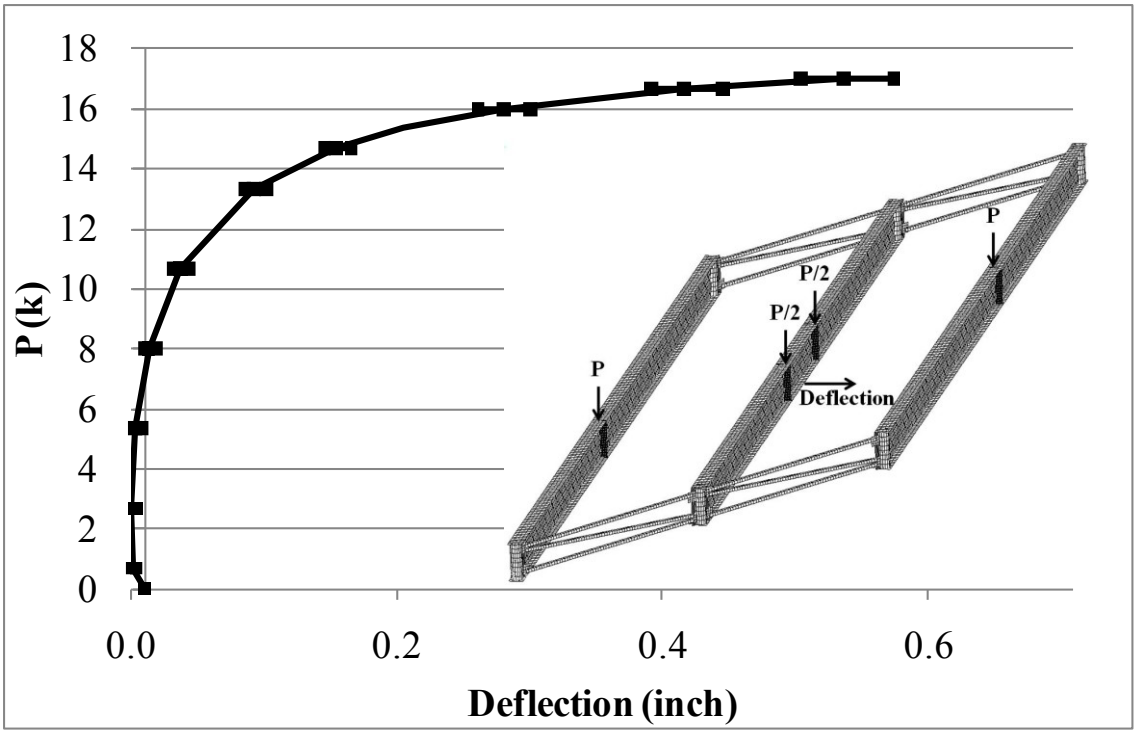

Figure A.41: GSP2 mid-span bottom flange lateral deflection

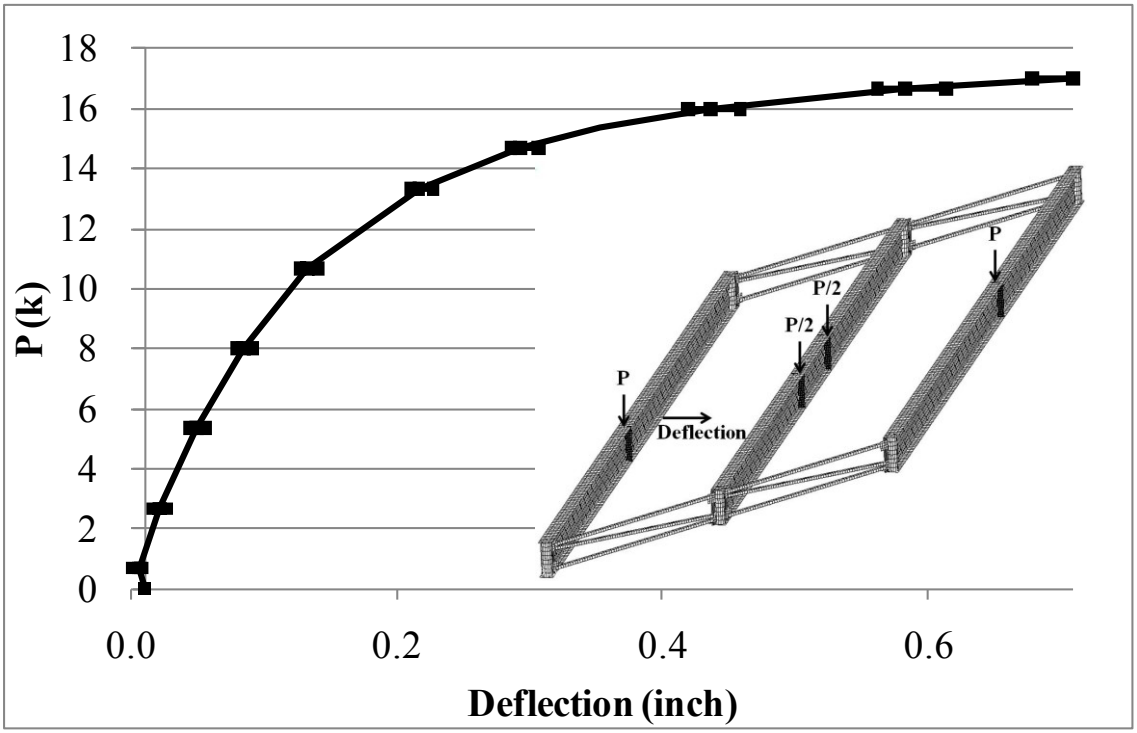

Figure A.42: GSP3 mid-span bottom flange lateral deflection

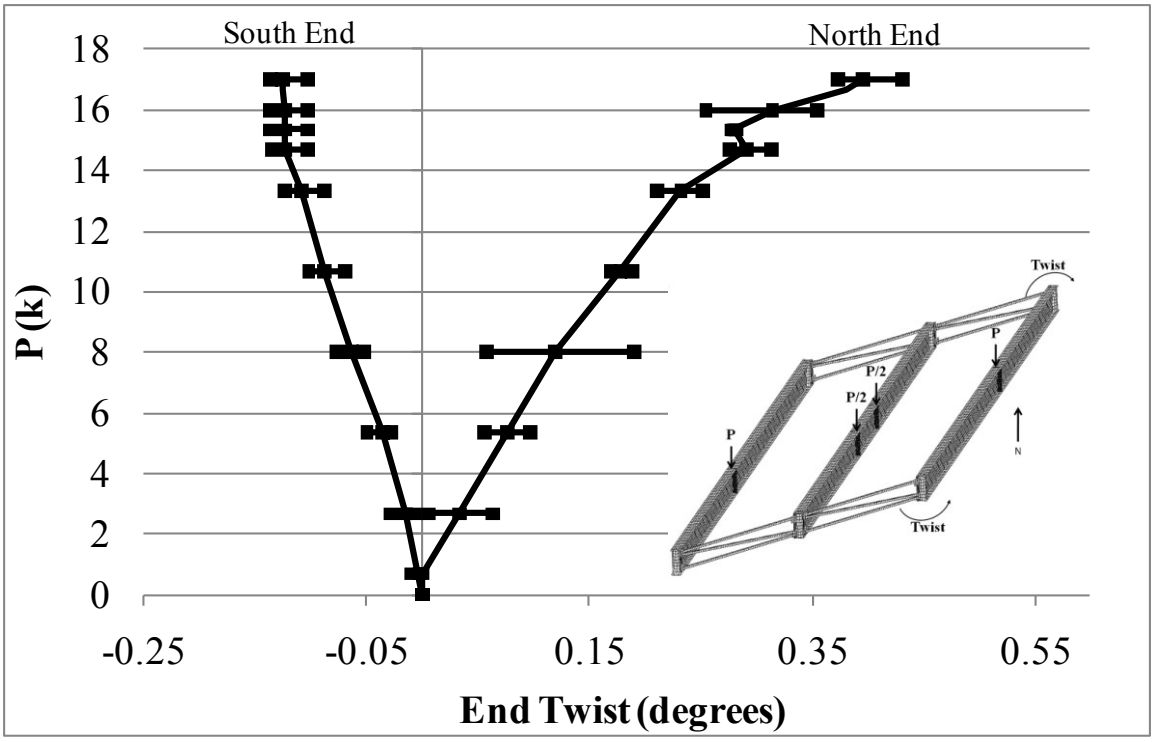

Figure A.43: GSP1 end twists

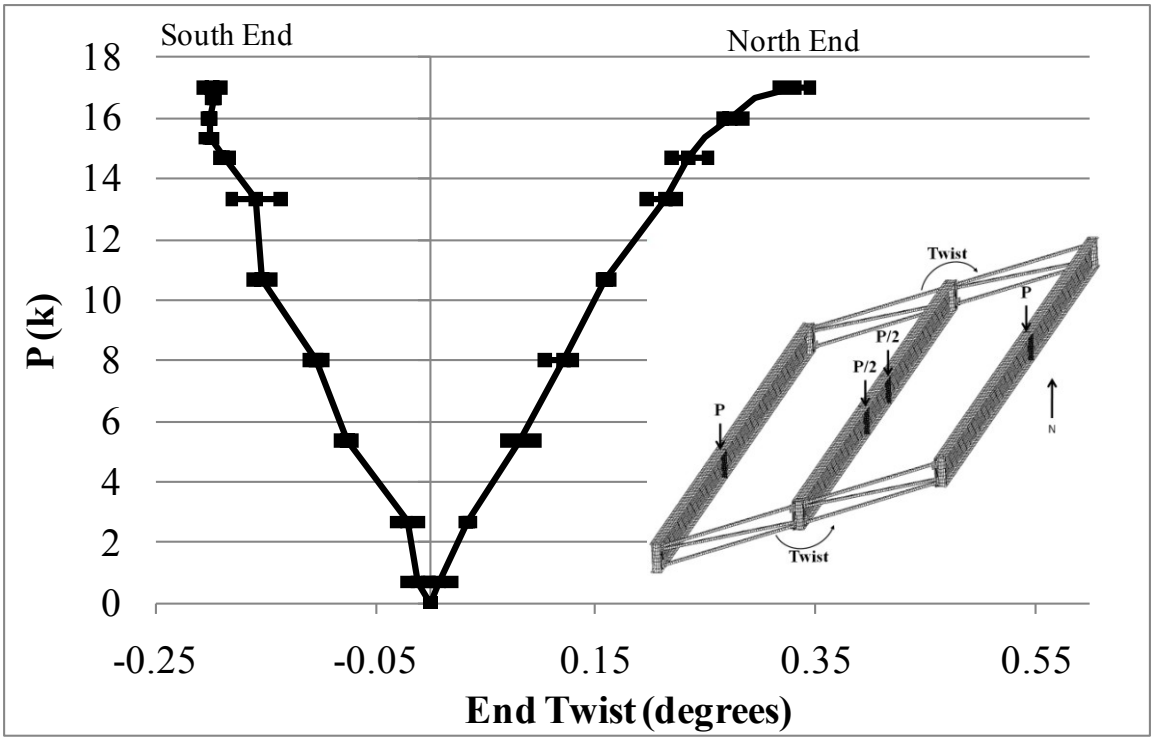

Figure A.44: GSP2 end twists

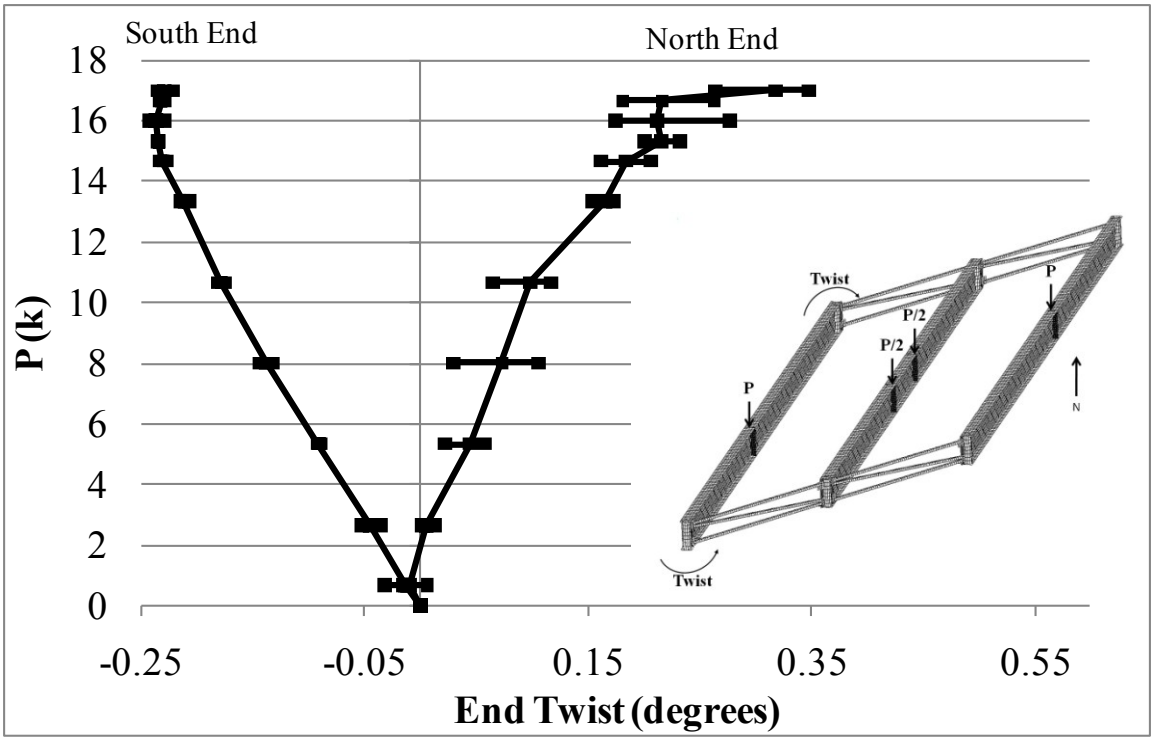

Figure A.45: GSP3 end twists

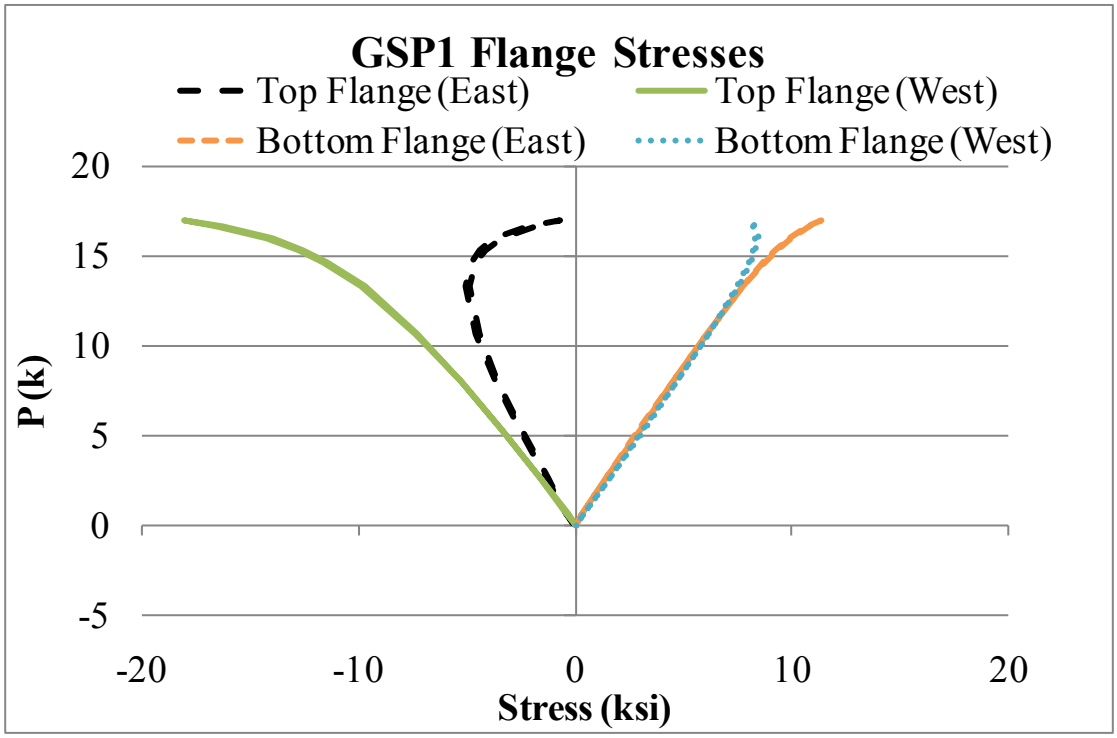

Figure A.46: GSP1mid-span flange stresses

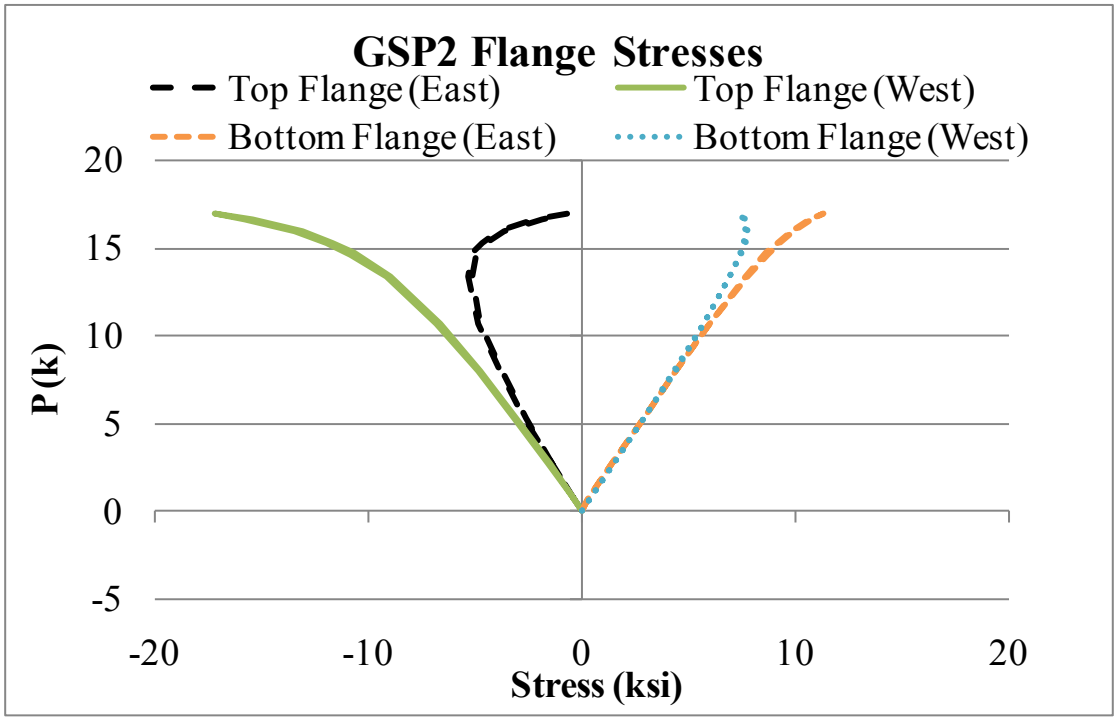

Figure A.47: GSP2 mid-span flange stresses

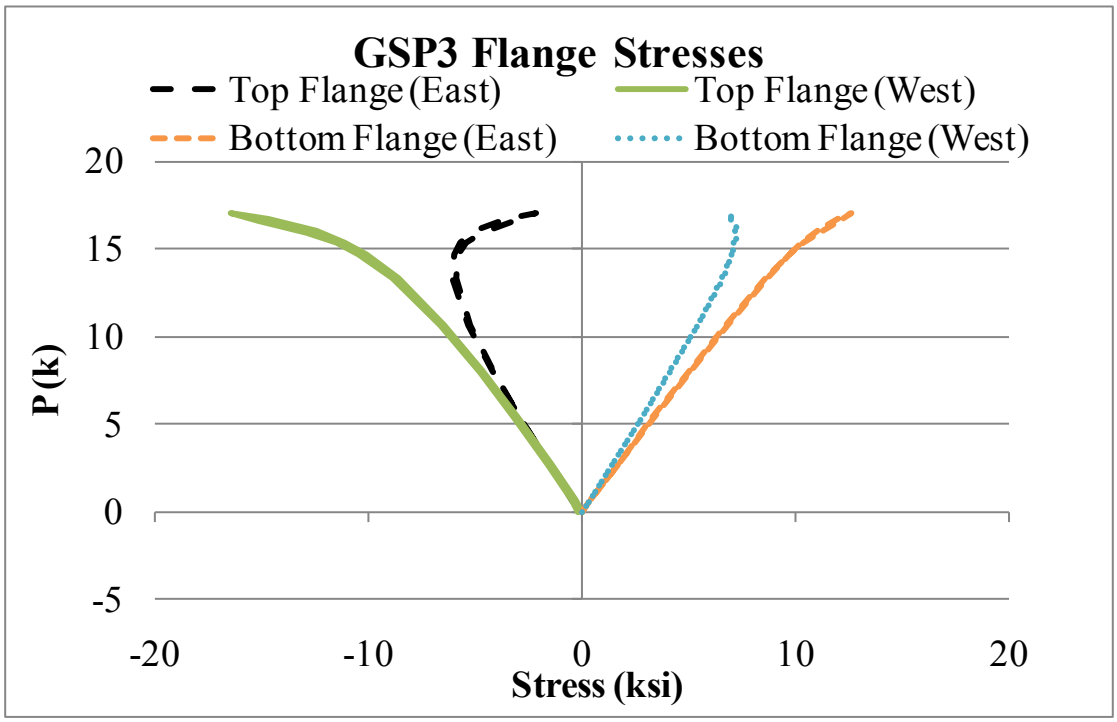

Figure A.48: GSP3 mid-span flange stresses

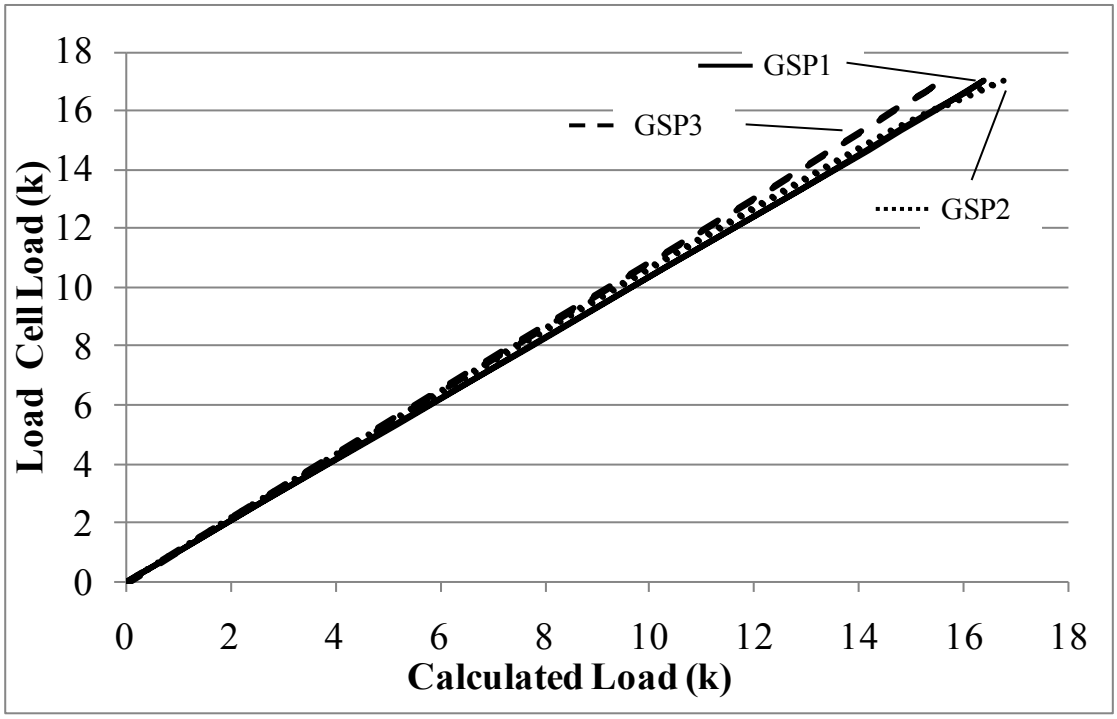

Figure A.49: Calculated girder loads from flange stresses

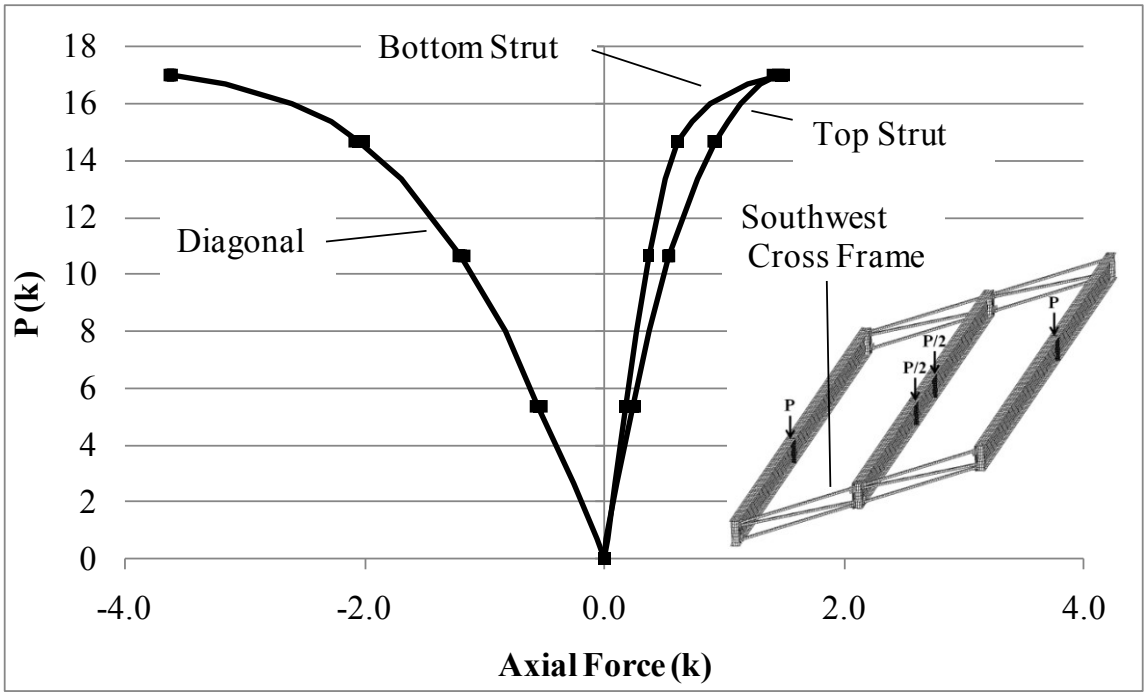

Figure A.50: Southwest cross frame axial brace forces

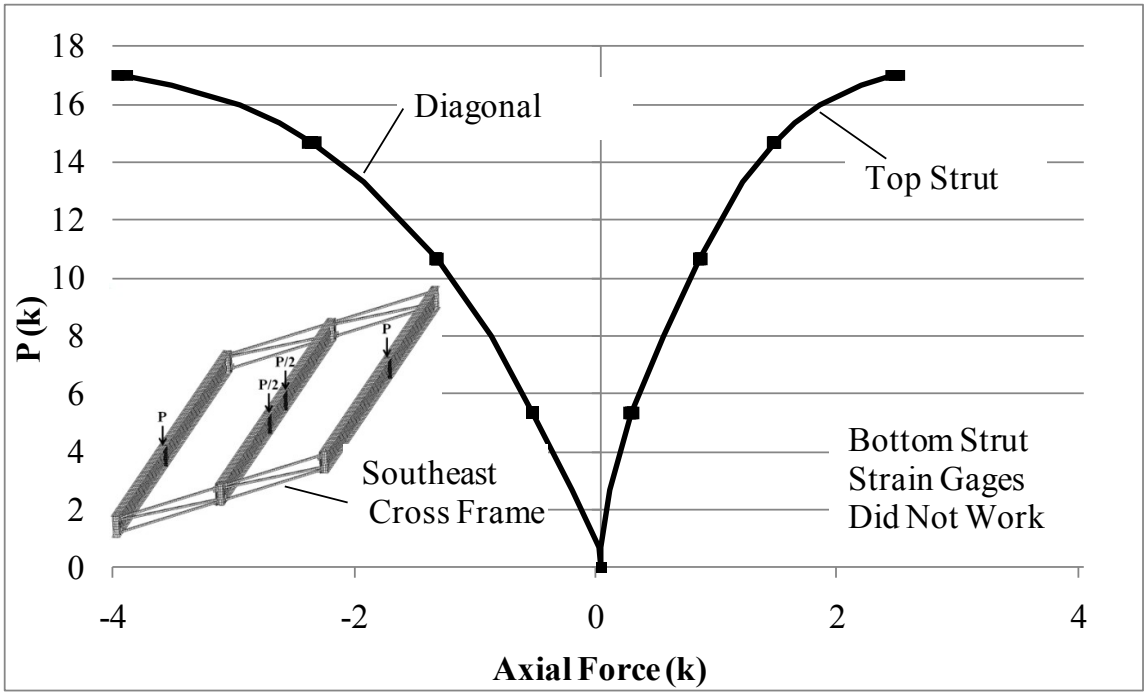

Figure A.51: Southeast cross frame axial brace forces

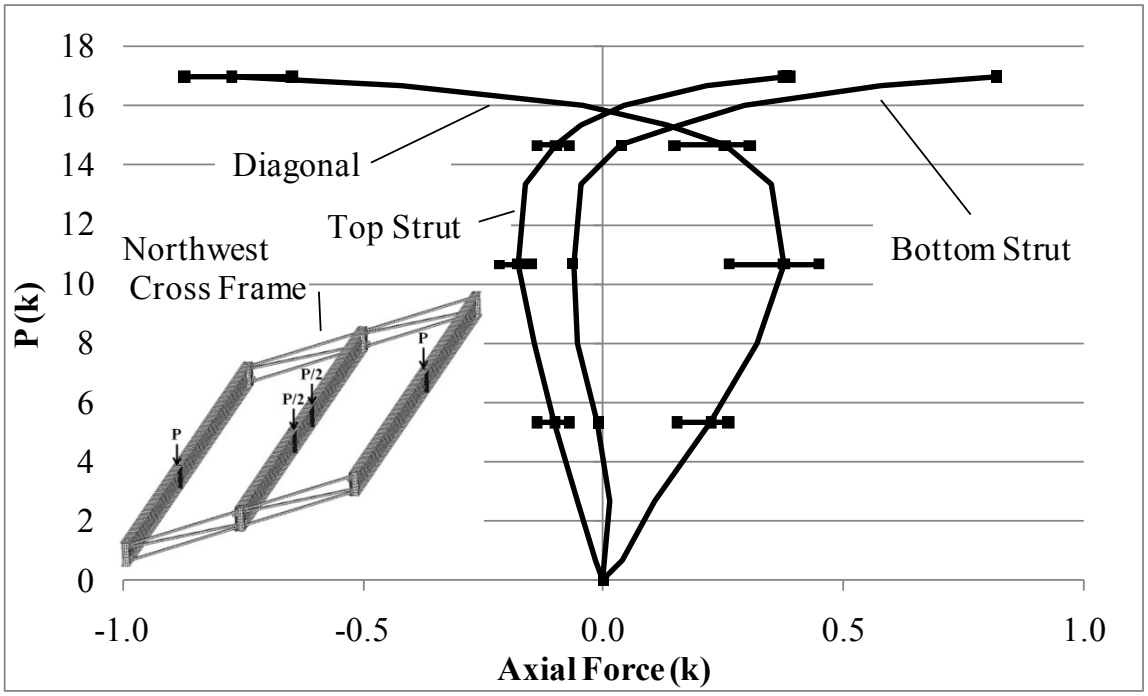

Figure A.52: Northwest cross frame axial brace forces

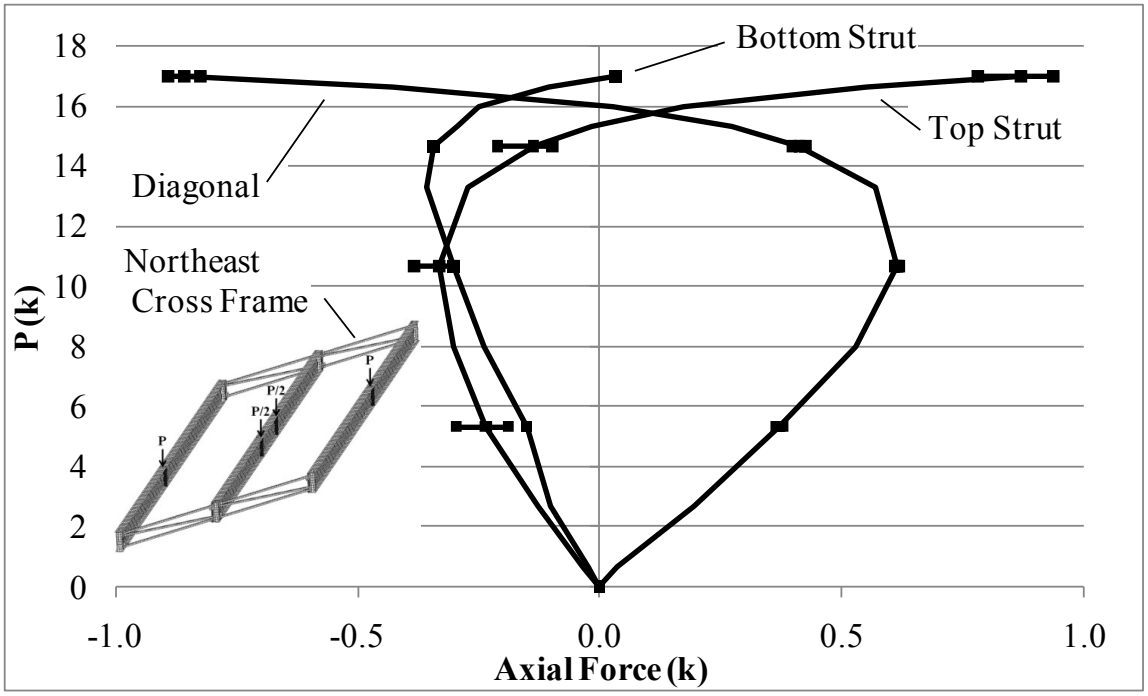

Figure A.53: Northeast cross frame axial brace forces

A.3.2 Thrust Washer Bearing with Staggered Intermediate Cross Frames

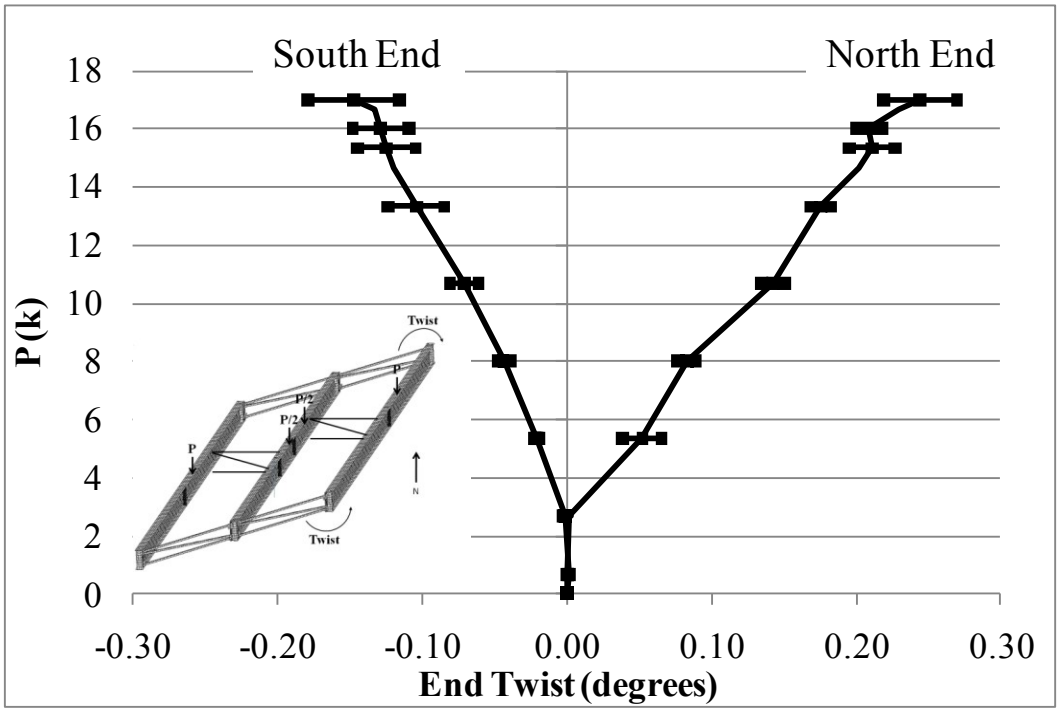

Figure A.54: GSP1 end twist

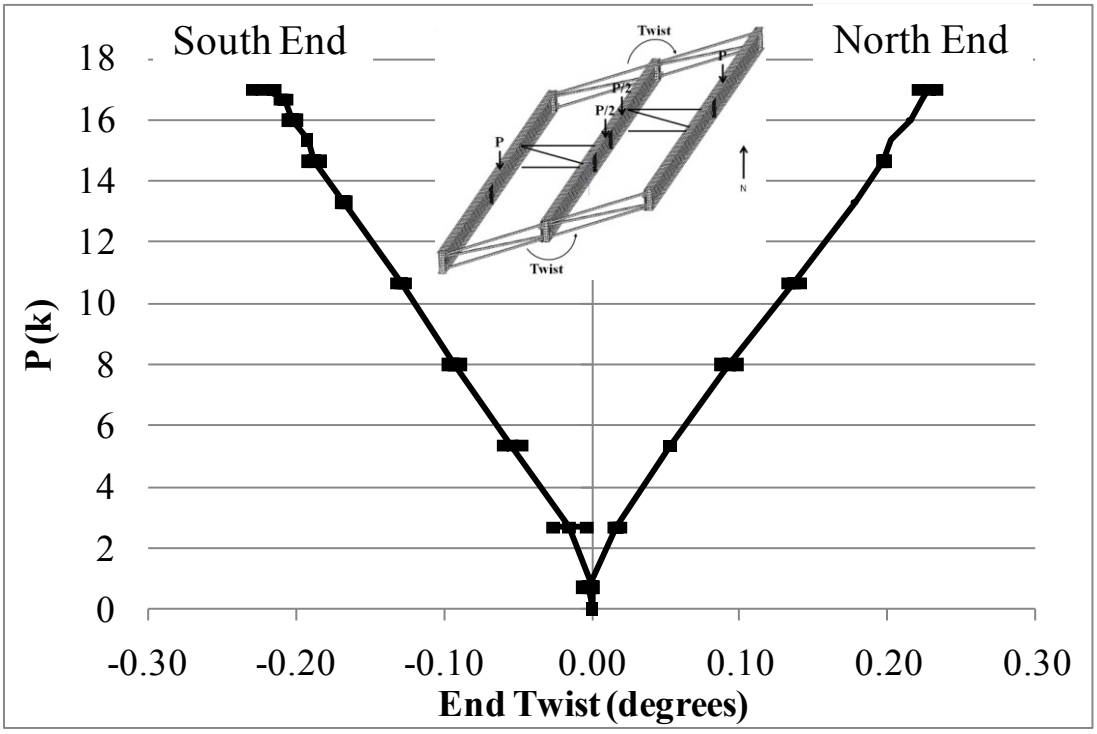

Figure A.55: GSP2 end twist

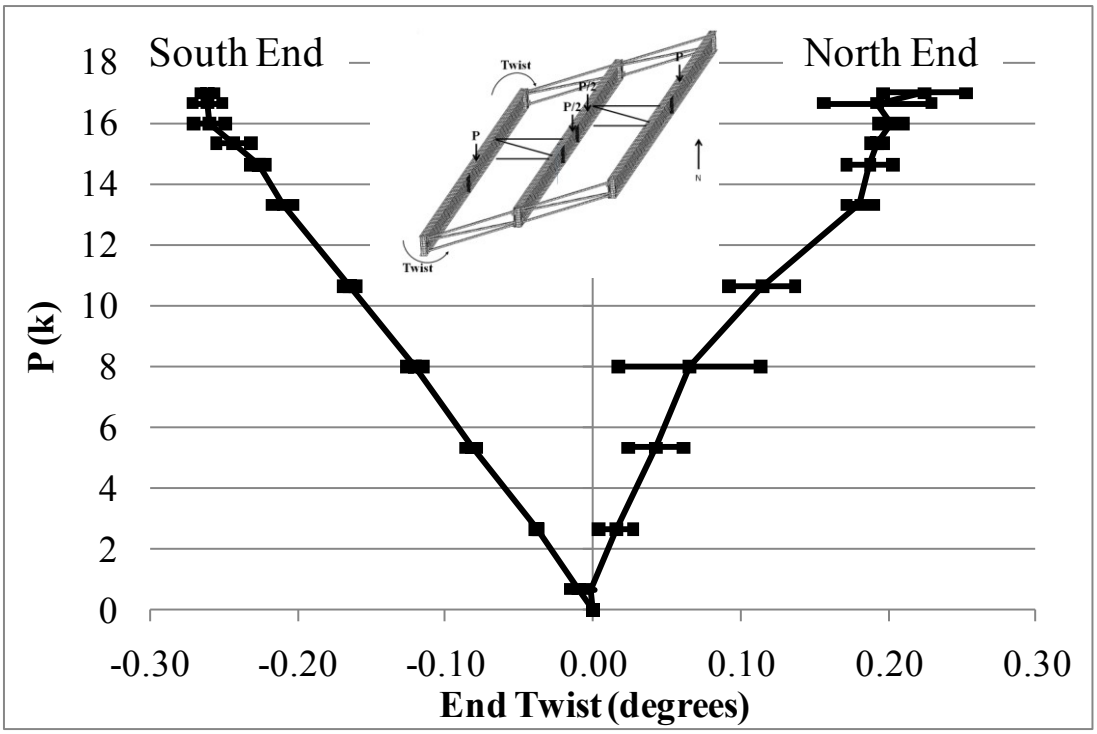

Figure A.56: GSP3 end twist

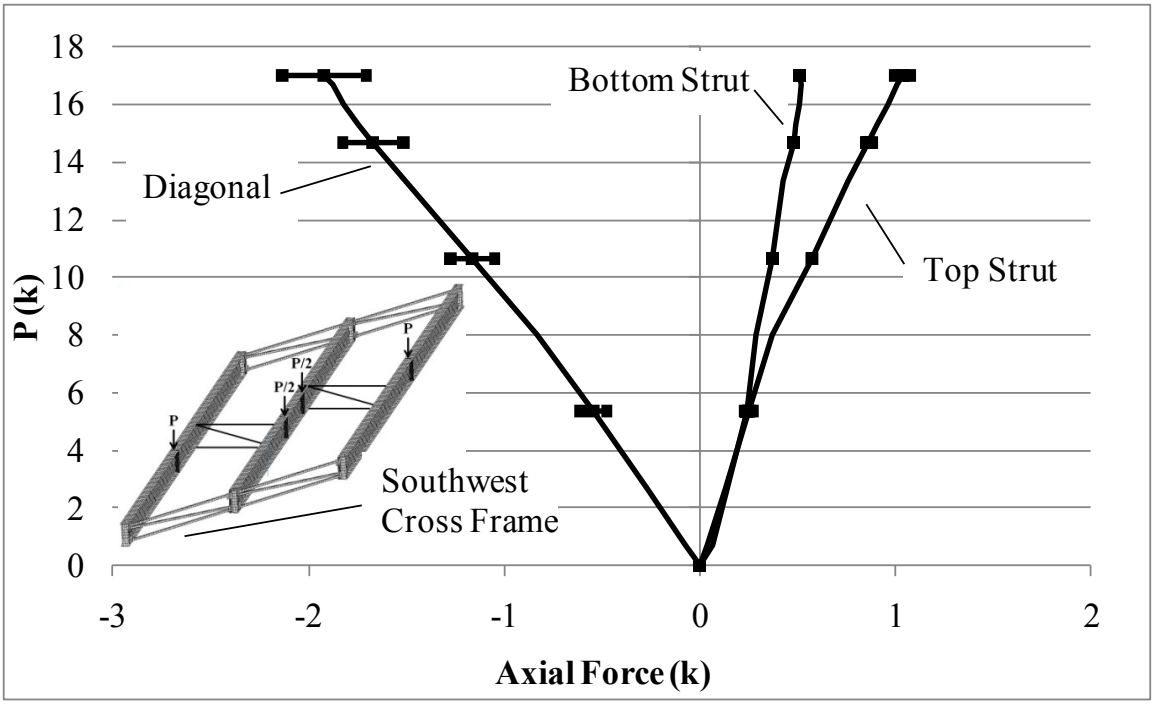

Figure A.57:SW end cross frame axial forces

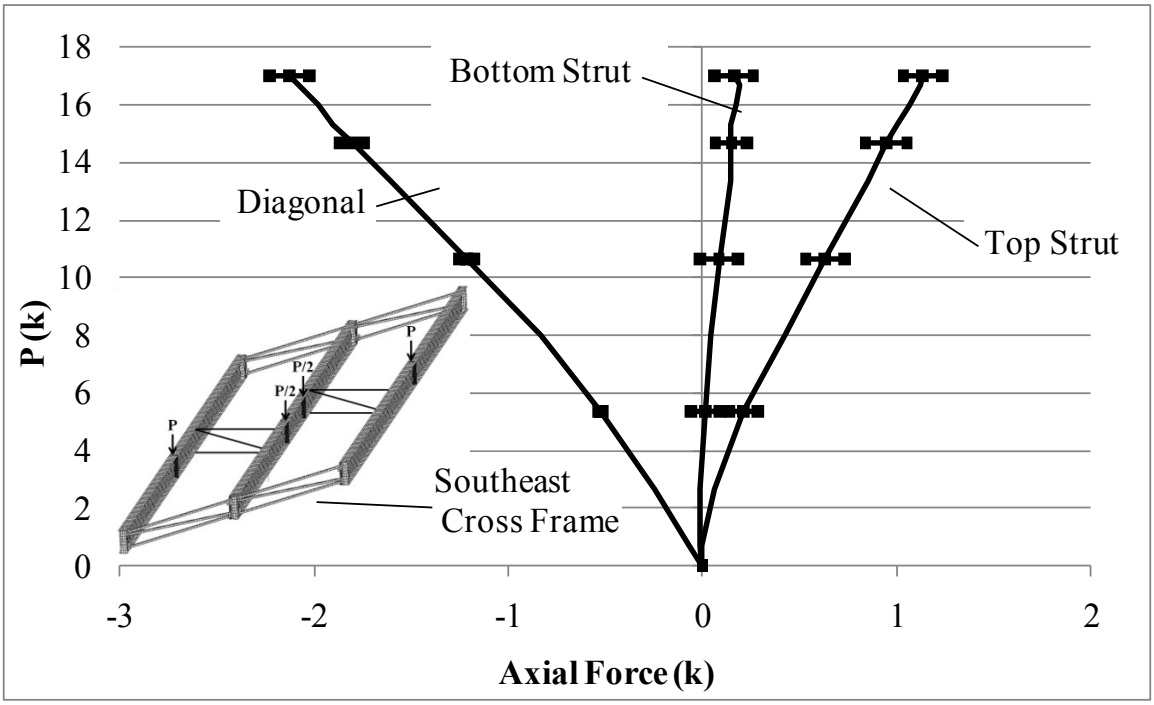

Figure A.58: SE end cross frame axial forces

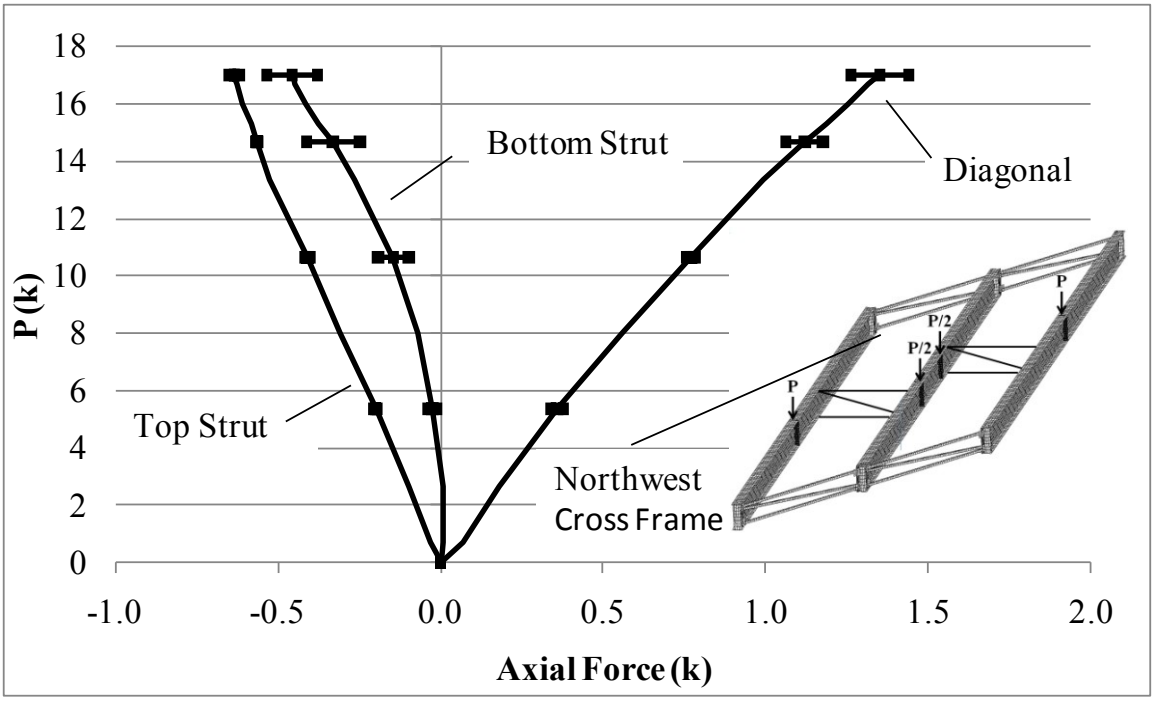

Figure A.59: NW end cross frame axial forces

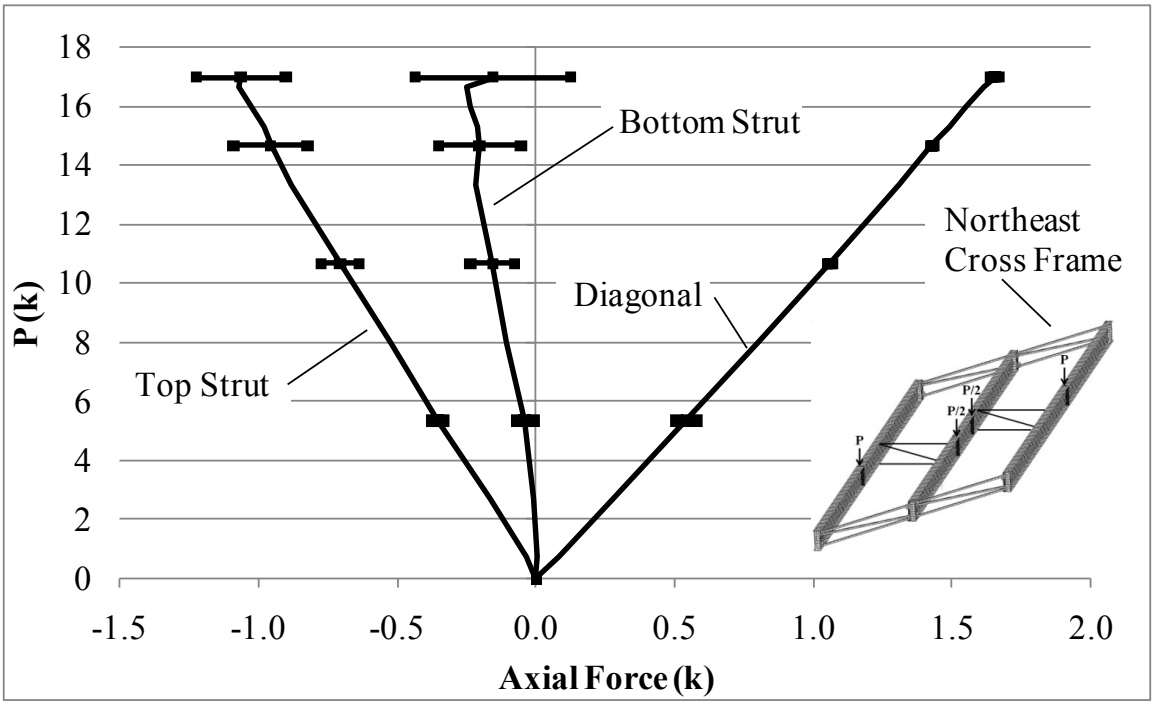

Figure A.60: NE end cross frame axial forces

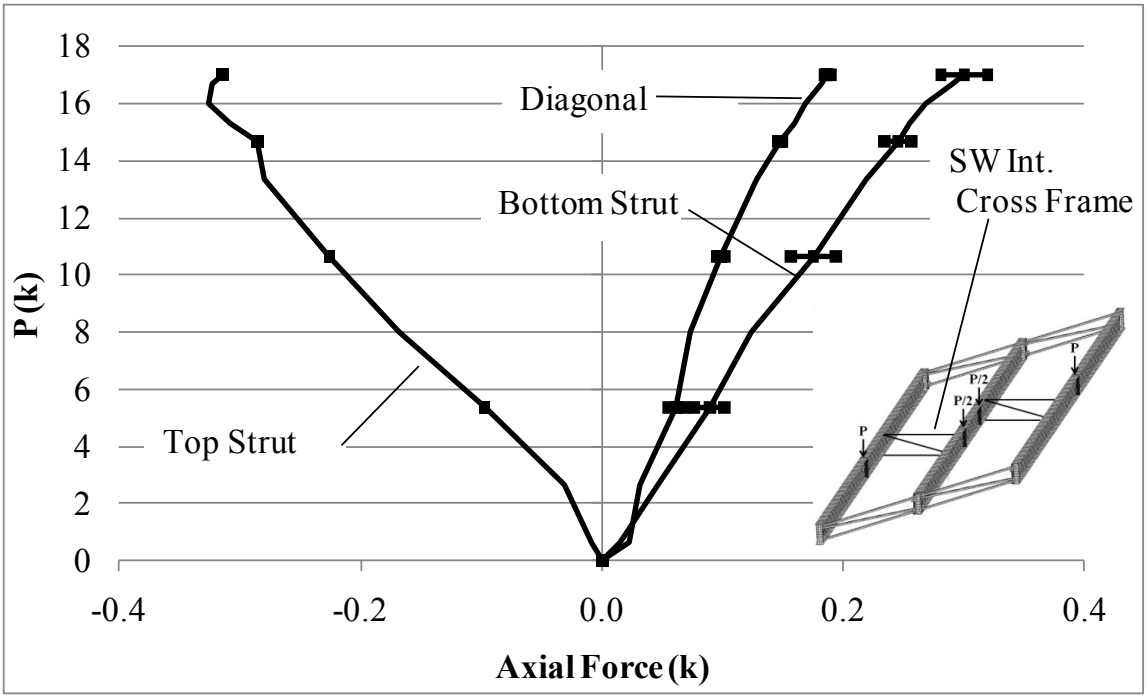

Figure A.61: SW intermediate staggered cross frame axial forces

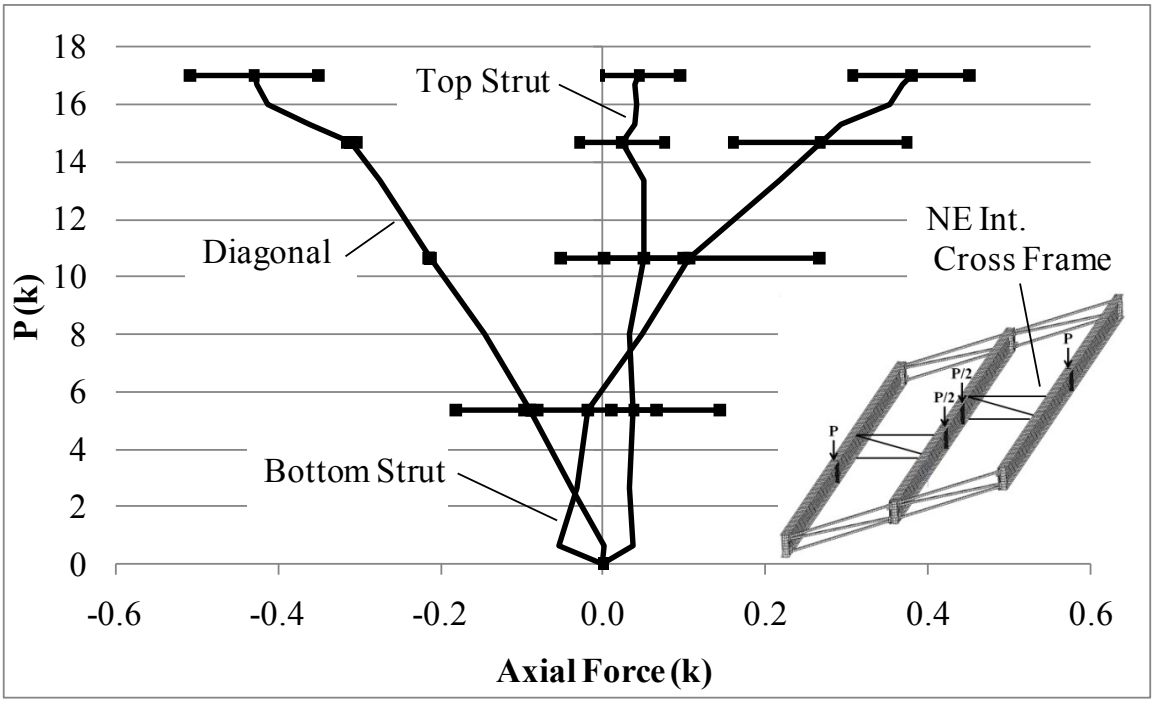

Figure A.62: NE intermediate staggered cross frame axial forces

A.3.3 Thrust Washer Bearing with Continuous Intermediate Cross Frames

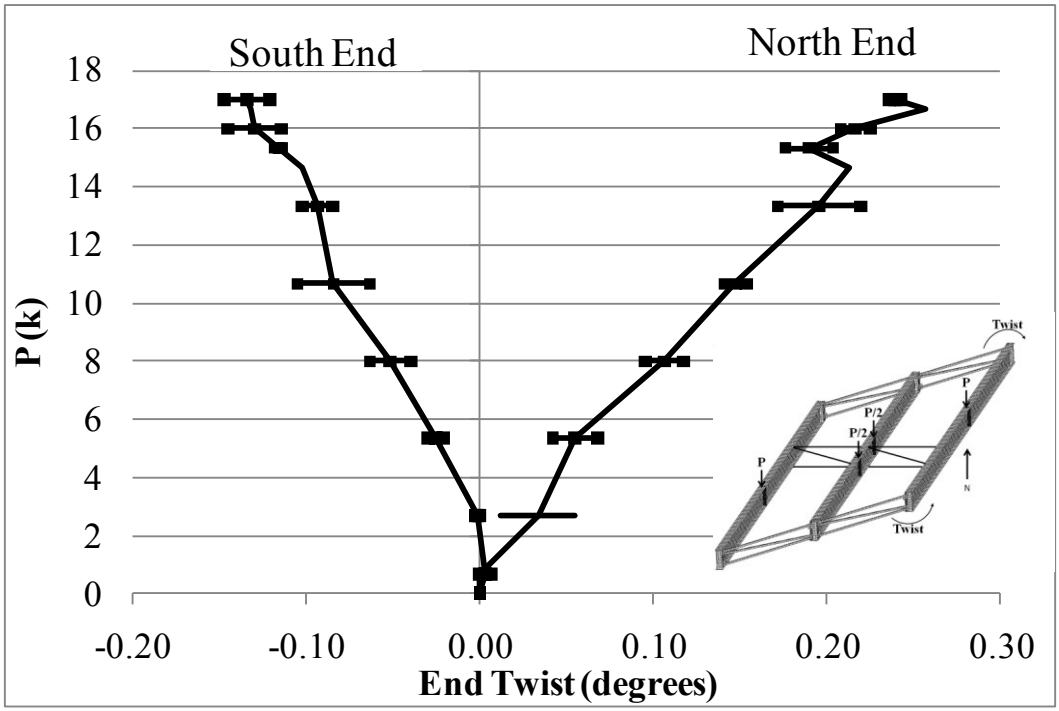

Figure A.63: GSP1 end twist

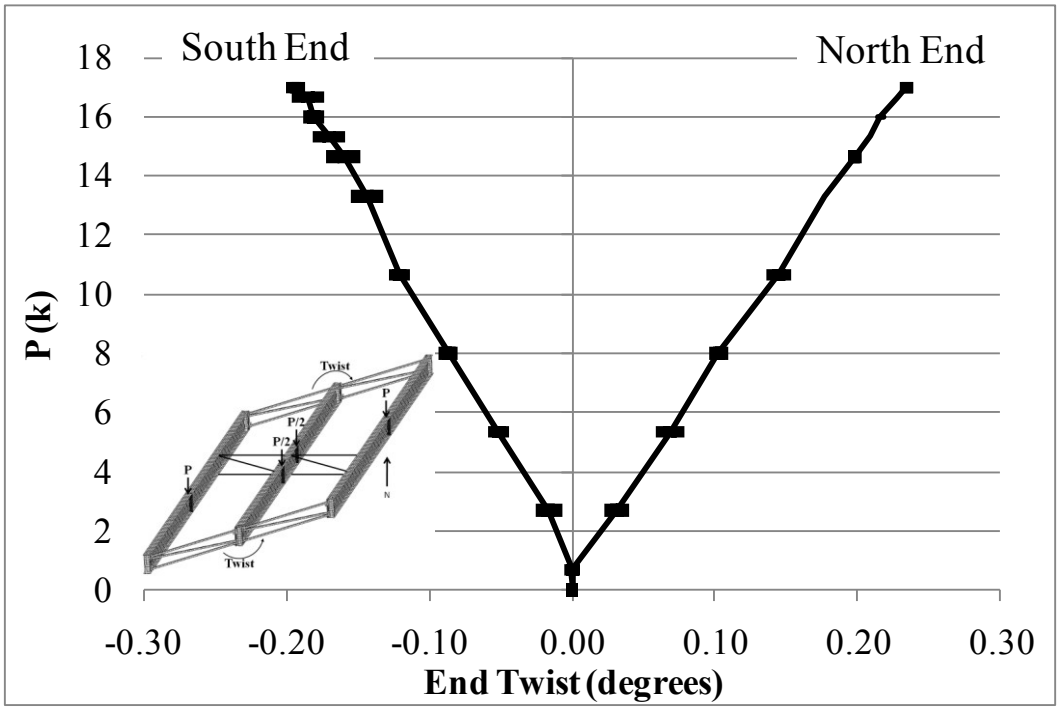

Figure A.64: GSP2 end twist

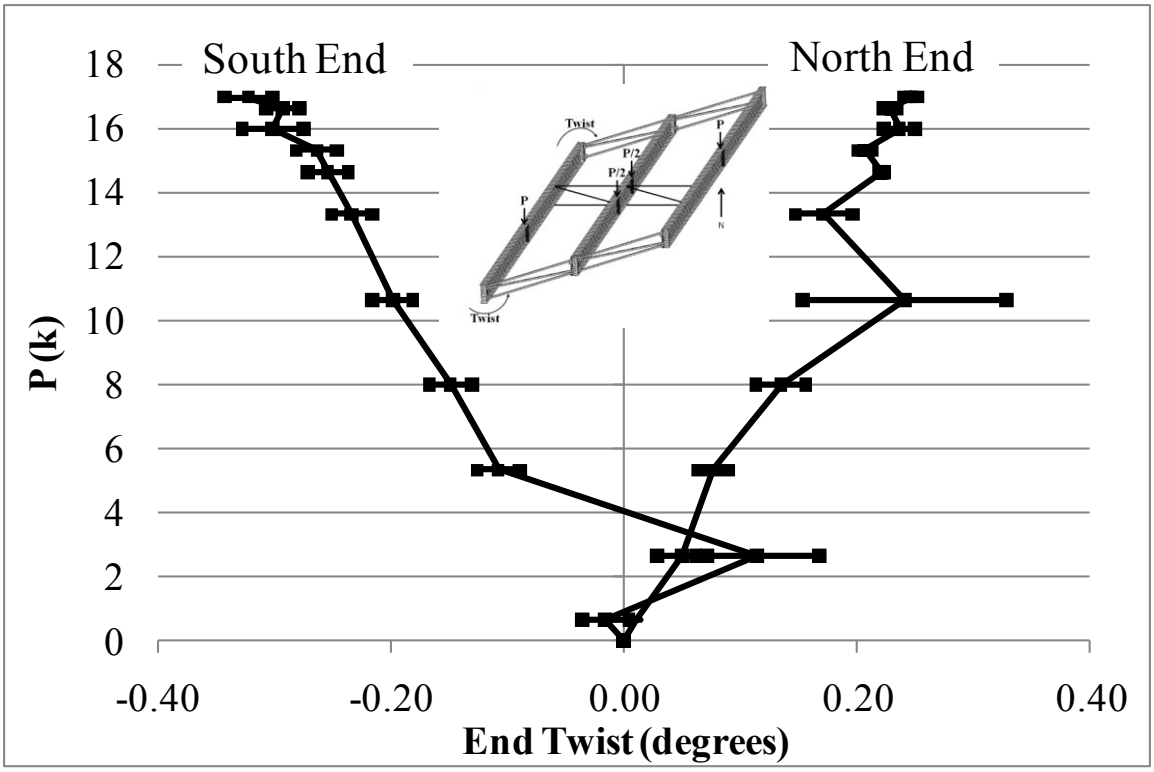

Figure A.65: GSP3 end twist

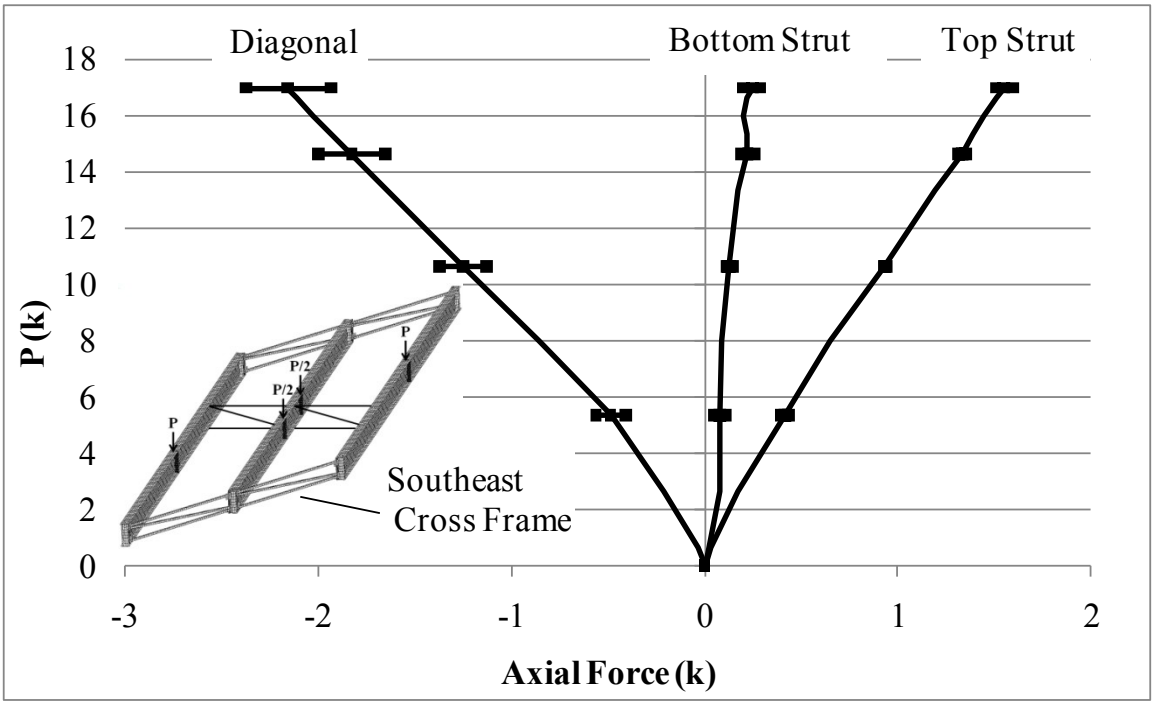

Figure A.66: SE end cross frame axial forces

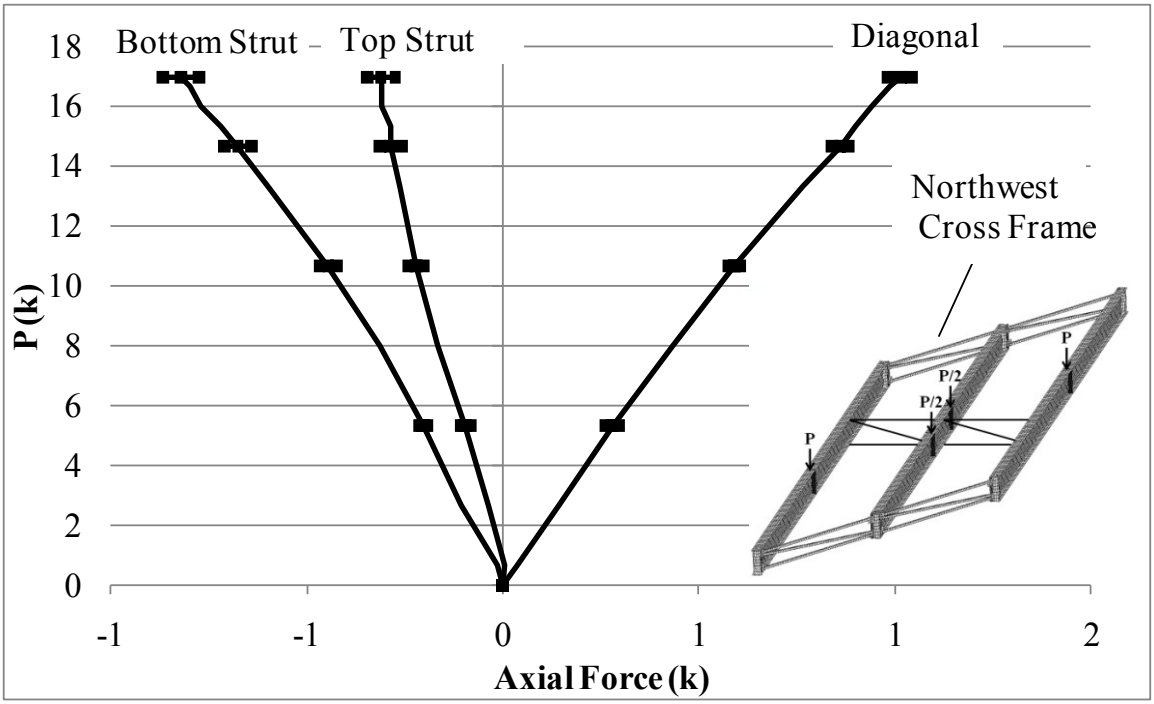

Figure A.67: NW end cross frame axial forces

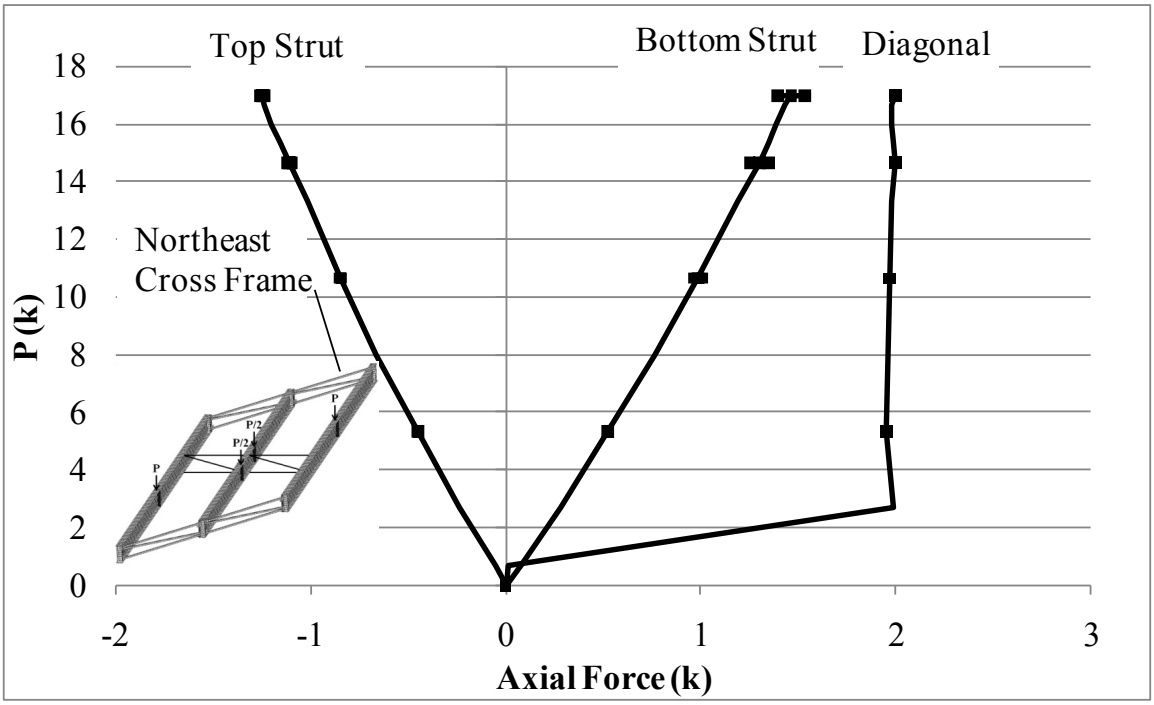

Figure A.68: NE end cross frame axial forces

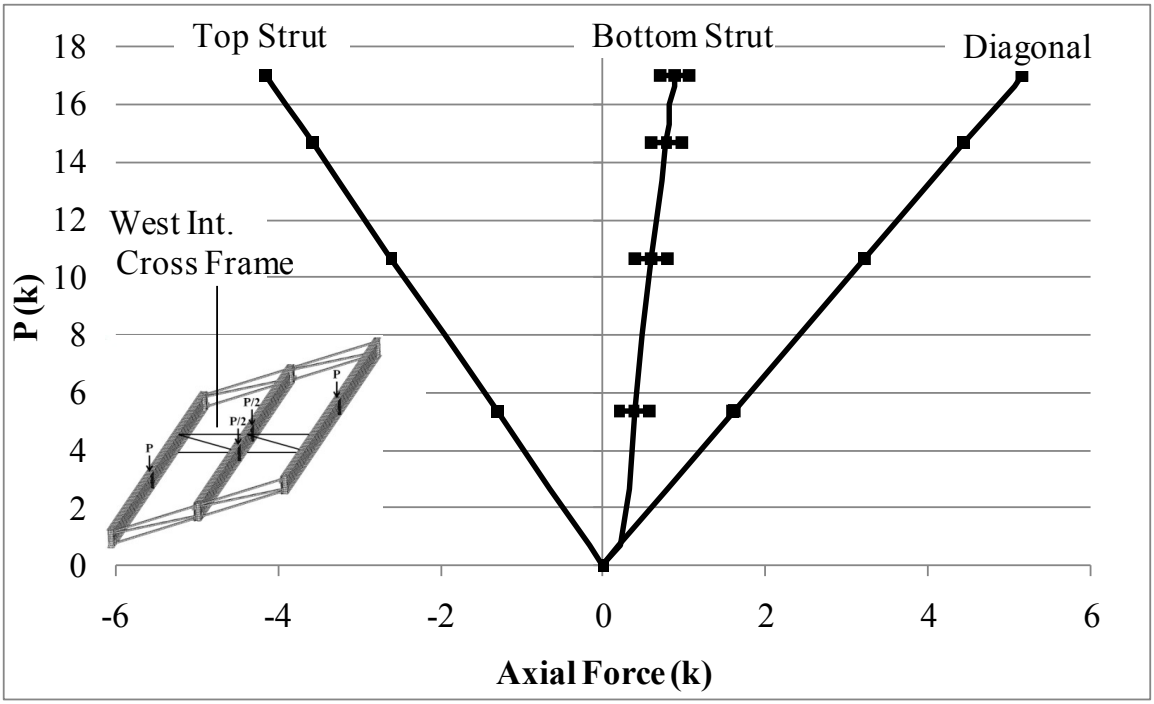

Figure A.69: West intermediate continuous cross frame axial forces

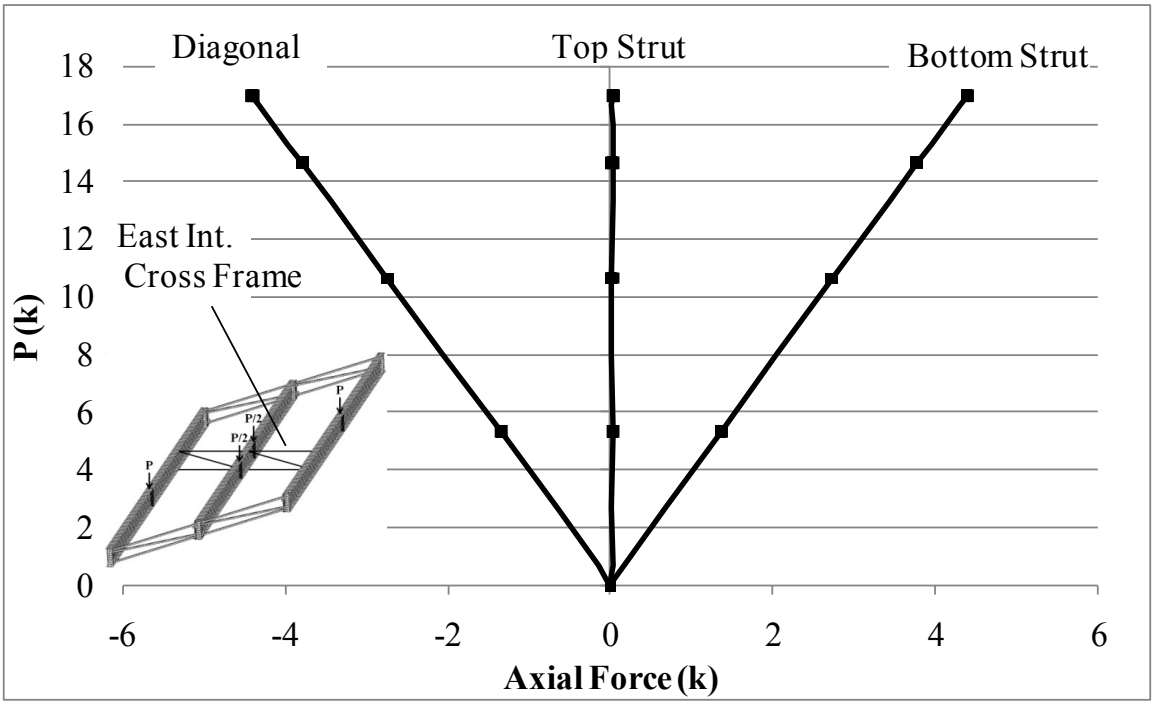

Figure A.70: East intermediate continuous cross frame axial forces

APPENDIX B

Finite Element Model Validation Results

B.1 CONNECTION MODEL VALIDATION

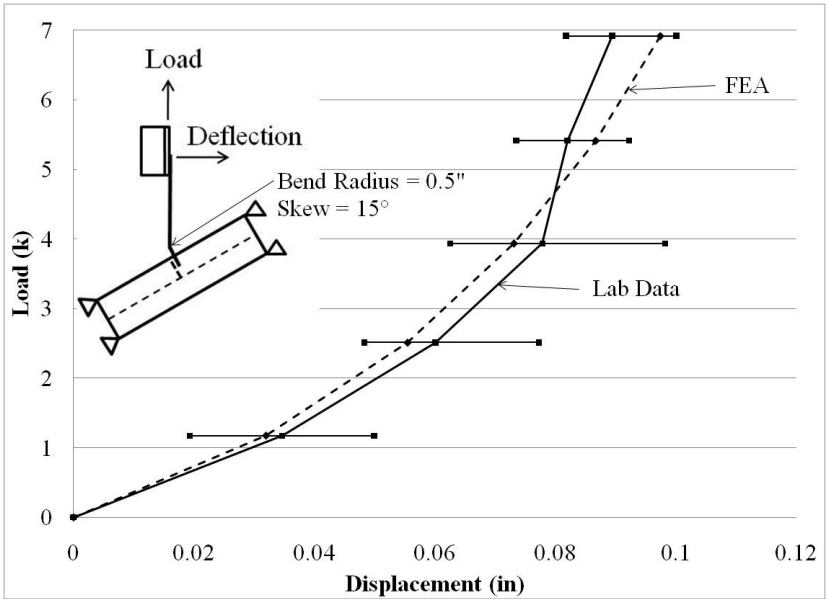

Figure B.1: 15° skew specimen and FEA lateral deflection results

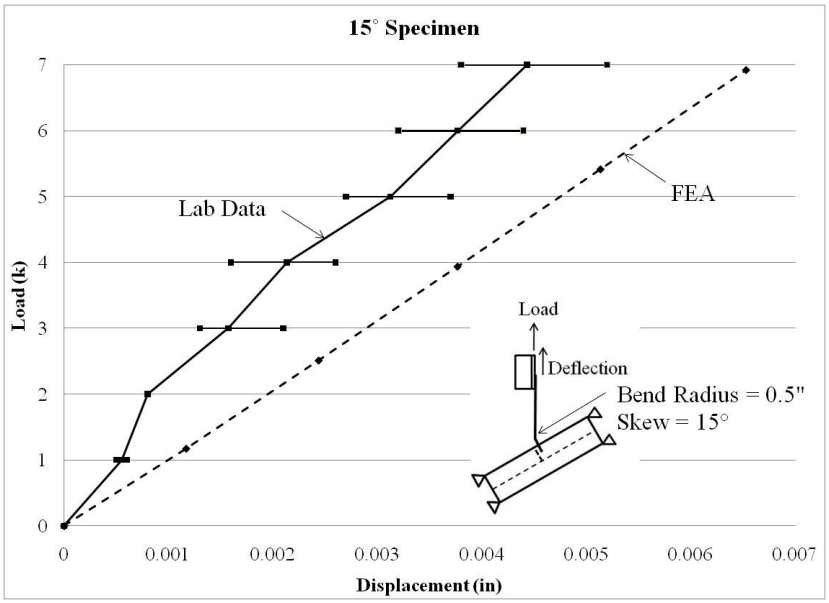

Figure B.2: 15° skew specimen and FEA lateral deflection results

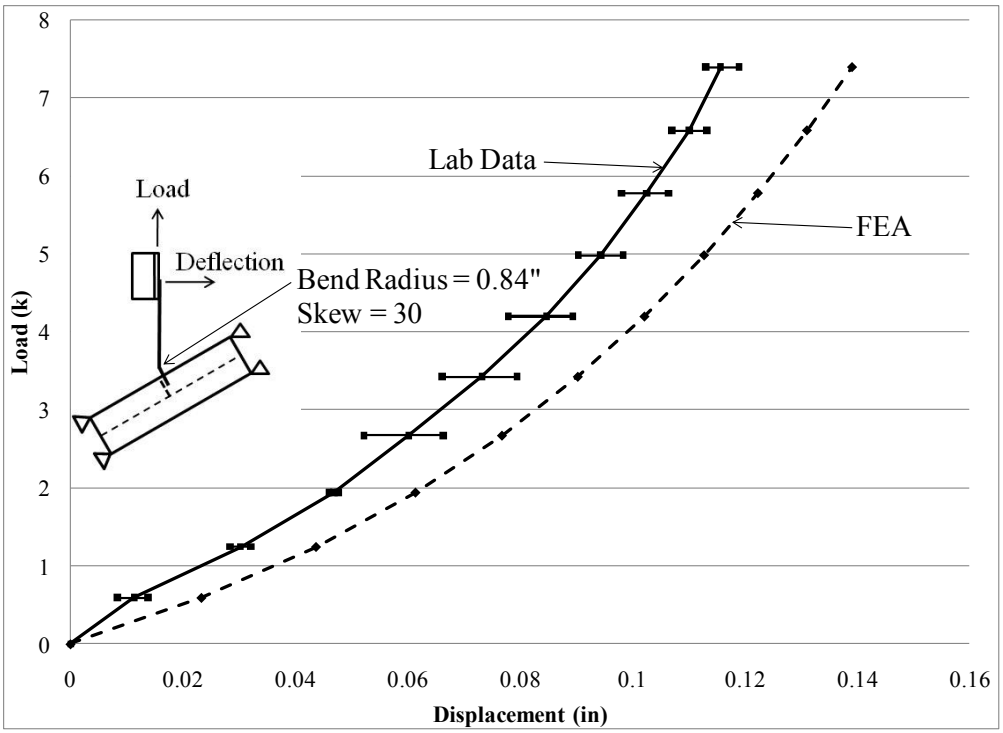

Figure B.3: 30° skew specimen and FEA lateral deflection results

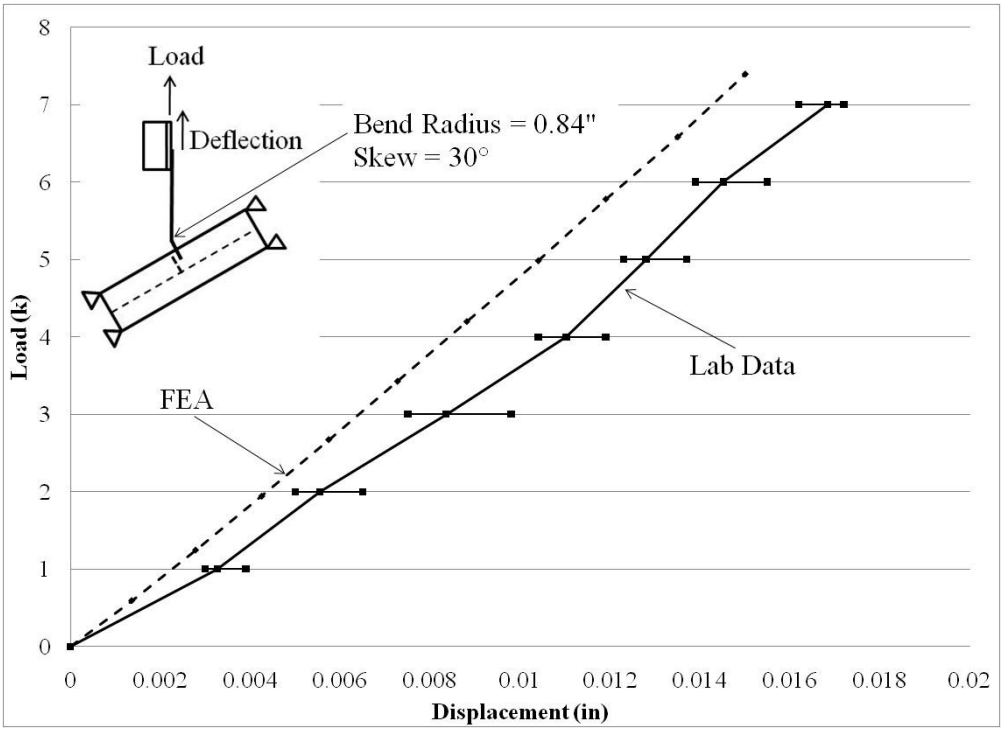

Figure B.4: 30° skew specimen and FEA vertical deflection results

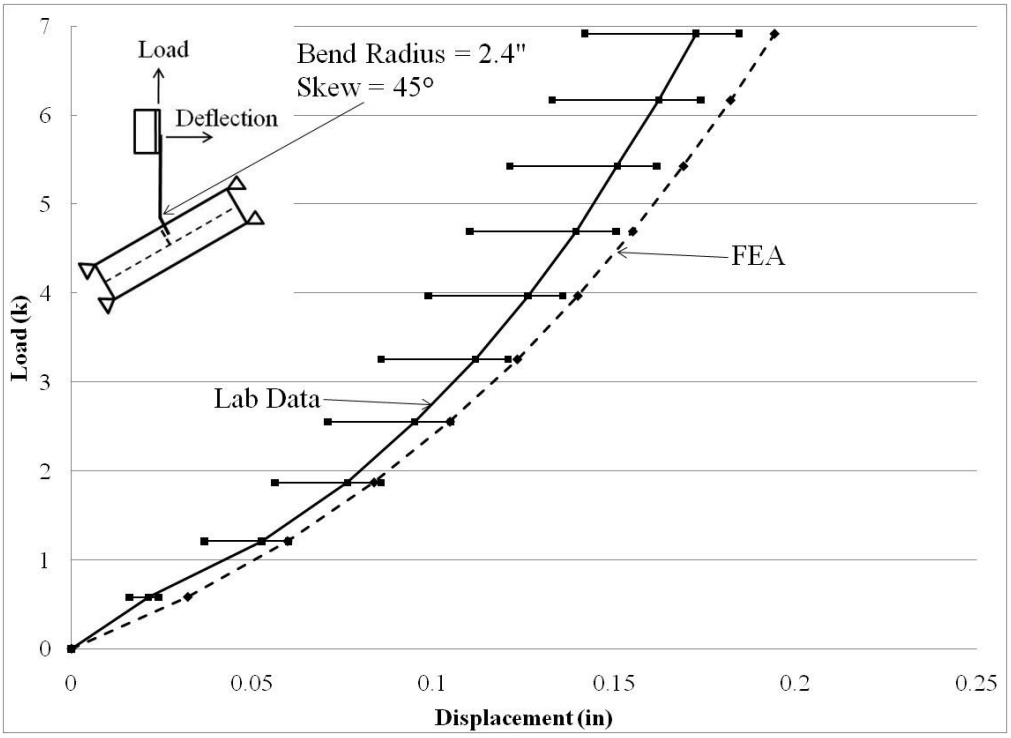

Figure B.5: 45° skew specimen and FEA lateral deflection results

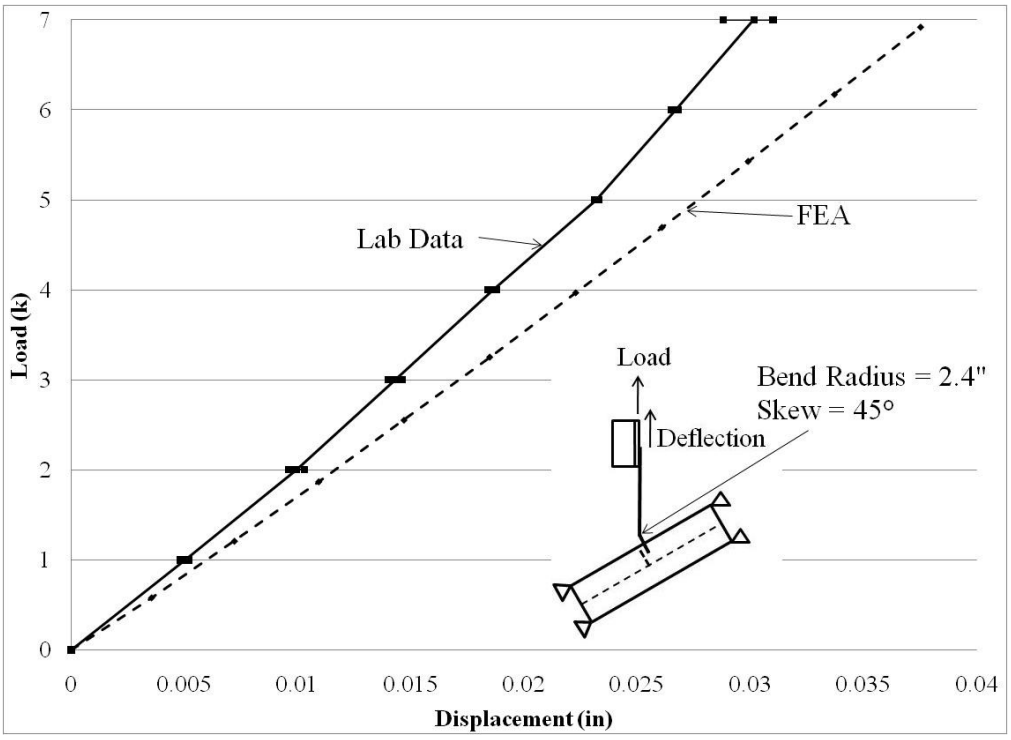

Figure B.6: 45° skew specimen and FEA vertical deflection results

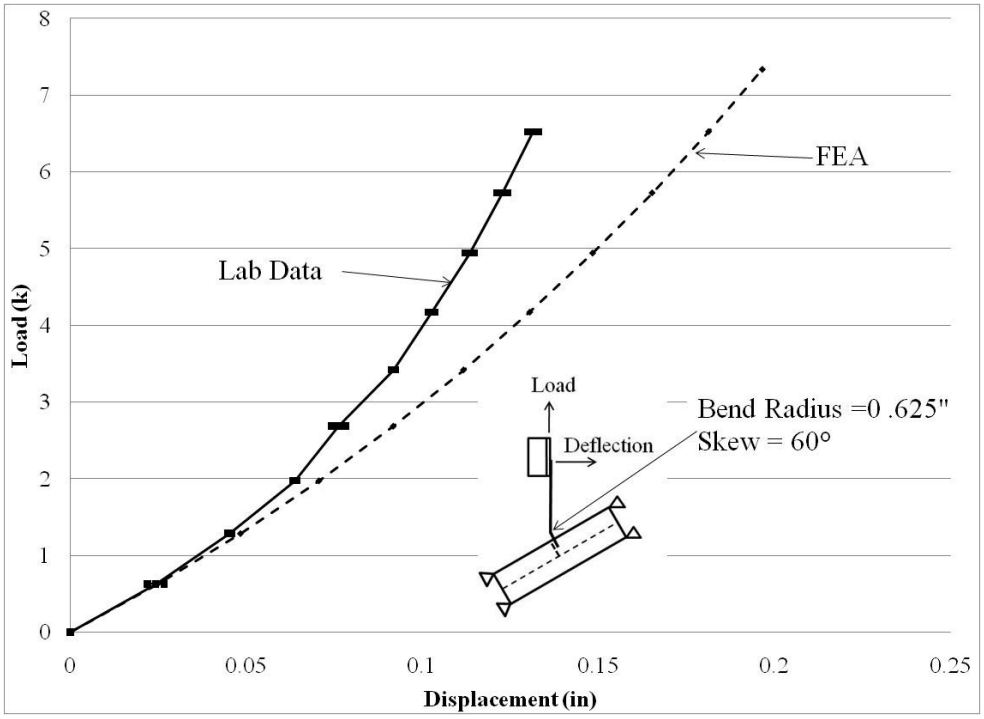

Figure B.7: 60° skew specimen and FEA lateral deflection results

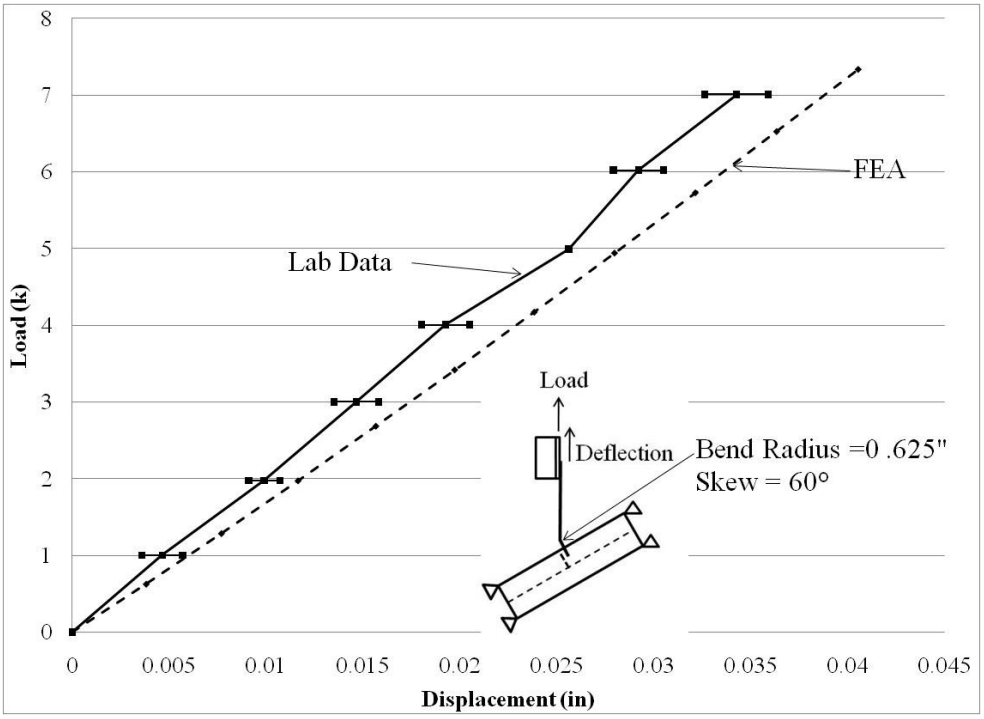

Figure B.8: 60° skew specimen and FEA vertical deflection results

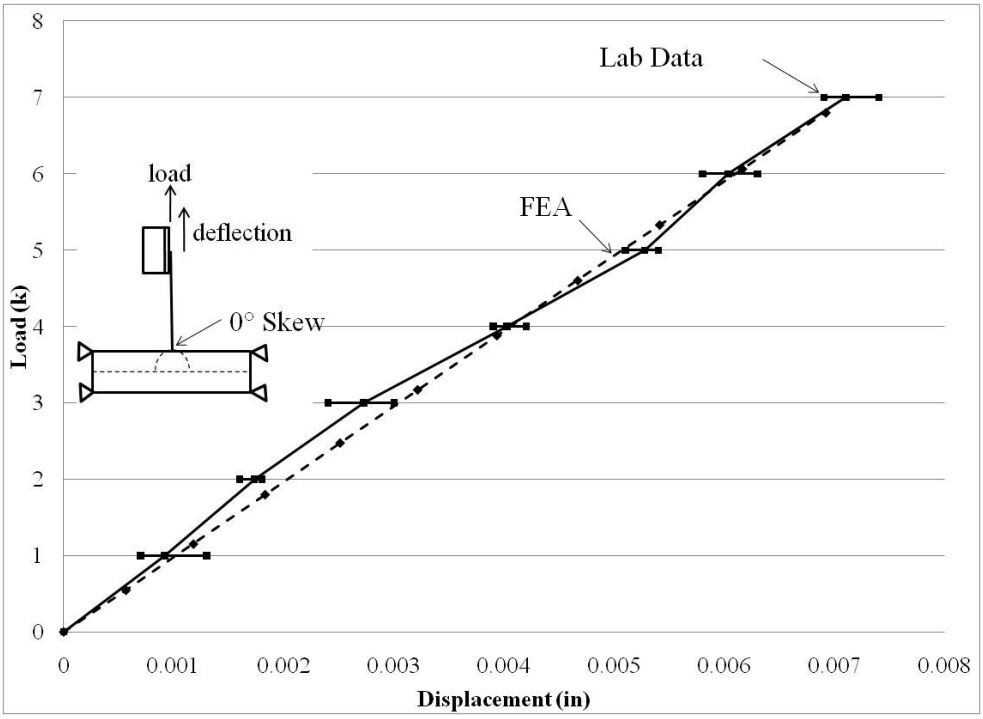

Figure B.9: 0° skew pipe specimen and FEA vertical deflection results

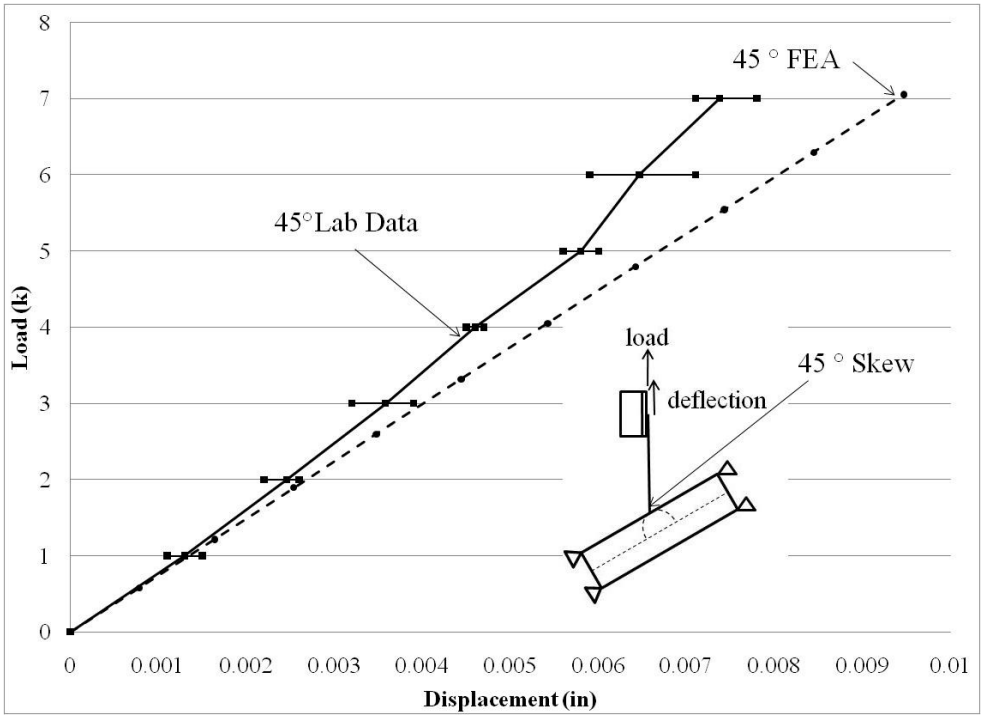

Figure B.10: 45° skew pipe specimen and FEA vertical deflection results

B.2 TWIN GIRDER VALIDATION RESULTS

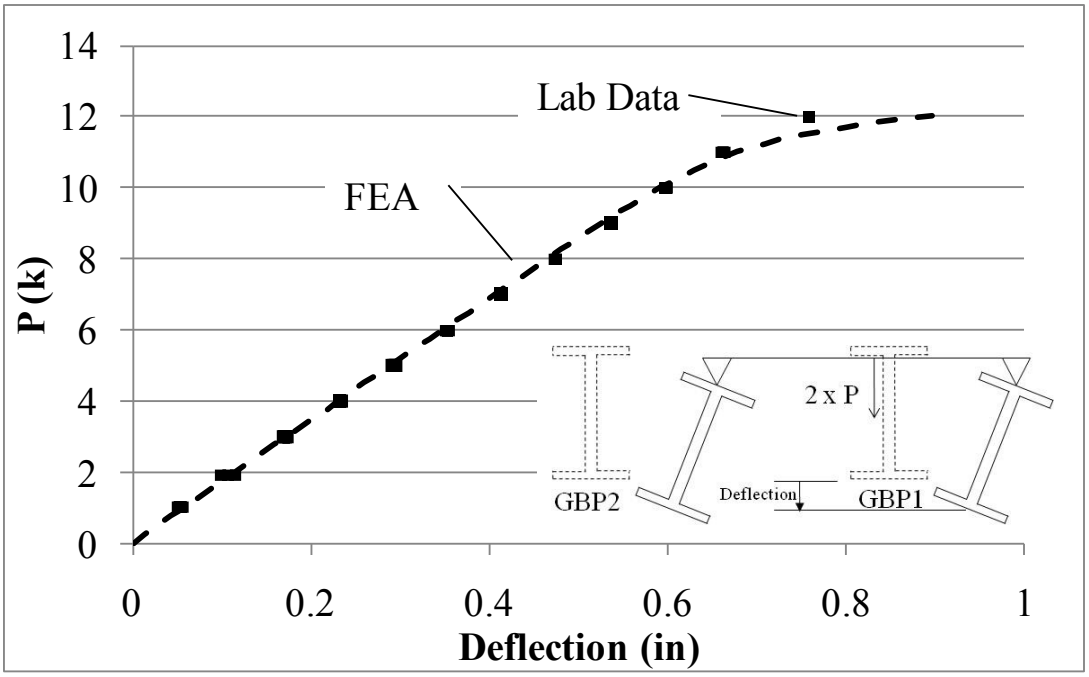

Figure B.11: GBP1 vertical deflection validation results

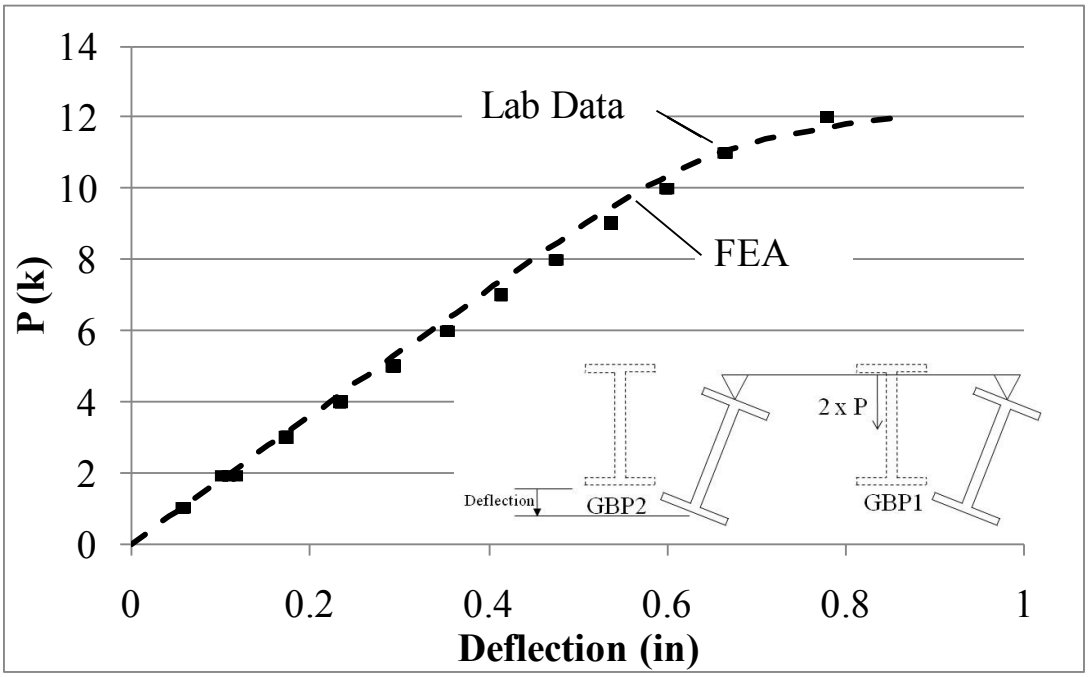

Figure B.12: GBP2 vertical deflection validation results

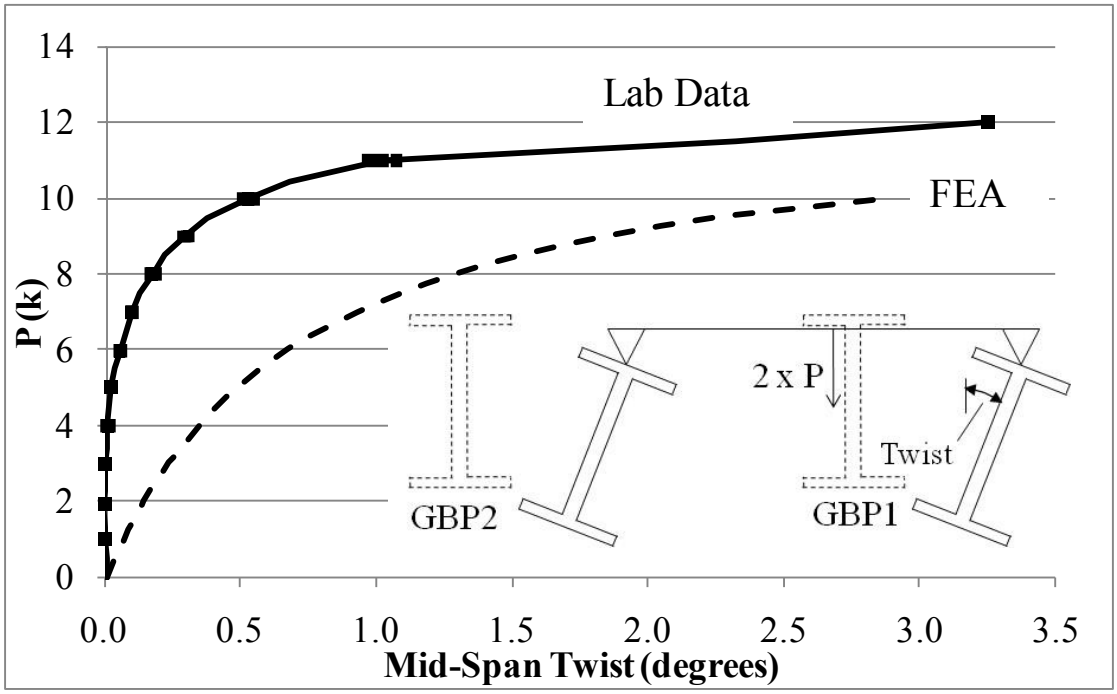

Figure B.13: GBP1 mid-span twist validation results

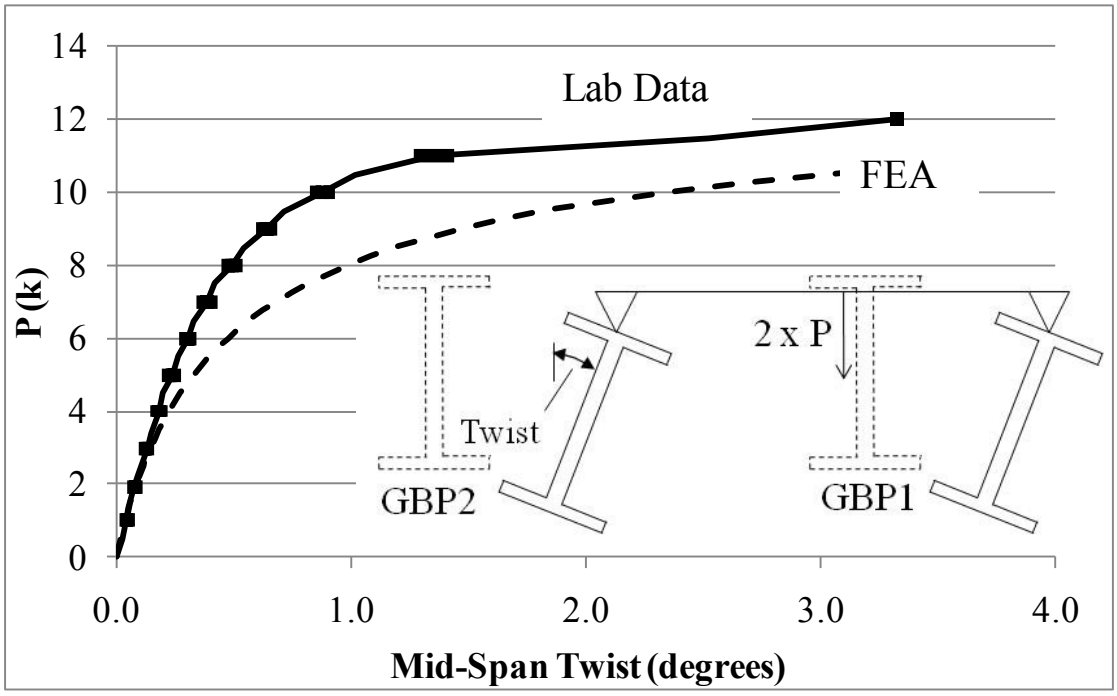

Figure B.14: GBP2 mid-span twist validation results

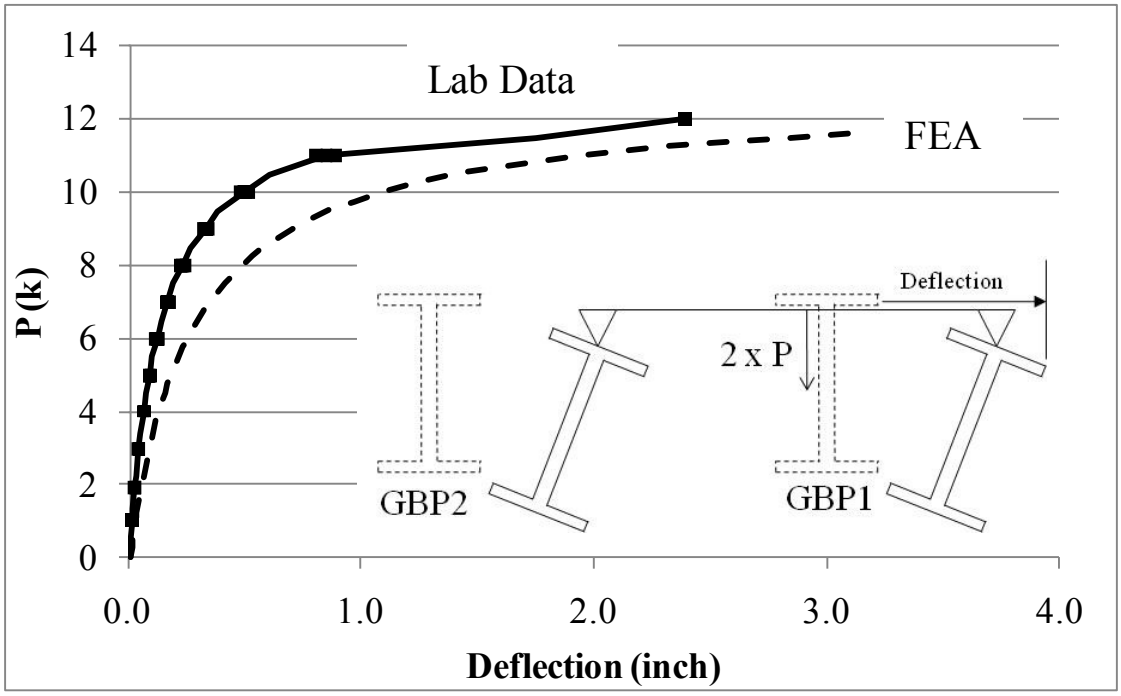

Figure B.15: GBP1 mid-span top flange lateral deflection validation results

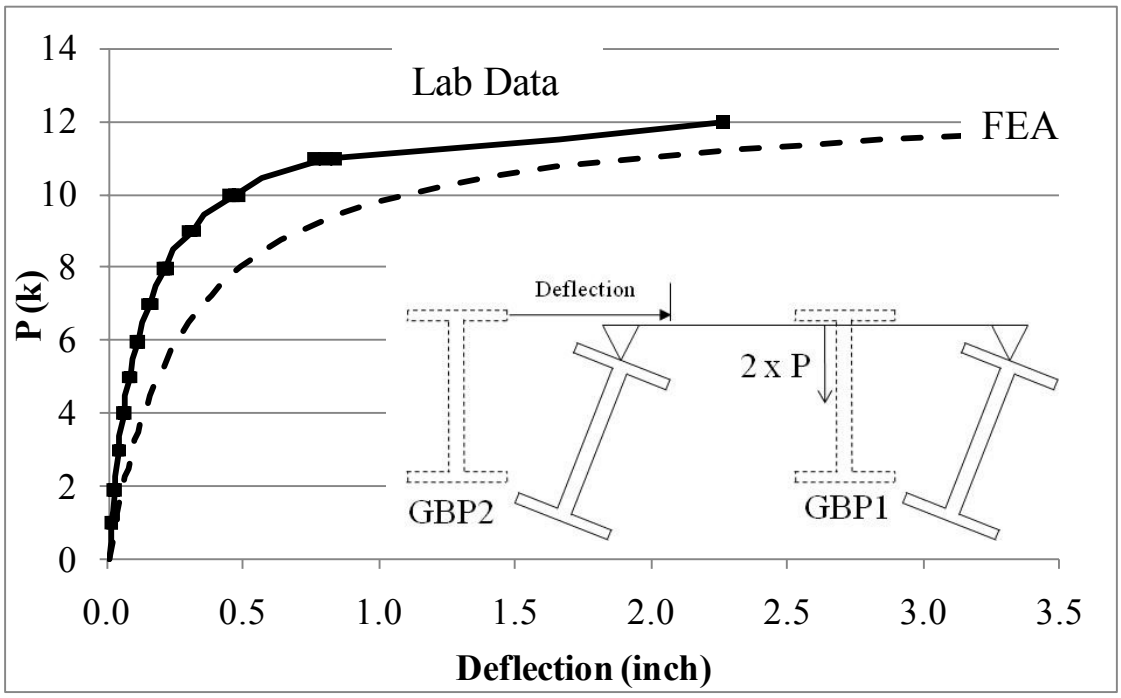

Figure B.16: GBP2 mid-span top flange lateral deflection validation results

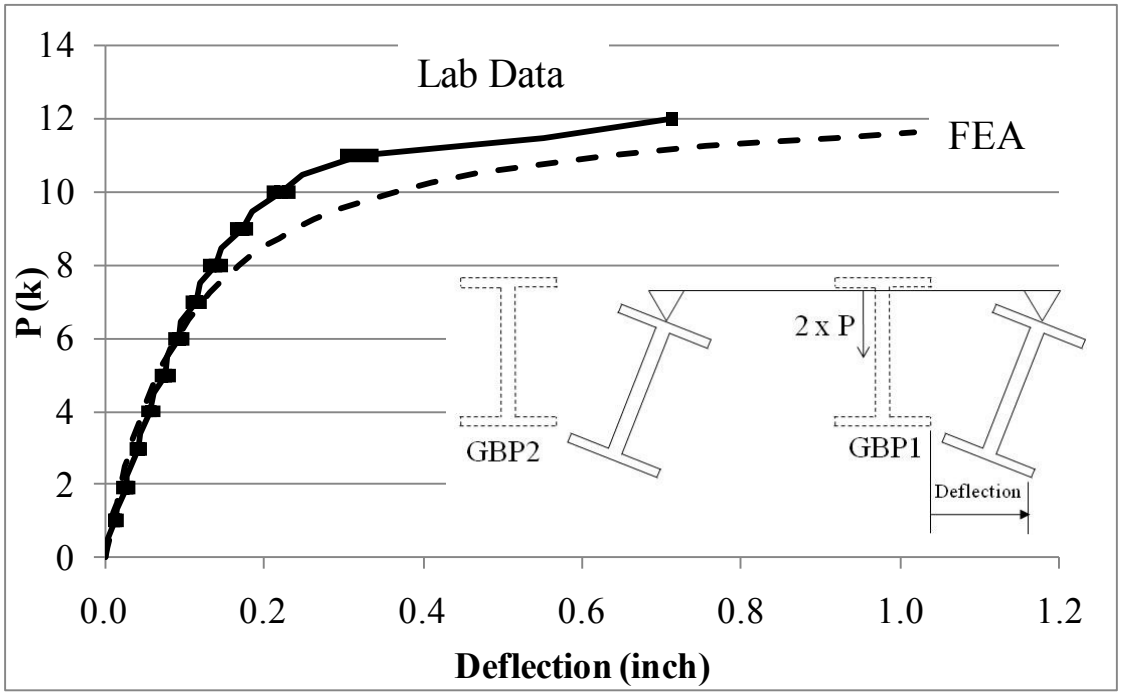

Figure B.17: GBP1 mid-span bottom flange lateral deflection validation results

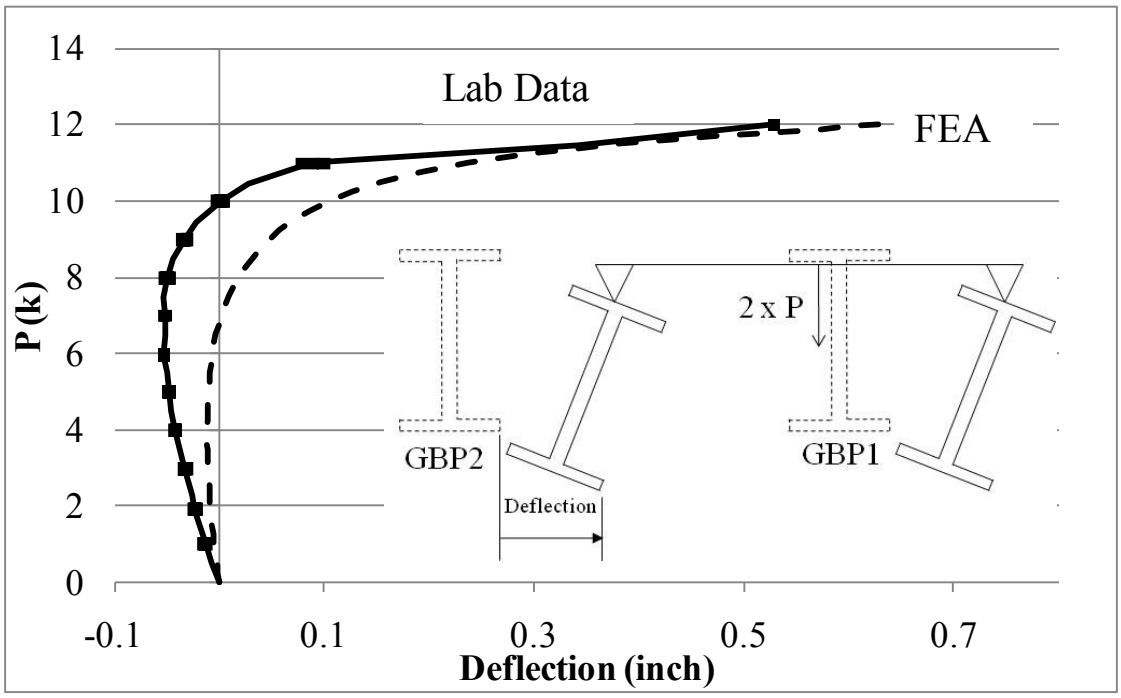

Figure B.18: GBP2 mid-span bottom flange lateral deflection validation results

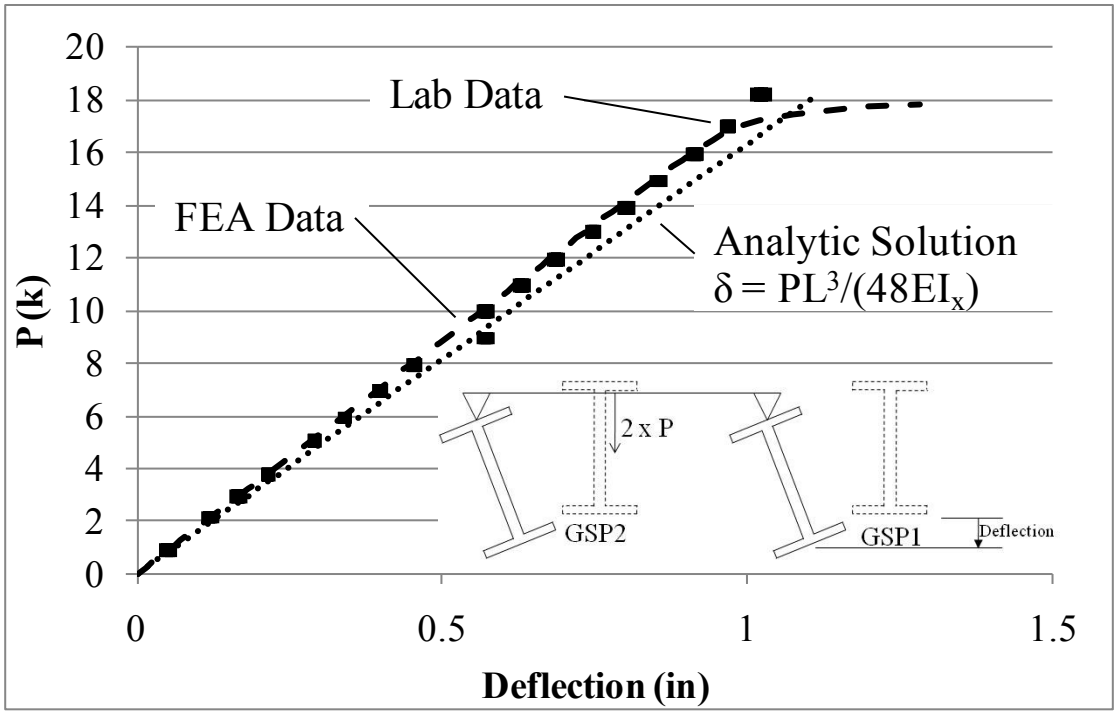

Figure B.19: GSP1 vertical deflection validation results

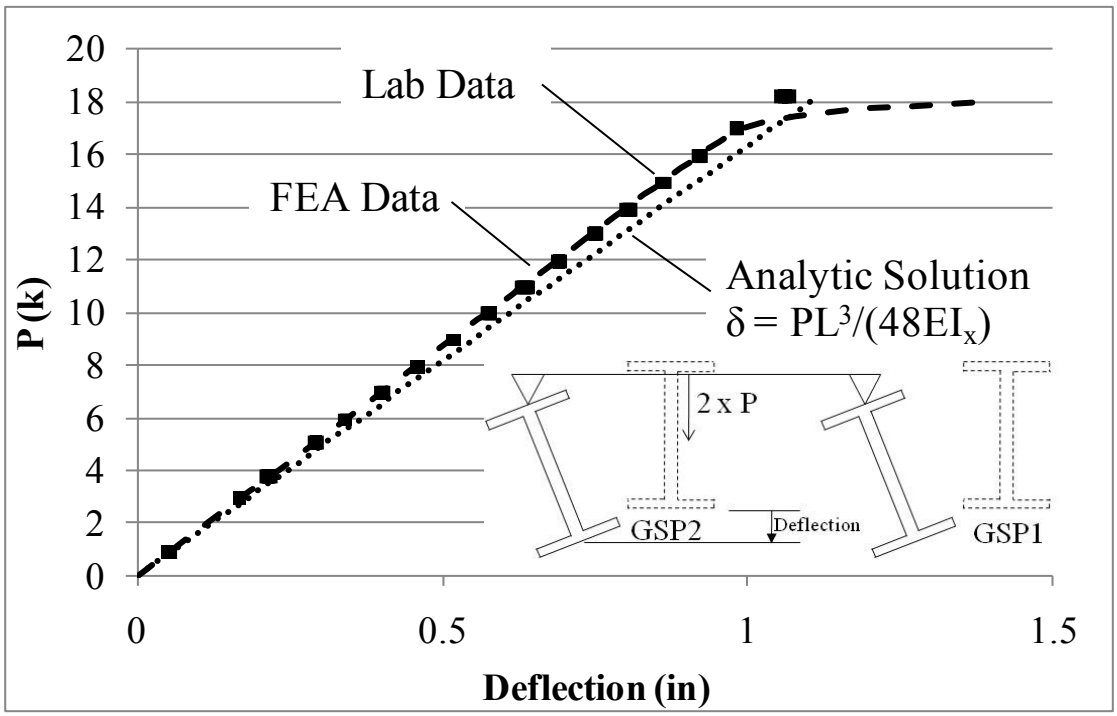

Figure B.20: GSP2 vertical deflection validation results

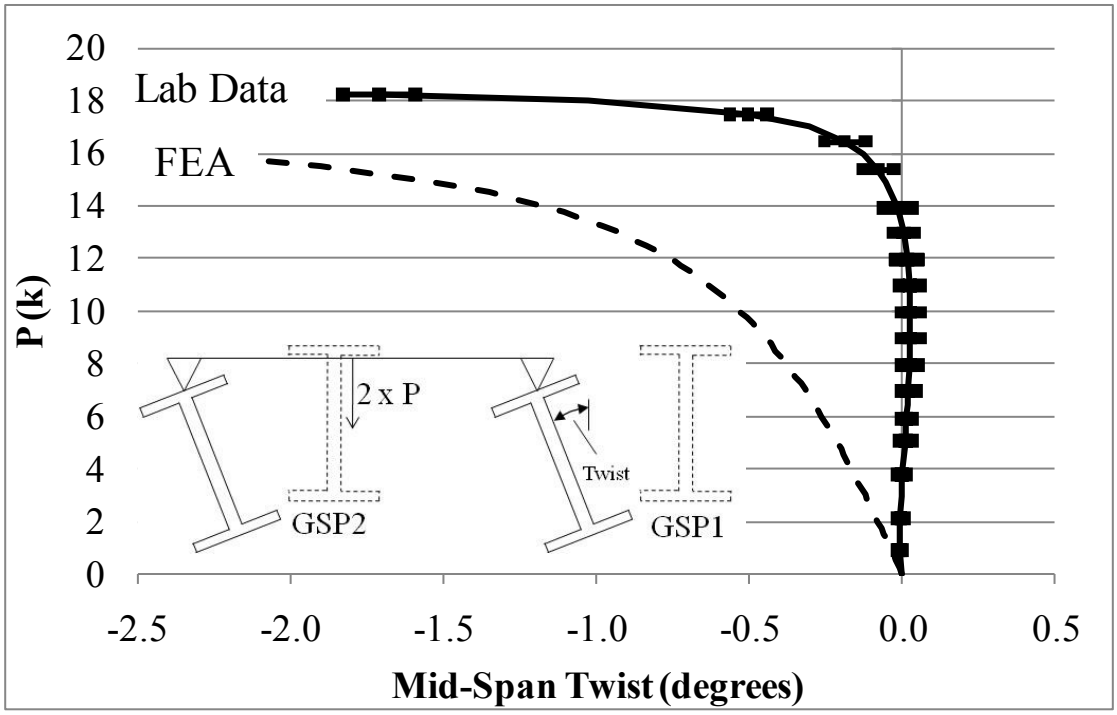

Figure B.21: GSP1 mid-span twist validation results

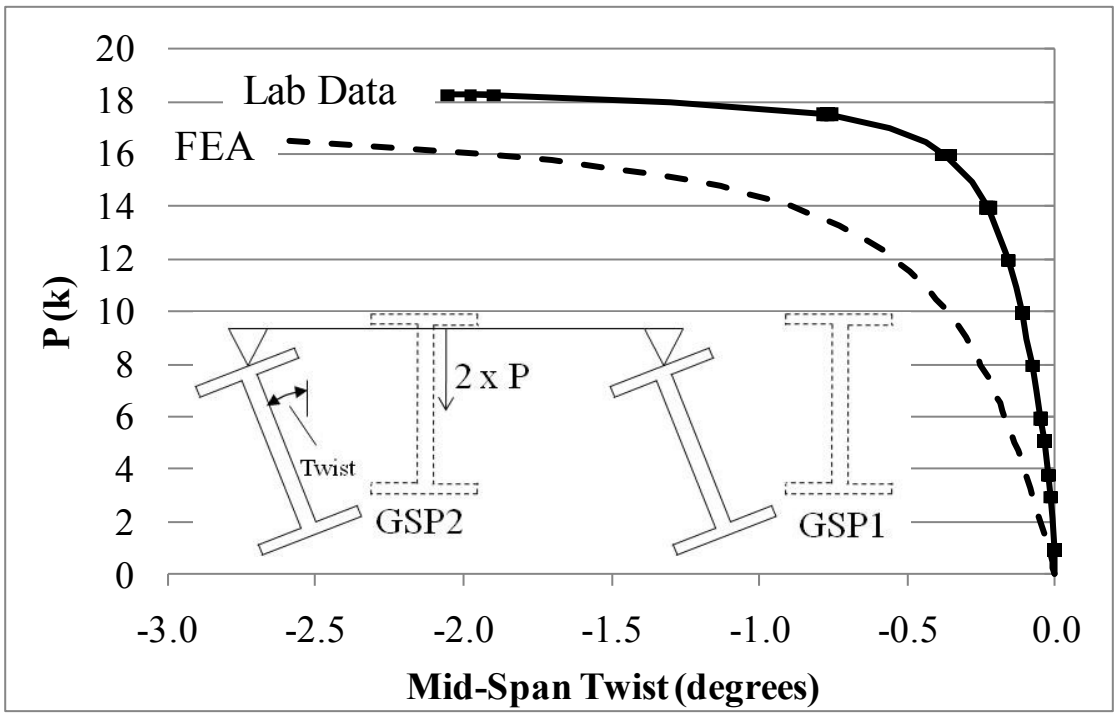

Figure B.22: GSP2 mid-span twist validation results

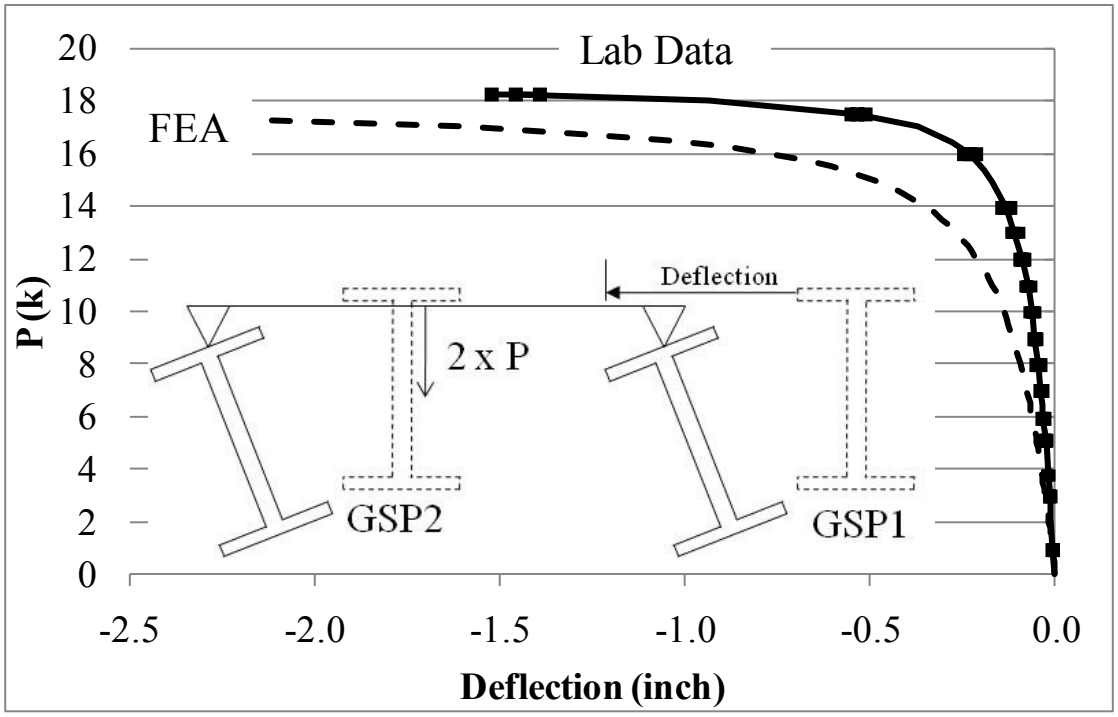

Figure B.23: GSP1 mid-span top flange lateral deflection validation results

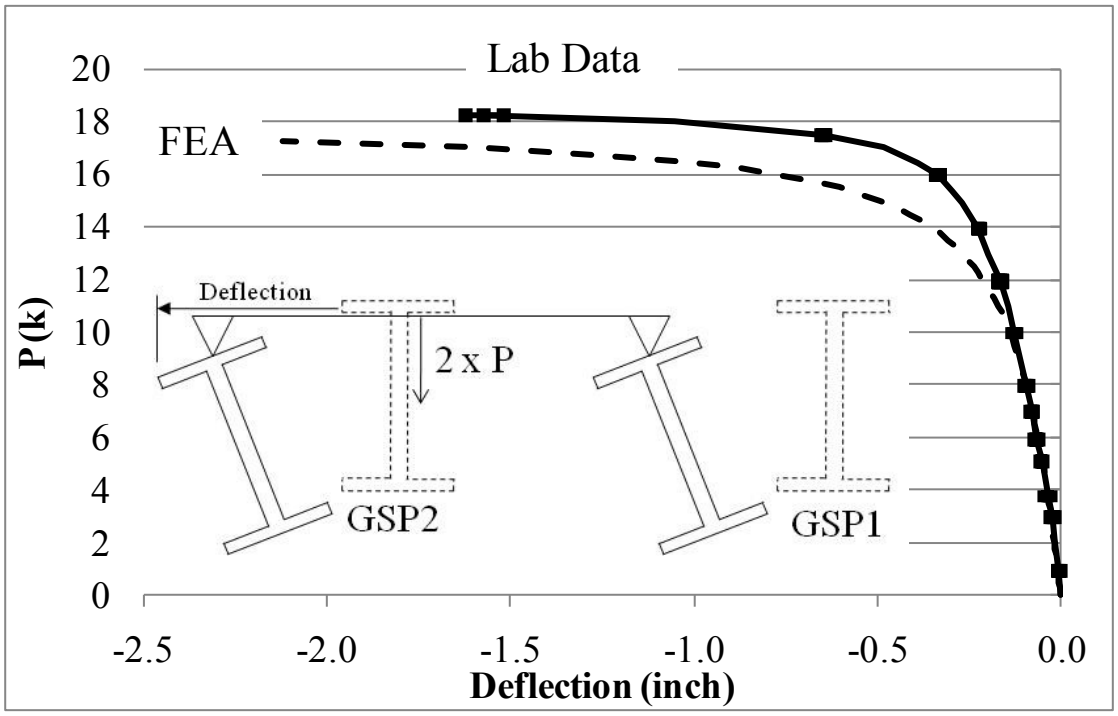

Figure B.24: GSP2 mid-span top flange lateral deflection validation results

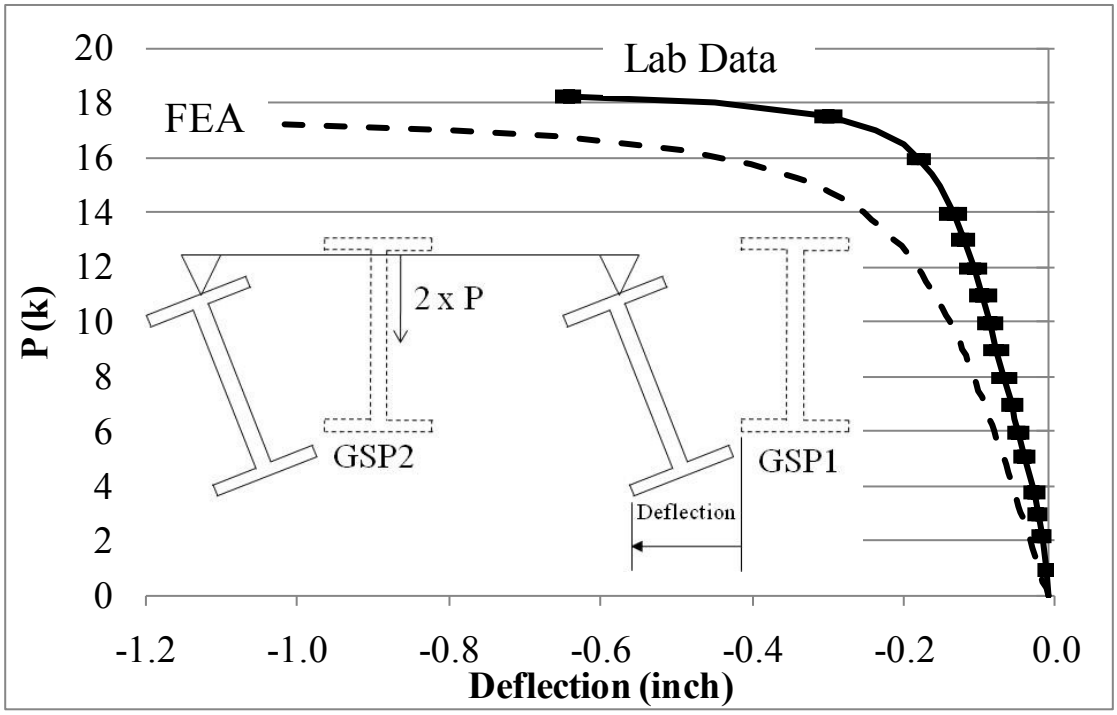

Figure B.25: GSP1 mid-span bottom flange lateral deflection validation results

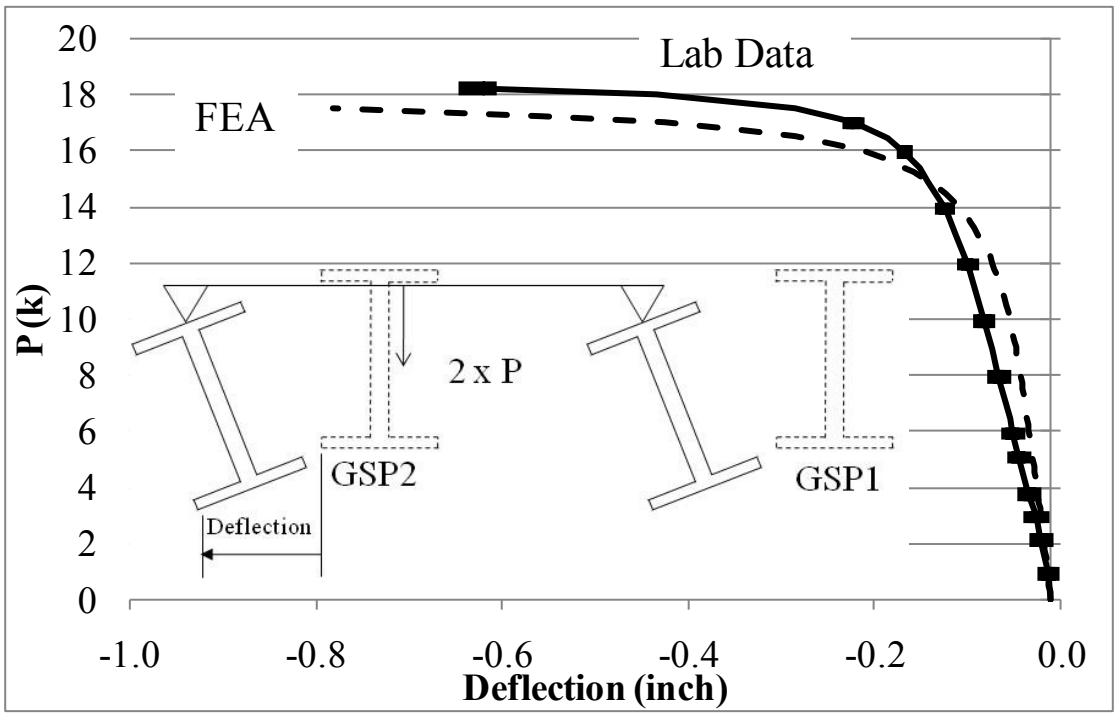

Figure B.26: GSP2 mid-span bottom flange lateral deflection validation results

B.3 THREE GIRDER PIPE-STIFFENER CROSS FRAME VALIDATION RESULTS

B.3.1 No Intermediate Cross Frames

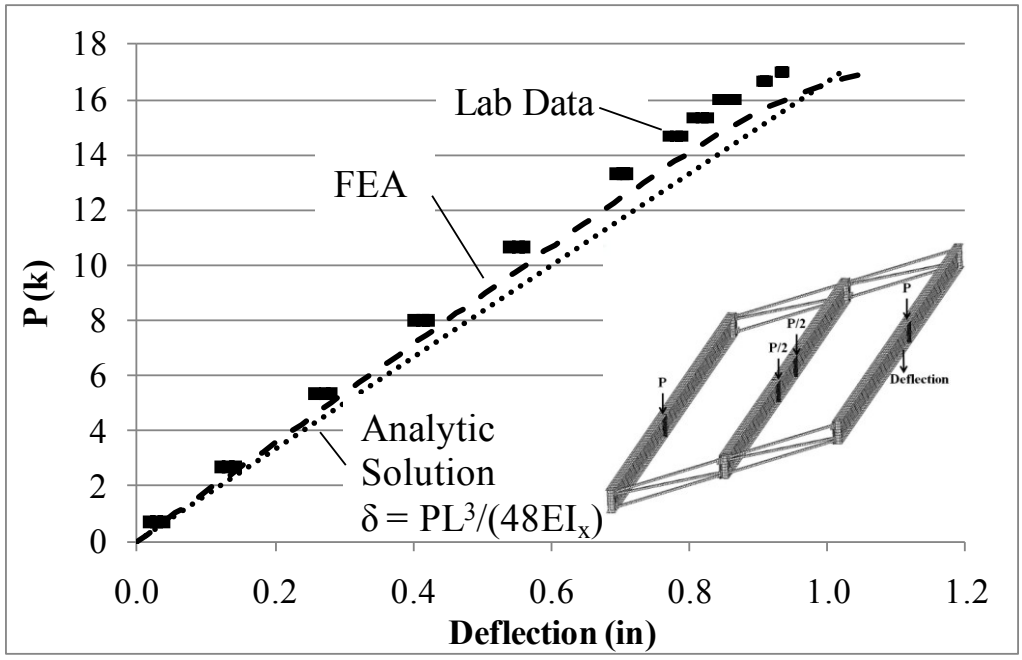

Figure B.27: GSP1 mid-span vertical deflection validation data

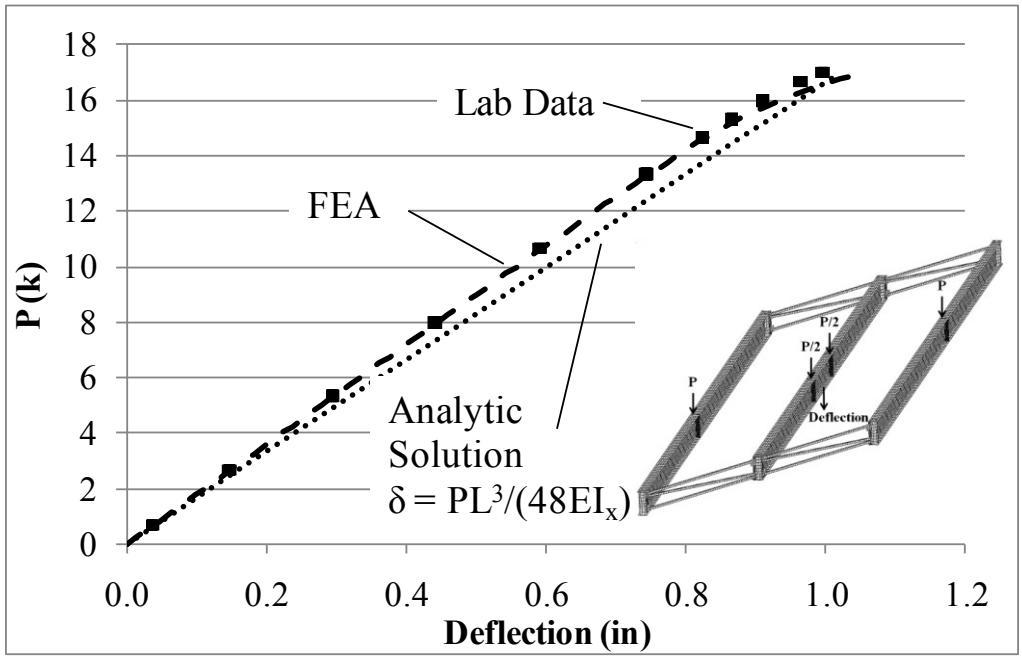

Figure B.28: GSP2 mid-span vertical deflection validation data

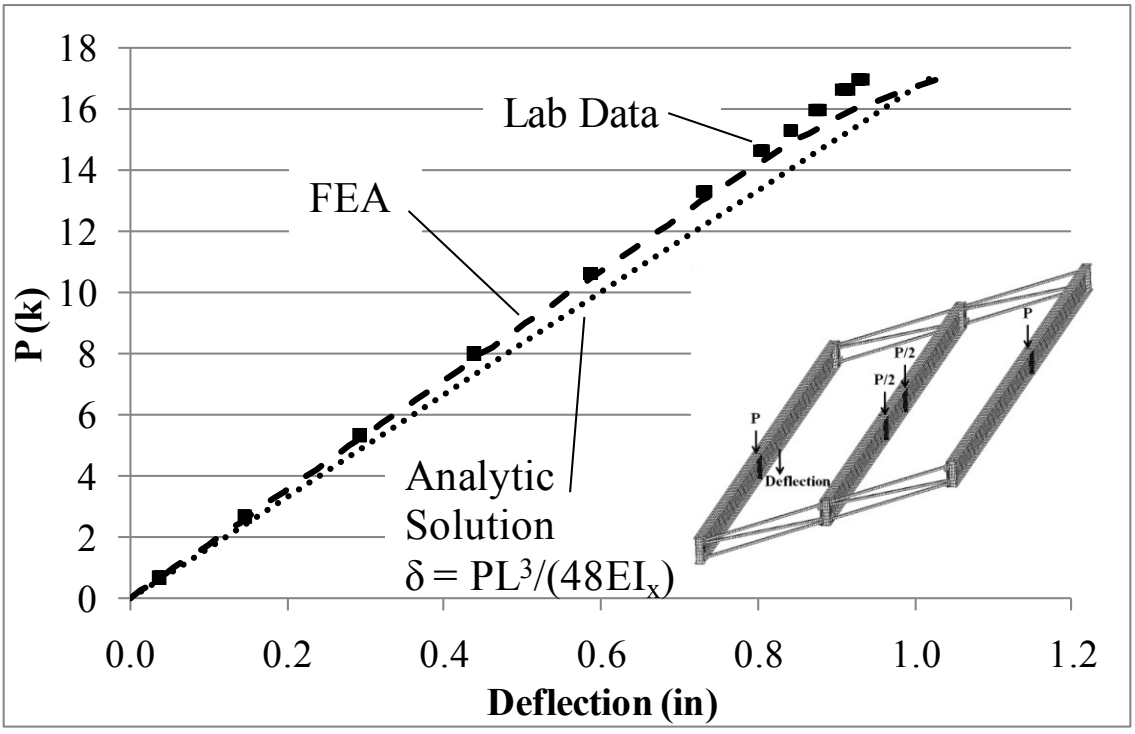

Figure B.29: GSP3 mid-span vertical deflection validation data

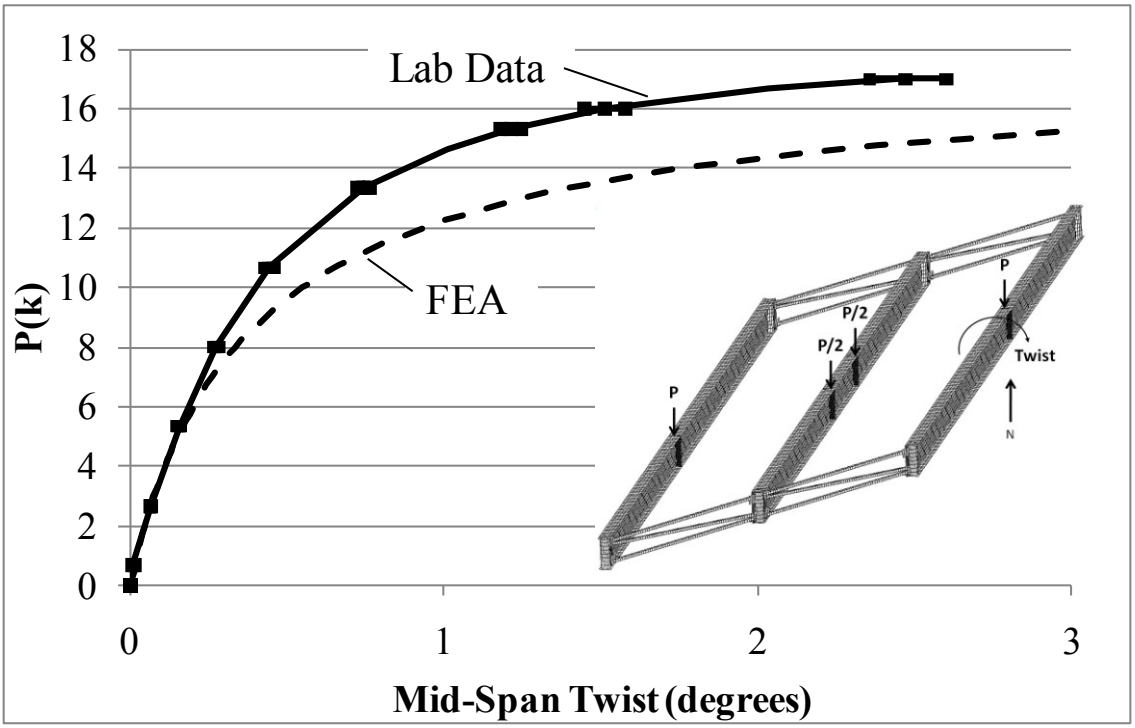

Figure B.30: GSP1 mid-span twist validation data

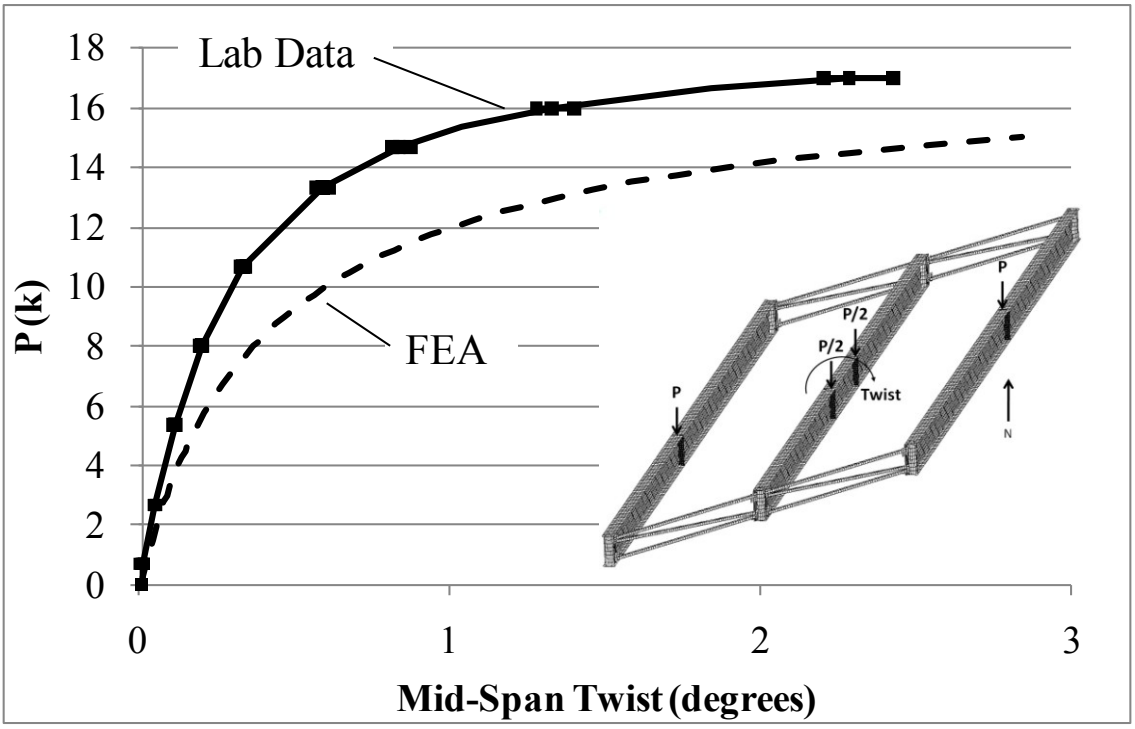

Figure B.31: GSP2 mid-span twist validation data

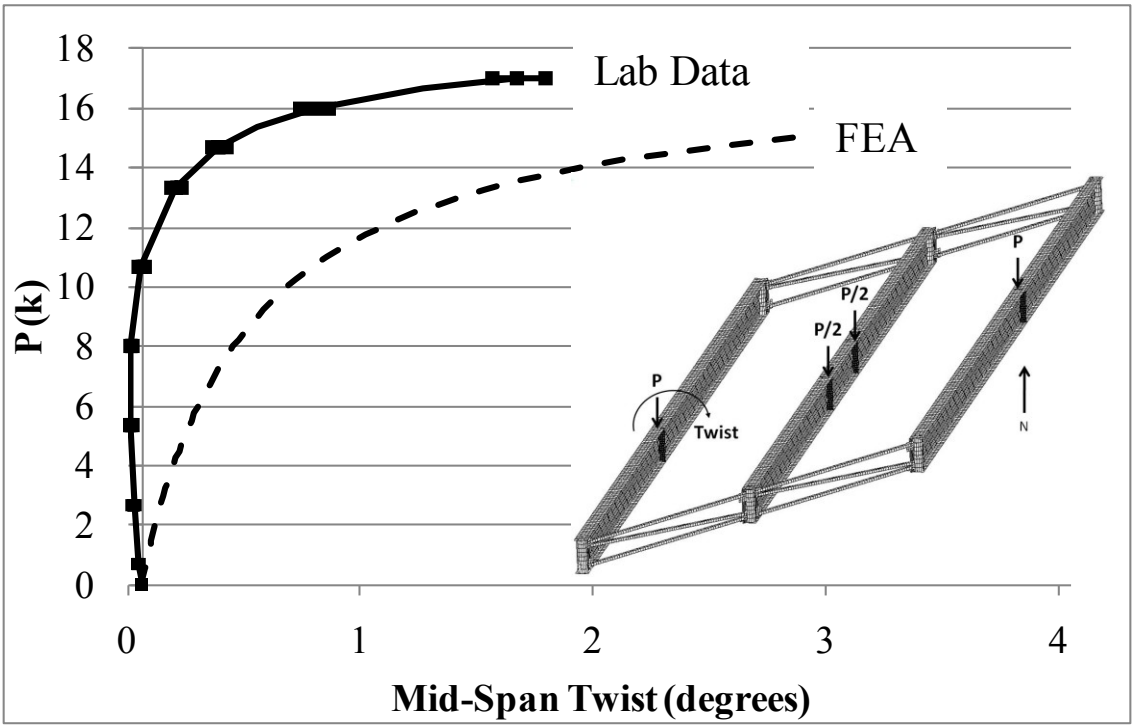

Figure B.32: GSP3 mid-span twist validation data

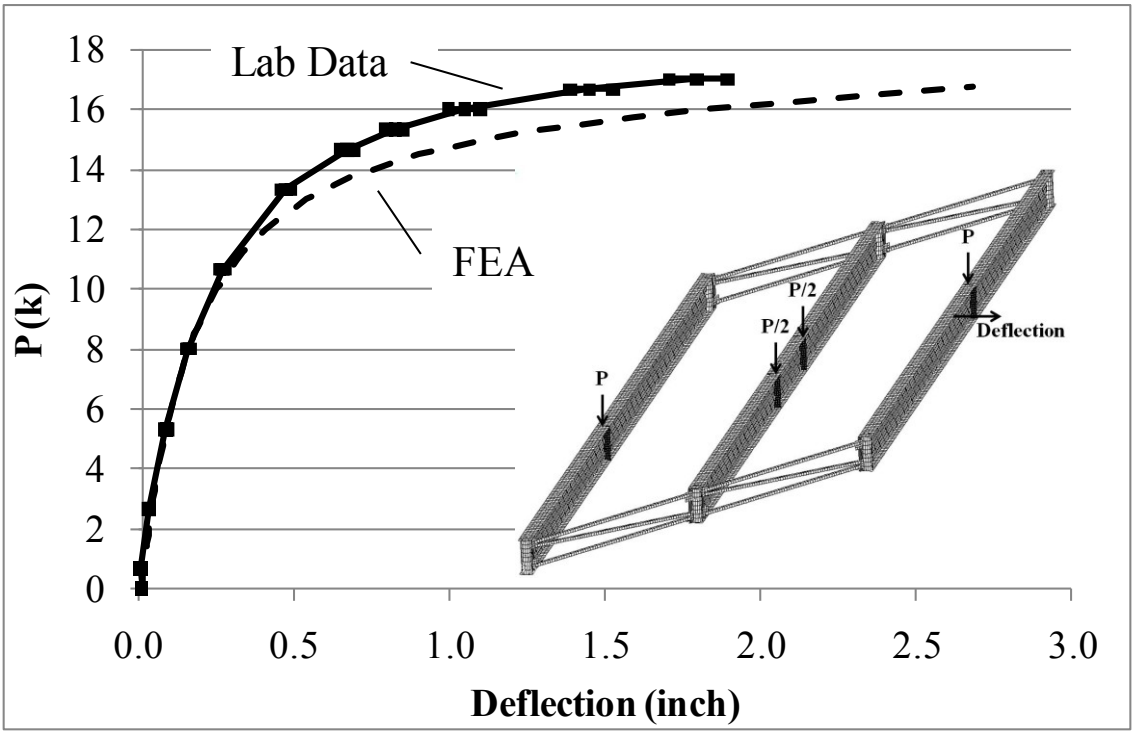

Figure B.33: GSP1 mid-span top flange lateral deflection validation data

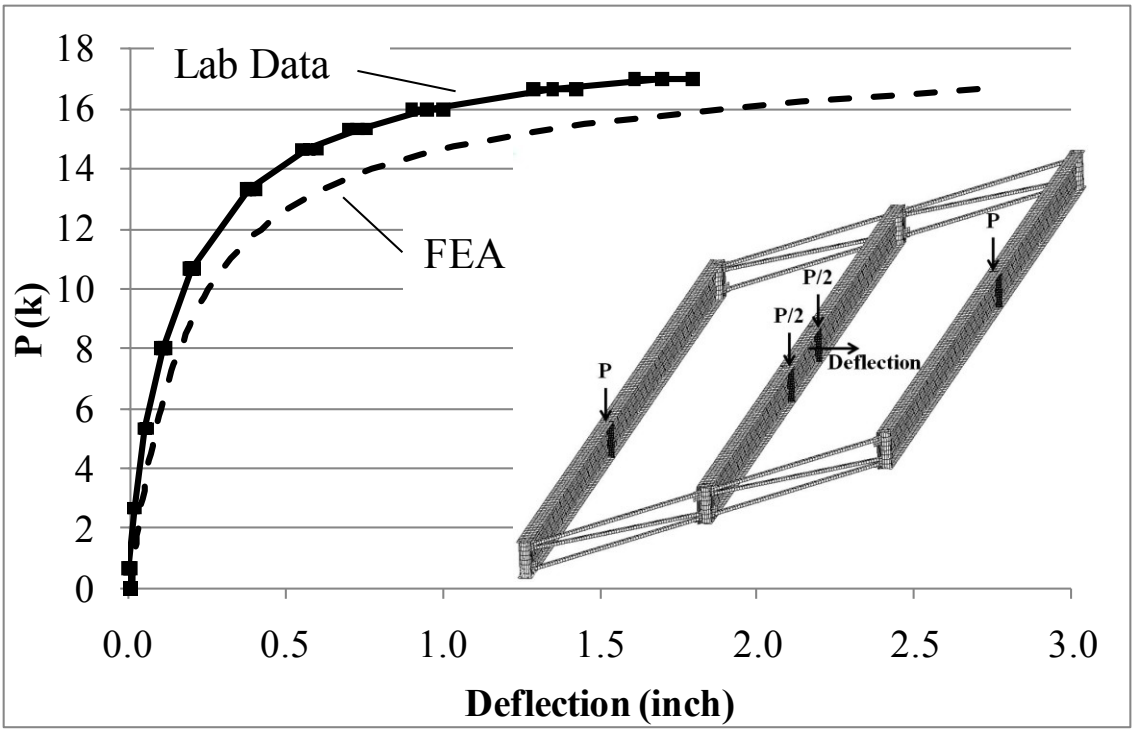

Figure B.34: GSP2 mid-span top flange lateral deflection validation data

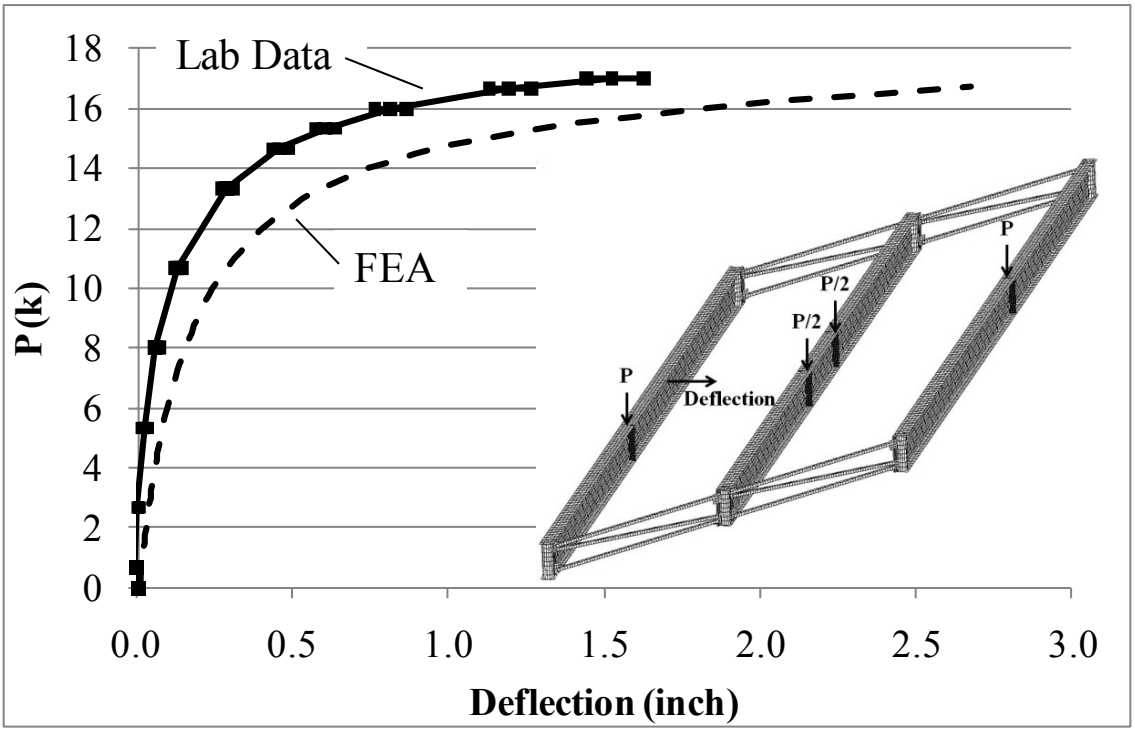

Figure B.35: GSP3 mid-span top flange lateral deflection validation data

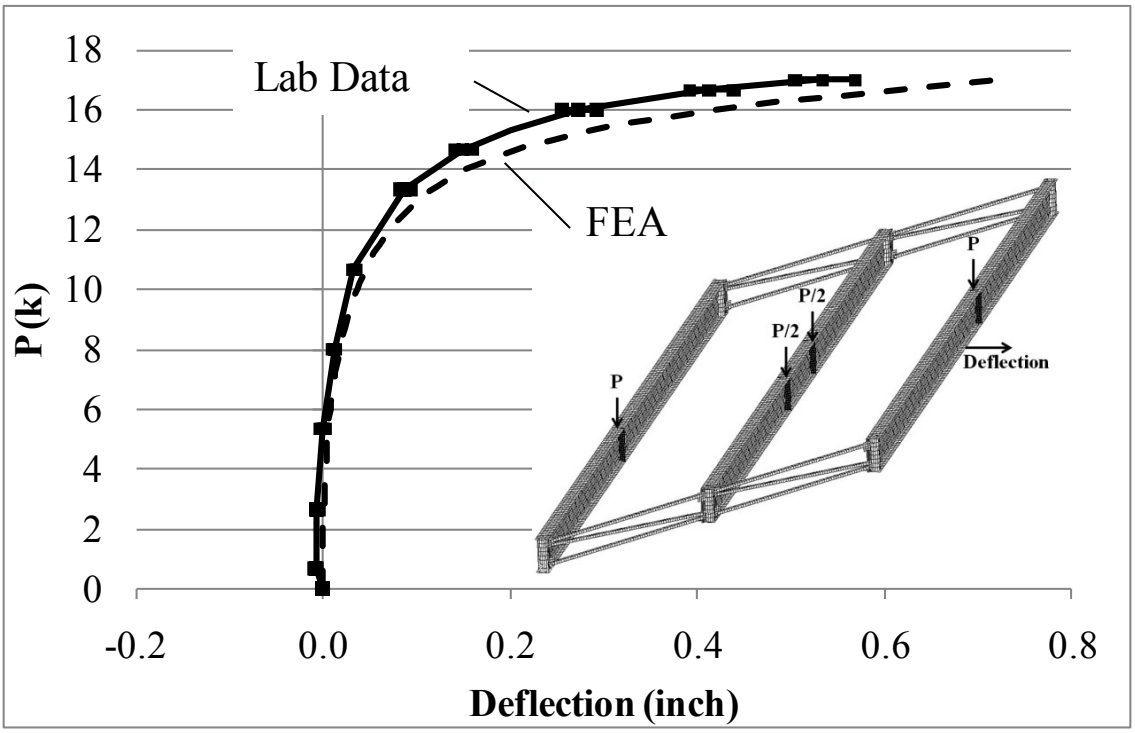

Figure B.36: GSP1 mid-span bottom flange lateral deflection validation data

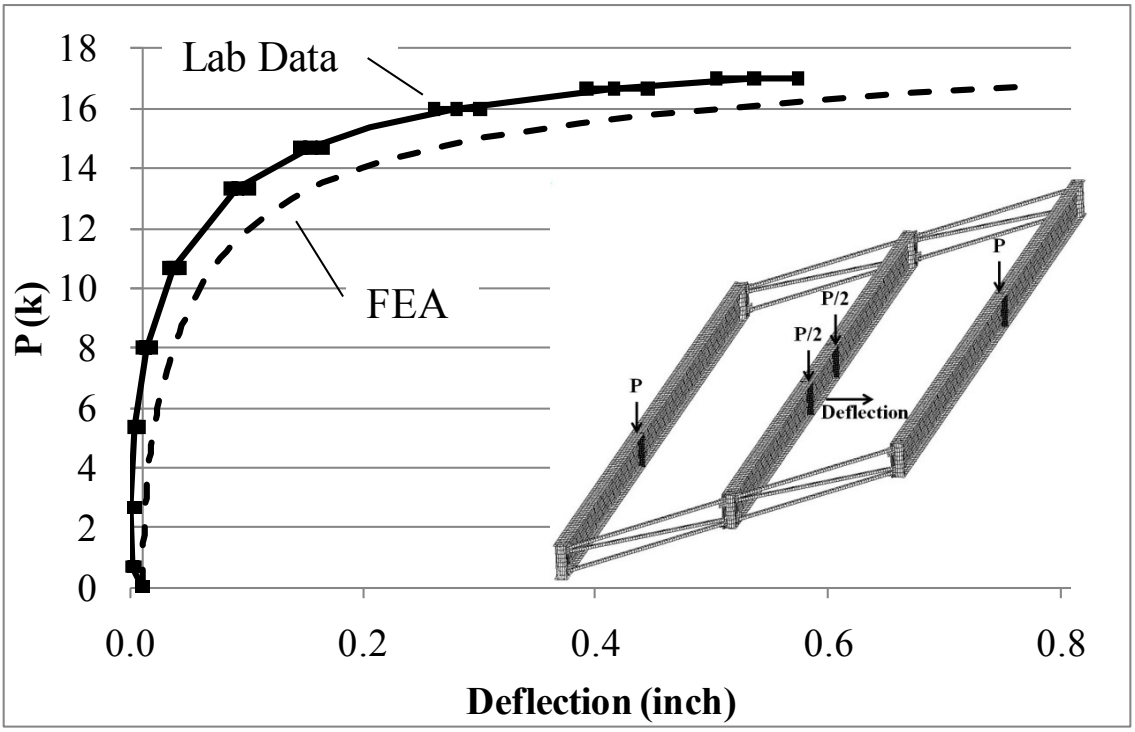

Figure B.37: GSP2 mid-span bottom flange lateral deflection validation data

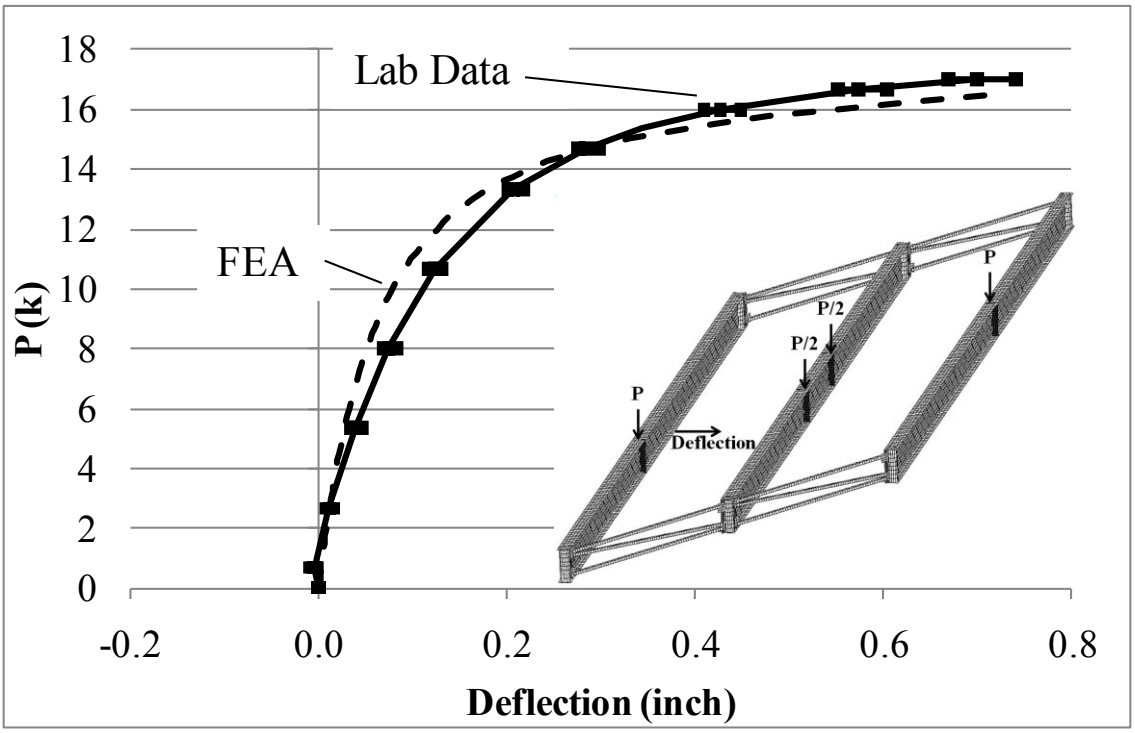

Figure B.38: GSP3 mid-span bottom flange lateral deflection validation data

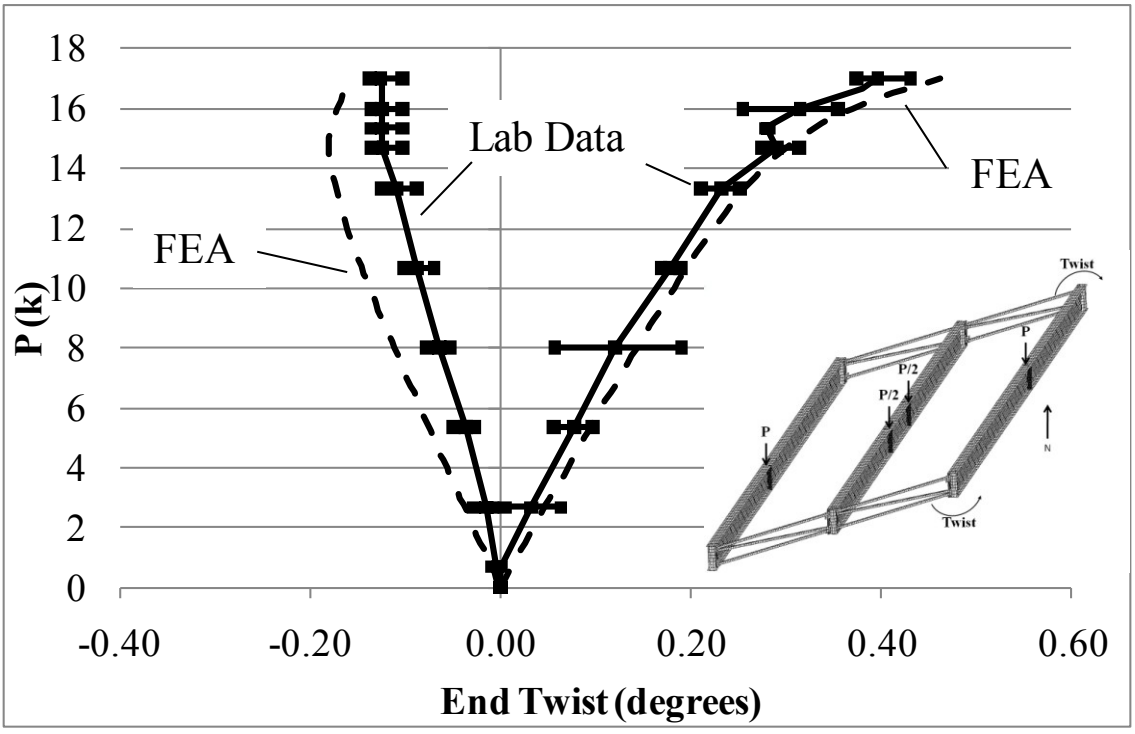

Figure B.39: GSP1 end twist validation data

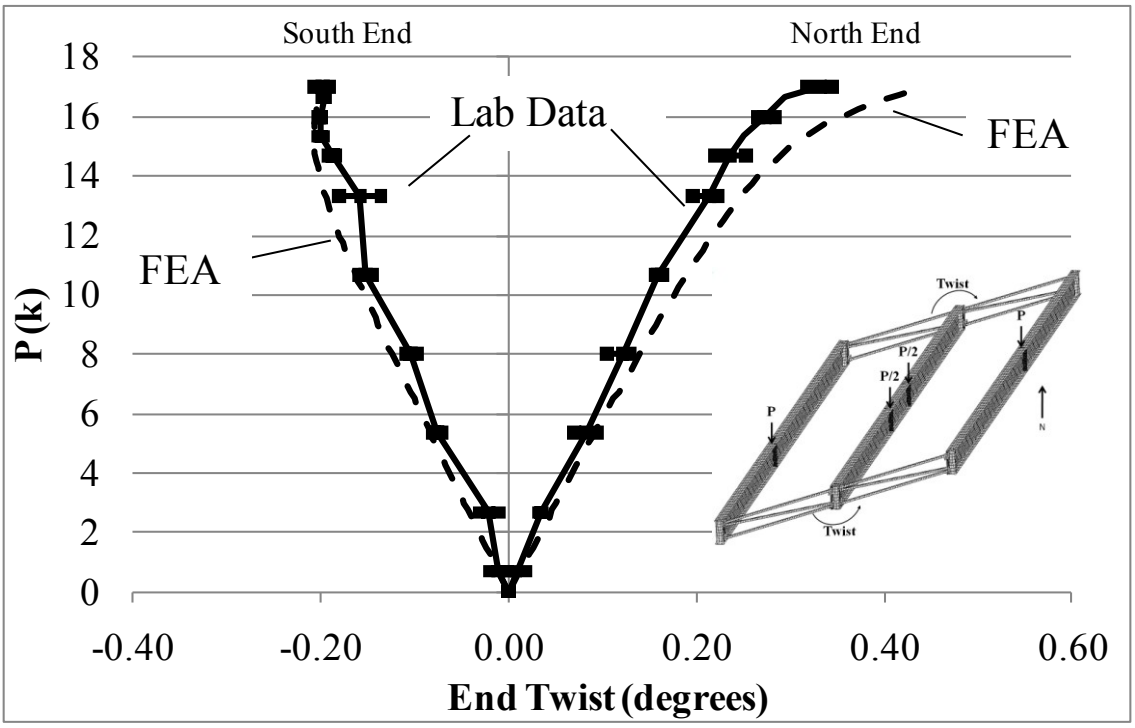

Figure B.40: GSP2 end twist validation data

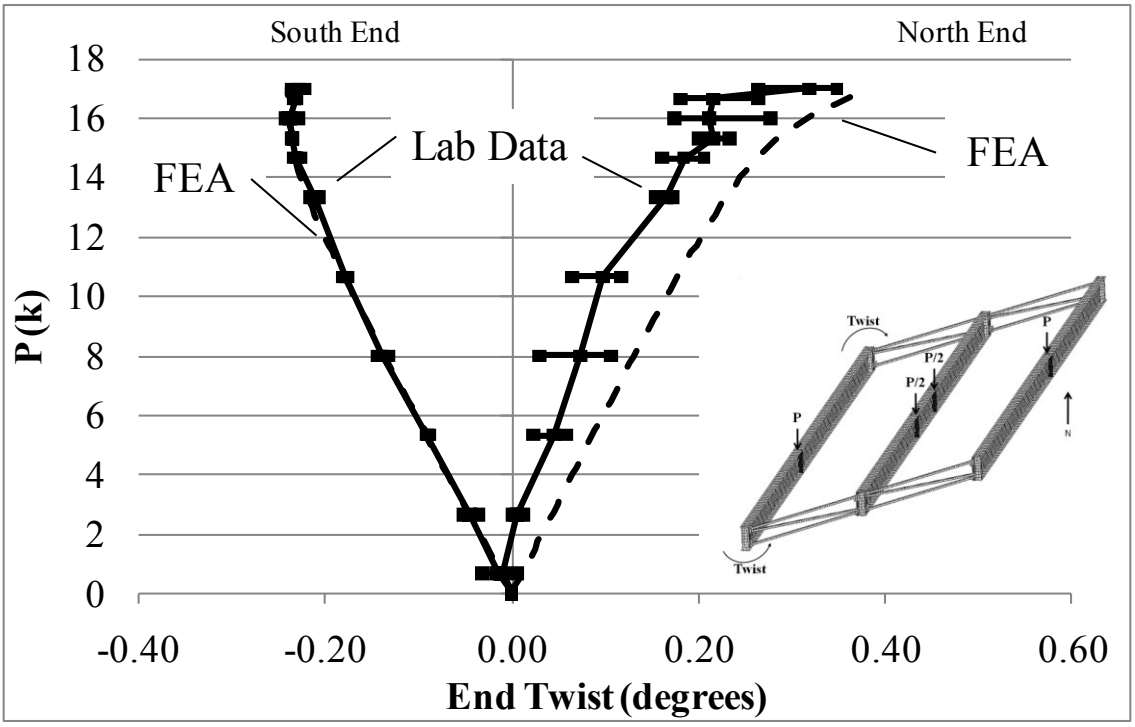

Figure B.41: GSP3 end twist validation data

B.3.2 Staggered Intermediate Cross Frames

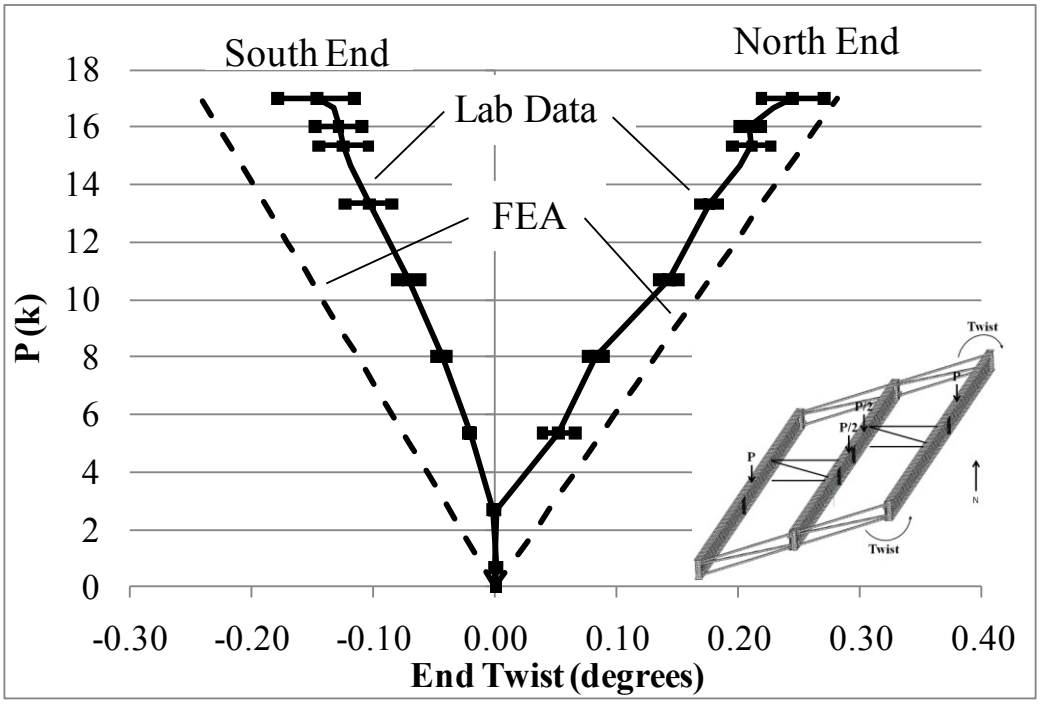

Figure B.42: GSP1 end twist validation data

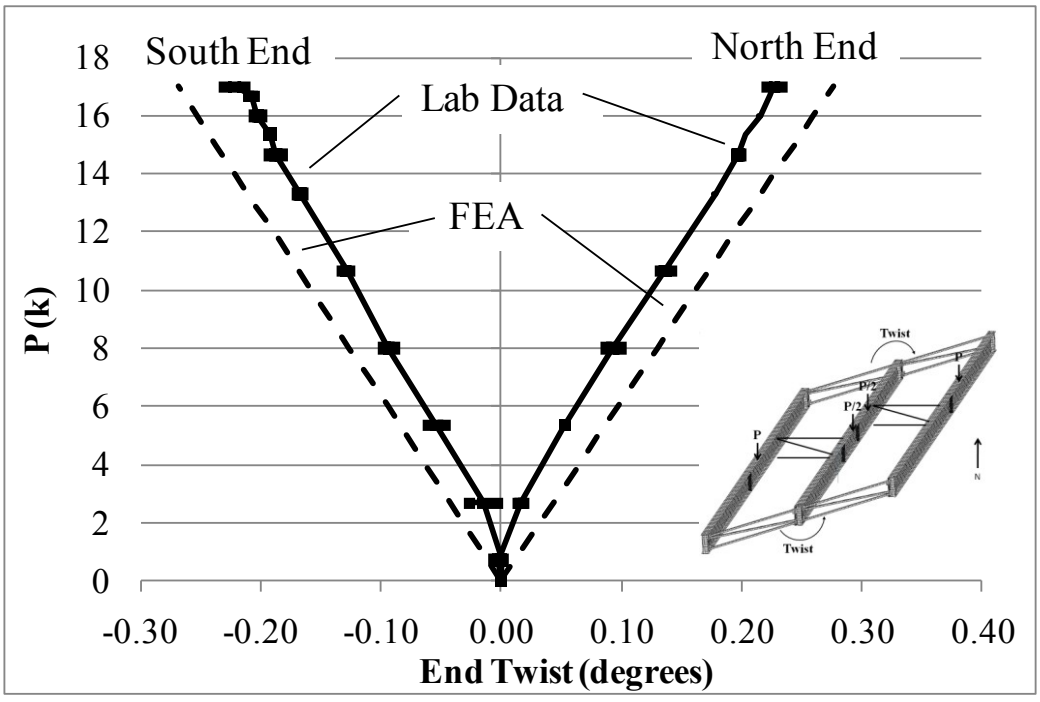

Figure B.43: GSP2 end twist validation data

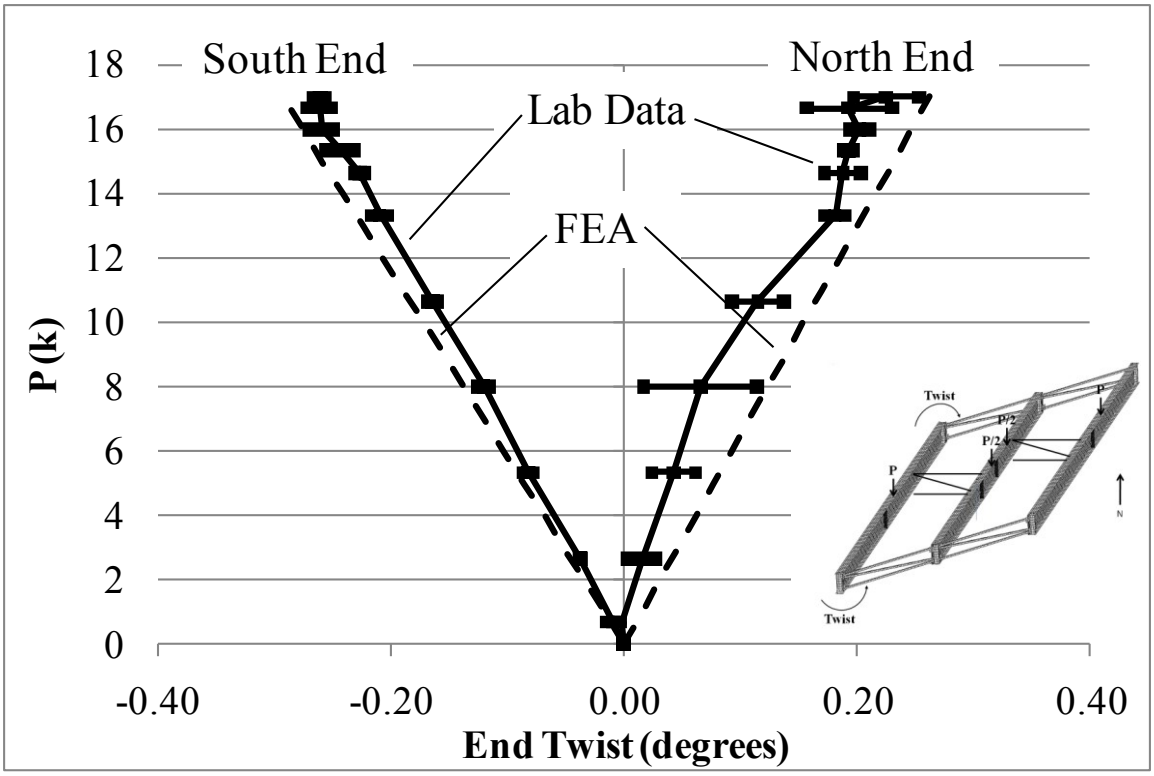

Figure B.44: GSP3 end twist validation data

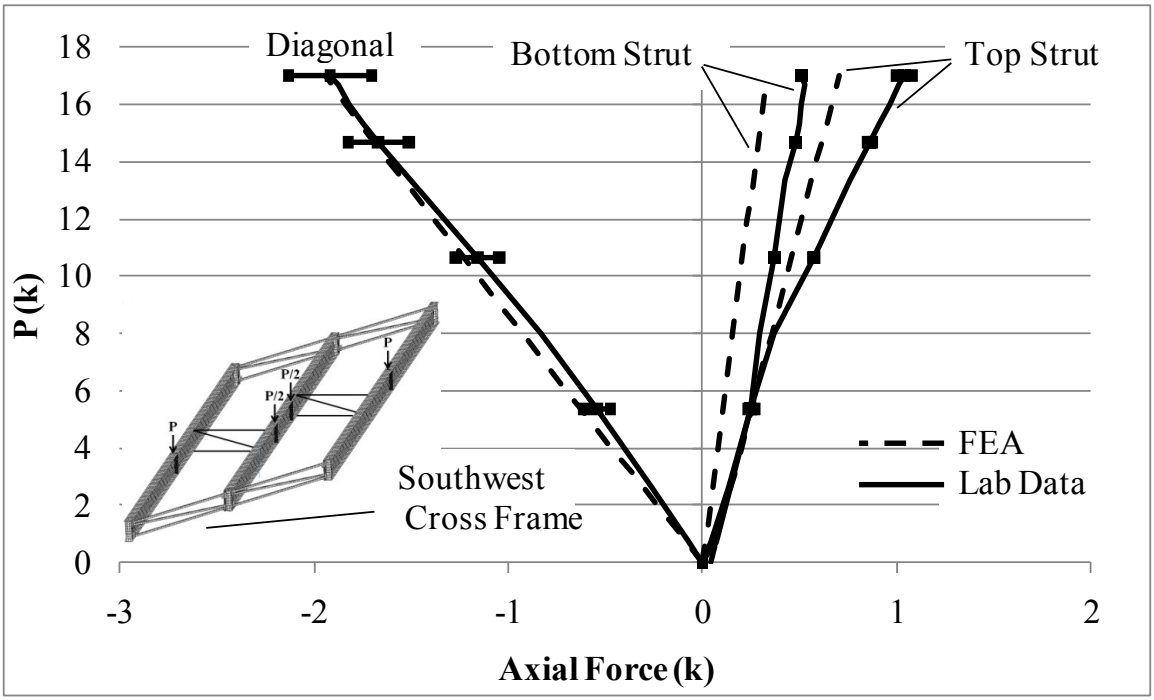

Figure B.45: SW end cross frame axial force validation data

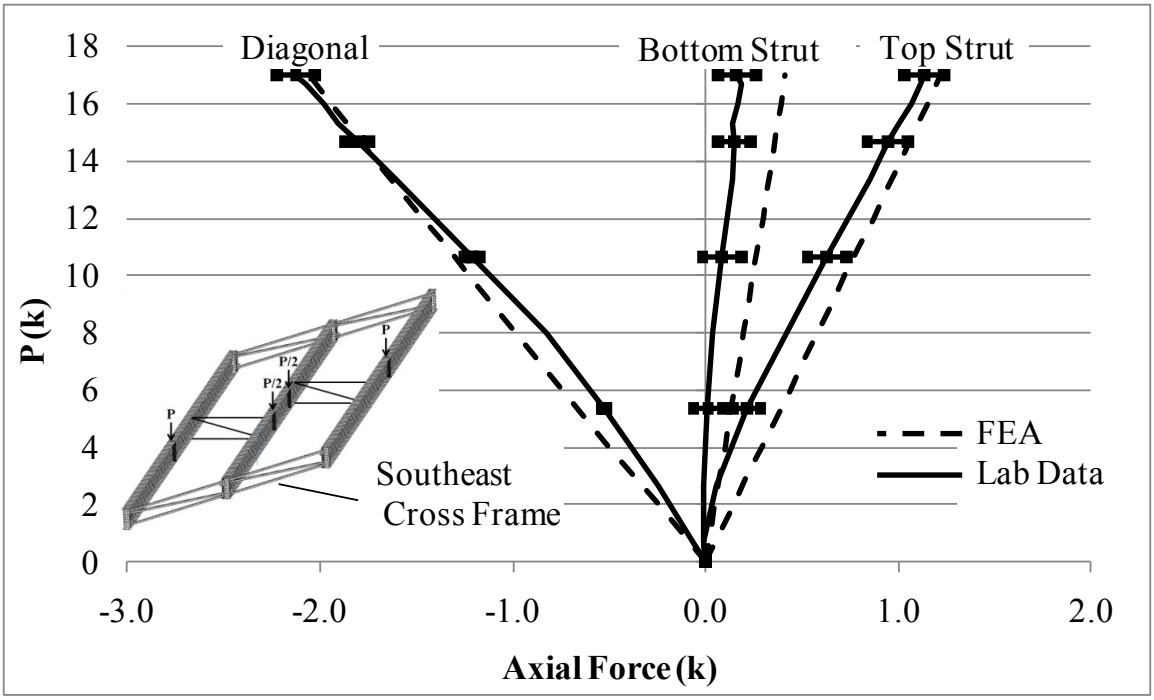

Figure B.46: SE end cross frame axial force validation data

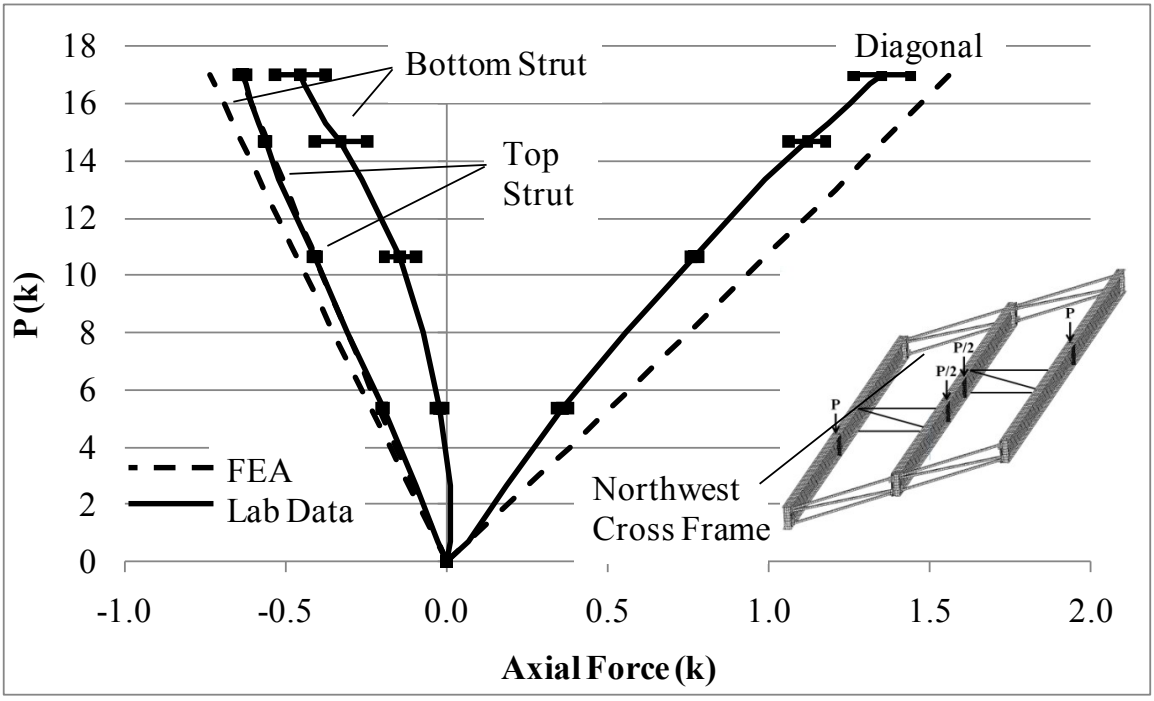

Figure B.47: NW end cross frame axial force validation data

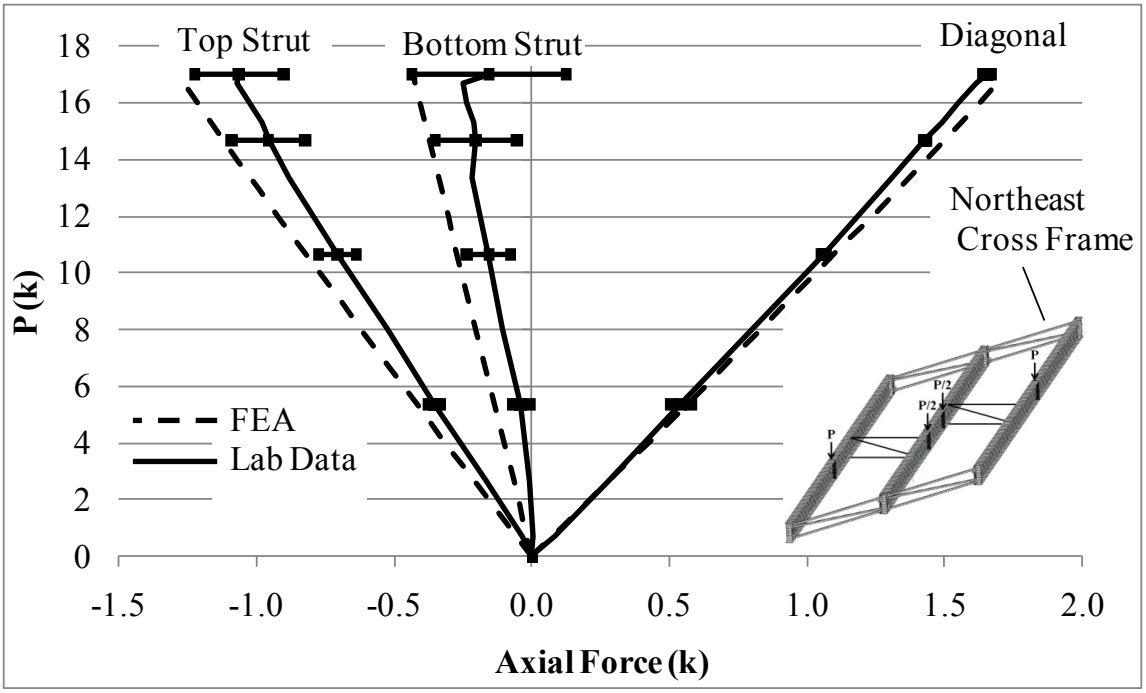

Figure B.48: NE end cross frame axial force validation data

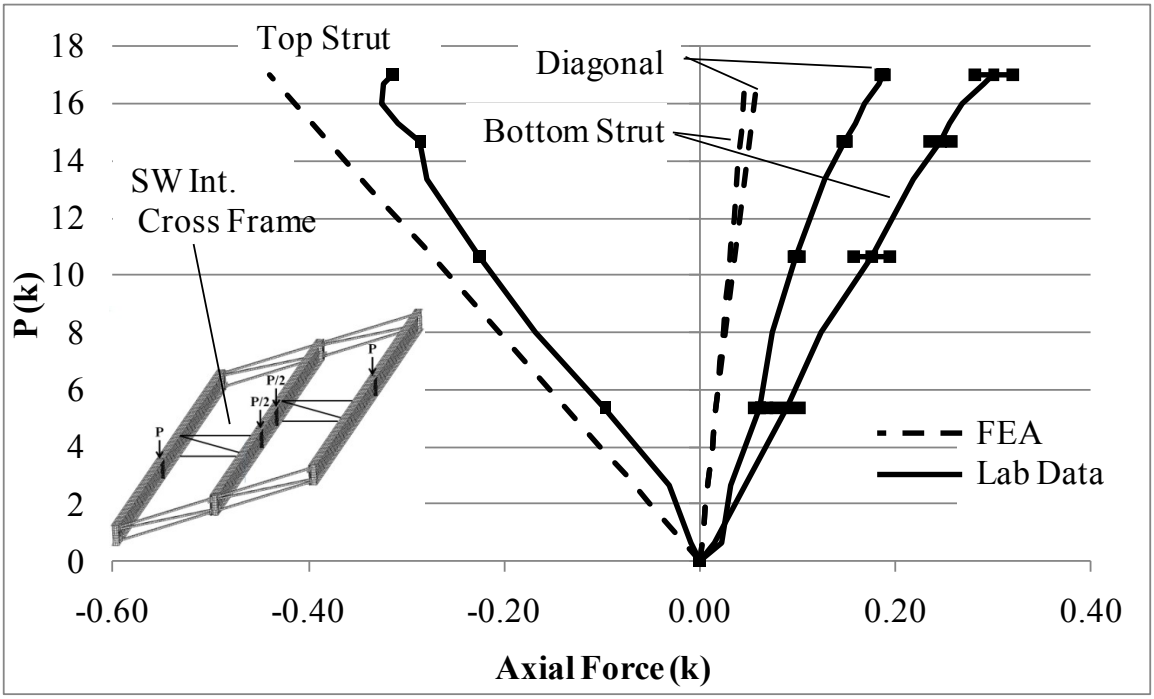

Figure B.49: SW intermediate cross frame axial force validation data

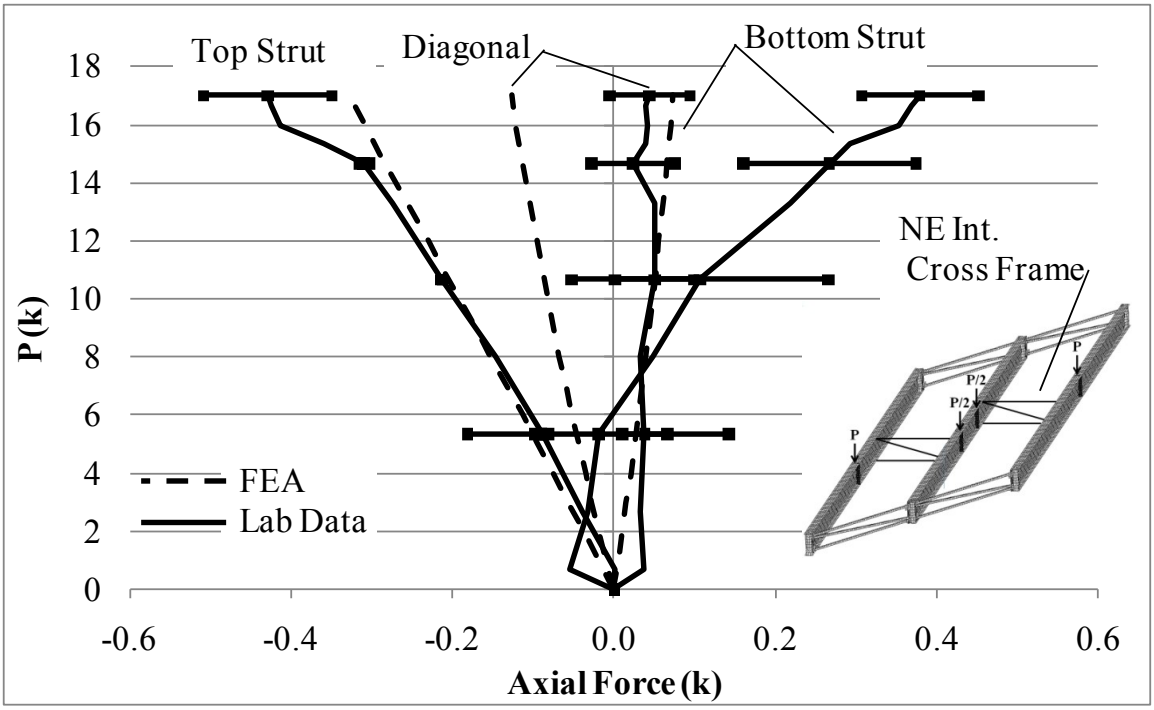

Figure B.50: NE intermediate cross frame axial force validation data

B.3.3 Continuous Intermediate Cross Frames

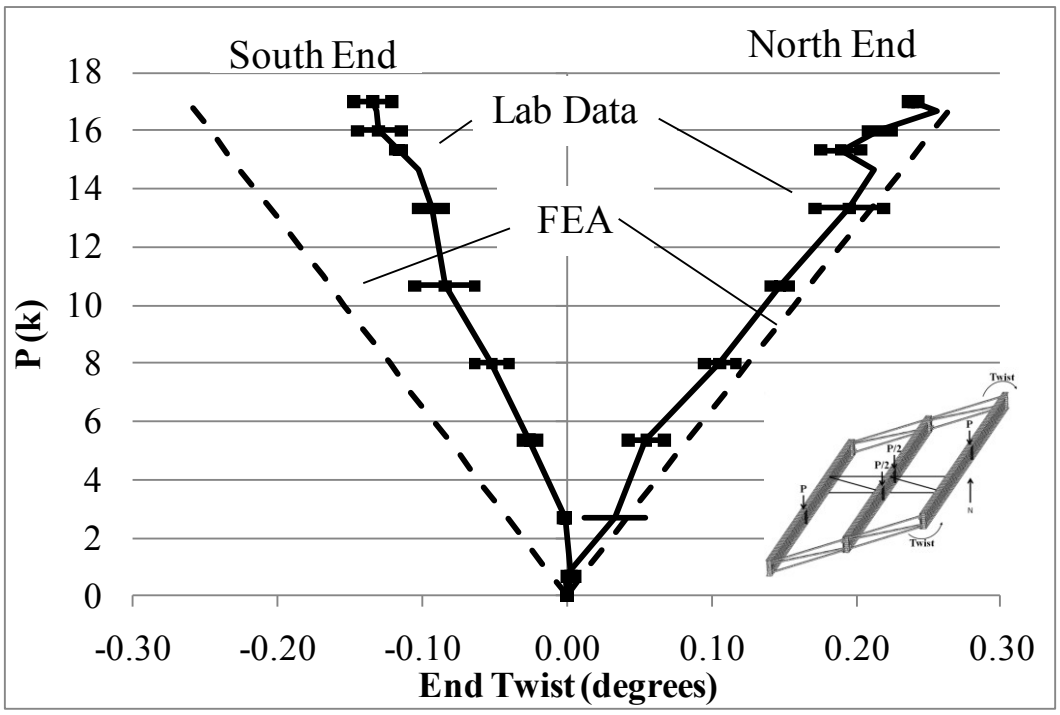

Figure B.51: GSP1 end twist validation data

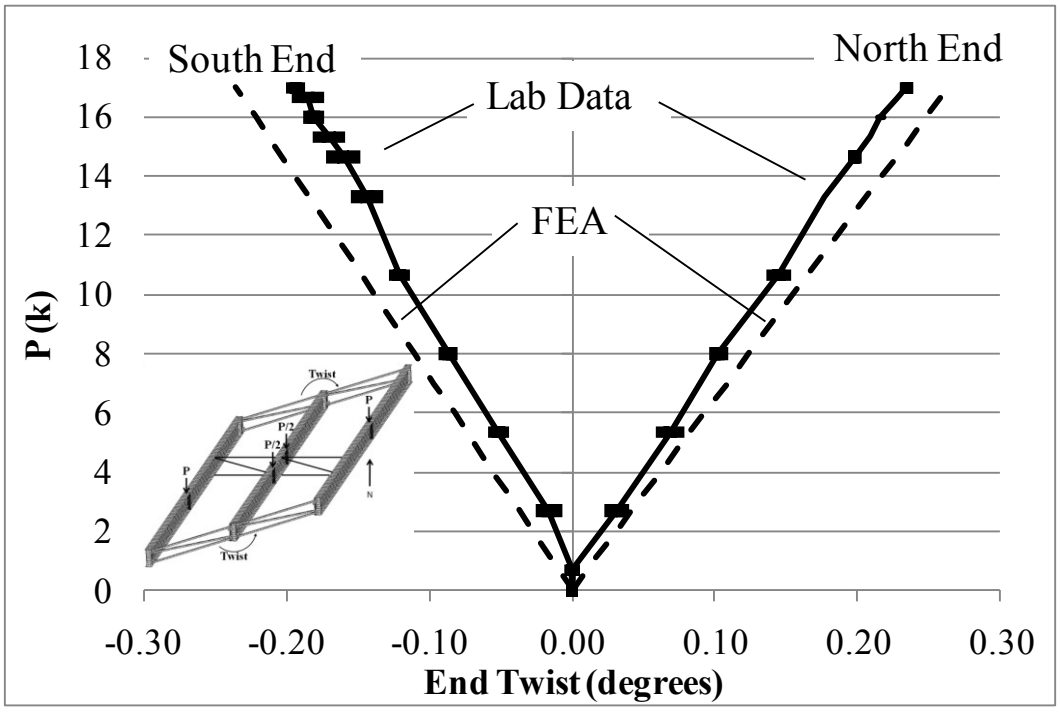

Figure B.52: GSP2 end twist validation data

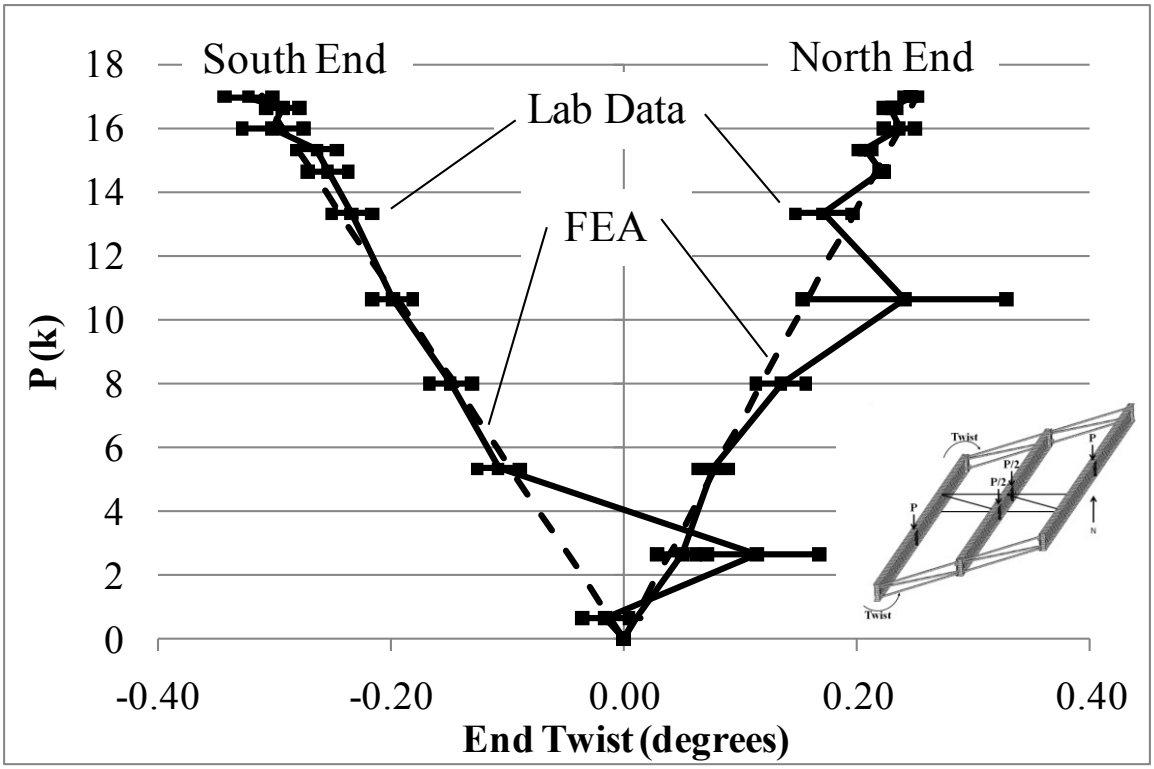

Figure B.53: GSP3 end twist validation data

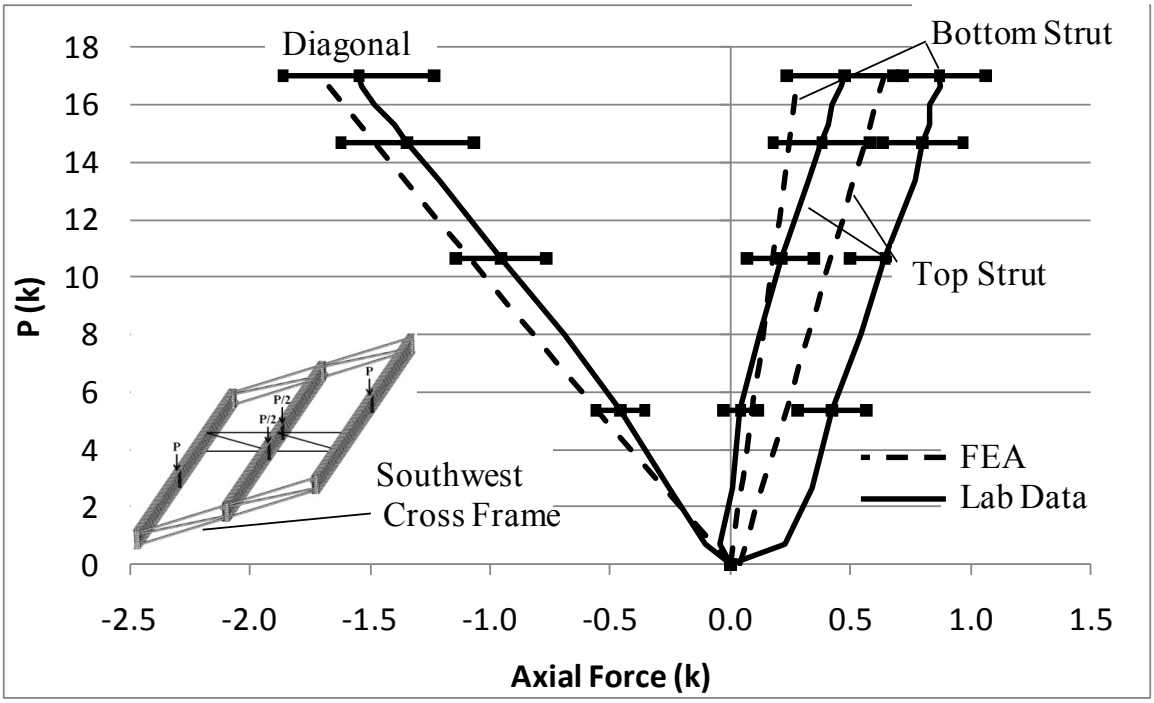

Figure B.54: SW end cross frame axial force validation data

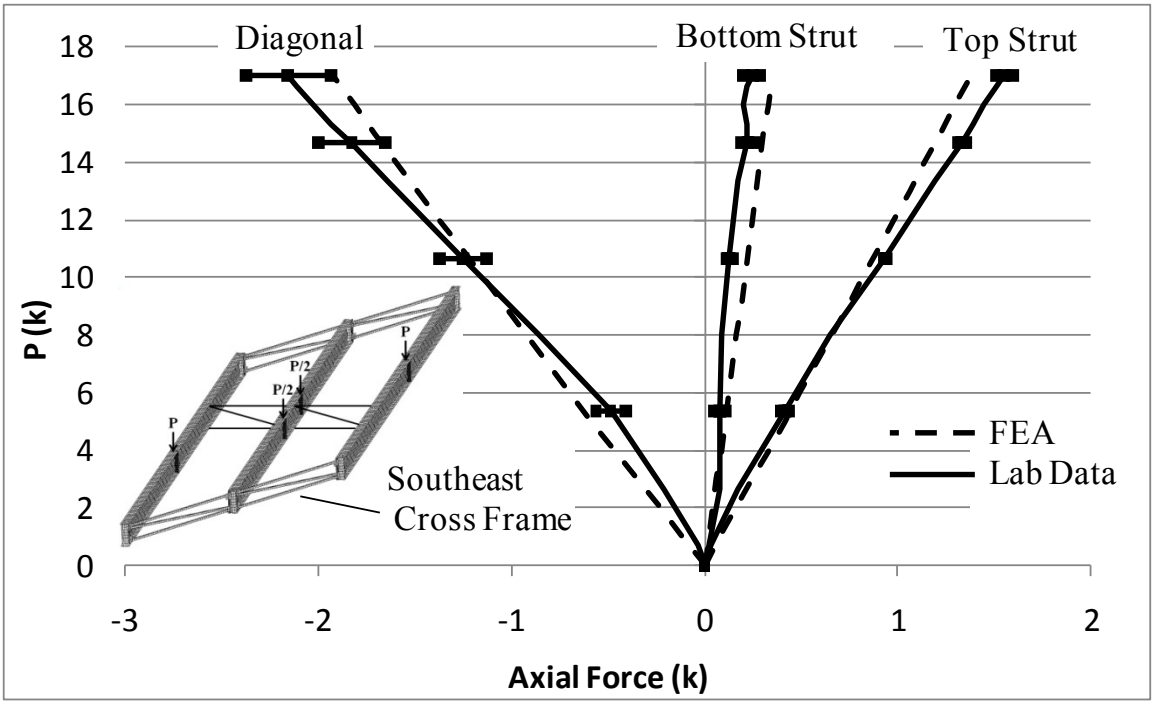

Figure B.55: SE end cross frame axial force validation data

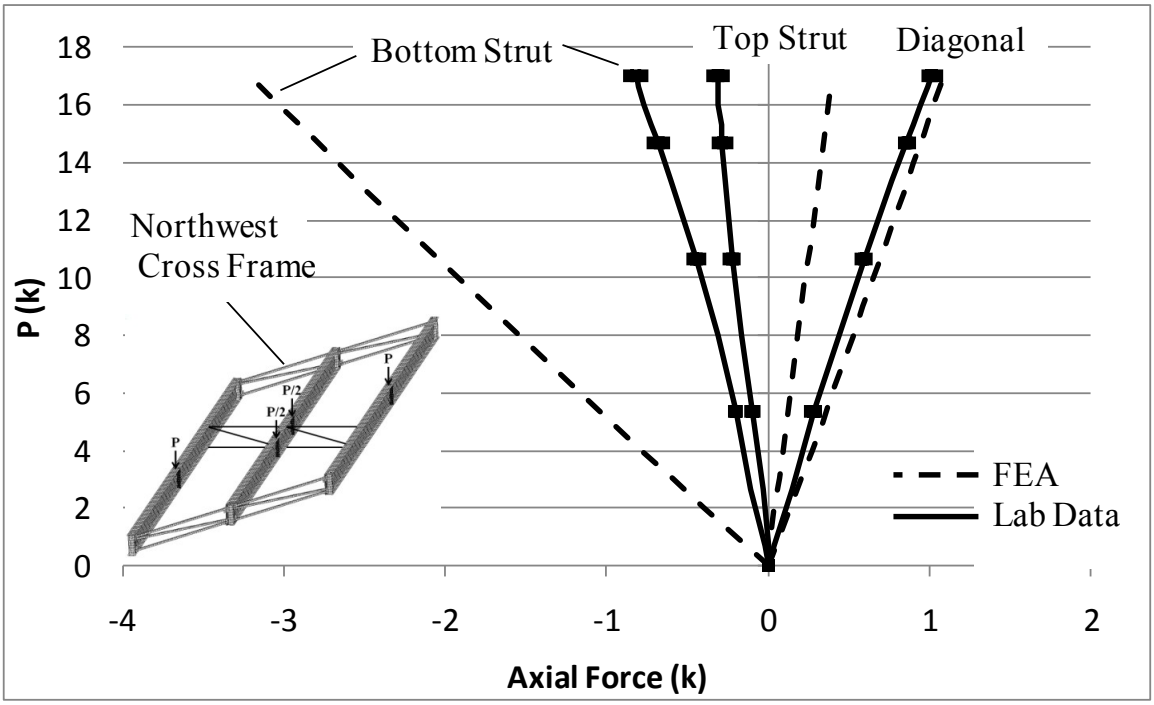

Figure B.56: NW end cross frame axial force validation data

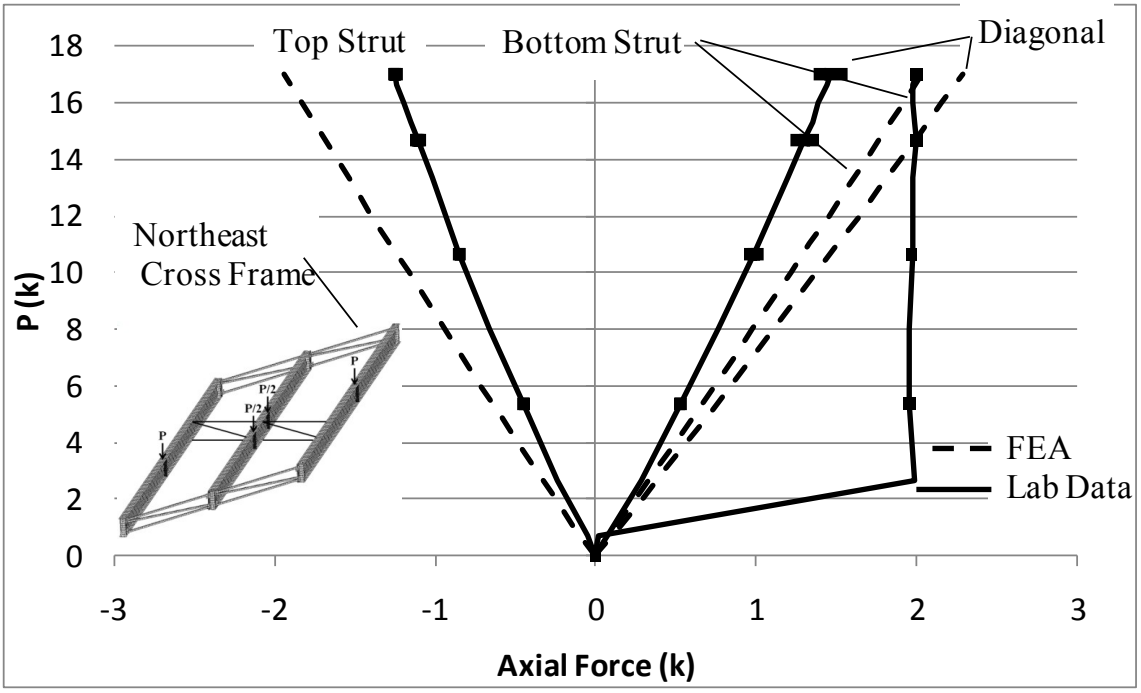

Figure B.57: NE end cross frame axial force validation data

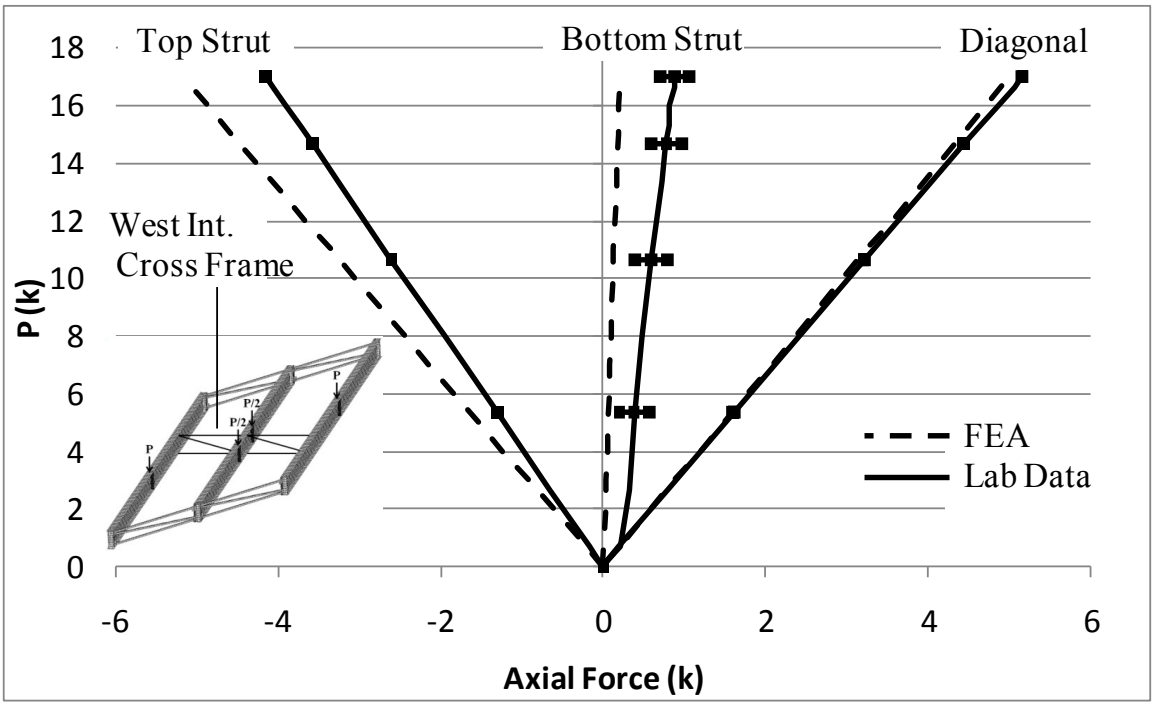

Figure B.58: West intermediate cross frame axial force validation data

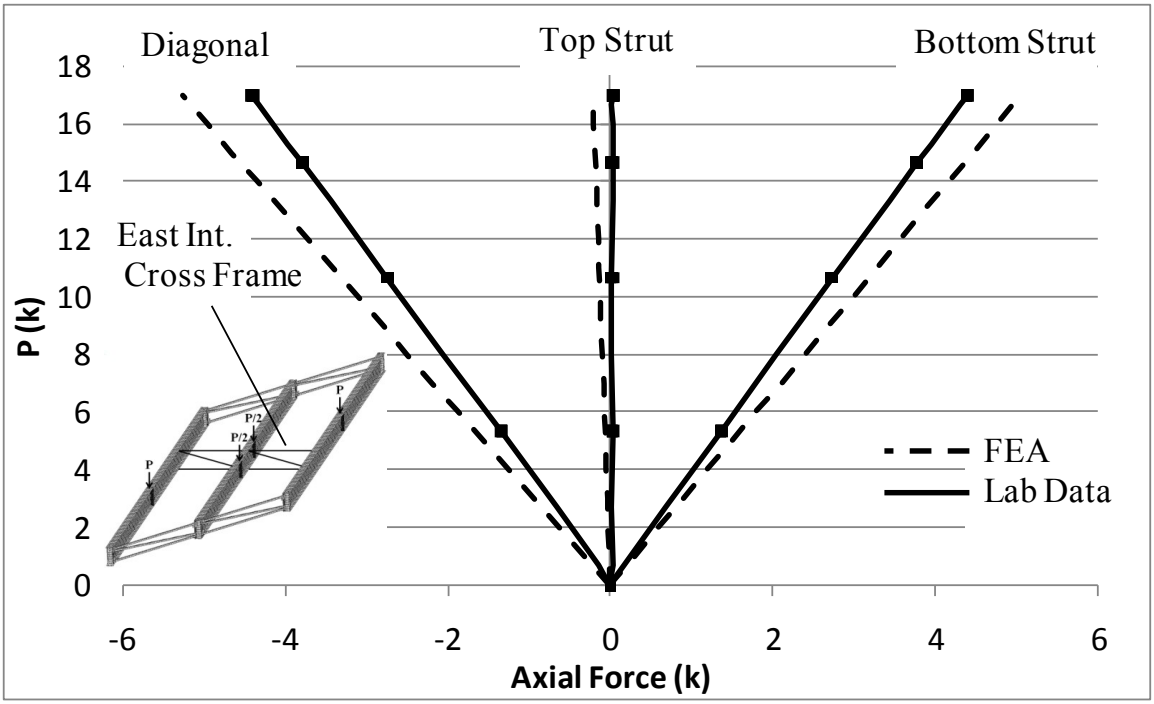

Figure B.59: East intermediate cross frame axial force validation data

APPENDIX C

Parametric Study Results

C.1 Analytic to FEA Bent Plate Cross Frame Stiffness Comparison

C.1.1 8' Girder Spacing

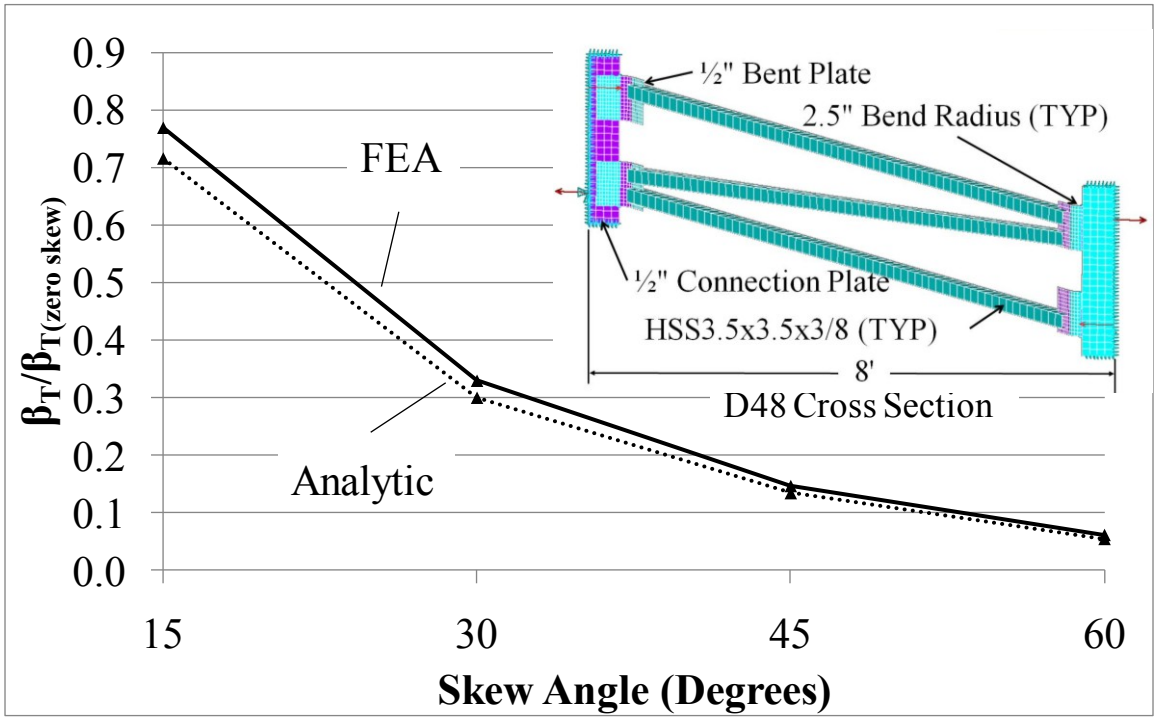

Figure C.1: D48 cross frame analytic to FEA comparison (S = 8')

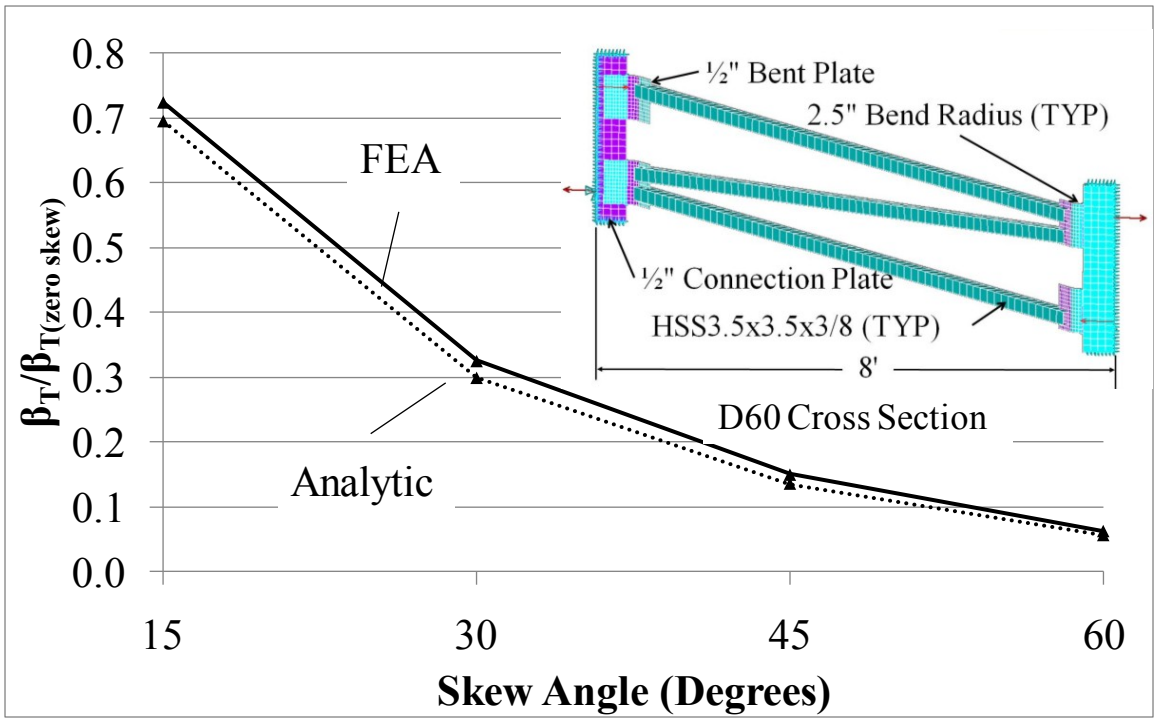

Figure C.2: D60 cross frame analytic to FEA comparison (S = 8')

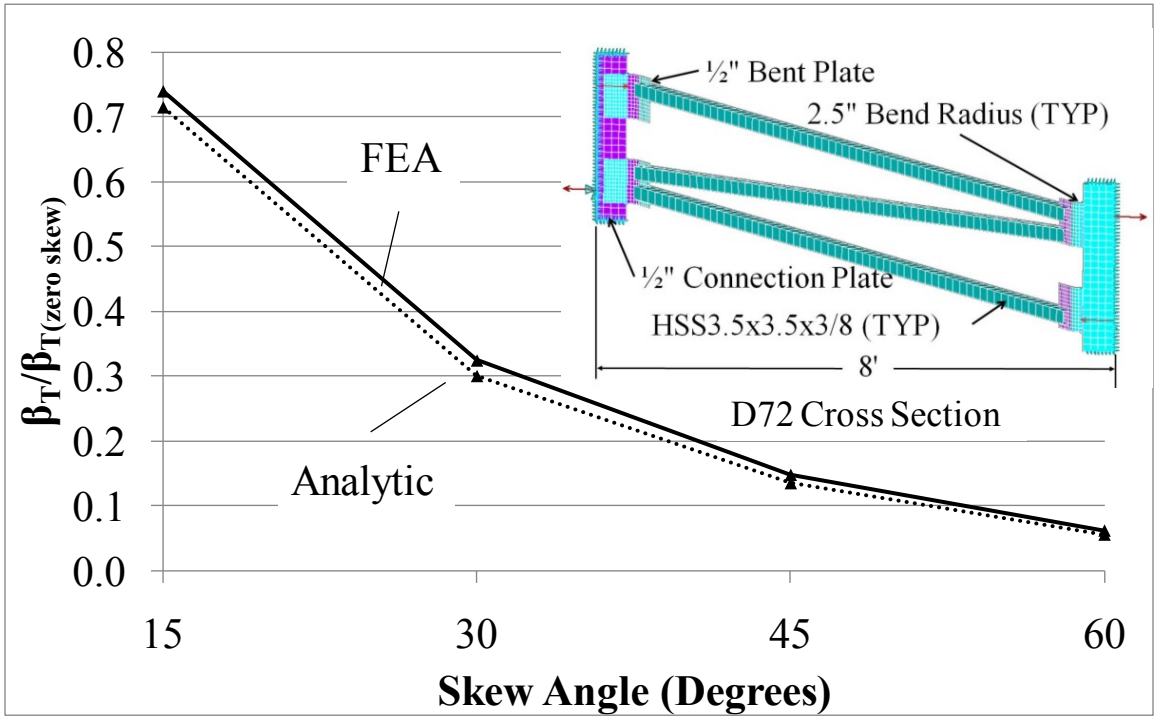

Figure C.3: D72 cross frame analytic to FEA comparison (S = 8')

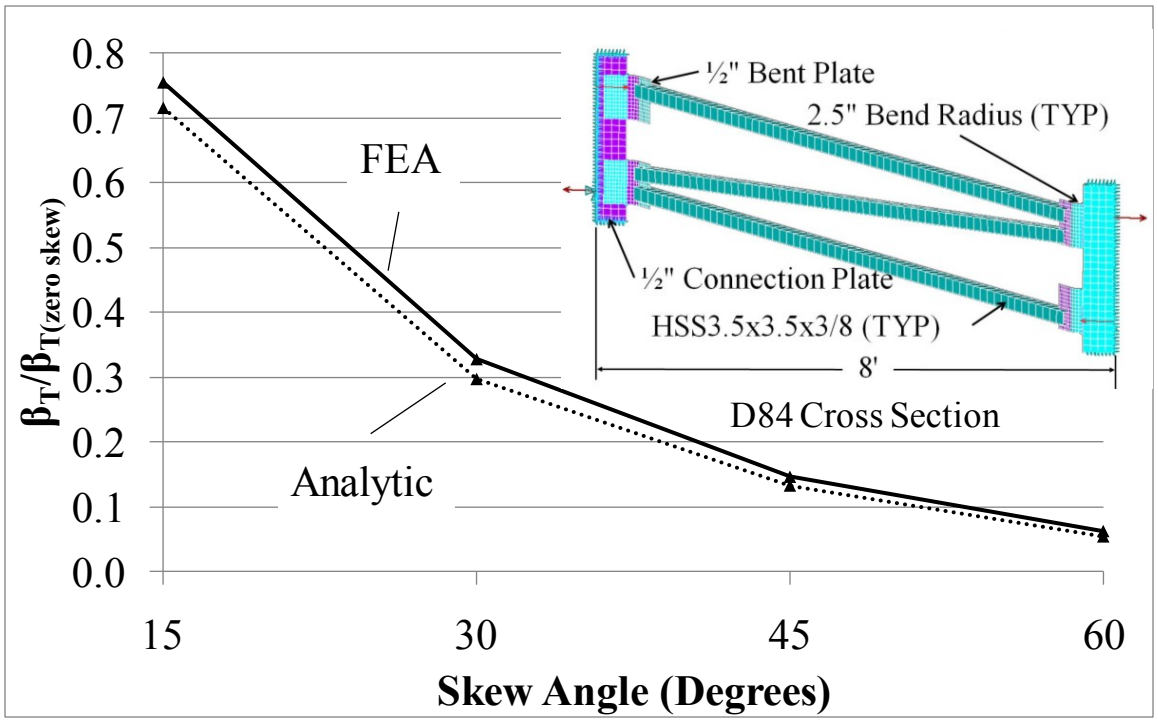

Figure C.4: D84 cross frame analytic to FEA comparison (S = 8')

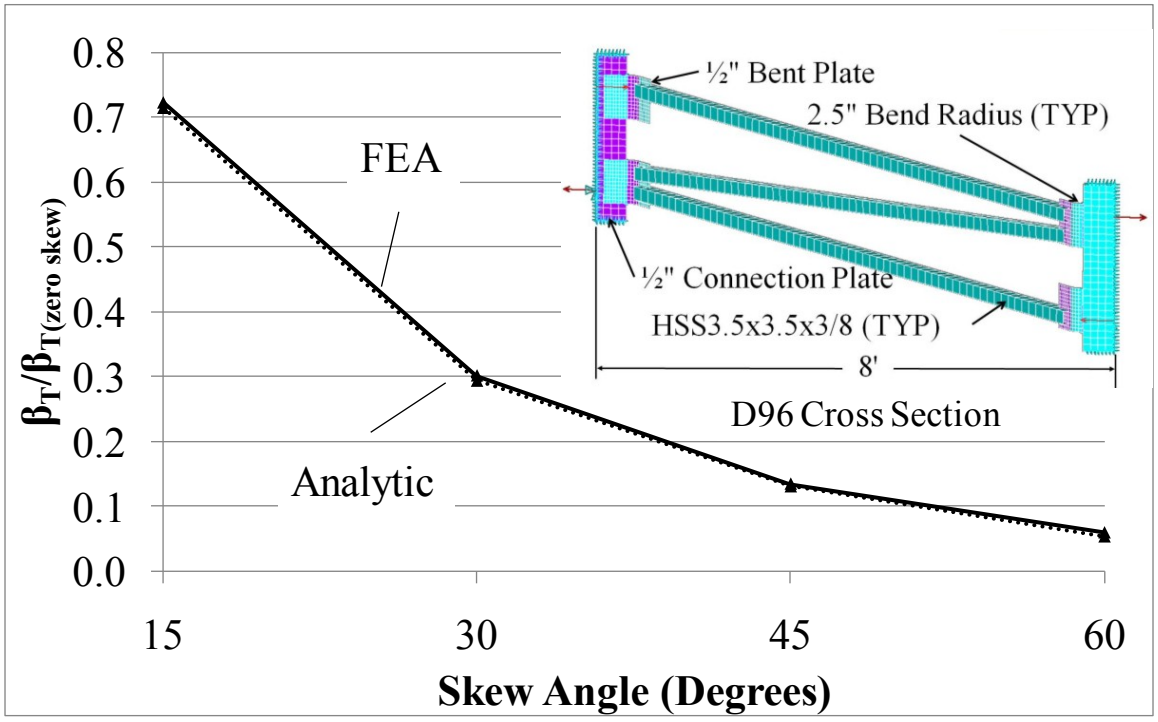

Figure C.5: D96 cross frame analytic to FEA comparison (S = 8')

C.1.2 10' Girder Spacing

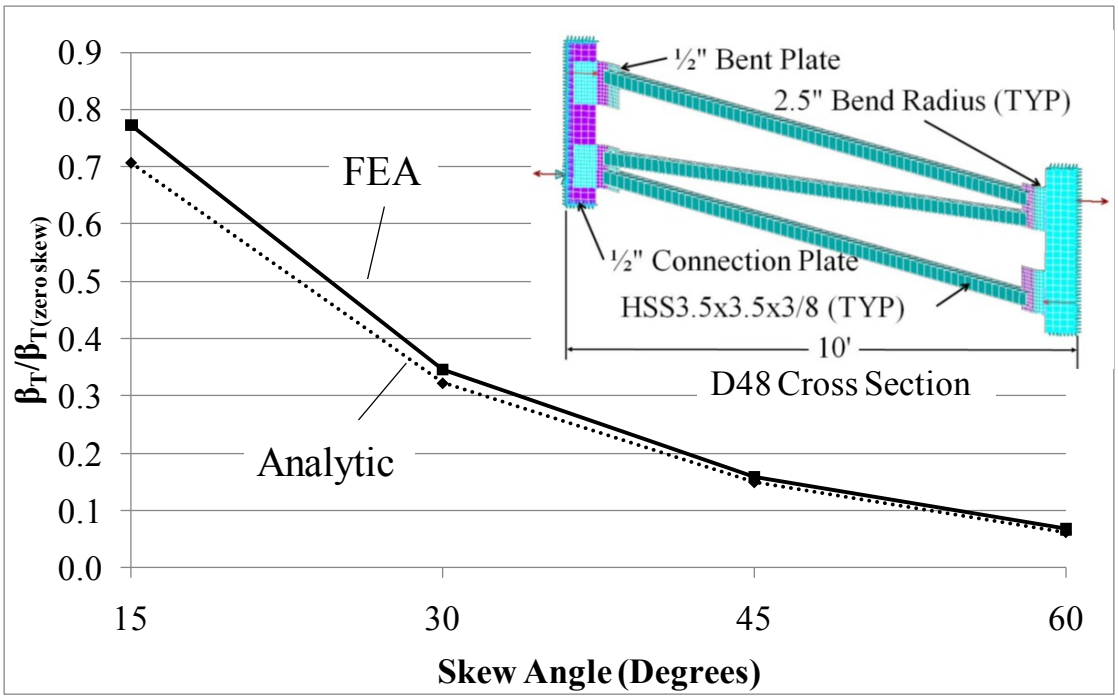

Figure C.6: D48 cross frame analytic to FEA comparison (S = 10')

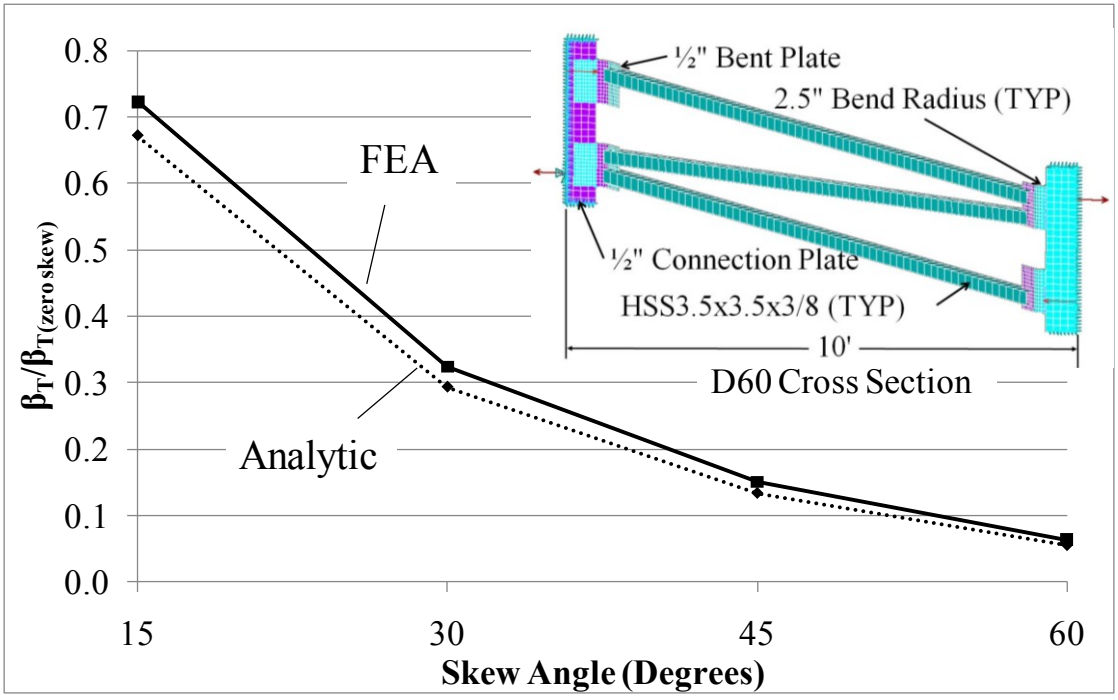

Figure C.7: D60 cross frame analytic to FEA comparison (S = 10')

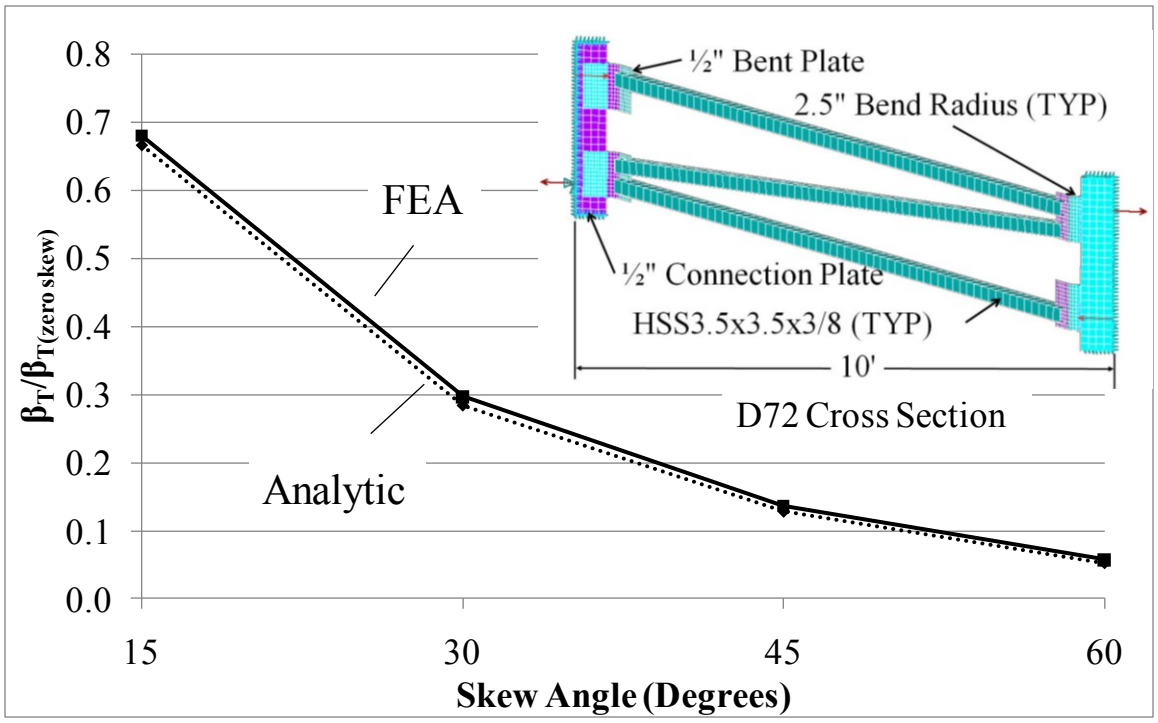

Figure C.8: D72 cross frame analytic to FEA comparison (S = 10')

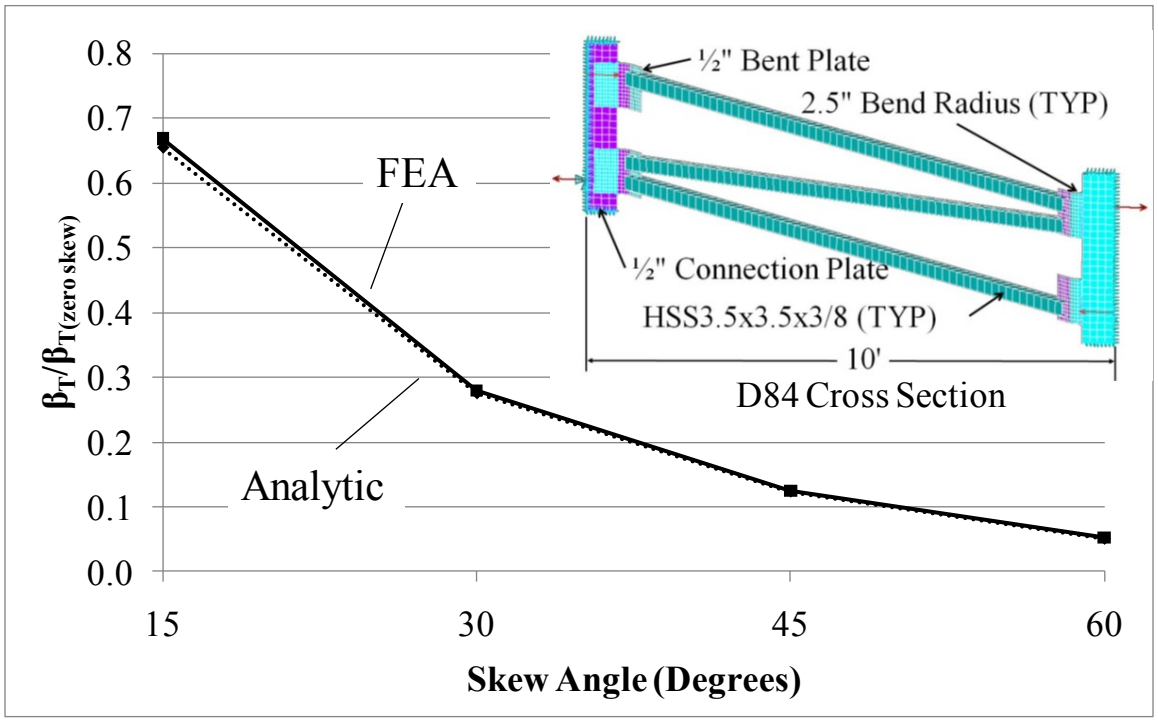

Figure C.9: D84 cross frame analytic to FEA comparison (S = 10')

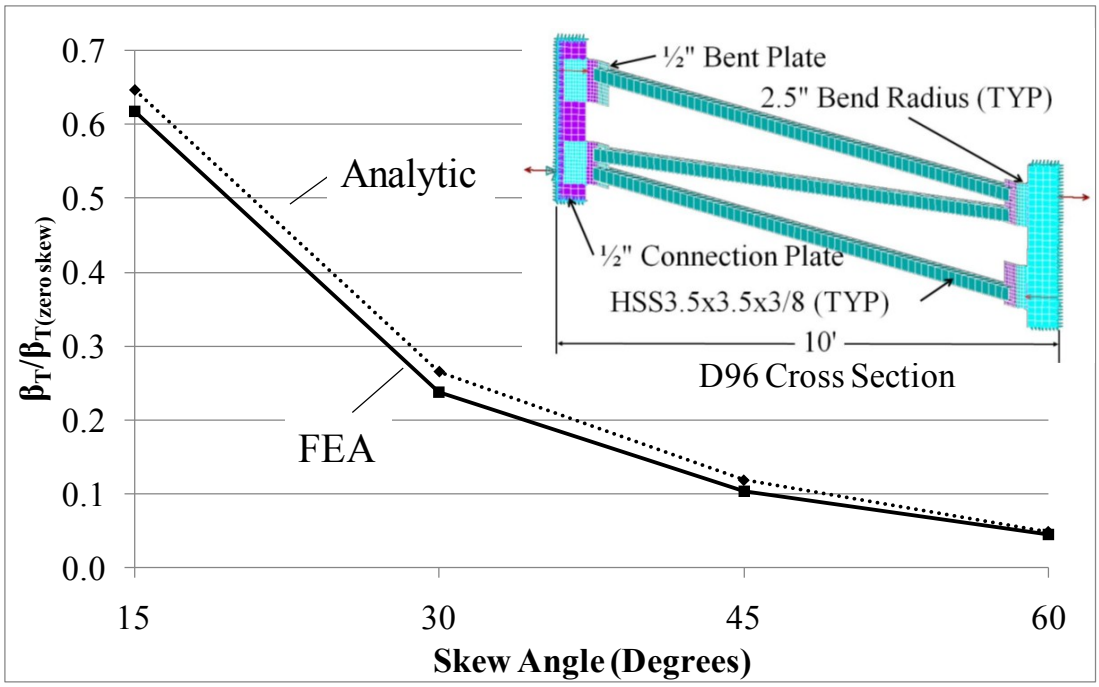

Figure C.10: D96 cross frame analytic to FEA comparison (S = 10')

C.1.3 6' Girder Spacing

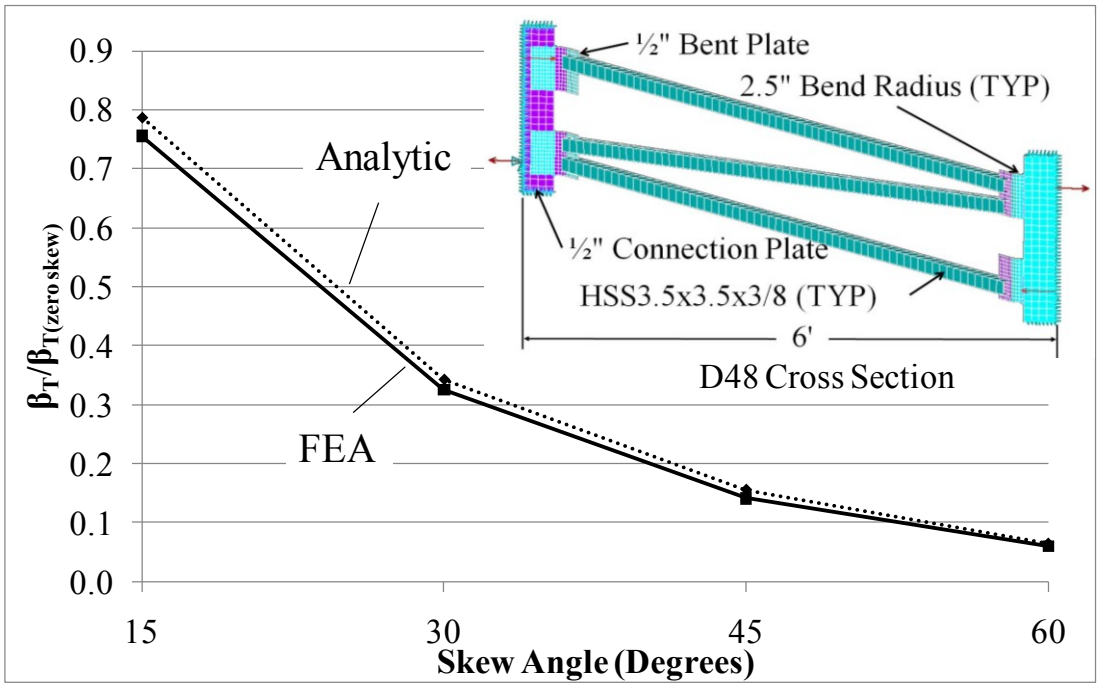

Figure C.11: D48 cross frame analytic to FEA comparison (S = 6')

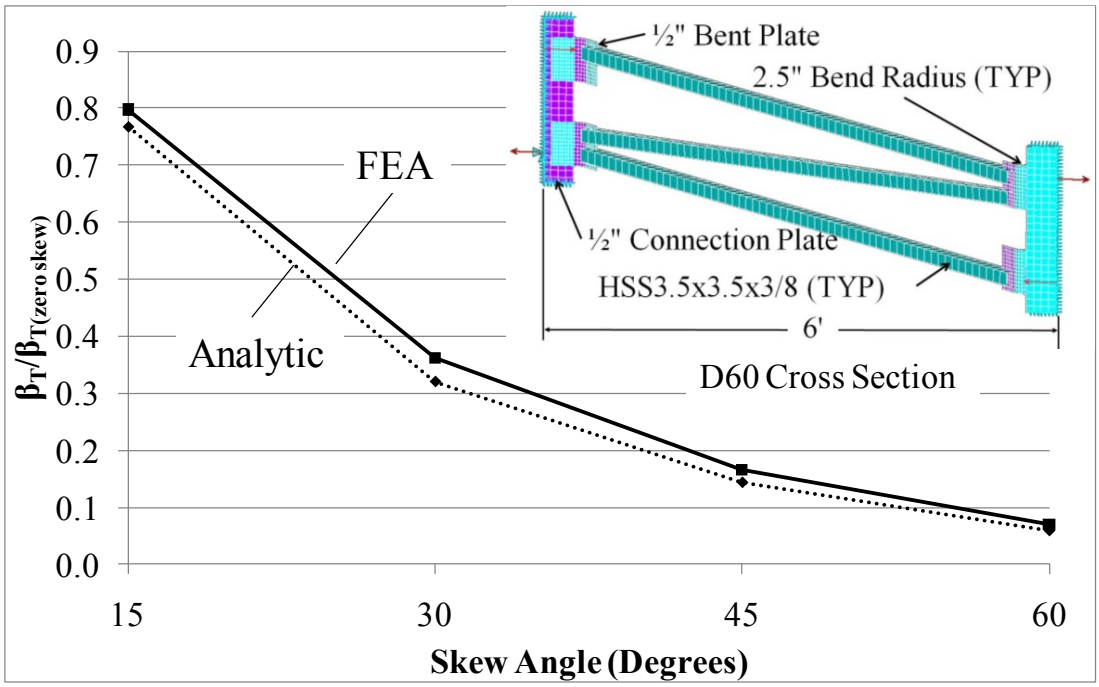

Figure C.12: D60 cross frame analytic to FEA comparison (S = 6')

C.2 Plate Thickness and Bend Radius Impact on Bent Plate Cross Frame Stiffness

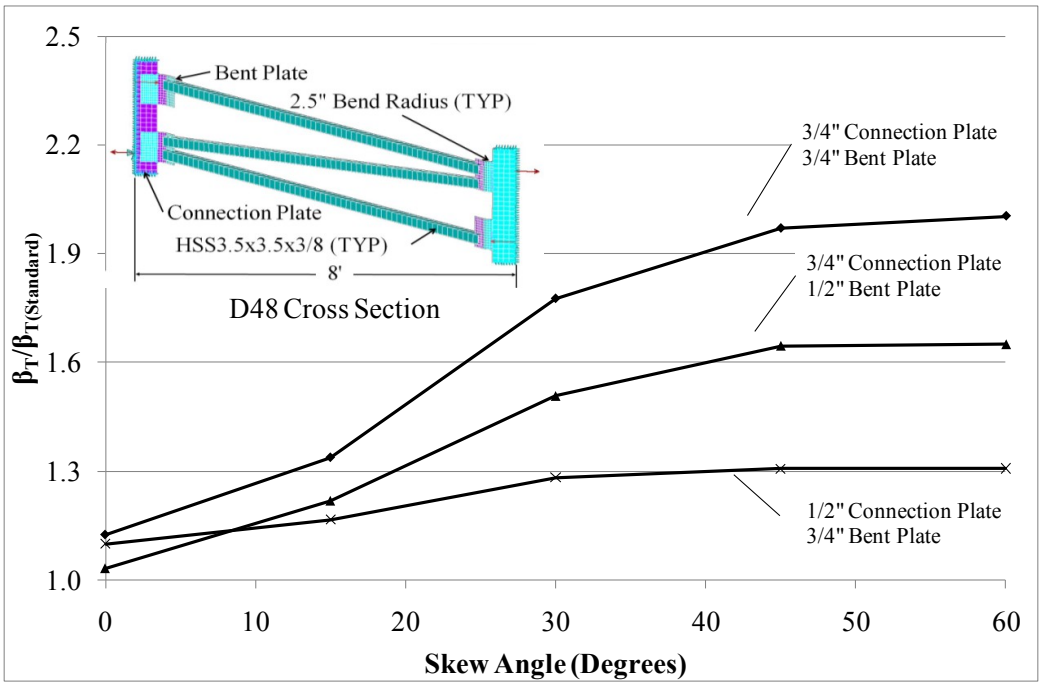

Figure C.13: D48 cross frame plate thickness impact on stiffness (2.5" bend radius)

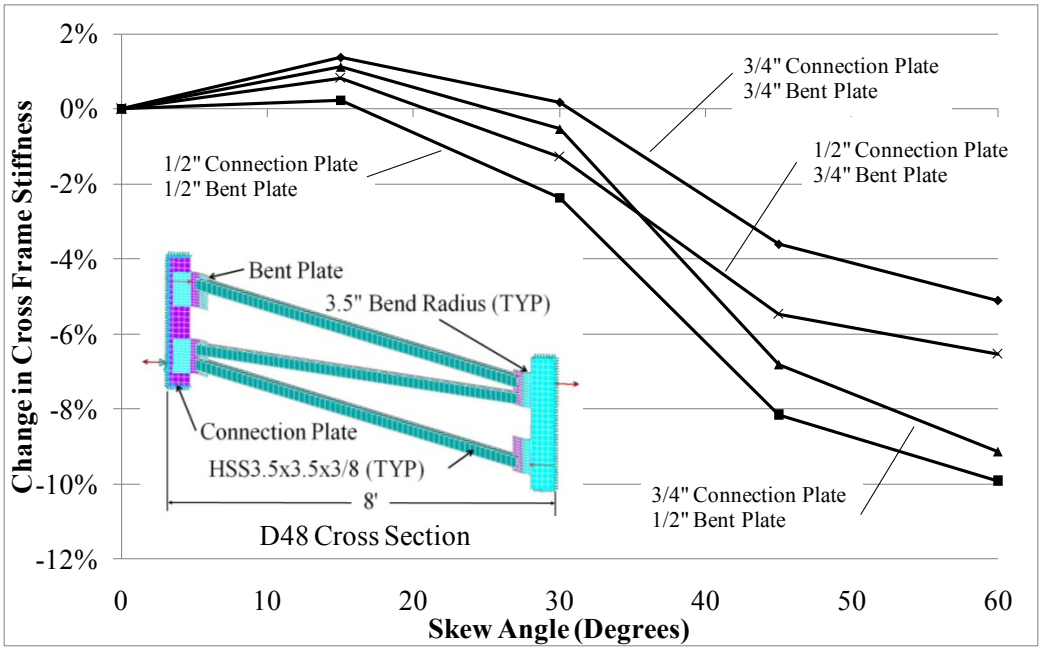

Figure C.14: D48 cross frame stiffness change (2.5" to 3.5" bend radius)

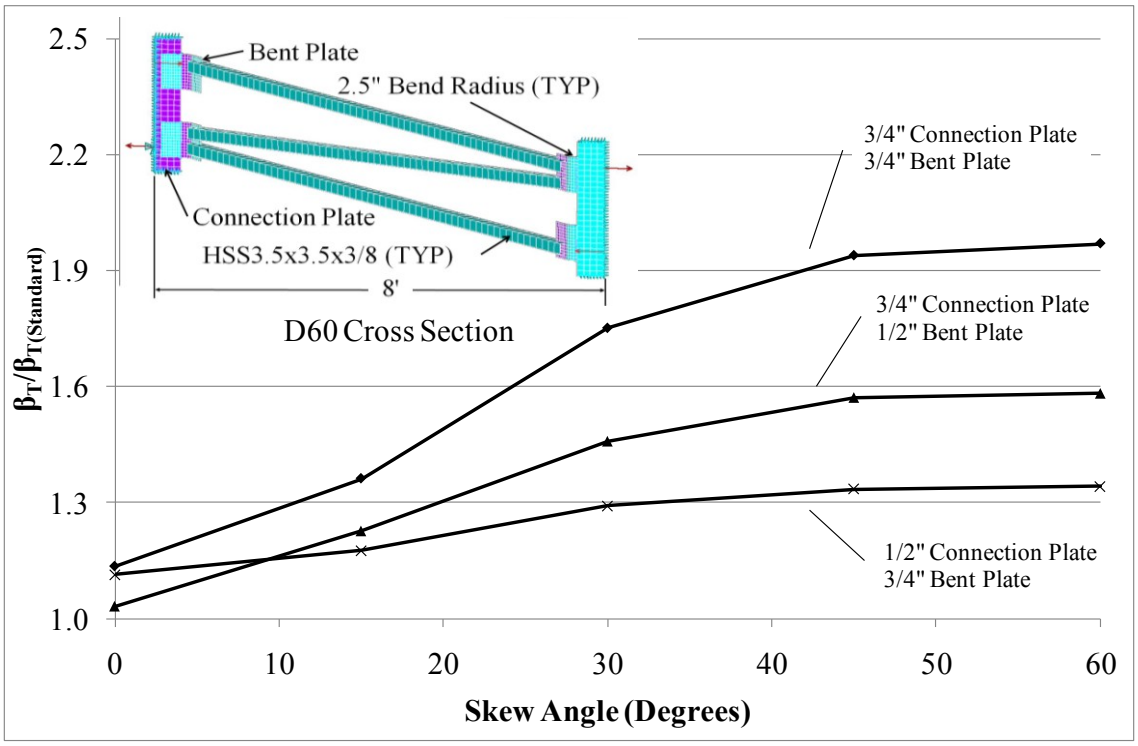

Figure C.15: D60 cross frame plate thickness impact on stiffness (2.5" bend radius)

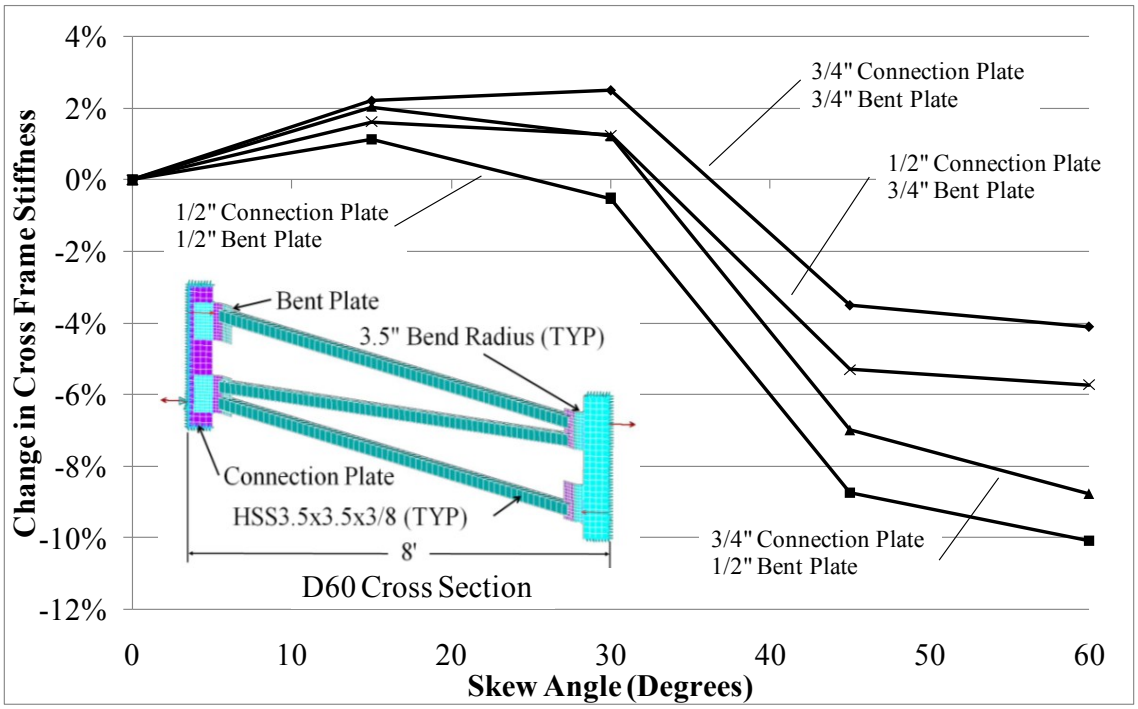

Figure C.16: D60 cross frame stiffness change (2.5" to 3.5" bend radius)

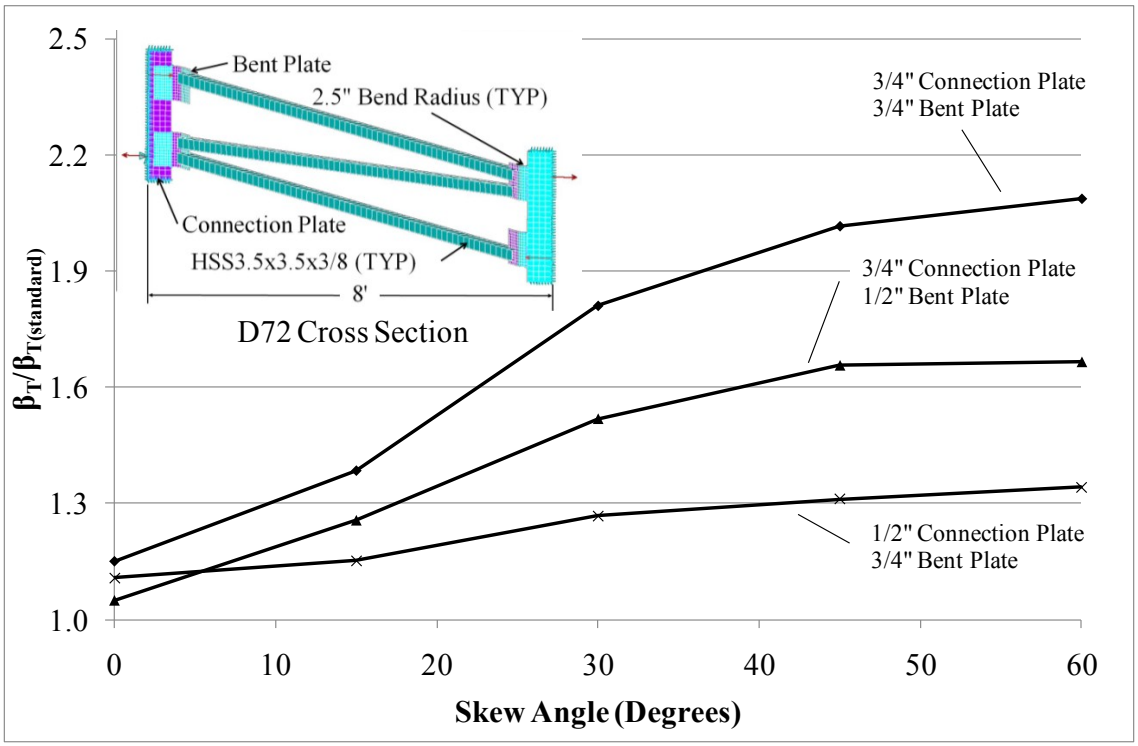

Figure C.17: D72 cross frame plate thickness impact on stiffness (2.5" bend radius)

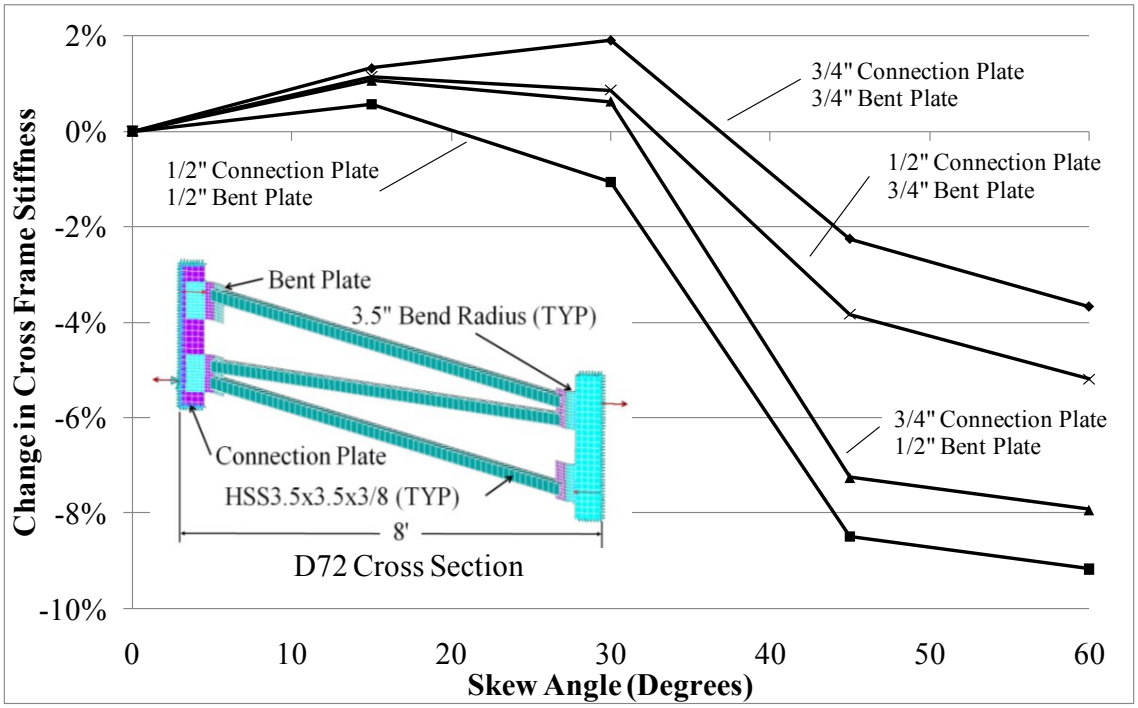

Figure C.18: D72 cross frame stiffness change (2.5" to 3.5" bend radius)

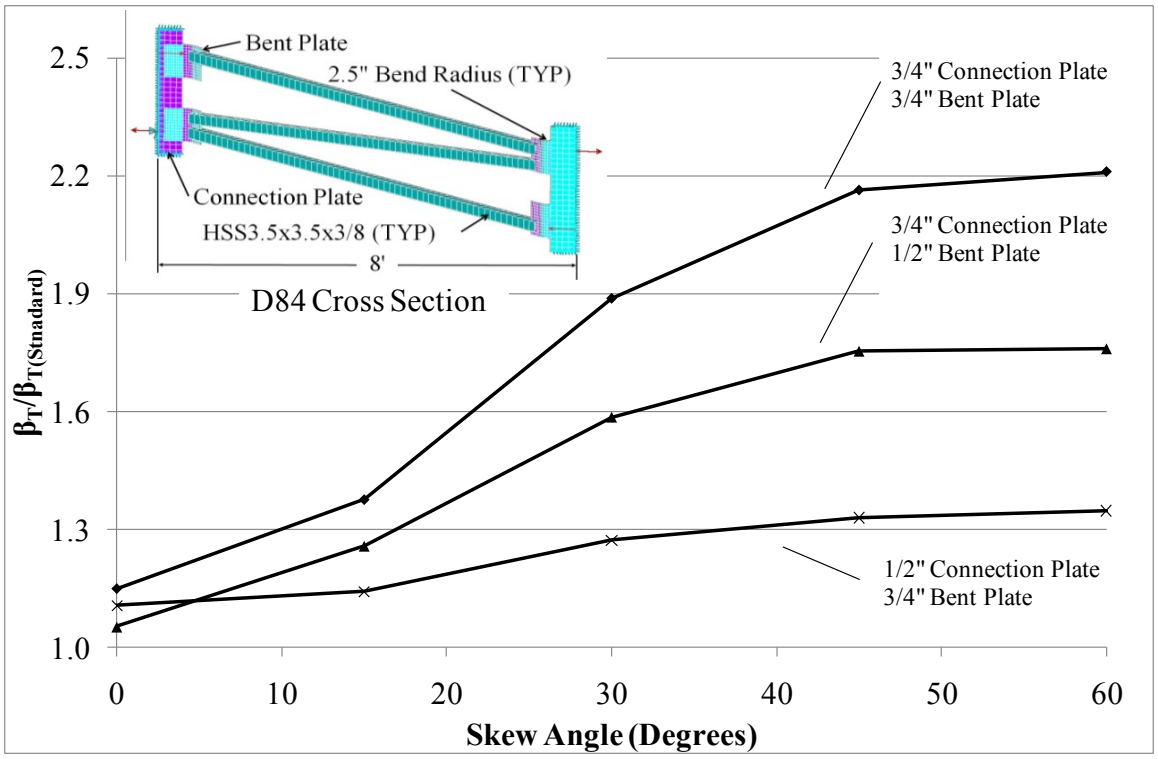

Figure C.19: D84 cross frame plate thickness impact on stiffness (2.5" bend radius)

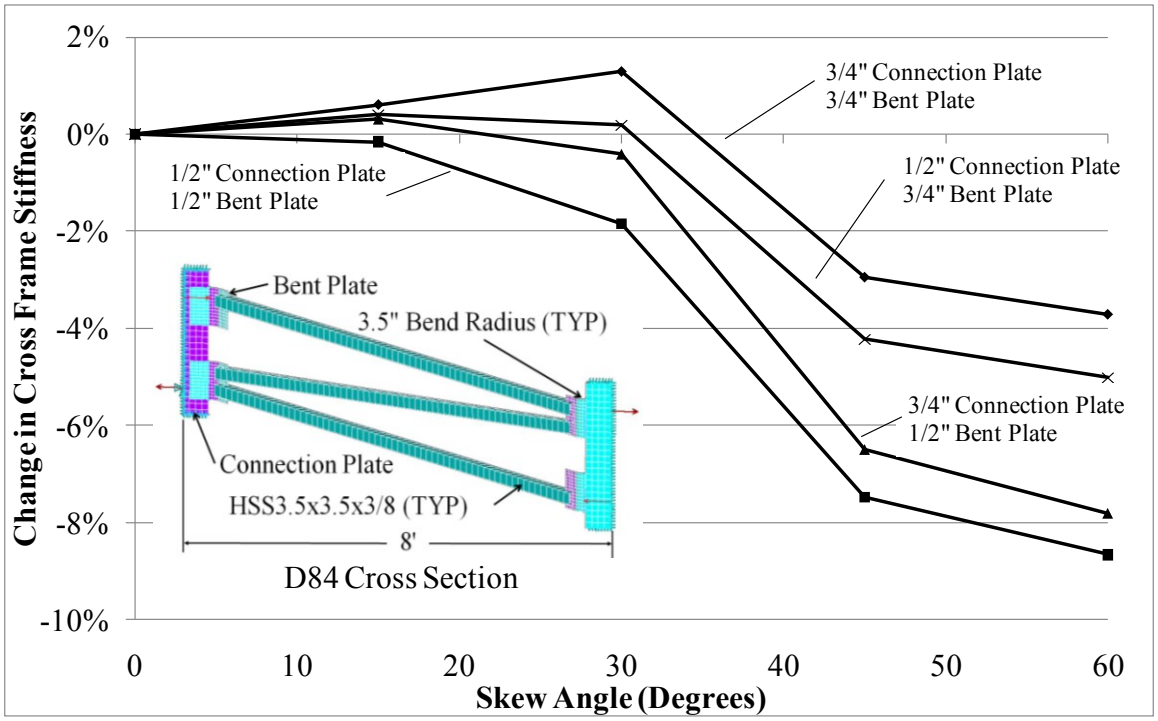

Figure C.20: D84 cross frame stiffness change (2.5" to 3.5" bend radius)

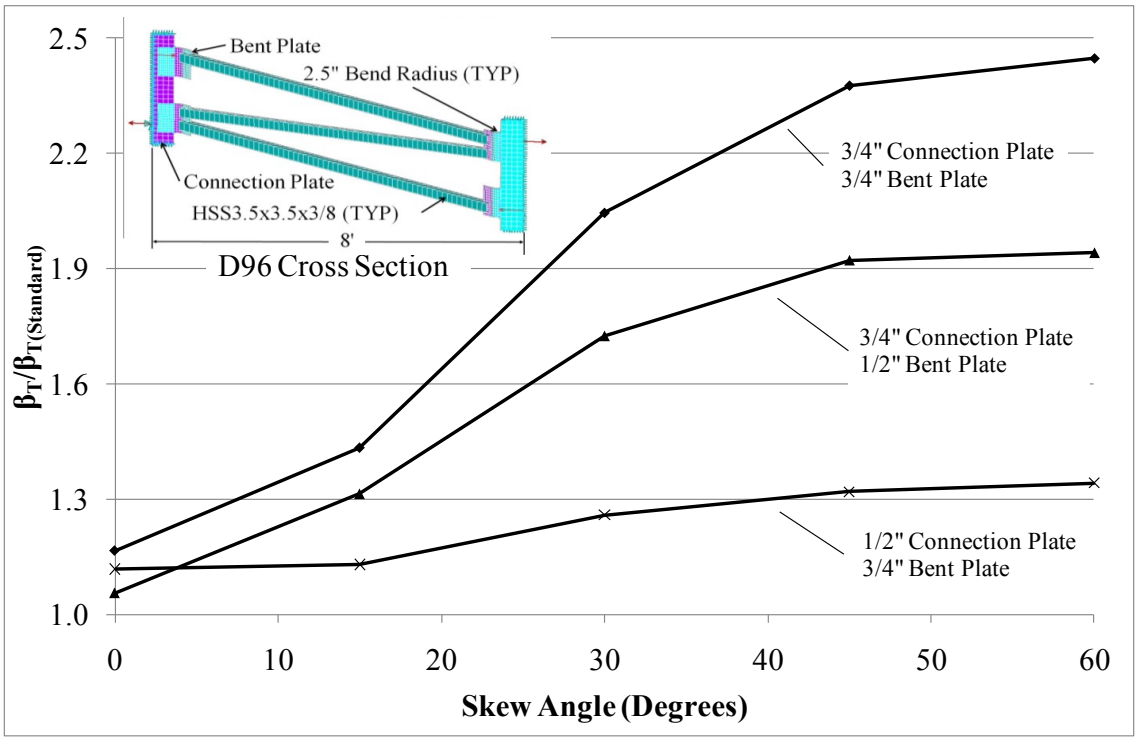

Figure C.21: D96 cross frame plate thickness impact on stiffness (2.5" bend radius)

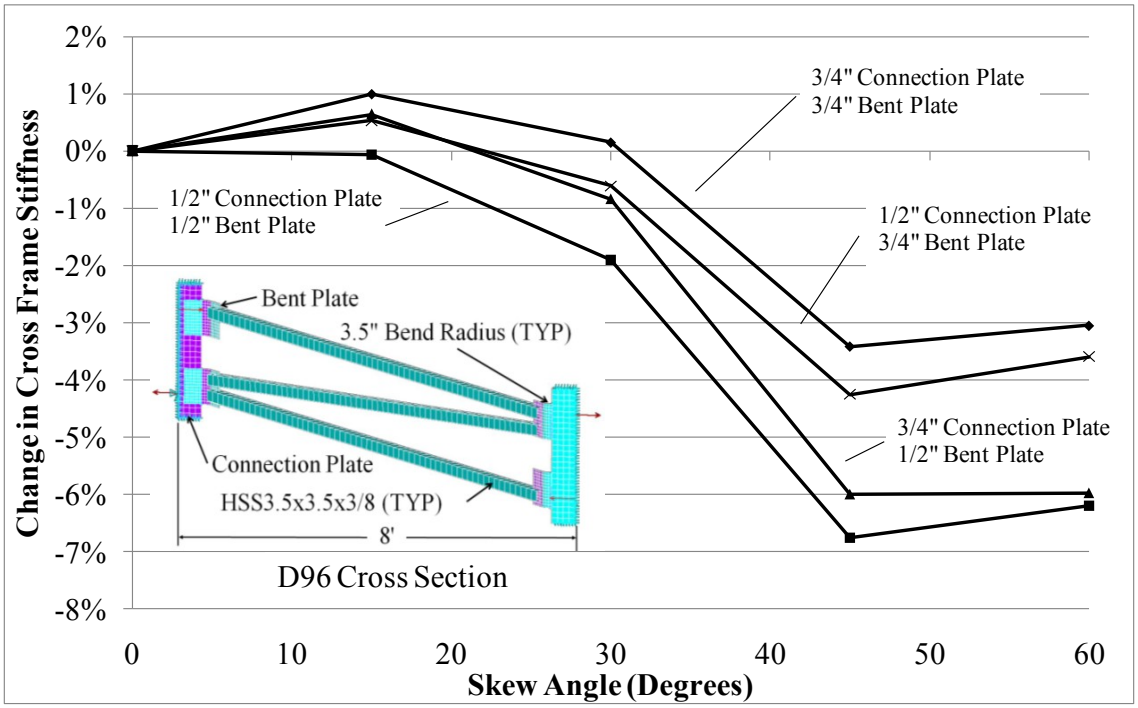

Figure C.22: D96 cross frame stiffness change (2.5" to 3.5" bend radius)

C.3 END TWIST IMPACT ON GIRDER BUCKLING STRENGTH

C.3.1 Bent Plate Cross Frame Connection

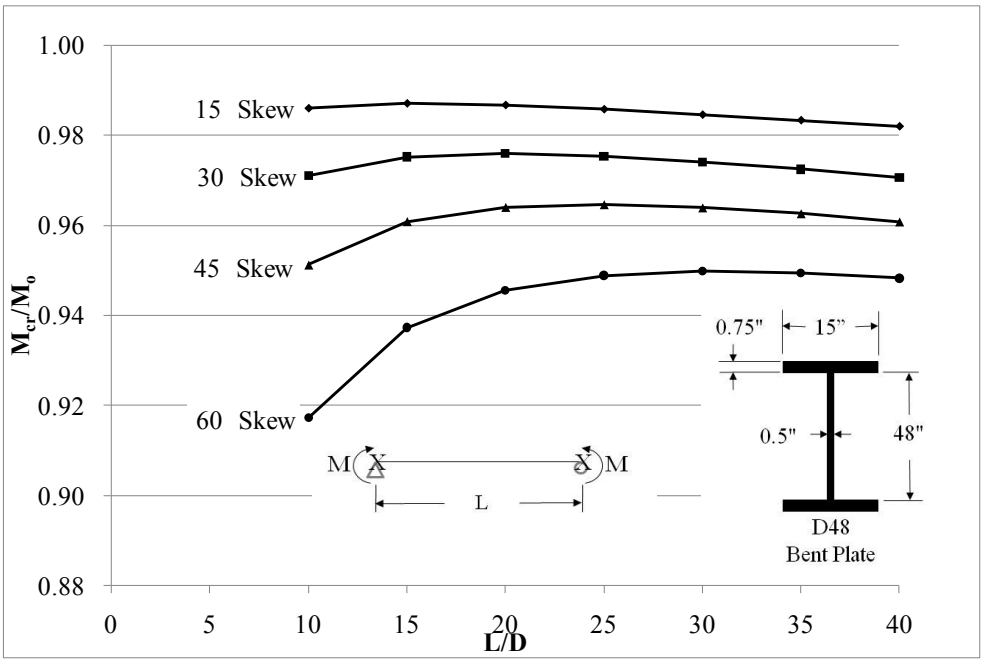

Figure C.23: D48 Cross section end twist affected buckling strength (bent plate)

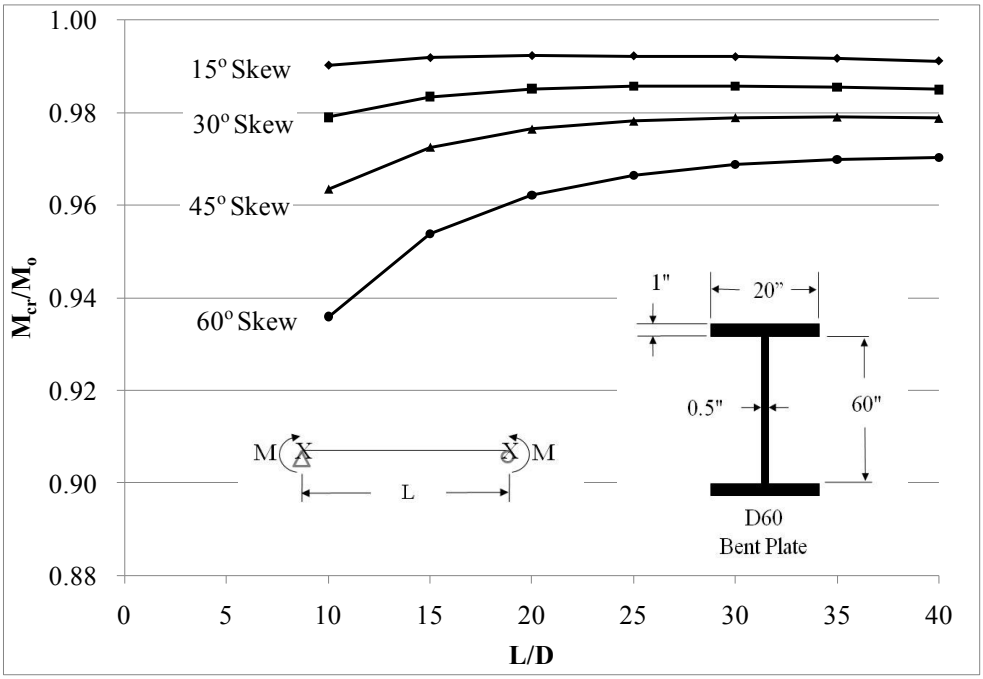

Figure C.24: D60 Cross section end twist affected buckling strength (bent plate)

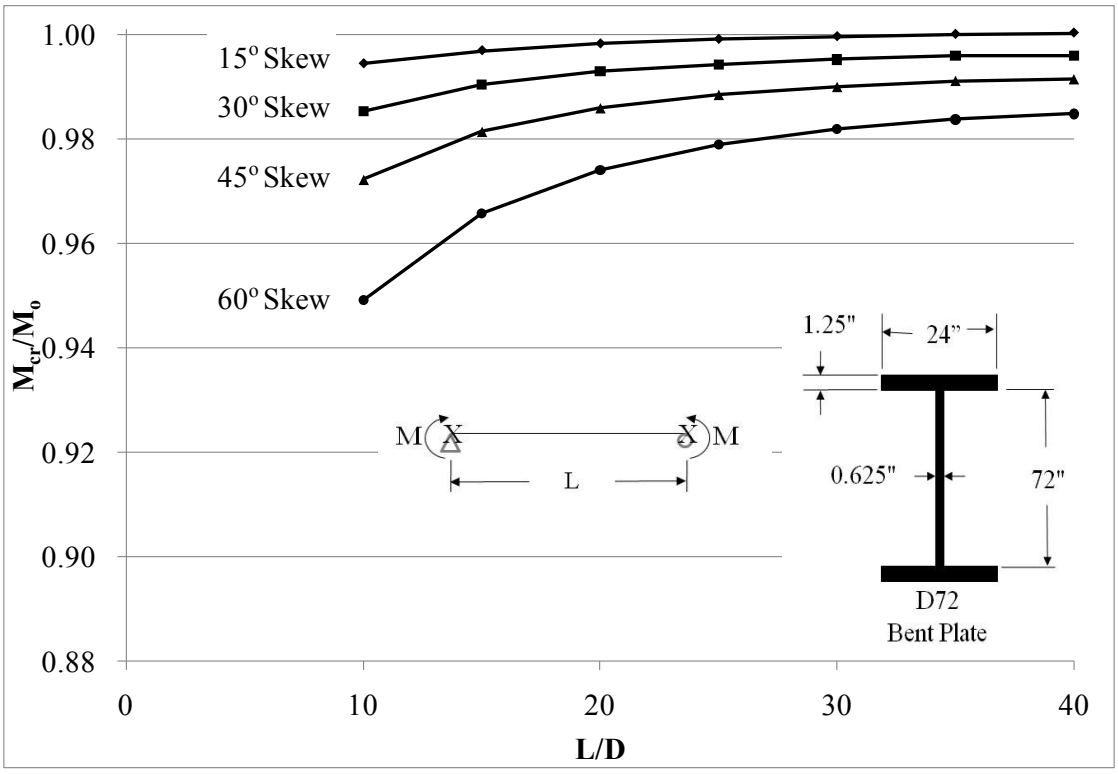

Figure C.25: D72 Cross section end twist affected buckling strength (bent plate)

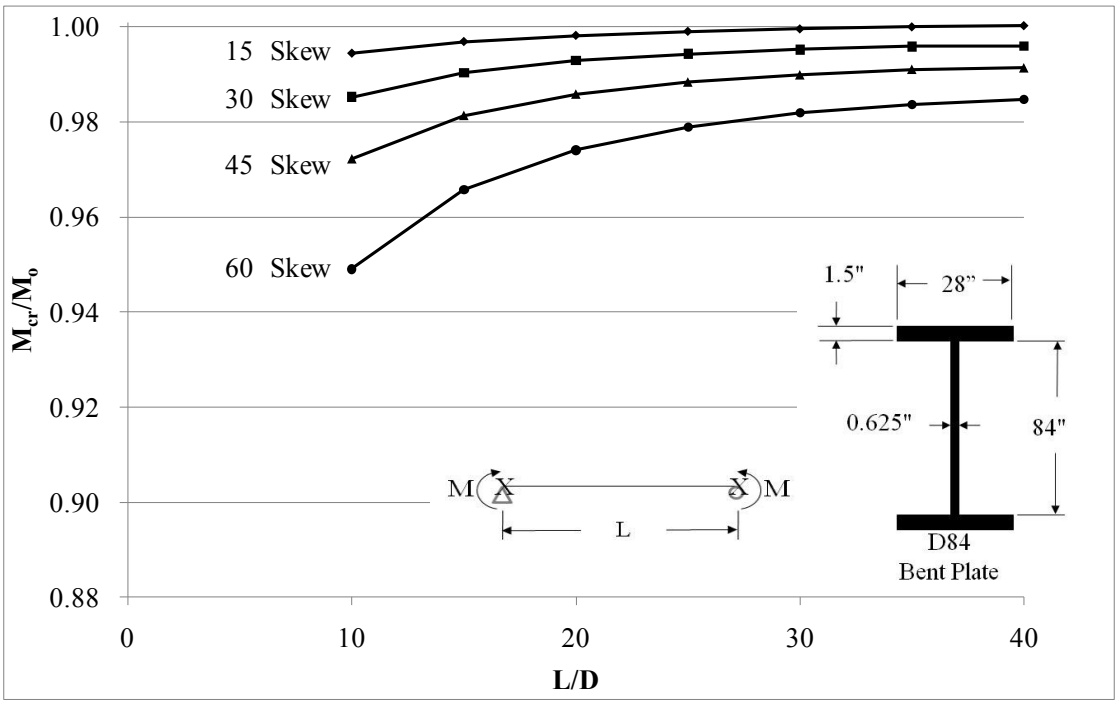

Figure C.26: D84 Cross section end twist affected buckling strength (bent plate)

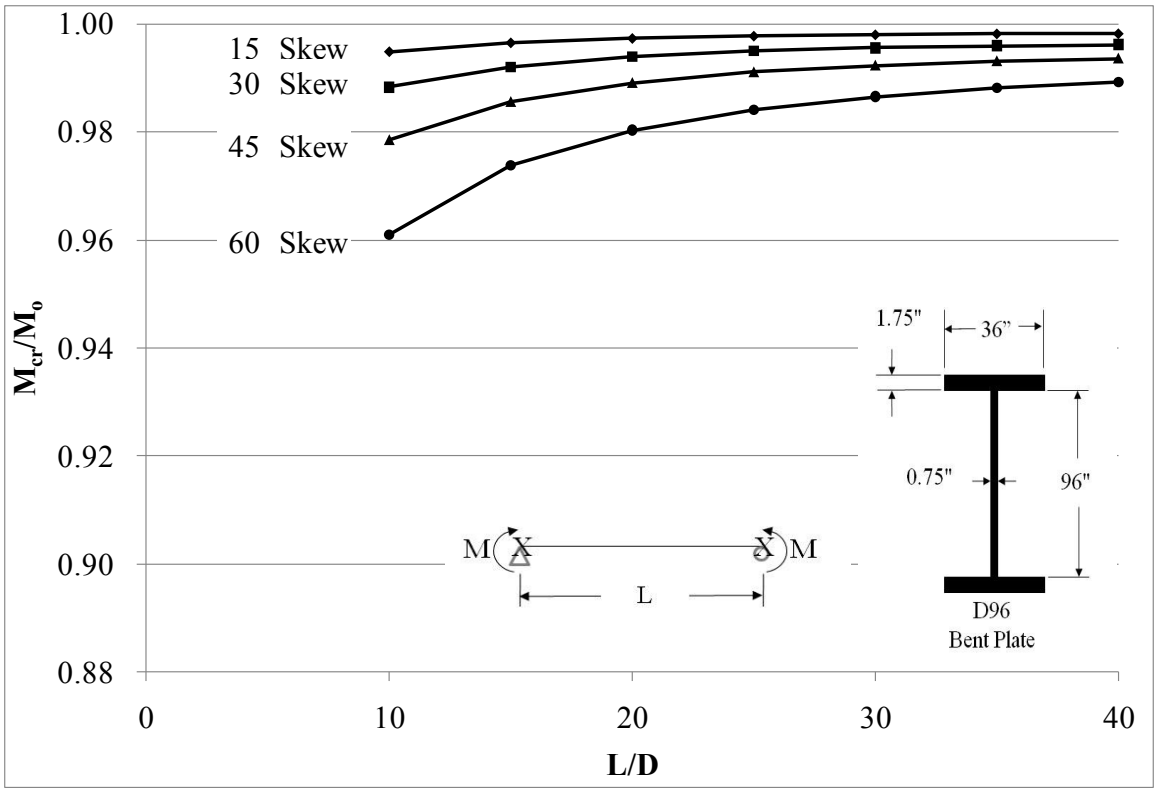

Figure C.27: D96 Cross section end twist affected buckling strength (bent plate)

C.3.2 Split Pipe Cross Frame Connection

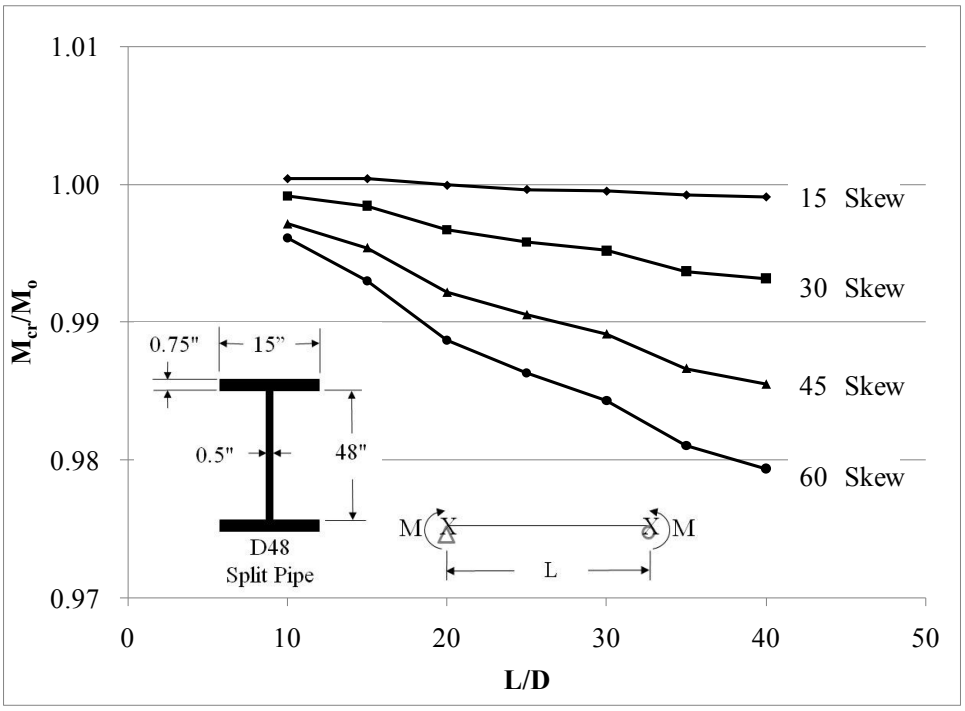

Figure C.28: D48 Cross section end twist affected buckling strength (split pipe)

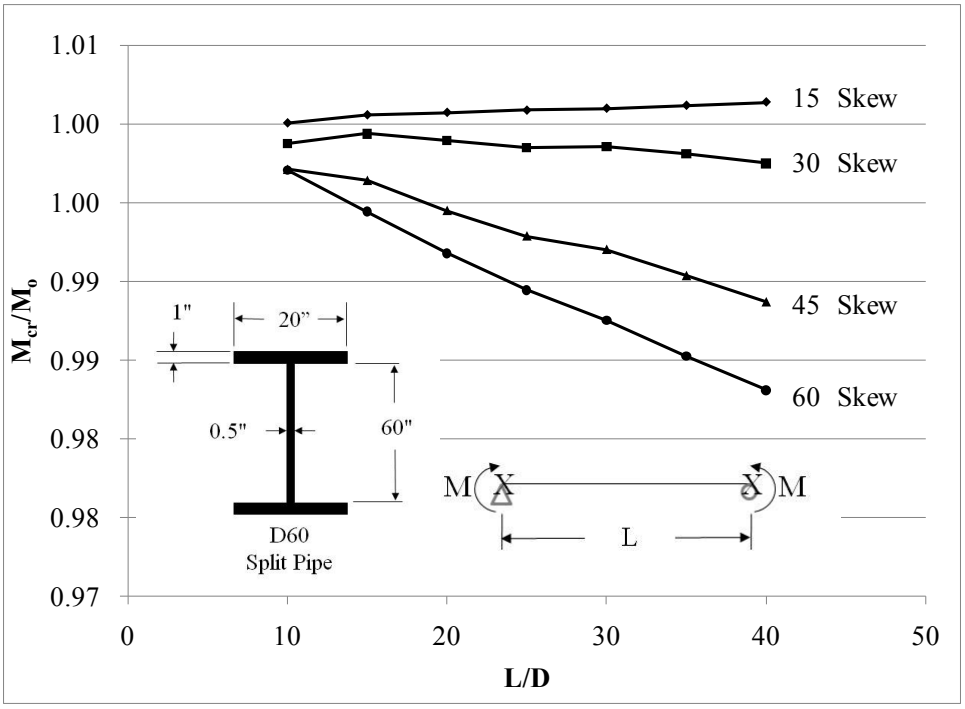

Figure C.29: D60 Cross section end twist affected buckling strength (split pipe)

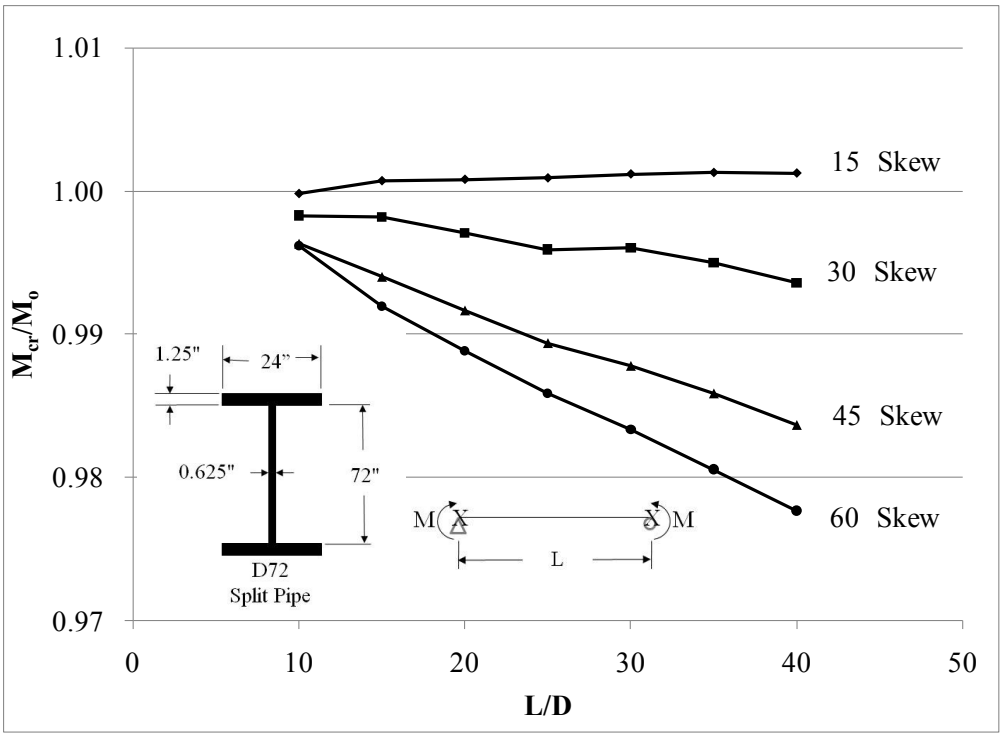

Figure C.30: D72 Cross section end twist affected buckling strength (split pipe)

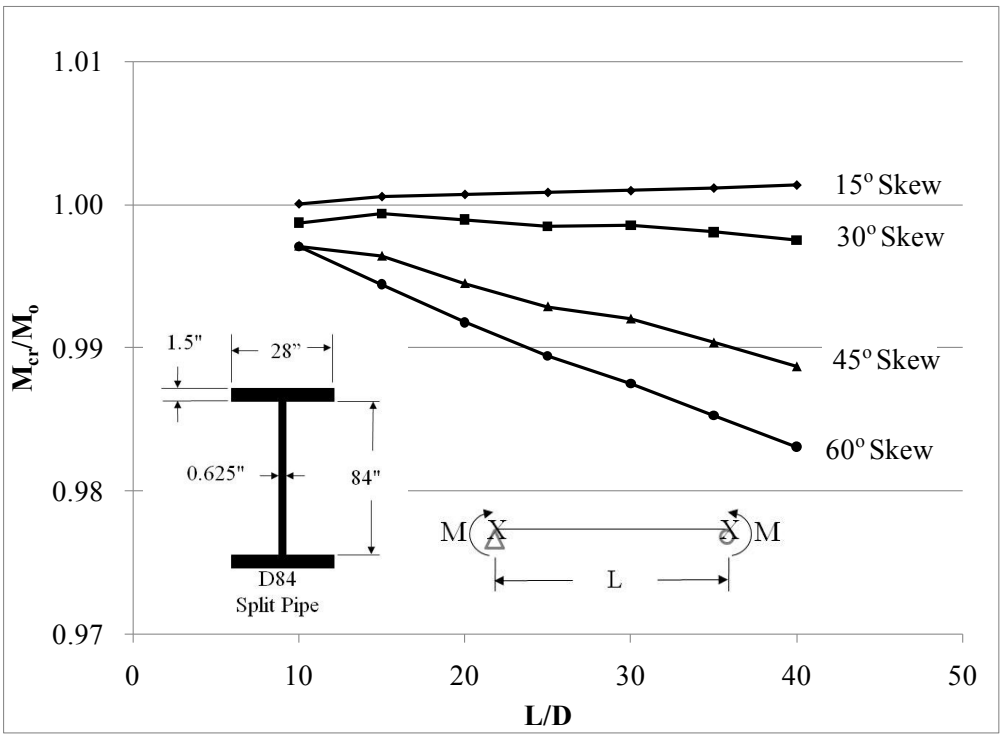

Figure C.31: D84 Cross section end twist affected buckling strength (split pipe)

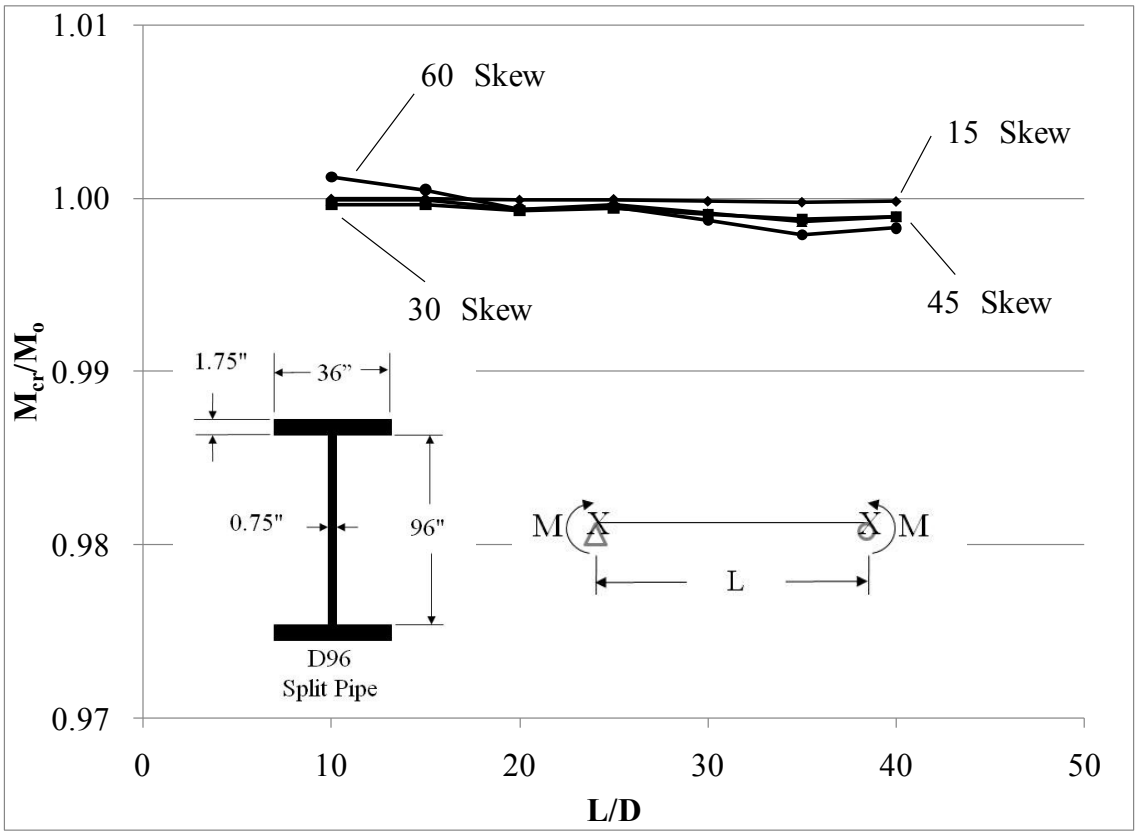

Figure C.32: D96 Cross section end twist affected buckling strength (split pipe)

C.4 PIPE STIFFENED GIRDER BUCKLING CAPACITY

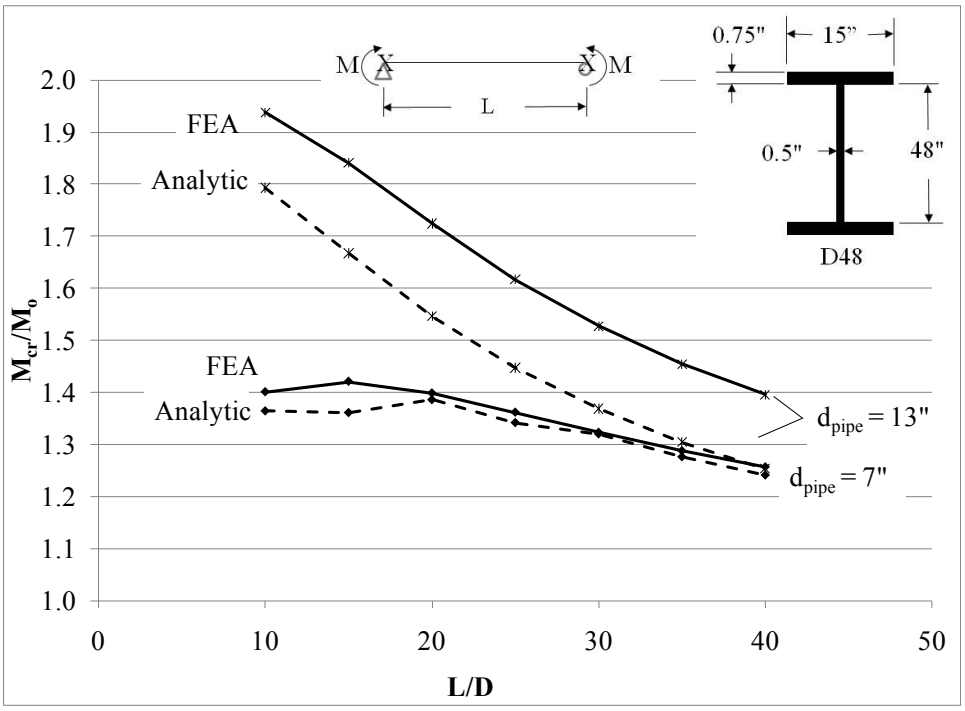

Figure C.33: D48 split pipe stiffened buckling capacity (uniform moment)

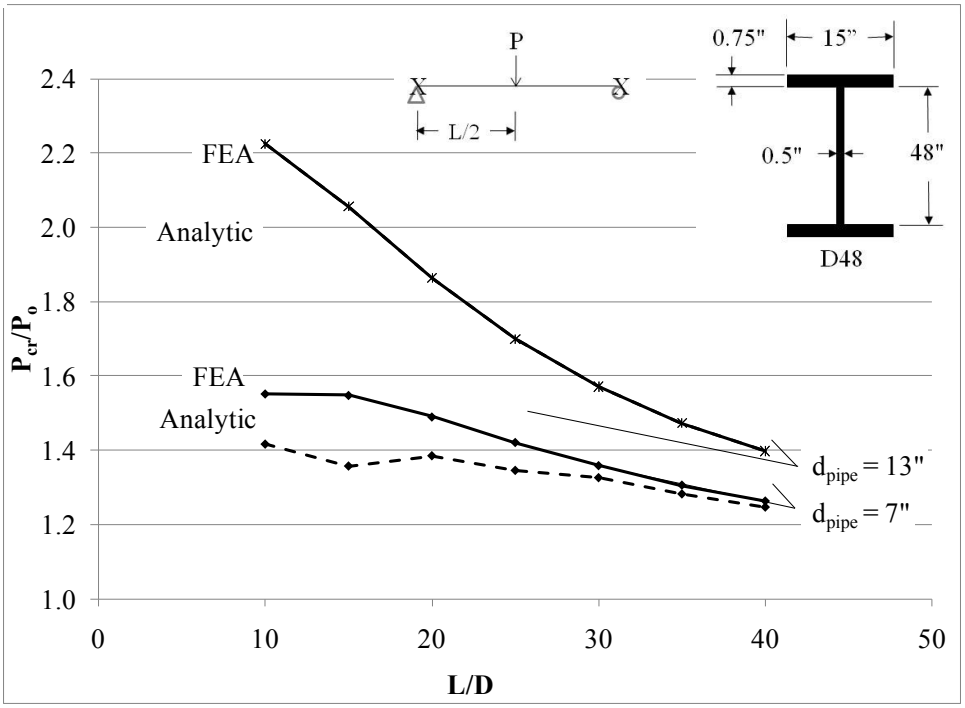

Figure C.34: D48 split pipe stiffened buckling capacity (mid-span point load)

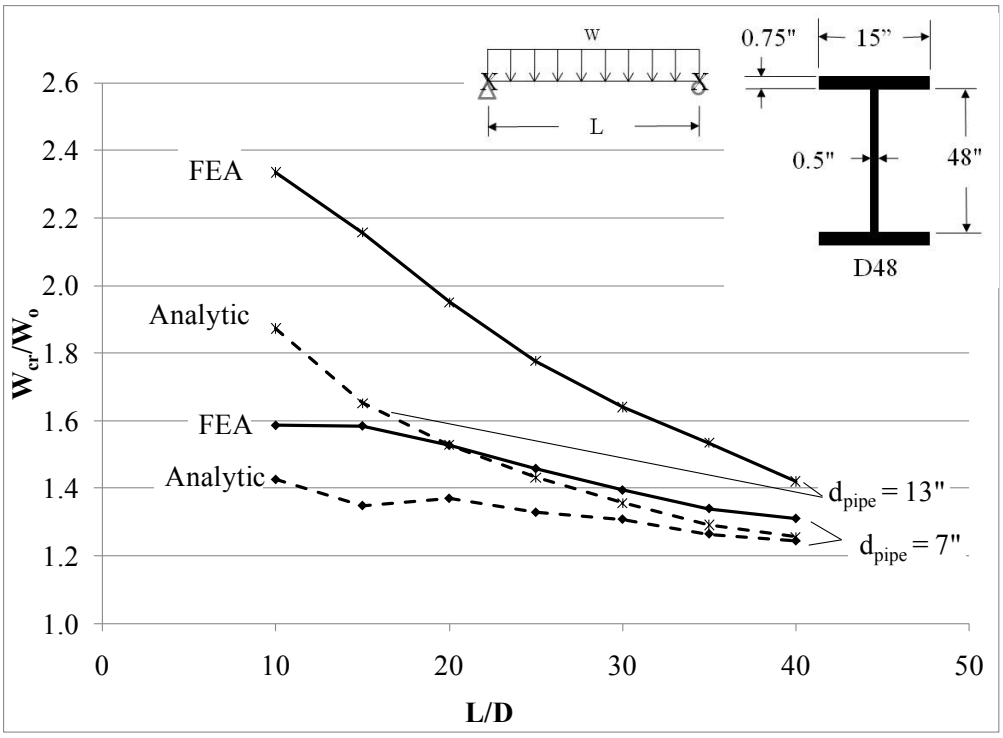

Figure C.35: D48 split pipe stiffened buckling capacity (distributed load)

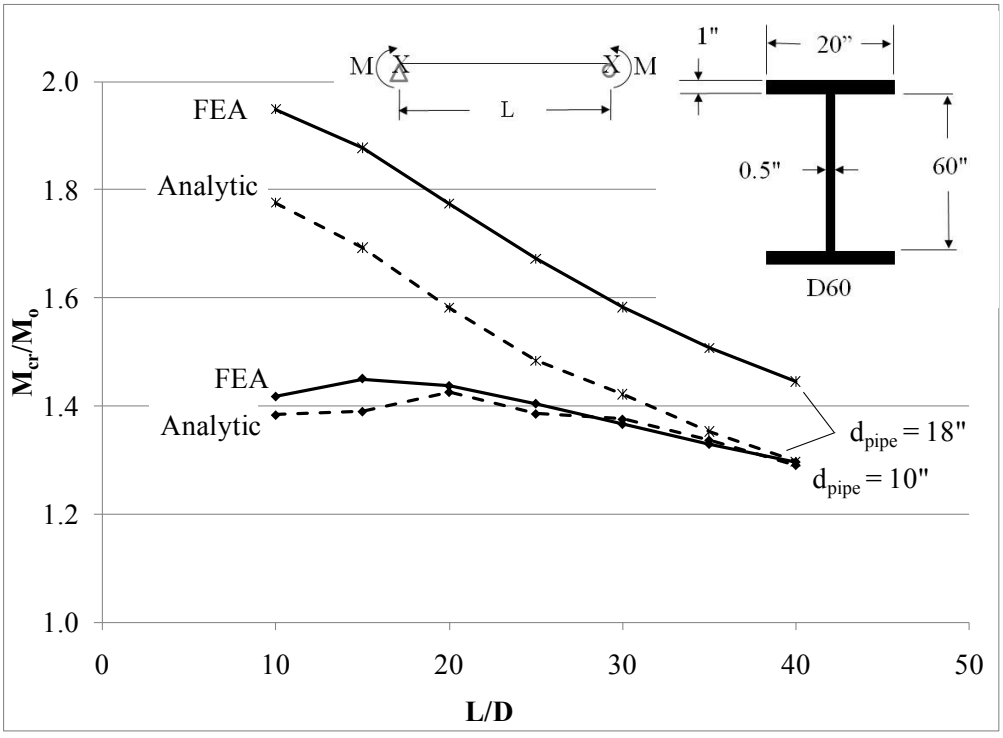

Figure C.36: D60 split pipe stiffened buckling capacity (uniform moment)

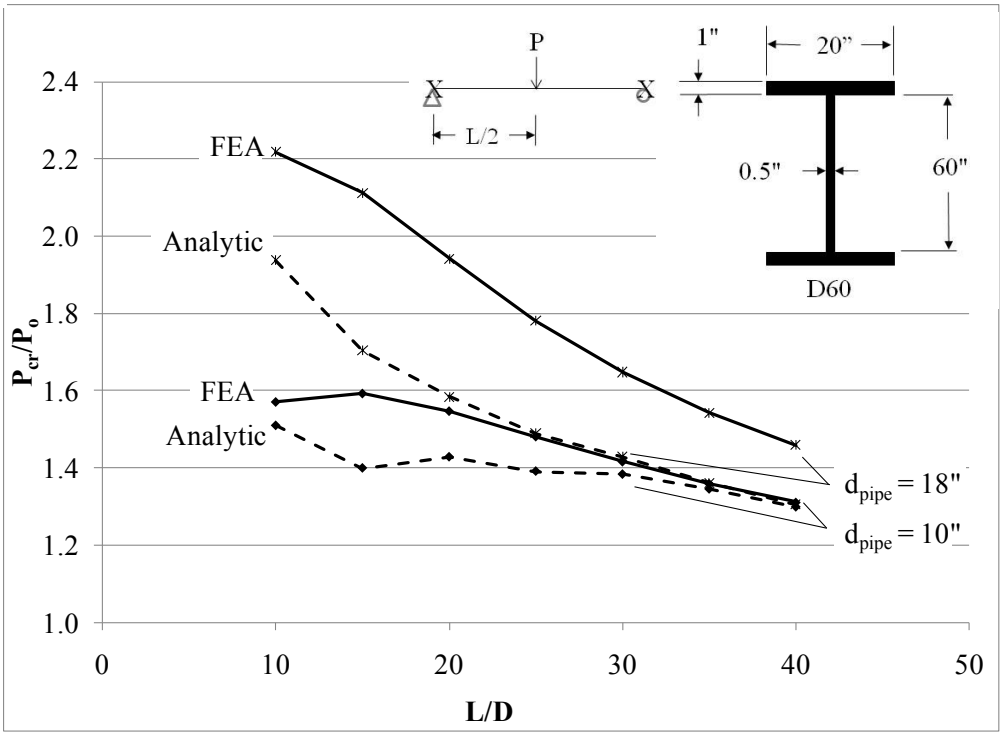

Figure C.37: D60 split pipe stiffened buckling capacity (mid-span point load)

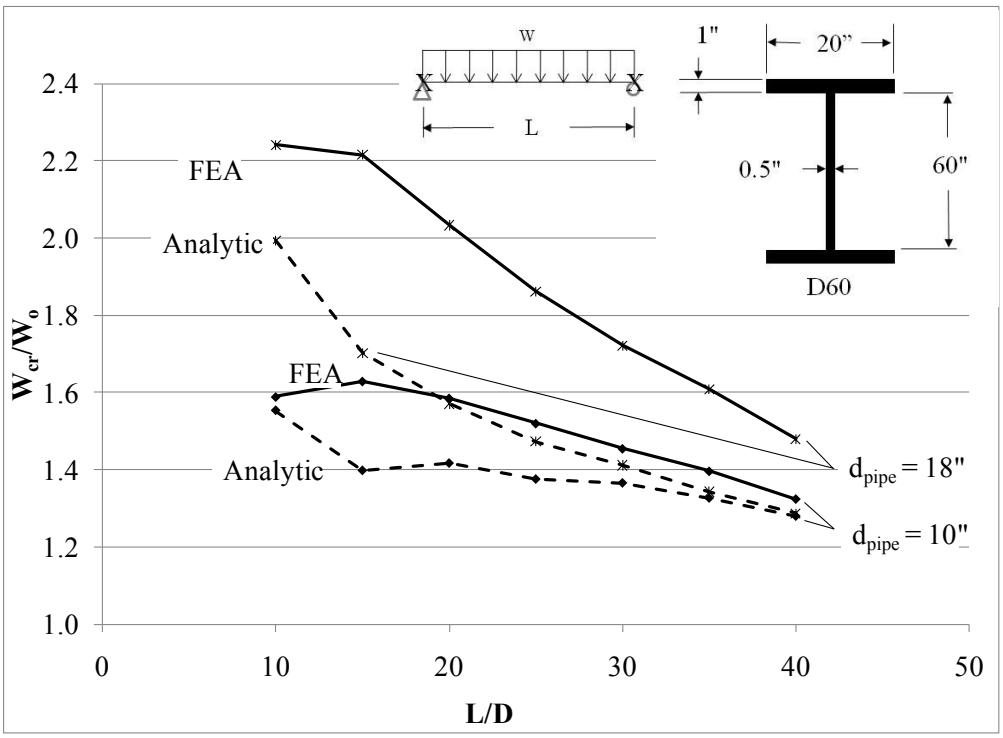

Figure C.38: D60 split pipe stiffened buckling capacity (distributed load)

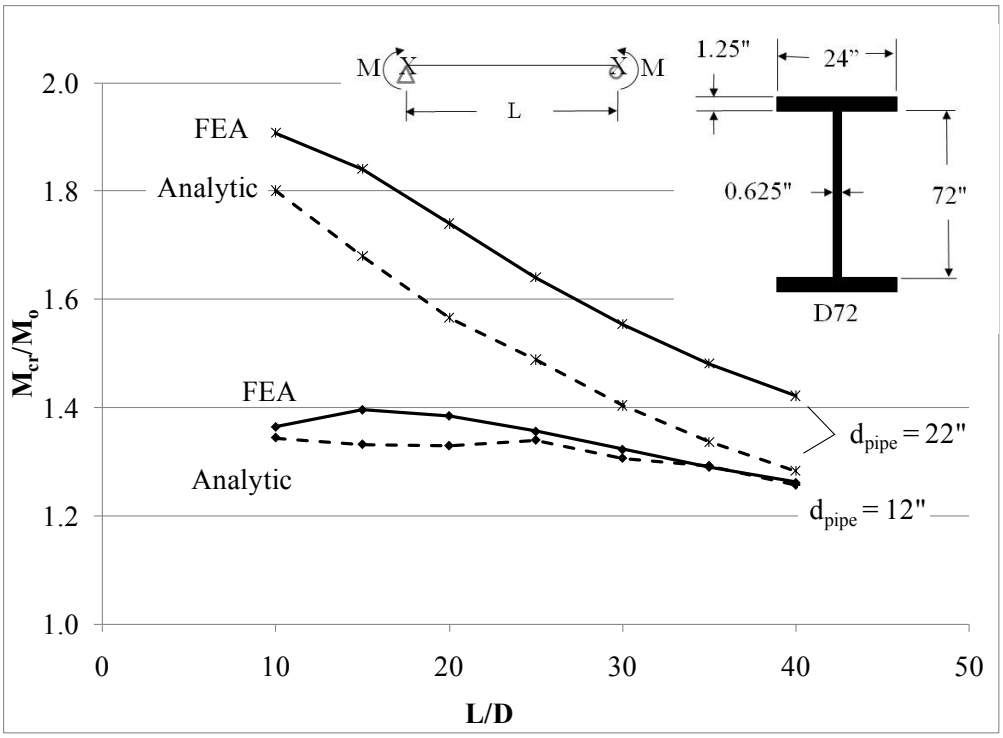

Figure C.39: D72 split pipe stiffened buckling capacity (uniform moment)

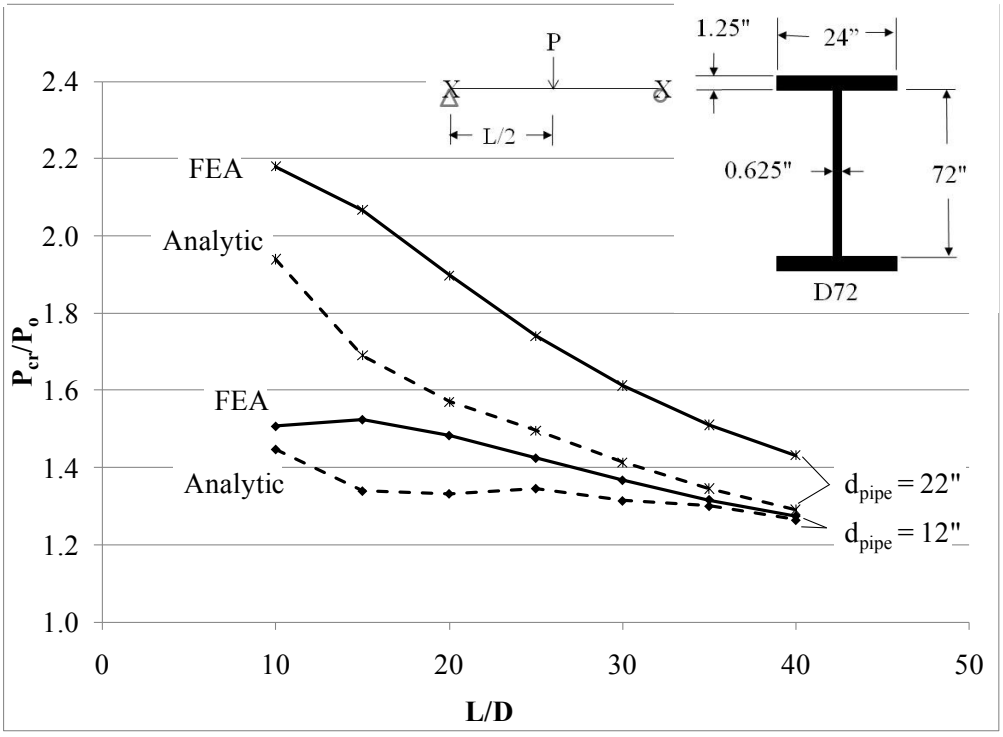

Figure C.40: D72 split pipe stiffened buckling capacity (mid-span point load)

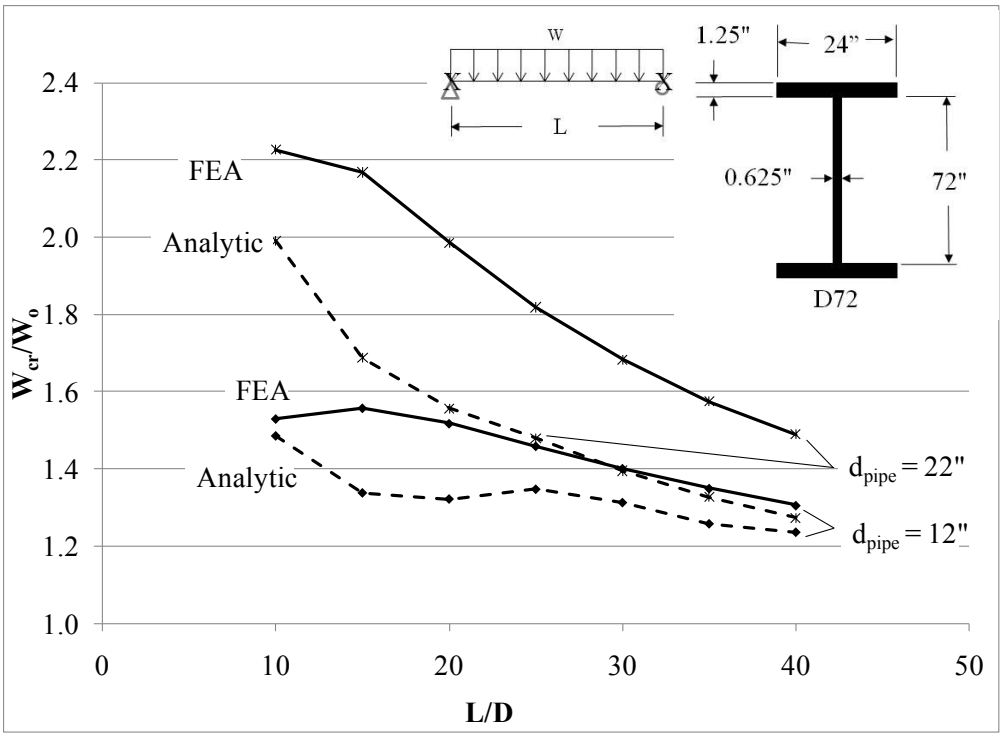

Figure C.41: D72 split pipe stiffened buckling capacity (distributed load)

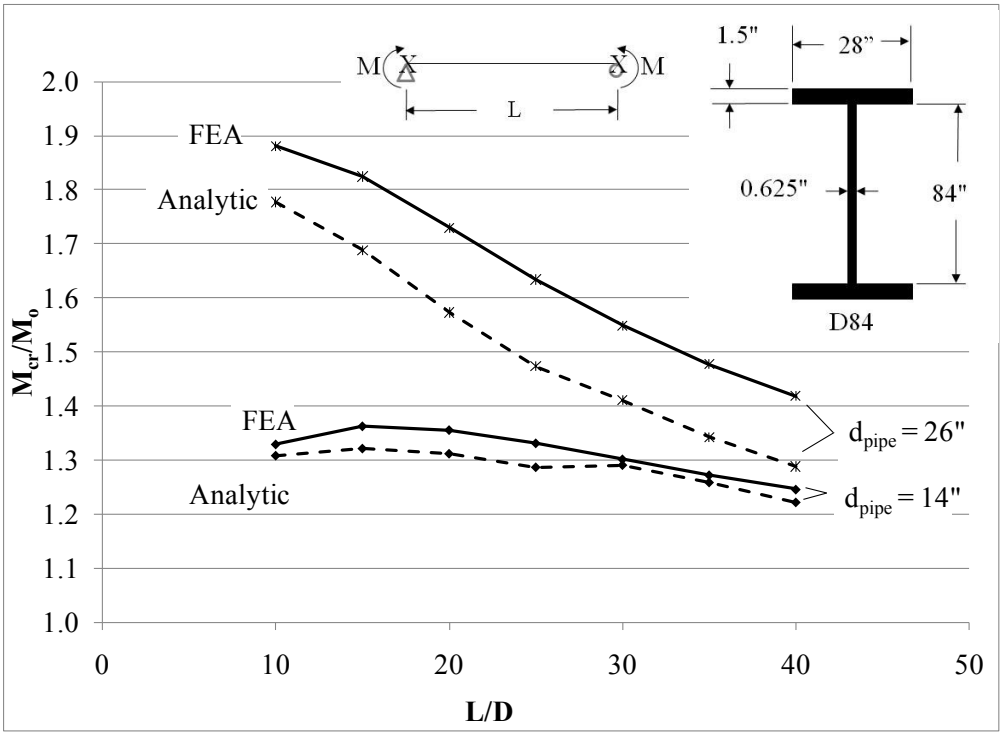

Figure C.42: D84 split pipe stiffened buckling capacity (uniform moment)

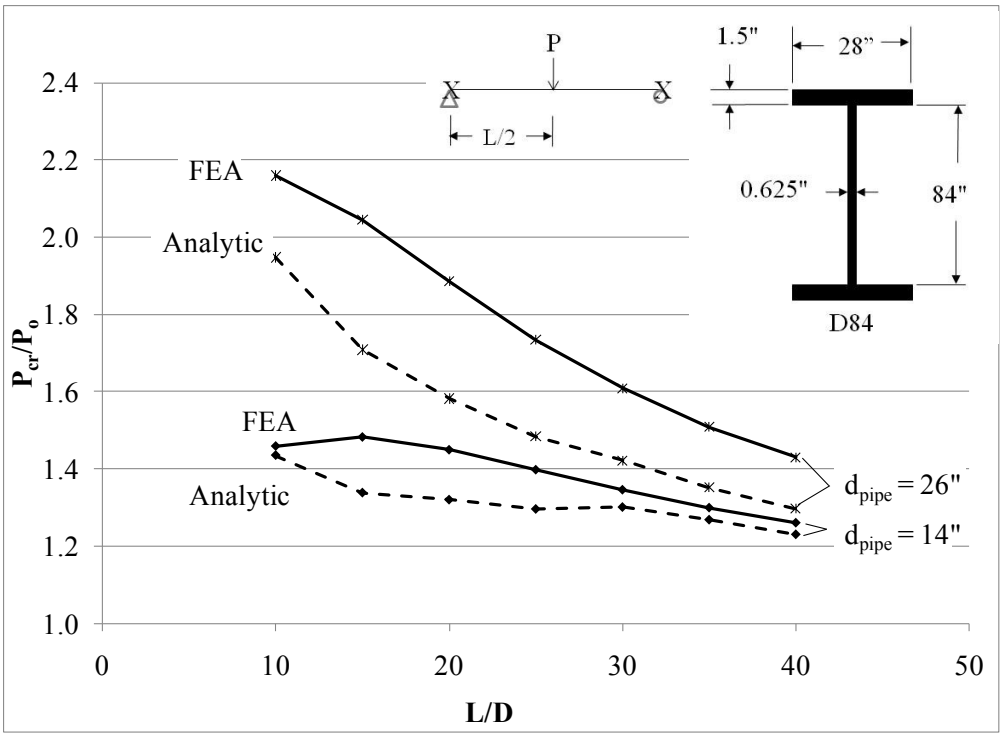

Figure C.43: D84 split pipe stiffened buckling capacity (mid-span point load)

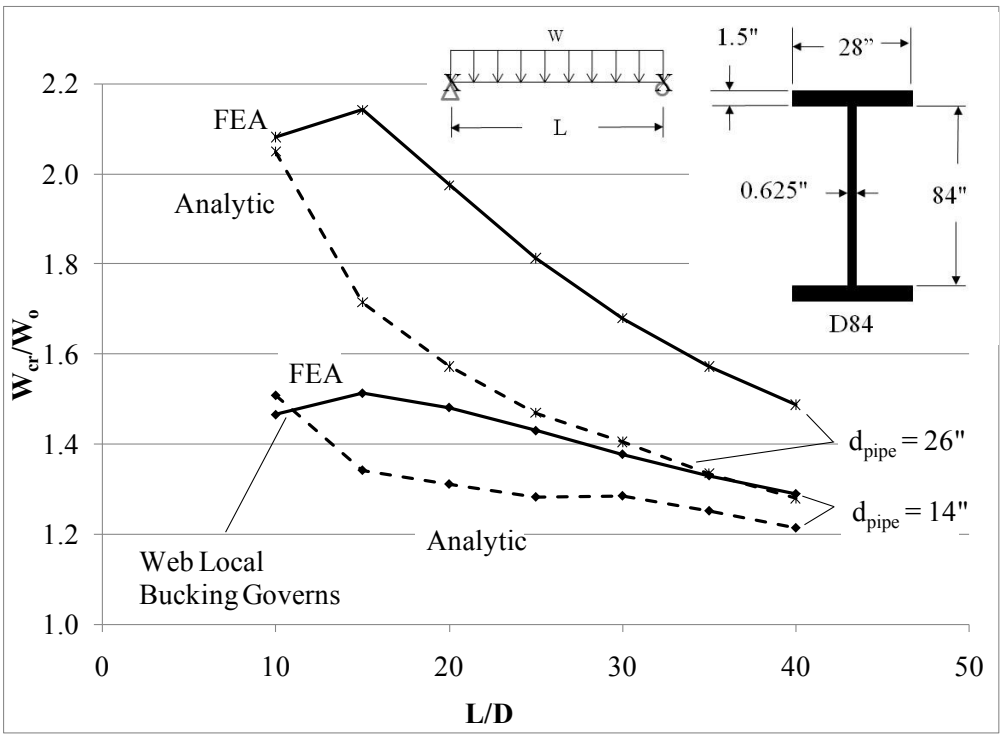

Figure C.44: D84 split pipe stiffened buckling capacity (distributed load)

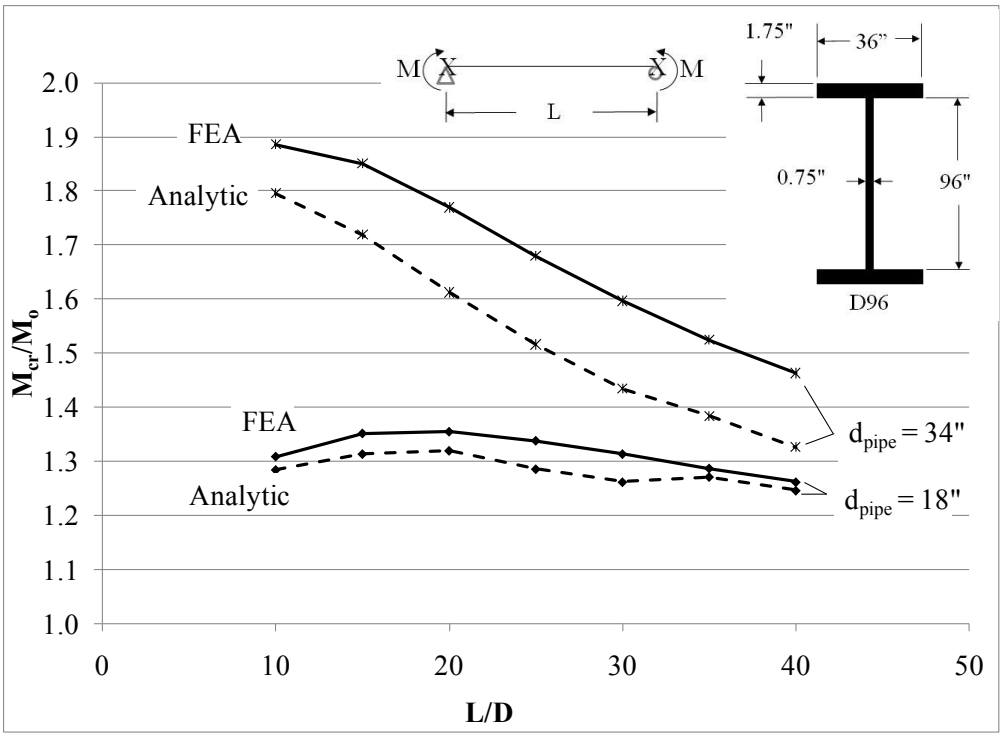

Figure C.45: D96 split pipe stiffened buckling capacity (uniform moment)

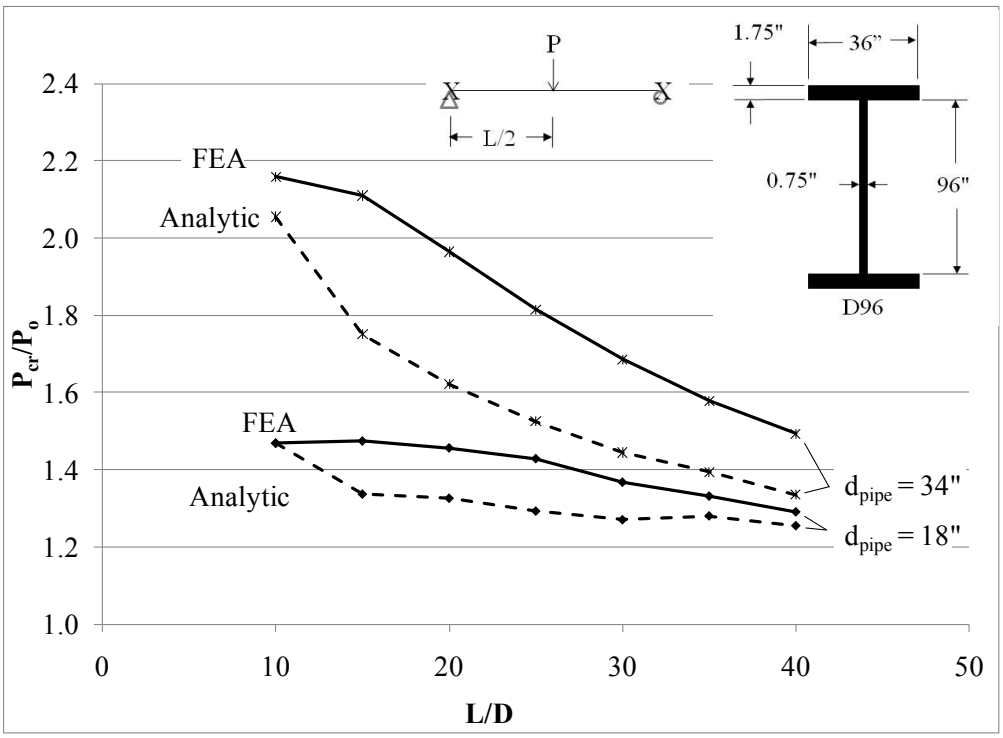

Figure C.46: D96 split pipe stiffened buckling capacity (mid-span point load)

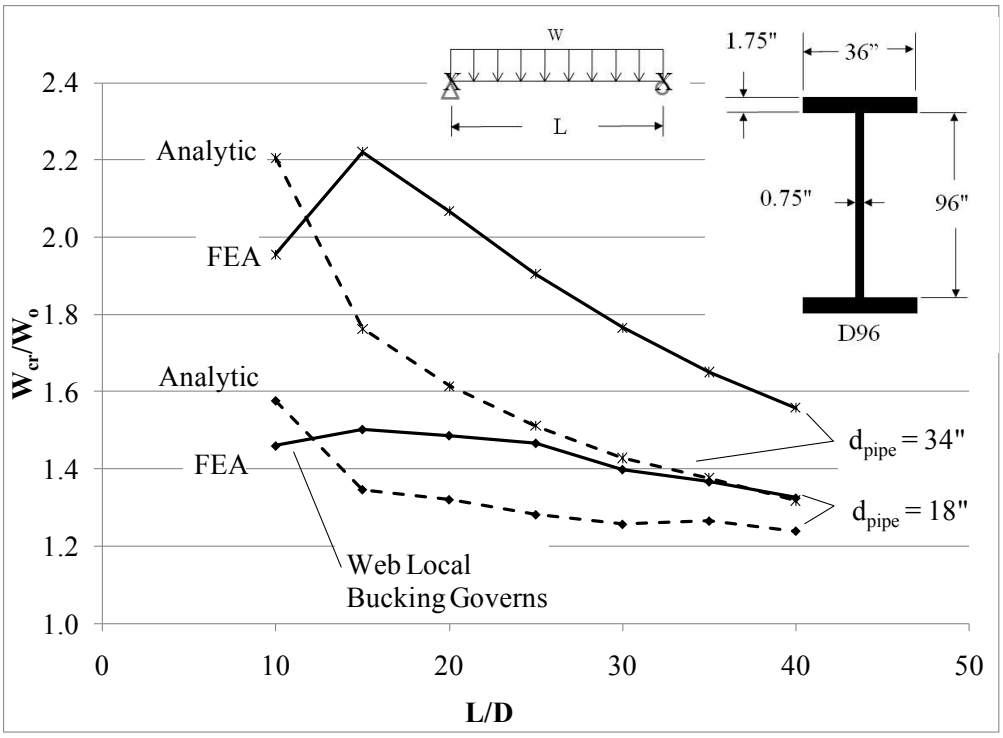

Figure C.47: D96 split pipe stiffened buckling capacity (distributed load)

References

AASHTO/NSBA Steel Bridge Collaboration. *Guidelines for Design for Constructibility.* AASHTO, 2003.

American Association of State Highway and Transportation Officials. *AASHTO LRFD Bridge Construction Specifications.* Washington, DC: AASHTO, 2004.

American Institute of Steel Construction. *Manual of Steel Construction.* Chicago: American Institute of Steel Constrution, 2005.

ANSYS Inc. "Elements Reference." *Release 11.0 Documentation for ANSYS.* 2010.

Battistini, Anthony. "Skewed Cross Frame Connection Stiffness." *Dissertation presented to The University of Texas.* Austin, TX, December 2009.

Bose, B. "The Influence of Torsional Restraint Stiffness at Supports on the Buckling Strength of Beams." *The Structural Engineer*, December 1982: 69-75.

Flint, A.R. "The Influence of Restraints on the Stability of Beams." *The Structural Engineer*, 1951: 235-246.

Heins, Conrad P., and Robert A. Potocko. "Torsional Stiffeneing of I-Girder Webs." *ASCE Journal of the Structural Division* (ASCE), August 1979: 1689-1698.

Helwig, Todd A. "Lateral Bracing of Bridge Girders by Metal Deck Forms." *PhD. Dissertation Submitted to University of Texas.* Austin, TX, August 1994.

Helwig, Todd A, Joseph A Yura, and Karl H. Frank. "Bracing Forces in Daphragms and Cross Frames." *Proceedings Structural Stalbility Research Council Conference.* Milwaukee: Structural Steel Sability Research Council, 1993. 129-140.

Herman, Reagan S, Todd A Helwig, and Zhou Chong. "Use of Lean-On Cross-Frame Bracing in Steel Girder Bridges." *Structures Congress: New Horizons and Better Practices.* Long Beach: ASCE, 2007. 79.

Hunt, Fred A. "The Suppression of Warping in Thin-Walled Beams." *M.S. Thesis Submitted to The Ohio State University.* 1973.

Meck, Harold R. "Experimental Evaluation of Lateral Buckling Loads." *Journal of The Engineering Mechanics Division*, April 1977: 331-337.

Ojalvo, M., and R.S. Chambers. "Effects of Warping Restraints on I-Beam Buckling." *ASCE Journal of the Structural Division* 103, no. ST12 (1977): 2351-2360.

Schmidt, Lewis C. "Restraints Against Elastic Lateral Buckling." *Journal of the Engineering Mechanics Diviaion*, December 1965: 1-10.

Southwell, R.V. "On the Analysis of Experimental Observations in Problems of Elastic Stability." *Proceedings of the Royal Society of London.* (The Royal Society) 135, no. 828 (April 1932): 601-616.

Structural Stability Research Council. *Guide to Stability Design Criteria for Metal Structrues.* Edited by T.V. Galambos. New York: John Wiley & Sons, 1988.

Texas Department of Transportation. "LRFD Design Manual." *Texas Departmant of Transportation.* April 2007. http://onlinemanuals.txdot.gov/txdotmanuals/lrf/lrf.pdf (accessed May 9, 2008).

Texas Department of Transportation "Miscellaneous Details Steel Girders and Beams." *Texas Department of Transportation.* April 2006. ftp://ftp.dot.state.tx.us/pub/txdot-info/cmd/cserve/standard/bridge/spgdste1.pdf (accessed February 2, 2008).

Texas Steel Quality Council. "Preferred Practices for Steel Bridge Design, Fabrication, and Erections." *Texas Depratment of Transportation.* April 1, 2007. http://www.dot.state.tx.us/publications/bridge/steel_bridge.pdf (accessed May 9, 2008).

Timoshenko, Stephen P., and James M. Gere. *Theory of Elastic Stability.* New York: McGraw-Hill, 1961.

Ude, Todd. "Field Study of Skewed I-Girders During Construction." *Proceedings of the World Steel Bridge Symposium.* San Antonio: National Steel Bridge Alliance, 2009.

Wahr, Andrew. "The Fatigue Performance of Cross Frame Connections." *Master's Thesis To Be Submitted to The University of Texas.* Austin, TX, 2010.

Wang, Liqun. "Cross-Frame and Diaphragm Behaviour for Steel Bridges with Skewed Supports." *Ph.D. Dissertation Submitted to the University of Houston.* Houston, TX, August 2002.

Wang, Liqun, and Todd A. Helwig. "Stability Bracing Requirements for Steel Bridge Girders with Skewed Supports." *Journal of Bridge Engineering* 13, no. 2 (March/April 2008): 149-157.

Whisenhunt, Todd Walter. "Measurement and Finite Element Modeling of the Non-Composite Deflections of Steel Plate Girder Bridges." *M.S. Thesis Submitted to North Carolina State University.* Raleigh, NC, 2004.

Winterling, Jason. "Monitoring Dead Load and Construction Stresses of a Heavily Skewed HPS Bridge." *M.S. Thesis Submitted to the University of Delaware.* Newark, DE, 2007.

Yarimici, Erol, Joseph A Yura, and Le-Wu Lu. *Techniques for Testing Structures Permitted to Sway.* Bethlehem: Lehigh University, 1966.

Yura, Joseph, Brett Phillips, Swarna Raju, and Stuart Webb. *Bracing of Steel Beams in Bridges.* Austin: Center for Transportation Research, 1992.

Yura, Joseph, Todd Helwig, Herman Reagan, and Chong Zhou. "Global Lateral Buckling of I-Shaped Girder Systems." *Journal of Structural Engineering* 134, no. 9 (2008): 1-8.

Zhou, Chong. "Utilizing Lean-On Cross-Frame Bracing for Steel Bridges." *Ph.D. Dissertation Submitted to the University of Houston.* Houston, TX, December 2006.

VITA

Craig Eugene Quadrato attended Bret Harte Union High School in Angel's Camp, California. In 1987 he entered the United States Military Academy and graduated in 1991 with a Bachelor of Science. in Civil Engineering and was commissioned a Second Lieutenant in the United States Army. After serving as a platoon leader and company executive officer, he graduated from The Missouri University of Science and Technology with a Master's of Science in Engineering Management in May 1995 and began his command of Bravo Company, 52nd Engineer Battalion in June 1995. . In September, 1999 he attended Stanford University and graduated with Masters of Science Degrees in Structural Engineering and Construction Engineering Management. He was assigned to the United States Military Academy as an Assistant Professor in June 2001. Upon completing his tour as Assistant Professor, Craig entered the United States Army Command and General Staff College and graduated in May, 2005 when he was assigned as Operations Officer for the 864th Engineer Battalion. In June 2005 Craig deployed and served as the Task Force Pacemaker Operations Officer in Kandahar and Paktika Province, Afghanistan. Upon completion of his tour, he was awarded the Bronze Star, Valorous Unit Award, and Meritorious Unit Citation for his service in the combat theater. In 2006, Craig was assigned as the Executive Officer for the 864th Engineer Battalion and deployed to Paktika Province, Afghanistan in January 2007. In August 2007, he accepted an appointment as an Academy Professor at the United States Military Academy and entered the Graduate School at The University of Texas at Austin.

Permanent Address: Department of Civil and Mechanical Engineering, United States Military Academy, West Point, NY 10996

This manuscript was typed by the author.